THE
PHYSICAL REVIEW

A journal of experimental and theoretical physics established by E. L. Nichols in 1893

SECOND SERIES, VOL. 80, No. 3 NOVEMBER 1, 1950

Photo-Neutron Thresholds of Beryllium and Deuterium*

R. C. MOBLEY AND R. A. LAUBENSTEIN
University of Wisconsin, Madison, Wisconsin, and Argonne National Laboratory, Chicago, Illinois
(Received July 5, 1950)

The photo-neutron thresholds of beryllium and deuterium have been measured by comparison with the $Li^7(p, n)$ threshold. For this purpose an electrostatic generator was used in which an electron beam and a positive ion beam were established simultaneously. Accurate control and measurement of the generator voltage was obtained by using an electrostatic analyzer on the H_2^+ component of the ion beam. Because the $Li^7(p, n)$ threshold lies between the $Be^9(\gamma, n)$ and $D(\gamma, n)$ thresholds, errors in extrapolation should be small. The electron beam was accelerated from ground to the accurately known potential of the high voltage electrode where x-rays were produced for the photo-disintegration process. From the photo-neutron thresholds the neutron binding energies of beryllium and deuterium were found to be 1.666 ± 0.002 and 2.226 ± 0.003 Mev, respectively.

I. INTRODUCTION

PERHAPS one of the most direct methods for determining the neutron binding energies of beryllium and deuterium is to measure their photo-neutron thresholds using x-rays produced by electrons accelerated in an electrostatic generator. Previous investigators[1,2] who measured the neutron binding energy in this manner used electrostatic generators which were designed only as electron accelerators and which had generating voltmeters for measurement and control of the electron energy. Because these generating voltmeters were calibrated at relatively low voltages, long extrapolations were necessary.

In this experiment an electron beam and a positive ion beam were established simultaneously in an electrostatic generator and the positive ion beam was used to control and measure accurately the energy of the electron beam. The energy scale was calibrated on the $Li^7(p, n)$ threshold and since this threshold lies between the $Be^9(\gamma, n)$ and $D(\gamma, n)$ thresholds, errors in extrapolation should be small.

II. APPARATUS

This experiment was performed with the pressure electrostatic generator of the Argonne National Laboratory. A schematic sketch of the arrangement is shown in Fig. 1.

The generator was operated in its normal fashion as a positive ion accelerator with the upper tube serving to accelerate positive ions and the lower tube providing differential pumping on the ion source. In addition, the differential pumping tube was used to accelerate a beam of electrons from ground to an x-ray target in the high potential electrode.

As shown in Fig. 1, the positive ion beam is separated by a magnetic analyzer into a proton and a H_2^+ beam. The H_2^+ beam is directed through a cylindrical electrostatic analyzer and onto a pair of slits where it is used to control the generator voltage at a value proportional to the voltage between the deflecting plates. Any inequality in division of current between the two exit slits is used to vary the corona current[3] electronically between the outside tank and the low potential shell so that the generator voltage is adjusted in the direction which minimizes this inequality.

The voltage between the analyzer plates is measured by means of a potentiometer and an oil-immersed resistor divider network. Calibration of the generator voltage scale in terms of the analyzer voltage was obtained by directing the proton beam onto a lithium target and making use of the $Li^7(p, n)$ threshold, which

* This work was supported in part by the AEC and in part by the Wisconsin Alumni Research Foundation.
[1] F. E. Meyers and L. C. Van Atta, Phys. Rev. **61**, 19 (1942).
[2] M. L. Wiedenbeck and C. J. Marhoefer, Phys. Rev. **67**, 54 (1945).
[3] R. M. Ashby and A. O. Hanson, Rev. Sci. Inst. **13**, 128 (1942).

has been determined to be 1.882 Mev±0.1 percent[4] on the absolute voltage scale.

In order to obtain reasonable counting rates within a few kilovolts of threshold, the x-ray target, the beryllium or deuterium sample, and the neutron counters (Fig. 2) were placed as close together as possible in the high voltage electrode of the generator. At energies above threshold, x-rays generated in the target by the electron beam produced photo-neutrons in the sample. The neutrons were detected by three BF_3 filled proportional counters.

Target Assembly

With the exception of a long circular hole 1 in. in diameter through which the electron beam reached the x-ray target, the target and sample were completely surrounded by a minimum thickness of 2 in. of lead to provide x-ray shielding for the neutron counters and other equipment in the high voltage electrode. As shown in Fig. 2, the steel tube containing the x-ray target was insulated and connected through a microammeter to the probe in order to obtain a rough measure of the electron current falling on the target. This meter could be read to an accuracy of about 1 μa by means of a telescope. A Vycor ring around the hole in the steel tube containing the x-ray target served as a visual aid in focusing the electron beam. Any electrons which missed the target caused fluorescence which could be observed by means of a mirror and window in the differential pumping tube.

The monoenergetic electron beam incident on the x-ray target produced x-rays of all energies up to that of the electron beam. Only x-rays with an energy greater than the photo-neutron threshold of the sample were effective in producing neutrons. Radiation of lower energy served only to produce an x-ray background in the neutron counters and ionization around other equipment. To minimize the intensity of low energy x-rays the target was constructed of a thin film of gold, with an absorption thickness of approximately 70 kev for 2-Mev electrons, on a thick carbon backing. Since data were taken to energies no greater than 50 kev above threshold, this target gave a thick gold target x-ray spectrum for all x-rays with an energy above threshold.

The sample placed close behind the x-ray target consisted either of a 286 g solid cylinder of beryllium metal or 145 g of deuterium oxide in a thin-walled brass container.

Neutron Detection and Data Transmission

The neutron counters shown in Fig. 2 consisted of three proportional counters filled with B^{10} enriched BF_3 to a pressure of 2 atmos. Voltage for the counters was provided by a 2100-v battery stack in a pressure-tight container. The counters had an i.d. of $\frac{1}{4}$ in., a 1.5-mil center wire, and an active length of 5-in. paraffin was placed behind the counters on the far side from the sample to give a maximum sensitivity for neutrons in the energy region near threshold. The position of the neutron counters was chosen to be as close to the sample as possible yet outside the region of highest x-ray intensity.

A special amplifier was built to modulate a small neon bulb[5] with a current proportional to the voltage output from the neutron counters. The amplifier consisted of a low noise triode coupled directly to the output from the neutron counters and followed by three stages of pentode amplification. All stages were highly degenerate

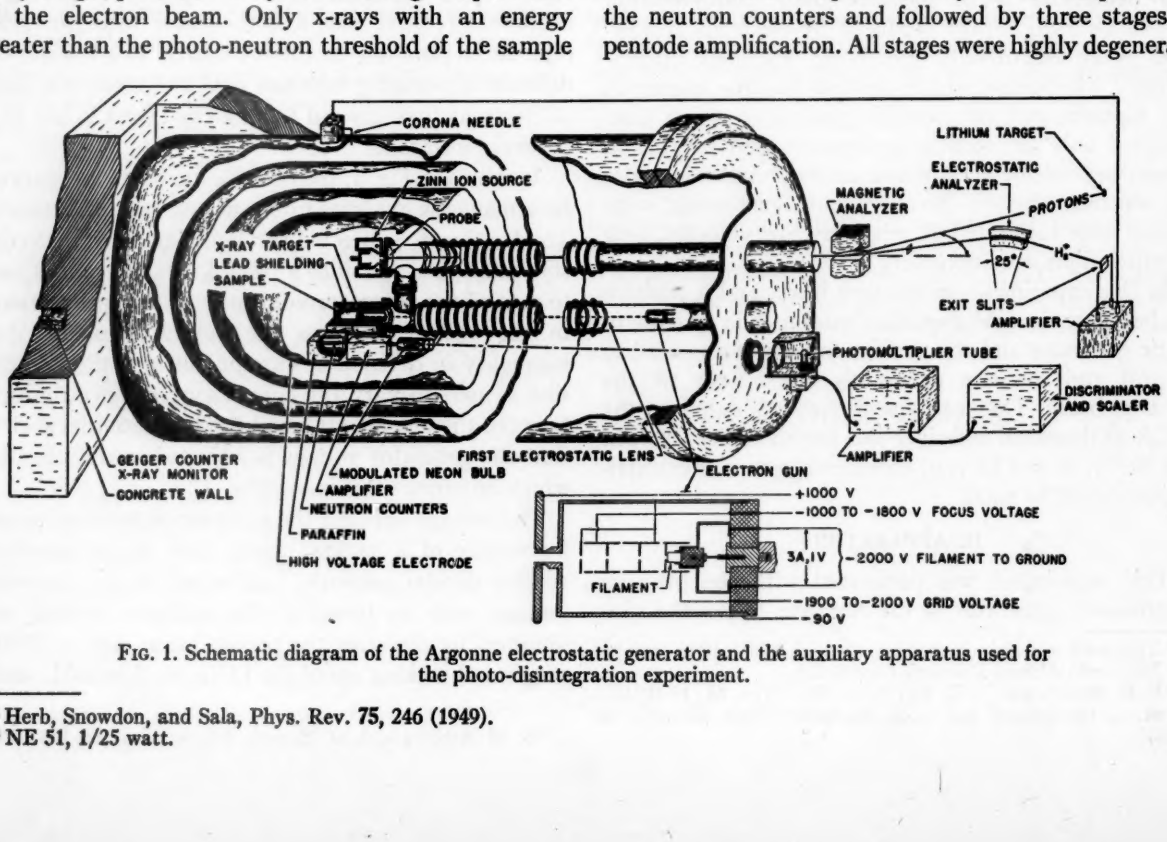

FIG. 1. Schematic diagram of the Argonne electrostatic generator and the auxiliary apparatus used for the photo-disintegration experiment.

[4] Herb, Snowdon, and Sala, Phys. Rev. **75**, 246 (1949).
[5] NE 51, 1/25 watt.

in order to insure linearity and good frequency response. The last stage was condenser coupled directly to one electrode of the neon bulb. A d.c. current was used to bias the neon bulb so that only one-half of one of the two parallel wire electrodes was surrounded by a cathode glow when there was no modulating current from the amplifier. The gain of the amplifier was then adjusted to about 10,000 where the maximum modulating current was never as large as the bias current. Viewed along its axis, the illuminated wire was essentially an intensity modulated point light source. Light in this direction was focused by a lens system through a port in the pressure tank enclosing the generator and into a photo-multiplier tube. The voltage output of the photo-multiplier tube was found to be closely proportional to the input voltage of the modulating amplifier at all frequencies up to 200 kc, while the gain of the system was found to be independent of frequency up to 50 kc, after which it decreased gradually. Whether this falling off above 50 kc was due to the circuit or to the neon bulb was not investigated, since the output from the photo-multiplier tube resembled the output from the neutron counters sufficiently well to permit it to be treated as such. The output of the photo-multiplier tube was amplified by a Model 100 amplifier which then drove a continuously variable discriminator and a scale-of-64.

Electron Gun

The electron beam was obtained from a well-shielded cathode-ray gun modified by replacing the oxide-coated cathode with a 6-mil tungsten filament. When this gun was initially mounted about 5 ft. from the first electrostatic lens in the ground portion of the differential pumping tube, a satisfactory focus could not be obtained at the high voltage electrode. After some check work using a mounting which made the gun fully adjustable in position, satisfactory results were obtained when the distance between the first electrostatic lens and the electron gun structure was between 4 and 10 in. At the distance of 8 in. which was used in the experiments, a spot about $\frac{1}{4}$ in. in diameter could be obtained at the target. For the final measurements the spot was defocused to a diameter of about $\frac{3}{4}$ in. to avoid local heating and to decrease possible variations in x-ray intensity which might accompany slight changes in position of a small image.

When the electron gun was initially placed near the first electrostatic lens, positive ions coming down the differential pumping tube and bombarding the electron gun shield released large numbers of secondary electrons which traveled back up the tube. To trap these secondary electrons, a circular plate at a positive potential of 1000 v was placed immediately in front of the electron gun shield as shown in Fig. 1.

A steel tube attached to the shield and extending through the plate was used to conduct the electron beam through the plate with a minimum disturbance

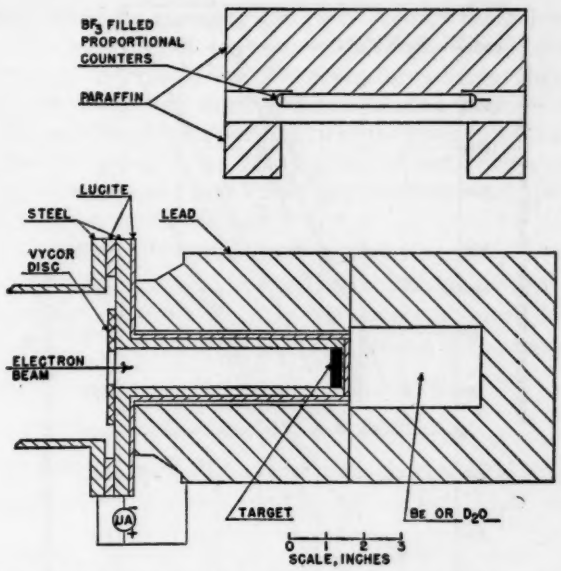

FIG. 2. Scale drawing of the x-ray target, sample, and neutron counters housed in the high voltage electrode.

to the focusing of the beam from the potential of the plate. Secondary electrons formed behind the electron gun were prevented from going up the differential pumping tube by a negative potential of 90 v on the electron gun shield. The current leaving the electron gun and that arriving at the x-ray target were the same within the accuracy of 1 μa with which the latter could be read.

III. EXPERIMENTAL PROCEDURE

Photo-neutron thresholds for beryllium and deuterium were obtained by extrapolating the neutron yield *versus* energy curve to zero yield. A Geiger counter outside the generator, behind 1 ft. of concrete and approximately on the axis of the electron beam, was used to monitor the high energy x-ray yield. A constant number of counts from the Geiger counter caused by x-rays from the electron beam were used to normalize the photo-neutron yield. During each run the number of x-ray counts was sufficiently large so that the probable error in normalization was 0.3 percent or less. Normalization in this manner should minimize errors due to fluctuations in the electron current or possible changes in x-ray intensity as the beam moved slightly on the target. With an electron current of 15 μa at an energy of 2.23 Mev the x-ray intensity around the box containing the Geiger counter was about 5 mr/hr., six percent of which was due to secondary electrons caused by the positive ion beam.

Data in this experiment were taken with electron currents of 10 or 15 μa. With an electron current of 15 μa, the x-ray background in the neutron counters was approximately one-quarter of the maximum neutron pulse height. Higher currents were not used because of lack of sufficient cooling for the target assembly and because higher x-ray intensity caused an undesirable

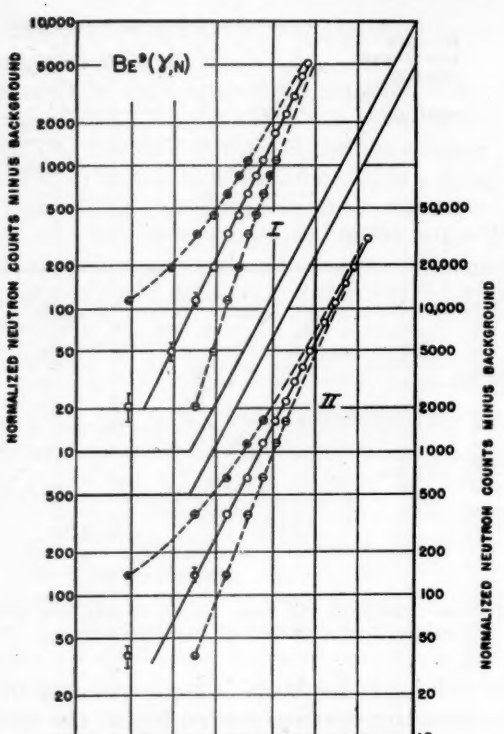

FIG. 3. Logarithmic plots of the photo-disintegration yield of beryllium *versus* the electron voltage above threshold. The solid lines are for an assumed threshold which gives a straight-line plot. The dotted curves result from assuming a threshold 0.93 kev either side of this. Statistical errors are smaller than the circles except where indicated. The neutron counts were normalized to a constant number of counts on the Geiger counter owing to x-rays from the electron beam. The number of Geiger counts chosen as a base for normalization was the average of all the 5-min. runs used in taking a set of data and the normalized neutron yield thus obtained is approximately equal to the actual neutron yield. The background below threshold for both curves was approximately six counts in 5 min. The electron current for both curves was 15 μa.

shortening of the plateau in the curve giving neutron counts *versus* discriminator bias.

High positive ion currents were observed to result in a secondary electron current in the ion accelerating tube sufficiently large to cause an objectionable x-ray background in the neutron counters. For this reason the generator was operated with the positive ion current as small as possible while still permitting effective operation of the energy control circuits.

The electron beam has not as yet been used for voltage control of the Argonne generator. At the Rice Institute this method of control has proved highly successful below[6] 2 Mev and electron currents up to about 20 μa were found to be sufficient. When the Argonne machine was operated at 2.2 Mev with an electron current of 15 μa, the x-ray intensity at the front of the machine and at the side and back of the machine beyond the shielding was approximately 1 mr/hr. or less. This intensity should be reduced appreciably when the present target is replaced by one consisting only of thick carbon. The shielding consists principally of the heavy lead immediately around the target and a concrete wall 2 ft. thick extending along one side of the machine and a concrete wall 32 in. thick across the back. If the x-ray intensity beyond the shielding varies approximately as the fifth power of the generator voltage, as indicated by the work at the Massachusetts Institute of Technology,[7] the shielding of the Argonne machine may be adequate for continuous use of the electron beam up to a generator voltage of about 4 Mev.

The beryllium and deuterium (γ, n) threshold voltages were each measured four times. Calibration of the voltage scale on the $Li^7(p, n)$ threshold were made before and after each (γ, n) threshold measurement. Although these two calibrations never differed by more than 0.05 percent, their average was used for calculation. Pure lithium targets about 5 kv thick were prepared by evaporation onto a tantalum backing while it was in place on the generator. Because the targets were heated to only about 80°C, they were renewed frequently to prevent any appreciable shift in the $Li^7(p, n)$ threshold due to surface accumulations on the target.

At the beginning of this experiment the electrostatic analyzer plates were polished to remove any non-

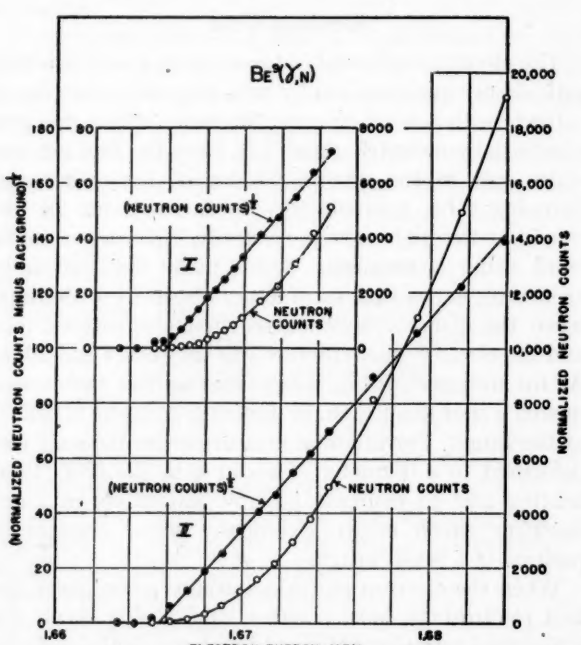

FIG. 4. The photo-neutron yield of beryllium near threshold. The neutron counts were normalized to a constant number of counts on the Geiger counter owing to x-rays from the electron beam. The number of Geiger counts chosen as a base for normalization was the average of all the 5-min. runs used in taking a set of data and the normalized neutron yield thus obtained is approximately equal to the actual neutron yield. The background below threshold for both curves was approximately six counts in 5 min.

[6] S. J. Bame, Jr., and L. M. Baggett, Rev. Sci. Inst. **20**, 839 (1949).

[7] Petrauskas, Van Atta, and Myers, Phys. Rev. **63**, 389 (1943).

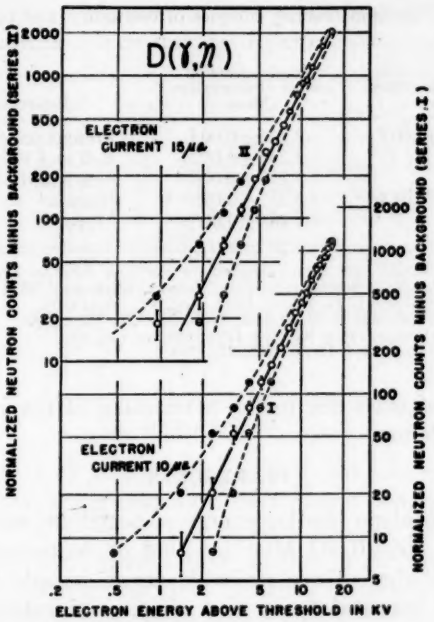
D(γ,n)
ELECTRON CURRENT 15 μa
ELECTRON CURRENT 10 μa
NORMALIZED NEUTRON COUNTS MINUS BACKGROUND (SERIES II)
NORMALIZED NEUTRON COUNTS MINUS BACKGROUND (SERIES I)
ELECTRON ENERGY ABOVE THRESHOLD IN KV

FIG. 5. Logarithmic plots of the photo-disintegration yield of deuterium *versus* the electron voltage above threshold. The solid lines are for an assumed threshold which gives a straight-line plot. The dotted curves result from assuming a threshold 0.93 kev either side of this. Statistical errors are smaller than the circles except where indicated. The neutron counts were normalized to a constant number of counts on the Geiger counter owing to x-rays from the electron beam. The number of Geiger counts chosen as a base for normalization was the average of all the 5-min. runs used in taking a set of data and the normalized neutron yield thus obtained is approximately equal to the actual neutron yield. The background below threshold for both curves was approximately six counts in 5 min.

conducting surface deposits. Since a current from 1 to 3 μa normally flowed between the plates of the electrostatic analyzer, small corrections (less than 0.04 percent) were made to the measured analyzer voltage in order to account for the voltage drop across the 1-megohm resistor in series with each plate.

Use of an electrostatic generator having a Zinn-type ion source[8] with a probe as a first ion accelerating electrode, suggested the possibility that the H_2^+ ions and the protons might originate in regions of different potentials lying between the potential of the arc and that of the probe, with the result that H_2^+ and proton beams would emerge from the probe with a difference in energy. Since the H_2^+ beam was used for measurement of the generator voltage and the proton beam for calibration of the voltage scale, a difference in energy between these two beams would result in a small error in calibration. Also, since the x-ray target was connected electrically through a microammeter and the metal structure near the ion source to the probe, changes in energy of the H_2^+ beam emerging from the probe as a function of the potential difference between the arc and the probe (probe voltage) would affect the position of the $Be^9(\gamma, n)$ threshold on the generator voltage scale.

[8] W. H. Zinn, Phys. Rev. **52**, 655 (1937).

Tests made by changing the probe voltage from 1 to 2.5 kv were found to raise both the $Li^7(p, n)$ and $Be^9(\gamma, n)$ thresholds on the generator voltage scale. Because of the shift in these thresholds as a function of probe voltage, all data were taken at the lowest practical probe voltage of 1 kv. Making use of test results at probe voltages of 1 and 2.5 kv, all data were extrapolated to zero probe voltage.

The filament of the electron gun was operated at a negative potential of 2 kv with respect to ground, and 2 kev was therefore added to the energy obtained by the electron beam in traveling from ground to the x-ray target.

III. EVALUATION OF DATA

At energies near the photo-neutron threshold the photo-neutron cross section for either beryllium[9] or

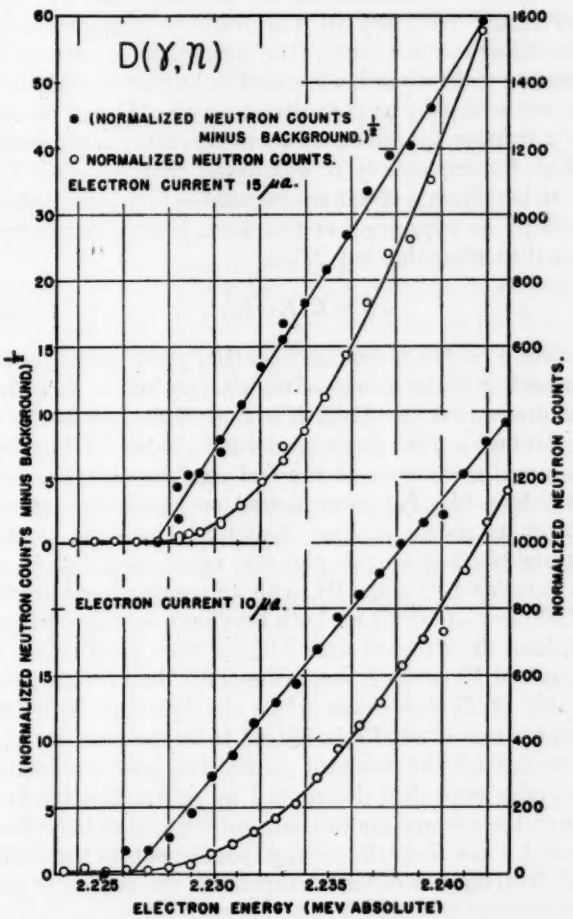

FIG. 6. The photo-neutron yield of deuterium near threshold. The neutron counts were normalized to a fixed number of counts on the Geiger counter owing to x-rays from the electron beam. The number of Geiger counts chosen as a base for normalization was the average of all the 5-min. runs used in taking a set of data and the normalization neutron yield thus obtained is approximately equal to the actual neutron yield. The background below threshold for both curves was approximately six counts in 5 min.

[9] E. Guth and C. J. Mullin, Phys. Rev. **76**, 234 (1949).

deuterium[10] should, according to theory, be approximately proportional to the square root of the energy above threshold. Also, if V_0 is the total potential difference traversed by the electrons in reaching the x-ray target and k is a constant, then experimentally[11] the intensity I_V of an isochromat corresponding to a voltage V which is less than V_0 is given by

$$I_V = k(V_0 - V). \quad (1)$$

Using this equation to represent the x-ray spectrum from threshold to the energy of the electron beam, some 50 kev or less above threshold, gives the expected neutron yield as proportional to

$$(E - E_0)^n, \quad (2)$$

where E_0 is the photo-neutron threshold energy, E is the energy of the electron beam, and $n = 2.5$. Owing to the method of normalizing the neutron yield and the decreasing efficiency of the neutron counters with increasing neutron energy, the normalized experimental neutron yield minus background would not be expected to rise as rapidly as is predicted by Eq. (1), but rather in a manner approximated by a somewhat lower value of n. Experimentally it was found that the data for both beryllium and deuterium could be fitted reasonably well by an expression of this form with a value of n equal to approximately 2, i.e.,

$$Y = K(E - E_0)^n, \quad (3)$$

where Y is the normalized neutron yield minus background, E is the energy of the electron beam, E_0 is the photo-neutron threshold, K is a constant, and $n = 2$.

To find n for a given yield curve, values of E_0 were assumed and curves of Y *versus* electron energy above threshold $(E - E_0)$ were plotted on logarithmic graph paper as shown in Figs. 3 and 5. The slope of the straightest line on this plot was taken as n. Values of n between 1.93 and 2.05, with an average very nearly 2.00, were obtained for both beryllium and deuterium. Taking the value of n as 2.00 for each yield curve, a graph of $Y^{\frac{1}{2}}$ *versus* E was made (Figs. 4 and 6) and the value of E_0 was taken to be the intercept with the energy axis of what was judged to be the best straight line through the resultant points. The neutron binding energies were then determined by subtracting 0.2 kev from the average photo-neutron threshold of beryllium and 1.3 kev from the average photo-neutron threshold of deuterium in order to correct for the motion of the center of mass due to the momentum of the incident x-ray photon.

[10] H. A. Bethe, *Elementary Nuclear Theory* (John Wiley and Sons, Inc., New York, 1947), p. 59.
[11] W. C. Miller and B. Waldman, Phys. Rev. **75**, 425 (1949).

TABLE I. Neutron binding energies of deuterium and beryllium.

Neutron binding energy of beryllium (Mev)	Neutron binding energy of deuterium (Mev)	Reference
1.666±0.002	2.226±0.003	Present paper
	2.230±0.007	Bell and Elliott[b]
	2.227±0.010	Smith and Martin[c]
1.681±0.013	2.221±0.013[a]	Hanson[d]
	2.181±0.005[a]	Meyer[e]

[a] These values have been corrected for the new value of 2.615±0.004 Mev for the ThC″ gamma-ray. A. L. Wolfson, Phys. Rev. **78**, 176 (1950).
[b] R. E. Bell and L. G. Elliott, Phys. Rev. **79**, 282 (1950).
[c] R. V. Smith and D. H. Martin, Phys. Rev. **77**, 752 (1950).
[d] A. O. Hanson, Phys. Rev. **75**, 1794 (1949).
[e] P. Meyer, Zeits. f. Physik **126**, 336 (1949).

IV. RESULTS

The neutron binding energy of beryllium was found to be 1.666±0.002 Mev and that of deuterium 2.226 ±0.003 Mev. These probable errors include the 0.1 percent uncertainty in the $Li^7(p, n)$ threshold. The agreement, as shown in Table I, between these results and other recent measurements is, with one exception,[12] within the probable errors.

The ratio of the deuterium to beryllium photo-neutron thresholds from this experiment is 1.337±0.001, which agrees very closely with the value of 1.338±0.004 given by Waldman and Miller.[13]

Using the value of 1.442±0.002 Mev obtained by Roberts and Nier[14] for the HH–D mass difference, together with the deuterium binding energy obtained in this experiment, the neutron-hydrogen mass difference is found to be 784±4 kev. This agrees within the probable errors with the value of 782±2 kev given by Taschek, Argo, Hemmendinger, and Jarvis,[15] with the value of 789±6 kev given by Tollestrup, Jenkins, Fowler, and Lauritsen,[16] and with the value of 783±4 kev given by Franzen, Halpern, and Stephens.[17]

We wish to thank Professor R. G. Herb for suggesting this problem and for his continued support and many helpful suggestions during the course of the experiment. We also wish to thank the staff of the Argonne National Laboratory, and particularly the Van de Graaff group, for their much appreciated cooperation.

[12] P. Meyer, Zeits. f. Physik **126**, 336 (1949).
[13] B. Waldman and W. C. Miller, Phys. Rev. **74**, 1225A (1948).
[14] T. R. Roberts and A. O. Nier, Phys. Rev. **77**, 746 (1950). The value they give for the HH-D mass difference is 1.442 Mev plus or minus a few kev.
[15] Taschek, Argo, Hemmendinger, and Jarvis, Phys. Rev. **76**, 325 (1949).
[16] Tollestrup, Jenkins, Fowler, and Lauritsen, Phys. Rev. **75**, 1947 (1949).
[17] Franzen, Halpern, and Stephens, Phys. Rev. **76**, 317 (1949).

Radioactive Isotopes of Ag and Cd

JANE R. GUM AND M. L. POOL
Ohio State University, Columbus, Ohio

(Received June 20, 1950)

Ag^{105}: An activity with a half-life of 40 days, has been produced by the following reactions: Rh(α,2n), Pd(α,p), Pd(d,2n) and Pd(p,n). This activity decays by K-electron capture only.

Ag^{110}: An activity with a half-life of 270 days previously reported as 225 days, has been produced by Pd(d,n) and Ag^{109}(d,p) reactions.

Cd^{105}: An activity with a half-life of 57 minutes has been produced by the Cd(n,2n) and Pd(α,n) reactions. Decay is accompanied by a 1.5-Mev positron and K-capture.

Cd^{109}: An activity with a half-life of 470 days, previously reported as 330 days, has been produced by the Ag(d,2n) and Pd(α,n) reactions.

I. 40-DAY Ag^{105}

AN activity with a 45-day half-life has been reported[1] as resulting from a 6.3-Mev proton bombardment of Pd. The decay of this activity was by K-capture with associated gamma-rays ranging in energies[2] from 0.28 to more than 1.0 Mev. The mass assignment of this activity in Ag was indefinite.

It seems reasonable to expect that the mass assignment could be arrived at by bombarding in a cyclotron the neighboring isotopes with the various projectiles available. When Rh is bombarded with 20-Mev alpha-particles a 40±0.7-day half-life activity was found produced[3] in Ag. This activity was confirmed by a 5.0-Mev proton bombardment of Pd. A Pd(α,p) reaction also produced the 40-day half-life. Fast neutron bombardment of Ag does not produce this activity. Thus, the mass assignment is Ag^{105}.

Figure 1 shows an electromagnetic absorption of the radiation of the 40-day activity obtained from a deuteron bombardment of Pd. The measuring technique employed a Wulf unifilar electrometer attached to a Freon filled ionization chamber. A magnetic field was placed between the radioactive source and the electrometer; all charged particles, if any, were deflected. Extrapolating the gamma-ray base line to zero thickness of absorber and subtracting from the total x-ray and gamma-ray activity, the net amount of radiation due to x-ray only is then obtained. The intensity of the x-ray ionization for zero absorption was determined from similar absorption curves at various intervals over a period of 300 days. These intensity values are plotted in Fig. 2. The point A of Fig. 1 is plotted as point A in Fig. 2. It is thus seen that an x-ray activity is decaying with a half-life of 40 days. Confirmation of the x-rays was made with a Cauchois spectrograph. A photographic exposure beginning 5 days after the Pd was bombarded with deuterons and extending 44 days showed the presence of the Pd K_α line. The ratio of the number of gamma-rays to x-rays is approximately two.

Beta-activities produced when Pd is bombarded with deuterons were measured concurrently during the 300-day interval and did not show a 40-day half-life. Therefore this 40-day activity decays by K-capture only.

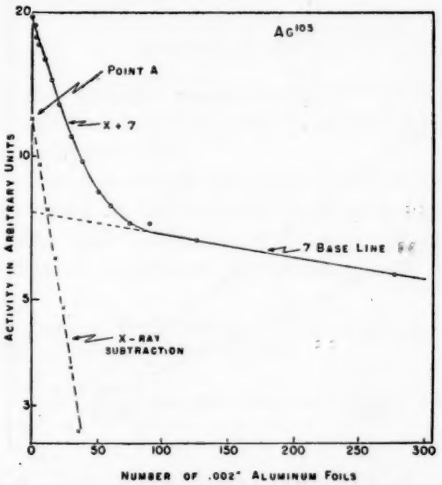

FIG. 1. Aluminum absorption taken during the decay of the 40-day half-life activity of Ag^{105}. A magnetic field prevented all charged particles from entering the ionization chamber.

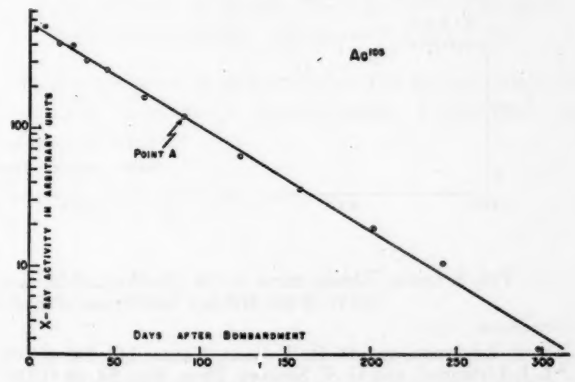

FIG. 2. Decay curve of the x-ray activity of the 40-day Ag material from a Pd+d bombardment. The point A of this figure is the same as point A of Fig. 1.

[1] T. Enns, Phys. Rev. **56**, 872 (1939).
[2] Deutsch, Roberts, and Elliott, Phys. Rev. **61**, 389 (1942).
[3] Gum, Thompson, and Pool, Phys. Rev. **76**, 184 (1949).

II. 270-DAY Ag^{110}

An isotope of Ag with a half-life activity of 225 days has long been known to be produced when Ag is bombarded with deuterons[4] or slow neutrons.[5]

Evidence is now available that the half-life value of this activity should be lengthened. After the previously discussed 40-day activity had decayed, a 270±4-day half-life was observed when Hilger Pd sponge was activated with deuterons. The Ag fraction of this bombardment was removed and the activity of the 270-day half-life material, as shown in the lower half of Fig. 3, followed a straight line decay for 5 years.

Ag enriched[6] in isotope 109 from 49 percent to about 92 percent, was bombarded with deuterons and the 270-day half-life was again found in the Ag fraction. This, together with the $Ag^{109}(n,\gamma)$ reaction,[7] adds to the evidence for the Ag^{110} mass assignment of the 270-day activity.

III. 57-MINUTE Cd^{105}

An activity with a half-life of 33 minutes has been reported[8] in Cd resulting from a $Cd(n,2n)$ reaction. No definite assignment was given to this activity.

A Cd activity with a 57±2-min. half-life was produced when Pd was activated with 20-Mev alpha-particles. The decay of the positron activity resulting from the $Pd(\alpha,n)$ reaction is shown in the upper curve of Fig. 4. A magnet was placed between the Geiger tube and the sample to separate positrons and electrons.

Cd bombarded with fast neutrons also yielded this activity. However, the activity is not observed when Ag is bombarded with deuterons or when Cd is bombarded with slow neutrons. These observations lead to the mass assignment of 105 for the 57-min. half-life activity.

In the lower curve of Fig. 4 an aluminum absorption is shown which was taken in the 57-min. half-life. A beta-end point was obtained at 0.7 g/cm² of aluminum,

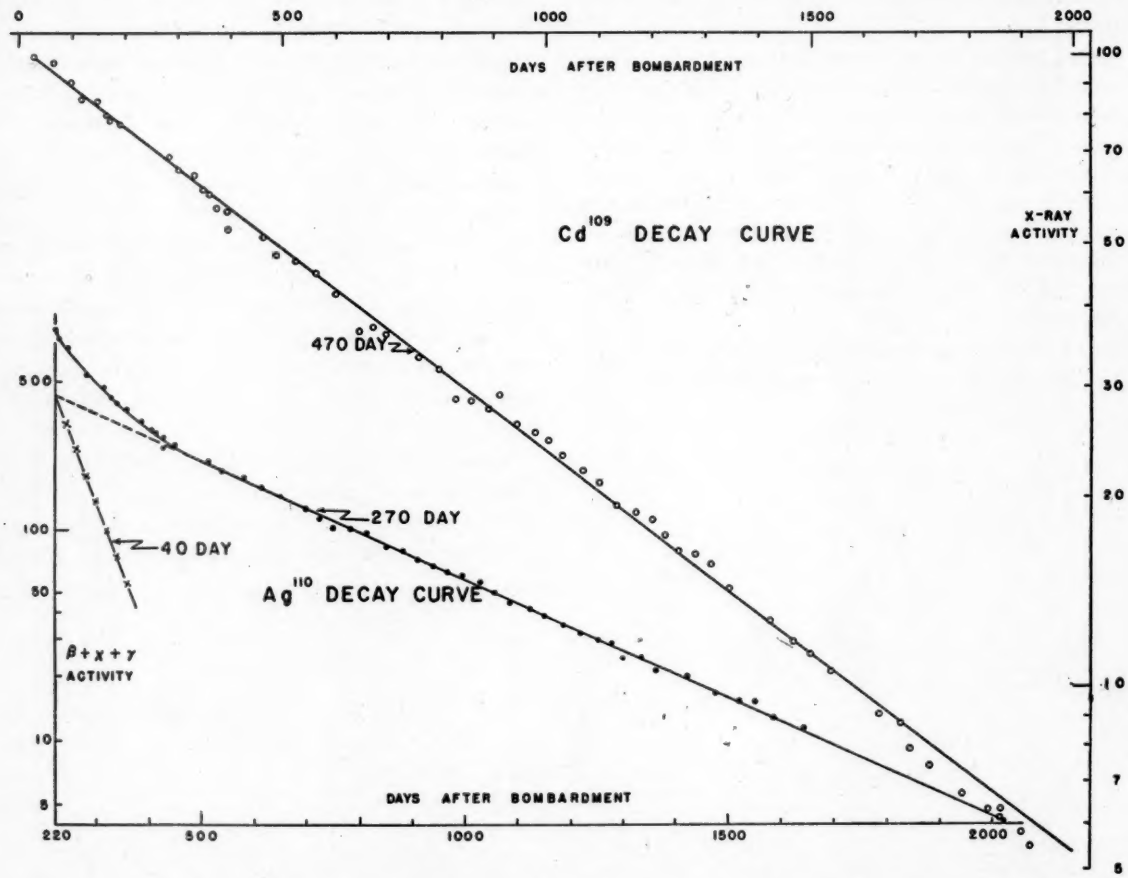

FIG. 3. Lower: Decay curve of the 270-day half-life activity of Ag produced by a Pd+d bombardment. Upper: Decay curve of the 470-day half-life activity of Cd produced by a Ag+d bombardment.

[4] R. S. Krishman, and D. H. T. Gant, Nature 144, 547 (1939).
[5] J. J. Livingood, and G. T. Seaborg, Phys. Rev. 54, 88 (1938); H. Reddemann, and F. Strassmann, Naturwiss. 26, 187 (1938).
[6] Supplied by the Y-12 Plant, Carbide and Carbon Chemicals Corporation through the Isotope Division, AEC, Oak Ridge, Tennessee.
[7] Goldhaber, Jacobs, and Williams, reported in Plutonium Project Report CP-3647 (October, 1946), p. 24 (unpublished).
[8] Pool, Cork, and Thornton, Phys. Rev. 52, 239 (1937).

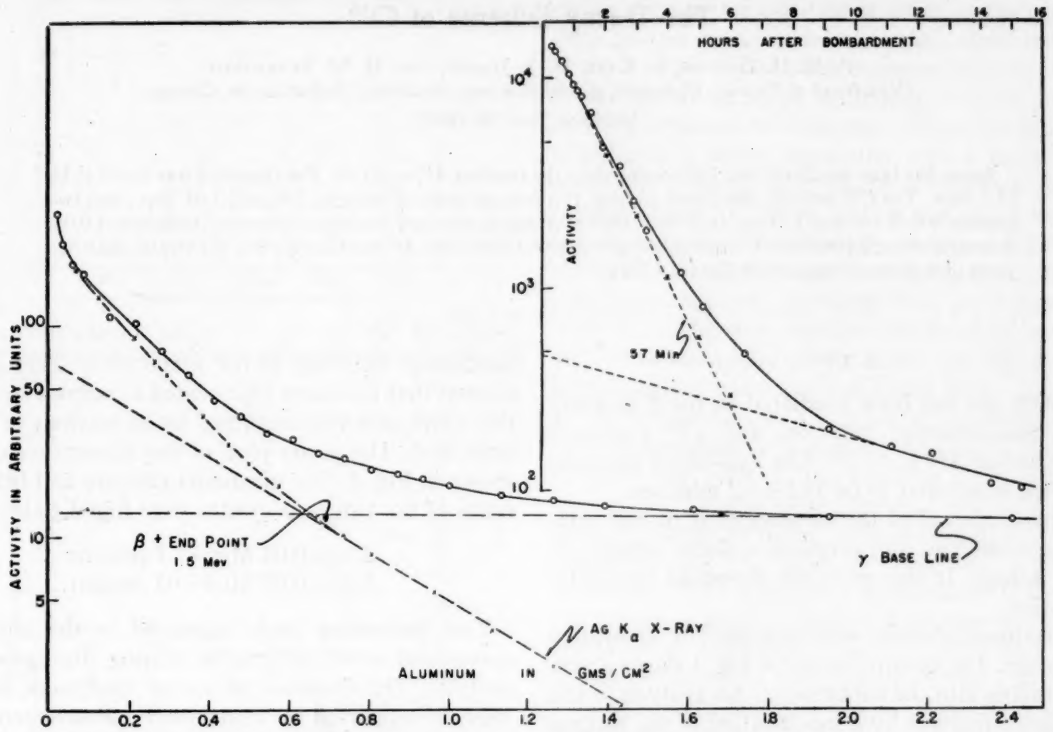

FIG. 4. Upper: Decay curve of the 57-minute Cd activity produced by a Pd+α bombardment. Lower: Aluminum absorption taken during the decay of the 57-minute Cd activity.

which corresponds to 1.5 Mev. In addition to the positron emission there is an x-ray and a gamma-ray associated with the activity. From the relative intensities of the beta-emission to that of x-ray, it is evident from Fig. 4 that the *K*-capture decay process is the most probable. With each *K*-capture process there is approximately one gamma-ray.

IV. 470-DAY Cd^{109}

A 330-day half-life has been reported[9] in Cd. This activity was found to decay by *K*-capture and assignment was made to Cd^{109}.

The value of this half-life seems to be appreciably longer as based on observations made over a period of 5 years. The upper half of Fig. 3 shows the decay of the Cd fraction of a deuteron bombardment of Ag. The activity which was measured on a Wulf electrometer decays with a 470±8-day half-life.

The Cd fraction from an alpha-bombardment of Pd also gives evidence of the 470-day half-life activity.

Observations made in a cloud chamber show that decay is accompanied by *K*-capture. Confirmation of *K*-capture was made by an aluminum absorption taken in the 470-day half-life. Beta-rays and gamma-rays were not observed; and if present, were very weak compared with the x-ray radiation.

Based upon the intensities of x-ray observations, the relative yields per atom of the following activities for the bombarding energy used are: $Pd(\alpha,n)Cd^{105}$, 57-min.: $Pd(\alpha,n)Cd^{107}$, 6.7-hour: $Pd(\alpha,n)Cd^{109}$, 470-day: $Pd(\alpha,n+\alpha,p)Ag^{105}$, 40 day = 1:4.5:1.7:23.7.

It is a pleasure to acknowledge the support received from the University Development Fund and the Graduate School.

[9] Bradt, Gugelot, Huber, Medicus, Preiswerk, Scherrer, and Steffen, Helv. Phys. Acta 19, 218 (1946).

The Decay Scheme of Cl^{39}

R. N. H. Haslam, L. Katz, H. J. Moody, and H. M. Skarsgard
Department of Physics, University of Saskatchewan, Saskatoon, Saskatchewan, Canada

(Received June 19, 1950)

Argon has been irradiated and Cl^{39} produced by the reaction $A^{40}(\gamma, p)Cl^{39}$. The threshold was found to be 14.2 Mev. The Cl^{39} activity was found to have two beta-particles of energies 2.96 and 1.65 Mev, and two gamma-rays of energies 1.31 and 0.35 Mev, the low energy gamma-ray having a conversion coefficient of 0.05. A decay scheme is proposed. Consideration of the results show that A^{39} must have a half-life greater than five years or a decay energy of less than 0.4 Mev.

I. Cl^{39}

ARGON gas has been irradiated in the University of Saskatchewan betatron, and Cl^{39} produced[1] by the reaction $A^{40}(\gamma, p)Cl^{39}$. The half-life of the chlorine isotope was found to be 55.5 ± 0.2 minutes.

This paper describes the measurement of the beta- and gamma-energies and proposes a decay scheme for the Cl^{39} isotope. It also gives the threshold energy for this reaction.

The maximum energies were measured by absorption in aluminum. The absorption curve Fig. 1 shows a very gradual tailing into the background. An analysis of this curve was carried out by a modification of the method previously described in the literature.[2,3] This analysis showed that the curve represented a complex spectrum; this conclusion was confirmed by an analysis in a magnetic field. The power plot[2] of the absorption curve is shown in Fig. 2. The maximum energies and branching ratios of the two beta-spectra were found to be:

2.96 ± 0.04 Mev— 7 percent
1.65 ± 0.03 Mev—93 percent.

Two conversion peaks appeared in the absorption curve and were subtracted during the process of analysis. The existence of one of the peaks, near 0.3 Mev, is supported by coincidence measurements. The second conversion peak is at about 3.2 Mev. It is of very low intensity, about 0.11 percent, but appears to be real. It appeared in three absorption curves. However, in only one case was sufficient accuracy obtained to confirm its existence. It is not supported by coincidence measurements, nor can it be explained by any combination of beta- and γ-energies. The conversion peak at 0.3 Mev constitutes about five percent of the total beta-count at zero absorber.

Coincidence measurements were undertaken to determine the decay scheme and to measure the γ-energies.

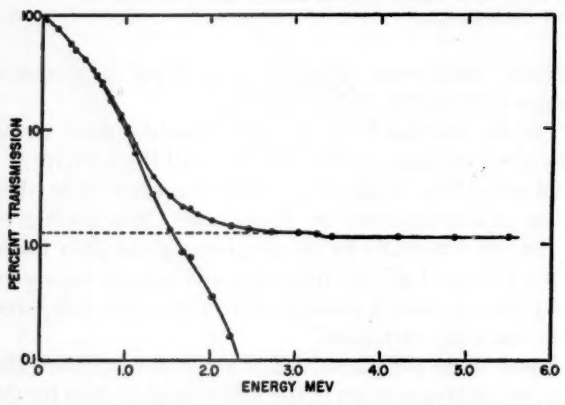

FIG. 1. Absorption of β^--particles from Cl^{39}. The breaks in the curve at 0.35 Mev and 3.2 Mev due to the two conversion peaks are clearly visible.

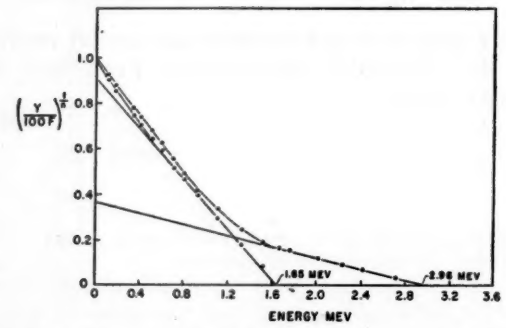

FIG. 2. The power plot of the absorption curve of Cl^{39}.

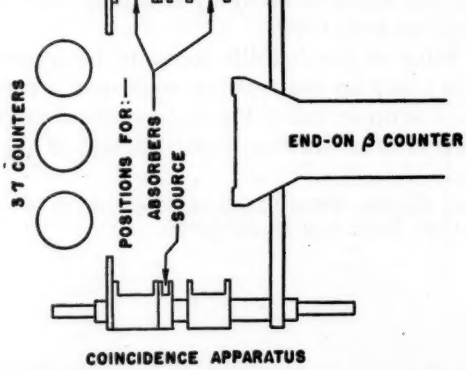

FIG. 3. The experimental arrangement used for the beta-beta and beta-gamma coincidence measurements with Cl^{39}.

[1] Haslam, Katz, Johns, and Moody, Phys. Rev. 76, 704 (1949).

[2] Katz, Penfold, Moody, Haslam, and Johns, Phys. Rev. 77, 289 (1950).

[3] A paper now in preparation on this modification will be published shortly.

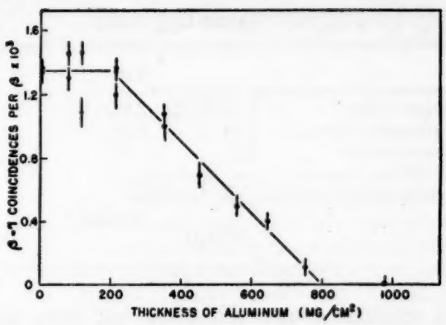

FIG. 4. Beta-gamma coincidences per recorded beta-particle from Cl^{39} plotted against the thickness of aluminum before the beta-counter.

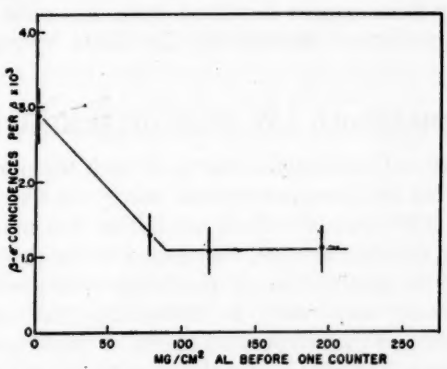

FIG. 5. Beta-beta coincidences per recorded beta-particle from Cl^{39} plotted against the thickness of aluminum before one counter.

The experimental arrangement is shown in Fig. 3. To obtain a high counting rate three cylindrical aluminum walled counters (30 mg/cm²) are connected in parallel and used as a γ-counter. The beta-counter is a mica window end-on counter. The signals from the beta- and gamma-counters are amplified in two preamplifiers and then fed into the coincidence mixer.

Gamma-gamma coincidences were observed, indicating the existence of two or more γ-rays in cascade. Beta-gamma coincidences were then measured. A plot of the number of coincidences per recorded beta-particle *versus* the thickness of aluminum between the source and the beta-counter is shown in Fig. 4. It displays the characteristic shape associated with a complex beta-spectrum. The end point of the coincidence absorption curve is about 1.75 Mev. This is due to the low energy beta-spectrum. The flattening at low energies is evidently due to a low energy beta-particle, presumably a conversion electron. To verify this, $\beta-\beta$ coincidences were measured with absorbers in front of one counter only. The resulting curve is shown in Fig. 5: the end point was determined at 0.35 ± 0.05 Mev.

Measurements were also made by coincidence absorption of secondary electrons to determine the highest energy γ-ray present. The resulting curve is shown in Fig. 6, with the end point plotted to an enlarged scale. The total range including the counter wall thickness was determined at 460 mg/cm². Using the range-energy curve[4] and the theoretical expression for the energy of the Compton electron ejected in the forward direction, the γ-energy was found to be 1.35 ± 0.05 Mev.

The difference in energy between the 2.96 Mev and 1.65 Mev beta-particles is 1.31 Mev. This obviously corresponds to the 1.35 Mev γ-ray measured by coincidence absorption of secondary electrons. The low energy γ-ray must then follow both beta-particles as shown in Fig. 7. This would mean that the high energy beta-particles should also show β-γ-coincidences. That these coincidences were not observed can be attributed to the low intensity of the high energy beta-particle, the decreased counting efficiency[5] of the 0.3-Mev γ-ray, and the low transmission through 800 mg/cm² of aluminum where these coincidences should have been

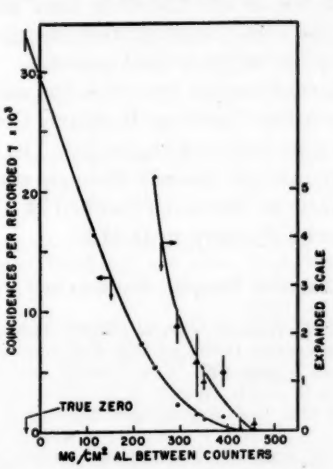

FIG. 6. The coincidence absorption curve of the secondary electrons from Cl^{39}. The lower portion of the curve is shown to an expanded scale with the standard deviation of the experimental points indicated.

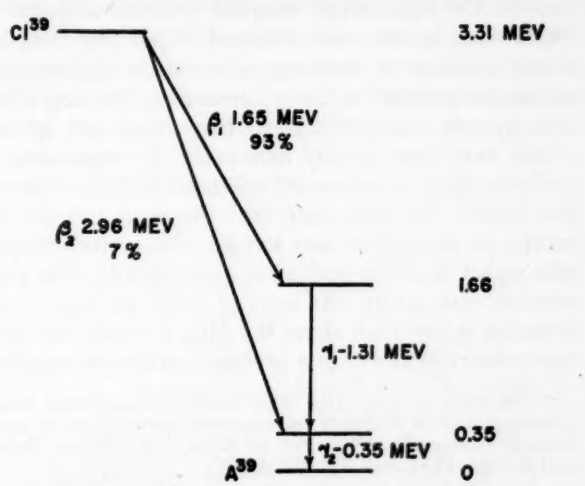

FIG. 7. The proposed decay scheme for Cl^{39}. The energies given do not include the rest mass of the beta-particle.

[4] C. Goodman, ed., *The Science and Engineering of Nuclear Power*, Vol. 1 (Addison-Wesley Press, Cambridge, 1947).

[5] Fowler, Lauritsen, and Lauritsen, Rev. Mod. Phys. **20**, 236 (1948).

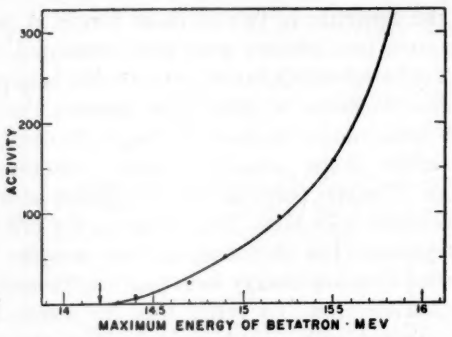

FIG. 8. The Cl^{39} activity curve plotted against the maximum energy of the betatron. The threshold energy for the reaction $A^{40}(\gamma, p)Cl^{39}$ is at 14.2±0.2 Mev.

observed. Assuming appropriate values for these factors one would expect a coincidence rate per recorded beta of about 0.04×10^{-3}. This is less than the statistical fluctuations of the measurements.

II. A^{39}

Since no activity that could be attributed to A^{39} was observed certain limits can be placed upon the half-life of this isotope.

A^{39} is formed when Cl^{39} disintegrates with the emission of a β^- particle. If the half-life of A^{39} were less than that of Cl^{39} then, when in equilibrium, the disintegration of a chlorine atom would on the average be accompanied by the disintegration of an atom of argon. This would mean that the β-spectra could be divided into two groups of equal intensities. The branching ratio of the two primary β particles is 0.93 and 0.07 with the conversion electrons contributing five percent of the total count. No division into equal parts is possible so it is concluded that the half-life of A^{39} is longer than that of Cl^{39}. An initial recorded chlorine activity of 78,500 counts/min. was obtained which was then allowed to decay to zero and an estimate made of the maximum possible activity remaining. No long-lived activity was observed though two counts per minute would have been readily detectable. A comparison of activities gives an estimated minimum half-life of about five years.* To make sure that the argon gas did not escape as soon as it was formed, the active chlorine was sealed in a thin-windowed glass capsule. The glass window was about 100 mg/cm² thick so that if the β-energy is less than about 0.4 Mev it would not have been observed at all. In a previous article[1] we reported a small residual count. This has not been observed since the procedure for removing the chlorine from the chamber has been altered. It is therefore thought that it may have been due to a slight amount of 12-hour activity from copper dissolved from the walls of the brass irradiation chamber by the dilute hydrochloric acid.

* *Note added in proof:* This value is not in disagreement with a minimum half-life of fifteen years recently reported for an argon isotope, presumably A^{39} formed by $K^{39}(n, p)A^{39}$. [Brosi, Zeldes, and Ketelle, Phys. Rev. 79, 902 (1950)].

TABLE I.

	Cl^{39}	A^{39}
Beta-energies (Mev)	1.65(93%); 2.96(7%)	—
Gamma-energies (Mev)	1.31 0.35	—
Total disintegration energy (Mev)	3.3	3.8
Conversion coefficient $\alpha=0.05$ for 0.35 Mev gamma		—
Mass	38.9826	38.9790

III. THRESHOLD AND MASS DETERMINATIONS

A series of irradiations was made with the purpose of measuring the gamma-threshold energy for the production of Cl^{39} from A^{40}. Each irradiation was made at a slightly different energy, the energy being determined by the integrator circuit previously described.[6] Extreme care was taken in performing the chemical separation so that conditions might be duplicated from run to run. The observed activity, after being corrected for dosage rate and irradiation time, was plotted against the maximum energy of the betatron. The curve is shown in Fig. 8. The threshold energy is determined at 14.2±0.2 Mev.

From the known mass[7] of the A^{40} isotope, the threshold energy for the production of Cl^{39}, and the total disintegration energy of the Cl^{39} isotope, the masses of Cl^{39} and A^{39} can be calculated. Also using the known mass of the K^{39} isotope the total disintegration energy of A^{39} can be determined. The results of these calculations are given in Table I. It should be noted that the mass of K^{39} is not as well known as that[8] of A^{40} and for that reason the total disintegration energy of A^{39} may be in error by an undetermined amount.

This work was carried out with the aid of a grant from the Canadian National Research Council, whose assistance is gratefully acknowledged. The authors also wish to acknowledge the aid through awards by the Canadian National Research Council of a studentship to H.J.M. and a Bursary to H.M.S.

[6] Katz, McNamara, Forsyth, Haslam, and Johns, Can. J. Research 28, 113 (1950).

[7] L. Rosenfeld, *Nuclear Forces* (North Holland Publishing Company, Amsterdam, 1948), pp. 501–528.

[8] See reference 7, page 499.

Energy Dependence of Proton-Proton Scattering, 18.8 to 31.8 Mev*

BRUCE CORK
Radiation Laboratory, Department of Physics, University of California, Berkeley, California
(Received June 22, 1950)

Measurements have been made of the absolute differential cross section of proton-proton scattering at 90° in the center-of-mass system. The energy of the incident protons was varied from 31.8 Mev down to 18.8 Mev, and an energy interval of ±1.0 percent was selected by means of a deflecting magnet. Apparatus using a proportional counter and a triple coincidence method was used to reduce the background. Measurements were made simultaneously, using apparatus for measuring the angular distribution at 31.8 Mev and a single charge integrator for collecting the incident proton beam.

The cross section at 90° in the center-of-mass system varies approximately as the reciprocal of the energy of the incident protons over the range investigated. Data are presented to show this dependence. Comparison is made with a Yukawa potential well, and with the tensor model selected by Christian and Noyes.

I. INTRODUCTION

MEASUREMENTS of the proton-proton differential cross section at 31.8 Mev[1–3] showed that the shape of the scattering cross-section curve was compatible with a pure *S*-wave. However, the magnitude of the cross section was approximately 1.3 times the value extrapolated from the low energy data[4,5] assuming a square well of depth 10.5 Mev, of range $\hbar/mc$, and *S*-wave scattering only. A more singular potential well, such as a Yukawa well has been selected[6] to be consistent with the angular distribution observed at 31.8 Mev, assuming that the *D*-wave scattering predicted for such a potential does not appear.

Measurements have been made by Herb *et al.*[4] over the range 0.860 Mev to 2.392 Mev; by Blair *et al.*[5] over the range 2.42 Mev to 3.53 Mev, and by others[7–12] up to energies of 14.5 Mev. Measurements have been made in the region of 240 Mev by Oxley[13] and in the region of 170 Mev to 340 Mev by Chamberlain and Wiegand.[14] The Berkeley 32-Mev linear accelerator has features which allow investigation of the region below 32 Mev.

II. METHOD

It was convenient to use the angular distribution apparatus[1] that was used at 31.8 Mev, to extend the measurements down to 25 Mev. The thickness of the aluminum window separating the hydrogen from the argon filled proportional counter limited the low energy range to 25 Mev for scattering angles of 90° in the center-of-mass system. To extend the measurements to still lower energy, a 90° coincidence method was used.

This apparatus was arranged so that the incident beam first passed through the angular distribution scattering chamber, then through the 90° coincidence chamber, and finally on into the charge integrator. This procedure allowed a direct comparison of the two geometries in the high energy region, and normalization of the 90° coincidence data to the 31.8-Mev data.

The 90° coincidence apparatus is shown in Fig. 1. To reduce the number of background counts, one of the 90° proportional counters was arranged as a double counter telescope. Thus scattered protons were counted by triple coincidences. The coincidence geometry is defined by the entrance apertures of each of the counters and the position of the incident beam. These apertures were of rectangular cross section 1 in.×2 in. and located at a distance of 7½ in. from the center of the scattering region. The scattered beam which could be accepted by the coincidence geometry was 45°±4° maximum and 45°±2° mean angle in the laboratory system of coordinates.

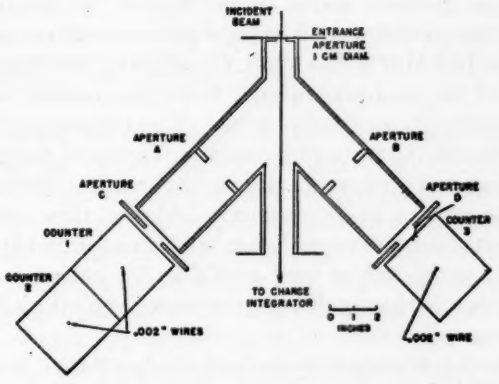

FIG. 1. Triple coincidence geometry for proton-proton scattering measurements.

* This work was sponsored under the auspices of the AEC.

[1] Cork, Johnston, and Richman, Phys. Rev. **79**, 71 (1950).
[2] W. K. H. Panofsky and F. L. Fillmore, Phys. Rev. **79**, 57 (1950).
[3] R. Christian and H. P. Noyes, Phys. Rev. **79**, 85 (1950).
[4] Herb, Kerst, Parkinson, and Plain, Phys. Rev. **55**, 998 (1939).
[5] Blair, Freier, Lampi, Sleator, and Williams, Phys. Rev. **74**, 553 (1948).
[6] Chew and Goldberger, Phys. Rev. **75**, 1637 (1949).
[7] May and Powell, Proc. Roy. Soc. **A190**, 170 (1947).
[8] R. R. Wilson, Phys. Rev. **71**, 384 (1947).
[9] R. R. Wilson and E. C. Creutz, Phys. Rev. **71**, 339 (1947).
[10] Wilson, Lofgren, Richardson, Wright, and Shankland, Phys. Rev. **71**, 560 (1947).
[11] Dearnly, Oxley, and Perry, Phys. Rev. **73**, 1290 (1948); J. Rouvina, private communication.
[12] F. Faris and B. Wright, private communication.
[13] C. L. Oxley, Phys. Rev. **76**, 461 (1949).
[14] O. Chamberlain and C. Wiegand, Phys. Rev. **79**, 81 (1950).

TABLE I. Measured values of $(d\sigma/d\Omega)_{90°\ c.m.}$ as a function of the energy of the incident protons.*

Energy (Mev)	$\frac{1}{E}\times10^3$	Run	Q coulombs $\times10^{-12}$	$\left(\frac{d\sigma}{d\Omega}\right)$ c.m. millibarns	Statistical error %	RMS N %	Assigned absolute probable error %	Relative errors
31.8	31.45	*A*		14.3	±0.7		±1.8	0
31.8	31.45	1*C*	2250	14.4	±2.2	±2.4		
31.45	31.8	1*T*	2250	14.5	±2.8	±3.1		
31.45	31.8	2*T*	856	14.3	±4.1	±2.6		
31.8	31.45	3*A*	1285	14.4	±0.9	±1.3		
31.8	31.45	3*C*	2185	14.3	±1.4	±1.5		
31.45	31.8	3*T*	3850	14.35	±2.4	±1.9		
31.45	31.8	Normalized Triple		25.45	—	—	±2.2	0
25.45	39.30	4*A*	2890	18.32	±0.7	±1.1		
25.45	39.30	4*C*	2890	18.4	±1.2	±1.4		
25.45	39.30	Weighted Mean		18.36	—	—	±2.1	±1.4
25.2	39.68	4*T*	5780	18.7	±1.7	±1.9	±2.6	±2.0
21.9	45.66	6*T*	1925	22.8	±2.5	±2.1	±2.3	±2.1
18.8	53.19	7*T*	1713	27.2	±2.5	±2.2	±2.4	±2.2

* Runs designated by "*A*" are with angular distribution singles geometry, runs designated *C* are with double coincidence angular distribution geometry, and runs designated *T* are triple coincidence geometry.

III. ENERGY SELECTION AND MEASUREMENT

The proton beam from the Berkeley 32-Mev linear accelerator[15] was collimated and then deflected in an analyzing magnet. Approximately 6 meters of further collimation gave a beam of 1 cm diameter and an angular divergence of ±0.001 radians. The energy spectrum was measured by observing the current at the charge integrator as a function of the deflecting magnet field.

The absolute energy was determined by measuring the deflection[16] of the proton beam in the magnetic field. The energy of the coincidence protons scattered at 90° in the center-of-mass (c.m.) system was also measured by determining their range in aluminum. Using the range data[17] extrapolated from low energies, the energy of the incident protons for the above deflecting magnetic field was observed to be 31.6±0.3 Mev.

Incident protons of energies less than 31.8 Mev were obtained by operating the linear accelerator in a manner different from the normal adjustment. Since beam currents of approximately 10^{-12} ampere were adequate to give a satisfactory counting rate, it was possible to adjust the energy of the injected protons and the voltage gradient at the output end of the linear accelerator so that a good beam of protons with energy as low as 18.8 Mev would result. By adjusting the magnetic field of the analyzing magnet to the appropriate value, protons with an energy spread of ±1.0 percent were incident at the scattering chamber. The mean energy of the incident protons was calculated from the deflection of the protons in the magnetic field, and these values, corrected for the energy loss in the Nylon foil and hydrogen, are the values used in Table I. Changes in the magnetic field over the range of energies used could be measured with an accuracy of ±⅓ percent. Thus the mean energy could be determined to ±⅔ percent.

IV. COUNTERS

Each proportional counter consisted of a rectangular chamber 1½ in.×3 in.×4 in. with a 0.002 in. diameter tungsten wire mounted along the major axis (Fig. 1). The scattered protons entered a 0.002-in. duraluminum foil mounted on the broad side of the counter. In the double counter these protons went on into the second counter, with no foil separating the two counters.

The signals from each of these counters were amplified by an amplifier having a gain of 3000 and a band width of 0.9 Mc. The output of each amplifier was coupled to a discriminator and gate circuit that generated a 0.7-μsec. pulse. These gated pulses associated with the various counters were then coupled into a triple coincidence circuit which recorded the coincidence scattered protons.

V. CORRECTIONS

The resolving time of the counter circuits was measured with a double pulse signal generator and observed to be 4 μsec. The counting rate of each counter was kept at a sufficiently low rate so that the correction for counts being missed by the triple coincidence circuit was less than ½ percent. This low counting rate also resulted in the corrections for accidental coincidences being less than ¼ percent.

The individual counting rates were kept approximately constant by varying the magnitude of the incident beam current. Thus the corrections to the relative cross section are very small due to counter resolving time.

As an additional check on the accidental coincidence rate, double coincidences were measured between one of the telescope counters and an auxiliary counter, measuring protons scattered from the same incident

[15] Bradner, Crawford, Gordon, and Woodyard, Phys. Rev. 73, 534A (1948).
[16] R. R. Wilson and E. C. Creutz, Rev. Sci. Inst. 17, 385 (1946).
[17] Livingston and Bethe, Rev. Mod. Phys. 9, 263 (1937).

beam. This counter was arranged so that it had approximately the same counting rate as the other counter, but scattered protons could not be in real coincidence.

All protons incident at the counters have greater than 8.0-Mev energy in the laboratory system. Multiple scattering of 8.0-Mev protons by 20 cm of hydrogen has been estimated using Williams formula[18] and found to have a root-mean-square scattering angle of 0.07°. This correction when applied to the coincidence geometry is estimated to be less than $\frac{1}{2}$ percent.

The root-mean-square multiple scattering angle in two of the 0.002 in. duraluminum foils (chamber exit foil and counter entrance foil) is estimated to be 1.5° at 8.0 Mev. The counter aperture was sufficiently large, compared with the entrance aperture, so that protons scattered by these foils would be counted, unless they were scattered at an angle of greater than 6.0°. Assuming a Gaussian distribution, the probability of scattering greater than 7.0° is 6×10^{-5}. No correction was made for multiple scattering by the foils.

An estimate of the correction for multiple nuclear scattering is made as follows. The cross section for single nuclear scattering of 8 Mev protons by protons was observed[9] to be 60.5×10^{-27} cm^2 at 90° c.m. Assuming the cross section is an order of magnitude greater than this in the forward direction in the laboratory system, the probability of an 8.0-Mev proton making an elastic collision in the 20 cm of hydrogen and possibly not being counted is estimated to be less than $\frac{1}{3}$ percent. No correction was made for multiple nuclear scattering.

The position of the incident proton beam was observed at the charge integrator by means of a photographic emulsion. It was observed that multiple scattering in the hydrogen did not cause a significant number of protons to be missed by the Faraday cage.

An investigation has been made of the effects of secondary electrons on the measurements of the charge integrated by the Faraday cup. The potential of the electron suppressor cylinder[1] was made variable. Measurements of protons scattered from helium were taken as a standard and the angular distribution apparatus[1] was used to obtain good statistics, a standard deviation of ±0.6 percent.

The total number of protons scattered into this apparatus for an indicated charge of 371×10^{-12} coulomb was 4.2 percent less for zero potential on the electron suppressor cylinder than for a potential of negative 100 volts.

The observed difference in the number of scattered protons for negative 420 volts was 1.1 percent greater, for protons of 31.8-Mev incident energy, and 0.7 percent less for protons of 25.9-Mev incident energy. An additional magnetic field of 75 gauss at the aluminum foil resulted in an observed decrease of 0.3 percent in the number of scattered protons. It is concluded that the bias potential of negative 135 volts used during the proton-proton scattering experiment was sufficient to suppress most of the secondary electrons from the aluminum foil and from the Faraday cage, over the range of 25.9 Mev to 31.8 Mev. Lower energy ranges have not been investigated. During the scattering experiments, the pressure was measured in the region of the Faraday cage and was always less than 10^{-5} mm of mercury.

[18] E. J. Williams, Proc. Roy. Soc. **169**, 531 (1939).

VI. PROCEDURE

The scattering chamber was evacuated and observed to be vacuum tight. Hydrogen was then admitted through a palladium tube until the pressure was slightly greater than one atmosphere. The excess hydrogen was then permitted to escape from the chamber via an oil-lock tube which regulated the pressure and prevented back diffusion of air into the system. The pressure was

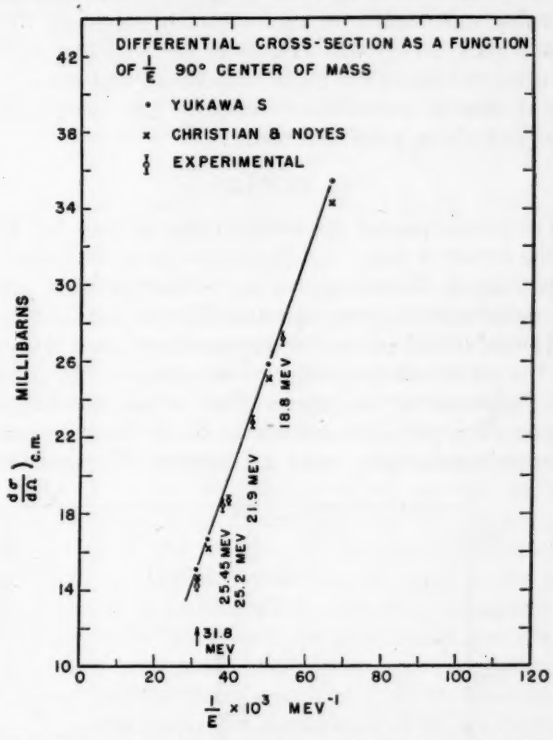

FIG. 2. Variation of the absolute differential cross section for proton-proton scattering at 90° center of mass as a function of the reciprocal of the energy of the incident protons.

calculated from the measurements of the height of the oil in this oil-lock column, the density of the oil, and the barometer reading. The temperature of the hydrogen was determined by measuring the temperature of the scattering chamber. It was possible to operate the proportional counters well up on the plateau for counting protons and still have a negligible number of background counts, using the triple coincidence method. The threshold for counting gamma-rays was determined for each counter, and then each counter was operated well above this point.

TABLE II. Calculated values of the differential cross section for proton-proton scattering at 90° c.m.

Energy (Mev)	$1/E\times10^3$	$(d\sigma/d\Omega)_{90°}$ c.m. Christian and Noyes	Millibarns Yukawa S	Yukawa S and D	Square S	Square S and D
5	200	100.21	100.37	99.63	99.60	99.64
10	100	52.05	53.51	52.73	50.70	52.73
15	66.6	34.23	35.40	34.33	31.72	34.33
20	50	24.95	25.84	24.58	21.85	24.58
29.4	34.01	16.11	16.62	15.15	12.47	15.15
32	31.25	14.59	15.00	13.51	10.89	13.51

TABLE III. Calculated values of the function $\bar{K}$ using the method of Blatt and Jackson.

Energy Mev	Christian and Noyes	Square S	$\bar{K}$ Yukawa S	$\bar{K}$ Yukawa S and D
5	6.018	6.052	6.025	6.052
10	8.318	8.540	8.113	8.235
15	10.424	11.165	10.053	10.354
20	12.416	13.932	11.894	12.524
29.4	15.908	19.536	15.248	16.660
32	16.843	21.188	16.188	17.846

Each run was made by opening a beam shutter and operating until a charge of 920.7×10^{-12} coulomb was collected on the Faraday cage. These runs were of approximately 20 minutes duration for protons of 31.8-Mev incident energy. This corresponds to a beam current of approximately 10^{-12} ampere. The incident beam current was reduced at lower energies in order that the counting rate would be approximately constant. The proton plus background counts of each counter were recorded as well as the triple coincidence and the accidental double coincidence counts. The corrections described above were then made.

VII. RESULTS

The proton-proton differential cross sections for 90° in the center of mass coordinates are given in Table I, Figs. 2 and 3. The energies of the incident protons, and the reciprocals of the energies are likewise tabulated.

The tabulated errors for the measured cross section are the statistical errors which were calculated by using the reciprocal of the square root of the number of counts. The probable errors due to temperature and pressure measurement were $\pm\frac{1}{3}$ percent. The probable error of the absolute cross section due to charge measurement was measured at 31.8 Mev and observed to be less than $\pm\frac{1}{2}$ percent, and the assigned probable errors of the absolute cross sections are tabulated.

The curve of Fig. 2 is normalized for the measured cross section of 14.3×10^{-27} cm² at 31.8 Mev, and all other points are plotted relative to this value. This procedure was more convenient than that of carefully evaluating the triple coincidence geometry.

The mean energy of the incident protons tabulated in Table I is the value calculated from the deflection in the magnetic field. The probable error in energy for each adjustment of the magnetic field is $\pm\frac{2}{3}$ percent.

Table II is a summary of the calculated values of the differential cross section for proton-proton scattering at 90° c.m. The third column is a tabulation of the values calculated by Christian and Noyes,[3] assuming a tensor model.

The curve of Fig. 2 is plotted through the values listed in Table III calculated by Christian and Noyes, assuming a Yukawa well of range $=1.417\times10^{-13}$ cm, and depth of 49.35 Mev. These are the parameters determined by Chew and Goldberger[6] selected to be con-

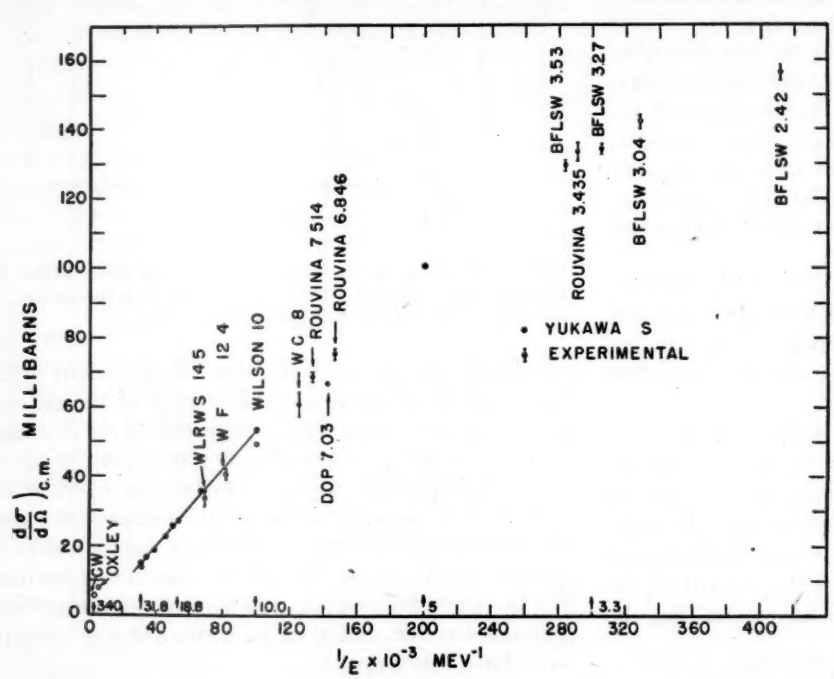

FIG. 3. Summary of proton-proton scattering data, 90° c.m. as a function of the reciprocal of the energy of the incident protons.

TABLE IV. Summary of measured values of the differential cross section for proton-proton scattering at 90° c.m. and calculated values of $\bar{K}$ assuming the measured cross sections.

Ref.	E(Mev)	Error %	$\frac{1}{E}\times 10^3$	$\left(\frac{d\sigma}{d\Omega}\right)_{90°\text{ c.m.}}$	Probable error %	Calculated $\bar{K}$
5	2.42			156.6	±2.1	4.86 ±0.05
5	3.04			142.1	±1.8	5.15 ±0.06
5	3.27			134.3	±1.4	5.24 ±0.06
5	3.53			129.4	±1.4	5.36 ±0.07
19	2.42			—		4.90 ±0.05
19	3.04			—		5.17 ±0.05
19	3.28			—		5.26 ±0.06
19	3.53			—		5.41 ±0.06
19	4.2			—		5.83 ±0.30
20	4.94	±0.04		99.57		6.02 ±0.18
11	7.03	±0.06		66.5		7.63 ±0.11
9	8.0	±0.1		60.46	±3.5	8.00 ±0.40
10	14.5	±0.7		33.4	±2.	10.78 ±0.80
11	3.435	±1.4	291.1	133.4	±2.4	5.30 ±0.067
	6.846	±0.58	146.1	146.48	±1.4	6.86 ±0.122
	7.514	±0.53	133.1	68.87	±1.3	7.18 ±0.130
12	12.4	±2.0	80.64	40.3	±2.0	9.683 ±0.2
Present work	18.8	±0.7	53.19	27.2	±2.4	11.67 ±0.27
	21.9	±0.7	45.66	22.8	±2.3	12.91 ±0.27
	25.2	±0.7	39.68	18.7	±2.6	14.65 ±0.33
	25.45	±0.7	39.30	18.36	±2.1	14.84 ±0.27
	31.45	±0.7	31.79	14.45	±2.2	16.73 ±0.30
	31.8	±0.7	31.45	14.3	$\pm^{1.8}_{1.5}$	16.76 $\pm^{0.25}_{0.21}$
1	31.8	3	31.45	14.3	$\pm^{1.8}_{1.5}$	16.76 $\pm^{0.25}_{0.21}$
2	29.4	±0.7	34.0	16.0	±3.0	15.84 ±0.39
13	250.		4.0	"8"		
14	170.		5.88	4.0		
	340.		2.94	4.0		

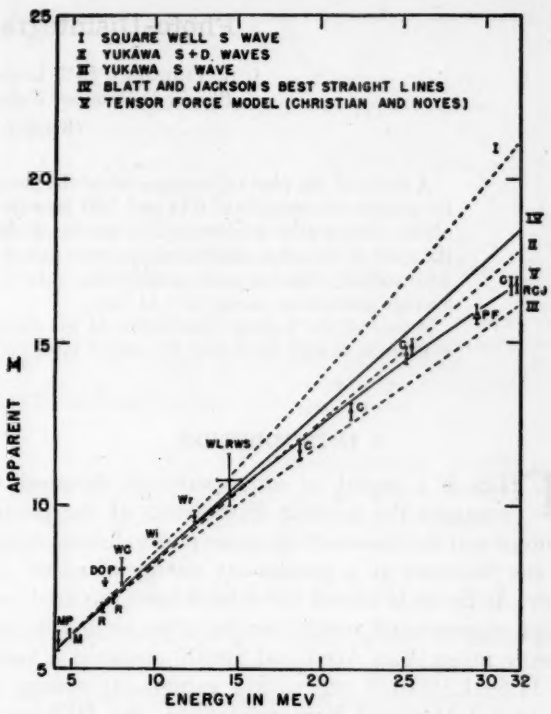

FIG. 4. Variation of the function $\bar{K}$ as a function of the energy of the incident protons.

sistent with the angular distribution observed at 31.8 Mev, assuming that somehow the D-wave scattering predicted for such a potential does not appear. Figure 3 is a summary of the measured values of the differential cross section for proton-proton scattering at 90° c.m. as a function of the reciprocal of the energy of the incident protons.

Table IV and Fig. 4 are a summary of the values of the function $\bar{K}$ defined by Blatt and Jackson.[19] The straight line labeled Blatt and Jackson, Fig. 4, is the best straight line fit for $K=3.755+0.4603E$ determined from low energy proton-proton scattering data.[20]

It is concluded that at present no potential model has been discovered having any effective range long enough to fit the low energy data, that also predicts negligible D-wave scattering at 32 Mev. Hence, there is no existing theoretical basis for such an S-wave model. The tensor model of Christian and Noyes[3] has been arranged to satisfy the experimental data at 250 Mev and 340 Mev, as well as the low energy data.

It is a pleasure to express my thanks to Professors Luis Alvarez and W. K. H. Panofsky for encouragement to continue this problem. Also, I am grateful to Professor Geoffrey Chew, Mr. Richard Christian, and Mr. H. P. Noyes for stimulating discussions, and for calculation of the values of the function $\bar{K}$. The linear accelerator crew under the direction of Mr. Robert Watt played an important role in making all the necessary adjustments for changing the energy and for satisfactory operation of the linear accelerator. The design and maintenance of the counting apparatus was done by G. O. Essex and A. J. Stripeika under the supervision of H. D. Farnsworth.

[19] J. D. Jackson and J. M. Blatt, Rev. Mod. Phys. 22, 77 (1950).
[20] See also R. E. Meagher, Ph.D thesis, University of Illinois, 1949; Phys. Rev. 78, 667 (1950).

Photo-Disintegration of the Deuteron*

J. A. PHILLIPS,† J. S. LAWSON, JR., AND P. GERALD KRUGER
Physics Department, University of Illinois, Urbana, Illinois

(Received June 26, 1950)

A study of the photo-disintegration of the deuteron using a cloud chamber as a detector has been made for gamma-ray energies of 6.14 and 7.00 Mev from the $F(p, \alpha)O^{16*}$ reaction. By observing the number of photo-disintegration protons and the number of electron pairs formed in the gas (CD_4) of the cloud chamber, the ratio of the photo-disintegration cross section to the pair cross section is obtained. Assuming a calculated value for the pair cross section these data yield $\sigma[D(\gamma, p)n] = 25.7$ (14 percent P.E.) $\times 10^{-28}$ cm² at an average gamma-ray energy of 6.55 Mev.

A plot of the angular distribution of the photo-disintegration protons agrees, within statistical limits, with $\sin^2\theta$, though there may be a slight asymmetry in the forward direction.

I. INTRODUCTION

THIS is a report of an experiment designed to measure the angular distribution of the photo-protons and the cross section of the photo-disintegration of the deuteron at a gamma-ray energy of about 6.5 Mev. As far as is known there have been reported two other experimental results for the cross section in this energy range. Van Allen and Smith[1] obtained a value of $11.6 \pm 1.5 \times 10^{-28}$ cm² with a gamma-ray energy of about 6.2 Mev and Barnes, Stafford, and Wilkinson[2] give $21.5 \pm 1.2 \times 10^{-28}$ cm² at about 6.2 Mev.

In the present experiment it was thought that the cross section might be obtained by observing the photo-disintegration of the deuteron together with a second process, pair production, whose cross section is rather well known. The cross section for the production of electron pairs has been experimentally determined by several observers[3] and found to agree with the theory for light elements. Thus, one might obtain the cross section for the photo-disintegration (σ_{pd}) by counting the number of disintegration protons (N_p) and electron pairs (N_{pairs}) occurring in a medium containing deuterium under the same conditions by

$$\sigma_{pd} = (Z^2)_{ef}\sigma_{\text{pairs}}N_p/N_dN_{\text{pairs}}, \quad (1)$$

where N_d is the number of deuterons per molecule, $(Z^2)_{ef}$, the effective Z^2 per molecule of the medium, and σ_{pairs} the cross section for the production of electron pairs.

A Wilson cloud chamber was used as the detector. Since the equipment and techniques were essentially the same as previously reported,[4] they will not be described here.

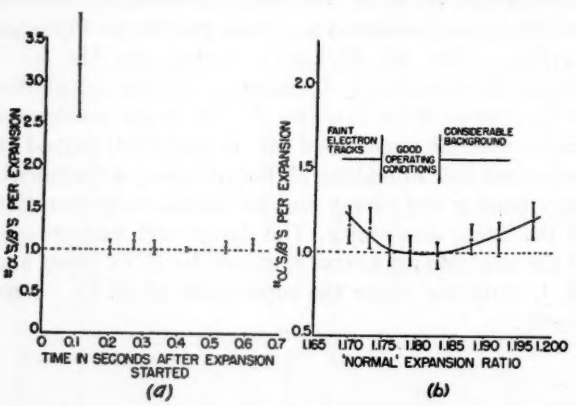

FIG. 1(a). The ratio of the number of alpha-tracks to the number of beta-tracks from a thin uranium nitrate source, observed as a function of time after the expansion started. For times larger than 0.2 sec., the average value of the ratio is 1.04.

FIG. 1(b). The ratio of the number of α-tracks to the number of β-tracks observed, as a function of the expansion ratio of the cloud chamber.

II. SENSITIVITY OF THE CLOUD CHAMBER

There may be some objection to the use of a cloud chamber as here employed, in that there is some question whether the sensitivity of a cloud chamber is the same for proton and electron tracks. It is well known that electron tracks may be discriminated against when it is desired to observe only heavy particle tracks by decreasing the expansion ratio. Thus, when a cloud chamber is adjusted for good electron tracks, is the cloud chamber equally sensitive for heavy particles and electrons?

To obtain information on the behavior of the cloud chamber a small quantity of uranium nitrate was placed on a thin foil of collodion which was then placed in the chamber. Assuming that the uranium was in secular equilibrium with its immediate daughter products there should, on the average, be one alpha-particle for every beta emitted by the uranium.

Figure 1 shows the data obtained from uranium; Fig. 1(a) the ratio of the number of alphas to betas as a function of the time after expansion. Within statistical error it is constant from 0.2 sec. to 0.6 sec. after ex-

* Assisted by the joint program of the ONR and the AEC.

† Now at Los Alamos Scientific Laboratory, Los Alamos, New Mexico.

[1] J. A. Van Allen and N. M. Smith, Jr., Phys. Rev. 59, 618 (1941).

[2] Barnes, Stafford and Wilkinson, Nature 165, 69 (1950).

[3] G. D. Adams, Phys. Rev. 74, 1707 (1948); J. L. Lawson, Phys. Rev. 75, 433 (1949); R. L. Walker, Phys. Rev. 76, 527 (1949).

[4] J. A. Phillips and P. G. Kruger, Phys. Rev. 76, 1471 (1949).

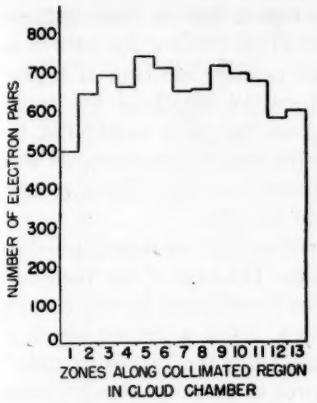

FIG. 2. Number of pairs observed per cylindrical volume element along the gamma-ray beam, in the usable portion of the chamber. These elements were 1.35 cm long and 2.54 cm in diameter. The usable portion of the chamber was 17.6 cm long, and was illuminated by a light beam 3.3 cm high. Thus, all tracks starting in this volume could be seen easily.

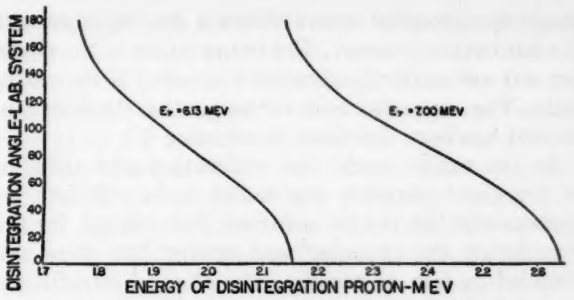

FIG. 3. Calculated values of the energy of the disintegration proton at various disintegration angles, θ, in the laboratory system, for gamma-ray energies of 6.13 Mev and 7.00 Mev. In this experiment, θ is defined as the angle made by the disintegration proton and the initial direction of the gamma-ray.

pansion, and accordingly the pictures were taken 0.45 sec. after expansion during the experiment.

The average value of the ratio during this time interval is 1.04 ± 3 percent. Actually, since beta-rays with energy less than 10 kev would probably not be seen in these pictures the observed ratio should be larger than unity. To obtain an idea of what ratio we should reasonably expect, an estimate of the ratio of the number of β's of energy less than 10 kev to the total number of β's from UX_1 and UX_2 has been made using Marshall's[5] data. This gives a ratio of 1.06 with an error which is difficult to assess. Since the observed ratio is 1.04 it is assumed that some but not all beta-rays of energy less than 10 kev are observed and that, essentially, the test agrees with the expected ratio.

The ratio of alphas to betas as a function of the expansion ratio is shown in Fig. 1b. The pictures were taken 0.45 second after the expansion of the cloud chamber. It is seen that if the chamber is adjusted for good electron tracks there is some latitude permissible in the expansion ratio without changing the ratio of alphas to betas.

A further check was made for the sensitivity of the cloud chamber for electron tracks. Figure 2 shows the distribution of the electron pairs obtained during the experiment as a function of the distance of the track origin along the axis of the collimated gamma-ray beam. Apparently the chamber was uniformly sensitive to electron tracks throughout the collimated region. Thus, it may be said from the data in Figs. 1 and 2, that whatever be the sensitivities of the chamber for protons and electrons they are constant within statistics under the conditions of the experiment.

III. SOURCE OF GAMMA-RAYS

The reaction $F^{19}(p, \alpha, \gamma)O^{16}$ was used as the source of gamma-rays with 5 Mev protons from the cyclotron of the University of Illinois. In the present experiment the energies of the gamma-rays were determined by measuring the range of the disintegration proton and its angle with respect to the incident gamma-rays.

[5] Marshall, Proc. Roy. Soc. London, A173, 397 (1939).

The energy, E_p, of the disintegration proton as a function of angle θ for the two gamma-ray energies of 6.13 Mev and 7.00 Mev has been calculated by the equation

$$2E_p = h\nu(1-h\nu/2Mc^2)+h\nu(P/Mc)\cos\theta - E, \quad (2)$$

where $h\nu$ is the energy of the gamma-ray, M is the mass of the proton, P is the momentum of the proton, and E is the binding energy of the deuteron, assumed to be 2.235 Mev. Figure 3 shows the results of these calculations. It is seen that there will be only a small energy region for which there will be doubt as to whether it is due to a 6.13-Mev gamma-ray and disintegrated in the forward direction or to a 7.00-Mev gamma-ray and disintegrated backwards.

The above equation can be solved for $h\nu$ and expanded by taking only the first two terms. There results

$$h\nu = \frac{2E_p+E}{(1+B\cos\theta)}\left\{1+\frac{2E_p+E}{2Mc^2(1+B\cos\theta)^2}\right\}, \quad (3)$$

where $B=v/c$ for the proton. This equation was used to calculate the energies of the gamma-rays from the energies of the disintegration protons.

IV. PROCEDURE

The procedure was essentially the same as that used previously.[4] The cyclotron was run continuously with a flop-gate preventing the beam from striking the target between expansions of the chamber. Immediately after the chamber had fully expanded the flop-gate was pulled aside. The average beam current was 9 μa of molecular hydrogen.

The cloud chamber was filled with CD_4 and its stopping power calculated using the Livingston and Bethe curves.[6] The composition of the gas with which the chamber was filled was determined by a mass spectrographic analysis. The pressure of the gas in the chamber (about 20 lb. gauge) as measured by a Bourdon type

[6] M. S. Livingston and H. A. Bethe, Rev. Mod. Phys. 9, 268 (1937).

gauge was recorded several times a day together with the barometric pressure. The temperature of the chamber was automatically controlled to $\pm 0.2°C$ by cooling coils. The magnetic field in which the chamber was located has been described in reference 4.

In the earlier work[4] the collimation and shielding of the cloud chamber was found to be sufficient for gamma-rays but not for neutrons. Accordingly, for this experiment the chamber and mirror box were surrounded by 6 in. of paraffin. Also 16 in. of paraffin was placed in front of the gamma-ray collimator, inside of the tanks surrounding the cyclotron to remove neutrons from the background radiation. Subsequent events show that this shielding may not have been completely adequate; this will be discussed later.

A total of 33,658 pictures were taken with the cloud chamber. These were examined on a Diebold microfilm reader by two observers. All electron pairs, electron triplets, and heavy particle tracks regardless of range were recorded. Those pictures containing possible proton tracks were later replaced in the original camera and optical system and measured.

V. ELECTRON PAIRS

The criteria for the selection of a countable electron pair were the same as previously used[4] with the added condition that the apex of an electron pair must lie in a

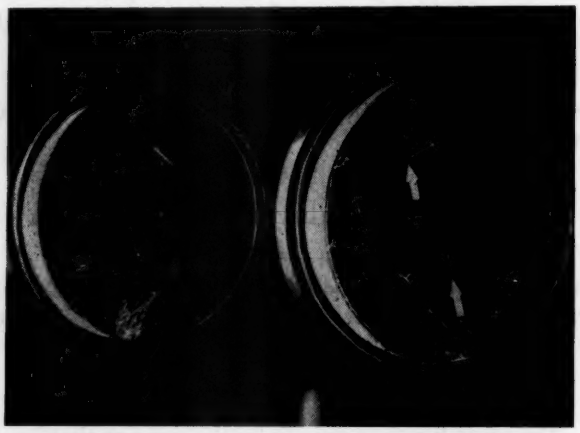

FIG. 4. Stereoscopic cloud chamber pictures showing a photoproton (upper arrow) and a pair (lower arrow) formed in the usable volume of the chamber.

volume covered by the collimated gamma-ray beam such that all of the range of a disintegration proton originating in this volume could be observed.

The distribution of the electron pairs in the usable volume of the cloud chamber is shown in Fig. 2. It is seen to be a constant within statistical limits except for the first and last two divisions. The first division is low as this division lies in the path of Compton electrons leaving the side wall of the chamber through which the gamma-rays pass as they enter the chamber making the apex difficult to be clearly observed. Protons, however, will easily be seen in this region due to their greater ionization. The last two divisions are low for here it is difficult to be sure that the positive electron of a pair has the right curvature since the length of the track observable is short. Thus, several pairs would not be counted. The average over the middle ten intervals was used to correct for these three intervals. There results 9007 ± 83 electron pairs that occurred.

There is one further correction that must be applied to the number of electron pairs. The end of the recorded interval of an expansion was determined by the closing of the shutter of the camera. Since a proton track is much denser than an electron track the "exposure time" for the film to record a proton track is shorter than that for an electron track. Thus the effective detection time for a proton track is longer than for an electron

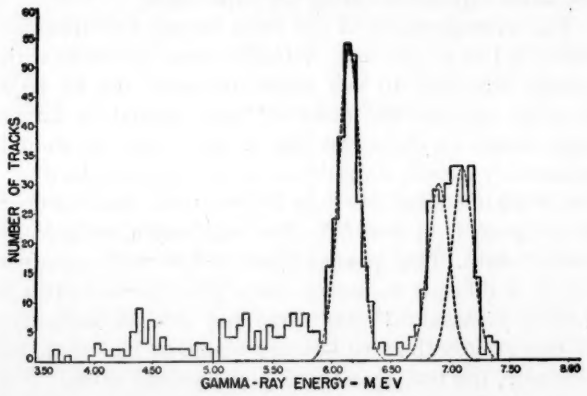

FIG. 5. Histogram of tracks starting in the collimated region showing the number of disintegration protons *vs.* the energy of the γ-ray causing the disintegration. This assumes that all measurable tracks whose full length was observable, were from the $D(\gamma, n)p$ reaction.

track. By varying the aperture of the lens and the shutter speed it was determined that the camera was sensitive to electron tracks 7.8 ± 5.2 percent shorter than to proton tracks. With this correction 9710 ± 476 (± 4.8 percent) electron pairs occurred.

VI. DISINTEGRATION PROTONS

All the proton tracks were viewed stereoscopically in the original optical system. The range, scattering angle, and azimuthal angle of each track were measured twice by a specially designed measuring engine.

Many of the proton tracks were observed to be badly "plumed," usually in the vertical direction. This is thought to be due to the chamber being overexpanded for proton tracks in order to obtain electron tracks. However, in most of these cases the original track could be observed through this plume and a reliable measurement made. An example of a sharp track is shown in Fig. 4.

The energies of the proton tracks whose entire range could be seen were calculated from their range and the stopping power, pressure and temperature of the gas. The energy of the incident gamma-ray was then calcu-

TABLE I. Calculation of angular distribution from tracks whose range can be measured.

7.00 Mev θ	N Experimental tracks in first div.	A Correction factor for geometry	$6NA$ (six div.)
10	0	1.00	3 (total)
30	4	1.02	24.4
50	25	1.04	156.0
70	35	1.06	222.2
90	44	1.09	287.2
110	24	1.05	151.0
130	19	1.02	116.0
150	6	1.00	36.0
170	0	1.00	2 (total)
			997.8
6.14 Mev			
10	0	1.00	0
30	5	1.01	30.3
50	9	1.02	55.0
70	27	1.03	166.9
90	24	1.03	148.2
110	16	1.02	97.9
130	19	1.01	115.2
150	8	1.00	48.0
170	3	1.00	0
			664.5

lated by Eq. (3). A histogram of the resulting gamma-ray energies are shown in Fig. 5. It is seen that there are two main groups, one at 6.14±0.05 Mev and the other at 7.00±0.06 Mev which are in good agreement with the authors[4] previous values from electron pair measurements and with reported values of others.[7]

The 7.00-Mev line appears to be much broader than the 6.14-Mev line. If one assumes a Gaussian distribution for the 6.14-Mev line and applies the same half-width to two lines at 6.90 and 7.10-Mev on can explain the total width of the 7.00-Mev line. The presence of two components in the 7.00-Mev line is also suggested by the report of three[8] groups of short range alphas to gamma-levels from this reaction. The gamma-ray energies of 6.9 and 7.1 would be in reasonable agreement with this picture. However, much better resolution would be necessary to show by this method that the 7.00-Mev group is double.

Since the light beam in the cloud chamber was not sufficiently high to permit the entire range of all tracks to be seen, there must be a correction to the number of tracks measured. The most straightforward method is to use only those tracks occurring in the first azimuthal distribution, 0 to 15°, interval. Correcting the number of tracks in the $\Delta\theta$ intervals of Table I by the calculated fraction of the total number in this interval which can be seen (correction factor for geometry in Table I) and multiplying by 6, the total number that would have been observed in all azimuths may be obtained. These calculations are given in Table I. There result 665±9.5 percent tracks in the 6-Mev line: 998±8 percent in the 7-Mev line and a total of 1663±6.1 percent tracks.

A second method of correction is as follows. From the range of the tracks (which varies with angle and with the energy of the gamma-ray) and the height of the light beam one can calculate the expected azimuthal distribution of these tracks where the entire range can be seen. Figure 6 shows this normalized, calculated, azimuthal distribution and the experimental distribution for the 6-Mev line. Assuming agreement within statistical error (since the data are divided into 9 groups for each line, the statistics in some intervals are very poor) the experimental numbers of protons observed can be corrected using the calculated fraction of the total number of tracks which would be observed. This calculation results in 642±6.5 percent tracks in the 6-Mev line: 1104±6 percent tracks in the 7-Mev line and a total of 1746±4.5 percent tracks.

While the results of both methods of correction agree within the standard deviation errors given, more confidence is placed in the first method because it involves only tracks whose full lengths could be seen and agree

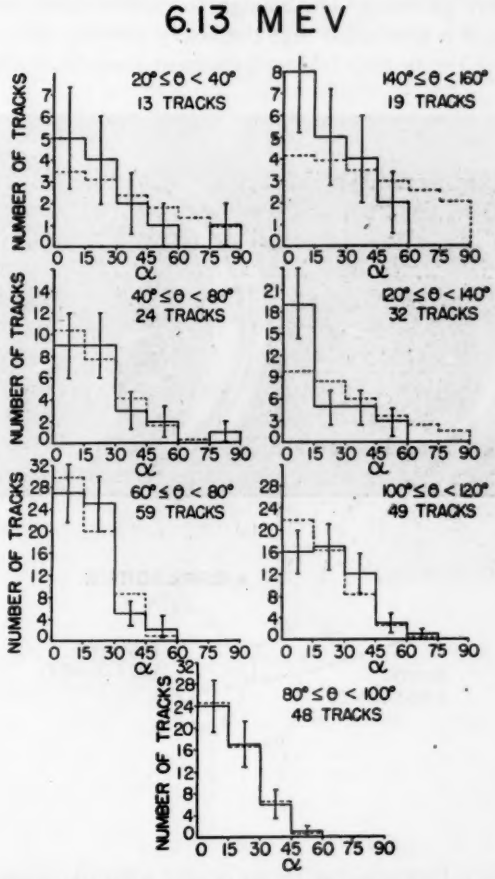

FIG. 6. Azimuthal distribution (folded 4 times) of observed tracks from the 6.13-Mev gamma-ray line, whose entire range was visible for various disintegration angles (θ). The solid curves give the experimentally observed numbers, while the dotted curves are the theoretical distribution calculated from the geometry of the light and gamma-ray beams and the range of a photo-proton falling in the θ-interval under consideration.

[7] Rasmussen, Hornyak, Lauritsen, and Lauritsen, Phys. Rev. 77, 617 (1950). R. L. Walker and B. D. McDaniel, Phys. Rev. 74, 315 (1948).

[8] W. E. Burcham and J. M. Freeman, Phys. Rev. 75, 1756 (1949). Chao, Tollestrup, Fowler, and Lauritsen, Phys. Rev. 78, 88 (1950).

TABLE II. Photo-disintegration cross section.

Gamma-ray energy Mev	Reference 12 σ(calc) $\times 10^{28}$ cm^2	Authors σ(expt) $\times 10^{28}$ cm^2	Barnes[a] σ(expt) $\times 10^{28}$ cm^2
6.14	22.4 20.1[c]	26.9±3.8	21.5±1.2[b]
6.55	21.4	25.7±3.7	—
7.04	20.2	24.2±3.4	—

[a] Barnes, Stafford, and Wilkinson, Nature 165, 69 (1950).
[b] A summary of other experimental results may be found in I. F. E. Hanson and L. Hulthin, Phys. Rev. 76, 1165 (1949).
[c] H. A. Bethe and C. Longmire, Phys. Rev. 77, 647 (1950).

with the data of Fig. 3. Thus, these numbers will be used below in calculating the photo-disintegration cross section.

VII. BACKGROUND CORRECTION

The background correction for heavy particle tracks is taken from the data of Fig. 5. Here it is seen that there are a number of heavy particle tracks that did not result from a photo-disintegration of a deuteron by either a 6-Mev or a 7-Mev gamma-ray. 583 electron pairs were measured and only 2.5 percent were found to have an energy low enough to explain these tracks. Thus, it is concluded that the heavy particle track outside of the 6- and 7-Mev lines must have been caused by deuteron recoils from neutrons that passed through the shielding around the cloud chamber, protons from the $D(n, 2n)p$ reaction or are protons from some similar process involving elements other than deuterium in the gas of the cloud chamber.

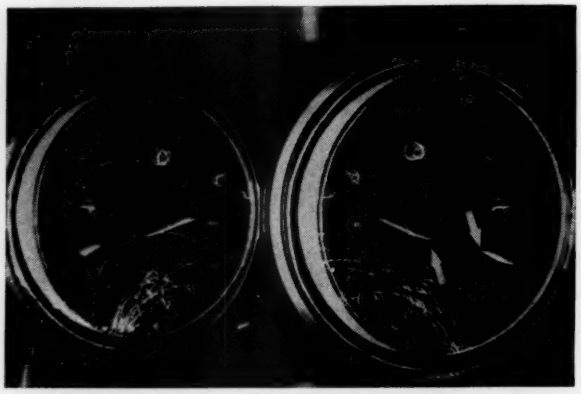

(a)

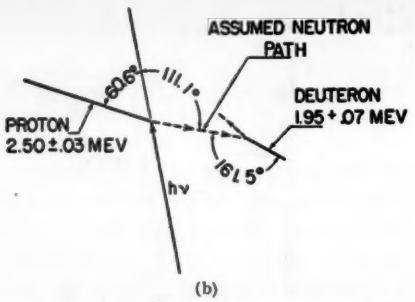

(b)

FIG. 7. Cloud-chamber picture (a) and schematic diagram (b) showing an $n-d$ scattering by a photo-neutron whose accompanying photo-proton is observable. The proton range and angle show the disintegration to have been caused by a 7.00-Mev gamma-ray. On this basis a deuteron scattered at 18.5° in the laboratory system by the photo-neutron should have 1.85 Mev, which agrees reasonably with the measured value of 1.95±0.07 Mev.

By taking the average background in Fig. 5 below 6 Mev and assuming that it remains constant up to 6.4 Mev, one must subtract 44/256 of 665 tracks (i.e., 114 tracks) in the 6-Mev line, giving a net number of 551±68 tracks (or ±12.3 percent) in the 6-Mev line. Between the two lines in the region of 6.5 Mev, there appear 14 tracks over a 0.3-Mev interval. Assuming this constant over the 7-Mev line, one must subtract 37/281 of 998 tracks which gives a net 867±90 tracks (10.3 percent) for the 7-Mev line. The total number of corrected proton tracks is now 1418±8 percent.

VIII. EFFECTIVE Z^2 FOR THE GAS

To obtain a cross section for the photo-disintegration of the deuteron by this method it is necessary to know the cross section for electron pair production.

This has been calculated from a formula given by Hough[9] and corrected by 1.4 percent for screening according to Walker[10] to give: $\sigma_{\text{pairs}}(6.13\text{ Mev})=0.0611$ barn; $\sigma_{\text{pairs}}(6.55\text{ Mev})=0.0653$ barn; $\sigma_{\text{pairs}}(7.04\text{ Mev})=0.0699$ barn.

The composition of the heavy methane gas was determined by a mass spectrographic analysis to be,

Component	Percent
CD_3H	9.2
CD_4	85.4
N_2	4.6
O_2	0.8

A 50:50 mixture by volume of heavy alcohol and heavy water was used. The vapor pressures of the vapors are 24.3 mm of Hg for C_2D_6O and 16.5 mm of Hg for D_2O as given by Das Gupta and Ghosh[11] at 22.1°C. From the above, the effective Z^2 per molecule[4] is calculated to be 44.98 and the number of deuterons per molecule is 3.71.

From the above data the value of the cross section for the photo-disintegration of the deuteron is calculated to be $25.7\pm3.7\times10^{-28}$ cm^2 at an average gamma-ray energy of 6.55 Mev. The values given in Table II for 6.14 and 7.04 Mev are calculated from the value at 6.55 Mev by taking the ratios of the theoretical values obtained from Levinger's[12] formula. The two latter values are in agreement with the values obtained from the number of disintegration protons in each line and the calculated number of electron pairs in each line assuming a ratio of gamma-ray intensities[4] of 1.7 for the two lines.

[9] P. V. C. Hough, Phys. Rev. 73, 266 (1948).
[10] R. L. Walker, Phys. Rev. 76, 527 (1949).
[11] N. R. Das Gupta and S. K. Ghosh, Rev. Mod. Phys. 18, 225 (1946).
[12] J. S. Levinger, Phys. Rev. 76, 699 (1949).

TABLE III. Angular distribution for all tracks whose lengths can be measured.

θ_{cm}	Number of tracks 6.15 Mev	Number of tracks 7.00 Mev	Total number both lines	Solid angle correction	Tracks per unit solid angle
10	0.0± 0.0	3.2± 1.3	3.2± 1.3	0.0603	53.1±21.6
30	25.6± 7.4	26.9± 7.4	52.5±10.5	0.1737	302.5±60.5
50	58.7±11.2	162.2±20.2	220.9±23.1	0.2660	830.0±86.8
70	176.0±20.0	246.8±25.5	422.8±32.4	0.3264	1292.0±99.3
90	150.0±18.7	290.6±28.1	440.6±33.7	0.3472	1270.0±97.2
110	116.0±15.6	171.5±20.7	287.5±25.9	0.3264	879.0±79.2
130	87.8±14.4	118.0±16.4	205.8±21.8	0.2660	773.0±82.0
150	36.4± 8.8	29.4± 8.1	65.8±11.9	0.1737	379.0±68.0
170	3.0± 1.2	2.0± 1.0	5.0± 1.56	0.0603	83.0±25.9

The experimental values obtained here are higher than those predicted by theory, and higher than the experimental value of Barnes. The calculated error (standard deviation) for the authors cross sections given in Table II is 10 percent. This calculated error does not include an error in the electron pair cross section nor in the value for the number of deuterons per molecule. Furthermore, no possible systematic or unknown errors are taken into account. If the second method of correcting for azimuthal distribution were considered a probable eror of 14 percent would be a more realistic value. The values in Table II are 14 percent probable errors.

One picture is of some interest and a reproduction is shown in Fig. 7. Here a photo-disintegration took place in the center of the chamber with the proton shown. The neutron went off in almost the opposite direction and scattered a deuteron in its path. From the measured energy and angle of the proton the neutron has the expected energy and angle within experimental error, (the energy of the neutron being determined by the deuteron). Also the direction of the proton and the initial neutron direction, as defined by the proton and origin of the deuteron, lie in the same plane.

Table III gives the data on the angular distribution of the photo-disintegration protons. These data are plotted in Fig. 8 and as expected, agree with a $\sin^2\theta$ distribution, with perhaps a slight assymetry in the forward direction. For comparison a curve described by Marshall and Guth[13] is included also.

[13] J. F. Marshall and E. Guth, Phys. Rev. **76**, 1879 (1949).

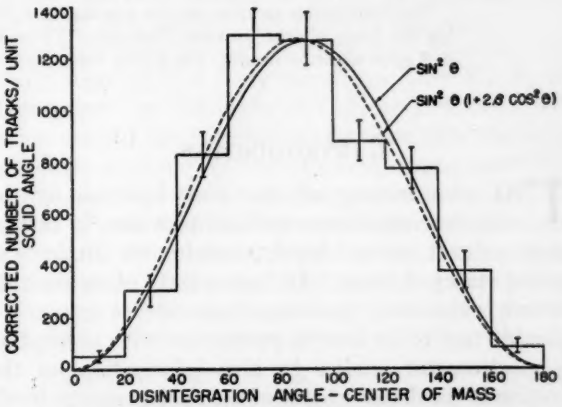

FIG. 8. Histogram of number of tracks corrected for azimuthal geometry, as a function of angle in the center-of-mass system. Also included are curves for $\sin^2\theta$ and the prediction of Marshall and Guth $f(\theta)=$(small const.)$+\sin^2\theta(1+2\beta\cos^2\theta)$. The difference between the two curves at this energy is too small to allow a clear choice of fit. Both curves are normalized to the experimental number at 90°.

IX. TRIPLETS

A total of 499 electron triplets were observed during the present experiment. The treatment of these triplets was the same as was used previously.[4] The value of $(Z^2)_{ef}/Z_{ef}$ for this gas is calculated to be 4.31. Having observed a total of 8620 electron pairs, the ratio of the cross section for electron pair production to triplet production results to be

$$\frac{\sigma_p(Z)_{ef}}{\sigma_t(Z^2)_{ef}}=4.01\pm0.12.$$

This compares favorably with the value 3.92±0.26 obtained previously.[4]

Short-Lived Isomers* of Ta^{181}

W. C. BARBER
Stanford University, Stanford, California
(Received July 3, 1950)

Excited states of Ta^{181} which result from the 46-day β-decay of Hf^{181} were investigated by the method of delayed coincidences. Using *trans*-stilbene scintillation counters and a coincidence system of about 1.3×10^{-8}-sec. resolving time, a state with a half-life of $(1.08\pm0.05)\times10^{-8}$-sec. was observed. Delayed coincidence absorption experiments indicated that the radiation following the delayed state arises chiefly from a transition of about 0.5-Mev energy.

The radiations preceding and following the 2.2×10^{-5}-sec. state were also investigated and, in agreement with other recent results, no γ-rays were observed in the preceding radiation.

Possible assignments of spin and parity to the excited states of the Ta^{181} nucleus are discussed.

The scintillation counter system was also used to search for delayed coincidences in the radiations following the decay of other isotopes. Sources of 5.3-yr. Co^{60}, 225-day Ag^{110}, 2.7-day Au^{198}, 2.6-hr. Mn^{56}, and 34-hr. Br^{82} gave negative results. The 8×10^{-8}-sec. state of Cd^{111} was observed in the decay of 2.8-day In^{111}.

I. INTRODUCTION

THE measurement of short-time intervals by the delayed coincidence method provides, in certain cases, a direct method for determining the lifetimes of excited states of nuclei.[1] In case a state of measurable lifetime is observed, the delayed coincidence system is a valuable tool to be used in connection with absorption or spectrometer studies to give information on the position in the decay scheme of the nuclear energy levels involved. Knowledge of the lifetime and positions of the energy levels is of importance in obtaining further valuable information about the nuclear states (e.g., spins and parities).

This paper is chiefly a report of a delayed coincidence investigation of the radiations emitted in the decay of Hf^{181}. Evidence is presented for the existence of a new short-lived isomer of Ta^{181}, and the sequence of the transitions of this latter nucleus is discussed in the light of delayed coincidence absorption experiments.

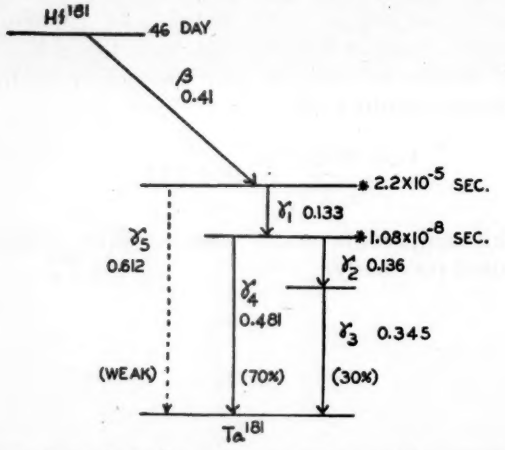

FIG. 1. Level diagram showing the major radiations produced by Hf^{181}. Transition energies are given in Mev. The γ-rays are labeled in order of increasing energy.

The radiations of Hf^{181} have been studied by a number of observers, and there is agreement among recent investigators as to the general features of the decay scheme.[2–5] However, there are several details of the level scheme which are still in doubt, and a recent investigation[5] indicates that the radiation spectrum may be more complicated than was previously supposed.* The facts generally agreed upon can be summed up in the level scheme shown in Fig. 1. In this figure the γ-ray energies have been taken from reference 5. The branching ratio for parallel transitions has been calculated from data given in reference 2. The assignment of the 1.08×10^{-8}-sec. level is made on the basis of investigation herein reported.

II. APPARATUS

Figure 2 shows a block diagram of the delayed coincidence apparatus as used in studying the very short-lived states.

The source was placed in position "*S*" and various absorption foils were inserted between the source and either counter.

The particle detectors were scintillation counters employing anthracene or *trans*-stilbene crystals mounted on 931-A photo-multiplier tubes.[6] The multiplier tubes were usually operated at room temperature, but in a few experiments, where multiplier noise counts were troublesome, the tubes were cooled with dry ice.

Cathode follower tubes sent the output pulses from

* Assisted by the joint program of the ONR and AEC.

[1] S. DeBenedetti and F. K. McGowan, Phys. Rev. **74**, 728 (1948).

[2] K. Y. Chu and M. L. Wiedenbeck, Phys. Rev. **75**, 226 (1949).

[3] E. N. Jensen, Phys. Rev. **76**, 958 (1949).

[4] Arne Lundby, Phys. Rev. **76**, 1809 (1949).

[5] Cork, Stoddard, Rutledge, Branyan, and Le Blanc, Phys. Rev. **78**, 299 (1950).

* *Note added in proof:* It has recently been shown [M. Deutsch and A. Hedgran, Phys. Rev. **79**, 400 (1950)] that most of the radiation which had previously been attributed to γ_3 is due to a longer-lived activity than that of Hf^{181}. However, the investigation of Cork *et al.* indicates the presence of two different γ-rays of about 0.345-Mev energy and coincidence spectrometer studies [C. M. Fowler and R. G. Shreffler, Rev. Sci. Inst. **21**, 740 (1950)] indicate that γ_3 has a place in the Hf^{181} decay scheme.

[6] The stilbene crystals used in the investigation were kindly supplied by Professor Robert Hofstadter of Princeton University.

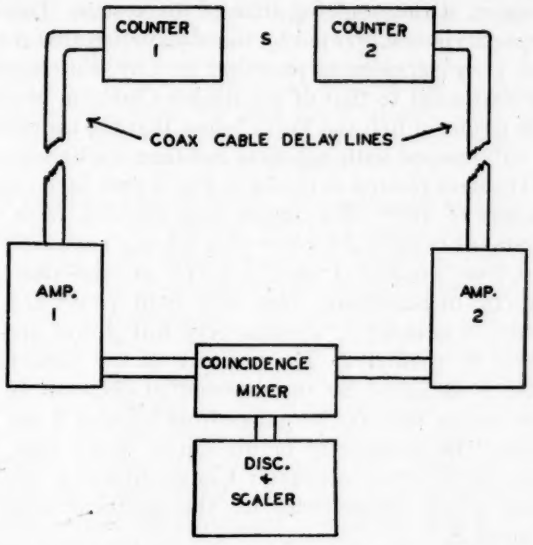

FIG. 2. Block diagram of the delayed coincidence apparatus. Scintillation counters are used. The amplifiers (amp.) are of the distributed type (reference 7).

the multiplier tubes into the coaxial cables which served as delay lines. The cables were Type *RG-7/U* which have a characteristic impedance of 97.5 ohms and a propagation velocity of 0.84 c. The amplifiers were of the distributed type,[7] having a voltage gain of about 25 and a band width (to the half-power point) of about 60 Mc/sec.

The coincidence system was a Rossi-type circuit which operated reliably for input pulses greater than 2 volts.[8]

The 2.2×10^{-5}-sec. state of Ta^{181} was investigated using vacuum-tube univibrator circuits to shape the pulses and produce the delays. Pulse widths and delay intervals were measured on a synchroscope. Pulses from the counters were amplified by conventional high gain amplifiers.[9] Except for the fact that both scintillation counters and Geiger counters were used as particle detectors, the arrangement of the apparatus into a delayed coincidence system was the same as that described by DeBenedetti and McGowan.[1]

III. SOURCES

The sources of Br^{82}, Au^{198}, and Mn^{56} were prepared by irradiation of the stable isotopes of these elements with neutrons produced by the Stanford cyclotron. The Co^{60}, Ag^{110}, and Hf^{181} sources were produced at Oak Ridge by pile irradiation. The In^{111} source was produced at the University of California at Berkeley and kindly supplied to the author by Professor A. C. Helmholz.

The first investigation of the Hf radioactivity was made with a source which was more than one year old. This source showed the presence of an electron component of energy slightly greater than that of any of the electrons reported[2] from the 46-day Hf^{181}. These energetic electrons were observed to be in immediate coincidence with γ-rays capable of penetrating several g/cm^2 of lead,[10] a situation which is at variance with the decay scheme shown in Fig. 1. A second source of Hf^{181}, which had been produced shortly prior to the time measurements were made, showed no evidence for an appreciable number of energetic electrons in coincidence with hard γ-rays, so the early results must be due either to a longer-lived[5] Hf or an impurity.

The radiation spectrum of the second Hf source was kindly observed in a β-ray spectrograph by Mr. R. W. Hayward of the University of California. This investigation showed the spectrum to be essentially the same as that reported for Hf^{181} by other experimenters.[2,3] The continuous β-spectrum and the conversion lines of γ_1, γ_3, and γ_4 were observed in one experiment. In a second experiment Compton electrons from an aluminum radiator were measured. Those produced by γ_4 were

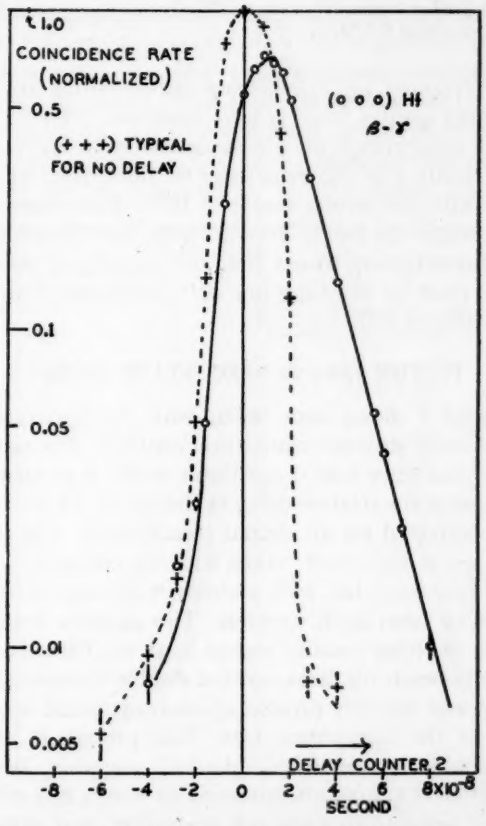

FIG. 3. Curves of coincidence rate as a function of delay, taken with the apparatus of Fig. 2. The points (+++) were taken with "simultaneous" events in each counter. The points (o o o) represent electron-γ-coincidences produced by Hf^{181}, where the electrons are admitted into counter 2 only. The two curves have been normalized to include the same area on a linear plot. The vertical lines indicate statistical standard errors.

[7] Ginzton, Hewlett, Jasberg, and Noe, Proc. I.R.E. **36**, 956 (1948).

[8] Interested persons may secure a diagram of the coincidence circuit by writing to the author.

[9] Some of the equipment used in this study was kindly lent to the Stanford Physics Department by the Department of Physics of the University of Illinois.

[10] W. C. Barber, Phys. Rev. **78**, 82 (1950).

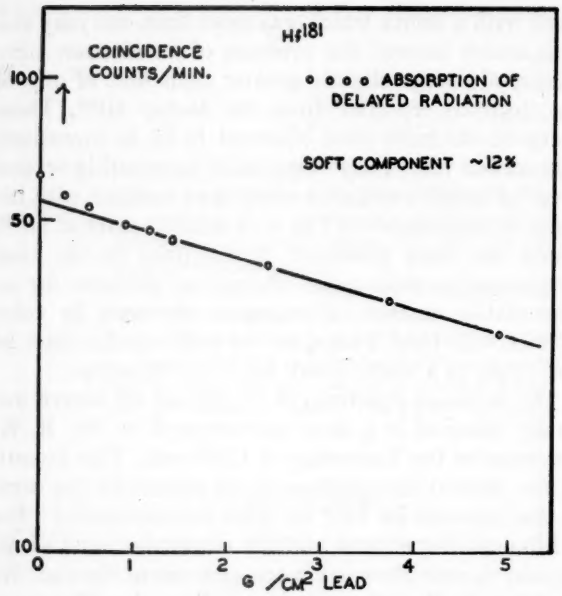

FIG. 4. Absorption in lead of the γ-radiation which is in delayed coincidence with electrons. In taking this curve the pulses from the electron counter were electrically delayed by 4×10^{-8} sec. more than the pulses from the γ-counter. The hard γ-component has an energy of about 0.5 Mev.

easily detected, but no electrons corresponding to γ-rays of energy greater than γ_4 were observed.

The experiments on the radioactivity of Hf^{181} which are described in the remainder of this paper were all made with the second source of Hf^{181}. This source may also contain the longer-lived activity, but the spectrometer investigation shows that the amount of such activity must be less than one or two percent of the activity due to Hf^{181}.

IV. THE 1.08×10^{-8}-SEC. STATE OF Ta^{181}

Figure 3 shows data taken with the apparatus of Fig. 2 using stilbene scintillation counters. The normalized coincidence rate (logarithmic scale) is plotted as a function of the relative delay in channel 2. All data have been corrected for accidental coincidences. The points (+++) in Fig. 3 were taken with the counters in their usual geometry, but with a strong γ-ray source located far away from both counters. The distance from the source to either counter was at least ten times the distance between counters, so that double Compton scattering was the only process which contributed appreciably to the coincidence rate. This process is not so improbable as the word "double" suggests, because almost all of the counts produced by γ-rays in a stilbene crystal are due to Compton scattering, and since the two counters are close together, there is a good chance of detecting the scattered photon in the second counter. Since it is likely that any delays in the Compton process are small compared with the resolving time of this apparatus,[11] the curve (+++) in Fig. 3 is taken as a measure of the resolving time of the system. This interpretation is supported by the observation that $\beta-\gamma$- and $\gamma-\gamma$-coincidences produced by Co^{60} sources yield curves similar to that of the double Compton process. The results of Bell and Petch[12] show that the transitions in Ni^{60} proceed with half-lives less than 3×10^{-9} sec.

The data plotted as circles in Fig. 3 were taken using sources of Hf^{181}. The source was shielded from the crystal of counter 2 by less than 0.4 mg/cm² of Nylon and from counter 1 by 3.2 g/cm² of lead plus 350 mg/cm² of aluminum. Thus only hard γ-rays are detected in counter 1, whereas very soft β-rays are detected in counter 2. The presence of the metastable state is indicated by the exponential decrease in the coincidence rate as the pulses from counter 2 are delayed. The asymmetry of the curve shows that the particles detected in counter 1 have suffered a nuclear delay which compensates for the electrical delay in channel 2.

The solid line in Fig. 3 represents the curve to be expected if all of the coincidences arise from events where the particles detected in counters 2 and 1, respectively, precede and follow a nuclear state of half-life 1.08×10^{-8} sec. Computation of this curve is as follows: Let $f(\delta)$ represent the curve (+++) in Fig. 3 (i.e., $f(\delta)$ is the experimental delay curve when the two particles are simultaneous). Here δ stands for the electrical delay introduced in channel 2. If the particles are separated by a nuclear state of decay constant λ the frequency distribution of pairs of particles separated by a time between t and $t+dt$ is given by $\lambda e^{-\lambda t}$. The probability of detecting this pair of particles in the coincidence circuit with delay setting δ is proportional to $f(\delta-t)$ and hence the over-all delay curve $F(\delta, \lambda)$ is given by

$$F(\delta, \lambda)=\int_0^\infty f(\delta-t)\lambda e^{-\lambda t}dt. \qquad (1)$$

Differentiation of Eq. (1) with respect to δ and then integration of the resulting equation by parts gives the result

$$\partial F(\delta, \lambda)/\partial\delta=\lambda[f(\delta)-F(\delta, \lambda)], \qquad (2)$$

which means that $F(\delta, \lambda)$ has its maximum where it intersects $f(\delta)$.[13]

The solid curve of Fig. 3 was computed by numerical integration of Eq. (1), using a value of λ determined by the slope of the experimental delay curve at large values of δ.

The good agreement between the computed and the experimental delay curves permits the following conclusions:

(1) A metastable state is present and its half-life is about 1.08×10^{-8} sec. A probable error of 0.05×10^{-8} sec. is assigned to

[11] R. Hofstadter and J. A. McIntyre, Phys. Rev. **78**, 24 (1950).

[12] R. E. Bell and H. E. Petch, Phys. Rev. **76**, 1409 (1949).

[13] This result has been derived independently by T. D. Newton who has given a general discussion of the evaluation of delayed coincidence experiments, Phys. Rev. **78**, 490 (1950).

the result from consideration of the statistical errors in the determination of the delay curves as well as the uncertainty in the propagation velocity of the cable (two or three percent).

(2) The decay of the Hf^{181} source produces few electrons in immediate coincidence with hard γ-rays. If such coincidences were present they would produce a delay curve like $f(\delta)$ and the experimental delay curve would not agree with $F(\delta, \lambda)$.

In order to investigate the position of the metastable state in the level scheme of Ta^{181}, absorption studies were made of the delayed and preceding radiation.

The presence of γ-radiation preceding the metastable state was demonstrated by detecting $\gamma-\gamma$-delayed coincidences. With counter 1 shielded by 3.2 g/cm² of lead and counter 2 shielded by 450 mg/cm² of aluminum a delay curve similar to that of the circles in Fig. 3 was obtained. An absorption study of the preceding γ-rays is difficult because of the high ratio of accidental to true delayed coincidences. However, data were taken which indicated that the preceding γ-rays are strongly absorbed by lead (half-value thickness less than 0.5 g/cm²) and hence consist mostly of photons of energy less than 200 kev.

Figure 4 represents the absorption in lead of the electromagnetic radiation which follows the metastable state. Statistical errors are less than or equal to the size of the plotted circles. In taking this curve the delay in channel 2 was fixed at 4×10^{-8} sec. and the lead absorbers were placed between the source and counter 1. An absorber of 180 mg/cm² of Celluloid was kept directly in front of counter 1 to prevent β-rays or secondary electrons from entering this counter. The half-value thickness of the delayed hard component is 5.3 g/cm², which indicates a quantum energy of about 0.5 Mev. The absorption of the delayed soft component is consistent with the interpretation that it consists of γ-rays of about 140 kev with perhaps some K x-rays of Ta as well. The absorption curve shows the amount of the soft component to be between 10 and 15 percent of the total, but since the efficiency of the counters for soft radiation is much less than for hard, the actual amount of soft component is more than this.

Figure 5 shows the absorption in Celluloid of the electrons which precede and follow the metastable state. Counts caused by γ-rays have not been subtracted, but the data were taken using thin stilbene crystals which had low efficiency for detecting γ-rays. Both of these curves were taken with an electrical delay of 4×10^{-8} sec. Statistical standard deviations are indicated by the vertical lines.

Absorption of the particles following the metastable state (shown by the circles in Fig. 5) indicates the presence of energetic electrons not completely absorbed by 85 mg/cm² of Celluloid as well as a softer electronic component. These two electron components are presumably due to the conversion of the transitions which produce the two γ-components indicated by Fig. 4. The data are consistent with the level scheme in Fig. 1 where γ_2 is responsible for the delayed soft component and γ_4 (and perhaps γ_3 as well) for the delayed hard component.

The crosses in Fig. 5 show the absorption of the particles preceding the metastable state. Ninety percent of these particles are absorbed by 13 mg/cm² of Celluloid, indicating that the particles are electrons of about 100-kev energy. This result is also consistent with the level scheme of Fig. 1, where the preceding electrons are the result of the K and L conversion of the γ_1-transition.

V. THE 2.2×10^{-5}-SEC. STATE OF Ta^{181}

The radiations preceding and following the 2.2×10^{-5}-sec. state were also investigated by absorption measurements. The delayed coincidences were produced by the system of univibrators mentioned earlier.

The delayed radiation showed the presence of γ-rays as well as electrons. The γ-radiation contained a component with a half-value thickness greater than 3 g/cm² of lead and is thus probably due to γ_4, γ_3, or both. The half-life of the state was observed to be about 20 μsec., but an accurate determination was not attempted.

All attempts to detect γ-rays or x-rays in the radiation preceding the 2.2×10^{-5}-sec. state yielded negative results. Experiments to detect $\gamma-\gamma$-delayed coincidences were made at first, using anthracene scintillation counters and later using Geiger counters with plated silver cathodes. The counters were shielded from β-rays by 200 mg/cm² of Celluloid and the immediate as well as the delayed coincidences were recorded. The sta-

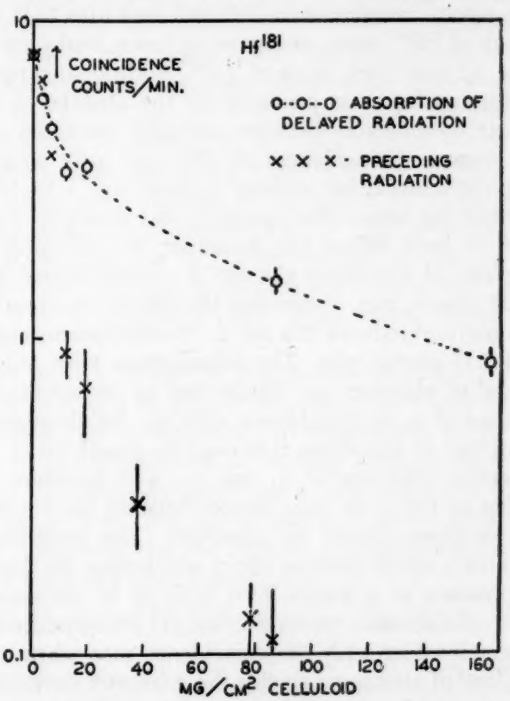

FIG. 5. Absorption in Celluloid of electron-electron delayed coincidences. The points (x–x–x) were obtained when the absorber was placed in front of the counter whose pulses were electrically delayed. In taking each curve the electrical delay was fixed at 4×10^{-8} sec.

TABLE I. Calculated γ-radiation decay constants for the transitions in Ta^{181}.

γ-energy (Mev)	λ_γ(sec.)$^{-1}$ $l=2$	$l=3$	$l=4$	$l=5$
γ_1 0.133	1.1×10^{8}	4×10^{2}	8×10^{-4}	...
γ_2 0.136	1.3×10^{8}	5×10^{2}	1×10^{-3}	...
γ_3 0.345	1.6×10^{10}	3×10^{5}	...	...
γ_4 0.481	8×10^{10}	3×10^{6}	8×10	...
γ_5 0.612	...	1×10^{7}	7×10^{2}	2.5×10^{-2}

TABLE II. Half-lives of the states of Ta^{181}, calculated from Table I but taking into account experimental values of internal conversion and γ-ray branching. Experimental half-lives are given for comparison.

γ-energy (Mev)	Calculated $T_{\frac{1}{2}}$ (sec.) $l=2$	$l=3$	$l=4$	$l=5$	Experimental $T_{\frac{1}{2}}$ (sec.)
γ_1 0.133	4×10^{-10}	1×10^{-4}	6×10	...	2.2×10^{-5}
γ_2 0.136	8×10^{-10}	2×10^{-4}	...	...	
γ_3 0.345	1×10^{-11}	7×10^{-7}	...	...	
γ_4 0.481	6×10^{-12}	1.5×10^{-7}	6×10^{-3}	...	1.08×10^{-8}
γ_5 0.612	...	7×10^{-10}	1×10^{-5}	2.7×10^{-1}	2.2×10^{-5}

tistical significance of the negative result is indicated by the ratio of total delayed to total immediate coincidences which (after correction for accidental coincidences and for the finite gate widths of the delayed coincidence system) was 0.013 ± 0.020. The $\pm$ figure gives the statistical standard deviation.

The negative result of the attempts to detect $\gamma-\gamma$-delayed coincidences is in agreement with the results of other recent investigations[4,14,15] and indicates that the β-decay of Hf^{181} must, in almost all cases, lead directly to the 2.2×10^{-5}-sec. state of Ta^{181}. Additional support for this conclusion is provided by the absence of immediate coincidences between energetic electrons and hard γ-rays. Coincidences of this sort were sought, using the scintillation counter system with 1.3×10^{-8}-sec. resolving time. The γ-counter was shielded by 2.3 g/cm^2 of lead. When the β-counter was shielded by 7 mg/cm^2 of aluminum the net $\beta-\gamma$-coincidence rate was 28 counts/min. Increasing the aluminum absorber to 33 mg/cm^2 reduced the net $\beta-\gamma$-coincidence rate to (0.8 ± 0.3) counts/min. The coincidences with only 7 mg/cm^2 of absorber are chiefly due to the conversion electrons of γ_1 in coincidence with γ_4. An absorber of 33 mg/cm^2 of aluminum is enough to absorb all of the conversion electrons of γ_1 and γ_2, and therefore according to Fig. 1 no coincidences between hard γ-rays and electrons should be observed. The experiment indicates a small positive effect which may be due to the presence of a longer-lived activity in the source. (Refer to discussion under Section III.) Comparison of this small effect with the coincidence rate when only 7 mg/cm^2 of aluminum shields the β-counter shows that the amount of such activity must be small. Because of the presence of the 1.08×10^{-8}-sec. state, only about one-half of the soft electron-hard γ-events are close enough in time to be detected by the coincidence system. Furthermore, the efficiency of the scintillation counters is much less for the soft electrons than for the hard ones. Taking these corrections into account, it can be concluded that the number of coincidences between hard γ-rays and penetrating electrons is fewer than one or two percent of the number of Ta^{181} disintegrations.

VI. DISCUSSION OF THE Ta^{181} ENERGY LEVELS

The delayed coincidence absorption experiments are in good agreement with the level scheme of Fig. 1, but attempts to make complete spin and parity assignments to the levels of Ta^{181} meet with difficulty.

The assignment of the multipole character of γ-ray transitions on the basis of lifetime measurements is somewhat uncertain, because the calculation of the radiative transition probability requires a detailed knowledge of the nucleus. However, various nuclear models have been used successfully to estimate transition probabilities. A recent survey of nuclear isomers[16] indicates that the formula

$$\lambda_\gamma=\tfrac{1}{3}(\rho^{2l}/(l!)^2)(W/137)^{2l+1}(mc^2/\hbar)$$

is a good approximation for the average decay constant of γ-ray transitions, but that individual cases may be expected to vary by factors of 10 to 100 from this value. In this formula l is the multipole order for electric radiation, W is the transition energy in units of mc^2, and ρ is the nuclear radius in units of e^2/mc^2. Application of the formula to the γ-rays of Ta^{181} yields the values which are given in Table I.

The entries in Table I are the decay constants for γ-emission only. Any competing processes, such as internal conversion or γ-ray branching, make the total decay constant of a state larger. Table II gives the expected half-lives of the states of Ta^{181} as computed from the γ-decay constants of Table I, taking into account the experimentally determined correction for internal conversion and branching. The half-life is calculated from the relation

$$T_{\frac{1}{2}}=0.693f/\lambda_\gamma(1+\alpha),$$

where α=conversion coefficient and f=fractional branching. Except for γ_5, the data necessary to calculate the conversion coefficients and branching ratios have been taken from the paper of Chu and Wiedenbeck.[2] The relative intensity of γ_5 has not been measured, but it is certainly small. In order to give a half-life in Table II, a value of one percent has been assumed for the branching of γ_5.

As has been pointed out by Lundby,[4] the observed lifetime and conversion coefficients of γ_1 lead to the conclusion that this transition is mixed electric octopole and magnetic quadrupole. The transition thus involves a parity change and a spin change of 2 units.

[14] D. Walker and E. W. Fuller, Nature **164**, 226 (1949).
[15] S. B. Burson and K. W. Blair, Phys. Rev. **78**, 89 (1950).
[16] P. Axel and S. M. Dancoff, Phys. Rev. **76**, 892 (1949).

Gamma-5 also arises from the 22-μsec. state, and to account for the fact that this transition is not observed with appreciable intensity, an l value of at least 4 is required.

Gamma-4 is the most prominent of the radiations following the 10^{-8}-sec. state. An l value of 3 for this transition predicts a lifetime of 1.5×10^{-7} sec., which is 14 times longer than the experimental value. However, any other l assignment gives discrepancies by factors greater than 1000. The value $l=3$ corresponds to electric octopole or magnetic quadrupole radiation. This assignment can be checked by the measurements of the conversion coefficient. The data of Chu and Wiedenbeck give $\alpha_k=0.031$, whereas the calculations of Rose *et al.*[17] predict 0.04 if the transition is electric octopole and 0.13 if magnetic quadrupole. The experimental value is uncertain because the branching ratio is uncertain. For this reason the discrepancy is not serious, provided the transition is mostly electric.

Either γ_2 or γ_3 must also originate from the 10^{-8}-sec. state. For γ_3 the value $l=2$ predicts a half-life of 10^{-11} sec., and $l=3$ predicts 7×10^{-7} sec. For γ_2 the choice $l=2$ yields 8×10^{-10} sec., which is in slightly better agreement with the experimental result than either choice for γ_3. For this reason, Fig. 1 has been drawn with γ_2 preceding γ_3; however, the order of these γ-rays is not important in the argument which follows.

On the basis of the level scheme of Fig. 1 and the foregoing classification of the γ-transitions, it is possible to draw some conclusions concerning the spins of the Ta^{181} levels. Consideration of γ_1, γ_4, and γ_5 leads to a requirement for a spin change of at least 4 units between the ground state and the 2.2×10^{-5}-sec. state. Since the ground state of Ta^{181} has a spin of 7/2, the upper state must have a spin of 15/2 or more. A possible assignment of spins and parities is shown in Fig. 6(a).

A level diagram which avoids the high spin assignments of 15/2 can be made, provided special assumptions about the γ-transitions are introduced. One such scheme is shown in Fig. 6(b). The difficulty here is that electric dipole radiation is allowed for γ_4, and the transition should proceed with a lifetime much shorter than 10^{-8} sec. The scheme is tenable, provided only that some special property of the nucleus reduces the electric dipole matrix element by an exceedingly great amount.

VII. OTHER ISOTOPES

The delayed coincidence apparatus has been used to search for short-lived isomers of some other isotopes.

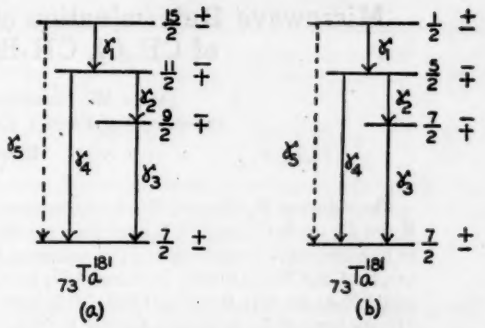

FIG. 6. Possible energy level schemes for Ta^{181}. Spins and parities are indicated at the right-hand side of each scheme.

Stilbene scintillation counters were used to measure the coincidences produced by sources of 5.3-yr. Co^{60}, 225-day Ag^{110}, 2.6-hr. Mn^{56}, and 2.8-day In^{111}. The delay curves produced by the $\beta-\gamma$-coincidences of Co^{60}, Ag^{110}, and Mn^{56} were similar to the instantaneous curve (+++) in Fig. 2. It can therefore be concluded that the states of Ni^{60}, Cd^{110}, and Fe^{56}, which give rise to γ-rays of appreciable intensity, do not have lifetimes in the range detectable by this apparatus (from about 3 or 4×10^{-9} sec. to 2 or 3×10^{-7} sec.).

The delay curve of coincidences produced by the In^{111} source showed the presence[18] of the 8×10^{-8}-sec. state of Cd^{111}, and provided the first direct evidence that the apparatus was capable of detecting metastable states.

An early version of the apparatus, using anthracene scintillation counters, was used to measure the coincidences produced by 2.7-day Au^{198}, and 34-hr. Br^{82}, as well as the Co^{60}. Due chiefly to the longer decay time of the anthracene, the delay curves were wider (resolving time about 2.3×10^{-8} sec.) than the "no delay" curve of Fig. 3. For each of the three sources, the $\beta-\gamma$-delayed coincidence curves were symmetrical about the zero delay axis. Analysis of the curves indicated that no states of lifetime greater than 10^{-8} sec. were playing an appreciable role in the production of the coincidences. The negative results in the case of Au^{198} and Co^{60} are in agreement with other recent investigations.[12,18]

The author wishes to express his appreciation to Mr. B. S. Baldwin, Jr., for his aid in the construction and testing of the apparatus, to Professor A. C. Helmholz for his cooperation in making research facilities at the University of California available for the spectometer part of this investigation, and to Professor W. E. Meyerhof for his interest and valuable advice in the working out of this problem.

[17] Rose, Goertzel, Spinrod, Harr, and Strong, Phys. Rev. **76**, 1883 (1949).

[18] M. Deutsch and W. E. Wright, Phys. Rev. **77**, 139 (1950).

Microwave Determination of the Centrifugal Distortion Constants of CH_3Cl, CH_3Br, CH_3I, BrCN, and ICN*

JAMES W. SIMMONS** AND WALLACE E. ANDERSON†
Department of Physics, Duke University, Durham, North Carolina

(Received June 16, 1950)

The values of B, D_J, and D_{JK} in the ground vibrational state for the heavier methyl halides, and values of B and D_J for BrCN and ICN have been calculated from microwave spectroscopic measurements in the three to five-mm wave-length region. The values of B_0 in Mc/sec., D_J in kc/sec., and D_{JK} in kc/sec. in that order are, for CH_3Cl^{35}: 13292.95, 26.4, and 189; for CH_3Cl^{37}: 13088.24, 27.0, and 184; for CH_3Br^{79}: 9568.188, 11.1, and 129.4; for CH_3Br^{81}: 9531.845, 10.7, and 129.0; for CH_3I: 7501.310, 7.95, and 99.4. Values of B_0 in Mc/sec. and of D_J in kc/sec. are, for $Br^{79}CN$: 4120.230 and 0.91; for $Br^{81}CN$: 4096.804 and 0.81; for ICN: 3225.578 and 0.88. Frequencies of observed lines are given in tables for calibration purposes.

I. INTRODUCTION

IN order to obtain additional information concerning the chemical bonds existing in the methyl halides and in the cyanogen halides, the rotational spectra of the above-named molecules have been measured in the three to five-mm wave-length region. A secondary purpose was to establish some standard frequencies for calibration purposes in this region. The results of this investigation have been combined with information gained from other J-transitions already reported[1] to determine the values of B, D_J, and D_{JK} in the expression for the frequency of a given J transition for a non-rigid symmetric-top molecule:[2]

$$\nu_r = 2B(J+1) - 4D_J(J+1)^3 - 2D_{JK}(J+1)K^2 \quad (1)$$

which, for a linear molecule, reduces to:

$$\nu_r = 2B(J+1) - 4D_J(J+1)^3. \quad (2)$$

II. APPARATUS

The absorption cell consisted of a section of coin silver K-band wave guide approximately seven feet long into which energy was introduced at either the second or third harmonic of the reflex klystron oscillator tube fundamental using multipliers of a type already described.[3] The single-crystal detection system was employed. Frequencies were measured at the oscillator tube fundamental by means of a secondary frequency

TABLE I. The hyperfine structure of the rotational transition $J=2\rightarrow3$ for CH_3Cl^{35}.

F Transition	ν(observed) (Mc/sec.)	ν(calculated)[a] (Mc/sec.)	Calculated relative intensity
		$K=0$	
7/2→9/2, 5/2→7/2	79755.68±0.16	79755.74	100*
3/2→5/2, 1/2→3/2	79751.02	79751.09	52**
7/2→7/2	79736.96	79736.96	17†
5/2→5/2	79764.56	79764.51	4
3/2→3/2	79769.94	79769.87	3
		$K=1$	
7/2→9/2	79755.68	79755.73	Included in * above
5/2→7/2, 3/2→5/2	79751.02	79751.04, 79750.90	Included in ** above
1/2→3/2	79755.68	79755.60	Included in * above
		$K=2$	
7/2→9/2	79755.68	79755.68	Included in * above
5/2→7/2	79736.96	79736.89	Included in † above
1/2→3/2	79768.98	79769.09	5
7/2→7/2	79755.68	79755.68	Included in * above
5/2→5/2	79736.96	79736.89	Included in † above

[a] Calculated using the constants given in Table III. Second-order effects are negligible here.

TABLE II. The hyperfine structure of the rotational transition $J=2\rightarrow3$ for CH_3Cl^{37}.

F Transition	ν(observed) (Mc/sec.)	ν(calculated)[a] (Mc/sec.)	Calculated relative intensity
		$K=0$	
7/2→9/2, 5/2→7/2	78527.10±0.16	78527.22	100*
3/2→5/2, 1/2→3/2	78523.32	78523.56	61**
7/2→7/2	78512.80	78512.46	4
		$K=1$	
7/2→9/2	78527.10	78527.00	Included in * above
5/2→7/2, 3/2→5/2	78523.32	78523.31, 78523.21	Included in ** above
1/2→3/2	78527.10	78526.90	Included in * above
		$K=2$	
7/2→9/2	78526.14	78526.32	22†
5/2→7/2	78511.68	78511.56	16††
3/2→5/2	78522.00	78522.10	11¶
7/2→7/2	78526.14	78526.32	Included in † above
5/2→5/2	78511.68	78511.56	Included in †† above
3/2→3/2	78522.00	78522.10	Included in ¶ above

[a] Calculated using the constants given in Table III. Second-order effects are negligible here.

* This work was supported by the Geophysical Research Directorate of the Air Force Cambridge Research Laboratories. It is published for technical information only and does not represent recommendations or conclusions of the sponsoring agency.

** Present address: Emory University, Atlanta, Georgia.
† Present address: The Citadel, Charleston, South Carolina.

[1] See individual tables for references.

[2] G. Herzberg, *Infra-Red and Raman Spectra of Polyatomic Molecules* (D. Van Nostrand Company, Inc., New York, 1945), p. 31. See also reference 7.

[3] Smith, Gordy, Simmons, and Smith, Phys. Rev. **75**, 260 (1949).

TABLE III. Frequencies of hypothetical unsplit rotational lines, ν_0, and resulting molecular constants for methyl chloride from the rotational transitions $J=0\rightarrow1$ and $J=2\rightarrow3$.

K	ν_0 (Mc/sec.)	B_0 (Mc/sec.)	D_J (kc/sec.)	D_{JK} (kc/sec.)	I_B (10^{-40} g cm^2)
		CH_3Cl^{35}			
	$J=0\rightarrow1$				
0	26585.77[a]				
	$J=2\rightarrow3$	13292.95±0.01	26.4±0.3	189±1	63.10_{00}[b]
0	79754.85				
1	79753.75				
2	79750.30				
		CH_3Cl^{37}			
	$J=0\rightarrow1$				
0	26176.37[a]				
	$J=2\rightarrow3$	13088.24±0.02	27.0±0.4	184±2	64.09_{61}[b]
0	78526.51				
1	78525.47				
2	78522.05				

[a] Gordy, Simmons, and Smith, Phys. Rev. **74**, 243 (1948).
[b] Using $h=6.62373\times10^{-27}$ erg sec. as given by J. W. M. DuMond and E. R. Cohen, Rev. Mod. Phys. **21**, 651 (1949).

TABLE IV. The hyperfine structure of the rotational transition $J=3\rightarrow4$ for CH_3Br.

F Transition	ν(observed) (Mc/sec.)	ν(calculated)[a] (Mc/sec.)	Calculated relative intensity
	CH_3Br^{79}		
	$K=0$		
9/2→11/2	76538.02±0.18	76538.31	67
7/2→9/2		76538.30	
5/2→7/2	76554.82	76554.96	100*
3/2→5/2		76555.03	
	$K=1$		
9/2→11/2	76532.88	76533.13	36
7/2→9/2	76547.24	76547.49	27
5/2→7/2	76554.82	76555.00	Included in * above
3/2→5/2	76540.20	76540.52	15
	$K=2$		
9/2→11/2	76517.36	76517.59	29
7/2→9/2	76575.22	76575.18	22
5/2→7/2	76554.82	76555.07	Included in * above
3/2→5/2	76496.60	76497.16	12
	$K=3$		
9/2→11/2	76491.36	76491.62	43
7/2→9/2	76621.78	76621.59	33
5/2→7/2	76554.82	76555.09	Included in * above
3/2→5/2	76425.18	76425.40	18
	CH_3Br^{81}		
	$K=0$		
9/2→11/2	76248.32	76248.39	67
7/2→9/2		76248.38	
5/2→7/2	76261.96	76262.30	100*[b]
3/2→5/2		76262.35	
	$K=1$		
9/2→11/2	76243.66	76243.89	36
7/2→9/2	76255.68	76255.90	27
5/2→7/2	76261.96	76262.16	Included in * above
3/2→5/2	76249.94	76250.08	15
	$K=2$		
9/2→11/2	76230.18	76230.40	29
7/2→9/2	76278.16	76278.52	22
5/2→7/2	76261.96	76261.71	Included in * above
3/2→5/2	76213.16	76213.36	12

TABLE IV.—*Continued.*

F Transition	ν(observed) (Mc/sec.)	ν(calculated)[a] (Mc/sec.)	Calculated relative intensity
		$K=3$	
9/2→11/2	76207.66	76207.88	43
3/2→5/2	76152.28	76152.54	18

[a] Calculated using the constants given in Table VI. Second-order effects are also included here.
[b] This value includes the intensity of the line for $F=5/2\rightarrow7/2$, $K=3$, since this line was not resolved at the pressures used.

TABLE V. They hyperfine structure of the rotational transition $J=4\rightarrow5$ for CH_3Br.

F Transition	ν(observed) (Mc/sec.)	ν(calculated)[a] (Mc/sec.)	Calculated relative intensity
		CH_3Br^{79}	
		$K=0$	
11/2→13/2	95673.51±0.27	95673.33	57
9/2→11/2		95673.32	
7/2→9/2	95683.62	95683.16	100*
5/2→7/2		95683.19	
		$K=1$	
11/2→13/2	95669.97	95669.71	30
9/2→11/2	95677.20	95676.90	25
7/2→9/2	95683.62	95683.26	Included in * above
5/2→7/2	95676.39	95676.04	16
		$K=2$	
11/2→13/2	95659.20	95658.87	26
9/2→11/2	95688.27	95687.65	21
7/2→9/2	95683.62	95683.55	Included in * above
5/2→7/2	95654.73	95654.58	14
		$K=3$	
11/2→13/2	95640.87	95640.80	40
9/2→11/2	95706.12	95705.65	33
7/2→9/2	95683.62	95683.98	Included in * above
5/2→7/2	95619.24	95618.95	21
		$K=4$	
11/2→13/2	95615.73	95615.48	11
		CH_3Br^{81}	
		$K=0$	
11/2→13/2	95310.78	95310.58	57
9/2→11/2		95310.58	
7/2→9/2	95319.12	95318.81	100**[b]
5/2→7/2		95318.83	
		$K=1$	
11/2→13/2	95307.48	95307.35	30
7/2→9/2	95319.12	95318.68	Included in ** above
		$K=2$	
11/2→13/2	95297.55	95297.68	26
9/2→11/2	95322.15	95321.73	21
5/2→7/2	95253.89	95294.12	14
		$K=3$	
11/2→13/2	95281.53	95281.54	40
9/2→11/2	95336.01	95335.72	33
5/2→7/2	95263.47	95263.29	21
		$K=4$	
11/2→13/2	95259.24	95258.92	11

[a] Calculated using the constants given in Table VI. Second-order effects are also included here.
[b] This value includes the intensities of the lines for $F=7/2\rightarrow9/2$, $K=2$, and $F=7/2\rightarrow9/2$, $K=3$, since these lines were not resolved at the pressures used.

TABLE VI. Frequencies of hypothetical unsplit rotational lines, ν_0, and resulting molecular constants for methyl bromide from the rotational transitions $J=1\rightarrow2$, $J=3\rightarrow4$ and $J=4\rightarrow5$.

K	ν_0 (Mc/sec.)	B_0 (Mc/sec.)	D_J (kc/sec.)	D_{JK} (kc/sec.)	I_B (10^{-40} g cm^2)
		CH_3Br^{79}			
	$J=1\rightarrow2$				
0	38272.40[a]				
1	38272.04[a]				
	$J=3\rightarrow4$				
0	76542.43				
1	76541.37				
2	76538.27	9568.188±.025	11.1±0.8	129.4±0.3	87.67_{68}[b]
3	76533.13				
	$J=4\rightarrow5$				
0	95676.65				
1	95675.36				
2	95671.48				
3	95664.89				
4	95655.88				
		CH_3Br^{81}			
	$J=1\rightarrow2$				
0	38126.97[a]				
1	38126.61[a]				
	$J=3\rightarrow4$				
0	76251.80				
1	76250.79				
2	76247.68	9531.845±.015	10.7±0.7	129.0±0.2	88.01_{08}[b]
3	76242.49				
	$J=4\rightarrow5$				
0	95313.35				
1	95312.10				
2	95307.96				
3	95301.64				
4	95292.78				

[a] See Table III, reference a.
[b] Using $h=6.62373\times10^{-27}$ erg sec., see Table III, reference b.

standard.[4] The absorption cell was maintained at dry ice temperature during measurements and gas pressures of about 10^{-3} mm Hg were used.

III. RESULTS

In order that some standard absorption lines for frequency comparison in the three- to five-mm wavelength region might be made available, the observed frequencies of the hyperfine structure lines for each of the J-transitions studied have been presented in Tables I, II, IV, V, VII, IX, and X. Frequencies falling within the range from 60,000 to 85,000 Mc/sec. were second harmonics of the klystron oscillator, those higher were the third harmonics with larger probable errors as given in the tables. No accurate measurement of relative intensities was attempted; only a general comparison of observed values with the calculated tabular values was made for line identification purposes.

Tables III, VI, VIII, and XI give the frequencies, ν_0, of the hypothetical unsplit absorption lines for the

[4] R. Unterberger and W. V. Smith, Rev. Sci. Inst. 19, 580 (1948).

TABLE VII. The hyperfine structure of the rotational transition $J=4\rightarrow5$ for CH_3I^{127}.

F Transition	ν(observed) (Mc/sec.)	ν(calculated)[a] (Mc/sec.)	Calculated relative intensity
		$K=0$	
13/2→15/2	75019.28±0.16	75019.35	78
11/2→13/2	75027.58	75027.47	63
9/2→11/2	75004.28	75004.11	50
7/2→9/2	74977.62	74977.65	69*
5/2→7/2	74967.66	74967.67	31
3/2→5/2	74986.14	74986.15	24
		$K=1$	
13/2→15/2	75026.20	75026.22	75
11/2→13/2	75016.20	75016.11	61
9/2→11/2	74993.28	74993.30	48
7/2→9/2	74976.22	74976.18	38
5/2→7/2	74977.62	74977.61	Included in * above
		$K=2$	
13/2→15/2	75046.48	75046.72	66
11/2→13/2	74982.18	74982.21	53
9/2→11/2	74960.76	74960.75	42
7/2→9/2	74971.76	74971.79	33
5/2→7/2	75007.62	75007.59	26
		$K=3$	
13/2→15/2	75081.02	75080.70	100
11/2→13/2	74926.04	74926.43	81
7/2→9/2	74964.36	74964.51	51
		$K=4$	
11/2→13/2	74849.92	74849.85	23
9/2→11/2	74829.54	74829.45	18

[a] Calculated using the constants given in Table VIII. Second-order effects are also included here.

respective molecules investigated. In every case except that of methyl chloride it was found that the second order nuclear quadrupole effects predicted by Bardeen and Townes[5] had to be taken into account in addition to first order nuclear quadrupole interactions before satisfactory agreement between observed and calculated line positions could be obtained. The resulting molecular B_0 and centrifugal distortion constant values

TABLE VIII. Frequencies of hypothetical unsplit rotational lines, ν_0, and resulting molecular constants for methyl iodide from the rotational transitions $J=1\rightarrow2$ and $J=4\rightarrow5$.

K	ν_0 (Mc/sec.)	B_0 (Mc/sec.)	D_J (kc/sec.)	D_{JK} (kc/sec.)	I_B (10^{-40} g cm^2)
	$J=1\rightarrow2$				
0	30004.98[a]				
1	30004.61[a]				
	$J=4\rightarrow5$	7501.310±0.007	7.95+0.09	99.4±0.5	111.8_{34}[b]
0	75009.15				
1	75008.15				
2	75005.09				
3	75000.10				
4	74993.30				

[a] See Table III, reference a.
[b] Using value of $h=6.62373\times10^{-27}$ erg sec., see Table III, reference b.

[5] J. Bardeen and C. H. Townes, Phys. Rev. 73, 627, 1204 (1948).

TABLE IX. The hyperfine structure of the rotational transition $J=8\rightarrow9$ for BrCN.

F Transition	ν(observed) (Mc/sec.)	ν(calculated)[a] (Mc/sec.)	Calculated relative intensity
	$Br^{79}CN$		
19/2→21/2	74162.76±0.18	74162.78	100
17/2→19/2			89
15/2→17/2	74159.48	74159.44	80
13/2→15/2			71
	$Br^{81}Cn$		
19/2→21/2	73741.20	73741.20	100
17/2→19/2			89
15/2→17/2	73738.42	73738.41	80
13/2→15/2			71

[a] Calculated using the constants given in Table XI. Second-order effects are also included here.

TABLE X. The hyperfine structure of the rotational transition $J=10\rightarrow11$ for ICN.

F Transition	ν(observed) (Mc/sec.)	ν(calculated)[a] (Mc/sec.)	Calculated relative intensity
25/2→27/2	70961.30±0.18	70961.27	100
23/2→25/2	70963.90	70963.71	91
21/2→23/2	70959.14	70959.22	83
19/2→21/2	—[b]	70952.99	76
17/2→19/2	70949.66	70949.79	69
15/2→17/2	—[b]	70953.54	63

[a] Calculated using the constants given in Table XI. Second-order effects are also included here.
[b] Observed but not measured since these lines were unresolved at the pressures used.

are shown in the same tables. In all the methyl halides the decrease in unsplit line frequency with increasing K values is quite marked for each J transition. It is interesting to note that even in the case of the $J=0\rightarrow1$ transition for methyl chloride the distortion effects are significant. Consequently, all values of B_0 are higher than those previously reported for the respective molecules. (See references accompanying the tables.) Somewhat lower values of I_B result from these, where I_B is the moment of inertia of the molecule about an axis through the center of mass perpendicular to the figure axis.

The values of line frequencies calculated using the constants for the respective molecules are given also in the tables alongside the observed frequencies and may be seen to agree rather well with these observed values.

IV. DISCUSSION

In Table XII are summarized the centrifugal distortion constants for the methyl halides. The bond-stretching and bond-bending force constants calculated by Linnett[6] for these molecules are listed there also for comparison purposes.

Since I_B for the methyl halides depends more heavily on $|\cos\angle XCH|$, where X represents the halogen, than on the sine of this angle, then the decreasing values

[6] J. W. Linnett, J. Chem. Phys. 8, 91 (1940).

TABLE XI. Frequencies of hypothetical unsplit rotational lines, ν_0, and resulting molecular constants for BrCN and ICN from the rotational transitions indicated below.

J Transition	ν_0 (Mc/sec.)	B_0 (Mc/sec.)	D_J (kc/sec.)	I_B (10^{-40} g cm^2)
	$Br^{79}CN$			
2→3	24721.14[a]	4120.230±0.018	0.91±0.09	203.6_{08}[c]
3→4	32961.79[b]			
8→9	74161.49			
	$Br^{81}CN$			
2→3	24580.56[a]	4096.804±0.018	0.81±0.09	204.7_{71}
3→4	32774.38[b]			
8→9	73740.12			
	ICN			
3→4	25804.22[a]	3225.578±0.018	0.88±0.09	260.9_{79}
4→5	32255.55[b]			
10→11	70958.06			

[a] Townes, Holden, and Merritt, Phys. Rev. 74, 1113 (1948).
[b] Smith, Ring, Smith, and Gordy, Phys. Rev. 74, 370 (1948).
[c] Using value of $h=6.62373\times10^{-27}$ erg sec., see Table III, reference b.

of D_J in the chloride, bromide, iodide series would indicate that $\angle XCH$ is decreasing sufficiently in the heavier compounds to offset the greater stretching of the C−X bond in these compounds which would be expected from the values of the C−X bond force constants.

The large shift in unsplit line frequencies, ν_0, with increasing K and the positive sign for D_{JK} would indicate a considerable lengthening of the C−H bond. This is especially true since both the effect of rotation about the figure axis and the probable increase in the ionic character of the C−X bond when it stretches would lead to a decrease in $\angle XCH$. Values of D_{JK} which decrease for the chloride, bromide, iodide sequence would follow from the sequence of C−H bond force constants in these molecules as well as from the decreasing values of the $\angle XCH$ bond-bending constants.

In the cases of BrCN and ICN the C≡N bond-stretching force constant should be the same in both molecules (about 17×10^5 dyne/cm) and we should then

TABLE XII. A tabulation of the centrifugal distortion constants for the methyl halides with values of corresponding bond-stretching and bond-bending force constants.

Molecule	D_J (kc/sec.)	D_{JK} (kc/sec.)	Force constants[a] C−H (10^5 dyne/cm)	C−X (10^5 dyne/cm)	X−C−H (10^{-11} dyne-cm/rad)	H−C−H (10^{-11} dyne-cm/rad)
CH_3Cl^{35}	26.4	189	4.90	3.35	0.701	0.523
CH_3Cl^{37}	27.0	184				
CH_3Br^{79}	11.1	129.4	4.95	2.83	0.632	0.516
CH_3Br^{81}	10.7	129.0				
CH_3I	7.95	99.4	5.00	2.32	0.550	0.516

[a] The values of force constants listed here are as given by Linnett (Ref. 6). Those calculated by B. L. Crawford, Jr., and S. R. Brinkley, Jr., J. Chem. Phys. 9, 69 (1941) with the assumption of a more general force field follow principally the same trend although they are somewhat different in magnitude.

expect the value of D_J to increase in going from BrCN to ICN due to the larger stretching of the C−X bond. The rather large limits of error prevent any definite conclusions here, although the value of D_J for ICN is larger than the average BrCN value.

It is interesting to compare the distortion constant values obtained here for the methyl halides with those calculated by Slawsky and Dennison.[7] Using dimensions and force constants determined principally from infra-red data, they obtained values of D_J which are roughly one-tenth of the values given here. Their computed values of D_{JK} have the correct order of magnitude, being 1.6 to 2.5 times the experimental values, but have the opposite algebraic sign. Frequencies of the unsplit lines for $K=0$ computed with their values of D_J but with the I_B evaluations reported here differ by about two or three megacycles from the observed frequencies. Within the limits of experimental error, however, the variation of the line frequency shift due to centrifugal distortion expressed as a function of the values of J and K appears to be correctly predicted by Eq. (1).

The authors wish to thank Dr. Walter Gordy for his continued interest in this investigation and Messrs. O. R. Gilliam and C. M. Johnson for assistance with the third-harmonic frequency measurements.

[7] Z. I. Slawsky and D. M. Dennison, J. Chem. Phys. 7, 509 (1939).

PHYSICAL REVIEW VOLUME 80, NUMBER 3 NOVEMBER 1, 1950

Pile Neutron Absorption Cross Sections

S. P. HARRIS, C. O. MUEHLHAUSE, S. RASMUSSEN, H. P. SCHROEDER, AND G. E. THOMAS
Argonne National Laboratory, Chicago, Illinois

(Received June 14, 1950)

Neutron absorption cross sections for over 50 elements have been measured in the neutron flux of the Argonne heavy water reactor. Measurements were made by observing the oscillating component of reactor power as a neutron absorber sample was oscillated in and out of the central flux of the pile. Calibration was effected with boron.

I. INTRODUCTION

IT was originally suggested by Fermi that neutron absorption cross sections for pile neutrons could be measured by inserting absorbers in the center of a pile in equilibrium and adjusting one of the control rods to compensate for the absorption. The compensating motion, Δl, would then be proportional to the absorption, $n_a\sigma_a$, and could be evaluated in terms of a standard such as boron. This method, termed the "danger coefficient method" (because the absorber was thought of as a poison to the reactor), was applied successfully at Argonne by Wattenberg in the measurement of about 20 elements.

A modification of the "danger" or static method was later suggested by Fermi and Wigner. This method was dynamic in character and consisted in oscillating an absorbing sample in and out of the reacting flux of a pile, while observing the oscillating component of pile power, Δp, and the mean pile power $\bar{p}(\Delta p \ll \bar{p})$. For a thin sample:

$$\Delta p \propto \bar{p} n_a \sigma_a,$$

where n_a and σ_a are the number of absorbing nuclei and the neutron absorption cross section, respectively.

The apparatus for performing these measurements was developed by a group under the direction of A. Langsdorf at the Argonne National Laboratory. Measurements were made later on 55 elements by the authors.

II. APPARATUS

The equipment will be described in a paper by Langsdorf and his collaborators in a future publication. Briefly it consists of:

(1) A vertical mechanical oscillator which periodically lowers a 75-cc "can" containing the absorbing material into the center of the reacting neutron flux for 10 sec. and then raises the sample out of the flux for 10 sec. The stroke is five feet in length. All parts that oscillate in the reactor flux are made of Dow-Metal FS-1 with the exception of the sample cans, bronze clamp, and graphite bearings.[1]

(2) A BF_3 ionization chamber to record both the total current, $i \propto \bar{p}$, and the oscillating current, $\Delta i \propto \Delta p$. This neutron chamber is placed in the thermal column of the reactor, which location is suitable for indicating the power level of the pile.

(3) A bridge circuit (20 sec. sensitivity) with ohmic

[1] Measurement of the neutron absorption cross section of Mg by an all-Al oscillator was shown by Langsdorf and his group to be about 0.07×10^{-24} cm². This approximate value was also confirmed by Wattenberg (Argonne, 1945) and by Goldhaber and Muehlhause (University of Illinois, 1942). Dow metal FS-1 which consists of ~95 percent Mg, five percent Al, and 0.15 percent Mn has therefore an effective neutron absorption cross section of about 0.1 barn and is three times less absorptive per unit volume than is Al.

balancing resistor, R, which measures directly[2] the ratio $\Delta i/i$.

III. ADJUSTMENTS AND FLUX CONDITIONS

The adjustment of the in-position of the sample was determined by finding the in-point from which graphite (an almost pure scatterer) could be oscillated yet produce no pile effect. This position, so determined, also nearly coincided with the maximum flux position as determined by the activation of a series of Au foils placed at equal intervals in the central vertical tube of the reactor. This latter point should be, and in fact was, slightly higher in the tube than the point of maximum reacting flux.

TABLE I. Neutron absorption cross sections.

Element	σ_{pile} (barns)	Comments	Chemical forms
B	710	standard	B, B_2O_3, H_3BO_3
Na	0.52		Na, NaF
Mg	0.06		Mg
Al	0.22		Al
Si	0.16		SiO_2
S	0.51		S, CS_2
Cl	31.5		C_2Cl_6
K	2.11		K, KF
Ca	0.43		CaF_2, $CaCO_3$
Sc	31.8	impure	Sc_2O_3
Ti	5.88		Ti
V	4.93		$V_2O_{3.72}$
Cr	3.05		Cr, Cr_2O_3
Mn	12.3		Mn
Fe	2.48		Fe, Fe_2O_3
Co	35.7		Co, CoO
Ni	4.37		Ni, NiO
Cu	3.71		Cu, CuO
Zn	1.09		Zn
Ga	3.10		Ga
Ge	2.64		GeO_2
As	5.46		As_2O_3
Se	12.2		Se
Br	8.83	thick	CBr_4
Sr	1.53		SrF_2
Zr	~0.4		ZrO_2
Cb	1.51		Cb, Cb_2O_5
Mo	3.04		Mo, MoO_3
Ru	6.30	~150 mg/cm²	Ru
Rh	172	~15 mg/cm²	Rh
Pd	10.3	thick	Pd
Ag	90	~5 mg/cm²	Ag
Sn	0.72		Sn
Sb	8.15	~400 mg/cm²	Sb, Sb_2O_3
Te	5.82		Te
I	9.23	~250 mg/cm²	I, CHI_3, PbI_2
Cs	35.8		CsF, Cs_2SO_4
Ba	1.35		BaF_2
La	9.01		La_2O_3
Ce	~0.65	small sample	Ce_2O_3
Nd	52	perhaps rare earth impurity	Nd_2O_3
Sm	~8200		Sm_2O_3
Gd	36,500		$Gd_2(SO_4)_3$
Hf	171	~20 mg/cm²	HfO_2
Ta	36	~130 mg/cm²	Ta, Ta_2O_5
W	24	~130 mg/cm²	W, WO_3
Re	120	~15 mg/cm²	Re
Ir	~470	~10 mg/cm²	Ir
Pt	13.5		Pt
Au	~157	~3.5 mg/cm²	Au
Hg	~380		HgO, $Hg(CN)_2$
Tl	3.65		Tl
Pb	0.16		Pb
Bi	0.038		Bi

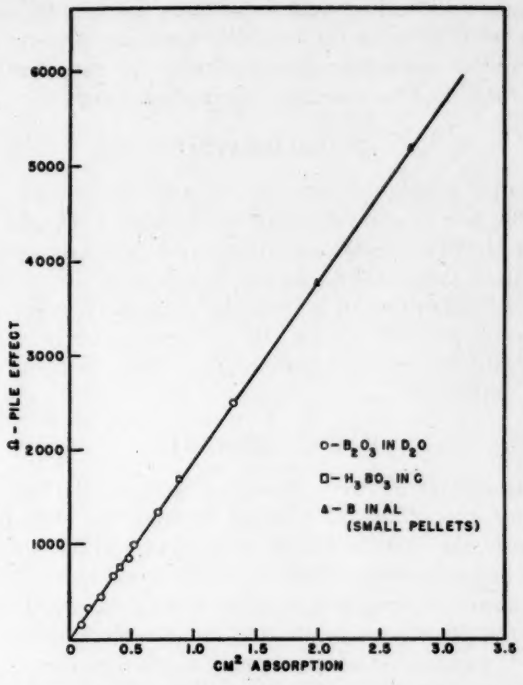

FIG. 1. Pile neutron absorption in boron *vs.* the pile effect (Ω).

An analysis of the pile flux was made by measuring the cadmium ratio for thin Au (0.15 mg/cm²) and assuming the Au resonance capture integral[3] (in excess of $1/v$ absorption) to be 1300 b. A value[4] of 93 b was taken for the Au thermal absorption cross section. Since boron was used to calibrate the pile effect, the measured pile cross section, σ_{pile}, can be written as

$$\sigma_{pile}=\sigma_{th}+k\Sigma_a,$$

where Σ_a is the resonance absorption integral for other than 1/v absorption. The 1/v resonance absorption was shown to be $\sim 0.45\sigma_{th}$ by several methods. Therefore:

$$k=\frac{\sigma_{th\text{-}Au}}{(\text{Cd ratio}-1)_{Au}(0.45\sigma_{th\text{-}Au}+\Sigma_{a\text{-}Au})}.$$

For a Cd-ratio of Au equal to 2.25, k was evaluated as 0.054. The pile absorption cross section is therefore:

$$\sigma_{pile}=\sigma_{th}+0.054\Sigma_a.$$

It should be understood that in the above Σ_a is the "effective" resonance absorption integral not including

[2] R is measured in ohms (Ω) and is adjusted to buck the oscillating component of current, Δi. This is done in such a way that $R\propto|\Delta i|/i$. The pile absorption effect is thereby translated into an "Ω-effect." Since the absorption is proportional to $n_a\sigma_a$ (Section I), then $\Omega\propto n_a\sigma_a$.

[3] M. Goldhaber, University of Illinois (Breit-Wigner fit to Columbia data).

[4] A. Wattenberg, Argonne National Laboratory (mechanical velocity selector).

1/v absorption. In a number of cases the samples used were so thick that the effective resonance absorption integral of the self-protected sample was considerably less than the true resonance absorption integral.

IV. CALIBRATION

Boron standards were run in various densities as H_3BO_3 fine mixture in graphite, B_2O_3 in D_2O, and as B in Al. All methods yielded the same calibration curve linear to about 6000Ω. In Fig. 1 is plotted the Ω-effect *vs.* cm^2 absorption of boron. The thermal cross section of boron was taken to be 710 b. The slope of the curve is $1890\Omega/cm^2$ which value was used throughout in the calculation of σ_{pile}.

V. MEASUREMENTS

Measurements were made by first oscillating the empty sample can plus empty powder can or bottle. That is, the blank or background effect for each sample was first determined. This was run several times. Next the absorbing sample with its container was oscillated, and the difference between the first and second measurements yielded the effect due only to the absorber.

To insure complete linearity all pile effects were kept at less than 3500Ω. The Dow metal empty sample can and moving hangar rods gave a reading of 730Ω. This was the least value to be subtracted from all others. For most samples, the net effect was determined by numbers of the following approximate magnitudes:

$$\text{net } \Omega = 3000 \pm 10 - 1000 \pm 10 = 2000 \pm 15.$$

This error is <one percent, and a given sample during a typical two-day run generally repeated to about two percent. For different samples from one run to any other (i.e. at least one month apart) measurements would repeat to less than five percent.

Each measurement took approximately 20 minutes since this much time was necessary for the pile to reach a new equilibrium. Though the readings were independent of pile power, control rod adjustments were made for each reading to bring the reactor back to about the same power level (~0.6 kw). Other factors that might have second- or third-order effects were also kept constant. Some of these were heavy water level in the reactor tank, and the positions of the shim rods.

VI. PREPARATION OF SAMPLES

The samples were the purest obtainable, being either reagent grade compounds or substances specially purified by S. Rasmussen. All materials were analyzed spectroscopically for traces of contaminants with special emphasis on impurities having a large neutron absorption cross section.

Most samples were of elemental, oxide, fluoride, carbonate, or sulfate form. They were run unmixed, mixed with graphite, or dissolved in D_2O. This latter substance had a negative pile effect owing to its high slowing-down power and low thermal absorption. Each element was run in the form of at least two independent samples, and usually in more than one chemical form. The average number of runs per cross section was four. This does not include blank or calibration runs.

VII. RESULTS

Table I lists the average values obtained for σ_{pile}. The internal consistency, except for strong resonance absorbers like Ta and W, was better than to five percent. Materials of this latter type, however, defy accurate measurement since in order to have the contribution to σ_{pile} from Σ_a linear with sample thickness, the amount of the sample had to be too small to measure properly. For this reason many of the pile absorption cross sections given in Table I are dependent on their exact thicknesses. Furthermore, in these cases, it is not possible to resolve σ_{pile} into σ_{th} and Σ_a unless σ_{th} is known. That is, Σ_a is in general only an effective value dependent on sample thickness in a non-linear way. Those substances having no comment on thickness may be assumed to have a pile cross section given by $\sigma_{pile} = \sigma_{th} + 0.054\Sigma_a$, where Σ_a is the true resonance absorption integral. A list of Σ_a values is given by Harris, Muehlhause, and Thomas.[5] These can be used to determine σ_{th} from σ_{pile}.

[5] Harris, Muehlhause, and Thomas, Phys. Rev. **79**, 11 (1950).

Protons and Deuterons Ejected from Nuclei by 90-Mev Neutrons*

JAMES HADLEY AND HERBERT YORK
Radiation Laboratory, Department of Physics, University of California, Berkeley, California
(Received February 16, 1950)

The angular and energy distributions of the fast charged particles emerging from nuclei bombarded by 90-Mev neutrons have been investigated. The results indicate that the nature of the collision process is determined predominantly by interactions of the bombarding particle with single nucleons rather than with the struck nucleus as a whole: angular distributions are found to be peaked in the forward direction for all emergent particles, the degree of peaking increasing with energy. Deuterons are found to be more concentrated in the forward direction than are protons. In the case of carbon, particles traveling in the forward direction with energies greater than 20 Mev consist of 60 percent protons, 36 percent deuterons, and about 4 percent tritons.

I. INTRODUCTION

THE inelastic processes which take place when nuclei are bombarded by nucleons with energies up to a few tens of Mev, or by alpha-particles with energies up to 50 Mev, are well described by Bohr's theory of the compound nucleus,[1] involving excitation of the whole nucleus with subsequent photon or particle emission. The energy of the incident particle is at first distributed among all of the constituent particles of the nucleus; a time long with respect to transit times of nucleons within the nucleus elapses before a sufficient amount of this energy chances to be concentrated in one nucleon to enable it to escape. Consequently the anisotropy contributed by the directed motion of the incident particle is almost entirely lost by the time of emission, and the emitted particle may take any direction with equal probability.

Since a basic assumption of this theory is that the mean free path for nucleons in nuclear matter is small compared with the dimensions of the nucleus, it may be expected to become less applicable with increase in energy of the bombarding particle and resulting decrease in nucleon-nucleon cross sections.

The total 90-Mev cross section measurements of Cook *et al.*[2] and the total and inelastic cross section measurements of DeJuren and Knable[3] and of Bratenahl *et al.*[4] indicate that loss of validity of the Bohr theory may be expected at that energy. Those measurements show a considerable transparency for 90-Mev neutrons, particularly in the case of light nuclei, demonstrating that the mean free path for these neutrons in nuclear matter is no greater than the order of size of the nuclear diameter. Fernbach, Serber, and Taylor[5] have calculated from data of this type that the mean free path is 4.5×10^{-13} cm, and a value close to this was previously estimated by Goldberger.[6] The mean free path is the same in all nuclei because of the constant density of nuclear matter.

Qualitatively then, the sequence of events in an inelastic collision at these high energies would be expected to take the following course (similar analyses pertaining to high energy cosmic-ray stars have been given by Heisenberg[7] and by Bagge[8]). The impinging neutron strikes a nucleon in the nucleus, imparting to it some of its energy; the struck nucleon is most likely to be a proton because the $n-p$ cross section is probably several times larger than the $n-n$ cross section.[9]

There are at this point two fast nucleons moving in the nucleus. They may, because of their high energy, either collide with additional particles or escape from the nucleus without further interaction. Thus the immediate emission of one or more fast particles may occur, followed by the formation of a relatively long-lived compound nucleus of the type described by Bohr. The fast secondaries may be charged or uncharged without prejudice, because of the relative smallness of the Coulomb barrier. Furthermore, the direction of emission of the secondaries should be correlated with that of the impinging neutron in roughly the same way as in $n-p$ scattering, where particles of high energies emerge in the forward direction and those of low energies emerge at wide angles.

Detailed quantitative predictions along this line have been given in Goldberger's paper in which he has taken into account such factors as the internal motion of the nucleons in the nucleus and the effect of the exclusion principle in a nuclear system considered as a degenerate Fermi gas.

The object of the present work was to make an experimental investigation of the high energy charged secondaries. The nuclei investigated were carbon, copper and lead. The observed phenomena do not closely agree with Goldberger's analysis, but do follow the general features outlined above except for one important

* This work was performed under the auspices of the AEC.

[1] N. Bohr, Nature **137**, 344 (1936).
[2] Cook, McMillan, Peterson, and Sewell, Phys. Rev. **72**, 1264 (1947).
[3] J. DeJuren and N. Knable, Phys. Rev. **77**, 606 (1950).
[4] Bratenahl, Fernbach, Hildebrand, Leith, and Moyer, Phys. Rev. **77**, 597 (1950).
[5] Fernbach, Serber, and Taylor, Phys. Rev. **75**, 1352 (1949).
[6] M. L. Goldberger, Phys. Rev. **74**, 1269 (1948).
[7] W. Heisenberg, Leipziger Berichte **89**, 369 (1937).
[8] E. Bagge, Ann. d. Physik **37**, 535 (1941).
[9] This fact is based primarily on statistical considerations; *i.e.*, $n-p$ scattering can take place in both singlet and triplet states for all values of l; $p-p$ scattering only in singlet states for even values of l. See for example reference 6.

difference. This difference lies in the comparatively large observed yields of secondary deuterons and tritons, which had not been predicted. Observations of the latter particles were made simultaneously and reported by Bradner[10] (photographic plates), Brueckner and Powell[11] (cloud chamber), and one of the authors.[12] High energy deuterons have also been observed among the fragments from cosmic-ray stars.[13]

II. GENERAL EXPERIMENTAL METHOD

1. Requirements

In this experiment we are concerned with measuring the angular and energy distributions of a mixture of several types of particles all of which have energies ranging from about 20 Mev to 100 Mev. The procedure

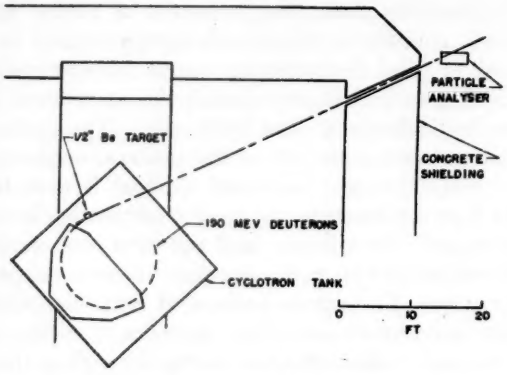

FIG. 1. General arrangement of apparatus.

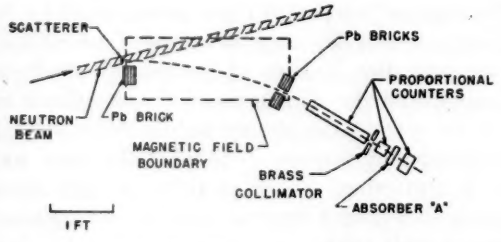

FIG. 2. Schematic diagram of particle analyzing system.

used is to measure the energy spectra at each of a series of angles.

For a known type of particle (i.e., proton, deuteron, or triton in the present case) the energy can be determined by a measurement of its $H\rho$, range, or specific ionization; conversely, for a particle of known energy the type can be determined by any one of these three measurements. In the present case it is necessary to measure simultaneously any two of the above quantities in order to determine both the type and energy of an observed particle.

[10] H. Bradner, Phys. Rev. **75**, 1467 (1949).
[11] K. Brueckner and W. Powell, Phys. Rev. **75**, 1274 (1949).
[12] H. York, Phys. Rev. **75**, 1467 (1949).
[13] Morand, Cüer, and Moucharafyeh, Comptes Rendus **226**, 1008 (1948); C. F. Powell and L. Leprince-Ringuet, Cosmic Ray Conference, Bristol, (1948).

2. Method Used

The measurements to be described here were made with $H\rho$-specific ionization combination, which makes possible the highest degree of resolution between types of particle. The $H\rho$ of the observed particles was fixed by requiring that they follow a fixed orbit in a magnetic field. The particles were then sorted according to specific ionization by passing them through a proportional counter connected to a pulse height analyzer. Protons, deuterons and tritons could be distinguished as groups of counts registered at three different levels in the pulse height analyzer. As an extra check on the results simultaneous range measurements were made in a few cases.

3. Arrangement of Components

Figures 1 and 2 show schematically the experimental arrangement used. The various components will be discussed in detail in Section III.

Neutrons of 90-Mev energy are produced by the stripping process[14] when 190-Mev deuterons strike a $\frac{1}{2}$ inch beryllium target in the 184-inch synchrocyclotron. These neutrons are collimated by a steel tube passing through the concrete shielding which surrounds the cyclotron. A neutron beam of rectangular cross section, 1 inch and $1\frac{1}{2}$ inches on the sides, emerges from this tube, and passes between the poles of the particle analyzing magnet, placed about 6 feet from the exit end of the collimator. A scatterer is placed in the beam where it enters the magnet, and a slit defined by lead bricks is placed at the other end of the magnet. A counter telescope consisting of three proportional counters is placed as shown, about 20 inches beyond the slit. Thus the charged secondaries from the scatterer travel along a circular path between the target and the slit, and along a straight path from the slit through the counters. The radius of curvature of the circular orbit is measured directly, and checked by range measurements to be described later.

III. APPARATUS

1. Counter System

The first of the three counters in the telescope is used to determine the specific ionization of the particles; the other two, which are placed in electrical coincidence with the first, are used to eliminate the large number of unwanted pulses produced in the first tube by particles entering from random directions. The ionization produced in the first tube is measured by means of a ten-channel pulse height analyzer. Absorbers can be placed in position A (Fig. 2), permitting a range measurement which can be used as an additional check on the nature of the radiation detected.

In the energy region of interest here the specific ionization is quite small. For this reason the first tube

[14] R. Serber, Phys. Rev. **72**, 1007 (1947).

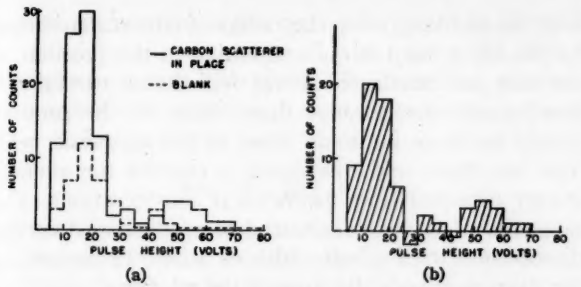

FIG. 3. Typical pulse-height histograms. (a) Counts from carbon scatterer and from blank; (b) Carbon-blank difference.

was made rather long (10 inches). This design also aids in reducing the importance of end effects in producing non-uniformity of pulse heights. The diameter of the first and second tubes is two inches, and that of the third tube about 4 inches. This increase in diameter was used in order to diminish loss of particles from scattering in the absorber sometimes placed at A, between the second and third tubes. The gas in the counters consists of 97 percent argon and 3 percent carbon dioxide, at a total pressure of about 1.1 atmospheres.

Various investigations of the operating characteristics of the first counter were made by placing a polonium alpha-gun inside in such a way as to emit alpha-particles either along a line parallel to the collecting wire or perpendicular to it. The gas amplification and the rate of change of gas amplification with collecting voltage (namely by a factor of two per hundred volts) were found to agree satisfactorily with results given by Diven and Rossi.[15] The pulse-height distribution produced by the alpha-particles consisted of a peak with a half-width of about 6 percent of the average pulse height, plus a low pulse height tail. The tail is presumably due to alphas which hit the walls of the counter before stopping, or which have suffered scattering collisions in the gun.

2. Magnet

The dimensions of the region of effective field in the magnet are 12 inches by 30 inches by $1\frac{3}{4}$ inches. The field can be adjusted to any value up to 15,000 gauss, and can be held constant to about $\frac{1}{2}$ of one percent, which corresponds to an energy variation of one percent.

3. Scatterers and Slits

The scatterers are carbon, copper and lead rectangles three inches long and one-half inch wide. They are placed in the beam with the long dimension vertical, and with the three by one-half inch face normal to the direction of emission of the particles being studied. The scatterer thus subtends the entire beam vertically, but only a small portion of it horizontally.

The thickness of the scatterers in the direction of the emitted particles under study is determined by a compromise between maximum secondary particle yield and minimum energy loss in the scatterer. The value chosen was $\frac{1}{8}$ inch for all three elements.

The first slit (Fig. 2) is formed by two lead bricks $\frac{1}{2}$ inch apart in the magnet gap near one edge. A second slit, about the same width, consists of a pair of brass plates placed between two of the proportional counters.

4. Electronics

The electronic equipment consists of two parts: a set of preamplifiers, amplifiers, and coincidence gate forming units built under the direction of H. Farnsworth, and a pulse-height analyzing system designed by Dexter and Sands[16] at the Los Alamos Scientific Laboratory, and built, with some modifications, by W. Goldsworthy and C. Wiegand at the Radiation Laboratory.

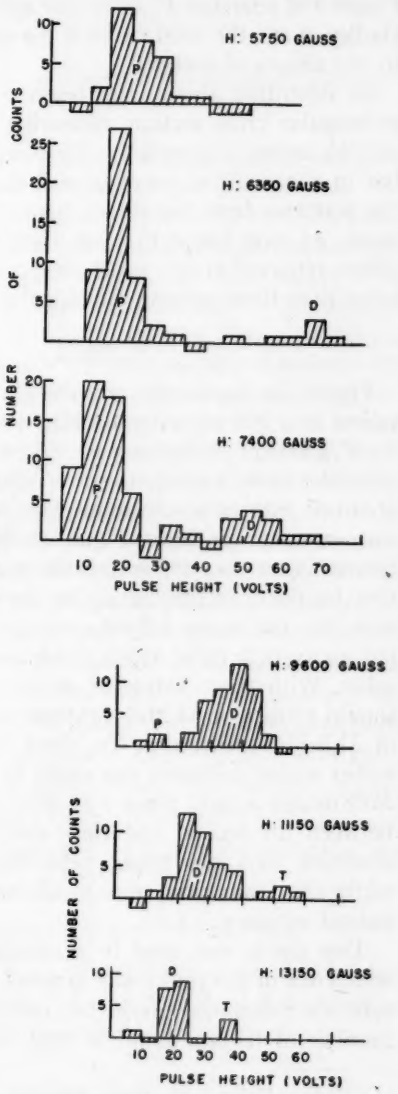

FIG. 4. Set of pulse height histograms for various magnetic fields showing proton (P), deuteron (D), and triton (T) peaks.

[15] B. C. Diven and B. Rossi, LADC-148, Los Alamos, (1944), (unpublished).

[16] E. Dexter and M. Sands, LADC 414, Los Alamos, (unpublished).

5. Monitor

The monitor consists of a boron trifluoride filled proportional counter which is inserted in the concrete cyclotron shielding a few inches from the high energy neutron collimating hole. High energy neutrons striking the steel collimator are inelastically scattered and in addition produce a number of secondary neutrons. Many of each enter the concrete, are moderated, and produce counts in the slow neutron sensitive monitor.

IV. NEUTRON BEAM

The neutron beam, produced and collimated as described in Section II, has a considerable energy spread. The spectrum as measured experimentally by Hadley *et al.*[17] and Brueckner *et al.*[18] in connection with $n-p$ scattering experiments show a peak with a maximum at about 90 Mev, and a half-width of 25 to 30 Mev. Figure 3 of reference 17 shows the spectrum as given by Hadley *et al.*; the solid curve is the spectrum predicted by the theory of Serber.[14]

As described above, the beam is collimated to a rectangular cross section measuring 1 inch vertically and $1\frac{1}{2}$ inches horizontally. By placing a long copper bar in the neutron beam in such a way as to shield the scatterer from the direct beam of collimated neutrons, we have found that less than one percent of the effects reported in this paper are produced by neutrons other than those coming through the collimating hole.

V. DATA

Figure 3a shows the pulse-height distribution obtained in a 300 second run using a scattering angle of $\theta=0°$, a field of 7400 gauss, $\rho=60$ inches, and the carbon scatterer (solid curve), together with the distribution obtained with no scatterer in place (dashed curve), for the same monitor count. Figure 3b shows the difference between these two and is thus the pulse-height distribution for particles originating in the carbon. It can be seen that the pulses fall into two groups, one of which has an average pulse height three times as large as the other. With these values of H and ρ the lower peak should consist of 63-Mev protons and the upper peak of 31.5-Mev deuterons. To check this, a carbon absorber whose thickness was equal to the range of a 45-Mev deuteron (and hence a 34-Mev proton) was placed between the second and third counters. It was then observed that the upper peak disappeared entirely while the lower peak was unaffected within the statistical accuracy.

This check was used in a number of instances in which one of the peaks was so small that its origin was somewhat doubtful, as in the case of the very small number of tritons found at high values of magnetic field. In addition, since the radius of curvature defined by the slit system is quite sensitive to the position of the slits and scatterer, it was felt that a careful determination of the range distribution of the protons should be made for some value of the magnetic field. This was done, and was found to confirm the average energy expected from geometrical considerations. The range distribution corresponded to a bell-shaped energy distribution with a half-width of about 13 percent of the average energy. Because of the relation

$$\Delta E/E=2\Delta\rho/\rho,$$

this energy resolution of 13 percent holds for all particles.

Figure 4 shows several histograms of the type presented in Fig. 3, taken at 0° scattering angle for a series of different values of magnetic field. The first graph shows the distribution obtained using a field of 5750 gauss. The duration of the run was 300 seconds, as in all the succeeding cases, for both the "scatterer in" count, and the background count. The monitor during this time recorded 86×64 slow neutron counts. At this value of magnetic field only one group of particles is seen, corresponding to 38-Mev protons. The 19-Mev deuterons which would have the same $H\rho$ are not able to penetrate all of the absorbing material along their potential path, such as the air and the counter windows. The succeeding graphs show the distributions obtained at the indicated values of H. The graphs are arranged in order of increasing H and therefore increasing energy of the particles. The proton peak can be seen moving steadily to lower values of pulse height since the specific ionization decreases with increasing energy. The first deuteron peak appears at 6350 gauss and corresponds to a deuteron energy of 23 Mev. At very high magnetic fields the protons are seen to disappear, and a new small peak to the right of the deuterons comes into existence. From its position, and from absorption measurements, this peak is ascribed to tritons.

Such histograms were obtained for 14 values of H, during each of three runs. Similar sets of data were obtained at 12°, 25°, and 45°.

VI. REDUCTION OF DATA AND DETERMINATION OF ABSOLUTE CROSS SECTIONS

1. Definition of Terms

The ultimate goal of this experiment is to determine the differential cross sections for the production of secondary charged particles of energy E at various angles θ. These cross sections will be denoted as $d\sigma_p(\theta, E)/d\Omega dE$ (abbreviated as $d\sigma_p$) where the subscript p stands for protons, and d and t for deuterons and tritons respectively. Because of the thickness of the targets and the finite acceptance interval of the slit system, the cross sections are not measured at single energies; instead their average values between two energy limits E_1 and E_2 are found. The above symbol will be understood as referring to such an average value.

[17] Hadley, Kelly, Leith, Segrè, Wiegand, and York, Phys. Rev. 75, 351 (1949).
[18] Brueckner, Hartsough, Hayward, and Powell, Phys. Rev. 75, 555 (1949).

Let us characterize the mean energy of the particles accepted by the magnet as E_m, and the width of the energy acceptance interval as ΔE. Then for a scatterer of infinitesimal thickness, E_1 and E_2 are $E_m-\frac{1}{2}\Delta E$ and $E_m+\frac{1}{2}\Delta E$ respectively, and

$$d\sigma_p=N_p/n_cN_n\Delta\Omega\Delta E,$$

where N_p=total proton count, N_n=total number of incident neutrons, n_c=carbon atoms/cm² in the target, and $\Delta\Omega$=solid angle presented to scatterer by slit system. Since, $\Delta E/E_m=2\Delta\rho/\rho$, and $\Delta\rho/\rho$ is a constant, $d\sigma_p$ may also be written $d\sigma_p=k(N_p/ME_m)$, where M=monitor count. The constant k contains several factors which are either difficult to determine absolutely or not well defined. It is therefore evaluated indirectly by integrating numerically, adding the various relative $d\sigma$'s involved, and setting this sum equal to the total cross section for these processes, which is in turn measured absolutely by a method to be described below.

In the case of a thick target both ΔE and the value of E_2 must be modified, because of energy loss suffered by particles in passing from their point of origin in the target to the face of the target. The energy interval E_2-E_1, over which the average value of $d\sigma$ is measured, becomes greater than the interval determined by the slit system alone. Further, ΔE, the energy interval at the point of origin corresponding to the energy interval of emergent particles which will be accepted by the slit system, depends upon the depth within the scatterer at which the particles originate, and must thus be averaged over the thickness of the scatterer. The calculation of these effects by means of range-energy curves is straightforward but tedious. The results have been used in preparation of the data.

2. Absolute Cross Section

The absolute cross sections for producing all secondary particles at a given angle θ were measured using an experimental arrangement identical to that used in the 90-Mev $n-p$ scattering experiments of Hadley *et al.*[17] The arrangement is given in Fig. 5. The location of the apparatus with respect to the cyclotron and collimating system was the same as in the part of the experiment done with the magnet.

The monitor used was a bismuth fission chamber, which is sensitive only to high energy neutrons.

The scatterers were 1″×2″ pieces of carbon (480 mg/cm²), copper (713 mg/cm²), lead (910 mg/cm²), and polyethylene (C_nH_{2n}) (420 mg/cm²). These thicknesses were chosen so that a high energy particle would lose the same amount of energy in passing through each target.

The polyethylene and carbon scatterers were bombarded first, with an absorber placed between the scatterers and counters such that a proton of energy 66 ($\cos^2\theta$) Mev originating at the center of the scatterer would just reach the end of its range upon entering the last counter. The difference between polyethylene counts per monitor count and carbon counts per monitor count is taken, giving the number of protons originating in $n-p$ collisions per monitor count. Use of the absorber mentioned above ensures that no protons recoiling from collisions with neutrons of energy less than 66 Mev will be counted. This is the same lower energy limit as that used in the 90-Mev $n-p$ scattering experiments, and we have, consequently, using the value of $\sigma_{n-p}(\theta)$ measured in that experiment, a direct proportion between number of scattered particles per

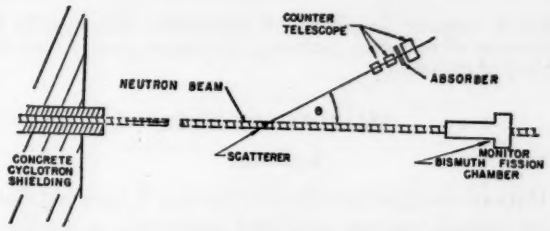

FIG. 5. Arrangement of apparatus for determining absolute cross sections.

bombarded nucleus per monitor count and the differential cross section for producing those particles.

If we are to count particles produced by neutrons of energy less than 66 Mev, the constant of proportionality must contain the factor N'/N, the ratio of the total number of effective neutrons in the beam to the number of neutrons of energy greater than 66 Mev. The carbon, copper, and lead scatterers are bombarded without the use of an absorber. Their thicknesses are such that the energies of particles originating at the scatterer center and just able to penetrate the last counter will be 20 Mev for protons, 27 Mev for deuterons, and 33 Mev for tritons. Because of the highly endothermic nature of the reactions involved, and because the cross sections for reactions of this kind typically are quite low at energies immediately above the threshold values, we can assume the lower energy limit of neutrons effective in producing observed particles to be not lower than about 50 Mev. Thus the factor N'/N above will be, at the greatest, equal to the ratio of number of neutrons of $E>50$ Mev to number of neutrons of $E>66$ Mev, or about 1.1. It may very probably be practically unity, and is taken so in the calculations of our results.

The quantities measured by this procedure are of the form

$$\sum(\theta)=[\sigma_{p>20}(\theta)+\sigma_{d>27}(\theta)+\sigma_{t>33}(\theta)],$$

where $\sigma_{p>20}(\theta)$ is the differential cross section for the production of protons of energy greater than 20 Mev at an angle θ to the direction of the incident neutrons, and so on.

Figure 6 is a plot of the results obtained. It gives the values of $\sum_c(\theta)$, $\sum_{cu}(\theta)$, and $\sum_{pb}(\theta)$ for angles ranging from 6° to 135°.

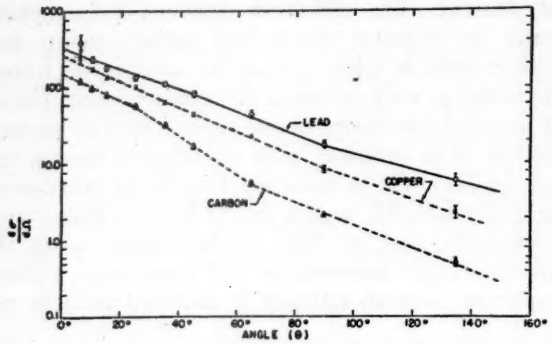

FIG. 6. Angular dependence of differential cross sections for production of secondary particles with ranges greater than 460 mg/cm² of carbon.

VII. FINAL RESULTS

1. Form

Data of the type described in Section V were obtained using carbon, copper, and lead scatterers, at angles of 0°, 12°, 25°, and 45° to the neutron beam. These data were analyzed using the methods described in Section VI to find the relative differential cross sections for each type of particle as a function of energy at each angle. A comparison with the values of $\sum(\theta)$ found by the procedure described in that section then provided absolute values for these cross sections. The final results are presented in graphical form in Figs. 7, 8, and 9.

The triton cross sections and some of the deuteron cross sections found are not plotted individually, but their average values over wide energy intervals are shown. The reason for this is that in each case the range of energies to which $d\sigma$ applies is so large, and so overlaps the neighboring values, that no spectral details could be seen.

Only in the case of the 0° carbon observations were any counts obtained which could with any real certainty be attributed to tritons. In that case they contributed 4 percent of the total cross section. Their contribution in all other cases is probably less than one percent.

2. Discussion of Error

The probable errors include only the expected statistical fluctuations in the relative values of the cross sections, and do not include the additional errors which can arise in the determination of the absolute scale. This latter error is probably of the order ±25 percent, and includes, besides the usual statistical factors, which are, in fact, quite small, two other factors. These are the uncertainty of the absolute value of the differential $n-p$ cross section involved in the calculations of the absolute cross sections, and the uncertainty involved in the numerical integration of the plots of the relative differential cross sections.

The case of the data at 0° deserves special attention in regard to these errors, for at that angle the absolute cross section for producing the secondaries was not measured at all. It can be seen in Fig. 6 that the cross sections at those points at which they were measured (6°, 10°, 25°, etc.) fall quite well on an exponential curve. This curve was extrapolated to 0°, and the extrapolated value was used in normalizing the 0° relative cross sections. This extrapolation is probably valid, since, as will be seen later, theoretical considerations indicate that there should be no marked singularities in the forward direction.

3. Total Cross Sections

In order to obtain total cross sections for the production of protons and deuterons having ranges in carbon

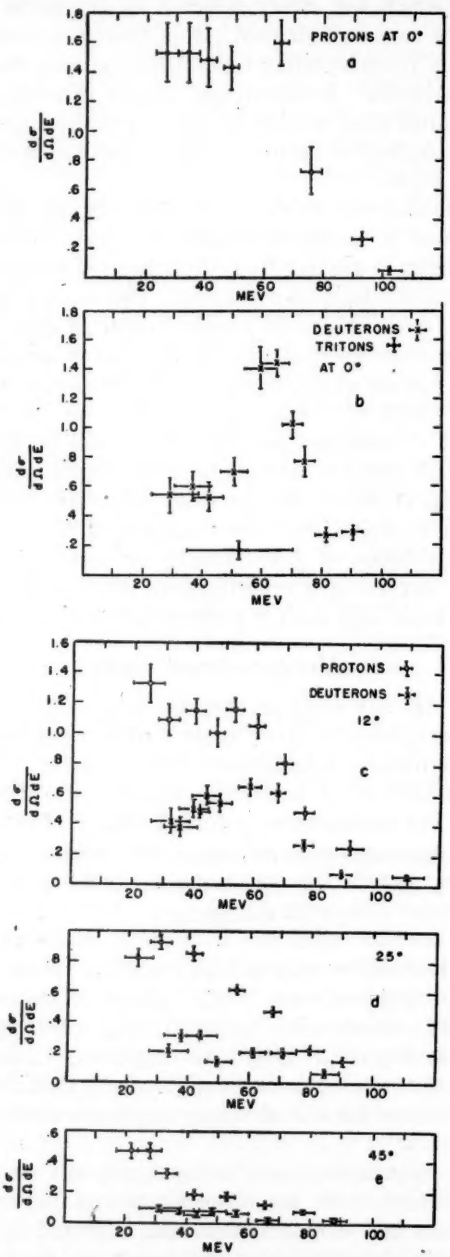

FIG. 7. Energy spectra of secondary particles from carbon $d\sigma/(d\Omega dE)$ in millibarns/steradian·Mev.

of 460 mg/cm² or more, it is necessary to make two assumptions about the values of the differential cross sections at angles other than the four at which they were measured.

In the first place, we have assumed that plots of differential cross section *vs.* angle would take the form of smooth curves passing through the measured points. Secondly, we have assumed that the cross sections for proton and for deuteron production are in the same ratio at angles greater than 45° as at the measured angles from 0° to 45°. The effect of the latter assumption on the final results is thought to be small, as the total cross sections are composed mostly of contributions from angles smaller than 45°; this can be seen by integration of the curves of Fig. 6, yielding the following values for the fraction of emitted particles falling in the range 0° to 45°:

Carbon	0.75
Copper	0.58
Lead	0.55.

By numerical integration of the quantities $d\sigma(E,\theta)/dEd\Omega$ over energy, we obtain the differential cross section

$$\left[\frac{d\sigma_p(\theta)}{d\Omega}\right]_{E>20\text{ Mev}}=\int_{E=20}^{\infty}\frac{d\sigma_p(E,\theta)}{d\Omega dE}dE$$

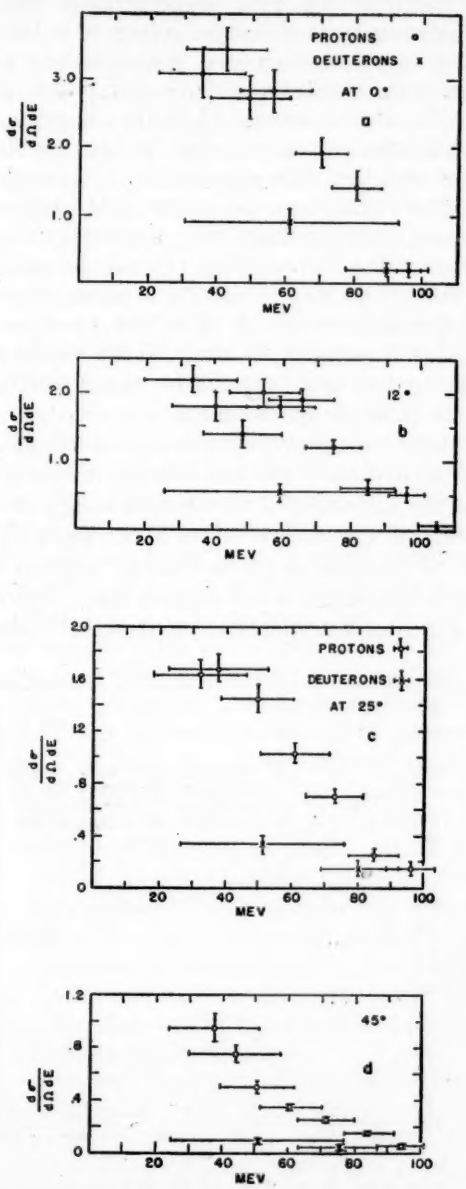

FIG. 8. Energy spectra of secondary particles from copper-$d\sigma/(d\Omega dE)$ in millibarns/steradian·Mev.

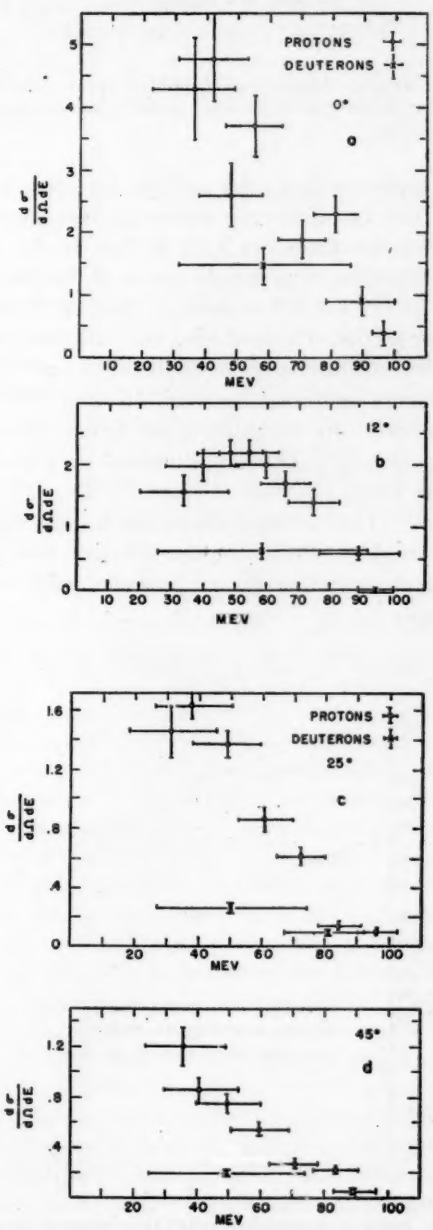

FIG. 9. Energy spectra of secondary particles from lead-$d\sigma/(d\Omega dE)$ in millibarns/steradian·Mev.

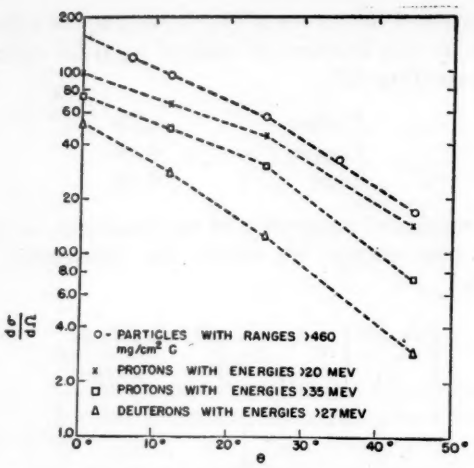

FIG. 10. Angular dependence of 90-Mev neutron-carbon cross sections for production of charged secondaries. $d\sigma/d\Omega$ in millibarns/steradian.

and the corresponding cross sections for protons above 35 Mev and for deuterons above 27 Mev plotted together with the quantities $\sum(\theta)$ in Figs. 10, 11, and 12.

By integrating appropriate parts of the curves in Figs. 10 to 12, Table I is derived. This table gives the total cross sections for producing the indicated particles within the indicated angular limits. The cross sections for producing deuterons between 45° and 180° (given in parentheses) are probable upper limits obtained by assuming the ratio between numbers of protons and deuterons found between 25° and 45° also holds from 45° to 180°. The corresponding proton cross section is then obtained by subtracting this deuteron cross section from the cross section for all particles, and is thus a lower limit.

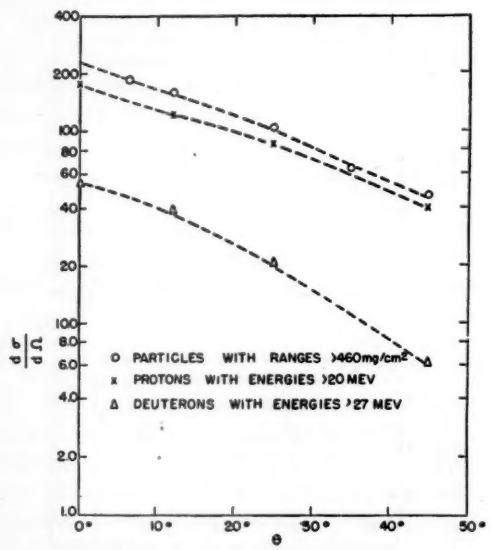

FIG. 11. Angular dependence of 90-Mev neutron-copper cross sections for production of charged secondaries. $d\sigma/d\Omega$ in millibarns/steradian.

VIII. DISCUSSION OF RESULTS

1. Shape of the Spectra

In the case of carbon, the only element for which there is much detailed information, the proton and deuteron spectra are seen to be fundamentally different. The proton spectrum at 0° is flat from 20 Mev to about 65 Mev, and then it decreases sharply as the energy increases further. While it is obviously impossible to deduce from this curve (Fig. 7) and the known neutron energy distribution (Fig. 3 of reference 17) the spectrum which would be obtained for monoenergetic neutrons, it may be worth while to point out the striking similarity of the observed curve to that derived from a rather simple assumption concerning the shape of the proton spectrum for such monoenergetic neutrons. For incident neutrons of energies of from 60 to 100 Mev, according to this assumption, the secondary proton spectrum in the forward direction is flat up to an energy equal to the neutron energy minus the energy required to make the reaction occur (about 15 Mev for 90-Mev neutrons) and then falls immediately to zero. On the basis of this assumption, the proton yield which would be obtained using neutrons with the energy distribution shown in Fig. 3 of reference 17 would be practically flat from 20 to 60 Mev, would fall to about one-half of the maximum value at 74 Mev, and to about one-eighth of that value at 90 Mev. All the values of the observed spectra at 0° and 12° fit such a distribution within the probable errors shown.

The deuteron energy distribution at 0° shows a peak at 60 to 65 Mev. The half-width of this peak is the same as the half-width of the neutron energy distribution, and the low energy tail is about twice as high relative to the peak as the low energy neutron tail is relative to the height of the neutron peak. This distribution fits the assumption that monoenergetic neutrons

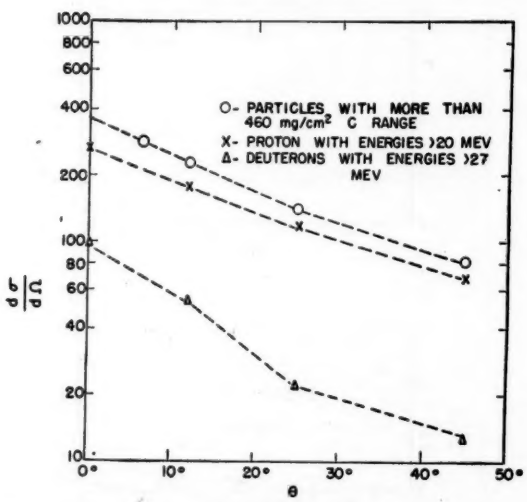

FIG. 12. Angular dependence of 90-Mev neutron-lead cross sections for production of charged secondaries. $d\sigma/d\Omega$ in millibarns/steradian.

would produce deuterons within a relatively narrow energy interval centered about 25 Mev below the neutron energy. As θ increases, the proton plateau and the deuteron peak both disappear. However, the average deuteron energy is higher than the average proton energy at all angles.

2. Total Cross Sections

The total cross sections for producing secondary protons of energy greater than 20 Mev are 0.090 barn for carbon, 0.24 barns for copper, and 0.42 barns for lead. The corresponding inelastic cross sections for 90-Mev neutrons as measured by DeJuren and Knable are 0.22, 0.78, and 1.79 barns. The ratios of these cross sections are 0.41 for carbon, 0.31 for copper, and 0.24 for lead. Since the cross section for striking at least one proton in the nucleus must be proportional to the inelastic cross section, the decrease in this ratio must be due to the increased difficulty which a proton has in leaving the larger nuclei.

For the case of carbon only, an additional total cross section is given, namely that for producing secondary protons of energy greater than 35 Mev. The reason for this particular choice of energy lies in the following arguments: In the $n-p$ scattering experiments performed at 90 Mev, the angular distribution of the scattered protons in the center-of-mass system is roughly symmetric about 90°. Consequently, in about one-half of the $n-p$ collisions the proton emerges with more than one-half of the energy of the incident neutron. Further, since the $n-p$ collision cross section is supposed to be three or four times larger than the $n-n$ cross section, about 0.8 of the inelastic cross section should produce $n-p$ collisions. If the nucleus were completely transparent, so that all struck protons could leave it without further collisions, we should expect that about 0.4 of the inelastic cross section would produce protons with more than half of the energy available to protons. Then since the maximum energy with which the proton can leave is about 70 Mev (taking 85 Mev as the mean energy of the impinging neutrons), the cross section for producing secondary protons with energies greater than 35 Mev would be about 0.4 of the inelastic cross section if the nucleus were completely transparent to the struck protons. In the case of carbon this would be about 100 millibarns. The observed cross section for this process is 52 millibarns, and hence about one-half of the protons leave without further interaction. The above arguments are too qualitative to allow a calculation of the mean free path, but the result is in agreement with the mean free paths estimated by Fernbach.

The total cross sections observed for deuteron production are given in Table I as 26 millibarns for carbon, 52 millibarns for copper, and 75 millibarns for lead. The ratios of these deuteron production cross sections to the inelastic cross sections are 0.12 for carbon, 0.067 for copper, and 0.042 for lead. Thus the deuteron production cross section, as well as the proton production cross section, increases more slowly with atomic number than does the inelastic cross section. The ratios of deuteron production cross section to proton production cross section are 0.29, 0.22, and 0.18 for carbon, copper, and lead respectively. This slower increase with Z of the deuteron cross section is to be expected, since in order for a deuteron to escape from a nucleus both of its component particles must escape without further interaction.

TABLE I. Total cross sections for the production of the particles indicated.*

	0°–25°	25°–45°	(0°–45°)	45°–180°	Total
Carbon					
All particles	48	39	87	30	117
All protons ($E>20$ Mev)	35	31	66	(24)	(90)
Protons ($E>35$ Mev)	24	19	43	(9)	(52)
All deuterons ($E>27$ Mev)	12	8	20	(6)	(26)
Copper					
All particles	88	82	170	123	293
Protons $E>20$ Mev	70	68	138	(103)	(241)
Deuterons $E>27$ Mev	18	14	32	(20)	(52)
Lead					
All particles	123	153	276	223	499
Protons $E>20$ Mev	100	132	232	(192)	(424)
Deuterons $E>27$ Mev	23	21	44	(31)	(75)

* All values are expressed in 10^{-27} cm².

3. The Origin of the Secondary Protons

An attempt was made by M. L. Goldberger[6] to predict the angular and energy distributions of the protons which would be ejected from heavy nuclei by 90-Mev neutrons. He used the Monte Carlo method, and treated the nucleus as a degenerate gas of nucleons. The experimentally determined $n-p$ differential cross sections were used to characterize the individual collisions which take place in the nucleus; the $n-n$ interactions were assumed to lead to the same angular distributions as in $n-p$ interactions, but with only one-fourth as large a total cross section. The angular distribution predicted by Goldberger gave a zero cross section for secondary particle production in the forward direction, and a maximum differential cross section at about 27°. The zero forward cross section was due to the action of the Pauli principle in forbidding small momentum transfers, which would leave one particle in a region of phase space already occupied by another particle.

The observed angular and energy distributions do not fit Goldberger's predictions. A possible explanation, suggested by R. Serber, for the lack of a minimum cross section in the forward direction is the following: The proton wave is refracted at the nuclear surface, since

the proton passes from a region in which there is a high negative potential to a region in which there is zero potential. The effect of this refraction then destroys completely any detailed structure such as that predicted around zero degrees.

The observed total cross section for producing secondary protons by bombardment of lead nuclei with 90-Mev neutrons is only about one-half of the predicted value. This indicates that the mean free path of particles in nuclear matter is smaller than the value given by Goldberger (6.2×10^{-13} cm) and is more nearly in agreement with that deduced by Fernbach *et al.*[5] (4.5×10^{-13} cm).

4. The Origin of the Secondary Deuterons

A possible mechanism for the origin of the secondary deuterons has been suggested by P. Cüer *et al.*[19] and by Chew and Goldberger,[20] and investigated in detail by the latter. This mechanism is characterized by a pick-up process, in which the impinging neutron combines with a proton from the nucleus to form a deuteron. Semiclassically, the process can be described as follows. Protons in the nucleus may have large components of momentum in the direction of the momentum of the impinging neutron. In fact, if the average kinetic energy of a bound nucleon is about 25 Mev, its root-mean-square momentum will be about one-half of the momentum of the impinging particle, and there may easily be nucleons present with momentum equal to that of the incident neutron. In such cases of high nucleon momentum, the nucleon and incident neutron may form a deuteron and so emerge from the nucleus. From this point of view, it would seem that the situation most likely to result in a secondary deuteron would be that in which the momenta of the proton and neutron were most nearly equal. However, for the case of equal momenta the deuteron would leave the nucleus with so much kinetic energy as to leave the nucleus in an impossibly low energy state. It can be seen qualitatively, though, that the energy of the deuteron would tend to be high, and that it would tend to emerge in the forward direction.

[19] Cüer, Morand, and Van Rossum, Comptes Rendus **228**, 481 (1949).
[20] G. F. Chew and M. L. Goldberger, Phys. Rev. **77**, 470 (1950).

5. Comparison to Other Experiments

Experimental investigations of some of the phenomena reported in this paper have also been made by Brueckner and Powell[11] and Bradner.[10] Brueckner and Powell have made a cloud chamber study of the angular and energy distributions of the particles emitted by carbon nuclei under bombardment with 90-Mev neutrons. Their method involved comparison of the $H\rho$'s of particles before and after passage through a plate of material of known stopping power. They found high energy protons, deuterons, and tritons, and their results are qualitatively in agreement with those obtained in the present experiment with respect to the ratios of number of protons to numbers of deuterons and tritons, and the general trends of the angular and energy distributions. There is a qualitative disagreement in the absolute values of the various cross sections, however, the values found in the present experiment being considerably larger than those determined in the cloud-chamber experiments.

Bradner's experiments used photographic plates, and were performed for the purpose of checking the existence of the secondary deuterons. The method involved a comparison of the grain density of tracks with a given residual range. The ratio of protons to deuterons in the forward direction as determined by his experiments is in agreement with that found in the present experiment.

The authors wish to express their gratitude to Professor Segrè and the other members of the committee who guided this research, for their frequent advice and encouragement. Thanks are also due Professor E. O. Lawrence and Dr. B. J. Moyer for their continued interest in this work; to Mr. Clyde Wiegand for the loan of equipment and for numerous suggestions; to Professor Serber, Dr. Chew, and Dr. Goldberger for many interesting discussions of the theoretical implications of this work; and to the cyclotron operating crew, especially Mr. Vale and Mr. Watt, who kindly supplied about 10^{12} high energy neutrons.

The Scattering of 100-Mev Electrons from a Heavy Nucleus*

GEORGE PARZEN†
Stanford University, Stanford, California
(Received June 8, 1950)

This paper describes and gives the results of a calculation of the scattering of 100-Mev electrons from a heavy nucleus with atomic number $Z=82.2$. For 100-Mev electrons the reduced de Broglie wave-length is about one-fourth of the radius of a lead nucleus and appreciable deviations from pure Coulomb scattering are to be expected. Three different models of the nucleus are considered. In the primary case, the nucleus is assumed to have a uniform charge distribution within its radius. The scattering for this model is calculated by the exact phase-shift method. In the two other models the effects on the scattering of varying the radius and non-uniform charge distributions are investigated. The last two calculations are carried out by perturbation on the first.

I. INTRODUCTION

IT is expected that high energy electron beams, of 100 Mev and higher, will soon be readily available from linear accelerators. It is the purpose of this paper to carry out some exploratory calculations to indicate the effectiveness of this tool in the investigation of the properties of the nucleus; in particular, the effects of the charge distribution within the nucleus and the radius of the nucleus are considered.

At the high energies the non-zero size of the nucleus will cause deviations from Coulomb scattering. Some calculations have already been performed along these lines by Rose.[1] However, these calculations were carried out using the Born approximation and it is known[2,3] that for heavy elements the Born approximation is not valid.

In this paper the exact phase-shift method as applied to the Dirac equation was used. The differential elastic cross section was calculated for the scattering of 100-Mev electrons from lead, $Z=82$ (more accurately, $Z=82.2$ was used in order to be able to use the results of Bartlett and Watson).

Three different cases were considered. In the primary case we assume the nucleus to have a uniform charge distribution within a radius a of the nucleus. The radius a was taken from the paper of Fernbach, Serber, and Taylor[4] and was in this case $a=8.09\times10^{-13}$ cm. For 100-Mev electrons, this radius gives a value of $ka=4.10$, k being the momentum divided by $\hbar$. That is, the de Broglie wave-length of the electron is about one-fourth of the radius of the nucleus. The scattering with this model of the nucleus was calculated exactly.

The scattering effects with two slightly different models of the nucleus were calculated by perturbation on the first case. These two variations were: (1) The radius was left unchanged, the charge density was allowed to increase by 43 percent in going from the center to the outer edge of the nucleus. This charge distribution is similar to that proposed by Feenberg[5] and was taken as $\rho=\rho_0(1+g(r/a)^2)$, where $g=0.43$. (2) The charge distribution was left uniform, but the radius was decreased by five percent. This was done to indicate the sensitivity of the scattering to the radius.

The potential due to a uniform charge distribution can be shown to be, for $r\leq a$,

$$V_0(r)=(Ze/2a)\{3-(r/a)^2\}. \tag{1}$$

For a charge distribution, $\rho=\rho_0[1+g(r/a)^2]$, the potential is

$$V_\rho(r)=\frac{Ze}{a}\left\{1+\frac{1}{2}\frac{10+3g}{10+6g}-\frac{1}{2}\frac{5}{5+3g}\left(\frac{r}{a}\right)^2-\frac{3}{4}\frac{g}{5+3g}\left(\frac{r}{a}\right)^4\right\} \tag{2}$$

and that due to a slightly decreased radius a', $a/a'=1+\epsilon$ where the density is still uniform,

$$\begin{aligned} V_a(r)&=(Ze/2a')\{3-(r/a')^2\}; && r\leq a' \\ V_a(r)&=Ze/r; && r\geq a'. \end{aligned} \tag{3}$$

The potential is very insensitive to the charge distribution, as can be seen by considering the two extreme cases of a uniform charge distribution and one in which the charge is concentrated on the surface.

Since for all charge distribution the value of the potential at $r=a$ is Ze/a, and the potential must increase monotonically as we go in toward the origin, a good way to compare the strengths of different potentials is to compare the value of the potentials at $r=0$, $V(0)$.

Thus for a uniform charge distribution, $V_0(0)=1.5Ze/a$. For a surface charge, $V(0)=Ze/a$. For a potential due to $\rho=\rho_0[1+g(r/a)^2]$ and taking $g=0.43$, $V_\rho(0)=1.45Ze/a$. This is only a change of five percent from $V_0(0)$ for the uniform charge distribution, although the density varies by almost 50 percent, showing the insensitivity of the potential to the charge distribution.

* Submitted in partial fulfillment of the Ph.D. requirements at Stanford University.
† Now at the Institute for Nuclear Studies, Chicago, Illinois.
[1] M. E. Rose, Phys. Rev. **73**, 279 (1948).
[2] Bartlett and Watson, Proc. Am. Acad. **74**, 53 (1940).
[3] W. McKinley and H. Feshbach, Phys. Rev. **74**, 1759 (1948).
[4] Fernbach, Serber, and Taylor, Phys. Rev. **75**, 1352 (1949).
[5] E. Feenberg, Phys. Rev. **59**, 593 (1941).

In general, we might note the useful relation which will give $V(0)$ directly from the charge distribution.

$$V(0)=4\pi\cdot\int_0^a \rho(r)\cdot r\cdot dr. \tag{4}$$

Thus if $\rho=\rho_0 u(r/a)$, then

$$V(0)=\frac{Ze}{a}\cdot\int_0^1 u(x)\cdot x\cdot dx\Big/\int_0^1 u(x)\cdot x^2\cdot dx. \tag{5}$$

II. METHOD OF CALCULATING CROSS SECTION FROM PHASE SHIFTS

If the scattering potential falls off at infinity like $-Ze^2/r$, then the radial part of the wave function will have the asymptotic form given by[6] **I**, Eq. (3),

$$g_l(r)\underset{r\to\infty}{\longrightarrow}\cos[kr+q\ln 2kr-\tfrac{1}{2}(l+1)\pi+\sigma_l] \tag{6}$$

where $q=Ze^2/\hbar v$, $v=$speed of electron. In terms of the phase shifts σ_l, the cross section $\sigma(\theta)$ for an unpolarized incident beam can be written as,[7]

$$\sigma(\theta)=|f_3(\theta)|^2+|f_4(\theta)|^2, \tag{7}$$

where

$$f_3(\theta)=(1/i2k)\sum_{l=0}\{(l+1)\exp(2i\sigma_l)+l\exp(2i\sigma_{-l-1})\}P_l(\cos\theta) \tag{8a}$$

and

$$f_4(\theta)=(1/i2k)\sum_{l=1}\{\exp(2i\sigma_{-l-1})-\exp(2i\sigma_l)\}P_l^1(\cos\theta) \tag{8b}$$

and

$$P_l^1=\sin\theta dp_l/d(\cos\theta).$$

In summing (8), which is a divergent series, one must first subtract out the scattering amplitude due to a pure Coulomb field. Let σ_l^c be the phase shifts for the Coulomb potential $-Ze^2/r$; then we can rewrite (8) as

$$f_3(\theta)=f_3^c(\theta)+(1/i2k)\sum_{l=0}\times\{(l+1)[\exp(2i\sigma_l)-\exp(2i\sigma_l^c)]+l[\exp(2i\sigma_{-l-1})-\exp(2i\sigma_{-l-1}^c)]\}P_l(\cos\theta) \tag{9a}$$

$$f_4(\theta)=f_4^c(\theta)+(1/i2k)\sum_{l=1}\times\{[\exp(2i\sigma_{-l-1})-\exp(2i\sigma_{-l-1}^c)]-[\exp(2i\sigma_l)-\exp(2i\sigma_l^c)]\}P_l^1(\cos\theta) \tag{9b}$$

where f_3^c, f_4^c are the Coulomb scattering amplitude.

The problem is now to calculate the phase shifts σ_l which appear in (4a) and (4b). This is done by matching at the point $r=a$, beyond which the potential is pure Coulomb. Thus we need to determine the regular solution of the wave equation for $r\leq a$, and both regular and irregular Coulomb wave functions for $r\geq a$.

The Coulomb wave functions were given by Gordon.[8] Instead of using the functions $g_l(r)$, $f_l(r)$, it is more convenient to use the function $S_l(r)$, defined by **I**, Eq. (35), and which has the asymptotic form, $S_l(r)\to\exp[i(kr+q\ln 2kr-\frac{1}{2}(l+1)\pi+\sigma_l)]$.

We may write the regular Coulomb wave function as

$$S_{l,R}=\exp(i\eta_l)\cdot\zeta_l(x;\rho_l) \tag{10}$$

where $x=kr$,

$$\zeta_l(x;\rho_l)=\frac{\Gamma(\rho_l+1+iq)}{\Gamma(2\rho_l+1)}\exp(\tfrac{1}{2}q\pi)\cdot\exp(i\tfrac{1}{2}\rho_l\pi)(2x)^{\rho_l}\cdot\exp(-ix)\cdot F(\rho_l+iq+1,\,2\rho_l+1;\,2ix), \tag{11}$$

and

$$\rho_l=[(l+1)^2-\alpha^2]^{\frac{1}{2}},\quad q=Ze^2/\hbar v,\quad \alpha=Ze^2/\hbar c.$$

$F(\alpha,\beta;x)$ is the confluent hypergeometric function[9] and

$$\exp(2i\eta_l)=\frac{l+1+iq'}{\rho_l-iq}\cdot\frac{\Gamma(\rho_l-iq)}{\Gamma(\rho_l+iq)}\cdot\exp(-i\pi\rho_l) \tag{12}$$

where $q'=(Ze^2/\hbar v)[1-(v/c)^2]^{\frac{1}{2}}$.

$\zeta_l(x;\rho_l)$ has the asymptotic form $\zeta_l\to\exp[i(kr+q\ln 2kr)]$. Thus $S_{l,R}\to\exp[i(kr+q\ln 2kr+\eta_l)]$ and so the Coulomb phase shifts are given by

$$\sigma_l^c=\eta_l+\tfrac{1}{2}(l+1)\pi. \tag{13}$$

The irregular solutions is obtained from (10) by simply replacing ρ_l by $-\rho_l$,

$$S_{l,I}=\exp(i\eta_l')\zeta_l(x;-\rho_l), \tag{14}$$

and

$$\exp(2i\eta_l')=\frac{l+1+iq'}{-\rho_l-iq}\frac{\Gamma(-\rho_l-iq)}{\Gamma(-\rho_l+iq)}\exp(i\pi\rho_l). \tag{15}$$

This procedure for obtaining the irregular solution breaks down in the non-relativistic theory since there $\rho_l=l+1$ as $\alpha\to 0$ and the hypergeometric function $F(\alpha,\beta;x)$ becomes infinite when β is a negative integer. Because of this there is no easily seen transition from some of our calculations to the corresponding non-relativistic calculations.

Thus, in contrast with the non-relativistic case η_l and η_l' do not differ by $\pi/2$, but approach each other for high l. In fact, we have after using the relation

$$\Gamma(-Z)=-\pi/\Gamma(Z+1)\sin\pi Z, \tag{16}$$

$$\exp[2i(\eta_l'-\eta_l)]=-\exp(2i\pi\rho_l)\times\sin\pi(\rho_l-iq)/\sin\pi(\rho_l+iq), \tag{17}$$

from which we can calculate $\eta_l'-\eta_l$.

[6] For some of the results used here the reader is referred to a previous paper, G. Parzen, Phys. Rev. **80**, 261 (1950), hereafter denoted by **I**.

[7] N. F. Mott, Proc. Roy. Soc. **A124**, 426 (1929).

[8] W. Gordon, Zeits. f. Physik **48**, 11 (1928).

[9] G. N. Watson, *Theory of Bessel Functions* (The Macmillan Company, New York, 1945), second edition, p. 100.

Having the above properties of the Coulomb functions, we can now match at $r=a$ to determine the phase shifts. Let $f_l(r)$, $g_l(r)$ be the regular solutions for $r\leq a$; let $f_{l,R}$, $g_{l,R}$ and $f_{l,I}$, $g_{l,I}$ be the regular and irregular Coulomb solutions.

Then at the point $r=a$,

$$\begin{aligned} f_l&=Cf_{l,R}+Df_{l,I}\\ g_l&=Cg_{l,R}+Dg_{l,I}. \end{aligned} \tag{18}$$

g_l would then have the asymptotic form,

$$\begin{aligned} g_l\rightarrow& C\cos(kr+q\ln 2kr+\eta_l)\\ &+D\cos(kr+q\ln 2kr+\eta_l')\\ &\rightarrow \text{const.}\cos(kr+q\ln 2kr+\eta_l+\delta_l) \end{aligned} \tag{19}$$

where

$$\tan\delta_l=\sin(\eta_l'-\eta_l)/[-(C/D)+\cos(\eta_l'-\eta_l)]. \tag{20}$$

From (18), we find for C/D,

$$C/D=-(g_{l,I}-\gamma_l f_{l,I})/(g_{l,R}-\gamma_l f_{l,R}),\quad \text{at}\quad r=a \tag{21}$$

where

$$\gamma_l=(g_l/f_l)|_{r=a}. \tag{22}$$

The above equations determine δ_l which is the phase shift in addition to the Coulomb phase shift. The phase shift defined in (6) is given then by

$$\sigma_l=\sigma_l^c+\delta_l. \tag{23}$$

III. COMPUTATIONAL PROCEDURE

The quantities to be calculated are the regular and irregular Coulomb functions and the interior regular solution, all at $r=a$. These functions are all calculated by finding a suitable series and summing it. Because the parameter involved in these series, which is ka, is of the order of 4, the series involved converge rather slowly and require from 12 to 20 terms to sum.

In calculating the Coulomb wave functions, the confluent hypergeometric function $F(\alpha,\beta;x)$ which appears converges too slowly requiring about 25 to 30 terms. It is more convenient to treat the function,[10]

$$H(\gamma,b;x)=\exp(-ix)F(\alpha,\gamma;2ix), \tag{24}$$

where $b=i(2\alpha-\gamma)$.

Since $F(\alpha,\gamma;u)$ satisfies the differential equation

$$\left(u\frac{d^2}{du^2}+(\gamma-u)\frac{d}{du}-\alpha\right)\cdot F=0, \tag{25}$$

then $H(\gamma,b;x)=\exp(-ix)\cdot F(\alpha,\gamma;2ix)$ satisfies the equation,

$$\left(x\frac{d^2}{dx^2}+\gamma\frac{d}{dx}+(x-b)\right)\cdot H=0 \tag{26}$$

where $b=i\cdot(2\alpha-\gamma)$.

[10] A. N. Lowen and W. Horenstein, J. Math. Phys. **21**, 264 (1942).

Note that if b is real, then H is a real function. This is the case in the non-relativistic theory. But in our case, $\gamma=2\rho_l+1$, $\alpha=\rho_l+iq+1$, so $2b=-q+i$.

Putting

$$H=\sum_{n=0}^{\infty}C_n\cdot x^n/n! \tag{27}$$

we find,

$$C_{n+1}=[1/(n+\gamma)]\{-nC_{n-1}+2bC_n\} \tag{28}$$

and $C_0=1$.

The C_n are complex. Writing $C_n=\alpha_n+i\beta_n$, we get the recurrence relations for the real quantities α_n, β_n,

$$\alpha_{n+1}=[1/(n+\gamma)]\{-n\alpha_{n-1}-q\alpha_n-\beta_n\}. \tag{29a}$$

$$\beta_{n+1}=[1/(n+\gamma)]\{-n\beta_{n-1}-q\beta_n+\alpha_n\}, \tag{29b}$$

and $\alpha_0=1$, $\beta_0=0$.

From (29) we can also show that we have the simple recurrence relation

$$\beta_{n+1}=(n+1)\alpha_n/(n+\gamma), \tag{30}$$

which can be used as a check.

It is only necessary to sum the series to calculate S_l; the function S_{-l-1} can be derived from S_l. For

$$S_{-l-1}=\exp(i\eta_{-l-1})\zeta_{-l-1}(x;\rho_{-l-1}), \tag{31}$$

and ζ_l depends on l only through $\rho_l=[(l+1)^2-\alpha^2]^{\frac{1}{2}}$.

Thus,

$$\zeta_{-l-2}=\zeta_l$$

and

$$S_{-l-2}=\exp[i(\eta_{-l-2}-\eta_l)]\cdot S_l. \tag{32}$$

Relation (32) holds for both regular and irregular Coulomb functions.

The solutions for $r\leq a$ are obtained by solving the differential equation for $S_l(r)$ by series. Thus, by I, Eq. (37),

$$\frac{d}{dx}S=\left(i-\frac{V}{k}\frac{E}{k}\right)S+\left(\frac{l+1}{x}-i\frac{V}{k}\cdot\frac{1}{k}\right)\bar{S}, \tag{33}$$

and for a uniform charge distribution we can write

$$VE/k^2=A-Bx^2, \tag{34}$$

where

$$A=-\tfrac{3}{2}(Ze/ka)\cdot(E/k)$$

and

$$B=\tfrac{1}{2}(Ze^2/ka)\cdot(E/k)\cdot 1/(ka)^2.$$

Putting

$$S=\sum_n a_n x^n,\quad \bar{S}=\sum_n \bar{a}_n x_n,$$

we get

$$\begin{aligned} a_m(m+s)=&i(1-A)a_{m-1}+iBa_{m-3}+(l+1)\bar{a}_m\\ &-iA'\bar{a}_{m-1}+iB'\bar{a}_{m-3} \end{aligned} \tag{35}$$

where $A'=A/E$, and $B'=B/E$;

$$s=l\ \text{ if }\ l\geq 0,\quad s=-l\ \text{ if }\ l<0.$$

Again writing $a_n=\alpha_n+i\beta_n$, we get for $l\geq 0$,

$$\alpha_n=-\frac{1-A+A'}{n}\beta_{n-1}-\frac{(B-B')}{n}\beta_{n-3}, \quad (36a)$$

$$\beta_n=\frac{1-A-A'}{n+2(l+1)}\cdot\alpha_{n-1}+\frac{B+B'}{n+2(l+1)}\alpha_{n-3}, \quad (36b)$$

and $\beta_0=0$, $\alpha_0=1$.

The ratio γ_l is given by,

$$\gamma_l=\left(\frac{E+1}{E-1}\right)^{\frac{1}{2}}\frac{\sum_n \alpha_n x^n}{\sum_n \beta_n x^n} \quad \text{at} \quad x=ka. \quad (37)$$

Also here it is not necessary to sum the series to determine γ_{-l-1}. Because the potential is an even function of x, one can show that for high enough energies

$$\gamma_{-l-1}'\cong>1/\gamma_l', \quad (38)$$

where

$$\gamma_l'=[(E-1)/(E+1)]^{\frac{1}{2}}\gamma_l$$

Relation (38) is not exactly true but numerical calculation of γ_{-1} and γ_{-2} showed it to be good to four figures.

IV. PERTURBATION METHOD

If the potential is changed somewhat in the region $r\leq a$, but remains $-Ze^2/r$ for r larger than a, then in the phase-shift method of the previous sections the only quantity which must be recalculated is γ_l.

To obtain an approximate method for calculating γ_l for a potential $V(r)$ which differs slightly from the uniform charge potential $V_0(r)$, consider the potential $U(r)$ constructed as follows:

$$\begin{aligned} U(r)&=V(r); \quad r\leq a \\ U(r)&=0; \quad r>a. \end{aligned} \quad (39)$$

If Eq. (33) is solved for $S_l(r)$, and thus f_l and g_l, then the ratio $\gamma_l=g_l/f_l$ at $r=a$ is the same for the potential $U(r)$ as for the potential $V(r)$, both potentials being identical for $r\leq a$.

Now the potential $U(r)$ will cause a certain phase shift which is connected to γ_l by the relation I, Eq. (64),

$$\gamma_l=\left(\frac{E+1}{E-1}\right)^{\frac{1}{2}}\frac{j_l(ka)-\tan\delta_l\cdot n_l(ka)}{j_{l+1}(ka)-\tan\delta_l\cdot n_{l+1}(ka)}. \quad (40)$$

Thus to determine the γ_l for the potential $V(r)$, one can equally well determine the phase shifts δ_l of the potential $U(r)$. The phase shift δ_l of $U(r)$ can be approximated by means of the variational result of paper I. There we showed that, I, Eq. (60),

$$\delta_l-\delta_l\cong-\frac{E+1}{2k}\cdot\int_0^\infty 2(V-V_l)\cdot\left\{\frac{g_l^2}{E+1}+\left(\frac{k}{E+1}\right)^2\frac{f_l^2}{E-1}\right\}dr. \quad (41)$$

Here we can choose for the trial potential $V_l(r)$, the potential $V_0(r)$ due to a uniform charge distribution. Further, instead of the wave functions of $V_0(r)$, we can put in (41), as a good approximation, the wave functions of a free particle. The integral then only involves Bessel functions and can be evaluated more easily. Thus (41) becomes

$$\delta_l-\delta_l{}^0\cong\tfrac{1}{2}(E+1)\{\Delta_l+[k/(E+1)]^2\cdot\Delta_{l+1}\}, \quad (42)$$

and

$$\Delta_l=-k\int_0^\infty 2\cdot(V-V_0)\cdot j_l^2(kr)\cdot r^2dr.$$

The application of (42) requires the evaluation of integrals of the form

$$k_{n,m}=\int_0^x t^m J_n^2(t)dt. \quad (43)$$

In some cases, for m even, the indefinite integral can be done. However, it is generally simpler to use a recursion formula which will be developed now. This will give $k_{n+1,m}$ in terms of $k_{n,m}$.

Using the Bessel function relation,

$$J_n(t)=(t/2n)(J_{n-1}+J_{n+1}),$$

we get from (43)

$$k_{n,m}=(1/2n)\{L_{n,m}+L_{n+1,m}\}, \quad (44)$$

where

$$L_{n,m}=\int_0^x t^{m+1}\cdot J_n(t)\cdot J_{n-1}(t)\cdot dt. \quad (45)$$

Now, using the relation $dJ_n/dt=\frac{1}{2}\{J_{n-1}-J_{n+1}\}$ we get for $L_{n,m}$ from (45)

$$L_{n,m}=L_{n+1,m}+\int_0^x t^{m+1}(dJ_m^2/dt)dt. \quad (46)$$

Integration by parts yields

$$L_{n,m}=L_{n+1,m}+x^{m+1}J_n^2(x)-(m+1)k_{n,m}. \quad (47)$$

Comparison of the expressions for $k_{n,m}$ as obtained from (47) and (44) gives the recursion formula for $L_{n,m}$,

$$L_{n+1,m}=\frac{2n+m+1}{2n-m-1}L_{n,m}-\frac{2n}{2n-m-1}x^m\cdot J_n^2(x). \quad (48)$$

Relation (48) together with (44) gives a recursion relation for $k_{n,m}$.

The recursion chain may be interrupted if we happen to arrive at a value of n for which $2n=m+1$.

The integral (45) for low values of n can usually be calculated easily in our case since we have Bessel functions of half-odd integer orders which involve only sines and cosines. For higher n, the recursion formula can be applied. The one disadvantage in the above procedure is that cancellation occurs in applying the

TABLE I. Phase shifts for the scattering of 100-Mev electrons from a lead nucleus with a uniform charge distribution. δ_l is the phase shift with the Coulomb phase shift subtracted.

l	$\delta_l=\sigma_l-\sigma_l^c$	$\delta_{-l-1}=\sigma_{-l-1}-\sigma_{-l-1}^c$
0	−.5339	
1	.2064−π	−.5307
2	.2507−π	.2091−π
3	.0678−π	.2572−π
4	.0115−π	.0711−π
5	.0013−π	.0124−π
6	.0001−π	.0015−π
7		.0001−π

recursion formula and one must start out with a great many figures in order to get a significant answer for large values of n.

V. DISCUSSION OF RESULTS

The behavior of the phase shifts at high energies is quite different from that met in non-relativistic scattering. As was pointed out in paper **I**, the phase shift δ_l, for a given l, does not approach zero when $k\to\infty$. By a slight modification of the argument presented in *I*, we can show that for the potentials considered in this paper, which go like $1/r$ at infinity but have no pole at the origin, δ_l approaches the value,

$$\delta_l \underset{k\to\infty}{\to} -\frac{1}{\hbar c}\int_0^a V(r)\cdot dr - \frac{Ze^2}{\hbar c}\ln ka - \sigma_l. \qquad (49)$$

In the case of the uniform charge distribution, this gives an asymptotic value of $\delta_0=-0.91$. Our calculated value of $\delta_0=-0.534$ agrees favorably with this as the deviation of δ_0 from its asymptotic value should be of the order of $1/ka=0.244$.

Our curve, Fig. 1, for the scattering due to a uniformly charged nucleus agrees qualitatively with what one would expect from the Born approximation, though it differs greatly quantitatively. The two minima in the curve should be at 66° and 142° according to the Born approximation but are actually at about 70° and 120°. The only feature not indicated by the Born approximation is the increase in the forward scattering as compared with pure Coulomb scattering at the angles of 15° and 30°. This increased forward scattering is due to the constructive interference of the higher order partial waves and would be a small effect at lower energies where the higher order phase shifts are small.

The effects of varying the density or the radius of the nucleus are almost identical although, for the cases chosen here, in opposite directions. Thus these two effects will tend to mask each other. However, the probable deviation of the charge distribution of the nucleus from a uniform one is equivalent to only a five percent change in the radius in affecting the scattering. The scattering at the larger angles, where the diffraction effects are most marked, is particularly sensitive to the above two factors. The large percentage deviation

TABLE II. Differential cross sections as a function of angle in units of $1/k^2=3.889\times10^{-26}$ cm². σ_c is the pure Coulomb cross section. σ_0 is the cross section in the case of a uniformly charged nucleus; σ_ρ refers to the case in which the density is not uniform; σ_a refers to the case in which the radius is decreased slightly but the charge density is uniform. The results at the angles 75°, 105°, and 135° are not as accurate as the results at the other angles since the Coulomb scattering amplitude at these angles were gotten by interpolation.

θ	σ_c	σ_0	$(\sigma_a-\sigma_0)/\sigma_0$ in %	$(\sigma_\rho-\sigma_0)/\sigma_0$ in %
0			0	0
15	347.8	420.8	0.68	−1.1
30	27.39	39.78	7.1	−7.8
45	7.001	5.421	14	−12
60	2.768	0.576	17	−14
75	1.3	0.40		
90	0.710	0.541	18	−21
105	0.37	0.28		
120	0.207	0.046	68	−45
135	0.10	0.069		
150	0.042	0.062	19	−25

shown in Table II at 120° occurs there since 120° happens to be the position of the second minimum of our scattering curve.

Some discussion of other quantities which will affect the scattering is given in the paper of Rose.[1] The screening of the orbital electrons would not be expected to have any effect except at small angles. Actual numerical calculations were carried out by Bartlett and Welton.[11] For an element like mercury; they found the screening to be important at less than 60° for 100-kev electrons,

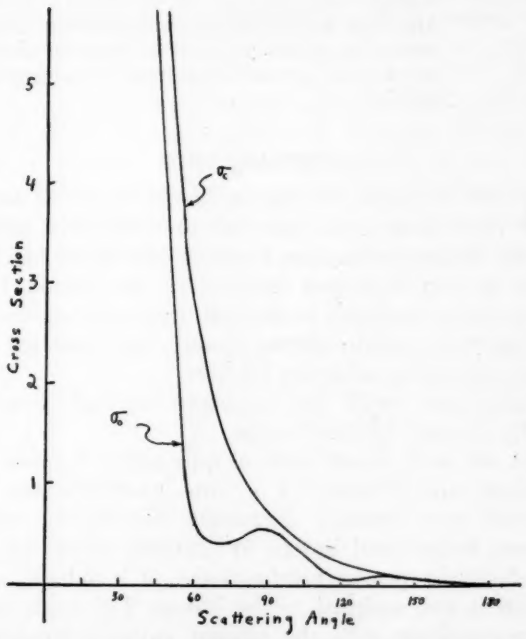

FIG. 1. The scattering of 100-Mev electrons from a lead nucleus ($Z=82.2$). σ_0 is the scattering with a uniform charge distribution. σ_c is the scattering with a pure Coulomb field. Units are $1/k^2=3.889\times10^{-26}$ cm².

[11] J. H. Bartlett, Jr. and T. A. Welton, Phys. Rev. **59**, 281 (1941).

and at less than 15° for 230-kev electrons; at 100 Mev we can expect the angle within which screening is important to be very small.

Radiative effects in the scattering as predicted by quantum electrodynamics may be large enough to mask the effect due to non-uniform charge density or to a slight change in the radius of the nucleus. Calculations for a pure Coulomb field based on Schwinger's[12] results would indicate this to be the case. However, since these results are based on the Born approximation, and give the deviation due to radiative effects from the Born approximation expression for the scattering, not from the actual scattering, their reliability in the case of heavy elements is doubtful. The order of magnitude given by them is probably still correct.

In our calculation, where we have assumed a continuous charge distribution within the nucleus, we have obtained a result which should approximate rather well the coherent elastic scattering of the electrons by the Z protons in the nucleus. The incoherent scattering[13] by the individual protons we expect to be much smaller than the coherent scattering by the nucleus as a whole. If we think of each proton as contributing to the entire scattering amplitude, which is proportional to Ze^2, an amount proportional to e^2, then the coherent scattering will be of the order of Z times larger than the incoherent scattering.

I would like to express my gratitude to Professor L. I. Schiff for suggesting this problem and for advice and many discussions. I would also like to thank Mrs. Sabra Driscoll for her excellent aid with the computations.

[12] J. Schwinger, Phys. Rev. 75, 898 (1949).

[13] L. I. Schiff, Microwave Lab., Stanford University Report No. 102 (November, 1949, unpublished).

PHYSICAL REVIEW VOLUME 80, NUMBER 3 NOVEMBER 1, 1950

The Disintegration of Ti^{45}

M. TER-POGOSSIAN, C. S. COOK, F. T. PORTER, K. H. MORGANSTERN, AND J. HUDIS*
Physics Department, Washington University,† St. Louis, Missouri
(Received May 22, 1950)

The positron and photo-electron spectra of 3.05-hr. Ti^{45} have been studied. At least 96 percent of the positron transitions are to the ground state of Sc^{45} with a maximum positron kinetic energy of 1.022±0.01 Mev. Less than four percent of the positron transitions are to an excited level of Sc^{45} at 450 kev. In addition, certain longer-lived activities are found in the chemically separated titanium fraction produced by both deuteron and proton bombardment of scandium oxide. Two of the activities are shown to be P^{32} and Sc^{46} impurities.

I. INTRODUCTION

BOTH deuteron and proton bombardment of scandium have been reported[1] to result in a radioactive isotope of titanium having a half-life of 3.05 hr. This activity has been assigned to the isotope Ti^{45}. Its positron spectrum, as obtained from a histogram resulting from cloud-chamber studies, has indicated an end-point energy of about 1.2 Mev.

Subsequent work[2] has confirmed the half-life originally reported for this isotope.

In the most recent table of radioactive isotopes by Seaborg and Perlman[3] a private communication is quoted from Dessauer indicating the presence of a second longer-lived isotope of titanium which can be produced by proton bombardment of scandium, and which is also assigned to the isotope Ti^{45}. In further correspondence with the present authors, Dessauer[4] has indicated that the 21-day half-life reported in the compilation of Seaborg and Perlman[3] is a typographical error. What he actually found in the titanium fraction after irradiating scandium with 7-Mev protons were two half-lives, 3.1 hr. and 3.1 days. At some time the 3.1 days was erroneously copied as 21 days.

It would thus appear that a beta-spectrometer study of the radioactive isotopes of titanium produced by either deuteron or proton bombardment of scandium could perhaps lead to interesting results.

In addition to the study of the disintegration schemes, the shape of the positron spectrum can also be of interest. Using the half-life and energy values reported in the literature Konopinski[5] has calculated a ft-value for the 3.05-hr. Ti^{45} corresponding to an allowed transition. Most recent evidence [6–9] indicates that simple allowed spectra should produce linear Fermi-Kurie plots. Since no gamma-rays had been reported,[1] it was

* Chemistry Department, Washington University.
† Assisted by the joint program of the ONR and AEC.
[1] Allen, Pool, Kurbatov, and Quill, Phys. Rev. 60, 425 (1941).
[2] Huber, Lienhard, and Wäffler, Helv. Phys. Acta. 16, 226 (1943); 17, 195 (1944).
[3] G. T. Seaborg and I. Perlman, Rev. Mod. Phys. 20, 585 (1948).
[4] G. Dessauer (private communication).
[5] E. J. Konopinski, Rev. Mod. Phys. 15, 209 (1943).
[6] Langer, Moffat, and Price, Phys. Rev. 76, 1725 (1949).
[7] G. E. Owen and C. S. Cook, Phys. Rev. 76, 1726 (1949).
[8] Lidofsky, Macklin, and Wu, Phys. Rev. 76, 1888 (1949).
[9] Langer, Motz, and Price, Phys. Rev. 77, 798 (1950).

assumed for the purpose of this study that the disintegration of the 3.05-hr. Ti^{45} most likely follows a single transition from the ground state of Ti^{45} to the ground state of Sc^{45}. This transition should thus yield a linear F-K plot.

Very recent work at Illinois,[10] however, has indicated the existence of two gamma-rays in the 3.05-hr. Ti^{45}. Since these two are reported as having different intensities, it appears that the assumption of a simple spectrum is probably not correct. The group at Illinois have also found activities in the titanium fraction other than the 3-hr. activity, in this case the reported half-lives being approximately 3.5 and in excess of 21 days.

II. APPARATUS

For the study of the beta- and gamma-spectra in the present investigation either a magnetic spectrometer or a cloud chamber were used, depending upon the relative activity of the source to be studied.

The magnetic spectrometer is of the uniform-field semicircular type and has a beta-particle radius of curvature of 14 cm. It has been described in some detail in previous papers.[11] For this reason no lengthy discussion of the spectrometer will be given here.

The cloud chamber[12] is of the standard type for nuclear work. The chamber has a diameter of 25 cm. It is normally operated with a filling mixture consisting of hydrogen and alcohol vapor. Chamber expansion and camera recording of the ion tracks are performed automatically at given intervals in order that a continuous record of any decaying radiations may be made.

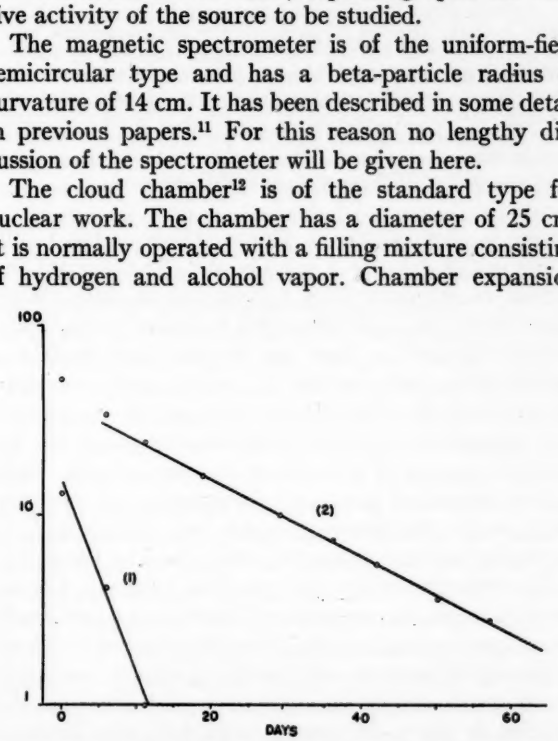

FIG. 1. Decay of titanium fraction beginning three days after completion of cyclotron bombardment. Curve (2) gives a 14-day half-life. Curve (1) gives a 3.4-day half-life produced by the difference between the earlier experimental points and the straight-line extrapolation of the 14-day half-life.

III. PREPARATION OF SOURCES

The active titanium has been produced through bombardment of scandium oxide with both 10-Mev deuterons and 5-Mev protons in the Washington University cyclotron.

The scandium oxide used was chemically pure according to Fairmount Chemical Company, the suppliers. In order to check the purity of the target material two samples were kindly analyzed spectroscopically for us by Dr. Keller at the Mallinckrodt Chemical Works. Both samples were found to be identical with major impurities being boron (impurity of 0.4 percent) and silicon (impurity 0.3 percent). Other impurities listed were calcium (about 0.1 percent), iron (about 0.05 percent), rubidium (less than 0.05 percent, if any), strontium (less than 0.10 percent, if any), and titanium (less than 0.01 percent, if any).

Following the bombardment the titanium was separated in accordance with the procedure outlined by the Ohio State group.[1] After the ScF_3 had been precipitated in the final step outlined by this group, leaving the titanium in solution, inactive $Sc(NO_3)_3$ was added to the solution and the scandium was again precipitated as ScF_3. The purpose of the last step is to dilute any scandium activity which might remain in solution after the first precipitation of ScF_3. Assuming that a small amount of scandium remains, the final dilution will leave most of the scandium in solution as inactive scandium.

In order to prepare beta-sources, the titanium solution was evaporated until only a small amount of liquid remained. A few drops of this solution was then deposited onto a backing consisting of a double layer of zapon, covered by a layer of *LC* 600. Zapon was used to provide mechanical strength, while the layer of *LC* 600

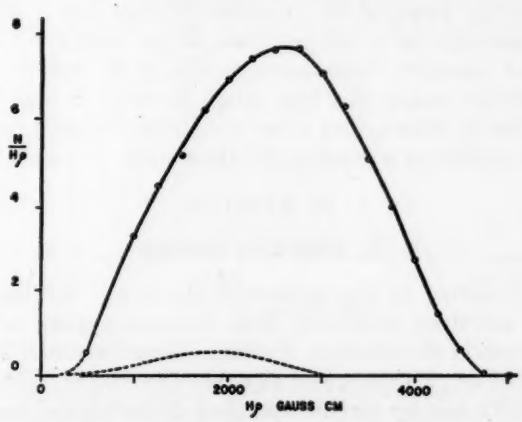

FIG. 2. Momentum distribution of the positrons from Ti^{45}. The dotted curve is the low intensity, low energy group of positrons obtained by subtracting the straight-line extrapolation of the F-K plot from the experimentally determined points.

[10] Kubitschek, Longacre, and Goldhaber, Phys. Rev. **77**, 742 (1950); A. Longacre (private communication); see *Note added in proof* at end of article.

[11] Ter-Pogossian, Cook, Goddard, and Robinson, Phys. Rev. **76**, 909 (1949) give the latest changes in this spectrometer. The basic operating principles of the electronic constant current supply mentioned in that paper are now described in some detail by Elmore and Sands, *Electronics, Experimental Techniques* (McGraw-Hill Book Company, Inc., New York, 1949), National Nuclear Energy Series, pp. 390–393, in addition to the relatively inaccessible AEC document referred to in the previous paper.

[12] K. H. Morganstern and K. P. Wolf, Phys. Rev. **76**, 1261 (1949).

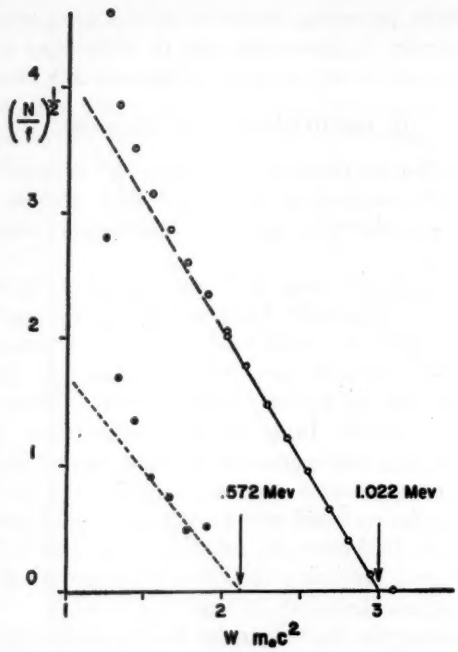

FIG. 3. F-K plot of the positrons from Ti^{45}. Open circles are experimentally determined points. Closed circles are values obtained after subtraction of the straight-line portion of the plot.

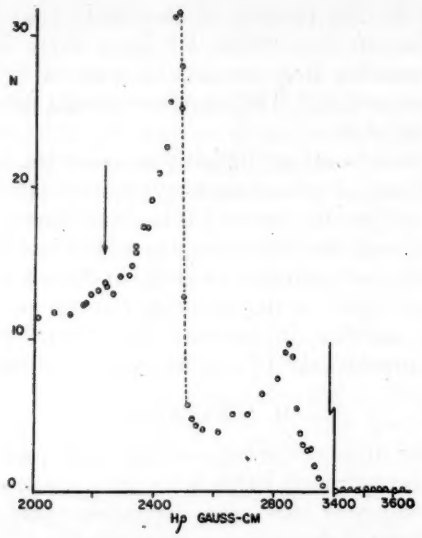

FIG. 4. Photo-electron spectrum of Ti^{45} electromagnetic radiation as produced in a 50-mg/cm² uranium radiator. In addition to the strong annihilation radiation photo-electron lines a small bump characteristic of a possible photo-electron from a gamma-ray of energy 450 kev is indicated by the arrow. The photo-electrons from the gamma-radiation reported by Kubitschek, Longacre, and Goldhaber (see reference 10) could not be found. They should have appeared at 2370 gauss-cm and 3600 gauss-cm.

provided an acid resistant layer,[13] this being necessary, since the titanium existed in a strongly acid solution. After deposition on the zapon-*LC* 600 backing the solution was brought to dryness under a heat lamp.

For the study of the gamma-ray spectrum of Ti^{45}, the concentrated solution prepared from the chemical separation was brought to dryness and the resulting powder was packed into a brass container on the face of which was cemented a strip of 50-mg/cm² uranium, 3 mm in width, which acted as a radiator of photo-electrons. This is the same procedure as was followed previously[11] for the study of secondary electron spectra resulting from gamma-radiation.

Cloud-chamber sources were prepared by deposition of a few drops of the titanium solution into a slight indentation on a special brass source holder for the cloud chamber. Subsequent drying of the source was made by means of a heat lamp. In order to hold the source in place a thin cover of "Krylon" plastic spray was applied as a covering for the source.

IV. RESULTS

A. Half-Life Studies

According to the measurements of the half-life of the activities produced, three isotopes appear to be present in the titanium fraction. These have half-lives of 3.05 hr., 3.4 days, and 14 days. The 3.05-hr. half-life activity has by far the strongest intensity and is the fairly well established Ti^{45} previously reported.[1]

A curve showing the decay of the longer-lived activities is given in Fig. 1. Curve (2) shows the results of the initial data, as a semilog plot. The straight-line section corresponds to a half-life of 14 days. When this straight line is extrapolated to earlier times, a subsequent subtraction from the original data leads to a second group, indicated by (1), which gives a resulting 3.4-day half-life. The relative efficiency of the counter was determined for each experimental point on the curve by means of a uranium standard source. Using a fixed standard geometry throughout the measurement, each experimental point was determined by measuring successive counting rates given by the sources in the following order: the uranium standard, the unknown sample, the uranium standard again, and finally the unknown sample again. In order to insure no change in geometry, sources were sealed in plastic containers which could always be replaced in the same position relative to the G-M counter used for these measurements. A thin mica-window counter was used in order to obtain both beta- and gamma-radiation from the unknown sample.

B. The Positron Spectrum of the 3.05-Hr. Activity

The positrons from the 3.05-hr. half-life Ti^{45} gave a momentum distribution as indicated in Fig. 2. The resulting F-K plot is indicated in Fig. 3. Extrapolation of the straight-line portion of the F-K plot in the higher energy region gives an end-point energy of $W_0=3.0m_0c^2$ ($E_0=1.022\pm0.01$ Mev). The experimental points, however, deviate from this straight line in the region of $W=2m_0c^2$. Subtraction of this straight-line section from the experimental points leads to a pos-

[13] L. M. Langer, Rev. Sci. Inst. **20**, 216 (1949).

sible second group, indicated by the solid circles in Fig. 3. These subtracted points do not form a good linear F-K plot. However, a straight line through the general vicinity of the higher energy points leads to the dotted line of Fig. 3. This gives the dotted line distribution of Fig. 2. The extrapolated end point is approximately $W_0=2.1\pm0.1m_0c^2$ ($E_0=0.57$ Mev). Comparison of areas leads to a relative abundance for this lower energy group of about four percent of the total number of positrons.

C. Photo-Electron Spectrum

The difference in the end-point energies of the two positron groups mentioned in Section IV-B is approximately 450 kev. This is rather close to the energy of one of the gamma-rays reported by the Illinois group.[10] Since this group had reported gamma-rays at 480 and 800 kev, searches were made for these gamma-rays.

Photo-electron sources prepared as described in Section III were studied in the region of energy where one would expect the K-shell photo-electrons from the uranium radiator for these two gamma-rays. The results of this search are shown in Fig. 4. The plot is divided into two parts, one covering the momentum range 2000 to 3000 gauss-cm and the other momentum range 3400 to 3650 gauss-cm. The K-shell photo-electron line from uranium for a gamma-ray having 480 kev energy should appear at 2370 gauss-cm and one for a gamma-ray having 800 kev energy should appear at 3600 gauss-cm. Within experimental limitations, and except for the photo-electron lines produced by the annihilation radiation, at only one place in the spectrum did a repeatable rise and fall occur which might possibly be explained as a photo-electron line. This is indicated by the arrow in Fig. 4. This was found on both gamma-ray sources which were used, the two sources having been prepared at different times from two different containers of scandium oxide. The intensity of this line is, however, only about two or three percent that of the annihilation line, and its momentum corresponds to a gamma-ray energy of 450 ± 10 kev. This intensity is somewhat lower than that reported by the Illinois group for their 480-kev gamma-ray. No indication of an 800-kev gamma-ray could be found.

D. Cloud-Chamber Studies

Cloud-chamber photographs indicated initially a very strong positron activity which died away with the known 3-hr. half-life for Ti^{45}. All photographs taken after sufficient time had elapsed for this 3-hr. activity to become negligible revealed an almost complete absence of any positrons. Negatrons, however, remained in appreciable quantities, though small compared with the original positron activity.

This means that the long-lived activity must be either an impurity emitting negative beta-particles or else a long-lived isomeric state of Sc^{45} following the

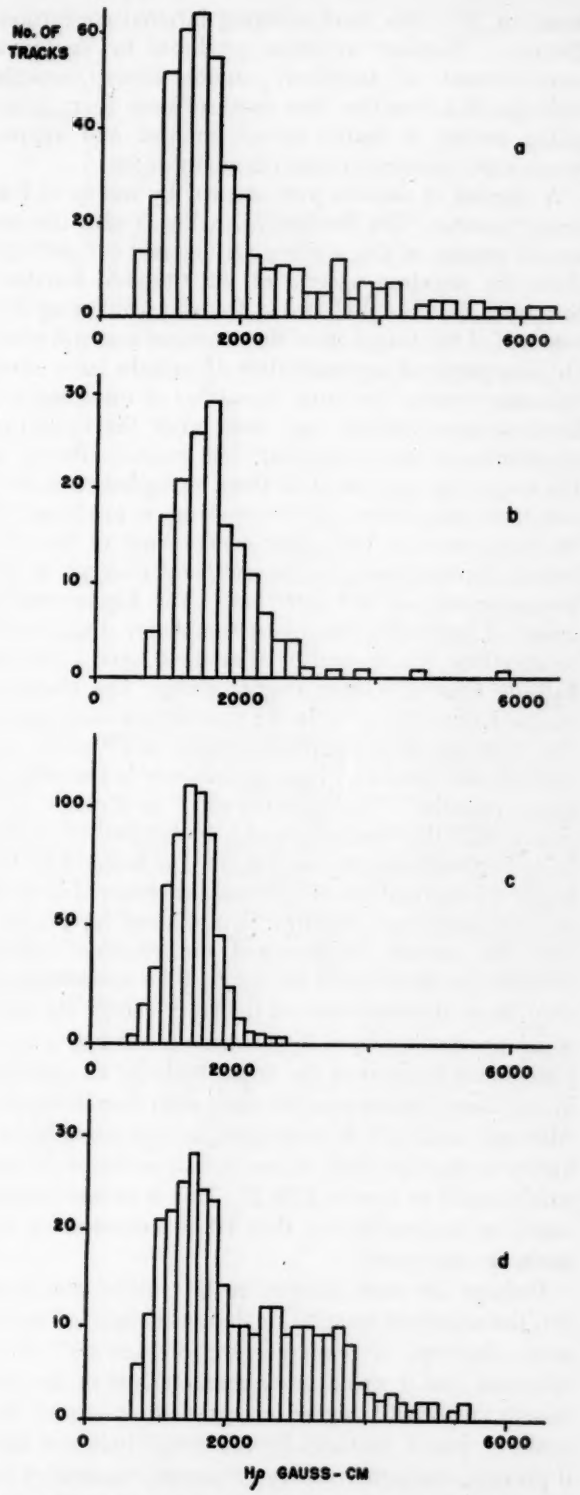

FIG. 5. Cloud-chamber studies of the particle radiations from the chemically separated fractions of the scandium oxide target. (a) The negatron spectrum of the titanium fraction a few days after the target had been removed from the cyclotron; (b) the same negatron spectrum approximately 1½ months later; (c) the scandium fraction a few days after the cyclotron bombardment was completed; (d) the phosphorus fraction a few days after the cyclotron bombardment was complete. Further discussion of the significance of these histograms is given in the text (Section IV-D).

decay of Ti^{45}, this state emitting internal conversion electrons. Titanium activities produced by deuteron bombardment of scandium cannot decay through emission of a negative beta-particle, since there is no stable isotope of higher atomic number and appropriate mass number to which it might decay.

A number of sources were studied by means of the cloud chamber. The histograms in Fig. 5 give the essential results of the studies. Histograms (a) and (b) show the negatron spectra of the titanium fraction. Spectrum (a) was prepared a few days following the removal of the target from the cyclotron and spectrum (b) was prepared approximately $1\frac{1}{2}$ months later using the same source. Spectrum (c) is that of the scandium fraction approximately one week after the cyclotron bombardment was completed. The great similarity in the low energy portion of all three histograms is indicative that this portion of the spectrum is produced by the same isotope. The upper energy limit of this distribution corresponds to the end-point energy[14] of the beta-spectrum of Sc^{46} (360 kev). The higher energy group of negatrons has almost completely disappeared in spectrum (b), indicating that these have a shorter half-life than the lower energy group. The chemical separations as discussed in the next section have shown that they are from the disintegration of P^{32} which apparently was produced from an impurity in the original target material.[15] The existence of P^{32} is of course consistant with the observation of a 14-day half-life in the half-life measurements (see Fig. 1). The reason why the longer 85-day half-life of Sc^{46} was not observed in these measurements can probably be explained by the fact that the counter window and the "Krylon" which covered the source used for the half-life measurements very likely absorbed most of the lower energy electrons which are emitted by Sc^{46}. Spectrum (d) of Fig. 5 is the phosphorus fraction of the target material as observed in the cloud chamber a few days after bombardment. Although some Sc^{46} still remains, the histogram gives a higher energy spectrum characteristic in shape to that which would be expected for P^{32}. This is merely another check on the assumption that P^{32} is present as an impurity in the source.

Perhaps the most interesting fact about histogram (c), the scandium fraction, is that, although 700 tracks were observed in preparing the 360-kev Sc^{46} beta-spectrum, not a single track characteristic of the previously reported[14] higher energy beta-group of Sc^{46} could be found. Statistically this result indicates that, if present, the higher energy beta-group consists of less than one-half of one percent of the total beta-transitions from Sc^{46}.

V. CHEMICAL STUDIES

Chemical studies have also been made in order to seek the source of the negatron radiations which have been observed in the titanium fraction. These studies are outlined in the following paragraphs.

Since a high specific activity of titanium was no longer necessary, titanium carrier was first added to the solution.

To a portion of this solution $CuCl_2$, $BiCl_3$, and $AsCl_5$ were added as carrier and precipitated with H_2S. The activity remained in solution.

$AlCl_3$ was added to the filtrate and the titanium was precipitated with excess NaOH. The activity followed the titanium.

To another portion of the active solution $LaCl_3$, $Sc(NO_3)_3$, and $Ti(SO_4)_2$ were added as carriers. The scandium and lanathanum were precipitated with HF, the titanium remaining in solution.[16] The activity remained with the titanium fraction.

A third portion of the active solution was taken, $ZrOCl_2$ added as carrier, and zirconium phosphate precipitated,[17] titanium being kept in solution by H_2O_2. All of the activity came with the zirconium phosphate.

A final chemical check consisted of adding enough Na_2HPO_4 to the active solution to allow precipitation of 60 mg of Ag_3PO_4. Sufficient $AgNO_3$ to precipitate approximately 20 mg of Ag_3PO_4 was added in three successive steps, Ag_3PO_4 being centrifuged away after each addition of the silver carrier. The three samples thus produced were weighed and counted and were found to have within 15 percent the same specific activity. The last two operations seemed to indicate that the activity was phosphorus.

Finally, an absorption curve was determined for the unknown activity and compared with an absorption curve made under identical experimental conditions from a sample of P^{32} which had been obtained from Oak Ridge. The results are indicated in Fig. 6. As can be seen, the curves of the unknown activity and of the known P^{32} sample are very similar in shape up to about 600 mg/cm^2 of aluminum (1.3 Mev). The counting rate was too low to follow the absorption curve accurately beyond this energy.

VI. DISCUSSION AND CONCLUSIONS

It would appear from this work that the only titanium activity produced in any significant quantities by bombardment of scandium with either 10-Mev deuterons or 5-Mev protons is the 3.05-hr. half-life positron emitter Ti^{45}.

[14] C. L. Peacock and R. G. Wilkinson, Phys. Rev. **74**, 297 (1948).

[15] Normally, production of P^{32} occurs through a (d, p) reaction on P^{31} or an (n, p) reaction on S^{32}. Subsequent check with Dr. Keller of Mallinckrodt Chemical Works revealed that either of these target impurities could have been missed in their spectroscopic analysis because of the absence of suitable strong spectral lines in the region of the spectrum studied.

[16] Noyes and Bray, *A System of Qualitative Analysis for the Rare Elements* (The Macmillan Company, New York, 1927) p. 221, outline this procedure in detail.

[17] Noyes and Bray, reference 16, pp. 207–208.

The difficult chemical procedure necessary to give a high specific activity titanium source for spectrometer studies apparently carries with the titanium a certain number of impurities. As discussed in Sections IV and V, the 14-day P^{32} and the 85-day Sc^{46} activities apparently are not easily eliminated from the titanium fraction. Deciding the exact nature of the 3.4-day activity presents a problem which cannot be answered accurately at the present time. It has been reported by all recent investigators[3,10] of the titanium activities produced from deuteron and proton bombardment of scandium. It definitely (but not strongly) appears in the half-life curve (Fig. 1), yet all search for a radiation which can be associated with this half-life has produced no results. All positron activity dies away with a 3.05-hr. half-life, after whose decay the cloud chamber shows no radiation other than that which can be accounted for by the negative beta-spectra of P^{32} and Sc^{46}.

It would appear, therefore, that most probably the only titanium activity present in the samples studied was the 3.05-hr. Ti^{45}. Its disintegration seems to consist almost entirely of transitions from the ground state of Ti^{45} to the ground state of Sc^{45}, with perhaps a small percentage (not more than five or six percent) of the transitions going to an excited state of Sc^{45} 450 kev above the ground state.

Since Ti^{45} emits positrons, it can also decay by the K-capture process. On the basis of the calculations of Feenberg and Trigg[18] the ratio K/β^+ for $W_0=3m_0c^2$, $Z=22$ is 0.50 and the ratio K/β^+ for $W_0=2.1m_0c^2$, $Z=22$ is 1.6.

These results lead to ft-values[19] for the 1.02-Mev transitions of 1.17×10^4 which on the basis of Konopinski's[5] empirical classification is an allowed transition. The lower energy K-capture and positron transition has a lower limit for its ft-value of 1.95×10^5 which means, if it exists, that it is most probably first forbidden.

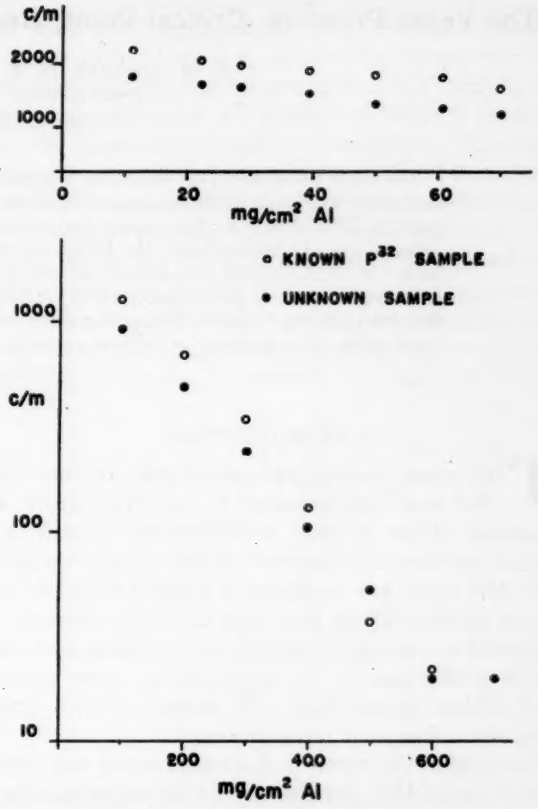

FIG. 6. Absorption curves for the unknown 14-day half-life activity in the chemically separated titanium fraction and for a known P^{32} sample from Oak Ridge. The P^{32} sample was prepared so that its total activity was of the same order of magnitude as the unknown sample. The absorber thickness indicated by the abscissa refers only to the total amount of aluminum interposed between sources and counter. In addition there was a 7-mg/cm² Duraluminum counter window and approximately 5 mg/cm² of air between sources and counter.

The authors are grateful to Mr. P. Hotz for help in scanning the cloud-chamber photographs.

[18] E. Feenberg and G. Trigg, Rev. Mod. Phys. (to be published).
[19] Values of f are again taken from calculations of Feenberg and Trigg.

The Vapor Pressure, Critical Point, Heat of Vaporization, and Entropy of Liquid He^3

B. M. Abraham, D. W. Osborne, and B. Weinstock
Argonne National Laboratory, Chicago, Illinois

(Received July 3, 1950)

The vapor pressure of pure liquid He^3 was measured from 1.025° to 3.35°K, and the data are represented accurately by the equation $\log_{10}p_{mm}=-0.97796/T+2.5\log_{10}T+0.000302T^2+1.91594$. The normal boiling point is 3.195±0.001°K. The critical temperature and pressure were determined to be 3.35±0.02°K and 890±20 mm Hg, respectively. The calculated heat of vaporization has a maximum value of 11.4±0.4 cal. $mole^{-1}$ at 2.1°K, and the extrapolated value at 0°K is 4.47 cal. $mole^{-1}$. The calculated entropy of liquid He^3, excluding the nuclear spin entropy, is 0.75±0.1 cal. $deg.^{-1}$ $mole^{-1}$ at 1°K, and the extrapolated value at 0°K is 0.42±0.1 cal. $deg.^{-1}$ $mole^{-1}$. This extrapolated value of the entropy suggests that below 1°K there is either a triple point or an anomaly in the heat capacity.

I. INTRODUCTION

THE vapor pressure and critical point of pure liquid He^3 were first measured by Sydoriak, Grilly, and Hammel.[1] Prior to their measurements certain theoretical considerations seemed to lead to the conclusion that He^3 could not condense to a liquid under its own vapor pressure.[2,3] De Boer and Lunbeck, however, by means of a quantum theory of corresponding states had made predictions of the approximate vapor pressure and critical temperature and pressure, which agreed with the subsequent measurements.[4]

Because of the theoretical importance of the properties of liquid He^3, particularly for an understanding of the behavior of liquid He^4, independent measurements seemed advisable. Furthermore, determinations of greater accuracy appeared necessary for the calculation of the heat of vaporization and the entropy of the liquid, as well as for the proper treatment of data on the vapor pressures of solutions of He^3 and He^4.

This paper presents comparative measurements of the vapor pressures of He^3 and He^4 from 1.025° to 3.35°K, measurements of the critical temperature and pressure, a vapor pressure equation which fits the He^3 data accurately, and calculations of the heat of vaporization and entropy of liquid He^3.

II. He^3 SAMPLE

The He^3 used in these experiments was obtained from the decay of tritium gas, which was prepared by neutron irradiation of lithium in a chain-reacting pile. The tritium was initially separated from He^4, also formed in the nuclear reaction, by diffusion of the tritium through a heated palladium thimble. Subsequently, the He^3 which had grown in was separated from the tritium by the same technique and was purified from traces of tritium by circulating the gas through a U-tube immersed in liquid helium. In this way 29.9 cc (NTP) of He^3 gas was obtained with a He^4 content, according to mass spectrometric analysis, of 0.03±0.03 percent.

III. APPARATUS

A schematic diagram of the cryostat is shown in Fig. 1. The nitrogen and helium dewars (*A* and *B*) had unsilvered viewing strips one cm wide. The helium dewar was held against a Neoprene gasket (*E*) in the cap (*D*) by means of three small stainless steel cables (*F*) and turnbuckles (*G*). The cap was bolted to an angle iron frame, which was in turn bolted to the floor. The vacuum space of the helium dewar was evacuated through tube (*C*), which was also used to admit dry nitrogen gas so that the apparatus could be precooled to liquid nitrogen temperatures. Ordinary helium was liquefied with a Collins liquefier and was transferred directly from the liquefier into the cryostat through the vacuum jacketed transfer tube[5] (*P*).

The pumping lead (*J*) was connected to a Kinney vacuum pump, with a displacement of 52 l/sec., through a 4-in. diameter iron pipe. A 4-in. diaphragm valve manufactured by the Hills-McCanna Company was used to regulate the pumping rate, so that the temperature could be held constant at any desired value between 1.025° and 4.2°K. An inclined differential manometer, filled with dibutyl phthalate, was connected to the cryostat pressure tube (*K*) and indicated the necessary adjustments of the valve. The reference volume was a 200-cc bulb immersed in an ice bath. Since this manometer had a 1:10 inclination, a one-mm change corresponded to a pressure difference of 0.008 mm of mercury. With this system the temperature could be held constant indefinitely to better than 0.001° for temperatures above about 1.4°K. Below this temperature the valve was set as closely as possible to maintain the desired pressure, and the pressure was then allowed to reach an equilibrium value.

The cryostat pressure tube (*K*) projected 43 cm below the top of dewar (*B*) into a region where the gas flow was laminar. A copper-constantan thermocouple was wound around the tube and soldered to the lower end, so that the temperature of that point could be measured for calculation of the thermomolecular pressure dif-

[1] Sydoriak, Grilly, and Hammel, Phys. Rev. **75**, 303 (1949).
[2] F. London and O. K. Rice, Phys. Rev. **73**, 1188 (1948).
[3] L. Tisza, Phys. Tod. **1**, 4 (1948).
[4] J. de Boer and R. J. Lunbeck, Physica **14**, 510 (1948).

[5] Similar to one described by M. C. Desirant and W. J. Horvath, Rev. Sci. Inst. **19**, 718 (1948), with the exception that the liquid nitrogen shield was omitted.

ference. The tube was connected to a dibutyl phthalate manometer (1.2 cm i.d.) for measuring pressures below 20 mm of mercury and to a mercury manometer (1.85 cm i.d.) for higher pressures, as well as to the inclined differential oil manometer.

The U-tube (*N*) was used for purification of the He^3 from traces of tritium.

In the first set of vapor pressure measurements (Series I), duplicate bulbs (*M*) were used for He^3 and He^4. These were drilled into a single block of copper and were of 0.05-cc capacity. The bulbs were suspended from the top of the cap by monel tubes (*L*) (0.051 cm i.d.), which were in turn connected to the manometers and filling line by means of small copper tubing. A constant volume mercury manometer (1.8 cm i.d.) was used for measuring the He^3 pressures. A similar mercury manometer was used for measuring He^4 pressures above 20 mm of mercury, and a dibutyl phthalate manometer (1.2 cm i.d.) was used for He^4 pressures below 20 mm of mercury. The metal tubes were protected from mercury vapor by means of glass capillary U-tubes immersed in liquid nitrogen.

The apparatus was modified for the critical point measurements (Series II). The connecting tubes were replaced with 0.05 cm i.d. glass capillary, and the bulbs were replaced by 3.5-cm lengths of 0.15 cm i.d. glass capillary. In addition, a stirrer for the helium bath was added. This consisted simply of a copper cage which was alternately raised and lowered by a solenoid at the top of the cryostat.

A further modification of the apparatus was made for Series III. As in Series I, the vapor pressure bulbs were made of a single block of copper, but the He^4 bulb was increased in volume to 0.20 cc, and the monel connecting tubes were made larger. The connecting tubes for the He^4 were of 0.508 cm i.d. and 0.005-cm wall thickness, and those for the He^3 were of 0.097 cm i.d. and 0.013-cm wall thickness. A radiation baffle was soldered into the He^4 connecting tube 20 cm above the bulb. The reasons for making these changes will be discussed below.

IV. VAPOR PRESSURE MEASUREMENTS

The entire sample of 29.9 cc (NTP) of He^3 gas was used for the vapor pressure measurements from 3.35° to 2.8°K, but to avoid possible overfilling of the bulb a smaller quantity was used at lower temperatures. The presence of a condensed phase was assured at the highest temperature for each sample size by establishing that the pressures in the He^3 and He^4 systems were independent of changes in the volumes of the systems.

Before each pressure measurement the temperature was held constant for at least 10 minutes. The stopcocks to the manometers were then closed simultaneously, and the manometer levels were read with cathetometers. Two cathetometers were used, one a Gaertner cathetometer which could be read to 0.03 mm, and the other a Henry Wild cathetometer which could be read to 0.01 mm. Both instruments were checked against a standard meter bar. The observed pressure readings were corrected to mm of mercury at 0°C and to the standard acceleration of gravity of 980.665 cm/sec.^{2} (i.e., to international mm of mercury). The local acceleration of gravity[6] was taken to be 980.278 cm/sec.^{2} Corrections were also applied for the temperature of the cathetometer scale, for the pressure exerted by the gas column in the tubes leading from the vapor bulbs to the manometer, and for the thermomolecular pressure difference.[7] The differences in meniscus heights were always small enough to make the meniscus corrections negligible. A factor to convert the readings of the

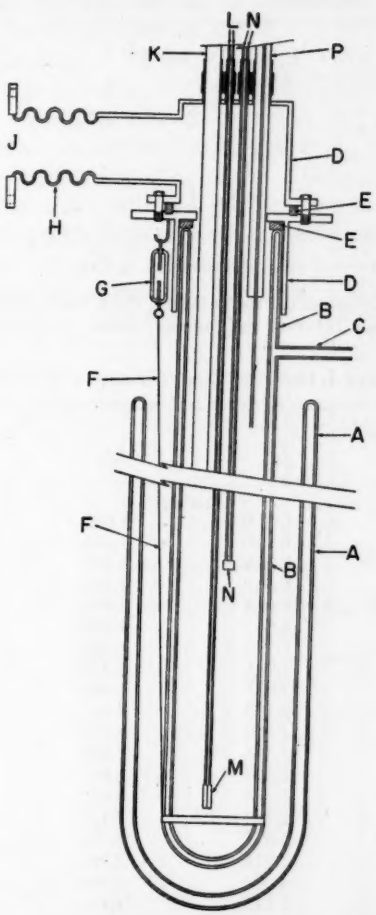

FIG. 1. Cryostat. A: liquid nitrogen dewar (Pyrex, 11.7 cm i.d., 90 cm inside length); B: liquid helium dewar (Pyrex, 5.9 cm i.d., 105 cm inside length); C: pumping lead for vacuum space of helium dewar; D: stainless steel cap; E: Neoprene gaskets; F: stainless steel cable; G: turnbuckle; H: brass bellows; J: pumping lead; K: cryostat pressure tube (monel, 0.823 cm i.d., 0.013 cm wall thickness); L: connecting tubes to vapor pressure bulbs (monel below cap, 0.051 cm i.d., 0.025-cm wall thickness; copper above cap); M: copper vapor pressure bulbs (0.05-cc capacity); N: monel U-tube for purification of He^3; P: vacuum-jacketed transfer tube from Collins helium liquefier.

[6] *International Critical Tables* (McGraw-Hill Book Company, New York, 1926), Vol. I, p. 396.

[7] Weber, Keesom, and Schmidt, Communs. Kamerlingh Onnes Lab. Univ. Leiden No. 246a (1936); S. Weber and G. Schmidt, Communs. Kamerlingh Onnes Lab. Univ. Leiden No. 246c (1936).

dibutyl phthalate manometers at room temperature to international mm of mercury was determined in each series of measurements by comparing the readings of the oil and mercury manometers at a pressure of approximately 20 mm of mercury.

Above the lambda-point the pressure in the He^4 vapor pressure bulb rather than that in the cryostat was always used to indicate the temperature of the He^3. This was done in order to eliminate any uncertainty regarding the temperature of the He^3 arising from heat leak down the connecting tubes, temperature gradients in the bath, and possible cold spots on the connecting tubes.

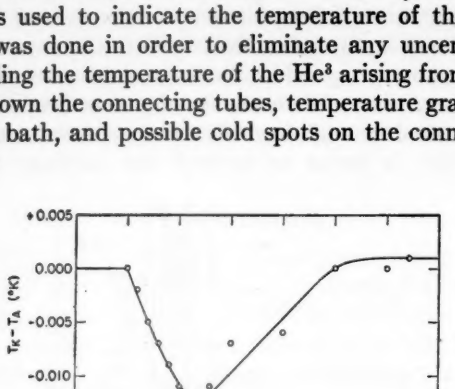

FIG. 2. Deviations of the temperature, T_K, according to Kistemaker (reference 11) from the "agreed" scale, T_A (reference 8).

TABLE I. Observed vapor pressure of liquid He^3.

$P(He^4)$ (int. mm Hg)	T_A (°K)	T_K (°K)	$P(He^3)$ (int. mm Hg)
	Series I		
0.152	1.025	1.025	9.71
0.346	1.121	1.121	14.74
0.551	1.183	1.183	18.68
1.746	1.363	1.363	34.16
3.811	1.513	1.513	52.59
6.853	1.647	1.644	72.78
11.94	1.792	1.785	99.65
19.82	1.945	1.935	135.0
27.40	2.057	2.046	165.1
37.17	2.175	2.162	201.1
46.60	2.269	2.257	234.2
61.44	2.393	2.382	282.7
80.78	2.527	2.517	342.4
96.89	2.623	2.614	389.8
117.1	2.729	2.722	446.6
132.7	2.802	2.796	489.0
157.7	2.911	2.906	555.3
181.5	3.004	2.999	616.9
213.5	3.115	3.112	697.4
241.4	3.206	3.203	765.6
278.8	3.314	3.312	856.0
	Series II		
0.154	1.026	1.026	9.81
0.179	1.042	1.042	10.46
0.205	1.058	1.058	11.29
267.2	3.282	3.280	827.7
276.3	3.307	3.305	849.9
278.9	3.314	3.313	856.5
280.3	3.318	3.316	859.5
292.4	3.351	3.350	888.7
	Series III		
0.172	1.038	1.038	10.41
0.549	1.182	1.182	18.79
1.192	1.298	1.298	28.00

Below the lambda-temperature there were neither temperature gradients in the bath nor cold spots on the connecting tubes. The effect of heat leak was overcome by having the bulbs immersed in the bath to a depth of at least 2.5 cm. Under these conditions, the pressures in the cryostat and He^4 vapor pressure bulb were expected to agree in the range where the thermomolecular pressure corrections could be neglected, since the impact pressure and pressure drop due to gas flow in the cryostat were negligible. Experimentally, they were found to agree within a pressure difference corresponding to 0.001°K from the lambda-temperature down to 1.7°K.

Below 1.7°K the cryostat pressure in Series I and II did not agree with that of the He^4 vapor pressure bulb, even after correction for thermomolecular pressure differences. This was due chiefly to the impracticably long time required for pressure equilibrium in the He^4 vapor pressure bulb system. The cryostat pressure was therefore used to determine the temperature of the He^3. This choice was further desirable because the thermomolecular pressure corrections which had to be applied to the He^4 vapor pressure bulb were too large to be made with sufficient accuracy and because there was an uncertain (although probably negligible) correction due to film flow.

In Series III the diameter of the connecting tube for the He^4 vapor pressure bulb was large enough for the pressure equilibrium time to be short and for the thermomolecular pressure corrections to be small even at the lowest temperature. In this series the cryostat and He^4 vapor pressure bulb agreed within 0.001°K.

For the He^3, the pressure equilibrium time was short and the thermomolecular pressure correction was negligible in all three series.

The experimental results are given in Table I. Columns 1 and 4 are the observed He^4 and He^3 vapor pressures, respectively, each entry being the average of two or more independent measurements. Column 2 is the "agreed" temperature, T_A, calculated from the He^4 pressure and the table given by van Dijk and Shoenberg,[8] which is essentially the Leiden 1937 scale[9] down to 1.6°K and the Bleaney and Simon scale[10] below 1.6°K. Column 3 is the temperature, T_K, calculated by applying to column 2 the corrections of Kistemaker,[11] smoothed as shown in Fig. 2. T_K rather than T_A was used in the derivation of the He^3 vapor pressure equation and in the thermodynamic calculations. This choice appears to be desirable because the heat of vaporization of He^4 at 0°K, calculated from Kistemaker's data, is much more nearly constant than that calculated from the 1937 scale. Also, van Dijk has recently obtained

[8] H. van Dijk and D. Shoenberg, Nature **164**, 151 (1949).
[9] G. Schmidt and W. H. Keesom, Physica **4**, 963 (1937); **4**, 971 (1937).
[10] B. Bleaney and F. Simon, Trans. Faraday Soc. **35**, 1205 (1939).
[11] J. Kistemaker, Physica **12**, 272, 281 (1946).

TABLE II. Vapor pressure of liquid He³ at even temperature intervals, from Eq. (4).

T_K (°K)	T_A (°K)	P (int. mm Hg)	dP/dT (mm/°)
1.0	1.000	8.68	41.3
1.1	1.100	13.51	55.9
1.2	1.200	19.93	72.7
1.3	1.300	28.13	91.7
1.4	1.400	38.33	112.6
1.5	1.500	50.72	135.5
1.6	1.603	65.50	160.3
1.7	1.705	82.85	186.9
1.8	1.807	102.94	215.2
1.9	1.909	125.94	245.2
2.0	2.011	152.04	276.9
2.1	2.112	181.38	310.2
2.2	2.213	214.13	345.1
2.3	2.312	250.46	381.6
2.4	2.411	290.50	419.6
2.5	2.510	334.44	459.3
2.6	2.609	382.41	500.5
2.7	2.708	434.59	543.2
2.8	2.807	491.13	587.6
2.9	2.906	552.18	633.6
3.0	3.005	617.89	681.1
3.1	3.104	688.45	730.3
3.2	3.203	764.02	781.2
3.3	3.302	844.74	833.8
3.195	3.198	760	

preliminary confirmation of Kistemaker's scale by magnetic measurements.[12]

It can be shown by equating the expressions for the Gibbs free energies of the liquid and of the saturated vapor, and neglecting the effects of nuclear spin, that the vapor pressure equation must be

$$\ln p = -\frac{\Delta H_0^0}{RT} + 2.5 \ln T + \ln(2\pi m)^{3/2} k^{5/2} h^{-3} - \frac{1}{RT}\int_0^T S_{\text{liq}} dT + \frac{1}{RT}\int_0^T V_{\text{liq}} \left(\frac{dp}{dT}\right)_{\text{sat}} dT - \frac{Bp}{RT} + \frac{1}{2}\left(\frac{Bp}{RT}\right)^2, \quad (1)$$

provided the liquid exists in equilibrium with the vapor at 0°K and the equation of state of the vapor can be expressed by

$$pV = RT[1 + B(T)/V]. \quad (2)$$

ΔH_0^0 is the heat of vaporization at 0°K, R is the gas constant, m is the mass of a He³ atom, k is Boltzmann's constant, h is Planck's constant, S_{liq} is the molal entropy of the liquid, V_{liq} is the molal volume of the liquid, and $(dp/dT)_{\text{sat}}$ is the slope of the vapor pressure curve. Equation (1) can be written in the form

$$\log_{10} p_{\text{mm}} = -A/T + 2.5 \log_{10} T + C + f(T), \quad (3)$$

where A and C are constants and $f(0) = 0$.

[12] H. van Dijk, Proceedings of the International Conference on the Physics of Very Low Temperatures, Massachusetts Institute of Technology (1949), p. 117.

Since $f(T)$ is only a correction term, it seemed reasonable to try $f(T) = DT^n$, and this function with $n = 3$ was found to be satisfactory. The constants A, C, and D were evaluated from the vapor pressure data in columns 3 and 4 of Table I by a least squares procedure in which the sum of the squares of the temperature deviations was minimized. The resulting vapor pressure equation is

$$\log_{10} p_{\text{mm}} = -0.97796/T_K + 2.5 \log_{10} T_K + 0.000302 T_K^3 + 1.91594. \quad (4)$$

Values of the pressure and of dp/dT calculated from Eq. (4) at 0.1° intervals from 1° to 3.3°K are given in Table II. The normal boiling point calculated from this equation is 3.195±0.001°K, in agreement with the previously reported value[1] of 3.20°K.

The deviations of the experimental data from Eq. (4) are plotted in Fig. 3 as temperature differences, $\Delta T = (p_{\text{calc}} - p_{\text{obs}})(dp/dT)^{-1}$, where p_{calc} and dp/dT are the pressure and slope calculated from the vapor pressure equation, and p_{obs} is the observed pressure. The deviations are within 0.001° except at the temperature extremes. In the neighborhood of the critical temperature there is a maximum deviation of 0.003°, and at the lowest temperature the deviations are within

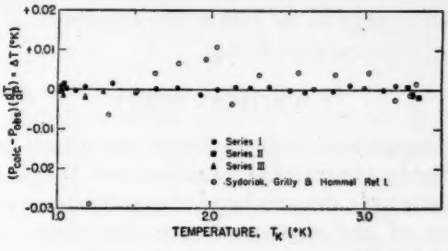

FIG. 3. Deviations from vapor pressure Eq. (4).

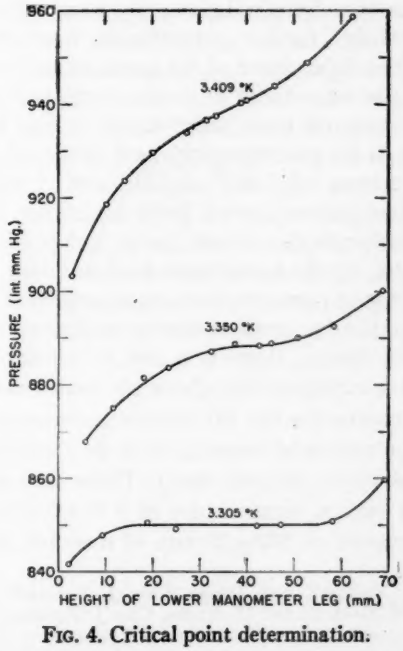

FIG. 4. Critical point determination.

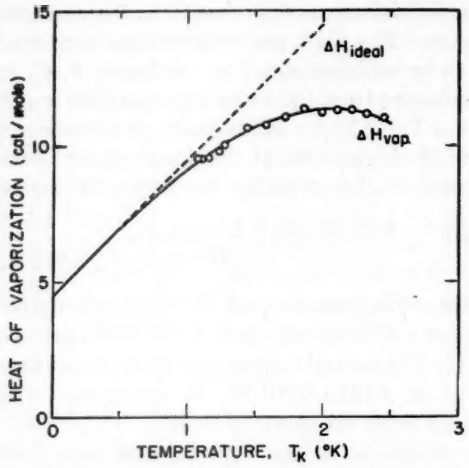

FIG. 5. Heat of vaporization of liquid He^3.

0.002°. It can also be seen from this figure that the three series of measurements are in excellent agreement with one another.

The deviations of the data of Sydoriak, Grilly, and Hammel[1] (corrected to the Kistemaker temperature scale) from Eq. (4) are also given in Fig. 3. Their deviations are considerably larger than those in the present work but appear to be within the experimental uncertainty of their measurements.

V. CRITICAL POINT

An attempt was made to locate the critical point of liquid He^3 by the classical visual method. Within experimental error the temperatures of appearance and disappearance of the meniscus were the same, namely, 3.317±0.001°K, and the corresponding measured pressure was 860±1 mm of mercury.

Since the visual method gives only a lower limit to the critical point,[13] further experiments were made by studying the dependence of the pressure on the volume of gas in the manometer at various temperatures. The observed pressures have been plotted in Fig. 4 against the height of the lower mercury level in the manometer, at temperatures of 3.305°, 3.350°, and 3.409°K. Although these curves are not $p-V$ isotherms, they can be used to locate the critical point. Below the critical temperature, as the manometer level is raised, there is an initial rise in pressure due to compression of the gas; next, there is a flat portion due to condensation to the liquid; and finally, there is a rise in pressure as the liquid in the capillary rises above the bath level. At the critical temperature the flat portion becomes an inflection with a horizontal tangent, since the densities of the liquid and vapor become equal. These measurements indicate a critical temperature of 3.35±0.02°K and a critical pressure of 890±20 mm of mercury, in agreement with the previously reported values of 3.34°K and 875 mm of mercury obtained by the same method.[1]

VI. HEAT OF VAPORIZATION

The heat of vaporization of He^3 was calculated from the thermodynamic relation,

$$\Delta H_{vap}=T(V_{gas}-V_{liq})dp/dT. \quad (5)$$

The molal volume of the gas, V_{gas}, was obtained from the equation of state (2), where the second virial coefficient, B, was taken from the computations of van Kranendonk, Compaan, and de Boer.[14] The molal volume of the liquid, V_{liq}, was taken from the experimental results of Grilly, Hammel, and Sydoriak,[15] and values of p and dp/dT were computed from Eq. (4).

The results are given in column 2 of Table III and by the solid curve in Fig. 5. The dashed curve in this figure shows the ideal heat of vaporization,

$$\Delta H_{ideal}=RT^2(d\ln p/dT). \quad (6)$$

The circles in Fig. 5 were obtained by using in Eq. (5) $\Delta p/\Delta T$ calculated from the successive experimental points of Series I and III (Table I) instead of dp/dT from Eq. (4). No calculations were made above 2.5°K because Eq. (2) is inadequate for the saturated vapor above this temperature.

The uncertainty in the heat of vaporization shown in Table III was estimated in the following way. Since the calculated values[14] of B for He^4 agree with the experimental ones[16] within about 10 percent, the uncertainty in the values of B calculated[14] for He^3 was taken to be 10 percent. An error in B of this magnitude causes an error in the heat of vaporization of 0.5 cal./mole at 2.5°K, 0.03 cal./mole at 1.0°K, and less at lower temperatures. The estimated error in the experimental values of the molal volume of the liquid is two to three percent,[15] and this results in an error in the heat of vaporization of 0.05 cal./mole at 2.5°K and less than 0.01 cal./mole at 1.0°K. Uncertainties in the slope of the temperature scale and in the measurements of the pressures together cause a one percent uncertainty in the heat of vaporization.

TABLE III. Heat of vaporization and entropy of liquid He^3.

T_K (°K)	ΔH_{vap} (cal. mole^{-1})	$\Delta H_{vap}/T$ (e.u.)[a]	$S_{ideal\ gas}$ (e.u.)	$S_{real}-S_{ideal}$ (e.u.)	S_{liq} (e.u.)
0	(4.47)	∞	∞	0.00	(0.42±0.11)
0.5	(6.95)	(13.89)	(14.34)	0.00	(0.45±0.12)
1.0	9.12±0.12	9.12	9.87	0.00	0.75±0.14
1.5	10.65±0.24	7.10	8.37	−0.02	1.25±0.17
2.0	11.34±0.41	5.67	7.62	−0.06	1.89±0.22
2.5	10.81±0.69	4.32	7.16	−0.11	2.73±0.29

[a] e.u. = cal. deg.$^{-1}$ mole^{-1}.

[13] Mason, Naldrett, and Maass, Can. J. Research **18B**, 103 (1940); S. N. Naldrett and O. Maass, Can. J. Research **18B**, 118 (1940).

[14] van Kranendonk, Compaan, and de Boer, Phys. Rev. **76**, 1728 (1949).

[15] Grilly, Hammel, and Sydoriak, Phys. Rev. **75**, 1103 (1949).

[16] J. Kistemaker and W. H. Keesom, Physica **12**, 227 (1946).

The values of the heat of vaporization previously reported by others[15] are in poor agreement with those presented here, chiefly because they were calculated from less accurate vapor pressure data.

VII. ENTROPY OF He^3

The entropy of liquid He^3 was calculated from the difference between the entropy of the saturated vapor and the entropy of vaporization. The entropy of the vapor was obtained from the Sackur-Tetrode equation,

$$S=2.5R\ln T-R\ln p_{\text{atmos}}+1.5R\ln M-2.314, \quad (7)$$

to which was added a small correction for non-ideality, calculated from Eq. (2). The effect of the Fermi-Dirac statistics is included in this correction. In accordance with the usual convention, the contribution of nuclear spin, $R\ln 2=1.377$ cal. deg.$^{-1}$ mole^{-1} for He^3, was not included. The entropy of vaporization was calculated from the heat of vaporization. The values of the fundamental constants used were those adopted in tabulations at the National Bureau of Standards.[17] The atomic weight, M was taken as 3.0162 on the chemical scale.[18]

The results are given in Table III. The indicated uncertainty in the entropy of the liquid from 1.0° to 2.5°K was calculated from the uncertainty in the heat of vaporization and an uncertainty of 0.002 to 0.004° in the temperature.

It is interesting to note that the entropy of the liquid at 0°K calculated by extrapolating the vapor pressure Eq. (4) is 0.42 ± 0.11 cal. deg.$^{-1}$ mole^{-1}. Since one would expect a value of zero from the third law of thermodynamics, it seems advisable to discuss the way in which the uncertainty in this value was obtained. The method was to estimate the limits of error in C, the constant term in the vapor pressure equation (3) or (4), since

$$S_{\text{liq},\,0^\circ\text{K}}=(2.0085-C)R\ln 10. \quad (8)$$

For this purpose, a vapor pressure equation was fitted to the data from 1.0° to 1.5°K. The data at higher temperatures were not used because it was desired to reduce the effect on C of the correction terms, which are more important above 1.5°K. The equation

$$\log_{10}p_{\text{mm}}=-(0.9807/T)+2.5\log_{10}T+1.9198 \quad (9)$$

was found to fit the experimental data with the same precision as Eq. (4) from 1.0° to 1.5°K, and the corresponding value of the entropy of the liquid at 0°K is 0.41 cal. deg.$^{-1}$ mole^{-1}, which is in agreement with the previous value.

Further, the effect of uncertainties in the temperature scale and in our experimental measurements were considered. Kistemaker[11] has estimated that the uncertainty in his measurement of the vapor pressure of He^4 against a gas thermometer is 0.003° at 1.5°K. The vapor pressure-temperature relation for He^4 below 1.5°K is a calculated one,[10,11] which joins Kistemaker's experimental results at 1.5°K. It can be shown that an error of 0.003° at 1.5°K will cause an error at 1.0°K of 0.0022° in the same direction. This error at 1.0°K could be changed by ±0.0016° if the error in the virial coefficient of gaseous He^4 at 1.5° is 10 percent, and by an additional ±0.0002° from the estimated one percent error[11] in the terms arising from the molal heat capacity and volume of liquid He^4 at lower temperatures. Our experimental error is 0.002° at 1.0°K and less than 0.001° at 1.5°K. The most unfavorable combination of these errors will change the temperature interval from 1.0° to 1.5°K by ±0.006°. This will result in a change in C of ±0.025, and hence a change in the entropy of the liquid at 0°K of ±0.11 cal. deg.$^{-1}$ mole^{-1}.

Another effect which must be considered is the possible alignment of the nuclear spins in the liquid at low temperatures, with a consequent loss of amount $R\ln 2$ in the entropy. Since this alignment cannot occur in the gas in the absence of a magnetic field, the entropy of the liquid at 0°K as calculated here would be smaller or negative, if there were any alignment in the liquid at 1°K. Hence, this effect cannot be used to explain the residual entropy of 0.4 cal. deg.$^{-1}$ mole^{-1}.

These considerations suggest that the extrapolation of the vapor pressure equation is not valid because there is a transition in liquid He^3 below 1°K. This transition may be to a solid in equilibrium with the vapor, with an entropy of fusion of 0.4 cal. deg.$^{-1}$ mole^{-1}, or there may be a hump in the heat capacity which will account for the remaining 0.4 cal. deg.$^{-1}$ mole^{-1}. The existence and nature of this transition, which is obviously of fundamental importance to the theory of liquid He^3 and He^4, will need to be investigated experimentally.

[17] Rossini, Pitzer, Taylor, Ebert, Kilpatrick, Beckett, Williams, and Werner, *Selected Values of Properties of Hydrocarbons*, National Bureau of Standards Circular C461 (U. S. Government Printing Office, Washington, D. C., 1947), p. 8.

[18] J. Mattauch and A. Flammersfeld, "Isotopic report," Zeits. f. Naturforsch. (1949).

On the Space Exchange Magnetic Moments of Light Nuclei*

LARRY SPRUCH**†
Massachusetts Institute of Technology, Cambridge, Massachusetts
(Received April 3, 1950)

The calculations were based on Sachs' phenomenological theory and on the independent particle model. Spin exchange moments were not included. Uncertainties in the parameters required to characterize the shell dimensions and the neutron-proton interaction, which was assumed to be of an entirely exchange nature, cause the calculated values to be uncertain by a factor of about 3; they are probably too large. For L-S coupling, the values found in the $1p$ shell for ^2P states for Li^7, Be^9, B^{11}, C^{13}, and N^{15}, and in the $1d$ shell for ^2D states for Ne^{21}, Na^{23}, Cl^{37}, and K^{39} were -0.04, -0.01, 0.1, 0.05, 0.1, -0.4, -0.1, 0.4, and 0.4 nuclear Bohr magnetons, respectively. For j-j coupling, the values found for $B^{11}(p_{3/2})^{-1}$, $C^{13}(p_{1/2})$, and $N^{15}(p_{1/2})$ were 0.2, -0.09, and 0.1, respectively. The signs and ratios of these values are such as to lead to the conclusion that the simple models used here cannot be brought into agreement with the data by the addition of space exchange contributions alone. The magnitudes are nevertheless reasonably large in some cases, and indicate that they must be included in any consistent theory of nuclear magnetic moments.

I. INTRODUCTION

NO theory thus far has accounted adequately for the experimental magnetic moments of even the light nuclei. The measure of success enjoyed by the various models is due largely to the spin contribution, which is the same for most of them. While it may well be that these models are inadequate, the possibility remains that agreement with the data might be achieved by the inclusion of the space and spin exchange magnetic moment contributions.

The complete exchange moment operator can only be derived by meson theory and as such is rather questionable. However, Sachs showed that the space exchange part, henceforth denoted by M_x, can be arrived at phenomenologically;[1] the potential is still arbitrary. While no definitive conclusion can be reached by a calculation which omits the spin exchange contribution,[2] the values of M_x obtained for a given model should be helpful in judging the validity of that model.

Sachs calculated M_x for the case of H^3 and obtained an extremely small value.[1] This was to be expected, since, as will be shown, M_x vanishes for an S state so that its non-zero value in H^3 is due to the small admixture of D state in H^3. We shall consider nuclei whose ground states are predominantly other than S states. We shall treat our ground states as pure states.

II. PROPERTIES OF THE SPACE EXCHANGE MAGNETIC MOMENT OPERATOR

The expression derived by Sachs can be written in the form

$$M_x=b\sum_\nu\sum_\pi\int(\psi, O_{\pi\nu x}\psi)d\tau, \qquad (1)$$

where

$$O_{\pi\nu x}=(i/a_0{}^2J_0)(\mathbf{r}_\pi\times\mathbf{r}_\nu)_x J_{\pi\nu}P_{\pi\nu},$$

and

$$b=J_0a_0{}^2M/\hbar^2.$$

Here M_x is in nuclear Bohr magnetons, the index x indicating its exchange nature, the indices ν and π refer to neutrons and to protons, respectively, $P_{\pi\nu}$ is the space exchange operator, $J_{\pi\nu}P_{\pi\nu}$ is the space exchange interaction, M is the proton mass, $\mathbf{r}$ is the distance of the nucleon from the center of gravity, and the subscript z represents the z component; a_0 and J_0, the range and strength of the space exchange interaction, have been introduced to make b and the integral dimensionless. The scalar product represents the summation over spins, and the space integration is over all particles.

There are a number of immediate consequences of the above form.

(a) To within the approximation of the equality of neutron-neutron and proton-proton forces, the M_x's of conjugate pairs of nuclei, that is, mirror nuclei, are equal in magnitude and opposite in sign.[1] This follows from the antisymmetry of the operator $O_{\pi\nu z}$ in neutrons and protons.

(b) As a special case of (a), we have that the M_x's of self-conjugate nuclei vanish.[1]

(c) The contribution to M_z of a neutron and a proton in a completely space symmetric or completely space antisymmetric state vanishes. This follows from the antisymmetry of the operator $O_{\pi\nu z}$ in neutrons and protons.

(d) The contribution to M_z of a neutron and a proton in space states which do not overlap vanishes. This follows from the presence of the operator $P_{\pi\nu}$.

(e) The M_x's of nuclei with zero orbital angular momentum vanish. In the independent particle model, since closed shells have no angular momenta, the contribution to M_z of a closed shell of neutrons interacting with a closed shell of protons vanishes. These follow from the fact that $O_{\pi\nu z}$ has the transformation properties of an $L=1$ function under space rotation.

* Originally reported at the meeting of the Am. Phys. Soc. (February 1950) at New York.
** AEC postdoctoral fellow.
† Now at New York University, Washington Square, New York, New York.
[1] R. G. Sachs, Phys. Rev. 74, 433 (1948).
[2] R. K. Osborne and L. L. Foldy have recently derived the spin exchange moments phenomenologically; the radial functions are however arbitrary. Phys. Rev. 79, 795 (1950).

The fact that a nucleon pair which contributes to M_x must consist of a neutron and a proton is physically evident since space exchange magnetic moments are due to exchange currents, and therefore charge must be exchanged.

III. MATRIX ELEMENTS ON THE INDEPENDENT PARTICLE MODELS[3]

The only models which we shall consider are the independent particle models, which are the ones which have enjoyed the most over all success. There are then three types of non-vanishing contributions to M_x:

(A) One of the nucleons is in a closed shell and the other is in an incomplete shell.

(B) The nucleons are in the same incomplete shell.

(C) The nucleons are in different incomplete shells. We shall have no occasion to consider contributions of this type.

We first study the case of *L-S coupling*. We consider type (A), and define $M_x(nl\gamma n'l')$ as the contribution to M_x due to the interaction between an incomplete shell of neutrons and protons with radial, orbital, and other quantum numbers n, l, and γ, respectively, and radial functions R_{nl}, and a complete shell of $2(2l'+1)$ neutrons and $2(2l'+1)$ protons with quantum numbers n' and l' and radial functions $R_{n'l'}$. We then find, as shown in Appendix I, that

$$M_x(nl\gamma n'l')=b\langle L_{\pi z}-L_{\nu z}\rangle_{\gamma l}2(2l'+1)I(nln'l'), \quad (2)$$

where $\langle L_{\nu z}\rangle_{\gamma l}$ and $\langle L_{\pi z}\rangle_{\gamma l}$ are the z components of the orbital angular momenta of the neutrons and protons, respectively, in the incomplete shell, and

$$I_{nln'l'}=(i/4\pi ma_0^2J_0)\int R_{nln'l'}(\pi,\nu)(\mathbf{r}_\nu\times\mathbf{r}_\pi)_z J_{\pi\nu}$$
$$\times Y_{lm}^*(\nu)Y_{lm}(\pi)P_{l'}(\cos\theta_{\pi\nu})d\tau_\pi d\tau_\nu.$$

m is any projection of l, Y_{lm} is a spherical harmonic, $P_{l'}$ is a Legendre function, and

$$R_{nln'l'}(\pi,\nu)=R_{nl}(r_\pi)R_{nl}(r_\nu)R_{n'l'}(r_\pi)R_{n'l'}(r_\nu).$$

Contributions of type (B) must usually be calculated explicitly by means of Eq. (1). However, if either the neutrons or the protons in the incomplete shell n, l form a closed subshell, Eq. (2) will be valid with $n'=n$, $l'=l$. Furthermore the number of explicit calculations can be reduced by means of hole theory. Thus the magnetic quantum numbers which are absent in the wave function of a nucleus are opposite in sign to those which are present in the nucleus which is its hole with respect to both neutrons and protons. For the contribution within an incomplete shell, $M_x(nl\gamma)$, if the nucleus and its hole have the same total angular momentum, J, we find[4]

$$M_x(nl\gamma)=-M_x(nl\gamma)(\text{hole})$$
$$+b\langle L_{\pi z}-L_{\nu z}\rangle_{\gamma l}2(2l+1)I_{nlnl}. \quad (3)$$

We turn now to *j-j coupling*. Though the elimination of the spin coordinates is no longer completely trivial,

TABLE I. Magnetic moments of the light nuclei with *L-S* coupling.

	M(exp)	State	$\langle L_{\pi z}\rangle$	M(non)	M_x		ΔM
Li^7	3.26	$^2P_{3/2}$	1/3	$\mu_p+1/3 = 3.12$	$-b(1/3)2I_{1110}$	≈-0.04	+0.14
Be^9	−1.18	$^2P_{3/2}$	1/3	$\mu_n+1/3 = -1.58$	$-b(1/3)2I_{1110}+b(3/5)I_{1111}$	≈-0.01	+0.40
B^{11}	2.69	$^2P_{3/2}$	2/3	$\mu_p+2/3 = 3.46$	$b(1/3)2I_{1110}+b(13/5)I_{1111}$	≈ 0.1	−0.77
C^{13}	0.70	$^2P_{1/2}$	4/9	$-(1/3)\mu_n+4/9 = 1.08$	$b(2/9)2I_{1110}+b(4/3)I_{1111}$	≈ 0.05	−0.38
N^{15}	(−)0.28	$^2P_{1/2}$	2/3	$-(1/3)\mu_p+2/3 = -0.26$	$b(2/3)(2I_{1110}+6I_{1111})$	≈ 0.1	−0.02
Ne^{21}		$^2D_{5/2}$	0	$\mu_n = -1.91$	$-b(2)(A)$	≈-0.4	
Ne^{21}		$^2D_{3/2}$	0	$-(3/5)\mu_n = 1.15$	$-b(9/5)(A)$	≈-0.4	
Na^{23}	2.22	$^2D_{3/2}$	3/5	$-(3/5)\mu_p+3/5 = -1.07$	$-b(3/5)(A)$	≈-0.1	+3.29
Cl^{37}	0.68	$^2D_{3/2}$	9/5	$-(3/5)\mu_p+9/5 = 0.13$	$b(9/5)(A+10I_{1212})$	$\approx+0.4$	+0.55
K^{39}	0.39	$^2D_{3/2}$	9/5	$-(3/5)\mu_p+9/5 = 0.13$	$b(9/5)(A+10I_{1212})$	$\approx+0.4$	+0.26

M(exp) is the experimental value of the magnetic moment in nuclear Bohr magnetons.
M(non) is the theoretical non-exchange value for *L-S* coupling.
$A=2I_{1210}+6I_{1211}+2I_{1230}$
$\Delta M=M(\text{exp})-M(\text{non})$.

TABLE II. Magnetic moments with *j-j* coupling.

	M(exp)	State	$\langle L_{\pi z}\rangle$	M(non)	M_x		ΔM
B^{11}	2.69	$(p_{3/2})^{-1}$	1	$\mu_p+1 = 3.79$	$b(2I_{1110}+4I_{1111})$	$\approx+0.2$	−1.10
C^{13}	0.70	$(p_{1/2})$	0	$-(1/3)\mu_n = 0.64$	$b(-2/3)(2I_{1110}+4I_{1111})$	≈-0.09	+0.06
N^{15}	(−)0.28	$(p_{1/2})$	2/3	$-(1/3)\mu_p+2/3 = -0.26$	$b(2/3)(2I_{1110}+(4+2)I_{1111})$	$\approx+0.1$	−0.02

M(exp) is the experimental value of the magnetic moment in nuclear Bohr magnetons.
M(non) is the theoretical non-exchange value for *j-j* coupling.
$\Delta M=M(\text{exp})-M(\text{non})$.

[3] An excellent review of the merits of the various models and a useful list of references to papers dealing with shell models is contained in a recent article by E. Feenberg, Phys. Rev. 77, 771 (1950). See also M. G. Mayer, Phys. Rev. 78, 16, 22 (1950).

[4] This is a functional rather than a numerical relationship, the parameters appearing in the I_{nlnl} being different for the nucleus and for its hole.

arguments similar to those of Appendix I lead to the result that the contribution to M_x due to the interaction of an incomplete shell with quantum numbers n, l, j, and γ, and of a closed shell with quantum numbers n', l', and j', is given by

$$M_x(nlj\gamma n'l'j')=b(L_{\pi z}-L_{\nu z})_{\gamma lj}(2j'+1)I_{nln'l'}. \quad (2')$$

As is quite reasonable, this differs from $M_x(nl\gamma n'l')$ in that $2(2l'+1)$ has been replaced by $(2j'+1)$, the number of particles in a closed shell of particles with quantum number j'. Here too the expression is valid within an incomplete shell, if either the neutrons or the protons form a closed subshell, with $n'=n$, $l'=l$, $j'=j$.

IV. APPLICATION TO LIGHT NUCLEI WITH *L–S* COUPLING

By argument (b) above, the only stable nuclei in the $1p$ shell with non-vanishing M_x's are Li^7, Be^9, B^{11}, C^{13}, and N^{15}. The theoretical values of $\langle L_{\pi z}\rangle$ and of $\langle L_{\nu z}\rangle$ (and of the non-exchange magnetic moments) are known for these nuclei.[5] The contributions due to the interaction of the particles in the $1p$ shell with the particles in the $1s$ shell follow immediately from Eq. (2). By (c), $M_x(11\gamma)(Li^7)=0$, since the proton and the two neutrons in the $1p$ shell are assumed to be in a space symmetric state; this is true for $j=3/2$ and for $j=1/2$. Only in the case of Be^9 must an explicit calculation be performed; using the wave function in Appendix II, one finds $M_x(11\gamma)(Be^9)=(3/5)bI_{1111}$. The others now follow from Eqs. (2) and (3).

The M_x's of O^{17} and F^{19} vanish to a first approximation, by (e), since these are predominantly in S-states. In the $1d$ shell we choose only some simple cases at the beginning and end of the shell. For Ne^{21}, Cl^{37}, and K^{39}, we have one neutron, three proton holes, and one proton hole, respectively, in the $1d$ shell, so that the specification of J, L, and S, uniquely determines the non-exchange magnetic moment and the M_x, the latter following from Eq. (2). We assume that the $(1d)(1d)^2$ configuration in Na^{23} is completely symmetric, in which case the state is $^2D_{3/2}$, $M_x(12\gamma)=0$, and $L_{\pi z}=(1/3)L_z$. Table I gives our results.

The numerical evaluation of the M_x's is discussed in Appendix III; since all of the relevant $I_{nln'l'}$ are positive and since b is positive, the signs of all of the M_x's but that of Be^9, where a difference of terms appears, are determined. The uncertainties in the parameters required to characterize the exchange interaction and the radial functions make the values uncertain by a factor of about two for the $1p$ shell nuclei and of about three for the $1d$ shell nuclei.

V. APPLICATION TO LIGHT NUCLEI WITH *j–j* COUPLING

We restrict our calculations to the simple cases where the assumption that the $p_{3/2}$ and $p_{1/2}$ shells fill in that order uniquely determines the wave functions, namely, B^{11} ($p_{3/2}$ proton hole), C^{13} ($p_{1/2}$ neutron), and N^{15} ($p_{1/2}$ proton). N^{15} has the same wave function and therefore the same M_x as in the case of L-S coupling. By Eq (2'), we have the results of Table II. In general M_x can be expected to be greater in absolute magnitude for j-j than for L-S coupling since in the latter case the wave functions are so constructed as to be as space-symmetric as possible. To put it in another way, where M_x within a shell does not vanish under either assumption, the two values will be of the same order of magnitude, but there will be cases, such as Li^7, where M_x within a shell will vanish for L-S but not for j-j coupling.

VI. CONCLUSIONS

While the magnitudes of the M_x's are uncertain by a factor of as much as 3 in some cases (the values given are probably too large), the signs of the M_x's are uniquely determined for all cases except possibly Be^9. These signs are in the wrong direction for the three j-j coupling cases considered (Table II) and for all of the L-S coupling cases other than Cl^{37} and K^{39} (Table I). The last two nuclei have the same non-exchange magnetic moments and their M_x's differ only very slightly due to the small difference in their dimensions and hence in their integrals. They should therefore have the same magnetic moments, which is again in contradiction with the data. One must therefore conclude that while the space exchange magnetic moments can be significantly large, the simple models used here can not be brought into agreement with the data by the addition of space exchange contributions alone.

The author takes pleasure in thanking Professor H. Feshbach for some interesting discussions. He should like also to thank Professor Weisskopf for the suggestion which led to the wave function representation used in Appendix II.

APPENDIX I

Evaluation of the $M_x(nl\gamma n'l')$

We define $M_x(nl\gamma n'l')$ as the contribution to M_x due to the interaction between an incomplete shell of s neutrons and t protons with quantum numbers n, l, and γ and a closed shell of $2(2l'+1)$ neutrons and $2(2l'+1)$ protons with quantum number n' and l'. (Many of the terms used in this appendix have been defined in Section III.) We need not antisymmetrize with respect to particles in different shells, and we thus have as our normalized wave function

$$\psi=\chi_1\chi_2\sum_{q,r}C_{qr}\Theta_q\Omega_r.$$

$\chi_1(1,\cdots 4l'+2)$ and $\chi_2(1,\cdots 4l'+2)$ are the same normalized wave functions, antisymmetric in the space and spin coordinates of the neutrons and protons, respectively, and constructed from the one particle functions $\varphi_{n'l'm_l'm_s'}$, where m_l' and m_s' are the projections of the orbital and intrinsic spin momenta. All values of m_l' and of m_s' appear in the closed shell functions χ_1 and χ_2. $\Theta_q(4l'+2+1,\cdots 4l'+2+s)$ and $\Omega_r(4l'+2+1,\cdots 4l'+2+t)$ are each an orthonormal set of functions, antisymmetric in the space and spin coordinates, constructed from the one particle functions $\varphi_{nlm_l^q m_s^q}$ and $\varphi_{nlm_l^r m_s^r}$ respectively. The superscripts q and r

[5] L. Rosenfeld, *Nuclear Forces* (Interscience Publishers, Inc., New York), Vol. II, p. 409. These values can in fact be calculated without the use of normalized wave functions. See Appendix II.

specify which set of values of m_l and m_s appear in that particular function. The C_{qr} are the expansion coefficients.

$M_x(nl\gamma n'l')$ can be broken up into the contribution due to the interaction of the neutrons in the (n, l) shell and the protons in the closed shell, $M_{x\nu}(nl\gamma n'l')$, and the contribution due to the interaction of the protons in the (n, l) shell and the neutrons in the closed shell, $M_{x\pi}(nl\gamma n'l')$. Since $O_{\pi\nu z}$ affects only one neutron and one proton at a time, all cross terms vanish and we find

$$M_{x\nu}(nl\gamma n'l')=b\sum_{\pi=1}^{4l'+2}\sum_{q,r}|C_{qr}|^2\sum_{m_l^q}\sum_{m_s^q}\times\int(\varphi_{nl}(\nu)_{m_l^q m_s^q}\chi_2(1,\cdots 4l'+2),$$

$$O_{\pi\nu z}\varphi_{nl}(\nu)_{m_l^q m_s^q}\chi_2(1,\cdots 4l'+2))d\tau.$$

Since the closed shell function χ_2 has no angular momenta, the angular momenta of $\varphi_{nlm_l^q m_s^q}\chi_2$ are those associated with $\varphi_{nlm_l^q m_s^q}$. We make use of the matrix relation[6]

$$(l, m_l^q, m_s^q|O_{\pi\nu z}|l, m_l^q, m_s^q)=m_l^q\times(1/m)(l, m|O_{\pi\nu z}|l, m),$$

where m is any projection of l. The spin coordinates give the factor unity, since $O_{\pi\nu z}$ is independent of spin. Proceeding along identical lines, we find for $\langle L_{\nu z}\rangle$, which is due to the neutrons in the (n, l) shell,

$$\langle L_{\nu z}\rangle_{\gamma l}=\sum_{q,r}|C_{qr}|^2\sum_{m_l^q}m_l^q.$$

Combining these results,

$$M_{x\nu}(nl\gamma n'l')=b\langle L_{\nu z}\rangle_{\gamma l}\sum_{\pi=1}^{4l'+2}(1/m)\int(\varphi_{nlm}(\nu)\chi_2, O_{\pi\nu z}\varphi_{nlm}(\nu)\chi_2)d\tau.$$

We now write $\varphi_{nlm}(\mathbf{r})=R_{nl}(r)Y_{lm}(\theta, \varphi)$, express $\chi_2(1, \cdots 4l'+2)$ in terms of its one particle components, use the Legendre addition theorem to perform the sum over m', the projection of l', and find, with a factor of 2 appearing due to summation over spins,

$$M_{x\nu}(nl\gamma n'l')=b\langle -L_{\nu z}\rangle_{\gamma l}2(2l'+1)I_{nln'l'}.$$

$I_{nln'l'}$ is independent of the m which appears in its definition. We write

$$I_{nln'l'}=(1/m)K_{nlmn'l'},$$

and shall choose values of m for convenience in integration.

To obtain $M_{x\pi}(nl\gamma n'l')$ we must replace $\langle -L_{\nu z}\rangle_{\gamma l}$ by $\langle L_{\pi z}\rangle_{\gamma l}$. The change in sign is due to the antisymmetry in neutrons and protons of $O_{\pi\nu z}$. Adding the expressions $M_{x\nu}(nl\gamma n'l')$ and $M_{x\pi}(nl\gamma n'l')$, we obtain Eq. (2) for $M_x(nl\gamma n'l')$.

APPENDIX II

Angular Dependence of the Ground-State Wave Functions of Odd Mass Nuclei in the lp Shell for L–S Coupling

While many properties of these nuclei depend only on their quantum numbers and symmetry properties, other properties depend in greater detail on the wave functions, which do not seem to have been tabulated for the assumption of the equality of nuclear forces. We let nucleons 5, 9, 13 and 6, 10, 14 and 7, 11, 15 and 8, 12, 16 represent, when present, neutrons with spin up or down, neutrons with spin down or up, protons with spin up or down, and protons with spin down or up, respectively, in the $1p$ shell. The functions must, of course, be antisymmetric in space in the particles with the same spin and isotopic spin. For any vectors **a**, **b**, and **c**, we define the completely symmetric vector

$$[\mathbf{a}, \mathbf{b}, \mathbf{c}]=(\mathbf{a}\cdot\mathbf{b})\mathbf{c}+(\mathbf{b}\cdot\mathbf{c})\mathbf{a}+(\mathbf{c}\cdot\mathbf{a})\mathbf{b}.$$

We let the unit vector $\mathbf{i}$ represent the i'th particle and $q=(4\pi)^{-1/2}$.

[6] E. U. Condon and G. H. Shortley, *Theory of Atomic Spectra* (Cambridge University Press, London, 1935), p. 63.

We define the vectors

$$\omega(\mathrm{Li}^7)=(9/5)^{1/2}q^3[5, 6, 7]$$
$$\omega(\mathrm{Be}^9)=(81/20)^{1/2}q^5(5\times 9)\times[6, 7, 8]$$
$$\omega(\mathrm{B}^{11})=(729/80)^{1/2}q^7[5\times 9, 6\times 10, 7\times 11]\times 8$$
$$\omega(\mathrm{C}^{13})=(3^7/80)^{1/2}q^9(5\cdot 9\times 13)[6\times 10, 7\times 11, 8\times 12]$$
$$\omega(\mathrm{N}^{15})=(3^8/16)^{1/2}q^{11}(5\cdot 9\times 13)(6\cdot 10\times 14)(7\cdot 11\times 15)(8\times 12).$$

The functions $\omega^{\pm 1}=(\omega_x\pm i\omega_y)/2^{1/2}$ and $\omega^0=\omega_z$ which have $L=1$, $m_L=\pm 1$ and 0, respectively, must be multiplied by the spin functions, antisymmetrized, and combined to obtain the function with the desired J and J_z. These functions have the greatest possible space symmetry consistent with the exclusion principle.

These functions, which are readily constructed, are convenient to handle and exhibit the relation between a nucleus and its hole with respect to both neutrons and protons. Furthermore, the non-exchange moments follow rather easily from them. Thus, in the case of the $^2P_{3/2}$ ground state of Be^9, for example, we have $J=J_z=3/2$, $L=L_z=1$, and $S=S_z=S_{\pi z}=1/2$. The $L=1$ function $(5\times 9)\times[6, 7, 8]$ is constructed from two functions, (5×9) and $[6, 7, 8]$, each with $L=1$, and each having $\langle L_z\rangle=1/2$. Since the function $[6, 7, 8]$ is completely symmetric, the protons 7 and 8 have $L_{\pi z}=2/3\times 1/2=1/3$, and thus $M(\mathrm{non})(\mathrm{Be}^9, {}^2P_{3/2})=\mu_p+1/3$. The normalization factors are not used.

APPENDIX III

Evaluation of the Integrals

For the explicit evaluation of the $I_{nln'l'}$ we set

$$J_{12}=-J_0\exp(-r_{12}^2/a_0^2)$$

and take oscillator functions for the R_{nl}. In particular,

$$R_{1l}=\left(\frac{2^{3l+7/2}l!}{\pi^{1/2}(2l+1)!}\right)^{\frac{1}{2}}(\alpha_{nl}/a_0)^{3/2}\rho^l\exp(-\rho^2),$$

$$R_{20}=(2^{9/2}/3\pi^{1/2})^{1/2}(\alpha_{20}/a_0)^{3/2}(2\rho^2-3/2)\exp(-\rho^2),$$

where we have let $\rho=\alpha_{nl}r/a_0$. a_0/α_{nl} is a measure of the dimension of the nl shell. It is then always possible to throw $I_{nln'l'}$ into the form

$$I_{nln'l'}=\int g(\rho_1^2, \rho_2^2, \boldsymbol{\rho}_1\cdot\boldsymbol{\rho}_2)\exp(-\beta\rho_1^2-\beta'\rho_2^2+p\boldsymbol{\rho}_1\cdot\boldsymbol{\rho}_2)d\tau_1 d\tau_2$$

$$=g\left(-\frac{\partial}{\partial\beta}, -\frac{\partial}{\partial\beta'}, \frac{\partial}{\partial p}\right)8\pi^3(4\beta\beta'-p^2)^{-3/2},$$

where $\beta=\beta'=1+\alpha_{nl}^2+\alpha_{n'l'}^2$ and $p=2$. The desired form can be obtained by taking $I_{11n'l'}=(1/1)K_{111n'l'}$ and

$$I_{12n'l'}=1/5[(1/1)K_{121n'l'}+4(1/2)K_{122n'l'}].$$

One finds

$$I_{1110}=(1/4)\alpha_{11}^5\alpha_{10}^3\gamma_{1110}^5$$
$$I_{1111}=(5/24)\alpha_{11}^3(\alpha_{11}^2+1)^{-7/2}$$
$$I_{1210}=(1/8)\alpha_{12}^7\alpha_{10}^3\gamma_{1210}^7$$
$$I_{1211}=(1/48)\alpha_{12}^7\alpha_{11}^5\gamma_{1211}^9(7+4\gamma_{1211}^{-2})$$
$$I_{1220}=(1/192)\alpha_{12}^7\alpha_{20}^3\gamma_{1220}^9\{(40\alpha_{20}^2+36\alpha_{20}^2\alpha_{12}^2)+(7\alpha_{20}^4+4\alpha_{20}^2+4\alpha_{20}^2\alpha_{12}^2-6\alpha_{12}^2-3\alpha_{12}^4)^2\}$$
$$I_{1212}=(7/32)\alpha_{12}^3(\alpha_{12}^2+1)^{-11/2}(9+4\alpha_{12}^2+4\alpha_{12}^4)$$

where

$$\gamma_{nln'l'}=2(\alpha_{nl}^4+2\alpha_{nl}^2+2\alpha_{nl}^2\alpha_{n'l'}^2+2\alpha_{n'l'}^2+\alpha_{n'l'}^4)^{-1/2}.$$

The nuclear range is taken as $a_0=1.5\times 10^{-13}$ cm, and the magnitude of the exchange interaction is taken as $J_0=55$ Mev. This J_0 is some average over the singlet and triplet state interactions, where it has been assumed that the entire interaction is of an exchange nature, so that J_0 may be too large by a factor of as much as two. The α_{nl} are fixed by setting $\bar{r}=1.4\times 10^{-13}B^{1/3}$, where $\bar{r}$ is the average value of r and B is the number of nucleons up through and including the shell under consideration. The $I_{nln'l'}$ are uncertain to within a factor of about two.

Electron Removal in Helium Afterglows*

R. A. JOHNSON, B. T. MCCLURE, AND R. B. HOLT
Department of Physics, Harvard University, Cambridge, Massachusetts

(Received June 1, 1950)

Observations of the electron density, visible and near ultraviolet light intensity, and spectrum associated with a 3000 Mc/sec. pulsed electrodeless discharge have been made. Our electron density data indicate recombination-type electron removal with a constant $\alpha = 1.0 \times 10^{-8}$ cm³/ion-sec. in reasonably good agreement with previous data. During the discharge, the spectrum of atomic helium predominates. In the afterglow, the band spectrum of He_2 predominates. The total energy radiated in the wave-length range 2000 to 8000A is estimated as 0.5 electron volts per electron removed. A maximum in the light intensity occurs a few hundred microseconds into the afterglow. The following mechanism is quantitatively consistent with all of our data: He^+ forms He_2^+ by undergoing a triple collision with two neutral atoms, after which the molecular helium ions combine with electrons.

I. INTRODUCTION

THE afterglow following a pulsed microwave electrodeless discharge through spectroscopically pure helium at pressures between 10 and 27 millimeters of mercury has been investigated. The spectral distribution and total intensity of light emitted between 2000 and 8000A, as well as the electron density, have been observed as a function of time after the end of the discharge pulse. The electron density measurements were made by observing the shift of the resonant frequency of a cavity in which the discharge occurred.[1] The total intensity of light emitted in various narrow wave-length regions was determined by using a gated photo-multiplier tube in conjunction with suitable optical filters. The spectral distribution of the emitted light was examined in detail by use of a rapidly rotating wheel having a slot through which the light passed (giving a time resolution of a few microseconds), in conjunction with a standard spectrograph. The entire apparatus has been described in some detail in a previous paper.[2]

Measurements of this type are of particular value in investigating the mechanism by which the electrons are removed from the plasma. It is frequently possible to choose conditions (such as pressure and electron density) so that only one mechanism is responsible for the removal of a large fraction of the electrons disappearing. It is possible to differentiate clearly (by means of electron density decay curves, pressure effects, etc.) between recombination, attachment, and ambipolar diffusion as methods of electron removal. Conditions were chosen in the present investigation to favor recombination as the principle method of electron removal.

II. MEASUREMENTS

Figure 1 shows the method of computing the recombination coefficient, α, defined by $dn/dt = -\alpha n^2$, where n is the electron density. When electrons are removed by recombination according to this formula, $1/n$ is a linear function of time with slope α. We assume that the total light intensity, I, is proportional to the rate of loss of electrons, and hence to n^2. The validity of this assumption is established by the linearity of the $1/I^{\frac{1}{2}}$ *vs.* t plot. A time in the afterglow at which experimental conditions particularly favor an accurate determination of the electron density is selected for the simultaneous determination of relative intensity, I, and the absolute electron concentration, n. This enables the assignment of the ordinate scale in $1/n$ which completes the determination of α by this method. Figure 2 shows the directly measured values of $1/n$ as a function of time. Observe that the value of α computed on this basis agrees with the more reliable value determined above to well within the experimental errors involved.

The purity and uniformity of our gas samples are attested to by the absence of the spectra of oxygen, nitrogen, or neon in bottles filled to pressures between 11 and 27 mm Hg by three independent methods. Spectrograms of our samples continuous wave excited show all the prominent atomic lines of un-ionized helium within the range of our instruments, but none of ionized helium. In addition to the line spectra, we observe the prominent molecular bands of He_2 with considerable intensity.

Spectra taken of the pulsed discharge at various times indicate a predominance of the molecular bands in the afterglow. In the presence of the strong field, i.e., during the discharge proper, the line spectrum predominates, presumably due to a high degree of excitation without ionization and to a relatively low concentration of molecules. It is interesting to note in this connection that previous work[3] has also shown the presence of strong band spectra in helium afterglows. It has even been noted that a shift in the relative intensities of the various bands occurs under appropriate conditions at times of the order of several milliseconds after the discharge. At any rate, the presence of this spectrum in helium afterglows indicates strongly that excited helium molecules are certainly formed during the after-

* This work was assisted by the ONR.

[1] M. A. Biondi and S. C. Brown, Phys. Rev. **76**, 1697 (1949).

[2] Holt, Richardson, Howland, and McClure, Phys. Rev. **77**, 239 (1950).

[3] L. Herman, Comptes Rendus **228**, 2016 (1949).

glow and have lives long enough to allow radiation. Any explanation of the electron removal process must take this into account.

The determination of the time variation of the relative light intensities has been supplemented by accurate estimates of the absolute intensities. We measure up to 3×10^{-2} watts radiated during the discharge. A comparison of the absolute intensity at some particular time in the afterglow with the corresponding value of αn^2 yields a value of 0.5 ev radiated (between 2000 and 8000A) per electron removed. This figure suggests that radiative recombination is a very important part of the mechanism of electron removal in helium, and may well account for essentially all of the electron removal.

The linear variation of $1/I^{\frac{1}{2}}$ used in measuring the recombination coefficient is observed only several hundred microseconds after the beginning of the afterglow. Immediately following the end of the discharge pulse, the intensity falls by a factor of about 30 and then rises to a rather broad maximum which occurs at a time varying from 50 to 1000 μsec. depending upon experimental conditions. The time at which this maximum occurs is found to be a sensitive function of the power fed to the discharge and thus of the number of ions existing at the end of the discharge. At an initial concentration of about 10^{12} ions/cm^3, the maximum occurs at 60 μsec. and is very well defined. As the power is decreased, the maximum occurs at later times and becomes broader until at about 1100 μsec. it is no longer discernable. This behavior suggests the mechanism outlined below.

III. THEORY

Let A denote the concentration of atomic ions; M, the concentration of molecular ions; α_1, the recombination coefficient between molecular ions and electrons; α_2, the recombination coefficient between atomic ions and electrons; and β, a constant characterizing the formation of molecular ions from atomic ions. We suppose that the atomic ions disappear in two ways. The usual recombination with electrons contributes the term $-\alpha_2 An$. Atomic ions are also removed by forming molecular ions in triple collisions. This process proceeds at the rate βA. Thus, the rate of change of A is $-\beta A-\alpha_2 An$. The molecular ions produced in the above reaction then disappear by recombination with electrons at the rate $-\alpha_1 Mn$. Thus, the rate of change of M is $\beta A-\alpha_1 Mn$. We also have the relation $n=M+A$ from conservation of charge within the plasma. In summary, the equations determining the concentrations as a function of time are:

$$\text{(a)}\quad \dot{A}=-\beta A-\alpha_2 An,$$
$$\text{(b)}\quad \dot{M}=\beta A-\alpha_1 Mn,$$
$$\text{(c)}\quad \dot{n}=-\alpha_1 Mn-\alpha_2 An,$$
$$\text{(d)}\quad n=M+A.$$

These equations are highly non-linear and not susceptible of analytic integration. A numerical integration has been performed in an attempt to fit a solution of these equations to the observed light intensity as a function of time. The constants and initial conditions needed for this numerical integration have been determined as follows.

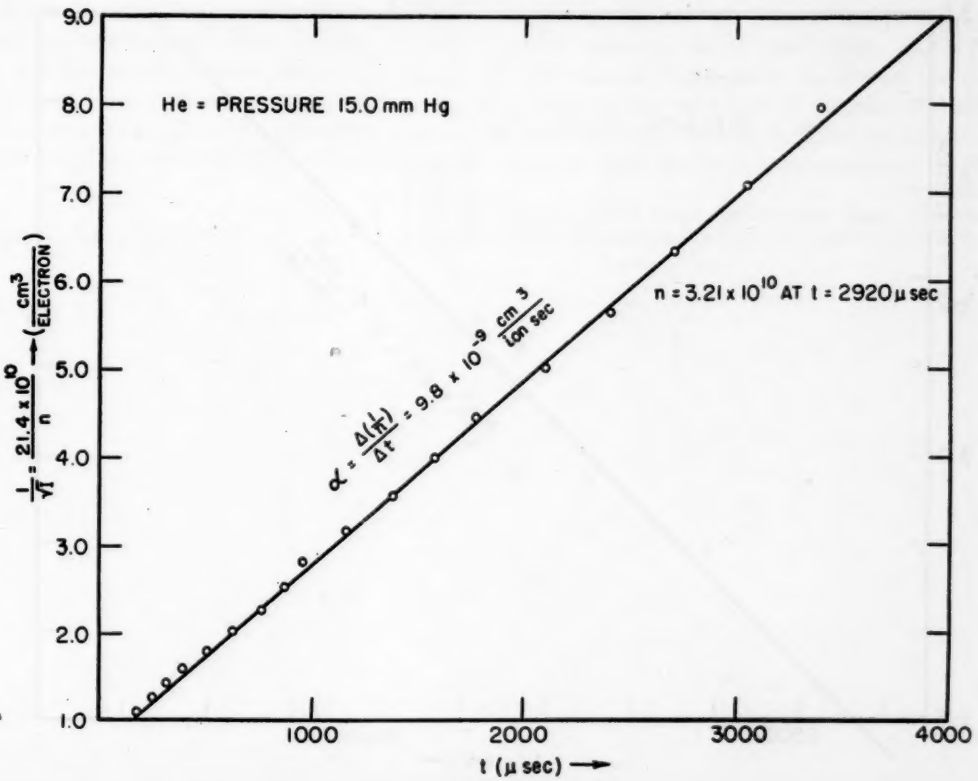

FIG. 1. Computation of α from light intensity data.

We assign the value 1.0×10^{-8} cm^3/ion-sec. (the value of α we measure for times far in the afterglow) to α_1 (the molecular recombination coefficient) since at these times we observe only the spectrum of the molecule. The choice of α_2 is of no consequence so long as it is of the same order of magnitude as α_1, or smaller. This will be apparent when we have evaluated the remaining constants. The concentration of electrons at the beginning of the afterglow, n_0, can be estimated quite accurately from an extrapolation of the observed electron density from times when this measurement is feasible. The remaining initial condition is the ratio of A_0 to M_0 (the initial atomic ion concentration to the initial molecular ion concentration). This ratio, when chosen to fit the observed light intensity just after the discharge, turns out to be about 10, which is a reasonable value. All of the ions created by the discharge are atomic ions (the neutral molecule is unstable), but some of the molecular ions created during the previous afterglow are still present in the plasma. Also a small number of molecular ions will be formed by triple collisions during the 8 μsec. discharge. The solutions of the equations are not markedly different for wide variations of the ratio A_0/M_0; therefore, no great accuracy is needed in determining it.

The remaining constant, β, is chosen to make the time of the maximum value of $\alpha_1 Mn$ (which is proportional to the light intensity due to recombination of molecular ions and electrons) agree with the observed maximum in the light intensity. Investigation of the solutions of the equations shows that the maximum value of $\alpha_1 Mn$ occurs only slightly before the maximum value of $\alpha_1 M^2$. Therefore, an approximate value of β can be determined by setting $dM/dt=\beta A-\alpha_1 Mn=0$ where all of the variables are assigned estimated values at the time of the maximum. Values of β which satisfy this condition are of the order of 10^4. Thus in Eq. (a) the term $\alpha_2 An$ is negligible if $\alpha_2 n$ is much less than 10^4. Since in our experiments n is less than 10^{11} and α_2 must be of the order of 10^{-8} or less we can neglect term $\alpha_2 An$ throughout. This is experimentally justified by the absence of atomic helium spectrum in the afterglow. The equation for the atomic ion concentration can now be integrated directly yielding $A=A_0e^{-\beta t}$. Substituting this into the approximate condition for the maximum in the light intensity, we get $t_{max}=(1/\beta)\ln(\beta A_0/\alpha_1 Mn)$ or still more approximately $t_{max}=(1/\beta)\ln(\beta/\alpha_1 A_0)$ which shows the dependence of the time of the maximum on the initial atomic ion concentration. Since the parameter β is the probability that an atomic ion make a triple collision multiplied by the probability that a molecular ion result from a collision between an atomic ion and two neutral atoms, it should vary as the pressure squared. A check on the variation of β with pressure was attempted by plotting various approximate functional relationships between measurable quantities. These showed an increase of β with pressure, but not as the pressure squared. It is thought that the approximations made were not sufficiently accurate to exhibit the correct dependence. The actual value of $\beta=10^4$ sec.$^{-1}$

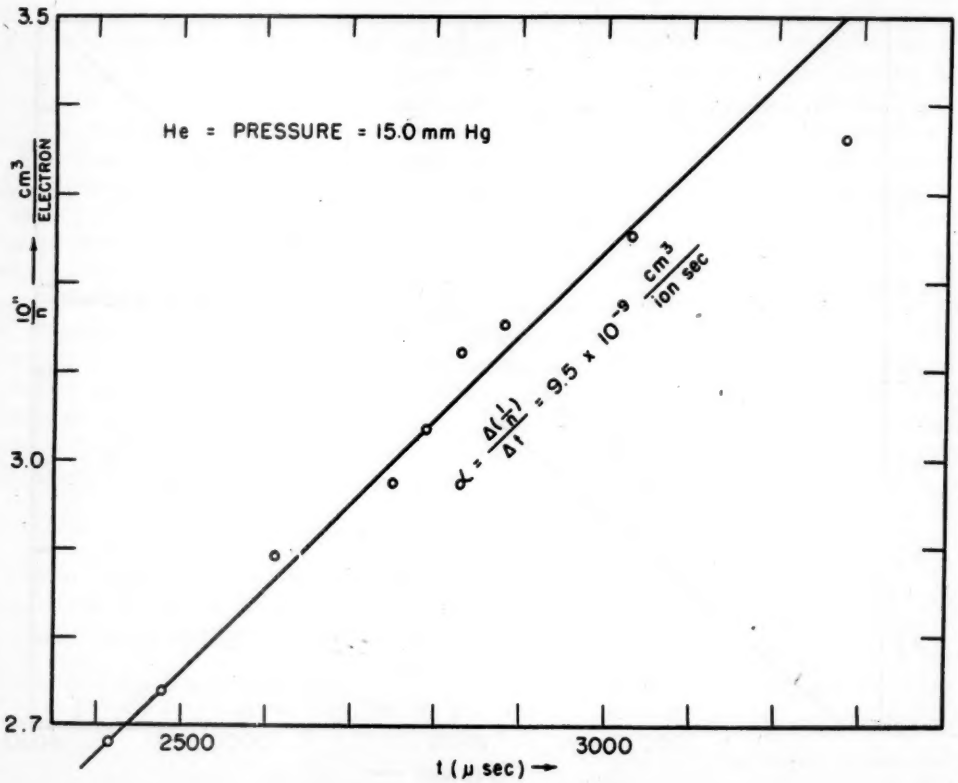

FIG. 2. Electron density as a function of time.

at 27 mm Hg (checked by comparing the results of numerical integrations with an experimental curve) corresponds to an effective radius of 2.0×10^{-8} cm for a collision between an atomic ion and two neutral atoms. This is to be compared with the kinetic theory value of 1.1×10^{-8} cm for neutral atoms in two-body collisions. Presumably, very accurate (and tedious) experimental and integration techniques would enable the pressure dependence of β to be determined by fitting curves. This did not appear to be practicable with the equipment at hand.

The integration was performed by Euler's method using Eqs. (a) and (c). The values of $A(t)$ can be written down immediately since the dependence is exponential. In (c) the term α_2An is negligible compared to α_1Mn after a very short time because of the rapid decrease in A and rapid increase in M. Therefore, α_2An can be neglected without materially affecting the results. The value of n at a time t_1 is determined from

$$n(t_1)=n(t_0)+(dn/dt)_{t_0}(t_1-t_0),$$

where

$$(dn/dt)_{t_0}=\alpha_1[n(t_0)-A(t_0)]n(t_0).$$

Convergence was indicated by comparing integrations using various time intervals. The results of an integration are given in Fig. 3, together with the experimental light intensity data. The relevant data on integration are: $A_0=9.5\times10^{10}$ ions/cm^3, $M_0=0.5\times10^{10}$ ions/cm^3, $\alpha_1=1.0\times10^{-8}$ cm^3/ion-sec., $\alpha_2=1.0\times10^{-8}$ cm^3/ion-sec., $\beta=10^4$ sec.$^{-1}$, and $\Delta t=10$ μsec.

Dissociative recombination has been proposed by Bates[4] as a possible mechanism for electron removal in cases where molecular ions are formed. It is thought that this is probably not the mechanism of the He_2^+ removal process in this case, since a *molecular* spectrum of high intensity is observed rather than the spectrum of excited *atoms* which would be expected from such a process.

[4] D. B. Bates, Phys. Rev. **77**, 718 (1950).

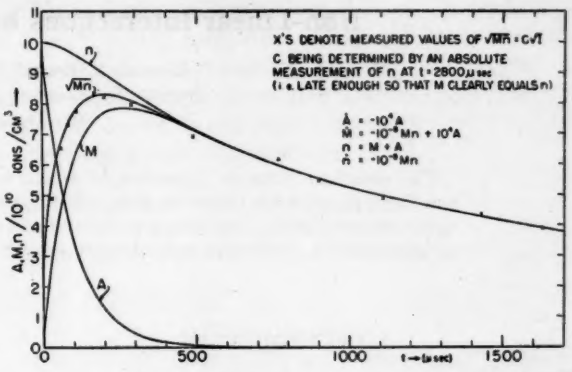

FIG. 3. The variation of time of M, A, n and $(Mn)^{\frac{1}{2}}$ as predicted by (a), (b), and (c).

It should be noted that an actual increase in electron density immediately after a microwave discharge in helium has been observed by Biondi.[5] This increase in initial density has been attributed to the formation of large numbers of metastables during the discharge and subsequently release of the energy so stored in the form of an increase of ionization in the plasma. No such increase in the electron density after the discharge was terminated was observed in our case, probably because of the higher initial electron densities present in our experiments and the higher pressures (helping to destroy metastables) used in the present investigation. Biondi's work does indicate, however, that the metastable population is quite large, which may well account for the collision cross section which we obtained for the formation of molecular ions being higher than that which would be expected on the basis of kinetic theory.

The authors wish to thank the group at MIT under the direction of Professor S. C. Brown for the preparation of one of the pure helium samples, and also to express appreciation to Mr. Al Redfield for assisting with the absolute light intensity measurements.

[5] M. A. Biondi, private communication and paper presented before the MIT conference on Physical Electronics, April 1950.

Non-Linear Interactions between Electromagnetic Fields

ROBERT KARPLUS*,† AND MAURICE NEUMAN‡
Institute for Advanced Study, Princeton, New Jersey
(Received June 12, 1950)

The covariant S-matrix formalism of Dyson has been applied to the calculation of the fourth order non-linear polarization of the vacuum, which is related to the lowest order non-linear interaction between electromagnetic fields. The finiteness and the gauge invariance of the interaction are exhibited explicitly by an expression for the fourth-rank vacuum polarization tensor in momentum space.

I. INTRODUCTION

IT has long been recognized that higher order corrections in quantum electrodynamics include non-linear interactions between electromagnetic fields.[1] They arise from the polarizability of the vacuum, from the possibility that transitions involve pairs only in intermediate states. Since such a correction depends on the operators of the electromagnetic field alone, it can be thought of as an addition of fourth degree in the field strengths to the electromagnetic Lagrangian density or as a non-diagonal contribution to the scattering matrix between matter-free states. The scattering of light by light, which has received some treatment in the literature,[2–5] is an example of a process which can be described by a specific interaction between photons.

Since the corrections we are discussing are necessarily at least of the order e^4, their calculation has involved considerable complications both because the treatment of effects involving virtual pairs has been traditionally accompanied by divergence and gauge-invariance difficulties and because the expressions encountered were lengthy and tedious to manipulate. With the promise the recent developments in quantum electrodynamics[6–9] give of eliminating the former and reducing the latter of these obstacles, it seemed worth while to re-examine the problem in spite of the smallness of the effects and the consequent difficulties attending their experimental detection. We have therefore rearranged the appropriate portion of the fourth order correction to the S-matrix to display explicitly its finiteness and gauge-invariance. To this end it has been expressed as a sum of terms each of which is a scalar product of derivatives of field strengths multiplied by a finite scalar non-local operator. The Fourier transforms of these are given as integrals over three parameters of rational functions of the momentum variables. The computation of a cross section requires only the well-known manipulations of the appropriate element of the scattering matrix in addition to the evaluation of the above-mentioned integrals for those values of the momenta which are of interest. The length of the expressions involved, however, makes the calculation of cross-sections very tedious except for simple special cases.

A quantity which plays an important role in the calculation is the vacuum polarization tensor $G_{\mu\nu\lambda\sigma}$ of fourth rank,

$$\delta j_\mu(x) = -(\alpha^2/12\hbar)\int G_{\mu\nu\lambda\sigma}(x, x', x'', x''')A_\nu(x') \times A_\lambda(x'')A_\sigma(x''')dx'dx''dx''', \quad (1)$$

where $\delta j_\mu(x)$ is that part of the current induced in the vacuum which is intrinsically cubic in the potential, and which cannot be reduced to lower order effects. This tensor, it will be shown, is finite and divergenceless with respect to all indices,

$$\frac{\partial}{\partial x_\mu}G_{\mu\nu\lambda\sigma}(x, x', x'', x''') = 0, \qquad \frac{\partial}{\partial x_\nu'}G_{\mu\nu\lambda\sigma}(x, x', x'', x''') = 0, \text{ etc.} \quad (2)$$

It will appear further that the tensor depends only on the mass of the pair field and on the nature of the coupling between the pair and vector fields. Hence Eq. (1) is valid even when $A_\mu(x)$ refers to a neutral vector meson fields, coupled vectorially to the pair field. The effective interaction Lagrangian density, $L(x)$, and the contribution to the scattering matrix, $S^{(4)}$, are simply related to the polarization tensor:

$$S^{(4)} = -\frac{i}{\hbar c}\int d^4x L(x) = \frac{-i\alpha^2}{(\hbar c)^2}\frac{1}{12}\int G_{\mu\nu\lambda\sigma}(x, x', x'', x''')A_\mu(x)A_\nu(x') \times A_\lambda(x'')A_\sigma(x''')dxdx'dx''dx'''. \quad (1')$$

---

* Frank B. Jewett Fellow.
† Now at Harvard University, Cambridge, Massachusetts.
‡ Now at Brookhaven National Laboratory, Upton, Long Island, New York.
[1] For a summary of the literature on this subject the reader is referred to A. Pais, "Developments in the Theory of the Electron" (Institute for Advanced Study and Princeton University, 1948), pp. 21–26.
[2] O. Halpern, Phys. Rev. 44, 855 (1934).
[3] H. Euler, Ann. d. Physik, 26, 398 (1936).
[4] W. Heisenberg and H. Euler, Zeits. f. Physik 98, 714 (1936).
[5] A. Achieser, Physik Zeits. Sowjetunion 11, 263 (1937).
[6] S. Tomonaga, Prog. Theor. Phys. 1, 27 (1946) and subsequent publications with co-authors.
[7] J. Schwinger, Phys. Rev. 73, 416 (1948); 74, 1439 (1948).
[8] R. P. Feynman, Phys. Rev. 76, 749, 769 (1949).
[9] F. J. Dyson, Phys. Rev. 75, 1736 (1949).

II. THE POLARIZATION TENSOR

The fourth-order term of the electrodynamic S-matrix which describes the non-linear effects in which we are interested is given by the Feynman diagram (Fig. 1) or by the integral over four four-spaces[9]

$$S^{(4)}=-(1/64)(e/\hbar c)^4\int d^4x_1d^4x_2d^4x_3d^4x_4 \times A_\mu(x_1)A_\nu(x_2)A_\lambda(x_3)A_\sigma(x_4) \times Tr\{\gamma_\mu S_F(x_2-x_1)\gamma_\nu S_F(x_3-x_2)\gamma_\lambda \times S_F(x_4-x_3)\gamma_\sigma S_F(x_1-x_4)\}. \quad (3)$$

$A_\mu(x)$ is the vector potential of a photon and/or a fixed electromagnetic field; $S_F(x)$ is the function characteristic of the fluctuations in the pair field,[9]

$$S_F(x)=-\frac{2i}{(2\pi)^4}\lim_{\epsilon\to 0^+}\int d^4p\frac{i(\gamma p)-\kappa}{p^2+\kappa^2-i\epsilon}e^{-ipx} \qquad \begin{pmatrix} px=\mathbf{p}\cdot\mathbf{r}-p_0x_0 \\ \kappa=mc/\hbar \end{pmatrix}. \quad (4)$$

The transition to momentum space, with

$$A_\mu(x)=(\hbar c)^{\frac{1}{2}}\int A_\mu(k)e^{ikx}d^4k, \quad (5)$$

yields

$$S^{(4)}=-\frac{i}{4}\alpha^2\int d^4x\int d^4k^{(1)}d^4k^{(2)}d^4k^{(3)}d^4k^{(4)} \times\exp[i(k^{(1)}+k^{(2)}+k^{(3)}+k^{(4)})x]A_\mu(k^{(1)})A_\nu(k^{(2)}) \times A_\lambda(k^{(3)})A_\sigma(k^{(4)})\tfrac{1}{3}G_{\mu\nu\lambda\sigma}{}^{(\kappa)}(k^{(1)},k^{(2)},k^{(3)},k^{(4)}), \quad (6)$$

where

$$G_{\mu\nu\lambda\sigma}{}^{(\kappa)}(k^{(1)},k^{(2)},k^{(3)},k^{(4)}) =T_{\mu\nu\lambda\sigma}{}^{(\kappa)}(k^{(1)},k^{(2)},k^{(3)},k^{(4)})+T_{\mu\nu\sigma\lambda}{}^{(\kappa)}(k^{(1)},k^{(2)},k^{(4)},k^{(3)}) +T_{\mu\lambda\nu\sigma}{}^{(\kappa)}(k^{(1)},k^{(3)},k^{(2)},k^{(4)}) \quad (7)$$

and

$$T_{\mu\nu\lambda\sigma}{}^{(\kappa)}(k^{(1)},k^{(2)},k^{(3)},k^{(4)}) =\frac{1}{i\pi^2}\int d^4pTr\left\{\gamma_\mu\frac{i\gamma p-\kappa}{p^2+\kappa^2-i\epsilon}\gamma_\nu\frac{i\gamma(p-k^{(2)})-\kappa}{(p-k^{(2)})^2+\kappa^2-i\epsilon} \times\gamma_\lambda\frac{i\gamma(p-k^{(2)}-k^{(3)})-\kappa}{(p-k^{(2)}-k^{(3)})^2+\kappa^2-i\epsilon} \times\gamma_\sigma\frac{i\gamma(p-k^{(2)}-k^{(3)}-k^{(4)})-\kappa}{(p-k^{(2)}-k^{(3)}-k^{(4)})^2+\kappa^2-i\epsilon}\right\}. \quad (8)$$

It will be understood from now on that integrals which depend on ϵ are to be evaluated in the limit as ϵ tends to zero through positive values. $\frac{1}{3}G_{\mu\nu\lambda\sigma}{}^{(\kappa)}$ is equivalent to $T_{\mu\nu\lambda\sigma}{}^{(\kappa)}$ in the integrand of Eq. (6) because of the symmetry of the remaining factors with respect to simultaneous permutations of $k^{(1)}$, $k^{(2)}\cdots$ and $\mu,\nu,\cdots$. $G_{\mu\nu\lambda\sigma}{}^{(\kappa)}$, of course, is completely symmetric with respect to these operations. Furthermore,

$$G_{\mu\nu\lambda\sigma}{}^{(\kappa)}(k^{(1)},k^{(2)},k^{(3)},k^{(4)}) =G_{\mu\nu\lambda\sigma}{}^{(\kappa)}(-k^{(1)},-k^{(2)},-k^{(3)},-k^{(4)}), \quad (9)$$

because the trace of the spinor product of an odd number of Dirac matrices vanishes.

At this stage the quantities $S^{(4)}$ and $G_{\mu\nu\lambda\sigma}{}^{(\kappa)}$ must be defined more precisely because they depend on the logarithmically divergent tensor $T_{\mu\nu\lambda\sigma}{}^{(\kappa)}$. This is accomplished by regularization:[10,11]

$$\bar{T}_{\mu\nu\lambda\sigma}=T_{\mu\nu\lambda\sigma}{}^{(\kappa)}-T_{\mu\nu\lambda\sigma}{}^{(M)} \quad (10)$$

and, correspondingly,

$$G_{\mu\nu\lambda\sigma}=\lim_{M\to\infty}[G_{\mu\nu\lambda\sigma}{}^{(\kappa)}-G_{\mu\nu\lambda\sigma}{}^{(M)}],$$

$$S^{(4)}=-\frac{i}{12}\alpha^2\int d^4x\int d^4k^{(1)}d^4k^{(2)}d^4k^{(3)}d^4k^{(4)} \times\exp[i(k^{(1)}+k^{(2)}+k^{(3)}+k^{(4)})x]A_\mu(k^{(1)}) \times A_\nu(k^{(2)})A_\lambda(k^{(3)})A_\sigma(k^{(4)}) \times G_{\mu\nu\lambda\sigma}(k^{(1)},k^{(2)},k^{(3)},k^{(4)}). \quad (11)$$

To verify the consistency of the theory, the finiteness and gauge-invariance of $S^{(4)}$, one may observe that the polarization tensor $G_{\mu\nu\lambda\sigma}$ is finite and that it satisfies the Fourier transform of Eq. (2),

$$k_\mu{}^{(1)}G_{\mu\nu\lambda\sigma}(k^{(1)},k^{(2)},k^{(3)},k^{(4)})=0, \quad k_\nu{}^{(2)}G_{\mu\nu\lambda\sigma}(k^{(1)},k^{(2)},k^{(3)},k^{(4)})=0, \text{ etc.} \quad (12)$$

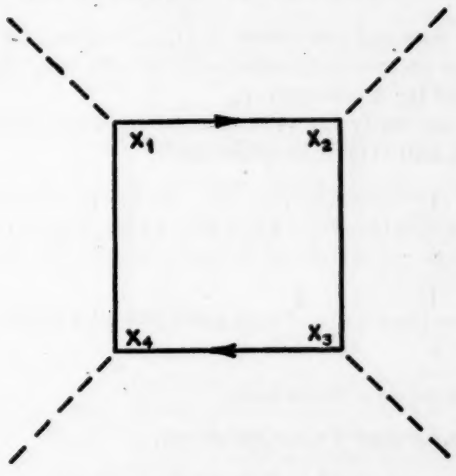

FIG. 1. The Feynman diagram.

[10] W. Pauli and F. Villars, Rev. Mod. Phys. 21, 434 (1949).

[11] Alternatively, the ambiguous integrals can be defined by demanding that $S^{(4)}$ be gauge-invariant. Equation (2) would then become a defining equation for $G_{\mu\nu\lambda\sigma}$.

Because $G_{\mu\nu\lambda\sigma}$ is symmetric these four equations are actually equivalent to one another.

That $G_{\mu\nu\lambda\sigma}$ is indeed finite may be seen more readily by separating the divergent terms in $T_{\mu\nu\lambda\sigma}{}^{(\kappa)}$ and $T_{\mu\nu\lambda\sigma}{}^{(M)}$:

$$\bar{T}_{\mu\nu\lambda\sigma}=T_{\mu\nu\lambda\sigma}{}^{0}+[T_{\mu\nu\lambda\sigma}{}^{(\kappa)}-T_{\mu\nu\lambda\sigma}{}^{(M)}-T_{\mu\nu\lambda\sigma}{}^{0}], \quad (13)$$

where

$$T_{\mu\nu\lambda\sigma}{}^{0}=\frac{1}{i\pi^2}\int d^4pTr\left\{\gamma_\mu\frac{i\gamma p-\kappa}{p^2+\kappa^2-i\epsilon}\gamma_\nu\frac{i\gamma p-\kappa}{p^2+\kappa^2-i\epsilon}\times\gamma_\lambda\frac{i\gamma p-\kappa}{p^2+\kappa^2-i\epsilon}\gamma_\sigma\frac{i\gamma p-\kappa}{p^2+\kappa^2-i\epsilon}-\gamma_\mu\frac{i\gamma p-M}{p^2+M^2-i\epsilon}\gamma_\nu\frac{i\gamma p-M}{p^2+M^2-i\epsilon}\times\gamma_\lambda\frac{i\gamma p-M}{p^2+M^2-i\epsilon}\gamma_\sigma\frac{i\gamma p-M}{p^2+M^2-i\epsilon}\right\}. \quad (14)$$

The quantity in brackets in Eq. (13) clearly approaches a finite limit as M becomes infinite. The tensor $T_{\mu\nu\lambda\sigma}{}^{0}$ is easily evaluated to be[12]

$$T_{\mu\nu\lambda\sigma}{}^{0}=\frac{1}{i\pi^2}\int d^4p\left\{(\delta_{\mu\nu}\delta_{\lambda\sigma}+\delta_{\mu\sigma}\delta_{\nu\lambda}-2\delta_{\mu\lambda}\delta_{\nu\sigma})\times\left[\frac{(4/3)(p^2)^2+4\kappa^2p^2}{[p^2+\kappa^2-i\epsilon]^4}-\frac{(4/3)(p^2)^2+4M^2p^2}{[p^2+M^2-i\epsilon]^4}\right]+(\delta_{\mu\nu}\delta_{\lambda\sigma}+\delta_{\mu\sigma}\delta_{\nu\lambda}-\delta_{\mu\lambda}\delta_{\nu\sigma})\times\left[\frac{\kappa^4}{[p^2+\kappa^2-i\epsilon]^4}-\frac{M^4}{[p^2+M^2-i\epsilon]^4}\right]\right\} \quad (15)$$

and so does not contribute to $G_{\mu\nu\lambda\sigma}$ because one term vanishes on symmetrization and the other on integration over the momentum p_μ.

One can verify Eq. (12), now, by the use of Eqs. (7), (8), (9), and (11), if he notes that

$$k_\mu{}^{(1)}\gamma_\mu=\frac{1}{i}[i\gamma(p-k^{(2)}-k^{(3)}-k^{(4)})+\kappa]-\frac{1}{i}[i\gamma p+\kappa] \quad (16)$$
$$=\frac{1}{i}[i\gamma p+\kappa]-\frac{1}{i}[i\gamma(p+k^2+k^3+k^4)+\kappa], \text{ etc.};$$

the resulting terms cancel in sets of four. A characteristic group is

$$(1/\pi^2)\int d^4pTr\left\{\frac{i\gamma p-\kappa}{p^2+\kappa^2-i\epsilon}\gamma_\nu\frac{i\gamma(p-k^{(2)})-\kappa}{(p-k^{(2)})^2+\kappa^2-i\epsilon}\gamma_\lambda\times\frac{i\gamma(p-k^{(2)}-k^{(3)})-\kappa}{(p-k^{(2)}-k^{(3)})^2+\kappa^2-i\epsilon}\gamma_\sigma-[\text{same with }\kappa\rightarrow M]-\frac{i\gamma p-\kappa}{p^2+\kappa^2-i\epsilon}\gamma_\lambda\frac{i\gamma(p+k^{(3)})-\kappa}{(p+k^{(3)})^2+\kappa^2-i\epsilon}\gamma_\nu\times\frac{i\gamma(p+k^{(2)}+k^{(3)})-\kappa}{(p+k^{(2)}+k^{(3)})^2+\kappa^2-i\epsilon}\gamma_\sigma+[\text{same with }\kappa\rightarrow M]\right\}=0. \quad (17)$$

These four terms come from $T_{\mu\nu\lambda\sigma}{}^{(\kappa)}(1234)$,

$$-T_{\mu\nu\lambda\sigma}{}^{(M)}(1234), \quad T_{\mu\lambda\nu\sigma}{}^{(\kappa)}(-1,-3,-2,-4),$$

and $-T_{\mu\lambda\nu\sigma}{}^{(M)}(-1,-3,-2,-4)$ in that order. (For simplicity, the $k^{(i)}$ have been replaced by i in the arguments of the tensors.) The displacement $p_\mu\rightarrow p_\mu-k_\mu{}^{(2)}-k_\mu{}^{(3)}$ in the third and fourth makes them equal to the first and second, respectively, except for sign.

III. METHOD OF CALCULATION

From Eqs. (7), (8) and (11) it is evident that the polarization tensor can be written

$$G_{\mu\nu\lambda\sigma}(1234)=\sum_{\substack{i=2,3,4\\j=1,3,4}}\sum_{\substack{l=1,2,4\\m=1,2,3}}A^{ijlm}(1234)k_\mu{}^{(i)}k_\nu{}^{(j)}k_\lambda{}^{(l)}k_\sigma{}^{(m)}+\sum_{\substack{l=1,2,4\\m=1,2,3}}B_1{}^{lm}(1234)\delta_{\mu\nu}k_\lambda{}^{(l)}k_\sigma{}^{(m)}+\sum_{\substack{j=1,3,4\\m=1,2,3}}B_2{}^{jm}(1234)\delta_{\mu\lambda}k_\nu{}^{(j)}k_\sigma{}^{(m)}+\cdots+C_1(1234)\delta_{\mu\nu}\delta_{\lambda\sigma}+C_2(1234)\delta_{\mu\lambda}\delta_{\nu\sigma}+C_3(1234)\delta_{\mu\sigma}\delta_{\nu\lambda}, \quad (18)$$

where the A, B, C are invariants which depend on scalar products of the four momenta. An expression of this form is obtained if the spinor summation and integration over p_μ, Eq. (8), are carried out. Because the four momenta are connected by the conservation equation, only three are independent; to maintain a symmetrical appearance of $G_{\mu\nu\lambda\sigma}$, the three were chosen in a way which is dependent on the vector index they carry, as illustrated by the restrictions on the summations in Eq. (18). The problem of obtaining an explicit expression for $G_{\mu\nu\lambda\sigma}$, and so $S^{(4)}$, can now be solved in a straight forward manner by obtaining the coefficients in Eq. (18) from Eqs. (7) to (11). This task is not as extensive as it seems, because the symmetry of the polarization tensor means that many invariants can be

[12] With the aid of the identities

(1) $\int p_\alpha f(p^2)d^4p=\int p_\alpha p_\beta p_\gamma f(p^2)d^4p=0,$

(2) $\int p_\alpha p_\beta f(p^2)d^4p=\frac{1}{4}\delta_{\alpha\beta}\int p^2f(p^2)d^4p,$

(3) $\int p_\alpha p_\beta p_\gamma p_\eta f(p^2)d^4p=\frac{1}{24}[\delta_{\alpha\beta}\delta_{\gamma\eta}+\delta_{\alpha\gamma}\delta_{\beta\eta}+\delta_{\alpha\eta}\delta_{\beta\gamma}]\times\int(p^2)^2f(p^2)d^4p.$

obtained from others by merely interchanging some of the momenta. Since $G_{\mu\nu\lambda\sigma}(k^{(1)}, k^{(2)}, k^{(3)}, k^{(4)})$ is invariant under simultaneous permutations of the arguments and indices, the following relations hold among the A's:

$$A^{2111}(1234)=A^{4441}(2341)=A^{3343}(3412)=A^{2222}(4123)$$
$$=A^{4111}(1432)=A^{2122}(2143)=A^{3222}(3214)=A^{4443}(4321)$$
$$=A^{3111}(1324)=A^{3313}(2413)=A^{2422}(3142)=A^{4442}(4231). \quad (19a)$$

$$A^{2121}(1234)=A^{4141}(2341)=A^{4343}(3412)=A^{2323}(4123)$$
$$=A^{2112}(1243)=A^{3113}(2314)=A^{3443}(3421)=A^{2442}(4132)$$
$$=A^{4422}(3142)=A^{3232}(4213)=A^{3311}(2413)=A^{4411}(3124). \quad (19b)$$

$$A^{2123}(1234)=A^{4121}(2341)=A^{4143}(3412)=A^{4323}(4123)$$
$$=A^{4341}(1432)=A^{2141}(2143)=A^{3221}(3214)=A^{2343}(4321)$$
$$=A^{3312}(1324)=A^{4311}(2431)=A^{4412}(3142)=A^{4232}(4213)$$
$$=A^{4421}(1342)=A^{3411}(2413)=A^{3321}(3124)=A^{3422}(4231)$$
$$=A^{2142}(1243)=A^{3112}(2314)=A^{3143}(3421)=A^{3422}(4132)$$
$$=A^{3413}(1423)=A^{2113}(2134)=A^{2412}(3241)=A^{2443}(4312). \quad (19c)$$

$$A^{2311}(1234)=A^{2441}(2341)=A^{3341}(3412)=A^{2342}(4123)$$
$$=A^{4113}(1432)=A^{4122}(2143)=A^{3123}(3214)=A^{4423}(4321)$$
$$=A^{3121}(1324)=A^{3441}(2431)=A^{2421}(3142)=A^{3423}(4213)$$
$$=A^{4113}(1342)=A^{4313}(2413)=A^{2312}(3124)=A^{4342}(4231)$$
$$=A^{2411}(1243)=A^{2313}(2314)=A^{4413}(3421)=A^{2423}(4132)$$
$$=A^{3141}(1423)=A^{3122}(2134)=A^{4143}(3241)=A^{3342}(4321). \quad (19d)$$

$$A^{2143}(1234)=A^{4321}(2341)=A^{3412}(1324). \quad (19e)$$

$$A^{2341}(1234)=A^{4123}(4321)=A^{2413}(1243)=A^{4312}(3124)$$
$$=A^{3142}(4312)=A^{3421}(2431). \quad (19f)$$

Some of these invariants, of course, are unchanged by certain interchanges of the momenta. Similar equations hold for the coefficients B and C, Eq. (18). These relations, therefore, considerably reduce the labor of finding all the coefficients.

One can, moreover, take advantage of the fact that the polarization tensor satisfies Eq. (12), in other words, that it is gauge-invariant. It is easy to show that a gauge-invariant tensor of the form Eq. (18) vanishes identically if all the coefficients A vanish. Hence, knowledge of the A's is sufficient to determine $G_{\mu\nu\lambda\sigma}$ completely and it becomes unnecessary to calculate the coefficients B and C at all.[13] They will therefore be ignored in the subsequent work. The terms which involve an A will be called "heads" or "leading terms."

One can take further advantage of the gauge-invariance of $G_{\mu\nu\lambda\sigma}$ by expressing this quantity as far as possible as the sum of simpler gauge-invariant tensors. These can be constructed from a consideration of scalar products of four field strengths, which will certainly give rise to gauge-invariant expressions. Thus one can define the tensors $g_{\mu\nu\lambda\sigma}{}^{(i)}$ as follows:

$$F_{\alpha\beta}(1)F_{\beta\alpha}(2)F_{\gamma\delta}(3)F_{\delta\gamma}(4)$$
$$=4A_\mu(1)A_\nu(2)A_\lambda(3)A_\sigma(4)g_{\mu\nu\lambda\sigma}{}^{(1)}(1234)$$
$$g_{\mu\nu\lambda\sigma}{}^{(1)}(1234)\sim k_\mu{}^{(2)}k_\nu{}^{(1)}k_\lambda{}^{(4)}k_\sigma{}^{(3)}, \quad (20)$$

$$F_{\alpha\beta}(1)F_{\beta\gamma}(2)F_{\gamma\delta}(3)F_{\delta\alpha}(4)$$
$$=A_\mu(1)A_\nu(2)A_\lambda(3)A_\sigma(4)g_{\mu\nu\lambda\sigma}{}^{(2)}(1234)$$
$$g_{\mu\nu\lambda\sigma}{}^{(2)}(1234)\sim k_\mu{}^{(2)}k_\nu{}^{(3)}k_\lambda{}^{(4)}k_\sigma{}^{(1)}$$
$$+k_\mu{}^{(4)}k_\nu{}^{(1)}k_\lambda{}^{(2)}k_\sigma{}^{(3)}, \quad (21)$$

$$F_{\alpha\beta}(1)F_{\beta\alpha}(2)k_\gamma{}^{(1)}F_{\gamma\delta}(3)F_{\delta\epsilon}(4)k_\epsilon{}^{(1)}$$
$$=-2A_\mu(1)A_\nu(2)A_\lambda(3)A_\sigma(4)g_{\mu\nu\lambda\sigma}{}^{(3)}(1234)$$
$$g_{\mu\nu\lambda\sigma}{}^{(3)}(1234)\sim[(k^{(3)}k^{(4)})k_\mu{}^{(2)}k_\nu{}^{(1)}k_\lambda{}^{(1)}k_\sigma{}^{(1)}$$
$$-(k^{(1)}k^{(3)})k_\mu{}^{(2)}k_\nu{}^{(1)}k_\lambda{}^{(4)}k_\sigma{}^{(1)}$$
$$-(k^{(1)}k^{(4)})k_\mu{}^{(2)}k_\nu{}^{(1)}k_\lambda{}^{(1)}k_\sigma{}^{(3)}], \quad (22a)$$

$$F_{\alpha\beta}(1)F_{\beta\alpha}(2)k_\gamma{}^{(2)}F_{\gamma\delta}(3)F_{\delta\epsilon}(4)k_\epsilon{}^{(1)}$$
$$=-2A_\mu(1)A_\nu(2)A_\lambda(3)A_\sigma(4)g_{\mu\nu\lambda\sigma}{}^{(4)}(1234)$$
$$g_{\mu\nu\lambda\sigma}{}^{(4)}(1234)\sim[(k^{(3)}k^{(4)})k_\mu{}^{(2)}k_\nu{}^{(1)}k_\lambda{}^{(2)}k_\sigma{}^{(1)}$$
$$-(k^{(2)}k^{(3)})k_\mu{}^{(2)}k_\nu{}^{(1)}k_\lambda{}^{(4)}k_\sigma{}^{(1)}$$
$$-(k^{(1)}k^{(4)})k_\mu{}^{(2)}k_\nu{}^{(1)}k_\lambda{}^{(2)}k_\sigma{}^{(3)}], \quad (22b)$$

$$k_\alpha{}^{(2)}F_{\alpha\beta}(4)F_{\beta\gamma}(1)[F_{\gamma\delta}(2)F_{\delta\epsilon}(3)-F_{\gamma\delta}(3)F_{\delta\epsilon}(2)]k_\epsilon{}^{(1)}$$
$$=A_\mu(1)A_\nu(2)A_\lambda(3)A_\sigma(4)g_{\mu\nu\lambda\sigma}{}^{(5)}(1234)$$
$$g_{\mu\nu\lambda\sigma}{}^{(5)}(1234)\sim[(k^{(2)}k^{(4)})(k_\mu{}^{(2)}k_\nu{}^{(3)}k_\lambda{}^{(1)}k_\sigma{}^{(1)}$$
$$-k_\mu{}^{(3)}k_\nu{}^{(1)}k_\lambda{}^{(2)}k_\sigma{}^{(1)})+(k^{(1)}k^{(4)})$$
$$\times(k_\mu{}^{(3)}k_\nu{}^{(1)}k_\lambda{}^{(2)}k_\sigma{}^{(2)}-k_\mu{}^{(2)}k_\nu{}^{(3)}k_\lambda{}^{(1)}k_\sigma{}^{(2)})]. \quad (23)$$

It should be noticed that Eq. (20) involves only heads in Eq. (19e), Eq. (21) those in Eq. (19f), Eq. (22) those in Eq. (19a–c), and Eq. (23) those in Eq. (19d). These few types of tensors, of course, need not be sufficient to express $G_{\mu\nu\lambda\sigma}$ completely. To find out to what extent they and their permutations are represented in $G_{\mu\nu\lambda\sigma}$ and what remainder is left after this is done, the coefficients A must be known more precisely. For this purpose we return to a consideration of $\bar{T}_{\mu\nu\lambda\sigma}$.

IV. EVALUATION OF THE POLARIZATION TENSOR

By the usual methods of carrying out the integration over the momenta of the virtual particles,[8] Eq. (10) can be transformed to

$$\bar{T}_{\mu\nu\lambda\sigma}(1234)=\frac{6}{i\pi^2}\int d\tau\int d^4p$$
$$\cdot Tr\left\{\frac{\gamma_\mu[i\gamma(p-\lambda^{(1)})-\kappa]\gamma_\nu[i\gamma(p-\lambda^{(2)})-\kappa]\times\gamma_\lambda[i\gamma(p-\lambda^{(3)})-\kappa]\gamma_\sigma[i\gamma(p-\lambda^{(4)})-\kappa]}{[p^2+\kappa^2-i\epsilon+(k^{(1)})^2y_4y_1+(k^{(2)})^2y_1y_2+(k^{(3)})^2y_2y_3+(k^{(4)})^2y_3y_4-(k^{(1)}+k^{(2)})(k^{(3)}+k^{(4)})y_2y_4-(k^{(1)}+k^{(4)})(k^{(2)}+k^{(3)})y_1y_3]^2}-[\text{same with }\kappa\to M]\right\}, \quad (24)$$

[13] The method of defining the ambiguous integrals by requiring gauge-invariance consists of calculating the coefficients A and constructing B's and C's that make the tensor gauge-invariant. This is the case because the A's are unambiguous while the C's are ambiguous. The method is therefore completely equivalent to regularization.

where

$$\begin{aligned}\lambda_\mu^{(1)} &= -k_\mu^{(1)}y_4 + k_\mu^{(2)}(y_2+y_3)+k_\mu^{(3)}y_3,\\ \lambda_\mu^{(2)} &= -k_\mu^{(2)}y_1+k_\mu^{(3)}(y_3+y_4)+k_\mu^{(4)}y_4,\\ \lambda_\mu^{(3)} &= +k_\mu^{(1)}y_1 - k_\mu^{(3)}y_2+k_\mu^{(4)}(y_4+y_1),\\ \lambda_\mu^{(4)} &= k_\mu^{(1)}(y_1+y_2)+k_\mu^{(2)}y_2 - k_\mu^{(4)}y_3,\end{aligned} \tag{25}$$

and

$$\int d\tau = \int\int\int\int_{y_i>0,\ \Sigma y_i=1} dy_1dy_2dy_3dy_4.$$

Since only the leading terms are of interest, the quantities $i\gamma p$ and κ or M in the numerators of the two terms may be dropped; as was already pointed out (see Eq. (9) and note to Eq. (15)), they contribute only quadratically and are then accompanied by a factor $\delta_{\mu\nu}$, so that they constitute part of a term B or C, Eq. (18). Then the regularizing term becomes of order M^{-4} and vanishes as the auxiliary mass tends to infinity. Hence, as far as head terms are concerned, the integration over the momentum p_μ in Eq. (24) becomes trivial, and

$$\bar{T}_{\mu\nu\lambda\sigma}(1234)\sim\frac{1}{\kappa^4}\int d\tau D(1234) \cdot Tr\{\gamma_\mu\gamma\lambda^{(1)}\gamma_\nu\gamma\lambda^{(2)}\gamma_\lambda\gamma\lambda^{(3)}\gamma_\sigma\gamma\lambda^{(4)}\}. \tag{26}$$

Here

$$\begin{aligned}D(1234) = \{1 &- i\epsilon' + (1/\kappa^2)[(k^{(1)})^2y_4y_1+(k^{(2)})^2y_1y_2\\ &+(k^{(3)})^2y_2y_3+(k^{(4)})^2y_3y_4-(k^{(1)}+k^{(2)})(k^{(3)}+k^{(4)})y_2y_4\\ &-(k^{(1)}+k^{(4)})(k^{(2)}+k^{(3)})y_1y_3]\}^{-2}\end{aligned} \tag{27}$$

with $\epsilon'=\epsilon/\kappa^2$.

A further simplification results from the consideration of heads only when the spin sum in Eq. (26) is carried out, because all but twenty-four terms may be ignored. Thus

$$\begin{aligned}&Tr\{\gamma_\mu\gamma\lambda^{(1)}\gamma_\nu\gamma\lambda^{(2)}\gamma_\lambda\gamma\lambda^{(3)}\gamma_\sigma\gamma\lambda^{(4)}\}\\ &\sim 4[(\lambda_\mu^{(1)}\lambda_\nu^{(2)}+\lambda_\mu^{(2)}\lambda_\nu^{(1)})(\lambda_\lambda^{(3)}\lambda_\sigma^{(4)}+\lambda_\lambda^{(4)}\lambda_\sigma^{(3)})\\ &\quad+(\lambda_\mu^{(1)}\lambda_\nu^{(3)}+\lambda_\mu^{(3)}\lambda_\nu^{(1)})(\lambda_\lambda^{(2)}\lambda_\sigma^{(4)}-\lambda_\lambda^{(4)}\lambda_\sigma^{(2)})\\ &\quad+(\lambda_\mu^{(1)}\lambda_\nu^{(4)}+\lambda_\mu^{(4)}\lambda_\nu^{(1)})(\lambda_\lambda^{(2)}\lambda_\sigma^{(3)}+\lambda_\lambda^{(3)}\lambda_\sigma^{(2)})\\ &\quad+(\lambda_\mu^{(2)}\lambda_\nu^{(3)}-\lambda_\mu^{(3)}\lambda_\nu^{(2)})(\lambda_\lambda^{(4)}\lambda_\sigma^{(1)}-\lambda_\lambda^{(1)}\lambda_\sigma^{(4)})\\ &\quad+(\lambda_\mu^{(4)}\lambda_\nu^{(2)}-\lambda_\mu^{(2)}\lambda_\nu^{(4)})(\lambda_\lambda^{(1)}\lambda_\sigma^{(3)}+\lambda_\lambda^{(3)}\lambda_\sigma^{(1)})\\ &\quad+(\lambda_\mu^{(3)}\lambda_\nu^{(4)}-\lambda_\mu^{(4)}\lambda_\nu^{(3)})(\lambda_\lambda^{(1)}\lambda_\sigma^{(2)}-\lambda_\lambda^{(2)}\lambda_\sigma^{(1)})].\end{aligned} \tag{28}$$

It must be remembered, of course, that the $\lambda^{(i)}$ have to be expressed in terms of the three momenta appropriate to the index the $\lambda^{(i)}$ carries in accordance with the convention adopted with Eq. (18). By substitution of Eq. (25) into Eq. (28) one can then express $\bar{T}_{\mu\nu\lambda\sigma}$ in the form

$$\bar{T}_{\mu\nu\lambda\sigma}(1234)\sim \sum_{\substack{i=2,3,4\\ j=1,3,4}}\ \sum_{\substack{l=1,2,4\\ m=1,2,3}} A_1^{ijlm}(1234)k_\mu^{(i)}k_\nu^{(j)}k_\lambda^{(l)}k_\sigma^{(m)}, \tag{29}$$

where the $A_1^{ijlm}(1234)$ are the contributions of $\bar{T}_{\mu\nu\lambda\sigma}(1234)$ to the coefficients A in Eq. (18). Because $\bar{T}_{\mu\nu\lambda\sigma}$ is less symmetric than $G_{\mu\nu\lambda\sigma}$, as many as fifteen of the A_1 must be obtained before the remainder can be generated by symmetry operations. Such a set may consist of the following:

$$A_1^{2111}(1234) = \frac{8}{\kappa^4}\int d\tau y_1(y_2+y_3+y_4)(y_1+y_2-y_3-y_4) \times(y_1+y_2+y_3-y_4)D(1234), \tag{30a}$$

$$A_1^{3111}(1234) = \frac{-8}{\kappa^4}\int d\tau (y_1+y_2)(y_3+y_4)(y_2+y_3+y_4-y_1) \times(y_1+y_2+y_3-y_4)D(1234), \tag{30b}$$

$$A_1^{2121}(1234) = \frac{-8}{\kappa^4}\int d\tau y_1(y_2+y_3+y_4)(y_1+y_3+y_4-y_2) \times(y_1+y_2+y_3-y_4)D(1234), \tag{31a}$$

$$A_1^{2112}(1234) = \frac{8}{\kappa^4}\int d\tau y_1(y_2+y_3+y_4)(y_1+y_2-y_3-y_4) \times(y_2+y_3-y_1-y_4)D(1234), \tag{31b}$$

$$A_1^{3311}(1234) = \frac{8}{\kappa^4}\int d\tau (y_1+y_2)(y_3+y_4)(y_1+y_3+y_4-y_2) \times(y_1+y_2+y_3-y_4)D(1234), \tag{31c}$$

$$A_1^{2113}(1234) = -\frac{8}{\kappa^4}\int d\tau y_1(y_2+y_3+y_4)(y_1+y_2-y_3-y_4) \times(y_1+y_2+y_4-y_3)D(1234), \tag{32a}$$

$$A_1^{3112}(1234) = -\frac{8}{\kappa^4}\int d\tau (y_1+y_2)(y_3+y_4)(y_2+y_3-y_1-y_4) \times(y_2+y_3+y_4-y_1)D(1234), \tag{32b}$$

$$A_1^{2141}(1234) = \frac{8}{\kappa^4}\int d\tau y_1(y_2+y_3+y_4)(y_1+y_2+y_3-y_4) \times(y_1+y_2+y_4-y_3)D(1234), \tag{32c}$$

$$\begin{aligned}A_1^{2311}(1234) = -A_1^{3121}(1234) = \frac{4}{\kappa^4}\int d\tau &(y_1+y_2+y_3-y_4)\\ &\times\{(y_1+y_3)[y_1y_2+(1-y_1)(1-y_3)]\\ &+(y_3+y_4)[y_1(1-y_2)+y_2(1-y_1)]\}D(1234),\end{aligned} \tag{33a}$$

$$\begin{aligned}A_1^{2411}(1234) = \frac{4}{\kappa^4}\int d\tau &(y_1+y_2-y_3-y_4)\\ &\times\{(y_1+y_4)[y_1y_4+(1-y_1)(1-y_4)]\\ &+(y_2+y_3)[y_4(1-y_1)+y_1(1-y_4)]\}D(1234),\end{aligned} \tag{33b}$$

$$\begin{aligned}A_1^{2413}(1234) = -\frac{4}{\kappa^4}\int d\tau \{&[(y_2+y_3)(y_3+y_4)\\ &+(y_1+y_2)(y_1+y_4)][y_1y_3+(1-y_1)(1-y_3)]\\ &+[(y_1+y_4)(y_3+y_4)+(y_1+y_2)(y_2+y_3)]\\ &\times[y_1(1-y_3)+y_3(1-y_1)]\}D(1234),\end{aligned} \tag{34a}$$

$$\begin{aligned}A_1^{2341}(1234) = \frac{4}{\kappa^4}\int d\tau \{&[(1-y_4)(1-y_3)+y_3y_4]\\ &\times[(1-y_1)(1-y_2)+y_1y_2]\\ &+[(1-y_4)y_3+(1-y_3)y_4]\\ &\times[(1-y_2)y_1+(1-y_1)y_2]\}D(1234),\end{aligned} \tag{34b}$$

$$A_1^{2143}(1234) = \frac{32}{\kappa^4}\int d\tau y_1y_3(1-y_1)(1-y_3)D(1234), \tag{35a}$$

$$A_1^{3412}(1234) = \frac{32}{\kappa^4}\int d\tau (y_1+y_2)(y_2+y_3)(y_3+y_4) \times(y_4+y_1)D(1234). \tag{35b}$$

Now, with the help of the symmetrization procedure indicated in Eq. (7), one can write down the coefficients A in terms of the A_1. From the nature of the A_1 one can also deduce certain identities among the A's, and these are indicated in Eqs. (36) to (41).

$$A^{2111}(1234) = A_1^{2111}(1234)+A_1^{2111}(1243)+A_1^{3111}(1324) = A^{2111}(1243), \tag{36}$$

$$A^{2121}(1234) = A_1^{2121}(1234)+A_1^{2112}(1243)+A_1^{3311}(1324) = A^{2121}(2143), \tag{37}$$

$$A^{2123}(1234) = A_1^{2113}(2134)+A_1^{3112}(2314)+A_1^{2141}(2143), \tag{38}$$

$$A^{2311}(1234) = A_1^{2311}(1234)+A_1^{3121}(1324)+A_1^{2411}(1243) = -A^{3121}(1234), \tag{39}$$

$$A^{2143}(1234) = A_1^{2143}(1234)+A_1^{2143}(1243)+A_1^{3412}(1324), \tag{40}$$

$$A^{2341}(1234) = A_1^{2341}(1234)+A_1^{2413}(1243)+A_1^{2413}(4132) = A^{4123}(1234). \tag{41}$$

To apply these relations to $G_{\mu\nu\lambda\sigma}$, it is helpful to consider a piece $G_{\mu\nu\lambda\sigma}'(1234)$ of this tensor:

$$\begin{aligned}G_{\mu\nu\lambda\sigma}'(1234) = &A^{2111}(1234)k_\mu^{(2)}k_\nu^{(1)}k_\lambda^{(1)}k_\sigma^{(1)}\\ &+A^{2121}(1234)k_\mu^{(2)}k_\nu^{(1)}k_\lambda^{(3)}k_\sigma^{(1)}+A^{2121}(1243)k_\mu^{(2)}k_\nu^{(1)}k_\lambda^{(1)}k_\sigma^{(2)}\\ &+A^{2111}(2143)k_\mu^{(2)}k_\nu^{(1)}k_\lambda^{(3)}k_\sigma^{(2)}+A^{2123}(1234)k_\mu^{(2)}k_\nu^{(1)}k_\lambda^{(2)}k_\sigma^{(3)}\\ &+A^{2123}(1243)k_\mu^{(2)}k_\nu^{(1)}k_\lambda^{(4)}k_\sigma^{(3)}+A^{2123}(2143)k_\mu^{(2)}k_\nu^{(1)}k_\lambda^{(4)}k_\sigma^{(1)}\\ &+A^{2123}(2134)k_\mu^{(2)}k_\nu^{(1)}k_\lambda^{(1)}k_\sigma^{(3)}+A^{2311}(1234)[k_\mu^{(2)}k_\nu^{(3)}k_\lambda^{(1)}k_\sigma^{(1)}\\ &-k_\mu^{(3)}k_\nu^{(1)}k_\lambda^{(2)}k_\sigma^{(1)}]+A^{2311}(2314)[k_\mu^{(2)}k_\nu^{(3)}k_\lambda^{(1)}k_\sigma^{(2)}\\ &-k_\mu^{(3)}k_\nu^{(1)}k_\lambda^{(2)}k_\sigma^{(2)}]+A^{2311}(3124)[k_\mu^{(2)}k_\nu^{(3)}k_\lambda^{(1)}k_\sigma^{(3)}\\ &-k_\mu^{(3)}k_\nu^{(1)}k_\lambda^{(2)}k_\sigma^{(3)}]+A^{2143}(1234)k_\mu^{(2)}k_\nu^{(1)}k_\lambda^{(4)}k_\sigma^{(3)}\\ &+A^{2341}(1234)[k_\mu^{(2)}k_\nu^{(3)}k_\lambda^{(4)}k_\sigma^{(1)}+k_\mu^{(4)}k_\nu^{(1)}k_\lambda^{(2)}k_\sigma^{(3)}].\end{aligned} \tag{42}$$

A look at Eqs. (20)–(28) suggests that $G_{\mu\nu\lambda\sigma}'(1234)$ be rearranged

as follows:

$$G_{\mu\nu\lambda\sigma}'(1234)=A^{2143}(1234)g_{\mu\nu\lambda\sigma}^{(1)}(1234)$$
$$+A^{2341}(1234)g_{\mu\nu\lambda\sigma}^{(2)}(1234)$$
$$+\frac{1}{(k^{(3)}k^{(4)})}[A^{2111}(1234)g_{\mu\nu\lambda\sigma}^{(3)}(1234)$$
$$+A^{2111}(2134)g_{\nu\mu\lambda\sigma}^{(3)}(2134)+A^{2121}(1234)g_{\mu\nu\lambda\sigma}^{(4)}(1234)$$
$$+A^{2121}(1243)g_{\mu\nu\sigma\lambda}^{(4)}(1243)]$$
$$+\frac{1}{(k^{(2)}k^{(4)})}[A^{2311}(1234)g_{\mu\nu\lambda\sigma}^{(5)}(1234)$$
$$-A^{2311}(3124)g_{\lambda\nu\mu\sigma}^{(5)}(3214)]+a(1234)k_\mu^{(2)}k_\nu^{(1)}k_\lambda^{(2)}k_\sigma^{(3)}$$
$$+a(1243)k_\mu^{(2)}k_\nu^{(1)}k_\lambda^{(4)}k_\sigma^{(3)}+a(2143)k_\mu^{(2)}k_\nu^{(1)}k_\lambda^{(4)}k_\sigma^{(1)}$$
$$+a(2134)k_\mu^{(2)}k_\nu^{(1)}k_\lambda^{(1)}k_\sigma^{(3)}+b(2314)$$
$$\times(k_\mu^{(2)}k_\nu^{(3)}k_\lambda^{(1)}k_\sigma^{(2)}-k_\mu^{(3)}k_\nu^{(1)}k_\lambda^{(2)}k_\sigma^{(2)}), \quad (43)$$

where

$$a(1234)=\frac{1}{(k^{(3)}k^{(4)})}[(k^{(3)}k^{(4)})A^{2123}(1234)$$
$$+(k^{(2)}k^{(4)})A^{2111}(2143)+(k^{(1)}k^{(4)})A^{2121}(1234)], \quad (44a)$$

$$b(2314)=\frac{1}{(k^{(2)}k^{(4)})}[(k^{(2)}k^{(4)})A^{2311}(2314)$$
$$+(k^{(1)}k^{(4)})A^{2311}(1234)+(k^{(3)}k^{(4)})A^{2311}(3124)]. \quad (44b)$$

The major part of the polarization tensor has now been expressed in terms of the tensors $g_{\mu\nu\lambda\sigma}^{(i)}$ derived from field strengths. The remainder

$$\sum_{24\text{ perm}} a(1234)k_\mu^{(2)}k_\nu^{(1)}k_\lambda^{(2)}k_\sigma^{(3)}+b(2314)(k_\mu^{(3)}k_\nu^{(3)}k_\lambda^{(1)}k_\sigma^{(2)}$$
$$-k_\mu^{(3)}k_\nu^{(1)}k_\lambda^{(2)}k_\sigma^{(2)})+b(2413)(k_\mu^{(2)}k_\nu^{(4)}k_\lambda^{(2)}k_\sigma^{(1)}-k_\mu^{(4)}k_\nu^{(1)}k_\lambda^{(2)}k_\sigma^{(2)})$$
$$+b(4312)(k_\mu^{(4)}k_\nu^{(4)}k_\lambda^{(1)}k_\sigma^{(3)}-k_\mu^{(3)}k_\nu^{(4)}k_\lambda^{(4)}k_\sigma^{(1)})$$
$$+b(2341)(k_\mu^{(2)}k_\nu^{(3)}k_\lambda^{(4)}k_\sigma^{(2)}-k_\mu^{(2)}k_\nu^{(4)}k_\lambda^{(2)}k_\sigma^{(3)}) \quad (45)$$

is still gauge-invariant and must satisfy Eq. (12) with appropriate B and C terms. It is therefore identically zero. The reason for this result is the fact that each head in Eq. (45) contains only three different momenta. The third-rank tensor that results from contraction, as in Eq. (12), with the fourth momentum then does not contain this fourth momentum. The third-rank tensors that result from the application of Eq. (12) to terms other than heads, terms that contain a Kronecker delta, will always contain the momentum vector with which they were multiplied. Hence the heads in Eq. (45) must satisfy Eq. (12) alone, and this means that every term in Eq. (45) vanishes. As a check on the calculation, $a(1234)$ and $b(2314)$ were computed explicitly as functions of null-vector momenta; they were indeed found to vanish identically.

The vacuum polarization tensor can therefore be written

$$G_{\mu\nu\lambda\sigma}(1234)=\sum_{24\text{ perm}}\Big\{\frac{1}{8}A^{2143}(1234)g_{\mu\nu\lambda\sigma}^{(1)}(1234)$$
$$+\frac{1}{8}A^{2341}(1234)g_{\mu\nu\lambda\sigma}^{(2)}(1234)$$
$$+\frac{1}{2}\frac{1}{(k^{(3)}k^{(4)})}A^{2111}(1234)g_{\mu\nu\lambda\sigma}^{(3)}(1234)$$
$$+\frac{1}{2}\frac{1}{(k^{(3)}k^{(4)})}A^{2121}(1234)g_{\mu\nu\lambda\sigma}^{(4)}(1234)$$
$$+\frac{1}{3}\frac{1}{(k^{(2)}k^{(4)})}A^{2311}(1234)g_{\mu\nu\lambda\sigma}^{(5)}(1234)\Big\}. \quad (46)$$

The sum over permutations here refers to simultaneous permutations of the labels of the momentum variables and of the tensor indices of the $g^{(i)}$. The superscripts on the A's define their functional form [Eqs. (30) to (41)].

A calculation based on Eq. (46) of the cross section for the scattering of light by light is being prepared for publication.

V. LOW ENERGY APPROXIMATION

If the interacting fields vary so slowly in space and time that the Fourier transforms have appreciable values only for momenta whose absolute value is much smaller that the mass of the pair field, the function $D(1234)$ in Eq. (27) may be approximated by unity. The evaluation of the integrals Eqs. (30) to (35) then becomes trivial. In particular, the integrals are independent of the momenta. The values of the six basic ones, Eqs. (36) to (41) are

$$A^{2111}=A^{2121}=A^{2311}=A^{2123}=0,$$
$$A^{2143}=A^{3412}=A^{4321}=4/9\kappa^4, \quad (47)$$
$$A^{2341}=A^{2413}=A^{3412}=-14/45\kappa^4.$$

Hence

$$G_{\mu\nu\lambda\sigma}(1234)=\frac{4}{9\kappa^4}(g_{\mu\nu\lambda\sigma}^{(1)}(1234)+g_{\mu\lambda\nu\sigma}^{(1)}(1324)$$
$$+g_{\mu\sigma\nu\lambda}^{(1)}(1423))-\frac{14}{45\kappa^4}(g_{\mu\nu\lambda\sigma}^{(2)}(1234)$$
$$+g_{\mu\lambda\nu\sigma}^{(2)}(1324)+g_{\mu\sigma\nu\lambda}^{(2)}(1423)), \quad (48)$$

$$S^{(4)}=-i\frac{\alpha^2}{180}\frac{1}{(\hbar c\kappa^2)^2}\int d^4x[5(F_{\mu\nu}(x)F_{\mu\nu}(x))^2$$
$$-14(F_{\mu\nu}(x)F_{\nu\lambda}(x)F_{\lambda\sigma}(x)F_{\sigma\mu}(x))], \quad (49)$$

and the effective Lagrangian density

$$L(x)=\frac{\alpha^2}{180}\frac{1}{\hbar c\kappa^4}[5(F_{\mu\nu}(x)F_{\mu\nu}(x))^2$$
$$-14F_{\mu\nu}(x)F_{\nu\lambda}(x)F_{\lambda\sigma}(x)F_{\sigma\mu}(x)]. \quad (50)$$

This last quantity, when expressed in terms of electric and magnetic field intensities ($\mathbf{D}$ and $\mathbf{B}$) becomes identical with the result of Euler's calculation:[3]

$$L(x)=-(2\alpha^2/45\hbar c\kappa^4)[(\mathbf{D}^2-\mathbf{B}^2)^2+7(\mathbf{D}\cdot\mathbf{B})^2]. \quad (50')$$

It is a pleasure to thank Professor Oppenheimer for his encouragement and to acknowledge many enlightening discussions with Dr. Res Jost. One of us (M. N.) is indebted to the Institute for Advanced Study for having supported his research by a grant of AEC funds.

Polarization Correlation of Mixed Multipoles

IRVING ZINNES
New York University, New York, New York

(Received June 1, 1950)

The directional polarization results of Hamilton are extended to cases in which one of the two photons emitted by a nucleus is described by a pure 2^L multipole and in which the second is described by two mixed multipoles. While these polarization functions are still quite simply related to the parameters occurring in the functions describing the correlation between two successive photons neither of whose polarizations is being measured, the relationship is more complicated than for pure multipole photons on account of the explicit dependence of the mixture polarization function on the mixture components and on the interference arising from the mixture. The net result is that the correlation parameters $Q, R, S, \cdots$ obtained from a correlation experiment without polarization are insufficient to describe a polarization correlation experiment when mixtures are involved. A table of polarization correlation functions is given for all pure-mixture transitions up to and including octupoles. Two examples briefly indicating how this table may be used, as well as a table of some useful combinations of the elements of the representations of the three-dimensional rotation group are included.

I. INTRODUCTION

ONE of the methods used to aid in the determination of the three spin states of a nucleus which decays from an excited state to a ground state through a short-lived intermediate state by emitting two photons is that of an angular correlation experiment.[1] This work has been carried out chiefly by Deutsch and his co-workers.[2] The theory has been worked out by Hamilton[3] and in a very general way by Goertzel.[4] If each photon is a pure electric or magnetic 2^L multipole, then the angular correlation function for the two photons is independent of the electric or magnetic character of the multipole. Falkoff[5] and Hamilton[6] have shown that a polarization correlation experiment would yield results which are sensitive to the multipole character. In fact, Hamilton[6] has computed the distribution functions for cases in which the multipoles involved are at most quadrupole and when in the experiment the linear polarization of only one of the photons is measured. The interest in the multipole characters lies in their determining the relative parity of the three nuclear states involved.

This angular correlation theory applied to pure multipole transitions has been successful in some cases and has failed in others,[1,2] notably in Pd^{106} and Sr^{88}. Ling and Falkoff[2,7] have shown that the experimental correlation function for Sr^{88} could be explained by assuming that one of the transitions was a mixed multipole. They have extended Hamilton's[3] original correlation functions to include mixtures in one of the photons. Deutsch and Metzger[8] have performed a polarization correlation experiment on Pd^{106} and have obtained some parity information by using Hamilton's polarization functions.

In view of the continuing interest in multipole mixtures, Hamilton's polarization functions are here extended to the case in which one of the photons can be described by two multipoles and the other by a simple pure multipole. The general formalism of Goertzel[4] will be used. References will be made to the formulas in Goertzel's paper by enclosing his corresponding number-designations in square brackets, such as [G, 9], for example.

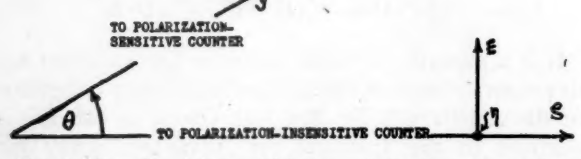

FIG. 1. Direction (x') in which the polarization of one photon is measured and the directions (z, ζ) in which both photons are detected.

II. FORMALISM AND RESULTS

The xyz coordinate system in Fig. 1 is obtained from the $\xi\eta\zeta$ system by applying to the latter system the Euler rotations $(0, \theta, 0)$, where θ is the angle of rotation about the η-axis, which is perpendicular to the page. Therefore, the x-, z-, ξ-, ζ-axes are all in the same plane. A second set of Euler rotations $(0, 0, \gamma)$ turns x into x'. Carrying out the two rotations (first the θ-rotation about the η-axis and then the γ-rotation about the z-axis) brings the ξ-axis into the x'-axis and the ζ-axis into the z-axis. If we neglect the hyperfine structure splitting of the intermediate states, then the probability that the two photons will be detected in the z- and ζ-directions with given polarizations is given by [G, 9] with $\nu_{\beta,\beta'}=0$ [or by Hamilton's[3] Eq. (10)];

$$W(\pi_1 z;\pi_2\zeta)=\sum\{l,n,n',p\}(al|H(\pi_1 z)|bn)^* \times(al|H(\pi_1 z)|bn')(bn|H(\pi_2\zeta)|cp)^* \times(bn'|H(\pi_2\zeta)|cp). \quad (1)$$

[1] E. Segrè and A. C. Helmholtz, Rev. Mod. Phys. **21**, 271 (1949).
[2] E. L. Brady and M. Deutsch, Phys. Rev. **72**, 870 (1947); **74**, 1541 (1948).
[3] D. R. Hamilton, Phys. Rev. **58**, 122 (1940).
[4] G. Goertzel, Phys. Rev. **70**, 897 (1946).
[5] D. L. Falkoff, Phys. Rev. **73**, 518 (1948).
[6] D. R. Hamilton, Phys. Rev. **74**, 782 (1948).
[7] D. S. Ling, Jr. and D. L. Falkoff, Phys. Rev. **76**, 1639 (1949).
[8] M. Deutsch and F. Metzger, Phys. Rev. **74**, 1542 (1948); **76**, 187 (1949).

Here, z and π_1 specify that the first photon is collected along the z-axis with polarization specified by π_1; similarly, ζ and π_2 specify the second photon. If a matrix element refers to a circularly polarized photon propagated along the z'-axis, then, in terms of the $\xi\eta\zeta$ coordinates from [G, 29] and [G, 30],

$$(al|H(Pz)|bn)$$
$$=\sum_L \alpha_L i^{L+\sigma} \sum_M D^{(L)}(0,\theta,\gamma)_{M,P}(al|Y_L{}^M|bn)P^\sigma$$
$$=\sum_L \alpha_L i^{L+\sigma} \sum_M e^{-iP\gamma} D^{(L)}(0,\theta,0)_{M,P} \times(al|Y_L{}^M|bn)P^\sigma. \quad (2a)$$

If the element refers to a photon linearly polarized along the x'-axis, then

$$(al|H(x',z)|bn)=\sum_{P=\pm1}(al|H(Pz)|bn). \quad (2b)$$

Here, α_L is independent of M, but depends on L and the unknown nuclear radial function; $\sigma=0$ or 1 depending on whether the multipole is magnetic or electric; and $P=1$ or -1, depending on whether the circular polarization is left- or right-handed. Equations (2) refer to a plane wave, which can be described by an infinite number of 2^L multipoles. When mixtures of only two multipoles are considered, then it is assumed that $\alpha_L=0$ except when $L=L_2$ and $L=L_3$. We shall usually set $\alpha_{L_2}=\alpha$ and $\alpha_{L_3}=\beta$. In the sequel it will always be assumed that the first transition is a pure multipole of order 2^{L_1} and that the second transition is made up of two multipoles of order 2^{L_2} and 2^{L_3}.[9]

Substituting (2) into (1) and summing over the two values of the circular polarization parameter of that photon whose polarization is not being measured, one obtains the following distribution functions: $[\sigma_1L_1;\ \sigma_2L_2,\ \sigma_3L_3]_\gamma$ is the probability that a 2^{L_1} photon of electric or magnetic character σ_1 is detected along the z-axis and is polarized along the x'-axis while a mixed 2^{L_2}, 2^{L_3} photon with characters σ_2 and σ_3 is detected along the ζ-axis; $[\sigma_2L_2,\ \sigma_3L_3;\ \sigma_1L_1]_\gamma$ is the distribution function when the paths of the photons are interchanged and the polarization along the x'-axis of the mixed photon is measured. These functions are given by

$$[\sigma_1L_1;\ \sigma_2L_2,\ \sigma_3L_3]_\gamma$$
$$=\sum_{n,M,P}\{|(an+M|Y_{L_1}{}^M|bn)|^2$$
$$\times[|\alpha|^2|(bn|Y_{L_2}{}^P|cn-P)|^2$$
$$+|\beta|^2|(bn|Y_{L_3}{}^P|cn-P)|^2$$
$$+2Re(\alpha\beta^* i^{L_2-L_3+\sigma_2-\sigma_3})P^{\sigma_2+\sigma_3}(bn|Y_{L_2}{}^P|cn-P)$$
$$\times(bn|Y_{L_3}{}^P|cn-P)][F_M{}^{(L_1)}(\theta)$$
$$+(-1)^{\sigma_1}\cos2\gamma f_M{}^{(L_1)}(\theta)]\}, \quad (3a)$$

[9] If the order of the pure and the mixed transitions is interchanged, one obtains the appropriate correlation function by considering the second transition and the final nuclear state as the first transition and the initial state, respectively.

TABLE I. Form functions as defined in Eq. (4).

L	$\lvert M\rvert$	$F_{\pm M}{}^{(L)}(\theta)$	$f_{\pm M}{}^{(L)}(\theta)$
1	1	$\frac{1}{2}(1+\cos^2\theta)$	$\frac{1}{2}(1-\cos^2\theta)$
	0	$1-\cos^2\theta$	$-(1-\cos^2\theta)$
2	2	$\frac{1}{2}(1-\cos^4\theta)$	$\frac{1}{2}(1-2\cos^2\theta+\cos^4\theta)$
	1	$\frac{1}{2}(1-3\cos^2\theta+4\cos^4\theta)$	$-\frac{1}{2}(1-5\cos^2\theta+4\cos^4\theta)$
	0	$3(\cos^2\theta-\cos^4\theta)$	$-3(\cos^2\theta-\cos^4\theta)$
3	3	$\frac{1}{32}(1-\cos^2\theta-\cos^4\theta+\cos^6\theta)$	$\frac{1}{32}(1-3\cos^2\theta+3\cos^4\theta-\cos^6\theta)$
	2	$\frac{5}{16}(1-3\cos^2\theta+11\cos^4\theta-9\cos^6\theta)$	$-\frac{5}{16}(1-11\cos^2\theta+19\cos^4\theta-9\cos^6\theta)$
	1	$\frac{1}{32}(1+111\cos^2\theta-305\cos^4\theta+225\cos^6\theta)$	$\frac{1}{32}(1-131\cos^2\theta+355\cos^4\theta-225\cos^6\theta)$
	0	$\frac{3}{8}(1-11\cos^2\theta+35\cos^4\theta-25\cos^6\theta)$	$-\frac{3}{8}(1-11\cos^2\theta+35\cos^4\theta-25\cos^6\theta)$

L_2	L_3	σ_3	$\lvert M\rvert$	$\mathfrak{F}_{\pm\lvert M\rvert}{}^{(L_2,L_3)}(\theta)$	$\mathfrak{G}_{\pm\lvert M\rvert}{}^{(L_2,L_3)}(\theta)$
1	2	$1-\sigma_2$	1	$\pm\frac{1}{2}(3\cos^2\theta-1)$	$\pm\frac{1}{2}(1-\cos^2\theta)$
			0	0	0
1	3	σ_2	1	$\frac{-1}{8}(1+6\cos^2\theta-15\cos^4\theta)$	$-\frac{1}{8}(1-16\cos^2\theta+15\cos^4\theta)$
			0	$\frac{-(6)^{\frac{1}{2}}}{4}(1-6\cos^2\theta+5\cos^4\theta)$	$\frac{(6)^{\frac{1}{2}}}{4}(1-6\cos^2\theta+5\cos^4\theta)$
2	3	$1-\sigma_2$	2	$\frac{\pm(10)^{\frac{1}{2}}}{8}(1-6\cos^2\theta+5\cos^4\theta)$	$\frac{\mp(10)^{\frac{1}{2}}}{8}(1-2\cos^2\theta+\cos^4\theta)$
			1	$\pm\frac{1}{8}(1-18\cos^2\theta+25\cos^4\theta)$	$\pm\frac{1}{8}(1+4\cos^2\theta-5\cos^4\theta)$
			0	0	0

$$[\sigma_2L_2,\ \sigma_3L_3;\ \sigma_1L_1]_\gamma$$
$$=\sum_{n,M,P}\{|(an+P|Y_{L_1}{}^P|bn)|^2$$
$$\times[|\alpha|^2|(bn|Y_{L_2}{}^M|cn-M)|^2$$
$$\times(F_M{}^{(L_2)}(\theta)+(-)^{\sigma_2}\cos2\gamma f_M{}^{(L_2)}(\theta))$$
$$+|\beta|^2|(bn|Y_{L_3}{}^M|cn-M)|^2(F_M{}^{(L_3)}(\theta)$$
$$+(-)^{\sigma_3}\cos2\gamma f_M{}^{(L_3)}(\theta))+2Re(\alpha\beta^* i^{L_2-L_3+\sigma_2-\sigma_3})$$
$$\times(bn|Y_{L_2}{}^M|cn-M)(bn|Y_{L_3}{}^M|cn-M)$$
$$\times(\mathfrak{F}_M{}^{(L_2,L_3)}(\theta)+(-)^{\sigma_3}\cos2\gamma\mathfrak{G}_M{}^{(L_2,L_3)}(\theta))]$$
$$+K_{n,M,P}\}. \quad (3b)$$

The functions used in (3) are defined as follows:

$$F_{\pm M}{}^{(L)}(\theta)=\sum_{P=\pm1}|D^{(L)}(0,\theta,0)_{|M|,P}|^2, \quad (4a)$$

$$f_{\pm M}{}^{(L)}(\theta)=\sum_{P=\pm1}D^{(L)}(0,\theta,0)_{|M|,P} \times D^{(L)}(0,\theta,0)_{|M|,-P}, \quad (4b)$$

$$\mathfrak{F}_{\pm M}^{(L_2,L_3)}(\theta)=(\pm)^{\sigma_2+\sigma_3}\sum_{P=\pm1}P^{\sigma_2+\sigma_3}\times D^{(L_2)}(0,\theta,0)_{M,P}D^{(L_3)}(0,\theta,0)_{M,P}, \quad (4c)$$

$$\mathfrak{G}_{\pm M}^{(L_2,L_3)}(\theta)=(\pm)^{\sigma_2+\sigma_3}\sum_{P=\pm1}P^{\sigma_2+\sigma_3}\times D^{(L_2)}(0,\theta,0)_{M,P}D^{(L_3)}(0,\theta,0)_{M,-P}. \quad (4d)$$

The functions in (4) continually occur in the theory and their explicit expansion is very useful in the calculations. They are therefore given in Table I up to $L=3$. For higher values of L, these functions are calculated somewhat tediously from [G, A19] and a table of normalized spherical harmonics with Condon and Shortley phase factors.[10] On the other hand,

$$K_{nMP}=(-)^{\sigma_2}2\sum_{P'=\pm1}|(an+P'|Y_{L_1}{}^{P'}|bn)|^2\times(bn|Y_{L_2}{}^{M}|cn-M)(bn|Y_{L_3}{}^{M}|cn-M)\times Im(\alpha\beta^*i^{L_2-L_3+\sigma_2-\sigma_3})\sin2\gamma P^{\sigma_2+\sigma_3+1}\times D^{(L_2)}(0,\theta,0)_{M,P}D^{(L_3)}(0,\theta,0)_{M,-P}. \quad (5)$$

However, $\sum_{nMP}K_{nMP}=0$ for all multipole mixtures. This can be readily seen in the following way.

$$(bn|Y_{L_2}{}^{M}|cn-M)=(-)^{J_b-L_2-J_c}(b-n|Y_{L_2}{}^{-M}|c-n+M),$$

where J_b and J_c are the angular momentum quantum numbers of the states b and c.[11] Therefore, $\sum_nK_{nMP}$ has the parity of L_2+L_3, relative to the sign of M. On the other hand,

$$\sum_P P^{\sigma_2+\sigma_3+1}D^{(L_2)}(0,\theta,0)_{M,P}D^{(L_3)}(0,\theta,0)_{M,-P}$$
$$=\sum_P P^{\sigma_2+\sigma_3+1}D^{(L_2)}(0,\theta,0)_{-M,-P}D^{(L_3)}(0,\theta,0)_{-M,P}$$
$$=(-)^{\sigma_2+\sigma_3+1}\sum_P P^{\sigma_2+\sigma_3+1}D^{(L_2)}(0,\theta,0)_{-M,P}\times D^{(L_3)}(0,\theta,0)_{-M,-P}$$

has the parity of $\sigma_2+\sigma_3+1$ relative to M. Therefore, the parity of $\sum_{n,P}K_{nMP}$ is $L_2+L_3+\sigma_2+\sigma_3+1$ in M. At this point it is convenient to recall that the interactions[12] $\mathbf{P}\cdot\mathbf{A}_\sigma(L,M)$ and $\boldsymbol{\alpha}\cdot\mathbf{A}_\sigma(L,M)$ have the parity of $L+1+\sigma$ relative to coordinate reflection and that the parity of the interactions arising from each of the mixture multipoles must be the same. Therefore, $L_2+\sigma_2\equiv L_3+\sigma_3$ (mod. 2), and $\sum_{nMP}K_{nMP}=0$. If the parity of the interactions arising from the mixture multipoles are not the same, then at least α or β must vanish, so that $\sum_{nMP}K_{nMP}$ still vanishes.

If the above calculation is repeated for two circularly polarized photons, whose polarizations are specified by P and P', respectively, two distribution functions are obtained: one describes the pure photon being detected with circular polarization P along the z-axis while the mixed photon is detected with polarization P' along the ζ-axis; the other distribution function describes the situation when the paths of the two photons are interchanged. Summing over the two values of P and P', one obtains two distribution functions describing the detection of two non-polarized photons. The result is precisely (3) with $\cos2\gamma=0$. Because of the symmetry of the problem when polarization is not investigated, the non-polarization distributions just obtained must be equal. We shall designate either distribution by $(L_1;\ \sigma_2L_2,\ \sigma_3L_3)$, where σ_1 is omitted, since it does not affect the non-polarization distribution. Since α and β can be looked upon as independent parameters in (3), it is evident that

$$|\alpha_{L_i}|^2\sum_{nMP}\{|(an+M|Y_{L_1}{}^{M}|bn)|^2\times|(bn|Y_{L_i}{}^{P}|cn-P)|^2F_M{}^{(L_1)}(\theta)$$
$$=|\alpha_{L_i}|^2\sum_{nMP}\{|(an+P|Y_{L_1}{}^{P}|bn)|^2\times|(bn|Y_{L_i}{}^{M}|cn-M)|^2F_M{}^{(L_i)}(\theta);\ (i=2,3) \quad (6a)$$

$$2Re(\alpha\beta^*i^{L_2-L_3+\sigma_2-\sigma_3})\sum_{nMP}|(an+M|Y_{L_1}{}^{M}|bn)|^2P^{\sigma_2+\sigma_3}\times(bn|Y_{L_2}{}^{P}|cn-P)(bn|Y_{L_3}{}^{P}|cn-P)F_M{}^{(L_1)}(\theta)$$
$$=2Re(\alpha\beta^*i^{L_2-L_3+\sigma_2-\sigma_3})\sum_{nMP}|(an+P|Y_{L_1}{}^{P}|bn)|^2\times(bn|Y_{L_2}{}^{M}|cn-M)\times(bn|Y_{L_3}{}^{M}|cn-M)\mathfrak{F}_M{}^{(L_2,L_3)}(\theta). \quad (6b)$$

Equation (6a) just expresses the equality between [G, 32] and [G, 32′], which are the same functions for pure-pure transitions without polarization described from different frames of reference. The specific polarization effect is therefore given by the $f_M{}^{(L)}$ and the $\mathcal{G}_M{}^{(L_2,L_3)}$ terms of (3). Looked upon as functions of θ, Eqs. (6) can be expanded in the following form, where the coefficients of the F's and the $\mathfrak{F}$'s are constants depending only on M:

$$(L_1;L_2)\doteq\sum_M A_MF_M{}^{(L_1)}(\theta)=\sum_M a_MF_M{}^{(L_2)}(\theta)=Q_2+R_2\cos^2\theta+S_2\cos^4\theta+T_2\cos^6\theta+\cdots, \quad (7a)$$

$$(L_1;L_3)=\sum_M B_MF_M{}^{(L_1)}(\theta)=\sum_M b_MF_M{}^{(L_3)}(\theta)=Q_3+R_3\cos^2\theta+S_3\cos^4\theta+T_3\cos^6\theta+\cdots, \quad (7b)$$

$$\sum_M D_MF_M{}^{(L_1)}(\theta)=\sum_M d_M\mathfrak{F}_M{}^{(L_2,L_3)}(\theta)=q+r\cos^2\theta+s\cos^4\theta+t\cos^6\theta+\cdots. \quad (7c)$$

$(L_1;L_i)$ are the non-polarization distribution functions corresponding to pure-pure transitions. The entire

[10] E. U. Condon and G. H. Shortley, *Theory of Atomic Spectra* (Cambridge University Press, Cambridge, 1935), p. 52.

[11] This relation follows immediately from Wigner, *Gruppentheorie* (reprint by J. W. Edwards in 1944), p. 206, Eq. (27), by identifying $(bn|Y_L{}^M|cn-M)$ with $S^{L,J_c}{}_{J_b,M,n-M}$.

[12] See Eq. (27) of reference 4.

mixture correlation function, assuming equal counter efficiencies and no polarization, is given by the sum of the three equations in (7):

$$\begin{aligned}(L_1;\sigma_2L_2,\sigma_3L_3)&=\sum_M(A_M+B_M+D_M)F_M{}^{(L_1)}(\theta)\\&=\sum_M[a_MF_M{}^{(L_2)}(\theta)+b_MF_M{}^{(L_3)}(\theta)\\&\qquad+d_M\mathfrak{F}_M{}^{(L_2,L_3)}(\theta)]\\&=(Q_2+Q_3+q)+(R_2+R_3+r)\cos^2\theta\\&\qquad+(S_2+S_3+s)\cos^4\theta+\cdots\\&=Q+R\cos^2\theta+S\cos^4\theta+T\cos^6\theta+\cdots.\end{aligned}\tag{8}$$

Q, R, $S\cdots$ are the numbers one would obtain from a correlation experiment without measuring the polarization. One would obtain Q_2, R_2, S_2, $\cdots$ from such a correlation experiment if the transitions could be described by pure 2^{L_1} and 2^{L_2} multipoles; similarly, for Q_3, R_3, S_3, $\cdots$. Using (7), (8) and the expansions of the F's and the $\mathfrak{F}$'s from Table I, one can obtain the coefficients of these polynomials in terms of the Q, R, S, $\cdots Q_2$, $\cdots S_3$, $\cdots$. Then the polarization correlation functions (3a, b) can be written in terms of the Q's, R's, S's, $\cdots$.

For purposes of tabulation and of ease in computation, the following procedure was adopted. Equations (3) can be written in the following form:

$$\begin{aligned}[\sigma_1L_1;\sigma_2L_2,\sigma_3L_3]_\gamma&=(L_1;\sigma_2L_2,\sigma_3L_3)+[\sigma_1L_1;\sigma_2L_{2\alpha}]\\&\quad+[\sigma_1L_1;\sigma_3L_3]_\beta+[\sigma_1L_1;\sigma_2L_2,\sigma_3L_3]_{\alpha\beta^*},\end{aligned}\tag{9a}$$

$$\begin{aligned}[\sigma_2L_2,\sigma_3L_3;\sigma_1L_1]_\gamma&=(L_1;\sigma_2L_2,\sigma_3L_3)+[\sigma_2L_2;\sigma_1L_1]_\alpha\\&\quad+[\sigma_3L_3;\sigma_1L_1]_\beta+[\sigma_2L_2,\sigma_3L_3;\sigma_1L_1]_{\alpha\beta^*}.\end{aligned}\tag{9b}$$

Each bracketed term on the right side of (9) is the $\cos2\gamma$ term in (3a) or (3b) which depends on $|\alpha|^2$ or $|\beta|^2$ or $Re(\alpha\beta^*)$. Regardless of its position, the subscript 1 always refers to the first photon; similarly, the subscripts 2 and 3 refer to the multipoles constituting the second photon. The first position in a bracket refers to that photon detected in the polarizer. Thus, $[\sigma_1L_1;\sigma_2L_2]_\alpha$ is the polarization contribution of the 2^{L_1} and the 2^{L_2} multipoles to the pure-pure distribution function describing the detection and polarization of the 2^{L_1} multipole and just the detection of the 2^{L_2} multipole. Similarly, $[\sigma_2L_2;\sigma_1L_1]_\alpha$ is the polarization contribution to the distribution function describing the situation when the paths of these two pure photons are interchanged. Therefore, $[\sigma_2L_2;\sigma_1L_1]_\alpha$ can be obtained from $[\sigma_1L_1;\sigma_2L_2]_\alpha$ by interchanging L_2 and σ_2 with L_1 and σ_1 in the expression for $[\sigma_1L_1;\sigma_2L_2]_\alpha$. On the other hand, the interference polarization terms in (9a, b), which are proportional to $Re(\alpha\beta^*)$, do not possess this symmetry. The polarization terms in (9) are given in Table II for all combinations of dipole, quadrupole and octupole multipoles in terms of the associated pure-pure and pure-mixture correlation parameters Q, $\cdots R_2$, $\cdots S_3$, $\cdots$.

TABLE II. Polarization terms of the associated pure multipole photons and of those arising from interference of the mixture multipoles.

A. $[\sigma_1L_1;\sigma_iL_i]_{\alpha L_i}=(-1)^{\sigma_1}E\cos2\gamma+(-1)^{\sigma_1}F\cos2\gamma\cos^2\theta+(-1)^{\sigma_1}G\cos2\gamma\cos^4\theta+(-1)^{\sigma_1}H\cos2\gamma\cos^6\theta$, $(i=2,3)$

L_1	L_i	E	F	G	H
1	1	R_i	$-R_i$	0	0
1	2	R_i	$-R_i$	0	0
1	3	R_i	$-R_i$	0	0
2	1	$-R_i$	R_i	0	0
2	2	$-(R_i+S_i)$	R_i+2S_i	$-S_i$	0
2	3	$-(R_i+S_i)$	R_i+2S_i	$-S_i$	0
3	1	$-\frac{3}{5}R_i$	$\frac{3}{5}R_i$	0	0
3	2	$-\frac{3}{5}R_i$	$\frac{3}{5}(R_i-6S_i)$	$4S_i$	0
3	3	$-\frac{1}{5}(2R_i-T_i)$	$\frac{1}{5}(2R_i-12S_i-19T_i)$	$4S_i+7T_i$	$-T_i$

B. $[\sigma_1L_1;\sigma_2L_2,\sigma_3L_3]_{\alpha\beta^*}=(-1)^{\sigma_1}e\cos2\gamma+(-1)^{\sigma_1}f\cos2\gamma\cos^2\theta+(-1)^{\sigma_1}g\cos2\gamma\cos^4\theta$

L_1	L_2	L_3	σ_3	e	f	g
1	1	2	$1-\sigma_2$	r	$-r$	0
1	1	3	σ_2	r	$-r$	0
1	2	3	$1-\sigma_2$	r	$-r$	0
2	1	2	$1-\sigma_2$	$-r$	r	0
2	1	3	σ_2	$-(r+s)$	$r+2s$	$-s$
2	2	3	$1-\sigma_2$	$-(r+s)$	$r+2s$	$-s$
3	1	2	$1-\sigma_2$	$-\frac{3}{5}r$	$\frac{3}{5}r$	0
3	1	3	σ_2	$-\frac{3}{5}r$	$\frac{3}{5}(r-6s)$	$4s$
3	2	3	$1-\sigma_2$	$-\frac{3}{5}r$	$\frac{3}{5}(r-6s)$	$4s$

C. $[\sigma_2L_2,\sigma_3L_3;\sigma_1L_1]_{\alpha\beta^*}=(-1)^{\sigma_2}e'\cos2\gamma+(-1)^{\sigma_2}f'\cos2\gamma\cos^2\theta+(-1)^{\sigma_2}g'\cos2\gamma\cos^4\theta$

L_1	L_2	L_3	σ_3	e'	f'	g'
1	1	2	$1-\sigma_2$	$-(1/3)r$	$(1/3)r$	0
1	1	3	σ_2	$(1/6)r$	$-(1/6)r$	0
1	2	3	$1-\sigma_2$	$-(1/2)r$	$(1/2)r$	0
2	1	2	$1-\sigma_2$	$-(1/3)r$	$(1/3)r$	0
2	1	3	σ_2	$(1/6)r$	$-(1/6)(r-6s)$	$-s$
2	2	3	$1-\sigma_2$	$-(1/10)(5r+4s)$	$(1/10)(5r+2s)$	$(1/5)s$
3	1	2	$1-\sigma_2$	$-(1/3)r$	$(1/3)r$	0
3	1	3	σ_2	$(1/6)r$	$-(1/6)(r-6s)$	$-s$
3	2	3	$1-\sigma_2$	$-(1/10)(5r+4s)$	$(1/10)(5r+2s)$	$(1/5)s$

It is clear from the form of (3a) that the distribution function describing a pure photon going to the polarization counter and the mixed photon going to the non-polarization counter depends only on Q, R, S, $\cdots$, the same parameters which describe the entire mixture angular correlation. Such a conclusion is not so easily drawn for (3b) and, in fact, is not correct in general as Table II shows. This was rather disappointing, since it was hoped that the total polarization correlation, which is essentially the sum of (3a) and (3b), would depend only on the non-polarization parameters just as for pure-pure transitions.[6]

Since the nuclear transitions occur in very rapid succession, one cannot tell which of the detected photons was emitted first. The entire polarization correlation is therefore given by a properly weighted sum of (3a) and (3b), the weights being the efficiencies of the detectors. We shall define their efficiencies as Hamilton[6] has done, so that ϵ_1 is the product of the efficiencies with which the polarization-sensitive counter detects

the pure photon (resulting from the first transition $a \rightarrow b$) and with which the polarization-insensitive counter detects the mixed photon. Similarly, ϵ_2 is the over-all efficiency for the detection of both photons when their paths are interchanged. The subscript of ϵ thus indicates the photon whose polarization is being measured. The total polarization correlation function is therefore given by

$$\{\sigma_1 L_1; \sigma_2 L_2, \sigma_3 L_3\}_\gamma = \epsilon_1[\sigma_1 L_1; \sigma_2 L_2, \sigma_3 L_3]_\gamma + \epsilon_2[\sigma_2 L_2, \sigma_3 L_3; \sigma_1 L_1]_\gamma. \quad (10)$$

Defining $\epsilon = \epsilon_1 + \epsilon_2$, one can expand (10) as a polynomial in $\cos^2\theta$, with the aid of Table II and Eqs. (9), as

$$\{\sigma_1 L_1; \sigma_2 L_2, \sigma_3 L_3\}_\gamma = [\epsilon Q + \mathfrak{A} \cos 2\gamma) + (\epsilon R + \mathfrak{B} \cos 2\gamma) \cos^2\theta + (\epsilon S + \mathfrak{D} \cos 2\gamma) \cos^4\theta + (\epsilon T + \mathcal{E} \cos 2\gamma) \cos^6\theta + \cdots. \quad (11)$$

It may be here emphasized that part A of Table II remains useful when for one of the three multipoles $L > 3$, since, as (9) shows, the polarization functions contain the terms $[\sigma_1 L_1; \sigma_i L_i]_{\alpha_{L_i}}$, which are independent of the mixture. An essentially complete set of the functions $\{\sigma_1 L_1; \sigma_2 L_2, \sigma_3 L_3\}_\gamma$ is given in Table III for all allowed dipole (D), quadrupole (Q), and octupole (O) combinations, both electric (E) and magnetic (M). The scheme ($ED; MD, EQ$), for example, refers to a pure electric dipole and a photon described by a magnetic dipole and an electric quadrupole. An essentially fourfold repetition has been avoided in Table III. The functions corresponding to transitions not explicitly given in the table may be obtained from those which are included in the following way. To replace E by M and M by E, replace ϵ_1 by $-\epsilon_1$ and ϵ_2 by $-\epsilon_2$. To interchange M and E in the mixture, replace ϵ_2 by $-\epsilon_2$. In both cases, however, the efficiency coefficients of $Q, R, \cdots$ in (11) remain unchanged in magnitude and sign: $\epsilon = |\epsilon_1| + |\epsilon_2|$.

For the specific combinations investigated here, Eqs. (7c) were sufficiently redundant to yield relations among the D's. The following useful results were thus obtained. For the transition schemes $(D; D, Q)$, $(D; D, O)$, $(D; Q, O)$, $(Q; D, Q)$ and $(O; D, Q)$, $q = -\frac{1}{3}r$. Therefore, for these schemes $Q + \frac{1}{3}R$ is independent of $Re(\alpha\beta^*)$. This relation can easily be verified from the table in reference 7. Also, for all these schemes, $s = 0$. For the remaining transitions, $(Q; D, O)$, $(Q; Q, O)$, $(O; D, O)$ and $(O; Q, O)$, $q = -\frac{1}{3}r - \frac{1}{5}s$. Therefore, for these schemes $Q + \frac{1}{3}R + \frac{1}{5}S$ is independent of $Re(\alpha\beta^*)$. Hamilton's[6] pure-pure polarization functions can be obtained from Table III by setting $\alpha = 0$ or $\beta = 0$ and $\gamma = 0$ (for his θ-component) and $\gamma = \pi/2$ (for his ϕ-component).

3. DISCUSSION

As already pointed out by Ling and Falkoff,[7] care must be taken to use appropriate tables such as theirs for $Q, R, S, T \cdots$. One may also obtain R_2, S_2, r, s from such a table by picking out those terms from R and S which are proportional to $|\alpha|^2$ (these define R_2 and S_2) and to $Re(\alpha\beta^*)$ (these define r and s).

An examination of Table III shows that when the

TABLE III. Polarization correlation function describing a pure 2^{L_1} multipole photon and a mixed 2^{L_2}, 2^{L_3} multipole photon when the linear polarization and direction of propagation of one of these photons and only the direction of propagation of the other are determined by counters with over-all efficiencies ϵ_1 and ϵ_2. ($\epsilon = |\epsilon_1| + |\epsilon_2|$)[a].

$$\{\sigma_1 L_1; \sigma_2 L_2, \sigma_3 L_3\}_\gamma = [\epsilon Q + \mathfrak{A} \cos 2\gamma] + [\epsilon R + \mathfrak{B} \cos 2\gamma] \cos^2\theta + [\epsilon S + \mathfrak{D} \cos 2\gamma] \cos^4\theta + [\epsilon T + \mathcal{E} \cos 2\gamma] \cos^6\theta.$$

Transition scheme	$\mathfrak{A}$	$\mathfrak{B}$	$\mathfrak{D}$[b]	$\mathcal{E}$[c]
$(ED; MD, EQ)$	$-\epsilon_1 R + \epsilon_2(R - 4/3r)$	$\epsilon_1 R - \epsilon_2(R - 4/3r)$	0	0
$(ED; ED, EO)$	$-\epsilon_1 R + (1/6)\epsilon_2(4R - 10R_2 - 5r)$	$\epsilon_1 R - (1/6)\epsilon_2(4R - 10R_2 - 5r)$	0	0
$(ED; MQ, EO)$	$-\epsilon_1 R + (1/6)\epsilon_2(4R - 10R_2 - 7r)$	$\epsilon_1 R - (1/6)\epsilon_2(4R - 10R_2 - 7r)$	0	0
$(EQ; MD, EQ)$	$\epsilon_1(R+S) + \epsilon_2(R+S-4/3r)$	$-\epsilon_1(R+2S) - \epsilon_2(R+2S-4/3r)$	$(\epsilon_1+\epsilon_2)S$	0
$(EQ; ED, EO)$	$\epsilon_1(R+S) + (1/6)\epsilon_2(4R - 10R_2 - 5r$	$-\epsilon_1(R+2S) - (1/6)\epsilon_2(4R - 10R_2 - 5r$ $-24S + 30s)$	$\epsilon_1 S - \epsilon_2(4S - 5s)$	0
$(EQ; MQ, EO)$	$\epsilon_1(R+S) + \epsilon_2[(1/6)(4R - 10R_2 - 7r)$ $-(1/5)(5S_2 + 2s)]$	$-\epsilon_1(R+2S) - \epsilon_2[(1/6)(4R - 10R_2 - 7r)$ $-(1/5)(20S - 10S_2 - 19s)]$	$\epsilon_1 S$ $-(1/5)\epsilon_2(20S - 15S_2 - 21s)$	0
$(EO; MD, EQ)$	$(2/3)\epsilon_1 R + \epsilon_2(R - 4/3r + S)$	$-(2/3)\epsilon_1(R - 6S) - \epsilon_2(R - 4/3r + 2S)$	$-4\epsilon_1 S + \epsilon_2 S$	0
$(EO; ED, EO)$	$(1/3)\epsilon_1(2R - T)$ $+(1/6)\epsilon_2(4R - 10R_2 - 5r - 2T)$	$-(1/3)\epsilon_1(2R - 12S - 19T)$ $-(1/6)\epsilon_2(4R - 10R_2 - 5r$ $-24S + 30s - 38T)$	$-\epsilon_1(4S + 7T)$ $-\epsilon_2(4S - 5s + 7T)$	$(\epsilon_1+\epsilon_2)T$
$(EO; MQ, EO)$	$(1/3)\epsilon_1(2R - T)$ $+(1/6)\epsilon_2(4R - 10R_2 - 7r - 6S_2$ $-12/5s - 2T)$	$-(1/3)\epsilon_1(2R - 12S - 19T)$ $-(1/6)\epsilon_2(4R - 10R_2 - 7r - 24S + 12S_2$ $+114/5s - 38T)$	$-\epsilon_1(4S + 7T)$ $-\epsilon_2(4S - 3S_2 - 21/5s + 7T)$	$(\epsilon_1+\epsilon_2)T$

[a] The absolute values of ϵ_1 and ϵ_2 are indicated to emphasize that the efficiency number multiplying Q, R, S and T remains unchanged in magnitude and sign when the procedure given in the text is used to obtain correlation functions corresponding to transition schemes with electric and magnetic characters different from those tabulated.

[b] When $\mathfrak{D} = 0$, $S = 0$.

[c] When $\mathcal{E} = 0$, $T = 0$.

interference terms do not vanish none of the distributions are independent of the counter efficiencies. This is in contrast with the results from pure-pure transitions,[6] for which some distributions are independent of the efficiencies. One can also observe from this table that the presence of two octupoles can be immediately detected by the presence of a $\cos^6\theta \cos 2\gamma$ term in the polarization distribution, at least as far as the transitions considered here are concerned.

In general, one knows the non-polarization parameters R/Q, S/Q, $\cdots$ and the ranges of $|\beta/\alpha|$ and the phase[7] of β/α from an angular correlation experiment. If, as in reference 8, one measures for the polarization correlation the ratio of photon coincidences when $\gamma=\pi/2$ to when $\gamma=0$, one obtains the ratio $\rho(\theta)$, which is given by

$$\rho(\theta)=\frac{(\epsilon Q-\mathfrak{A})+(\epsilon R-\mathfrak{B})\cos^2\theta+\cdots}{(\epsilon Q+\mathfrak{A})+(\epsilon R+\mathfrak{B})\cos^2\theta+\cdots}$$
$$=\frac{(1-\mathfrak{A}/\epsilon Q)+(R/Q-\mathfrak{B}/\epsilon Q)\cos^2\theta+\cdots}{(1+\mathfrak{A}/\epsilon Q)+(R/Q+\mathfrak{B}/\epsilon Q)\cos^2\theta+\cdots}. \quad (12)$$

The polarization experiment now yields the polarization parameters $\mathfrak{A}/\epsilon Q$, $\mathfrak{B}/\epsilon Q$, $\cdots$. If the pure photon is dipole, only the first two polarization parameters occur, and from Table III these are the negative of each other. (This is probably true for any mixture combination, that is, when either L_2 or L_3 or both are greater than 3.) To test whether the data can be explained, for example, by the transition scheme (ED; MD, EQ) for which $q=-\frac{1}{3}r$, one must have from Table III

$$\frac{\mathfrak{A}}{\epsilon Q}=\frac{\epsilon_2-\epsilon_1}{\epsilon}\frac{R}{Q}-\frac{4}{3}\frac{\epsilon_2}{\epsilon}\frac{r}{Q} \quad (13)$$

or

$$y=\Gamma=\frac{r}{Q}=\frac{\bar{r}Re(\beta/\alpha)}{q_2+|\beta/\alpha|^2q_3-(1/3)\bar{r}Re(\beta/\alpha)}, \quad (14)$$

where $Q_2=|\alpha|^2q_2$, $Q_3=|\beta|^2q_3$, $r=\bar{r}Re(\alpha\beta^*)$ and where, if ϵ_1 and ϵ_2 are known, Γ is a known constant. Just as in Fig. 2 of reference 7, one may plot y *vs.* $|\beta/\alpha|$ for different values of the phase of β/α. The intercepts of $y=\Gamma$ with these curves may lead to one or more possible values of $|\beta/\alpha|$ and $Re(\beta/\alpha)$. The final possible values of $|\beta/\alpha|$ and $Re(\beta/\alpha)$ must then lie in the common range of these intensity parameters as just determined and as determined from the correlation experiment.

As a last example, let us suppose[13] that $T=0$ and that therefore (EQ; MD, EQ) is a possible scheme. From the values of $\mathfrak{A}/\epsilon Q$ and $\mathfrak{B}/\epsilon Q$ in Table III, we find, just as in (14), that $\Gamma_1=r/Q$ and $\Gamma_2=r/Q$, where Γ_1 and Γ_2 are known constants; also, that $\mathfrak{D}/\epsilon Q=S/Q=S_3/Q$. These relations lead to two negative tests for the proposed scheme: (1) $\Gamma_1=\Gamma_2$, (2) $\mathfrak{A}/\epsilon Q+\mathfrak{B}/\epsilon Q+\mathfrak{D}/\epsilon Q=0$. However, the latter test is satisfied by all transitions considered here; that is, independently of the counter efficiencies, the sum of all the polarization parameters vanishes identically. This result is probably true for all values of L, at least for pure-mixture transitions. The second test must therefore be looked upon as a consistency test on the data.

By choosing a set of three angular momenta for the three states of the nucleus, r and δ_3, where $S=|\beta|^2\delta_3$, are determined. Then the solution of the two simultaneous equations

$$\Gamma_1=r/Q=\bar{r}Re(\beta/\alpha)/\{q_2+|\beta/\alpha|^2q_3-(1/3)\bar{r}Re(\beta/\alpha)\}$$

and

$$\mathfrak{D}/\epsilon Q=S/Q=|\beta/\alpha|^2\delta_3/\{q_2+|\beta/\alpha|^2q_3-(1/3)\bar{r}Re(\beta/\alpha)\}$$

may lead to admissible values of $|\beta/\alpha|$ and $Re(\beta/\alpha)$. (They are admissible, for example, if $|\beta/\alpha|>0$ and $|\beta/\alpha|\geq Re(\beta/\alpha)$ or if $|\beta/\alpha|=0$ and $Re(\beta/\alpha)=0$.) Such an admissible solution must now lie in the range of these parameters as determined from a non-polarization experiment. Similar considerations may be applied to any of the schemes in Table III.

In conclusion, I should like to express my appreciation to Professor Deutsch for suggesting this problem and to Professor Goertzel for his unfailing aid.

[13] It will be recalled from reference 4 that the maximum power of $\cos^2\theta$ appearing in the pure-pure correlation function of $\leq$Min.(L_1, L_2). In the present case, therefore, the maximum power $\leq$Max.$\{$Min.(L_1, L_2), Min.$(L_1, L_3)\}$.

Asymptotic Expansion of Irregular Coulomb Function for Angular Momentum Zero

G. Breit and M. H. Hull, Jr.
Yale University, New Haven, Connecticut*
(Received June 12, 1950)

A justification is given for an expansion of the irregular Coulomb function, usually denoted by G_0, in terms of Bessel functions of the second kind with an imaginary argument. This expansion has been considered speculatively by Yost, Wheeler, and Breit and explicitly verified by Breit and Bouricius for a number of terms. A general rule of replacement of the Bessel functions of the first kind with an imaginary argument in the corresponding expansion of the regular Coulomb function is here established. The formulas developed are convenient for the calculation of coefficients of the energy.

Notation

M, M' and Ze, $Z'e$, masses and charges of the particles.
μ=reduced mass; $\mu^{-1}=M^{-1}+(M')^{-1}$.
m=mass of electron.
v=relative velocity of the particles.
$k=\mu v/\hbar$.
$L\hbar$=angular momentum.
$a=\hbar^2/\mu ZZ'e^2$.
$\eta=1/ka=ZZ'e^2/\hbar v$.
$\rho=kr$.
$x=(8\rho\eta)^{\frac{1}{2}}=(8r/a)^{\frac{1}{2}}$.
F_0, G_0=regular and irregular solutions of the differential equation for $r\times$radial function for $L=0$; the signs and normalization are as in YWB.
$C_0^2=2\pi\eta/(e^{2\pi\eta}-1)$.
$\Phi_0=F_0/C_0\rho$ is a power series in ρ the first term of which is 1.
$\Theta_0=C_0G_0$.
$\Gamma(x)$=gamma-function of x.
$\gamma=0.5772\cdots$=Euler's constant.
$q=2\eta(2\gamma-1+\text{R.P.}\Gamma'(i\eta)/\Gamma(i\eta))$ for $L=0$.
$\Psi_0=\Theta_0-\rho(2\eta\ln 2\rho+q)\Phi_0$ is a power series in ρ beginning with the term 1 and having no term in ρ.
$p=2\eta$ for $L=0$.

I. INTRODUCTION

It has been shown by Yost, Wheeler, and Breit[1] that in the limit of zero energy the quotient $G_L/(D_L\rho^{-L})=\Theta_L$ approaches a finite limit,

$$\lim_{\eta=\infty}\Theta_L=-(2/(2L)!)(x/2)^{2L+1}K_{2L+1}(x), \qquad (1)$$

where $K_\nu(x)$ is the Bessel function of an imaginary argument of the second kind defined by Whittaker and Watson's[2] Eq. (17.71). It has been also stated in that reference[1] that the replacement of K_{2L+1} by a series obtainable from the series for the regular Coulomb function by the substitution of the K_ν for the Bessel functions of an imaginary argument I_ν leads to values which agree in some cases with results obtained by direct calculation also at finite values of the energy. At the time there was no proof that the expansion of Θ_L in the K_ν is justifiable. For $L=0$ the expansion has been used by Breit and Bouricius.[3] These authors have verified the expansion for a number of terms by a rearrangement of the standard series for Θ_0. The quantity $\Gamma'(i\eta)/\Gamma(i\eta)$ which multiplies the regular function in the expression for Θ_0 was replaced in these calculations by Stirling's series for the logarithmic derivative of the Γ function. These calculations have been preceded by some closely related ones made by the present authors. Since then a different treatment has been published by Jackson and Blatt.[4] An explanatory note concerning the procedure of Breit and Bouricius was inserted in a footnote by Breit and Hatcher[5] and the relationship to the work of Jastrow[6] was pointed out. In the present note considerations are presented which demonstater that the replacement of the I_ν by the K_ν in the series for the regular function should lead to the result of employing Stirling's approximation for $\Gamma'(i\eta)/\Gamma(i\eta)$ in the standard expression for Θ_0. The replacements are meant to be made by means of Eqs. (7.24), (7.26) of Breit and Bouricius. These give

$$\Phi_0=\varphi_0+\varphi_1/\eta^2+\varphi_2/\eta^4+\cdots,$$
$$\varphi_0=(2/x)I_1(x),\ \cdots, \qquad (2)$$
$$-2\Theta_0/x^2=\theta_0+\theta_1/\eta^2+\theta_2/\eta^4\cdots \qquad (3)$$

and here the φ_i can be obtained from Eqs. (7.3), (7.31) of the same reference,[3] while the θ_i follow by replacing the I_ν by the K_ν. A proof can be given as follows.

It will first be noted that the expression for Θ_0 in terms of Ψ_0, Φ_0, p, q of YWB contains a term in $\ln\eta$ when ρ is expressed in terms of $r/a=\rho\eta$. The quantity q_0 contains $\Gamma'(i\eta)/\Gamma(i\eta)$. When Stirling's series is used for the logarithmic derivative of the gamma-function the term in $\ln\eta$ is removed everywhere, the two compensating terms occurring in the single factor $p\ln 2\rho+q$ which multiplies the regular function. The series for Θ_0 can be rearranged, therefore, as in Eq. (3). The symbols θ_i are independent of η but are functions of x. The cancellation of terms in $\ln\eta$ is essential for the validity of this form. The absence of positive powers of η is readily seen from the structure of Eq. (10) of YWB. The step of the proof, just conducted, will be referred to as step A.

* Assisted by the joint program of the ONR and AEC.
[1] Yost, Wheeler, and Breit, Phys. Rev. **49**, 174 (1936), referred to as YWB.
[2] E. T. Whittaker and G. N. Watson, *Modern Analysis* (Cambridge University Press, London, 1920), third edition, Chapter XVII.
[3] G. Breit and W. G. Bouricius, Phys. Rev. **75**, 1029 (1949), referred to as BB.
[4] J. David Jackson and John M. Blatt, Rev. Mod. Phys. **22**, 77 (1950).
[5] G. Breit and R. D. Hatcher, Phys. Rev. **78**, 110 (1950).
[6] R. Jastrow, Phys. Rev. **73**, 60 (1948).

It will next be noted that Whittaker's integral representation of Whittaker's confluent hypergeometric function gives

$$F_0+iG_0=(ie^{-i\rho}/C_0)\int_0^\infty t^{-i\eta}(t+2i\rho)^{i\eta}e^{-t}dt$$

$$=(i/C_0)\int_{i\rho}^\infty(\tau-i\rho)^{-i\eta}(\tau+i\rho)^{i\eta}e^{-\tau}d\tau, \quad (4)$$

where each of the integrals may be taken along an arbitrary path from the lower limit to the infinitely remote part of the complex plane to the right of the axis of pure imaginaries. This requirement is essential because it is necessary to require that

$$e^{-t}t^{L-i\eta+1}(t+2i\rho)^{L+i\eta-1}$$

have vanishing values at both limits of integration. In terms of the variable τ the original path of integration from $t=0$ to $t=\infty$, along the axis of reals in the t plane, corresponds to integration along the straight line $Im\tau=\rho$. This path may be deformed into a path along two straight lines, the first from $\tau=i\rho$ to $\tau=0$, the second from $\tau=0$ to $\tau=\infty$. In the process of deforming the path one must vary $\arg t=\arg(\tau-i\rho)$ as well as $\arg(\tau+i\rho)$ continuously. Accordingly $\arg(\tau-i\rho)$ on the vertical part of the path is $-\pi/2$, while $\arg(\tau+i\rho)$ on this part of the path is $+\pi/2$. There results, therefore, the factor $\exp(-\pi\eta)$ which multiplies

$$|\tau-i\rho|^{-i\eta}|\tau+i\rho|^{i\eta}$$

in the integrand. It now follows that

$$C_0(F_0+iG_0)=e^{-\pi\eta}\rho\int_0^1(1-u)^{-i\eta}(1+u)^{i\eta}e^{-i\rho u}du$$

$$+i\int_0^\infty\exp[-\tau-2\eta\tan^{-1}(\rho/\tau)]d\tau. \quad (5)$$

Hence

$$\Theta_0=C_0G_0=\Theta_0{}^I+\Theta_0{}^{II}, \quad (6)$$

where

$$\Theta_0{}^I=\int_0^\infty\exp[-\tau-2\eta\tan^{-1}(\rho/\tau)]d\tau \quad (6')$$

and

$$\Theta_0{}^{II}=e^{-\pi\eta}\rho\int_0^1\sin\left[-\rho u+\eta\log\frac{1+u}{1-u}\right]du. \quad (6'')$$

The real part of Eq. (5) gives

$$F_0=(\rho e^{-\pi\eta}/2C_0)\int_{-1}^{+1}(1-u)^{-i\eta}(1+u)^{i\eta}e^{-i\rho u}du$$

$$=(\rho e^{-\pi\eta}/2C_0)[|\Gamma(1+i\eta)|^2/i\rho]M_{i\eta,\frac{1}{2}}(2i\rho)$$

$$=C_0M_{i\eta,\frac{1}{2}}(2i\rho)/(2i), \quad (7)$$

in agreement with the fact that F_0 is the regular solution which can be expressed as a power series having for the first term $C_0\rho$. The quantity $\Theta_0{}^I$ is readily transformed into

$$\Theta_0{}^I=(x/2)\int_0^\infty\exp[-(x/2)(v+1/v)]$$

$$\times\exp[2\eta(\xi-\tan^{-1}\xi)]_{\xi=x/4\eta v}dv. \quad (8)$$

The establishment of Eqs. (6)–(8) will be referred to as part B of the proof.

It will be shown next that the expansion defined by part A of the proof can be obtained from the following symbolic expression for G_0

$$C_0(G_0)_{\text{symb}}=(\Theta_0)_{\text{symb}}=(x/2)\int_0^\infty e^{-(x/2)(v+1/v)}$$

$$\times\exp\{-2\eta\Sigma_1{}^\infty(-)^n\xi^{2n+1}/(2n+1)\}_{\xi=x/4\eta v}dv. \quad (9)$$

The relation of Eq. (9) to Eq. (8) is that of replacing $\xi-\tan^{-1}\xi$ by its Taylor expansion. The employment of the symbolic expression for G_0 is meant in the sense that if one expands the exponential containing ξ in a power series in $1/\eta$ and integrates over v then one obtains a representation of $G_0=\Theta_0/C_0$ which is claimed to be identical with that obtained by the Stirling series procedure described in part A of the proof. In fact according to Eq. (3)

$$-x^2\theta_s/2=(1/s!)[\partial^s\Theta_0/\partial(\eta^{-2})^s]_{\eta=\infty}. \quad (10)$$

This relation is true irrespective of questions of convergence of the right side of Eq. (3). In fact Stirling's asymptotic series for $\Gamma'(y)/\Gamma(y)$ has the property that the coefficient of $1/y^2$ can be obtained by successive differentiation of

$$\Gamma'(y)/\Gamma(y)-\ln y+1/2y \quad (11)$$

and equating both sides of the resultant equation as though Stirling's series were a convergent rather than an asymptotic one. The reason for this circumstance is the fact that the above expression is

$$-2\int_0^\infty\frac{tdt}{(t^2+y^2)(e^{2\pi t}-1)}=I \quad (12)$$

and that Stirling's series is obtainable by expanding $1/(t^2+y^2)$ in ascending powers of t^2/y^2 and integrating term by term in accordance with Eq. (12). On the other hand,

$$\{\partial^s I/\partial(y^{-2})^s\}_{y=\infty}$$

$$=-2\int_0^\infty\frac{t}{e^{2\pi t}-1}\left\{\frac{\partial^s}{\partial(y^{-2})^s}(t^2+y^2)^{-1}\right\}_{y=\infty}dt, \quad (13)$$

and

$$\left\{\frac{\partial^s}{\partial(y^{-2})^s}(t^2+y^2)^{-1}\right\}_{y=\infty}=s!(-)^{s-1}t^{2s-2}. \quad (13')$$

The differentiation under the integral sign in Eq. (13) is legitimate because the integrals converge for all derivatives.

In the present application the variable $y=i\eta$. The The term $\ln\eta$ in Eq. (11) is removed by a similar term arising from $\ln\rho$. The term in $1/y$ does not enter because $1/y$ is purely imaginary. The expression listed as Eq. (11) is, therefore, the one of interest. The differentiation of Θ_0 involves the differentiation of Φ_0, p, q and Ψ_0, ρ. An inspection of Eq. (18) of YWB shows that $p\rho=2r/a$ does not bring in η and that Ψ_0, Φ_0, and the expression listed under Eq. (11) are the only ones containing η. Since Ψ_0, Φ_0 are absolutely convergent their differentiation with respect to η^{-2} can be performed as though they were polynomials. It has just been shown that the same may be done employing Stirling's series for the expression arising from q and listed under (11). It follows, therefore, that one may use Eq. (10) in order to evaluate θ_s even though the series for Θ_0 in powers of η^{-2} is an asymptotic one.

Returning to Eq. (6) it will now be sufficient to consider separately the contributions arising from the two parts of Θ_0. The presence of $e^{-\pi\eta}$ in Θ_0^{II} causes the disappearance of its contributions to the right side of Eq. (10). The form of Θ_0^I presented as Eq. (8) and the expansion

$$\tan^{-1}\xi=\Sigma_0^{\infty}(-)^n\xi^{2n+1}/(2n+1)$$

show that these derivatives can be obtained by forgetting temporarily that the expansion of $\tan^{-1}\xi$ is inapplicable for $\xi>1$ because this circumstance is irrelevant in the evaluation of successive derivatives for $\xi=0$. It now follows that the θ_s can be obtained by means of a formal expansion of Eq. (9) in powers of η^{-2}, successive differentiation with respect to η^{-2} and evaluation for $\eta=\infty$ by means of Eq. (10). The procedure of performing differentiations is unnecessary, however, because the symbolic expansion furnishes the coefficients directly. Eq. (10) had to be brought into the discussion only as a means of defining coefficients of an asymptotic series. Since the power series in ξ for the second exponential in Eq. (9) is a power series in η^{-2} it has been proved by now that the formal expansion of the integrand of Eq. (9) in ascending powers of η^{-2} yields a series which is identical with that obtained through the replacement of $\Gamma'(i\eta)/\Gamma(i\eta)$ by Stirling's series. The part of the proof just concluded will be referred to as part C. It demonstrated the equivalence of the symbolic expansion to the employment of Stirling's series.

It remains to show that the θ_s are obtainable from the φ_s by replacing the $I_\nu(x)$ by the $K_\nu(x)$. A proof of this can be given by noting that the recurrence relations for the $I_\nu(x)$ and $K_\nu(x)$ are the same, that the Taylor expansion of the second exponential factor in Eq. (9) brings in powers of x which combine with the Bessel functions and that the powers are in agreement with the lowest permissible ones occurring for Φ_0. It is hard to write out this proof briefly and unambiguously because of the necessity for distinguishing between operations on the I_ν and K_ν. A more usual type of proof will be given, therefore, making use of the possibility of expressing Φ_0 in a form similar to Eq. (9).

It follows from Eq. (7) that

$$\Phi_0=\frac{\sinh(\pi\eta)}{2\pi\eta}\int_{-1}^{+1}(1-u)^{-i\eta}(1+u)^{i\eta}e^{-i\rho u}du$$
$$=\frac{\sinh(\pi\eta)}{\pi\eta}\int_{-\infty}^{\infty}\left\{\exp\left[i\eta\theta-i\frac{x^2}{8\eta}\tanh\frac{\theta}{2}\right]\right\}e^{\theta}(e^{\theta}+1)^{-2}d\theta. \quad (14)$$

In the second form of Φ_0, listed above, the parts $e^{\pi\eta}/2$ and $e^{-\pi\eta}/2$ of $\sinh(\pi\eta)$ will be first considered separately. For the first, the path of integration is moved to the line $Im\theta=\pi$, going around the point $\theta=\pi i$ in a small semicircle from below. For the second part the path is moved to the line $Im\theta=-\pi$, going around $\theta=-\pi i$ in a small semicircle from above. The two integrals can then be combined into one since the contributions on the rectilinear portions of the paths cancel. One finds by a short calculation

$$\Phi_0=-\frac{1}{2\pi\eta}\int_C\left\{\exp\left[i\theta\eta-i\frac{x^2}{8\eta}(e^{\theta}+1)\Big/(e^{\theta}-1)\right]\right\}$$
$$\times e^{\theta}(e^{\theta}-1)^{-2}d\theta, \quad (14')$$

where C is a contour around $\theta=0$, taken counterclockwise. Expressing this result in terms of u and introducing a variable of integration

$$\zeta=ix/(4\eta u), \quad (15)$$

one obtains

$$\Phi_0=\frac{i}{\pi x}\int_C\left(1+\frac{ix}{4\eta\zeta}\right)^{i\eta}\left(1-\frac{ix}{4\eta\zeta}\right)^{-i\eta}e^{-x\zeta/2}d\zeta$$
$$=\frac{i}{\pi x}\int_C e^{-(x/2)(\zeta+1/\zeta)}$$
$$\times\exp\{-2\eta\,\Sigma_1^{\infty}(-)^n(x/4\eta\zeta)^{2n+1}/(2n+1)\}d\zeta. \quad (16)$$

In the last formula C denotes a counterclockwise contour around the origin in the ζ plane. This form of Φ_0 is directly comparable with

$$-(2/x^2)[\Theta_0]_{\text{symb.}}$$

It is seen by means of Eq. (9) that aside from the fact that the integrals in Eqs. (9), (16) are over different variables and different paths their integrands have the same form and that the formula for Φ_0 contains an

extra factor $1/(\pi i)$. The standard integral

$$K_\nu(x)=\frac{(x/2)^\nu\Gamma(\frac{1}{2})}{\Gamma(\nu+\frac{1}{2})}\cos(\pi\nu)\int_0^\infty e^{-x\cosh\theta}\sinh^{2\nu}\theta d\theta$$

may be expressed as

$$K_\nu(x)=\frac{(x/2)^\nu\Gamma(\frac{1}{2})}{2\Gamma(\nu+\frac{1}{2})}\cos(\pi\nu)\int_0^\infty e^{-(x/2)(v+1/v)}\times\left(\frac{v}{2}-\frac{1}{2v}\right)^{2\nu}\frac{dv}{v} \quad (17)$$

and one has also

$$I_\nu(x)=\frac{(x/2)^\nu\Gamma(\frac{1}{2})}{\pi\Gamma(\nu+\frac{1}{2})}\int_0^\pi\cosh(x\cos\varphi)\sin^{2\nu}\varphi d\varphi$$

$$=\frac{(x/2)^\nu\Gamma(\frac{1}{2})}{2\pi i\Gamma(\nu+\frac{1}{2})}\cos(\pi\nu)\int_C e^{-(x/2)(\zeta+1/\zeta)}\times\left(\frac{\zeta}{2}-\frac{1}{2\zeta}\right)^{2\nu}\frac{d\zeta}{\zeta}, \quad (18)$$

the last contour being in the same sense as in Eq. (16). It will be noted that the integrands in Eqs. (17), (18) differ only by a change of the letter v to ζ, that the contours differ in the same way as in the representations of $-2\Theta_0/x^2$ and Φ_0 by Eqs. (9), (16) and that the extra factor $1/(\pi i)$ occurs in the formula for I_ν, just accounting for its presence in Eq. (16). The collection of the same powers of $1/\eta^2$ in Eq. (16) must lead to the Bessel function expansion of YWB since there can be only one such expansion. The same process applied to $-2\Theta_0/x^2$ through Eq. (9) will give in accordance with Eqs. (9), (16)–(18) the same form for the θ_s as for the φ_s but with the I_ν replaced by K_ν.

It may be mentioned that the symbolic expansion of Θ_0 and the analogous form for Φ_0 are reasonably convenient for the calculation of coefficients of η^{-2s}. The absence of the I_ν in the series for Θ_0 means that all terms of the asymptotic expansion vanish exponentially with x for large x. These terms provide, therefore, a continuous passage to the solutions of negative energy for which the particles are bound to each other by a deviation from the Coulomb law at short distances.

It is clearly possible to subtract the term in $[\Gamma'(i\eta)/\Gamma(i\eta)-\log\eta]\rho\Phi_0$ from Θ_0, expressing it by means of Stirling's series and then to add it again without the use of Stirling's series. The calculations of Jackson and Blatt[4] give a formula which has this relation to the asymptotic expansion discussed here. The law of formation of the coefficients appears to be simplest, however, for the asymptotic series and it can be used as a starting point for the modification just mentioned avoiding the somewhat laborious operations which appear to be necessary in the solution of the chain of equations for the θ_s. Whether one does so or not does not matter in the calculation of Ψ_0. This quantity is the only one used by BB.

In connection with the calculations of BB, the Bessel function expansion of Ψ_0 was compared with series calculations of Breit, Thaxton, and Eisenbud[7] for proton-proton interaction in the energy range 0.2 to 2.8 Mev, and of Thaxton and Hoisington[8] in the energy range 3 to 9 or 10 Mev. It was found that the Bessel function expansion including the term in E^2 gave values of Ψ_0 0.05 percent smaller than exact calculations at 2.8 Mev for $r=0.75e^2/mc^2$ and 0.001 percent larger for $r=e^2/mc^2$. In the higher energy range, the Bessel function expansion gave a result smaller than the results of exact calculations at 10 Mev by 0.07 percent for $r=0.75e^2/mc^2$, and at 9 Mev by 2.4 percent for $r=e^2/mc^2$. A Bessel function expansion including only the linear term in E was found to give agreement within 0.4 percent below 2.8 Mev.

[7] Breit, Thaxton, and Eisenbud, Phys. Rev. **55**, 1018 (1939).
[8] H. M. Thaxton and L. E. Hoisington, Phys. Rev. **56**, 1194 (1939).

The Zeeman Effect in Oxygen*

ALLAN F. HENRY†
*Sloane Physics Laboratory, Yale University,** New Haven, Connecticut*
(Received June 19, 1950)

This paper describes the calculation of the energy of magnetic sub-levels belonging to the $^3\Sigma$-state of O_2 in an external magnetic field. A general secular determinant is derived, the roots of which yield the desired energies. The results are particularly useful in the investigation of levels associated with a low value of the rotational quantum number. The perturbation representing the external magnetic field is introduced together with the perturbations leading to the rotational triplets; thus the distortion of the rotational triplets is considered from the beginning of the calculation. The work is performed in two stages to avoid the mathematical difficulties of treating a ninth-order secular determinant. Comparison between theory and experiment is satisfactory.

I. INTRODUCTION

As a result of the application of microwave techniques to the examination of molecular Zeeman patterns, a need has arisen for more exact theoretical expressions for the Zeeman energy levels of a diatomic molecule. Recently a method for computing these levels has been applied to the $^2\Pi_{3/2}$-state of $N^{14}O^{16}$;[1] the results of the calculation are in good agreement with experiment. In the present paper the same method is used to compute the energy values of the magnetic sub-levels of the rotational triplets in $O^{16}O^{16}$. The mathematical details are somewhat different, since O_2 is an example of Hund's case (*b*), whereas NO corresponds closely to Hund's case (*a*).

A general method of computing the Zeeman effect in O_2 has been discussed in a paper by Schmid, Budó, and Zemplén.[2] Their procedure is to suppose that the rotational spin triplets in O_2 are examples of Hund's case (*b*); then, employing eigenfunctions representing case (*b*), they introduce the external magnetic field as a perturbation on the three state functions corresponding to a rotational triplet. Essentially the result is that the effect of the external magnetic field is superimposed on the rotational triplets. Unfortunately, when applied to the most intense lines in the spectrum, their work agrees only approximately with the experimental results of Beringer and Castle.[3]

In this paper we start with a set of eigenfunctions corresponding to Hund's case (*a*). Certain perturbations (discussed below) treated in conjunction with this set lead to the rotational triplets in O_2. We introduce the operator representing the effect of the external magnetic field along with these perturbations and thereby take into account from the beginning of the calculation the distortion of the energy levels of the rotational triplets by the external magnetic field. The results of this calculation reduce to those of Schmid, Budó, and Zemplén for large values of the rotational quantum number, K; the approximation is increasingly good for all $K>5$. Hence we are primarily interested in the magnetic sub-levels belonging to the rotational levels for which $K=1$ and 3. (States for which K is even are prohibited by the homonuclear character of O_2.)

II. THE VECTOR MODEL FOR O_2

The energy levels to be investigated belong to the $^3\Sigma$-state of the oxygen molecule. This state is a close approximation to Hund's ideal case (*b*). The quantum number Λ, which represents the projection along the internuclear axis of the total orbital angular momentum, is zero. The total electronic spin, **S**, has associated with it a quantum number, S, which has the value unity; we suppose that **S** is the result of the addition of the individual spins of two electrons. The sum of **S** and the rotational angular momentum vector, **K**, is represented by the vector **J**, the total angular momentum of the molecule; associated with **K** and **J** are the quantum numbers K and J. For a given value of K, there are three possible values of J; these depend on the three possible orientations of **S** relative to **K**. As a result, each rotational energy level of the $^3\Sigma$-state of O_2 (characterized by a particular value of the rotational quantum number, K) is divided into three sub-levels, the values of J associated with these sub-levels being $J=K$; $J=K\pm1$. There is a magnetic moment associated with **J**, and this magnetic moment interacts with an external magnetic field, **H**. The result is that each member of a rotational triplet is further divided into $2J+1$ sub-levels which depend on the $2J+1$ possible orientations of **J** relative to **H**. The quantum number M_J is used to designate the projection of **J** in the direction of this field. The energy level diagram for the case $K=1$ is shown qualitatively in Fig. 1. We use the notation $W(J, K, M_J)$ to represent the energy of a magnetic sub-level. $W(J, K, M_J)$ will of course be a function of the strength of the external magnetic field, H. We shall compare the theory to be developed with experiment by finding those values of the magnetic field strength,

* Part of a dissertation to be submitted in partial fulfillment of the requirements for the degree of Doctor of Philosophy at Yale University.

† Now with Westinghouse Electric Corporation; Atomic Power Division; Pittsburgh, Pennsylvania.

** Assisted by the ONR.

[1] H. Margenau and A. Henry, Phys. Rev. **78**, 587 (1950).

[2] Schmid, Budó, and Zemplén, Zeits. f. Physik **103**, 250 (1936).

[3] R. Beringer and J. G. Castle, Jr., Phys. Rev. **78**, 581 (1950).

H, for which

$$W(J, K, M_J)-W(J, K, M_J-1)=\nu_0 \qquad (1)$$

where ν_0 is the operating frequency.

III. THE QUANTUM-MECHANICAL CALCULATION

Oxygen is an example of Hund's case (*b*). Nevertheless we begin the calculation with a set of eigenfunctions corresponding to case (*a*). Such eigenfunctions are sharp with respect to the quantum numbers J, S, Σ, and M_J, where Σ is the quantum number representing the component of $\mathbf{S}$ along the internuclear axis. We use this set so that we may take advantage of the work of previous authors; we expect the final result to be independent of the particular basic set of eigenfunctions employed, provided we consider the interaction of a sufficient number of eigenfunctions from the basic set.

The symbol $|J, S, \Sigma, M_J)$ is to designate an eigenfunction of the basic set; explicit dependence on vibrational and electronic quantum numbers is not indicated.

The functions $|JS\Sigma M_J)$ which correspond to Hund's ideal case (*a*), are obtained as eigenfunctions of the Hamiltonian of the oxygen molecule in a magnetic field only when certain terms in that Hamiltonian are neglected. In order to obtain a more accurate state function for the molecule, these terms must be treated as perturbations.

In doing this we first consider the terms in the Hamiltonian neglected when the wave equation of the entire molecule is separated into electronic, vibrational, and rotational parts. We indicate these terms by the symbol H'. They are given explicitly by Van Vleck,[4] who computes the following matrix elements of H' between eigenfunctions, $|JS\Sigma M_J)$

$$(JS\Sigma M_J|H'|JS\Sigma\pm1M_J)=B[(S\pm\Sigma+1)(S\mp\Sigma)(J\pm\Sigma+1)(J\mp\Sigma)]^{\frac{1}{2}}, \qquad (2)$$

$$(JS\Sigma M_J|H'|JS\Sigma M_J)=B[S(S+1)-\Sigma^2],$$

$B\equiv\hbar^2/2m\rho^2$; $m\equiv$reduced mass of molecule; $\rho\equiv$internuclear distance.

Two other perturbations of importance in this calculation were first introduced by Kramers.[5] The first involves the interaction of the spins of the two outermost electrons; the sum of these spins gives the molecule a total spin of 1. The second perturbation takes into account the interaction of the magnetic moments associated with $\mathbf{K}$ and $\mathbf{S}$. Mathematically, the two are,

$$A[3S_{z'}^2-S^2] \quad \text{and} \quad \mu\mathbf{K}\cdot\mathbf{S},$$

where A and μ are proportionality constants; $S_{z'}$ is the operator representing the component of total electron spin along the internuclear axis. Kramers gives the matrix elements of the first as

$$(JS\Sigma M_J|A(3S_{z'}^2-S^2)|JS\Sigma M_J)=A[3\Sigma^2-S(S+1)]. \qquad (3)$$

[4] J. H. Van Vleck, Phys. Rev. **33**, 467 (1929).
[5] H. A. Kramers, Zeits. f. Physik **53**, 422 (1929).

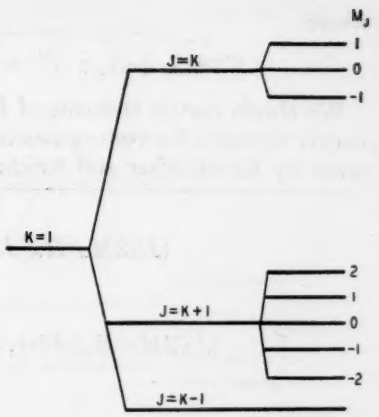

FIG. 1. Qualitative energy level diagram for the lowest rotational state of O_2 in a magnetic field.

He also provides matrix elements of the second between eigenfunctions corresponding to Hund's case (*b*) in which J, K, S, M_J are "good" quantum numbers. Following his work, we shall not introduce this perturbation until the stage at which we are dealing with state functions which correspond closely to case (*b*) eigenfunctions. The matrix elements then are

$$(JKSM_J|\mu\mathbf{K}\cdot\mathbf{S}|JKSM_J)=\tfrac{1}{2}\mu[J(J+1)-K(K+1)-S(S+1)]. \qquad (4)$$

Finally we consider the effect of the external magnetic field. Since Λ is 0, and O_2 has no nuclear spin, the only interaction with the external field is that involving S, the total electronic spin. This interaction may be written

$$H_m=2\mu_0\mathbf{H}\cdot\mathbf{S}; \quad \mu_0\equiv\text{the Bohr magneton.}$$

For the basic set of eigenfunctions $|JS\Sigma M_J)$, the total spin is quantized along the internuclear axis the projection being designated by the quantum number Σ. The arguments of the rotational part of $|JS\Sigma M_J)$ are the Eulerian angles θ and ψ. (See Kronig.[6] Without losing any generality we may let the Eulerian angle ϕ be zero.) These angles specify the position of an axis system, $X'Y'Z'$, with origin at the center of mass of the two nuclei and Z' lying along the internuclear axis of the molecule, relative to XYZ, another axis system having the same origin but with the X, Y, and Z directions fixed in space. We suppose that the external magnetic field of magnitude H is in the Z direction. Then, if we let $H_{x'}$, $H_{y'}$, and $H_{z'}$ be the components of $\mathbf{H}$ in the X', Y', and Z' directions, we obtain

$$H_{x'}=0; \quad H_{y'}=H\sin\theta; \quad H_{z'}=H\cos\theta.$$

Therefore

$$H_m=2\mu_0\mathbf{H}\cdot\mathbf{S}=2\mu_0[H_{x'}S_{x'}+H_{y'}S_{y'}+H_{z'}S_{z'}],$$
$$H_m=\mu_0H[2\cos\theta S_{z'}-i\sin\theta(S'^{+}-S'^{-})], \qquad (5)$$

[6] R. Kronig, *Band Spectra and Molecular Structure* (Cambridge University Press, London, 1930).

where

$$S'^{+}\equiv S_{x'}+iS_{y'};\quad S'^{-}\equiv S_{x'}-iS_{y'}.$$

We obtain matrix elements of H_m by employing the matrix elements between symmetric-top eigenfunctions given by Rademacher and Reiche[7] and by use of the relations

$$S'^{+}|S\Sigma)=[(S-\Sigma)(S+\Sigma+1)]^{\frac{1}{2}}|S,\Sigma+1),$$
$$S'^{-}|S\Sigma)=[(S+\Sigma)(S-\Sigma+1)]^{\frac{1}{2}}|S,\Sigma-1),$$

$|S\Sigma)$ being the spin part of $|JS\Sigma M_J)$. The matrix elements which we require are

$$\left.\begin{aligned}
(JS\Sigma M_J|H_m|JS\Sigma M_J)&=\frac{2\Sigma^2 M_J}{J(J+1)}\mu_0 H,\\
(JS\Sigma M_J|H_m|J+1,S\Sigma M_J)&=\frac{2\Sigma}{J+1}\left[\frac{[(J+1)^2-\Sigma^2][(J+1)^2-M_J^2]}{(2J+1)(2J+3)}\right]^{\frac{1}{2}}\mu_0 H,\\
(JS\Sigma M_J|H_m|JS,\Sigma+1,M_J)&=-\frac{\mu_0 H M_J}{J(J+1)}[(J-\Sigma)(J+\Sigma+1)(S-\Sigma)(S+\Sigma+1)]^{\frac{1}{2}},\\
(JS\Sigma M_J|H_m|J+1,S,\Sigma+1,M_J)&=\mu_0 H\left[\frac{(J+\Sigma+2)(J+\Sigma+1)(S+\Sigma+1)(S-\Sigma)[(J+1)^2-M_J^2]}{(J+1)^2(2J+1)(2J+3)}\right]^{\frac{1}{2}},\\
(JS\Sigma M_J|H_m|J-1,S,\Sigma+1,M_J)&=-\mu_0 H\left[\frac{(J-\Sigma)(J-\Sigma-1)(S+\Sigma+1)(S-\Sigma)(J^2-M_J^2)}{J^2(2J-1)(2J+1)}\right]^{\frac{1}{2}}.
\end{aligned}\right\}\quad(6)$$

In computing them we suppose $|JS\Sigma M_J)$ to be multiplied by a phase factor, $\exp[-i|\Sigma-M_J|\pi/2]$, so that the results given in the table of Rademacher and Reiche have a consistent sign.

Since we are interested in energy changes within a particular rotational level, we neglect the constant electronic and vibrational energies associated with that level. The total Hamiltonian of the molecule may then be written

$$H_0=H_T+H'+A[3S_{x'}^2-S^2]+\mu\mathbf{K}\cdot\mathbf{S}+H_m, \quad (7)$$

where H_T is the operator representing the rotational energy of the molecule in case (*a*); it is the Hamiltonian of the symmetric top for case (*a*) and has a matrix element which is the energy of the symmetric top. Thus

$$(JS\Sigma M_J|H_T|JS\Sigma M_J)=B[J(J+1)-\Sigma^2]. \quad (8)$$

In order to describe adequately the energy level belonging to a rotational triplet, it is necessary to use nine functions from the basic set in conjunction with the Hamiltonian (8). We avoid the ninth-order secular determinant which arises from such a procedure by performing the calculations in two stages. These stages are best described with the help of Fig. 2.

We begin with the nine eigenfunctions the energy levels of which are represented under the column "start" in Fig. 2; the values of the quantum numbers J and Σ which distinguish them are indicated on the figure; the energies associated with them are $B[J(J+1)-\Sigma^2]$. Since they are case (*a*) eigenfunctions, they have no correspondence to states of the O_2 molecule.

Next, we form a linear combination of

$$|J_1S,1,M_J),\quad |J_1S,0,M_J)\quad\text{and}\quad |J_1S,-1,M_J)$$

and diagonalize the Hamiltonian (8) with respect to it, omitting the term $\mu\mathbf{K}\cdot\mathbf{S}$ at this stage. This procedure gives rise to a secular determinant the roots of which are

$$\begin{aligned}
E(J_1,J_1+1)&=B[J_1(J_1+1)+1]-\frac{\lambda}{3}+\frac{\mu_0 H M_J}{J_1(J_1+1)}\\
&\quad+\left\{(2J_1+1)^2\left[B-\frac{\mu_0 H M_J}{J_1(J_1+1)}\right]^2\right.\\
&\quad\left.+\lambda^2-2B\lambda+\frac{2\lambda\mu_0 H M_J}{J_1(J_1+1)}\right\}^{\frac{1}{2}},\\
E(J_1,J_1)&=BJ_1(J_1+1)+\frac{2}{3}\lambda+\frac{2\mu_0 H M_J}{J_1(J_1+1)},\qquad(9)\\
E(J_1,J_1-1)&=B[J_1(J_1+1)+1]-\frac{\lambda}{3}+\frac{\mu_0 H M_J}{J_1(J_1+1)}\\
&\quad-\left\{(2J_1+1)^2\left[B-\frac{\mu_0 H M_J}{J_1(J_1+1)}\right]^2\right.\\
&\quad\left.+\lambda^2-2B\lambda+\frac{2\lambda\mu_0 H M_J}{J_1(J_1+1)}\right\}^{\frac{1}{2}},
\end{aligned}$$

where $\lambda\equiv\frac{3}{2}A$.

The notation $E(J_1, J_1+1)$, etc. will be explained below. By putting the roots (9) back into the three equations which led to the secular determinant, we evaluate the coefficients of the linear combination and obtain the

[7] H. Rademacher and F. Reiche, Zeits. f. Physik 41, 453 (1927).

eigenfunctions corresponding to the three roots. They are

$$\left.\begin{aligned}
\psi(J_1, J_1+1) &= a(J_1, J_1+1)|J_1S1M_J) \\
&\quad +b(J_1, J_1+1)|J_1SOM_J) \\
&\quad +c(J_1, J_1+1)|J_1S-1M_J), \\
a(J_1, J_1+1) &= c(J_1, J_1+1) \\
&= \frac{E(J_1, J_1+1)-E(J_1, J_1)}{\{2f^2+[E(J_1, J_1+1)-E(J_1, J_1)]^2\}^{\frac{1}{2}}}, \\
b(J_1, J_1+1) &= \frac{f}{\{2f^2+[E(J_1, J_1+1)-E(J_1, J_1)]^2\}^{\frac{1}{2}}}, \\
f &\equiv B[2J_1(J_1+1)]^{\frac{1}{2}}-\frac{2\mu_0 HM_J}{[2J_1(J_1+1)]^{\frac{1}{2}}},
\end{aligned}\right\} \quad (10)$$

$$\left.\begin{aligned}
\psi(J_1, J_1) &= a(J_1, J_1)|J_1S1M_J) \\
&\quad +b(J_1, J_1)|J_1SOM_J) \\
&\quad +c(J_1, J_1)|J_1S-1M_J), \\
a(J_1, J_1) &= c(J_1, J_1) = 1/\sqrt{2}; \quad b(J_1, J_1) = 0,
\end{aligned}\right\} \quad (11)$$

$$\left.\begin{aligned}
\psi(J_1, J_1-1) &= a(J_1, J_1-1)|J_1S1M_J) \\
&\quad +b(J_1, J_1-1)|J_1SOM_J) \\
&\quad +c(J_1, J_1-1)|J_1S-1M_J), \\
a(J_1, J_1-1) &= c(J_1, J_1-1) \\
&= \frac{E(J_1, J_1-1)-E(J_1, J_1)}{\{2f^2+[E(J_1, J_1-1)-E(J_1, J_1)]^2\}^{\frac{1}{2}}}, \\
b(J_1, J_1-1) &= \frac{f}{\{2f^2+[E(J_1, J_1-1)-E(J_1, J_1)]^2\}^{\frac{1}{2}}}.
\end{aligned}\right\} \quad (12)$$

If we let λ and H be zero, the energies (9) have the form $BK(K+1)$, where $K=J_1+1$ for $E(J_1, J_1+1)$, $K=J_1$ for $E(J_1, J_1)$ and $K=J_1-1$ for $E(J_1, J_1-1)$. Now $BK(K+1)$ is the form for the energy of a molecule in Hund's case (b) with $\Lambda=0$; hence the energies (9) are all associated with the same value of J but with the values of K: $K=J_1$; $K=J_1\pm1$. This accounts for the notation of Eq. (9). For instance, $E(J_1, J_1+1)$ signifies that the value of J associated with this energy level is J_1 and the value of K is J_1+1. It follows that the functions $\psi(J_1, J_1+1)$, $\psi(J_1, J_1)$ and $\psi(J_1, J_1-1)$ are eigenfunctions of the operators $\mathbf{K}$ as well as the operator $\mathbf{J}$; hence these functions correspond to Hund's case (b) and thus are a good representation for states in the O_2 molecule.

By repeating the above process for the cases $J=J_1+1$ and $J=J_1-1$, we obtain the energy level scheme shown in stage (1) of Fig. 2; if we were to include all possible levels arising from different values of J, stage (1) would

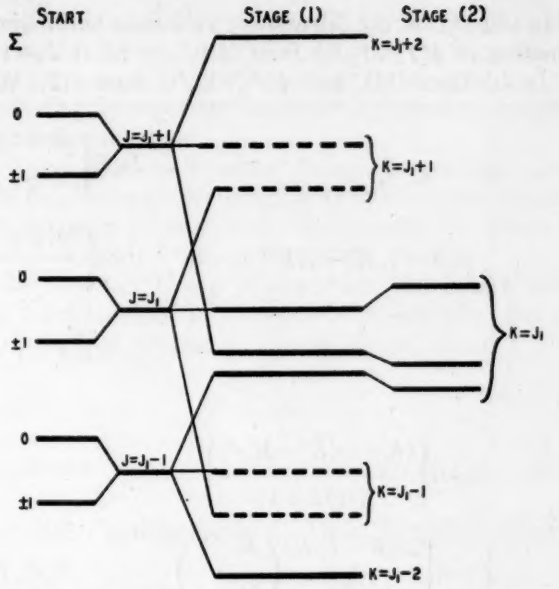

FIG. 2. Rotational energy levels at different stages of the calculation.

be a series of triplets, each set being associated with a different value of K. Except for the presence in the Hamiltonian of the operator representing the magnetic field and the temporary omission of the term $\mu\mathbf{K}\cdot\mathbf{S}$, the calculation and results at stage (1) are identical with those of Schlapp.[8] Since the state functions for O_2 must be antisymmetric in the exchange of the identical oxygen nuclei, states associated with even values of K do not exist; this result would appear automatically if we were to start with a basic set having the correct symmetry properties.

When $J=0$, Eq. (9) are not valid, since $[01, \pm1, M_J)$ does not exist. For this special case

$$\begin{aligned}
E(0, 1) &= -(4/3)\lambda+2B, \\
\psi(0, 1) &= a(0, 1)|011M_J)+b(0, 1)|010M_J) \\
&\quad +c(0, 1)|01-1M_J), \quad (13) \\
a(0, 1) &= c(0, 1) = 0; \quad b(0, 1) = 1.
\end{aligned}$$

TABLE I. Theoretical and experimental field strengths and line intensities for transitions between Zeeman components of first two rotational levels in O_2.

K	J	Transition $M_J \rightarrow M_J-1$	H (oersted) Calc.	Obs.	Relative intensity Calc.	Obs.
1	1	0→−1	5524.2	5527	0.35	0.60
1	1	1→0	~10,000.0	——	0.35	—
1	2	−1→−2	8703.6	8657	0.68	0.40
1	2	0→−1	7169.5	7149	1.00	1.00
1	2	1→0	6633.7	6620	0.99	1.00
1	2	2→1	6023.0	6014	0.66	0.60
3	2	0→−1	7447.5	7445	0.34	0.25
3	4	0→−1	8528.8	8500	0.68	0.80

[8] R. Schlapp, Phys. Rev. 39, 806 (1932).

In stage (2) of the calculation, we form a linear combination of $\psi(J_1-1, J_1)$ from (10), (or 13, if $J_1=1$), $\psi(J_1, J_1)$ from (11), and $\psi(J_1+1, J_1)$ from (12). We diagonalize the Hamiltonian (7) with respect to this combination, including now the term $\mu\mathbf{K}\cdot\mathbf{S}$. This leads to the secular determinant

$$\begin{vmatrix} E(K-1,K)-\mu(K+1)-W & 2\mu_0H\left[\frac{(K+1)(K^2-M_J^2)}{K^2(2K+1)}\right]^{\frac{1}{2}} \times\left[\frac{2a(K-1,K)}{\sqrt{2}}\left(\frac{K-1}{2K-1}\right)^{\frac{1}{2}} + b(K-1,K)\left(\frac{K}{2K-1}\right)^{\frac{1}{2}}\right] & 0 \\ 2\mu_0H\left[\frac{(K+1)(K^2-M_J^2)}{K^2(2K+1)}\right]^{\frac{1}{2}} \times\left[\frac{2a(K-1,K)}{\sqrt{2}}\left(\frac{K-1}{2K-1}\right)^{\frac{1}{2}} + b(K-1,K)\left(\frac{K}{2K-1}\right)^{\frac{1}{2}}\right] & E(K,K,-\mu-W & 2\mu_0H\left[\frac{K[(K+1)^2-M_J^2]}{(K+1)^2(2K+1)}\right]^{\frac{1}{2}} \times\left[\frac{2a(K+1,K)}{\sqrt{2}}\left(\frac{K+2}{2K+3}\right)^{\frac{1}{2}} - b(K+1,K)\left(\frac{K+1}{2K+3}\right)^{\frac{1}{2}}\right] \\ 0 & 2\mu_0H\left[\frac{K[(K+1)^2-M_J^2]}{(K+1)^2(2K+1)}\right]^{\frac{1}{2}} \times\left[\frac{2a(K+1,K)}{\sqrt{2}}\left(\frac{K+2}{2K+3}\right)^{\frac{1}{2}} - b(K+1,K)\left(\frac{K+1}{2K+3}\right)^{\frac{1}{2}}\right] & E(K+1,K)+\mu K-W \end{vmatrix} =0, \quad (14)$$

where quantities are labeled by the value of K; i.e., $E(K-1, K)$ is the energy for which $J=K-1$ and $K=K$. The roots of this determinant are the energy values required for the solution of Eq. (1). For large K or small H, (9) reduces to the analogous result in the paper of Schmid and Budó. Under the method of calculation used here it is necessary to consider the perturbation of neighboring rotational states in order to obtain for the energy a value which reduces to the Paschen-Back energy at very high fields.

We compute relative intensities by calculating for the transitions the numerical expression for the quantity

$$\begin{aligned}&\langle\psi(JKM_J)|S_x+iSy|\psi(JKM_J-1)\rangle^2 \times\exp\left[-\frac{W(JKM_J)}{kT}\right] \\ &=[-2a^2(J,K)+2a(J,K)b(J,K)(2J(J+1))^{\frac{1}{2}}]^2 \times\frac{1}{J^2(J+1)^2}(J+M_J)(J-M_J+1) \times\exp\left[-\frac{W(JKM_J)}{kT}\right], \quad (15)\end{aligned}$$

where the dependence of the eigenfunctions (10), (11) and (12) on the quantum number, M_J, is indicated in the notation $\psi(JKM_J)$. T stands for the absolute temperature of the oxygen in which the transition is taking place; k is the Boltzman constant.

IV. RESULTS

The values of H which are solutions of (1) and which lie in the experimental range of Beringer and Castle's apparatus are given in in Table I along with the intensities computed by use of (15). The expressions for the constants needed in the calculation are as follows: $B=1.4377$ cm^{-1}, $\mu=0.008$ cm^{-1}, $\lambda=1.985$ cm^{-1}, $\nu_0=0.31163$ cm^{-1}, $T=78°$ Kelvin, $\mu_0=4.66846\times10^{-5}$ cm^{-1}/oersted. The first three are taken from the article of Schlapp;[7] the third and fourth are experimental values. Results are given only for the energy levels for which K equals (1 or 3). For $K=3$, all values of the field strength other than the two given lie outside the experimental range (9200 oersted). All of the intense lines arise from transitions within these two levels. The principal cause of the discrepancies between theoretical

and experimental results is probably the proceedure of solving the problem in two stages. This proceedure neglects part of the distortion of the internal coupling by the magnetic field. Because the coupling in O_2 is quite small and is therefore easily broken down, this neglect may be significant. It is of no importance in NO (see reference 1) which has a large coupling energy.

Two more lines have been found in a preliminary investigation of the level for which $K=5$. The method of Schmid and Budó (which leads to results differing from experiment by about 200 oersteds for $K=1$) should be sufficient for the investigation of transitions within levels associated with values of K greater than 5. Even when this simpler formula is employed, the arithmetical work involved in identifying the entire spectrum resolved by Beringer and Castle is very laborious and has not been attempted.

I wish to thank Professor Henry Margenau for suggesting this problem and the method of solution and for helpful criticism and advice throughout the course of the calculation.

To Professor Robert Beringer and Mr. J. G. Castle, Jr. I am indebted for prepublication use of a part of their data on oxygen.

PHYSICAL REVIEW VOLUME 80, NUMBER 3 NOVEMBER 1, 1950

The Influence of a Transverse Magnetic Field on the Conductivity of Thin Metallic Films

E. H. SONDHEIMER*
*Research Laboratory of Electronics, Massachusetts Institute of Technology, Cambridge, Massachusetts***
(Received June 5, 1950)

The influence of a transverse magnetic field on the conduction properties of thin metallic films, of thickness comparable with the free path of the conduction electrons, is investigated. It is shown that, owing to scattering of electrons at the boundaries of the film, the Hall coefficient is increased, and the electrical resistance oscillates with the strength of the applied magnetic field.

I. INTRODUCTION

IN the theory of metals it is usual to assume that the conduction electrons may be treated as if they were free, the energy being proportional to the square of the wave vector. This assumption is sufficient to explain most of the conduction phenomena, but it leads to a zero change of resistance in a magnetic field, and to explain the usual type of magneto-resistance effect[1] it is necessary to employ more complicated models which take into account the departure of the energy surfaces from spherical symmetry.[2] However, in proving that there is no magneto-resistance effect for the free electron model it is tacitly assumed that all the dimensions of the specimen considered are large compared with the free path of the conduction electrons. This requirement is fulfilled under ordinary conditions, but it may break down in the case of thin films or wires at very low temperatures; under such conditions, where boundary scattering of electrons plays an essential part in determining the resistance, the alteration of the free electron trajectories in a magnetic field may lead to a finite magneto-resistance effect. This is a "geometrical" effect which is of a totally different type from the ordinary increase in resistance observed in the bulk metal, and, being essentially classical in nature, it is much simpler to understand. The details of the phenomena observed in any particular case depend, of course, upon the shape of the specimen and upon the relative configurations of specimen, electric current and magnetic field.

An effect of this type was first observed by MacDonald,[3] who found that the resistance of a thin sodium wire at low temperatures *decreased* when a longitudinal magnetic field was applied. In the present paper, however, we discuss only the case of a thin film placed in a magnetic field which is perpendicular to the plane of the film. Although this is perhaps not the simplest case to visualize, it is the easiest to analyze mathematically, and an exact solution can be obtained assuming only that the conduction electrons are quasi-free and that a time of relaxation can be defined for their collisions with the ionic lattice of the metal. These assumptions are sufficient to bring out all the essential features of the phenomena; a more general model, which leads also to a finite magneto-resistance effect in the bulk metal, will be examined in a later paper.

The increase in resistance of a thin metallic film in the absence of a magnetic field has been discussed by Fuchs,[4] and the present theory is a simple generalization of Fuchs' analysis. General formulas for the electrical conductivity and the Hall coefficient in a magnetic field of arbitrary magnitude are derived in Section II, both for the case in which the electrons suffer diffuse reflec-

---

* Now at Trinity College, Cambridge, England.

** This work has been supported in part by the Signal Corps, the Air Materiel Command, and the ONR.

[1] P. Kapitza, Proc. Roy. Soc. **A123**, 292 (1929).

[2] R. Peierls, Ann. d. Physik (5) **10**, 97 (1931).

[3] D. K. C. MacDonald, Nature **163**, 637 (1949).

[4] K. Fuchs, Proc. Camb. Phil. Soc. **34**, 100 (1938).

tion at the surface of the film and for the more general case of partially elastic surface scattering. In Section III we discuss the Hall coefficient in the limit of small magnetic fields, and find that it shows an increase above the bulk value analogous to the increase of the zero-field electrical resistance. The field variation of the magnetic effects is considered in Section IV, and it is shown in particular that, for films whose thickness is small compared with the free path, the resistance *oscillates* with the strength of the applied magnetic field. By measuring the position of the resistance maxima and minima it is possible to obtain a direct estimate of the momentum of the electrons at the surface of the Fermi distribution, and hence of the number of conduction electrons per unit volume.

II. GENERAL FORMULAS FOR THE MAGNETIC EFFECTS

(A)

We consider a metal film of thickness a, with its surfaces parallel to the xy-plane, which is subjected to an electric field $(\mathcal{E}_x, \mathcal{E}_y, 0)$ in the plane of the film and a transverse magnetic field $(0, 0, H)$. (For this particular arrangement, the condition $\mathrm{curl}\mathbf{E}=0$ ensures that the electric field components are constant across the thickness of the film.) The conduction electrons in the metal are regarded as free, in the sense that the energy E is related to the wave vector $\mathbf{k}$ by $E=\hbar^2|\mathbf{k}|^2/(8\pi^3 m)$, m being the effective mass of an electron. The distribution function f of the electrons is written in the form

$$f=f_0+f_1(\mathbf{v}, z), \tag{1}$$

where f_0 is the Fermi function $1/\{e^{(E-\zeta)/kT}+1\}$ (ζ being the Fermi energy level), $\mathbf{v}$ is the velocity of an electron, and f_1 is a function of $\mathbf{v}$ and z which must be determined. f_0 depends on the absolute value of $\mathbf{v}$ only.

Under the combined action of the applied fields and the collisions of the electrons with the lattice a steady state is set up, and the distribution function in the steady state is determined by the Boltzmann equation[5]

$$-(2\pi\epsilon/h)(\mathbf{E}+(1/c)\mathbf{v}\times\mathbf{H})\cdot\mathrm{grad}_{\mathbf{k}}f+\mathbf{v}\cdot\mathrm{grad}_{\mathbf{r}}f=-(f-f_0)/\tau, \tag{2}$$

where $-\epsilon$ is the electronic charge and τ is the time of relaxation of the conduction electrons. f is regarded as a function of the wave vector $\mathbf{k}$ and the space vector $\mathbf{r}$, and τ is assumed to depend on the absolute value of $\mathbf{k}$ only. The term $\mathbf{v}\cdot\mathrm{grad}_{\mathbf{r}}f$ must be included to take account of the non-uniform space distribution of the electrons in the z-direction.

On combining (1) and (2), using the relation $\hbar\mathbf{k}=2\pi m\mathbf{v}$ which holds for free electrons, and neglecting as usual the product of $\mathcal{E}$ with f_1 but retaining all the terms involving H, f_1 is found to satisfy the equation

$$\frac{\partial f_1}{\partial z}+\frac{f_1}{\tau v_z}-\frac{\epsilon H}{mcv_z}\left(v_y\frac{\partial f_1}{\partial v_x}-v_x\frac{\partial f_1}{\partial v_y}\right)=\frac{\epsilon}{mv_z}\left(\mathcal{E}_x\frac{\partial f_0}{\partial v_x}+\mathcal{E}_y\frac{\partial f_0}{\partial v_y}\right). \tag{3}$$

(B)

To solve this equation we put

$$f_1=(v_x c_1+v_y c_2)\partial f_0/\partial v, \tag{4}$$

where v is the absolute value of $\mathbf{v}$, and where c_1 and c_2 are functions of v, v_z and z which do not depend explicitly on v_x and v_y. From (3) and (4) we obtain the following simultaneous equations for c_1 and c_2:

$$\frac{\partial c_1}{\partial z}+\frac{c_1}{\tau v_z}+\frac{\epsilon H}{mcv_z}c_2=\frac{\epsilon}{mvv_z}\mathcal{E}_x, \tag{5}$$

$$\frac{\partial c_2}{\partial z}+\frac{c_2}{\tau v_z}-\frac{\epsilon H}{mcv_z}c_1=\frac{\epsilon}{mvv_z}\mathcal{E}_y. \tag{6}$$

Introducing the complex quantities $g=c_1-ic_2$, $\mathcal{F}=\mathcal{E}_x-i\mathcal{E}_y$, we can write these equations in the compact form

$$\frac{\partial g}{\partial z}+\frac{g}{\tau v_z}+\frac{i\epsilon H}{mcv_z}g=\frac{\epsilon}{mvv_z}\mathcal{F}. \tag{7}$$

The general solution is

$$g=\frac{\epsilon\tau\mathcal{F}}{mv[1+(i\epsilon H\tau)/mc]}\times\left[1+F(\mathbf{v})\exp\left\{-\left(1+\frac{i\epsilon H\tau}{mc}\right)\frac{z}{\tau v_z}\right\}\right], \tag{8}$$

where F is an arbitrary function of v and v_z.

The boundary conditions which are used to determine F depend on the nature of the scattering at the surface of the film. If we assume, as we shall do for the present, that the electrons are scattered entirely at random, with complete loss of their drift velocities, the distribution function of the electrons leaving each surface of the film must be independent of their directions of motion. This requirement is obviously satisfied if we take

$$F(\mathbf{v})=-1 \quad \text{for all } \mathbf{v} \text{ such that } v_z>0, \tag{9}$$

and

$$F(\mathbf{v})=-\exp\{[1+(i\epsilon H\tau)/mc](a/\tau v_z)\} \quad \text{for all } \mathbf{v} \text{ such that } v_z<0, \tag{10}$$

since these equations ensure that g (and therefore f_1) vanishes for electrons leaving the surfaces $z=0$ and $z=a$ respectively.

[5] A. H. Wilson, *The Theory of Metals* (Cambridge University Press, London, 1936), p. 158.

(C)

The current density $(J_x, J_y, 0)$ can now be calculated. For example, we have

$$J_x = -2\epsilon(m/h)^3 \int\int\int v_x f dv_x dv_y dv_z.$$

Using (1) and (4), introducing polar coordinates $(v, \theta, \tilde{\omega})$ in the v-space (with $v_z = v\cos\theta$) and integrating over $\tilde{\omega}$, this becomes

$$J_x = -2\pi\epsilon(m/h)^3 \int\int v^4 \sin^3\theta c_1 (\partial f_0/\partial v) dv d\theta.$$

There is a corresponding expression for J_y with c_1 replaced by c_2.

Introducing the complex current $\mathcal{J} = J_x - iJ_y$, and integrating over v by means of the formula

$$-\int \psi(v)(\partial f_0/\partial v)dv = \psi(\bar{v})$$

which holds for a degenerate electron gas, $\bar{v}$ being the velocity at the surface of the Fermi distribution, we obtain

$$\mathcal{J} = 2\pi\epsilon(m/h)^3 \bar{v}^4 \int_0^\pi \sin^3\theta g d\theta. \tag{11}$$

For comparison with experiment we require the *mean* current $\mathcal{J}_{Av}$, averaged across the thickness of the film. Combining (8), (9), (10) and (11), we obtain after some calculation

$$\mathcal{J}_{Av} = (1/a)\int_0^a \mathcal{J} dz = \kappa\sigma_0 \mathfrak{F}/\phi(s), \tag{12}$$

where

$$\frac{1}{\phi(s)} = \frac{1}{s} - \frac{3}{8s^2} + \frac{3}{2s^2}\int_1^\infty \left(\frac{1}{t^3} - \frac{1}{t^5}\right) e^{-st} dt, \tag{13}$$

and where s is a complex variable defined by

$$s = \kappa + i\beta, \tag{14}$$

with

$$\kappa = a/l, \quad \beta = a/r, \tag{15}$$

$l = \tau\bar{v}$ being the free path of the conduction electrons, and $r = m\bar{v}c/\epsilon H$ being the radius of the circular orbit of an electron in a magnetic field H. We have also used the expressions

$$\sigma_0 = ne^2 l/m\bar{v}, \quad n = (8\pi/3)(m\bar{v}/h)^3 \tag{16}$$

for the conductivity of the bulk metal and for the number of electrons per unit volume.

The formal similarity between Eq. (12) of the present paper and Eq. (17) of Fuchs' paper[4] should be noted.

(D)

Equation (12) contains all the results required for comparison with experiment. The electrical conductivity σ, for example, is measured by applying an electric field in, say, the x-direction and observing the current in this direction, no electric current being allowed to flow in the transverse direction. We therefore have $\sigma = \Re(\mathcal{J}_{Av})/\Re(\mathfrak{F})$, with $\Im(\mathcal{J}_{Av}) = 0$, where $\Re$ and $\Im$ denote the real and imaginary parts respectively. Using Eq. (12) for $\mathcal{J}_{Av}$ and eliminating $\mathfrak{F}$, we obtain for the ratio of the resistivity $1/\sigma$ to that of the bulk metal $1/\sigma_0$

$$\sigma_0/\sigma = \Re\{\phi(s)\}/\kappa. \tag{17}$$

The Hall coefficient is defined by $A_H = \mathcal{E}_y/HJ_x = -\Im(\mathfrak{F})/\{H\Re(\mathcal{J}_{Av})\}$, where $\mathcal{E}_y$ is the transverse electric field set up under the above experimental conditions, and we easily obtain

$$A_H/A_{H,0} = \Im\{\phi(s)\}/\beta, \tag{18}$$

where β is defined by (15), and where $A_{H,0} = -1/(ne\epsilon)$ is the Hall coefficient of the bulk metal. The ratios σ_0/σ and $A_H/A_{H,0}$ are therefore functions of the two dimensionless parameters κ and β only. Note that κ and β are both proportional to the thickness of the film; also that κ depends upon the temperature (its temperature variation being the same as that of the bulk electrical resistance), whereas β is proportional to the strength of the magnetic field but is independent of the temperature.

(E)

The theory is easily extended to apply to the more general case of partially elastic surface scattering, where a fraction, p, of the electrons arriving at the surface of the metal is supposed to be specularly reflected, retaining its drift velocity, while the rest are scattered diffusely. The analysis is formally identical with that given by Fuchs[4] for the case of zero magnetic field and will not be presented here in detail. (Note that our notation differs somewhat from that used by Fuchs, a, l, and p being used instead of t, λ_0, and ϵ.) It is found that all the results of the preceding sections apply, except that the function $\phi(s)$ defined by Eq. (13) must be replaced by $\phi_p(s)$, where

$$\frac{1}{\phi_p(s)} = \frac{1}{s} - \frac{3}{2s^2}(1-p)\int_1^\infty \left(\frac{1}{t^3} - \frac{1}{t^5}\right)\frac{1-e^{-st}}{1-pe^{-st}} dt. \tag{19}$$

This reduces to (13) when $p=0$, and to the bulk metal value $1/s$ when $p=1$.

III. THE HALL COEFFICIENT IN SMALL MAGNETIC FIELDS

When $\beta = 0$, Eq. (17) combined with (13) or (19) leads at once to expressions for the conductivity of a thin film in the absence of a magnetic field which have already been given by Fuchs [Eqs. (18) and (22) of his paper]. By expanding (13) and (19) in ascending powers of β and retaining only the linear term, corresponding expressions may be obtained for the Hall coefficient in the limit of vanishingly small magnetic fields. In this

limit $A_H/A_{H,0}$ is independent of β, and the resulting expression (for arbitrary p) can be written in the form

$$\frac{A_H}{A_{H,0}}=\frac{1-\frac{3}{4\kappa}(1-p)-\frac{3}{2\kappa}(1-p)^2\sum_{m=1}^{\infty}p^{m-1}\left\{\frac{m^4\kappa^4}{12}Ei(-m\kappa)-\exp(-m\kappa)\left(\frac{1}{2}-\frac{m\kappa}{6}+\frac{m^2\kappa^2}{12}-\frac{m^3\kappa^3}{12}\right)\right\}}{\left[1-\frac{3}{8\kappa}(1-p)-\frac{3}{4\kappa}(1-p)^2\sum_{m=1}^{\infty}p^{m-1}\left\{Ei(-m\kappa)\left(m^2\kappa^2-\frac{m^4\kappa^4}{12}\right)-\exp(-m\kappa)\left(\frac{1}{2}-\frac{5}{6}m\kappa-\frac{m^2\kappa^2}{12}+\frac{m^3\kappa^3}{12}\right)\right\}\right]^2}, \tag{20}$$

where

$$-Ei(-u)=\int_1^{\infty}(\exp[-ut]/t)dt. \tag{21}$$

When $p=0$, (20) reduces to

$$\frac{A_H}{A_{H,0}}=\frac{1-\frac{1}{8}\kappa^3Ei(-\kappa)-\frac{3}{4\kappa}(1-e^{-\kappa})-e^{-\kappa}\left(\frac{1}{4}-\frac{\kappa}{8}+\frac{\kappa^2}{8}\right)}{\left[1-\frac{3}{4}Ei(-\kappa)\left(\kappa-\frac{\kappa^3}{12}\right)-\frac{3}{8\kappa}(1-e^{-\kappa})-e^{-\kappa}\left(\frac{5}{8}+\frac{\kappa}{16}-\frac{\kappa^2}{16}\right)\right]^2}. \tag{22}$$

Equations (20) and (22) are to be compared with Eqs. (22) and (18) of Fuchs' paper. Figure 1 shows $A_H/A_{H,0}$ as a function of κ for three values of p, and should be compared with Fig. 1 of Fuchs' paper. It is seen that the Hall coefficient of thin films shows an increase above the bulk value analogous to, but smaller than, the increase of the electrical resistivity.[6] For very small values of κ, Eq. (20) reduces to

$$\frac{A_H}{A_{H,0}}=\frac{4}{3}\frac{1-p}{1+p}\frac{1}{\kappa(\ln\kappa^{-1})^2}; \tag{23}$$

the corresponding expression for the electrical resistance

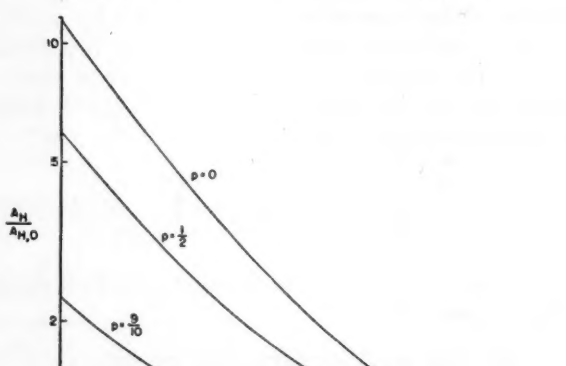

FIG. 1. The Hall coefficient of thin metallic films in the limit of small magnetic fields.

[6] As κ decreases from large values, A_H at first actually *decreases* slightly below the bulk value before increasing in the expected manner; the effect is very small, however, and is of no practical importance.

is[7]

$$\frac{\sigma_0}{\sigma}=\frac{4}{3}\frac{1-p}{1+p}\frac{1}{\kappa\ln\kappa^{-1}}=(\ln\kappa^{-1})\frac{A_H}{A_{H,0}}. \tag{24}$$

To my knowledge there are at present no experimental results with which to compare the theoretical predictions outlined above.

IV. THE FIELD VARIATION OF THE CONDUCTION PHENOMENA

(A)

The field dependence of σ and A_H is obtained from Eqs. (13), (17), (18) and (19) by keeping κ constant and varying β. Various methods have been used for evaluating the theoretical expressions numerically. Considering for the present the case $p=0$ only, we find that, for small $|s|$ (that is, for $\kappa^2+\beta^2\ll1$), $\phi(s)$ is most conveniently evaluated by means of the power series

$$\frac{1}{\phi(s)}=\frac{3}{4}(1-\gamma-\log s)+\frac{1}{2}s-\frac{1}{192}s^2(31-12\gamma-12\log s)+3\sum_{n=3}^{\infty}(-1)^n\frac{s^n}{(n-2)n(n+2)!}, \tag{25}$$

where γ is Euler's constant. For sufficiently large $|s|$, the asymptotic series

$$\frac{1}{\phi(s)}=\frac{1}{s}-\frac{3}{8s^2}+\frac{1}{16}e^{-s}\sum_{n=4}^{\infty}(-1)^n\frac{(n+4)(n-3)(n-1)!}{s^n} \tag{26}$$

may be used. For intermediate values of $|s|$, however,

[7] The expression given by Fuchs for σ_0/σ in the limit of small κ (Eq. (23) of his paper) differs from (24) and is incorrect.

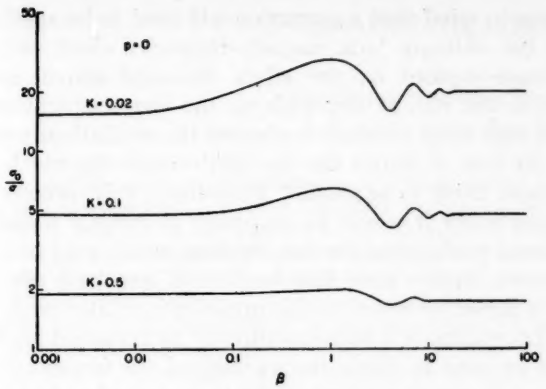

FIG. 2. The field variation of the resistivity, assuming diffuse surface scattering.

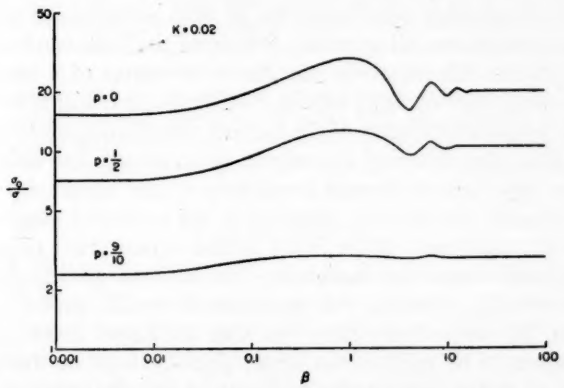

FIG. 3. The influence of the surface scattering coefficient on the field variation of the resistivity.

neither of these series is of practical utility, and numerical integration is necessary. The integrals required are of the form

$$\int_1^\infty \left(\frac{1}{t^3}-\frac{1}{t^5}\right)\exp(-\kappa t)\cos\beta t\,dt$$

and

$$\int_1^\infty \left(\frac{1}{t^3}-\frac{1}{t^5}\right)\exp(-\kappa t)\sin\beta t\,dt,$$

and cannot, in general, be expressed in terms of tabulated integrals. For small values of κ, however, approximate values can be obtained by replacing $\exp(-\kappa t)$ by $1-\kappa t+\frac{1}{2}\kappa^2 t^2$ and expressing the integrals in terms of the sine and cosine integrals for the argument β.

For non-zero values of p the calculations become very laborious. It is possible to write down expansions corresponding to (25) and (26), but in general it is simplest to evaluate the real and imaginary parts of (19) by direct numerical integration.

(B)

The results of the calculations are shown in Figs. 2 to 5 for some typical values of the parameters, sufficient to illustrate the general behavior and to show the effect of varying κ and p. The curves of Fig. 2 show σ_0/σ as a function of β for $p=0$ and for three values of κ, while those of Fig. 3 show σ_0/σ as a function of β for $\kappa=0.02$ and for three values of p. Figures 4 and 5 give the corresponding curves for $A_H/A_{H,0}$.

The most interesting result of these calculations is that the resistance of a thin metallic film oscillates with the strength of an applied transverse magnetic field. In the absence of a magnetic field the resistance is given by Fuchs' value; as the magnetic field is increased, the resistance increases initially and reaches its first maximum for a magnetic field such that β is approximately unity. The higher oscillations are of roughly constant spacing (successive maxima occurring for $\beta=1, 7, 13, 19, \cdots$ approximately) but decrease rapidly in amplitude, and in very strong magnetic fields the resistance tends to the constant asymptotic value

$$(\sigma_0/\sigma)_{\beta=\infty}=1+3(1-p)/8\kappa. \tag{27}$$

The oscillations die out and the resistance approaches the bulk value as κ tends to infinity or as p tends to unity; the *position* of the maxima and minima, however, is not appreciably affected.

The Hall coefficient, on the other hand, does not oscillate, and, as β increases from zero to infinity, A_H decreases steadily from the value (20) or (22) to the bulk metal value.[8]

(C)

It is interesting to compare Eq. (24) for the conductivity of a thin film when $H=0$ with Eq. (27) for the conductivity when $H=\infty$. The logarithmic dependence of σ on the ratio l/a when $l\gg a$ is due to the fact that,

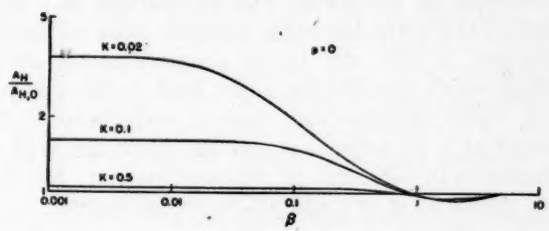

FIG. 4. The field variation of the Hall coefficient, assuming diffuse surface scattering.

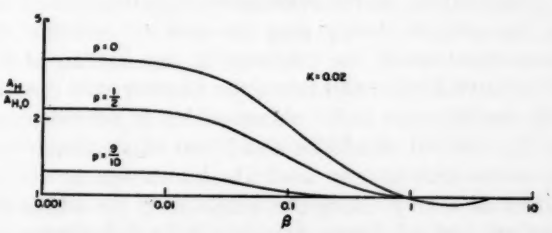

FIG. 5. The influence of the surface scattering coefficient on the field variation of the Hall coefficient.

[8] More precisely, A_H decreases to a value slightly below the bulk value, passes through a minimum and finally increases towards the bulk value. This behavior is similar to that of A_H for $H=0$ as a function of κ.

in the absence of a magnetic field, the dominant contribution to the current arises from electrons which, after reflection at the surface of the film, move in directions so nearly parallel to the surface that they do not travel freely to the opposite surface but make their next collision in the bulk of the metal. Equation (27) shows that the contribution of these "anomalous" electrons is eliminated in a strong transverse magnetic field, and the conductivity is given by an expression of the ordinary type (16), with a length of the order of the thickness of the film playing the part of an effective free path of the conduction electrons.

The oscillations in conductivity which occur for intermediate values of the magnetic field are connected with the oscillations in speed of an electron moving in perpendicular electric and magnetic fields, as pointed out by Chambers.[9] If we put $\mathcal{E}_y=0$ and regard $\mathcal{E}_x$ as the resultant of the applied electric field and the Hall field, kinetic arguments may be used to show that the distribution function is given by [compare Eq. (24) of Chambers' paper]

$$f(\mathbf{v},z)=f_0+\frac{ev_0\mathcal{E}_x}{mvv_z}\frac{\partial f_0}{\partial v}\int_{-z}^{0}\sin\left(\frac{\xi}{r\cos\theta}+\delta\right)e^{\xi/(l\cos\theta)}d\xi, \quad (28)$$

where $v_x=v_0\sin\delta$, $v_y=-v_0\cos\delta$, and the remaining symbols have their usual meanings. This expression is easily shown to be equivalent to the expression for f obtained by combining Eqs. (1), (4), (8) and (9) of the present paper and putting $\mathcal{E}_y=0$. The integrand of (28) represents the contribution to f of electrons which have traveled freely to the point considered from a distance ξ away in the z-direction, the limit of integration $-z$ corresponding to electrons which have traveled from the surface of the metal. The fluctuations in f as a function of z/r are due to the presence of an oscillating integrand in (28), and to the presence of the metal surface which provides an upper limit to the distance from which electrons can come to contribute to the current at z. In a metal of infinite extent the limit of integration in (28) may be replaced by $-\infty$, and f is then independent of z and no longer fluctuates.

(D)

Observations on the resistance oscillations predicted by the present theory may be used to estimate the momentum $m\bar{v}$ of the electrons at the surface of the Fermi distribution and hence the number n of conduction electrons per unit volume, which is related to $m\bar{v}$ by Eq. (16). It should be noted that this estimate can be made without any accurate knowledge as to the values of κ or p, since the values of β for which the maxima and minima occur are almost independent of the values of these parameters. It must, however, be borne in mind that a correction will need to be applied for the ordinary bulk magneto-resistance effect which is superimposed on the effect discussed above, and which will not be negligible at the low temperatures and high fields required to observe the oscillations even in the case of metals like the alkali metals for which it is most likely to be small.[10] To estimate this correction theoretically it would be necessary to employ a more general model than the free-electron model used in the present theory, since this leads to a zero bulk effect. It is hoped to return to this question in a later paper.

The values of n obtained directly as explained above can be used to check the validity of the free-electron theory by comparing them with the values of n obtained by combining estimates of l obtained from the increase in resistance of a thin film in the absence of a magnetic field (assuming some value for p) with estimates of $n^{\frac{1}{3}}l$ obtainable according to Eq. (16) from the bulk conductivity σ_0. Alternatively, the direct estimates of n may be used together with values of σ_0 to obtain l, and hence to obtain an estimate of the surface reflection coefficient p from the observed increase in resistance in the field-free case (which depends sensitively on the value[4] of p).

Finally, we give an estimate of the orders of magnitude which may occur in an actual experiment: these indicate that the resistance oscillations should be observable, though the experiment would probably not be easy. Note that the film thickness must be chosen to be neither too large, since it must be made small compared with the free path of the electrons, nor must it be too small, since otherwise it would not be possible to obtain sufficiently large values of β with the magnetic fields that are obtainable in practice. If we choose $a=10^{-4}$ cm, then a sufficiently long free path may be obtained by employing very pure unstrained specimens and liquid helium temperatures. Also, if the metal used is sodium, we have $n=2\cdot5\times10^{22}$, and we estimate that $\beta=1$ in a magnetic field of 60,000 gauss. Smaller magnetic fields would be required in the case of metals with a smaller number of conduction electrons.

The work described in this paper was begun at the H. H. Wills Physical Laboratory, University of Bristol, England and was completed at the Research Laboratory of Electronics of the Massachusetts Institute of Technology. The author would like to express his thanks to Professors N. F. Mott, J. C. Slater, and A. G. Hill for the hospitality extended to him at their laboratories. He also wishes to thank Mr. R. G. Chambers for showing him the manuscript of his paper before publication, and Miss Elizabeth J. Campbell of the Joint Computing Group of the Massachusetts Institute of Technology for patiently performing most of the heavy numerical work.

[9] R. G. Chambers, Proc. Roy. Soc. **A202**, 378 (1950).

[10] D. K. C. MacDonald, Proc. Phys. Soc. London A **63**, 290 (1950).

Photo-Disintegration of Silver and Aluminum*

B. C. DIVEN** AND G. M. ALMY
Physics Department, University of Illinois, Urbana, Illinois
(Received July 3, 1950)

The energy and angular distributions of protons emitted from Ag and Al nuclei when irradiated with the x-rays from a 22-Mev betatron were determined with the use of photographic nuclear emulsions. A maximum x-ray energy of 20.8 Mev was used with Ag and energies of 20.8, 17.1, and 13.9 Mev with Al.

With silver the number of neutrons emitted in the same irradiation was determined from the (γ, n) induced activity. The ratio of numbers of protons in each Mev interval to the total number of neutrons is compared to the same ratio calculated on the basis of various assumptions as to level density and nuclear reaction cross sections. The comparison suggests that the observed proton spectrum consists of two overlapping components. One is a lower energy group in rough quantitative agreement as to spectrum shape and numbers with calculations from reasonable assumptions as to statistical-model level densities and other nuclear parameters. The second group is a high energy tail (10–14 Mev) of protons definitely outside of the spectrum expected from the statistical model. Moreover, only the high energy group shows angular asymmetry with a preference for emission at 90° to the x-ray beam, which supports the hypothesis that these protons are emitted before the excitation energy is statistically distributed in the nucleus.

The ratio of total numbers of protons to neutrons emitted by Ag under 20.8-Mev bremsstrahlung radiation is 0.023 ± 0.008.

With Al protons are emitted with spherical symmetry and with a yield, for quanta above about 14 Mev, as large or larger than the (γ, n) yield determined by Hirzel and Wäffler at 17.6 Mev. The shape of the spectrum and the ratio of (γ, p) to (γ, n) cross sections are compatible with the assumption of a constant or slowly increasing level density in the residual nucleus, as expected for a light nucleus in the energy range involved. From the maximum energy of emitted protons the proton threshold was determined to be 8.6 ± 0.5 Mev.

For use with the theoretical calculation of the proton spectra, the (γ, n) cross sections as a function of x-ray quantum energy were determined for $Ag^{107,109}$, Al^{27}, and also for Cu^{63}. The cross section of Ag^{109} was found to have a maximum of 0.32×10^{-24} cm^2 at 16.5 Mev, Cu^{63} a maximum of 0.10×10^{-24} cm^2 at 17.5 Mev. For Al^{27} the cross section is still rising at 22 Mev.

I. INTRODUCTION

MEASUREMENTS of relative cross section of (γ, p) and (γ, n) reactions in a number of elements have been reported by Hirzel and Wäffler[1] and Perlman and Friedlander.[2] In all cases of elements of medium weight, where it is appropriate to apply the statistical theory of nuclear reactions, the observed proton yields were much larger than those predicted, often by a factor of a thousand. Attempts at explaining the large yield have been made by Courant,[3] by Levinger and Bethe,[4] and by Schiff.[5] Their suggestions will be discussed in the light of the results of this paper.

The present experiments were undertaken to see whether a more detailed study of the protons emitted in a (γ, p) reaction would shed light on the processes involved in the nuclear photo-effect. We have determined the energy and angular distributions of protons emitted from silver and aluminum when excited with x-rays from a 22-Mev betatron. We shall show in the last section of the paper that the experimental results do suggest a basis for explaining the anomalously large proton yields observed for many nuclei.

Similar studies with similar techniques have been made by Toms and others[6] with magnesium and by Curtis and others[7] with rhodium.

II. EXPERIMENTAL METHOD

The experimental arrangement is shown in Fig. 1. The betatron target T was the source of x-rays of which a thin pencil passed through the laminated lead collimator C and lead wall W, through the 0.003-in. aluminum entrance window of the evacuated exposure chamber, along the length of foil of the metal under study, out of the chamber, and through the monitors. The primary monitor was a Victoreen 100-roentgen thimble surrounded by 4 cm of aluminum wall whose response was calculated according to Fowler, Lauritsen, and Lauritsen.[8] The beam also passed through a tantalum foil, $0.002 \times 1 \times 1$ in., inducing, by a (γ, n) reaction, an 8.2-hr. activity which served as an additional monitor.

The collimator confined the x-ray beam to a cone of angular width 0.0115 radian. The beam diameter was 0.75 cm at the entrance window and 1.115 cm at the exit window. The collimator and lead wall interposed $12\frac{1}{2}$ in. of lead in the beam, except for the transmitted pencil.

The exposure chamber was a brass tube with a port on one side which held a pair of 1×3-in. photographic plates (Ilford C-2, 200μ emulsion). The surfaces of the plates were parallel and separated by 1.80 cm. The edges of the plates nearer the beam were 3.81 cm from the center of the beam and parallel to the beam.

The irradiated foil, 12 in. long, was supported by a half-cylinder of thin-walled aluminum $1\frac{1}{2} \times 13$ in. It was placed in the chamber nearly, but not quite, parallel to the center of the beam. The surface of the foil was perpendicular to the surfaces of the plates. The chamber was evacuated and water vapor was admitted

* Assisted by the joint program of ONR and AEC.
** AEC Predoctoral Fellow; now at Los Alamos Scientific Laboratory, Los Alamos, New Mexico.
[1] O. Hirzel and H. Wäffler, Helv. Phys. Acta **20**, 373 (1947).
[2] M. L. Perlman and G. Friedlander, Phys. Rev. **74**, 442 (1948); **75**, 988 (1949).
[3] E. D. Courant, Phys. Rev. **74**, 1226 (1948).
[4] J. S. Levinger and H. A. Bethe, Phys. Rev. **78**, 115 (1950).
[5] L. I. Schiff, Phys. Rev. **73**, 1311 (1948).
[6] Toms, Halpern, and Stephens, Phys. Rev. **77**, 753 (1950).
[7] Curtis, Hornbostel, Lee, and Salant, Phys. Rev. **77**, 290 (1950), and private communication from Dr. Hornbostel.
[8] Fowler, Lauritsen, and Lauritsen, Rev. Mod. Phys. **20**, 263 (1948).

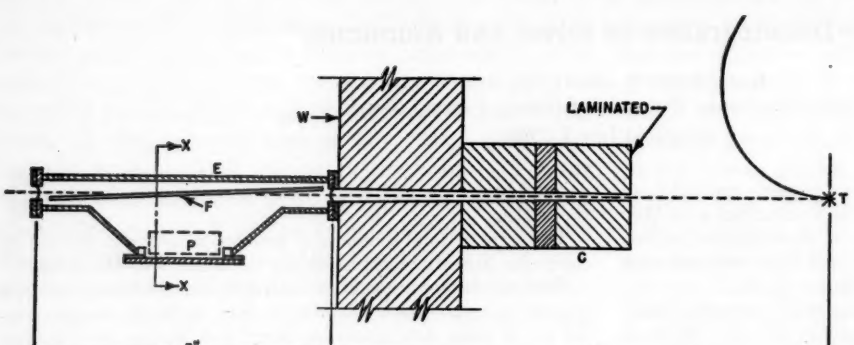

FIG. 1. Two sections of exposure chamber E and collimator C. T, betatron target; W, lead wall; F, foil; P, photographic plates; A and B, magnet pole pieces. Dashed circle indicates size of x-ray beam. The tilt of the foil is exaggerated.

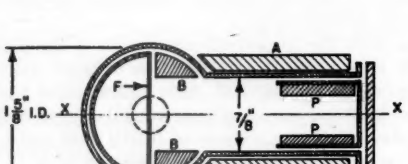

to a pressure of 18 mm Hg to avoid desiccation of the emulsion.

Troublesome fogging due to low energy electrons scattered from the foil was reduced adequately by applying a magnetic field of about 2000 gauss in the half of the chamber nearer the betatron. For this purpose permanent magnetron magnets with soft iron pole strips were used.

The exposures given were 2000 to 2500 roentgens at the foil. At the end of an exposure on silver the 24.5-min. activity induced in the foil by a (γ, n) reaction was counted for each of several one-cm sections along the length of the foil. This served, first, to measure the variation of x-ray intensity along the foil and, second, to determine the number of neutrons produced in the foil by the same irradiation for which the protons were observed and counted in the emulsions. As a further check on intensity variation along the foil, the 10-min. activity of 1-cm Cu strips placed as extensions of the foil at each end were counted at the end of each run. With an Al foil the 7.5-sec. (γ, n) induced activity decayed too rapidly to measure and the Cu strips alone were used.

For each proton track observed in the emulsion the projection of the range onto the plane of the plate, the angle to the beam, and the angle of dip as the proton entered the emulsion were measured. To be accepted a track was required to start at the surface of the emulsion and to have a direction compatible with an origin in the irradiated part of the foil. Angles to the beam from 20° to 160° were accepted.

The energy loss of the protons in the emulsion was obtained from the range-energy relations of Lattes, Fowler, and Cuer.[9] To these energies were added the energy which would have been lost if the proton traversed one-half of the foil thickness at the angle involved. The Ag foil weighed 12.58 mg/cm² and the Al foil 4.74 mg/cm². The uncertainty in energy due to foil thickness is equal to the correction added and varied for the foils chosen from about 0.1 Mev to 0.6 Mev, depending on the energy and angle of the proton. A calculation showed that scattering in the foils does not materially affect the angular distribution, plotted in 20° intervals.

Background exposures were taken at each betatron energy used, by removing the metal foil from the chamber and exposing a pair of plates in an otherwise normal run. The background plates were analyzed in the same manner as plates taken with silver or aluminum foils in place.

A source of background which is not subtracted by the above procedure is the (n, p) process in the foil itself. However, from an earlier approximate measurement of the fast neutron flux and approximate knowledge of the (n, p) and (γ, p) cross sections, it is estimated that with a silver foil less than 10^{-4} of the protons observed come from (n, p) reactions. For the Al foil the fraction is less than 10^{-2}. The distribution in dip angle of the proton tracks also indicates that nearly all of the protons come from the part of the silver foil irradiated by x-rays and not from the whole foil as would be expected for (n, p) protons.

III. EXPERIMENTAL RESULTS

Silver

An area of 291 mm² on two pairs of plates exposed at 20.8 Mev disclosed 676 tracks of protons, with energies greater than 3 Mev, which satisfied the selection criteria. After corrections for the measured variation of

[9] Lattes, Fowler, and Cuer, Proc. Roy. Soc. 59, 883 (1947).

x-ray intensity along the foil the number of protons per unit solid angle was plotted against angle between beam and proton emission, in Fig. 2, for three energy intervals. For energies up to 10 Mev the distribution appears to be spherically symmetrical. Above 10 Mev, however, there is pronounced asymmetry with emission at 90° to the beam most probable. The energy distribution is plotted in Fig. 3.

The total yield was 1.29 protons per r per mm length of foil. The number of neutrons produced in the foil in the same irradiations was found by counting, immediately after each run, the 24.5-min. activity extrapolated to saturation, induced by a (γ, n) reaction in Ag^{107}. For this purpose an end window counter was calibrated against a RaE source and its efficiency determined to be 0.135. We found 1.89 disintegrations per r per mm of foil leading to the observed 24.5-min. activity. The same reaction leads also to an 8.2-day isomer which we do not measure but we assume that the reaction leads with equal probability to the two isomers. We also measured the $Ag^{109}(\gamma, n)Ag^{108}$, 2.3-min. activity as well as the 24.5-min. activity in separate short irradiations with a thin foil and found the 2.3-min. activity to be 1.9 times as strong as the 24.5-min. activity. The total yield of neutrons was therefore $(2\times1.89+1.9\times1.89)/0.135$ or 54.6 neutrons per r per mm of foil.

Correcting for isotopic abundance, the 2.3-min. Ag^{108} activity was just 2.0 times the 24.5-min. Ag^{103} activity, as would be expected if (1) the two isomers of Ag^{106} are equally populated in the reaction, and (2) the (γ, n) cross sections of Ag^{107} and Ag^{109} are identical. The latter condition is supported by the observation that the (γ, n) thresholds and shapes of excitation curves (Fig. 7) of Ag^{107} and Ag^{109} are nearly identical.

Finally, the ratio of numbers of protons to neutrons emitted from silver during an exposure to a 20.8-Mev x-ray continuum is $1.29/54.6$ or 0.023 ± 0.008. The largest factor in the uncertainty came from errors in the determination of the neutron yield from the beta-activity and no allowance was made for the assumption that the isomers of Ag^{106} are equally populated in the reaction. The ratio of protons to neutrons is independent of variation and uncertainty in absolute intensity of x-rays along the foil (which are considerable in this arrangement), fluctuations of source intensity, and area of foil irradiated.

Aluminum

With an aluminum foil (4.74 mg/cm²) in the chamber, exposures were made at three betatron energies and the proton tracks were measured on four pairs of plates as shown in Table I.

The energy distributions are plotted in Fig. 4 and the angular distributions in Fig. 5. No pronounced angular asymmetry was observed.

An additional area of 549 mm² on the 17.1-Mev plates was searched for protons of energy more than 5 Mev to determine the maximum proton energy and hence the (γ, p) threshold. The highest energy observed was 8.5 Mev and 9 protons were found in the interval 8.0 to 8.5 Mev. We therefore estimate the proton threshold to be $17.1-8.5=8.6\pm0.5$ Mev. This is in reasonable agreement with the value 9.2 ± 0.4 Mev computed from the (γ, n) threshold (14.0 Mev)[10] and the energy of the positron emitted from Al^{26} (3.0 Mev).

(γ, p) cross sections averaged over wide bands of x-ray energies were obtained in the following manner. First, the number of protons per atom per r at 17.1 Mev was subtracted from the number per atom per r at 20.8 Mev. The difference arises from the effect of a band of x-rays obtained by subtracting the x-ray spectra (number of quanta *vs.* energy) for the two betatron energies each normalized to represent a spectrum which would produce 1 r response in the aluminum-shielded monitor. The band extends from 12 to 20.8 Mev with most of the quanta in the region from 16 to 20 Mev. Similarly, the difference in yields at betatron energies of 17.1 and 13.9 Mev is associated with a band of quanta extending from 11 to 17.1 Mev but mainly between 13 and 16 Mev. Finally, the protons observed at 13.9-Mev betatron energy are due to a band of x-rays from 11 to 13.9 Mev, since no protons of energy less than 2 Mev were recorded and the proton threshold is about 9 Mev. In the three intervals the cross sections were as given in Table II.

These values should be reliable to within a factor of two. They are of the same order of magnitude as the $Al(\gamma, n)$ cross section at 17.5 Mev, 3.2×10^{-27} cm², found by Wäffler and Hirzel.[11]

IV. ENERGY DEPENDENCE OF PHOTO-NEUTRON CROSS SECTIONS

In order to interpret the proton energy distributions we need to know the variation with energy of the (γ, n)

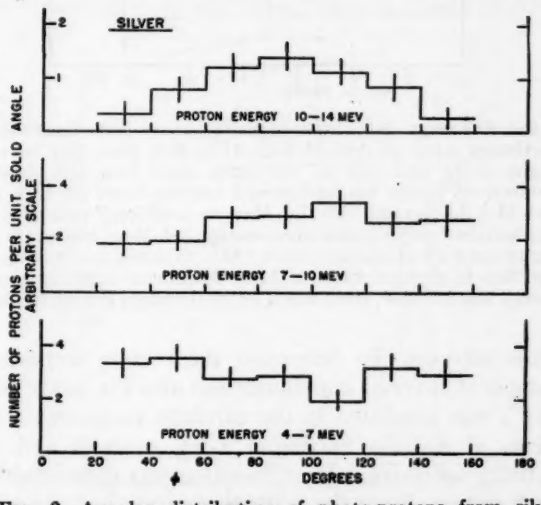
SILVER
PROTON ENERGY 10—14 MEV
PROTON ENERGY 7—10 MEV
PROTON ENERGY 4—7 MEV
NUMBER OF PROTONS PER UNIT SOLID ANGLE ARBITRARY SCALE
0 20 40 60 80 100 120 140 160 180
φ DEGREES

FIG. 2. Angular distribution of photo-protons from silver. Maximum x-ray energy, 20.8 Mev. ϕ is angle of proton emission with respect to x-ray beam.

[10] McElhinney, Hanson, Duffield, and Diven, Phys. Rev. 75, 542 (1949).
[11] H. Wäffler and O. Hirzel, Helv. Phys. Acta 21, 200 (1948).

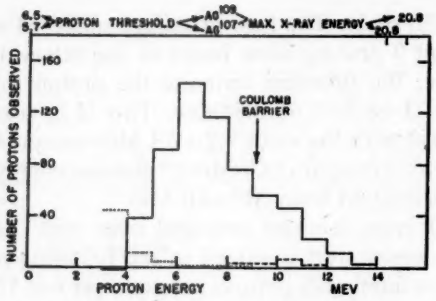

FIG. 3. Energy distribution of photo-protons emitted from silver between angles to the beam of 20° and 160°. Solid lines are numbers of proton tracks less background (dotted line). Dashed line represents tracks which penetrate entire emulsion plotted according to length of track in emulsion, and not included in solid-line plot.

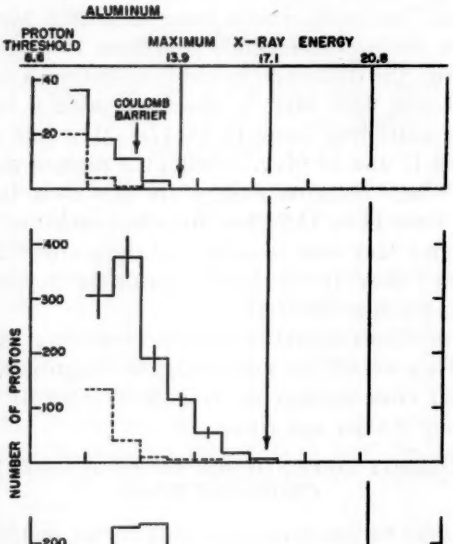

FIG. 4. Energy distribution of photo-protons from aluminum at maximum x-ray energies of 13.9, 17.1, 20.8 Mev, and between angles of 20° and 160° to the beam. Solid lines are observed numbers of tracks less background (dotted lines) for 13.9- and 20.8-Mev histograms. At 17.1 Mev an additional area of plate was searched only for protons of energy >5 Mev; histogram and background are normalized below 5 Mev to correspond to observed numbers of protons above 5 Mev. Maximum observed proton energy was 8.5 Mev, from which (γ, p) threshold is 8.6±0.5 Mev.

cross sections. To determine these cross sections, a sample of silver or aluminum, and also Cu, $0.005'' \times \frac{3}{4}'' \times 1''$, was irradiated in the carefully monitored x-ray beam at various maximum x-ray energies and the activity following a (γ, n) reaction was determined at each energy. From the activation curves and the x-ray spectrum, the energy dependence of the (γ, n) cross section can be deduced.

The observed saturated activity per r per min. per atom from a (γ, n) reaction of cross section $\sigma(E)$ in-

TABLE I. Protons from aluminum.

Betatron energy (Mev)	Exposure (r)	Area searched (mm²)	Protons observed	Net protons per atom per $r \times 10^{19}$
20.8	2010	114	560	2.8
20.8	2580	86	574	
17.1	2360	217	429	1.7
13.9	1500	217	109	0.3

TABLE II. Cross section for the (γ, p) reaction in Al.

Energy (Mev) Range (Mev)	Energy (Mev) Average (Mev)	$\sigma_{\gamma,p}$ (millibarns)
12–20.8	18	6
11–17.1	14.5	6
11–13.9	12.5	1.5

duced by the spectrum of x-rays with $N(E, E_m)$ quanta per unit energy interval per unit area is,

$$A = K \int_{B_n}^{E_m} \sigma_{\gamma,n}(E) N(E, E_m) dE \Big/ \int_0^{E_m} N(E, E_m) i(E) dE,$$

where E is the quantum energy, E_m the maximum x-ray energy, B_n the (γ, n) threshold, and $i(E)$ the sensitivity of the monitor in r per quantum of energy E per unit area of beam. We have computed the monitor response $i(E)$, following Fowler, Lauritsen, and Lauritsen.[8] The x-ray spectrum used was that given by Schiff.[12] Normalization was accomplished by computing the spectrum $N(E, E_m)$ for each E_m which would make the denominator in the expression for A correspond to 1 r. K is then the counter efficiency. $\sigma(E)$ was obtained by replacing the integral expression for A with the following equations and solving them step by

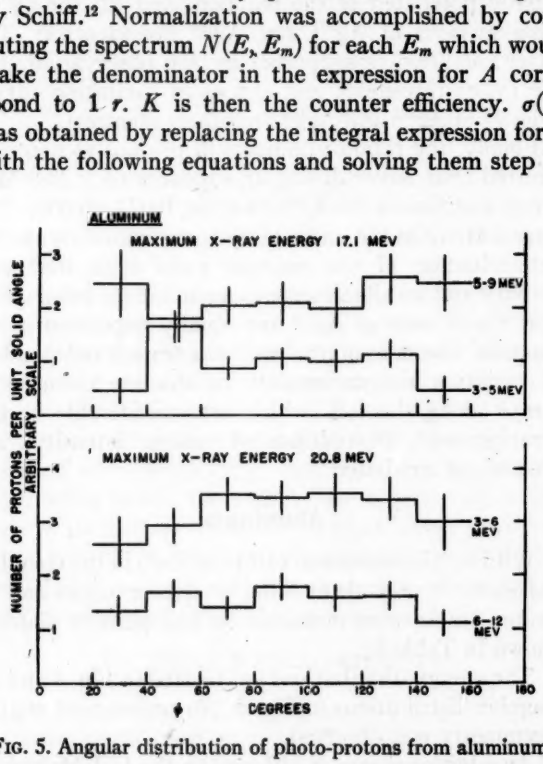

FIG. 5. Angular distribution of photo-protons from aluminum.

[12] L. I. Schiff, Phys. Rev. 70, 87 (1946); see G. D. Adams. Phys. Rev. 74, 1710 (1948).

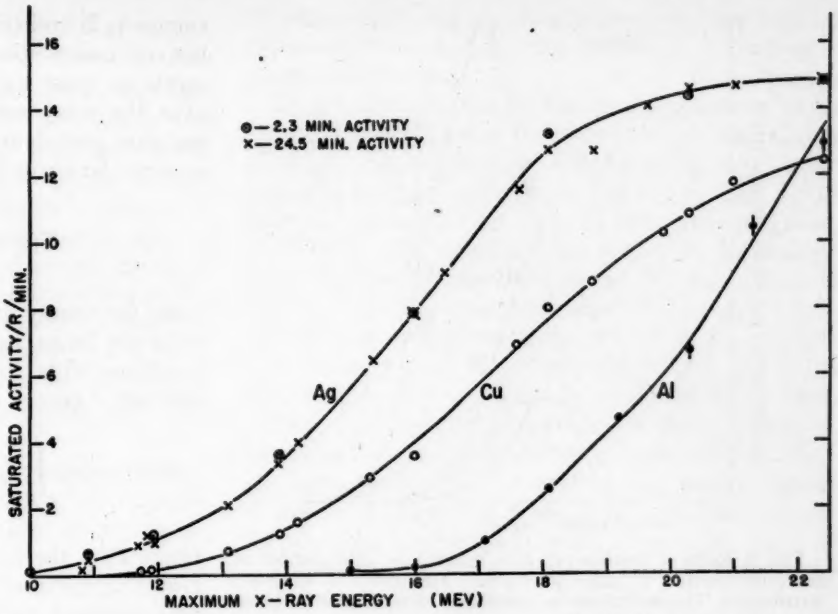

FIG. 6. Excitation curves for (γ, n) activities in silver, aluminum, and copper. The activity curve for Ag^{107} has been multiplied by a constant factor to show its similarity in shape to the activity curve for Ag^{109}. Some points for silver and copper are from unpublished data of J. McElhinney.

step:

$$A_1/K=N_{11}\sigma_1, \quad A_2/K=N_{21}\sigma_1+N_{22}\sigma_2, \quad \text{etc.},$$

where A_1 is the activity per r induced by an x-ray spectrum whose E_m is 1 Mev above B_n and which has N_{11} quanta in this 1-Mev interval. σ_1 is the average cross section for the interval. A_2 is the activity for the spectrum for which $E_m=B_n+2$ Mev, with N_{21} and N_{22} quanta in the first and second 1-Mev intervals above B_n. σ_2 is the cross section for the interval 1 to 2 Mev and so on.

Absolute values of cross section were obtained for Ag and Cu, since activities were determined with a calibrated counter and the monitor response $i(E)$ fixes the number of quanta at each energy of the spectrum when its shape is assumed. The uncertainty in the calculated cross section becomes very large at high energies, but it is certain that it drops rapidly to a low value a few Mev above the peak.

The activation and cross section curves are shown in Figs. 6 and 7 for the Ag isotopes, for Al^{27}, and also for Cu^{63}. The principal features for Ag^{109} and Cu^{63} are shown in Table III. As stated earlier, the activity per atom per r with Ag^{107} is just one-half that with Ag^{109}, and if it is assumed that both isomers of Ag^{106} are equally populated in the (γ, n) reaction, we conclude that the characteristics of the $\sigma_{\gamma, n}$-curve are the same for Ag^{107} as listed for Ag^{109}. Their activation curves are identical in shape, within errors of measurement.

The neutron yields for Cu and Ag, measured by Price and Kerst by neutron detection, are listed in comparison with ours in the above table. They did not distinguish the isotopes, but according to our interpretation the (γ, n) cross sections and yields should be the same for Ag^{107} and Ag^{109}. There is some uncertainty about the contribution of neutrons per atom of Cu^{65}, relative to Cu^{63}, but since the isotopic abundance of Cu^{65} is only 30 percent, the agreement in the yields for Cu can hardly be disturbed by more than the experimental errors in their determination.

The cross section curves are of the resonance type as first shown by Baldwin and Klaiber[13] for Cu^{63} and C^{12}. They found the peak for Cu^{63} at 22 Mev. The betatron group at Saskatoon[14] has, however, obtained a cross

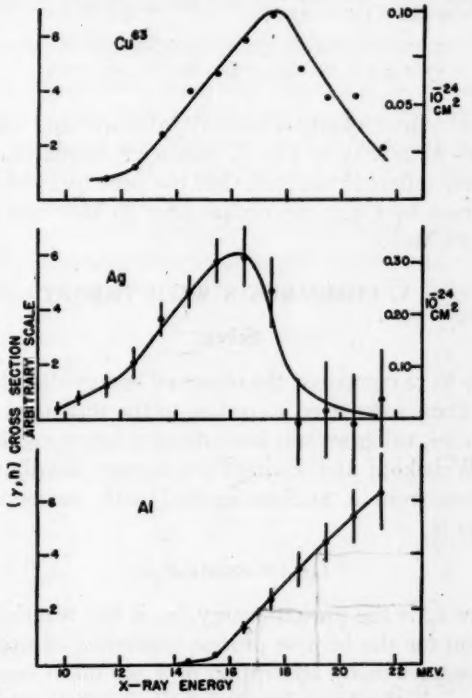

FIG. 7. (γ, n) cross sections for silver, aluminum and copper.

[13] G. C. Baldwin and G. S. Klaiber, Phys. Rev. 73, 1156 (1948).
[14] Leon Katz, University of Saskatchewan, Saskatoon (private communication).

FIG. 8. Ratio of protons per Mev interval to total number of neutrons emitted in same irradiation. Histogram is observed distribution. Theoretical curves calculated with parameters given in text for cases I, II, III, IV.

TABLE III. Results for Ag^{109} and Cu^{63}.

	Ag^{109}	Cu^{63}
Energy at peak (Mev)	16.5	17.5
$\sigma_{\gamma,n}$ at peak (barns)	0.32	0.10
$\int\sigma_{\gamma,n}dE$ (Mev-barns)	1.65	0.6
Neutrons/mole/$r\times10^{-6}$		
This work—20.8 Mev	7.3	2.6
Price and Kerst[a]—22 Mev	6.7	2.5

[a] G. A. Price and D. W. Kerst, Phys. Rev. 77, 806 (1950).

section curve nearly identical in shape and absolute values with that in Fig. 7. Strauch[15] estimates, by an entirely different method, that the principal absorption of x-rays by Cu nuclei occurs near 20 Mev and by Ag near 18 Mev.

V. COMPARISON WITH THEORY

Silver

We have compared the observed energy distributions with those calculated according to the statistical theory of nuclei, using several level density functions. Following Weisskopf and Ewing[16] the energy distribution of protons from a nucleus excited with monoenergetic x-rays is

$$I(\epsilon_p)=\text{const}\epsilon_p\sigma_p\omega_R,$$

where ϵ_p is the proton energy, σ_p is the reaction cross section for the inverse process consisting of excitation of the nucleus by absorption of a proton of energy ϵ_p, and ω_R is the level density of the residual nucleus at the excitation energy which remains when a proton of energy ϵ_p is emitted from the compound nucleus. For the continuous spectrum of x-rays used in this experiment we must use the appropriate integral of $I(\epsilon_p)$ over the x-ray spectrum. The average value of the emission probability per unit time of a particle b from a particular excited state is

$$\Gamma_b=\text{const}\int_0^{\epsilon_{b\,\max}}\epsilon_b\sigma_b\omega_R d\epsilon_b.$$

Then the energy distribution of protons per nucleus in the x-ray beam, excited with cross section $\sigma_\gamma(E)$ by a spectrum with $N(E, E_m)$ quanta per cm² per Mev interval at energy E and a maximum energy E_m, is

$$F(\epsilon_p)=\epsilon_p\sigma_p\int_{B_p}^{E_m}\frac{\sigma_\gamma(E)N(E,E_m)\omega_R(E-B_p-\epsilon_p)}{\sum_{b'}\Gamma_{b'}}dE,$$

where B_p is the (γ, p) threshold and the b'-summation is over all modes of disintegration of the excited nucleus, here assumed to be restricted to (γ, p) and (γ, n) processes. Then since

$$\sigma_\gamma/\sigma_{\gamma,n}=\sum_{b'}\Gamma_{b'}/\Gamma_n,$$

$$F(\epsilon_p)=\epsilon_p\sigma_p\int_{B_p}^{E_m}\frac{\sigma_{\gamma,n}(E)N(E,E_m)\omega_R(E-B_p-\epsilon_p)}{\Gamma_n}dE.$$

The total number of neutrons emitted is

$$N_n=\int_{B_n}^{E_m}\sigma_{\gamma,n}(E)N(E,E_m)dE,$$

or, alternatively, $\sum_{\epsilon_n}F(\epsilon_n)$, where $F(\epsilon_n)$ is calculated in a way similar to $F(\epsilon_p)$.

The calculations were carried through for each isotope and the distributions, weighted for isotopic abundance, were added. The calculated ratios of protons per Mev energy interval to total neutrons may be compared to the experimental ratio obtained directly without use of the absolute (γ, n) cross sections.

Four combinations of energy level density and reaction cross section have been used, as follows:[17–19]

$\omega_1=C\exp(aE)^{\frac{1}{2}}$, $a=A/5$ (reference 16); σ_p with $r_0=1.42\times10^{-13}$ cm, and σ_n from reference 17. (I)

$\omega_2=C\exp(aE)^{\frac{1}{2}}$, $a=1.6(A-40)^{\frac{1}{2}}$ (reference 18); σ_p with $r_0=1.30\times10^{-13}$ cm from reference 18, σ_n from reference 19. (II)

Same as (II), except $r_0=1.50\times10^{-13}$ cm (reference 18). (III)

[15] K. Strauch, Phys. Rev. 79, 241 (1950).
[16] V. F. Weisskopf and D. H. Ewing, Phys. Rev. 57, 472 (1940).
[17] Lecture Series in Nuclear Physics (MDDC 1175) U. S. Gov't Printing Office, pp. 100–105.
[18] V. F. Weisskopf, private communication, March, 1950, proposed ω_2 as giving better agreement with other current experiments and supplied recently calculated reaction cross sections, σ_p.
[19] H. Feshbach and V. F. Weisskopf, Phys. Rev. 76, 1550 (1949).

$\omega_3 = C \ln(E+b)/b$, $b = 20/A$ (reference 5); σ_p and σ_n as in I. (IV)

The (γ, n) thresholds for Ag^{107} (9.5 Mev) and Ag^{109} (9.3 Mev) have been determined by Baldwin and Koch.[20] The (γ, p) threshold for Ag^{107} is computed from the (γ, n) threshold and the positron energy of Ag^{106} (2.0 Mev) to be 5.7 Mev, which agrees to within 0.1 Mev of the value obtained from Fermi's semi-empirical formula.[21] From the latter formula the (γ, p) threshold of Ag^{109} is 6.5 Mev. The computed shape of the proton spectrum is not very sensitive to the thresholds, but the computed ratio of protons to neutrons is quite sensitive. The difference of 1.0 Mev in $B_n - B_p$ reduces the proton yield of Ag^{109} as compared with Ag^{107} by a factor of four.

The comparison of calculated and observed ratios of protons per Mev to total neutrons is presented in Fig. 8. There is no arbitrary fitting of curves at any point; the theoretical and experimental curves are entirely independent.

The areas under the curves, which are ratios of the total numbers of protons to the total numbers of neutrons emitted during 20.8-Mev bremsstrahlung irradiation, are:

Level density	N_p/N_n
(I) ω_1	0.022
(II) $\omega_2(r_0 = 1.3\times10^{-13}$ cm)	0.030
(III) $\omega_2(r_0 = 1.5\times10^{-13}$ cm)	0.075
(IV) ω_3	0.13
Observed	0.023 ± 0.008.

The disagreement between the observed proton spectrum and calculations (III) or (IV) appears to be definite. The agreements in cases (I) or (II) are satisfactory up to 8 or 9 Mev when one considers the uncertainties in the experiment and in the calculation, especially at low proton energies. At higher energies there are definitely more protons than are predicted from a statistical model (ω_1 or ω_2). A calculation showed that even if the (γ, n) cross section is assumed to rise linearly to 20.8 Mev instead of dropping rapidly from a peak at 16.5 Mev, there are definitely more protons observed than predicted above 10 Mev.

The significance of the results will be discussed in the following section.

Aluminum

A statistical treatment of energy levels is not appropriate in light nuclei in the energy range of interest, since the levels are widely spaced. For example, the nuclei[22,23] of Al^{27} and Si^{28} have been shown to have a rather widely spaced ($\sim$1 Mev) and slowly converging level structure for several Mev above the ground state. No structure in our observed proton spectrum is to be expected, however, since the nucleus is excited by a continuum of x-rays.

To get a rough idea of the proton spectrum to be expected with 20.8-Mev bremsstrahlung a calculation of $F(\epsilon_p)$ was made with the following simplifying assumptions: ω_R = constant, $\sigma_{\gamma,n}$ as in Fig. 7 for $E > 15$ Mev, σ_γ = constant from 11 to 15 Mev and equal to σ_γ at 15 Mev. The reaction cross section σ_n is obtained from reference 19 and σ_p from the W. K. B. method (see reference 17), admittedly unreliable for such a light element but unimportant since most of the protons have energy greater than the barrier height. The (γ, n) threshold is 14 Mev and the (γ, p) threshold is 9 Mev.

The calculated proton spectrum is shown in Fig. 9, normalized arbitrarily, since the neutrons emitted during the exposures were not counted, as they were for silver. If the level density were assumed to increase slowly with energy, as it certainly must, a better fit would be obtained, for the curve would be concave toward the axis above a proton energy of 4 or 5 Mev.

The simple assumption of a constant level density leads also to the result that at an x-ray energy of 17 or 18 Mev the yield of protons should be about 1½ times the yield of neutrons, in qualitative agreement with the ratio of two between our $\sigma_{\gamma,p}$ at 16 to 20 Mev and the value of $\sigma_{\gamma,n}$ at 17.6 Mev found by Hirzel and Wäffler.[11] The emission of protons is favored by the fact that the proton threshold is about 5 Mev less than the neutron threshold, which outweighs the restraining effect on protons of the Coulomb barrier.

VI. SUMMARY AND DISCUSSION

The observations on protons from the (γ, p) reaction in silver, excited by a 20.8-Mev bremsstrahlung spectrum which covers the resonance absorption with a maximum at 16.5 Mev, can be summarized qualitatively as follows:

(a) Protons of low energy (<8 or 9 Mev) are emitted with equal probability at all angles and with an energy distribution similar to that expected with reasonable

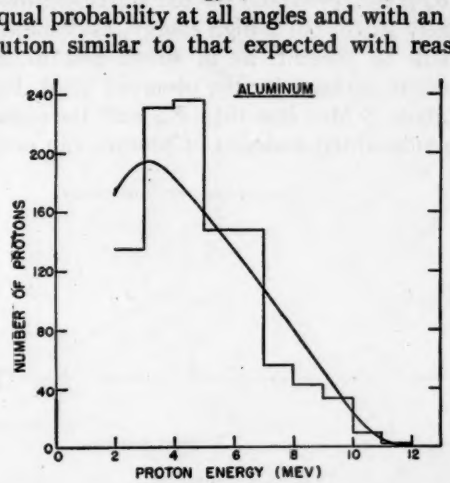

FIG. 9. Energy distribution of protons from aluminum with maximum x-ray energy 20.8 Mev, compared with distribution computed for constant level density.

[20] G. C. Baldwin and H. W. Koch, Phys. Rev. **67**, 1 (1945).
[21] "Table of Atomic Masses," N. Metropolis and others (unpublished).
[22] C. P. Swann and C. E. Mandeville, Phys. Rev. **79**, 240 (1950).
[23] R. A. Peck, Jr., Phys. Rev. **76**, 1279 (1949).

statistical level densities in the residual nucleus. These protons comprise more than half of the total number.

(b) There is a high energy tail on the proton spectrum (10–14 Mev) with numbers of protons definitely in excess of the prediction from statistical level densities. Only these protons show a pronounced angular asymmetry with a maximum at 90° to the x-ray beam.

(c) The ratio of total numbers of protons to neutrons (average of $\sigma_{\gamma,p}/\sigma_{\gamma,n}$ over the spectrum) is of the order predicted from statistical level densities and reaction cross sections in the range appropriate to other nuclear reactions. The Schiff assumption[5] of an effective, nearly constant, level density for a photo-nuclear processes predicts about 6 times as many protons as observed and at higher average energy.

Remarkably similar energy and angular distributions of protons from Rh^{103} have been obtained by Curtis and others.[7] According to the atomic mass calculations of reference 21, the proton and neutron thresholds are about the same in Rh^{103} as in the silver isotopes.

The essential features of nuclear absorption suggested by the observations on silver are (1) a resonance excitation as shown in Fig. 7, followed by (2) an emission of a group of protons of high energy and angular asymmetry which fall outside the distribution predicted from the statistical nuclear model, and (3) an emission of a group of protons of lower energy which in energy distribution and in numbers relative to the number of emitted neutrons fit approximately predictions based on the statistical model (Fig. 8).

Whatever the exact nature of the nuclear absorption process, the high energy spherically asymmetric protons which fall outside of the expected distribution provide an experimental basis for a possible interpretation of the high (γ, p) yields at 17.6 Mev, of many middle weight nuclei. In every such case which Hirzel and Wäffler[1] examined, the proton threshold, B_p, was greater than the neutron threshold, B_n. Consequently, the ratio $\sigma_{\gamma,p}/\sigma_{\gamma,n}$ predicted on the statistical model was extremely small, but a high energy, asymmetric group may still be present, as in silver, and in sufficient numbers to account for the observed yield. For silver B_p is about 3 Mev less than B_n, with the consequence that a substantial emission of protons can occur even on the statistical model. Hence, both groups of protons are to be expected and both are observed.

Levinger and Bethe, and Courant (reference 4, p. 128) propose a picture which contains just the above features for the purpose of explaining the high yield of protons in medium weight nuclei. The picture proceeds naturally from their view that the main process of nuclear absorption is the excitation of a single proton in the nucleus. The proton occasionally escapes immediately without transferring its excitation energy to the rest of the nucleus. In this process protons of high energy would be favored and they might be expected to emerge preferentially at 90° to the x-ray beam. Usually, however, the proton does interact with other nucleons and then the subsequent emission of neutrons and protons is in accordance with the statistical model.

In the case of the (γ, p) reaction in Al^{27}, excited with continua of x-rays which do not extend to the peak of the resonance absorption, the principal results may be stated as follows:

(a) Protons are emitted with energies up to the maximum available (maximum x-ray energy minus proton threshold) and the shape of the proton spectrum is compatible with the assumption of a constant or slowly increasing level density in the residual nucleus.

(b) The (γ, p) cross section in the range of x-ray energies 16 to 20 Mev is as large or larger than the (γ, n) cross section at 17.6 Mev, in agreement with calculation on the basis of constant level density.

(c) Protons of all energies observed, with x-ray excitation up to 20.8 Mev, are emitted with spherical symmetry.

Since the calculated emission of protons is large without the special assumption that a few escape immediately upon excitation of the nucleus, nearly spherical symmetry of the protons is to be expected. For, even though a few escape immediately and preferentially at 90° to the beam, they would not stand out among the great number which can emerge, after distribution of the excitation energy, with energies up to the maximum and with spherical symmetry.

According to Toms, Halpern, and Stephens[6] the protons from a (γ, p) reaction on the Mg isotopes are also approximately spherically symmetric.

Neutron Capture Gamma-Ray Spectra*

BERNARD HAMERMESH
Argonne National Laboratory, Chicago, Illinois
(Received June 13, 1950)

Photographic plates soaked in D_2O may be used for gamma-ray studies. By measuring the ranges of the photo-protons resulting from the photo-disintegration of the deuterons in the D_2O, the γ-ray energies can be found. The method is limited to γ-rays of energy above 3 Mev. The neutron capture γ-ray spectra of Al, Cl, Fe, Br, Cd, La, W, Au, and Hg have been obtained by this method. The results suggest a possible dependence of the shape of the spectra on the odd-even character of the compound nucleus.

I. INTRODUCTION

ALTHOUGH a large amount of research has been done on the problem of radiative capture cross sections for thermal neutrons, very little attention has been given to the study of the instantaneous gamma-rays emitted. Most of the studies[1] of these capture gamma-rays have been made by studying their absorption in some material for the purpose of finding either an average gamma-ray energy or a maximum energy. Since such spectra are usually complex, the absorption technique cannot be expected to yield very accurate average energies. As for the maximum energy determinations, here one is faced with finding the end point of a spectrum and only in those researches where neutron beams from a chain reacting pile have been used has the intensity been high enough for reasonably accurate measurements.

In all of the above-mentioned work no direct study of the spectra was made. Recently, studies made with a γ-ray pair spectrometer[2] have been reported. A pair spectrometer should be capable of giving good results at the high energy end of the γ-ray spectra. In the work of Kinsey *et al.*, the energy values reported do not go below 4.5 Mev.

The researches described in this paper were carried out for the purpose of obtaining some detailed knowledge about the instantaneous γ-ray spectra of various elements resulting from neutron capture. It was hoped that by studying various elements some information concerning the dependence of the shape of the spectrum on atomic number or nuclear type could be found.

II. EXPERIMENTAL METHOD

By introducing heavy water into a photographic emulsion[3] and then exposing the plate to γ-rays it is possible to obtain the energies of the γ-rays by measuring the ranges of the photo-protons resulting from the photo-disintegration of the deuterons in the D_2O. The energy of the γ-ray, E_γ, is related to the energy of the proton, E_p, by the relation

$$E_\gamma = 2E_p + 2.2 \text{ Mev}. \quad (1)$$

This formula neglects the effect on the energy of the angular dependence of the reaction. This effect will be a cause of poor resolution for the method unless one has sufficient γ-ray intensity to be able to collimate the gamma-ray beam. Furthermore, since it is difficult to measure accurately the range in an emulsion of a proton of energy very much below 0.5 Mev (6 microns), this method will be limited to γ-rays above 3 Mev.

Amounts of D_2O of at least 60 percent by weight can be introduced into an emulsion by soaking in D_2O. The emulsion need not be[3] stripped but may be left on a glass backing to simplify the handling problem.

Figure 1 shows the experimental arrangement used. A beam of neutrons from the thermal column of the Argonne heavy water moderated pile impinges on a calcium fluoride crystal. The crystal is rotated until a Bragg maximum is found at an angle of 30° to the incident neutron beam. In this manner one avoids placing the plates in the direct pile beam which contains many gamma-rays, which would cause a very large background of tracks and make the search for photo-proton tracks impossible.

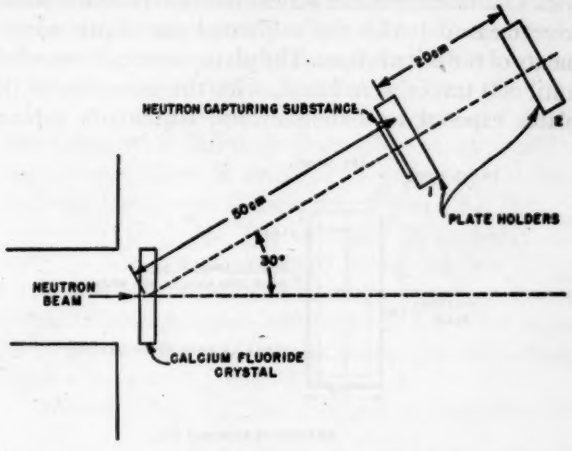

FIG. 1. Diagram of apparatus.

* A preliminary report of this work was presented at the Washington meeting of the American Physical Society, 1949; Phys. Rev. **76**, 182 (1949).

[1] H. E. Kubitschek and S. M. Dancoff, Phys. Rev. **76**, 531 (1949). This paper is the most recent one using the absorption method. It contains a list of references to the earlier work on capture gamma-rays.

[2] Kinsey, Bartholomew, and Walker, Phys. Rev. **77**, 723 (1950); **78**, 77 (1950); **79**, 218 (1950); Bartholomew, Kinsey, and Walker, Phys. Rev. **79**, 218 (1950).

[3] G. Goldhaber, Phys. Rev. **74**, 1725 (1948).

The Bragg reflected neutron beam then strikes the capturing material. Figure 1 shows the location of the plate holders and the (n, γ) source. The first plate (experimental plate) is right next to the gamma-ray source, whereas the second plate (background plate) is relatively very far from the gamma-ray source. On the other hand, the two plates are comparatively close together with respect to any source of background radiation such as fast neutrons from the pile.

The details of the plate holders are shown in Fig. 2. The holders are of $\frac{1}{8}''$ lead and are coated with a thick layer of boron carbide which has been painted on with Zapon. The holders are then covered with a thin sheet of aluminum foil to protect the boron carbide coating. The lead prevents the very low energy capture γ-rays from striking the plate. These would serve no useful purpose but would fog the plates. The boron carbide absorbs any thermal neutrons that may have penetrated the (n, γ) source and does not yield any capture gamma-rays that could photo-disintegrate deuterium. The plate holders are filled with D_2O. Ilford C_2 emulsions, 100 microns thick, have been used for all the elements that have been studied. The plates are immersed in the heavy water throughout the irradiation.

The thickness of the (n, γ) source has been chosen to be approximately one thermal neutron capture mean free path, provided this length is less than the mean free path for Compton scattering of a gamma-ray of 3 Mev. For small capture cross sections, the last criterion required using only a small fraction of a mean free path, in which case the searching of the plates was much more difficult.

The irradiations were of 30 to 50 hours duration. When longer irradiations were used, the background became too heavy to allow for easy searching of the plates.

III. DATA AND CORRECTIONS

After irradiation, the plates were processed and then searched with microscopes with oil immersion objectives. The projected lengths of the tracks were measured with calibrated eyepiece scales and the dips of the tracks were measured with the calibrated fine depth adjustments of the microscopes. The plates were each searched until 300 tracks were found, with the exception of the plates exposed to aluminum and lanthanum capture gamma-rays. The background plate corresponding to a given experimental plate was then searched over the same total area as had been covered on the experimental plate. The number of tracks found on the background plate averaged below 20 percent of the number found on an experimental plate.

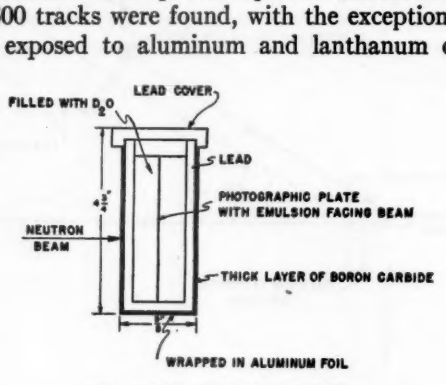

FIG. 2. Detail of plate holder.

The actual track lengths were calculated by correcting for emulsion shrinkage and for the dip of the track. In order to be able to use the Ilford range-energy[4] curves, a comparison of the range of protons in wet and dry emulsions was needed. Goldhaber[3] gives the range in dry emulsion as equal to 0.93 times the range in wet emulsion. This relation was used and then the energies of the photo-protons could be calculated. The γ-ray energy was then determined from Eq. (1). Figure 3 shows the range distribution of tracks from cadmium. The associated background tracks are shown on the same figure.

The range distribution must be corrected for the following: (1) the probability of tracks leaving the emulsion, (2) the variation with energy of the photo-disintegration cross section of the deuteron.

The first correction is purely a geometrical one. It may be calculated exactly in terms of emulsion thickness and track length. The second correction is more difficult to determine. The measurements[5] of the (γ, n) cross section of the deuteron have only been made at a few energies. The experiments are very difficult ones and the results are not very accurate. However, the theoretical calculations of the cross section should be reasonably good in the range of energies 3 to 9 Mev.

The values of $\sigma(\gamma, n)$ for the deuteron were obtained from a calculation based on the[6] simple theory of the effect, neglecting tensor forces. The calculations were extended to 5 Mev. Beyond 5 Mev, the formula for the photoelectric cross section was used, since the photomagnetic cross section is negligible at these energies. The recent measurements[7] at 6.13 and 17.6 Mev agree very well with the results of the above calculations.

Both corrections raise the number of high energy tracks relative to the number of low energy tracks. The corrected spectrum of cadmium is shown in Fig. 4.

Similar sets of histograms for the other substances studied were obtained. The background data for all the elements studied were then averaged and the distribution of the average background was determined. The histograms were then redrawn using the average background.

Finally, the data was smoothed by taking the average of the number of tracks in two adjacent blocks of the previously obtained histograms. A point corresponding to this average number of tracks was then plotted

[4] Lattes, Fowler, and Cuer, Proc. Phys. Soc. London **59**, 883 (1947).
[5] A. Wattenberg, *Photoneutron Sources*, Preliminary Report No. 6, Nuclear Science Series, Division of Math. and Phys. Sciences, Nat. Res. Council.
[6] H. A. Bethe and R. F. Bacher, Rev. Mod. Phys. **8**, 122 (1936).
[7] Barnes, Stafford, and Wilkinson, Nature **165**, 69 (1950).

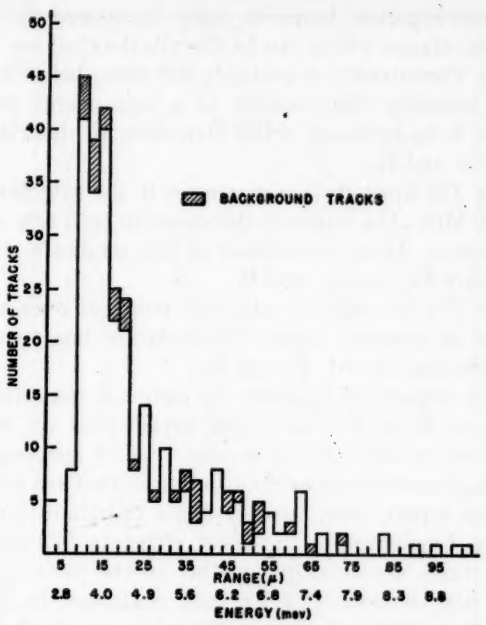

FIG. 3. Range distribution of tracks from cadmium.

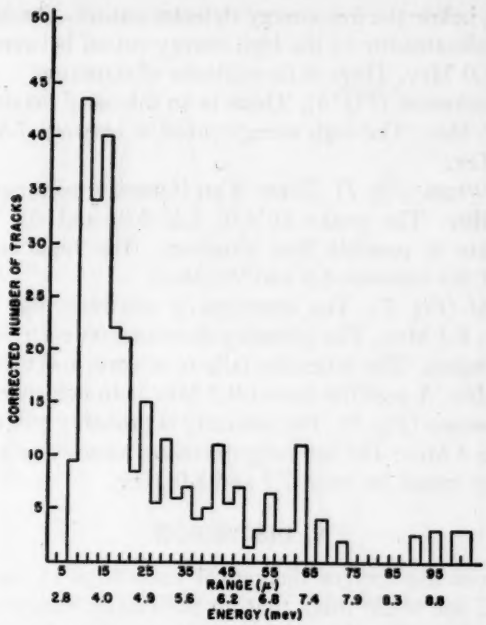

FIG. 4. Neutron capture γ-ray spectrum of cadmium.

against the average of the energy represented by the two corresponding blocks of the histograms. The points were then joined by straight lines. Figure 6 shows the smoothed spectrum of cadmium.

The energy resolution of the method is of the order of ±0.25 Mev. Most of this spread arises from the dependence of the energy of the photo-proton on the angle between the incident γ-ray and the proton's direction of motion. The thermal flux available after Bragg reflection was too low to permit collimation of the γ-rays so as to try to minimize the angular effect on the resolution.

IV. RESULTS

Before the capture γ-ray spectra are examined, it should be recalled that there is a low energy cutoff for the detector at about 3 Mev. Furthermore, by the very nature of the photographic method it will be difficult to determine a high energy cut-off of a spectrum. In addition, the poor resolving power of the method will tend to mask evidence of line structure in the spectra.

The elements reported herewith are Al, Cl, Fe, Br, Cd, La, W, Au, and Hg. The solid element was used in all cases except for Cl, Br, and Hg. For these C_2Cl_6, NaBr, and HgO were used. These were finely powdered and were placed in thin-walled aluminum containers. The thermal neutron capture mean free path of aluminum is 83 cm so that a thin-walled container gives a negligible contribution to the γ-ray spectrum that is being studied. The thickness of material used was one thermal neutron capture mean free path for all substances with the exception of Al, La, and Cd. In Al, only $\frac{1}{5}$ of a mean free path was used, since there is no advantage in using a thickness greater than a Compton mean free path. (For Al this is about 20 cm for 3 Mev gamma-rays.) In La, only enough material was available for $\frac{1}{2}$ a mean free path. For Cd, a thickness of 4 mean free paths was used.

In those cases where compounds were used (C_2Cl_6, NaBr, and HgO) the companion element in the compound yielded a negligible contribution to the capture γ-ray spectrum. In all cases, with the exception of Al and La, 300 tracks were obtained. In the two exceptions, 150 and 200 tracks respectively were obtained.

Aluminum (*Fig. 5*). There seem to be two possible peaks in the spectrum at 5.3 and 6.3 Mev. The group at 7.6 Mev reported by[2] Kinsey *et al.* does not stand out. The high energy cutoff is between 8.0 and 8.5 Mev.

Chlorine (*Fig. 5*). The spectrum is relatively flat over a wide range of energies beginning at the low energy cutoff of the detector. The intensity falls to a low value near 8.0 Mev and then a very intense group appears at 8.5 Mev. This is probably a single line. This γ-ray has been used to photo-disintegrate[8] various substances. The high energy cutoff is at about 9.2 Mev.

Iron (*Fig. 5*). The intensity is a maximum at 5.2 Mev. The intensity is definitely decreasing on each side of this energy. There is evidence of a line at 6.0 Mev. The high energy cutoff is between 7.5 and 8.0 Mev.

Bromine (*Fig. 6*). The intensity is probably still rising as one goes to energies below the low energy cutoff of the detector. The intensity decreases sharply towards higher energies. The peaks at 5.3, 6.3, 7.3, and 8.0 may be evidence of line structure. The high energy cutoff is between 8.5 and 9.0 Mev.

Cadmium (*Fig. 6*). The intensity is probably still

[8] B. Hamermesh and A. Wattenberg, Phys. Rev. **76**, 1420 (1949).

rising below the low energy detector cut-off. The intensity falls steadily to the high energy cut-off between 7.5 and 8.0 Mev. There is no evidence of structure.

Lanthanum (*Fig. 6*). There is an intensity maximum at 4.6 Mev. The high energy cutoff is between 7.5 and 8.0 Mev.

Wolfram (*Fig. 7*). There is an intensity maximum at 4.6 Mev. The peaks at 4.6, 5.3, 6.0, and 6.6 Mev indicate a possible line structure. The high energy cutoff lies between 8.5 and 9.0 Mev.

Gold (*Fig. 7*). The spectrum is relatively flat from 4.8 to 8.2 Mev. The intensity decreases on each side of this region. The intensity falls to a very low value at 8.8 Mev. A possible line at 9.2 Mev is in evidence.

Mercury (*Fig. 7*). The intensity is probably still rising below 3 Mev. The intensity decreases steadily to a high energy cutoff between 7.5 and 8.0 Mev.

V. DISCUSSION

From the meager theoretical knowledge at our disposal, one would think that for sufficiently heavy nuclei the predictions of a statistical theory of nuclear structure would apply. This theory predicts spectra of the form of the[9] cadmium spectrum. However, the types of spectra reported herewith may be placed in three general classes which can be described as follows:

(1) The intensity is probably still rising below 3 Mev. The intensity falls steadily to a high energy cut-off. There is no evidence of line structure. In this class we find Cd and Hg.

(2) The intensity is a maximum in the neighborhood of 5.0 Mev. The intensity decreases on each side of this maximum. There is evidence of line structure. In this class are Fe, Br, La, and W.

(3) The intensity is relatively constant over a wide range of energies. There is evidence of line structure. In this class are Al, Cl, and Au.

The strange thing about the results is that from the data on cadmium one might expect that all heavier elements would have a similar type of spectrum. Of those elements heavier than cadmium that are included in this report, only mercury has a cadmium-like spectrum. Furthermore, the three elements W, Au, and Hg, which are so close together in the periodic table and are so much heavier than cadmium, have very different spectra. In fact, in the above rough classification, they are in different classes.

If one considers the compound nuclei from which the γ-rays are emitted, a possible reason for the differences between W, Au, and Hg will appear. In the case of gold the capturing nucleus is Au^{197}. However, for the other elements there are several isotopes that need be considered. Fortunately, in each case there is one isotope which outweighs all others by virtue of its relatively very large capture cross section. These isotopes are W^{186} and Hg^{199}. The three compound nuclei which give rise to the capture gamma-spectra are of the types:

Even Z, odd $N-W_{74}^{187}$,
Odd Z, odd $N-Au_{79}^{198}$,
Even Z, even $N-Hg_{80}^{200}$.

The differences in shapes of the capture γ-ray spectra could be due to the differences in the nuclear types of the compound nuclei of W, Au, and Hg. This is not an unreasonable assumption, since level spacings should vary considerably from one nuclear type to another. Recent work[10] on capture γ-ray multiplicities indicates such a dependence on nuclear type. Additional elements are now being studied to check the above suggestion.

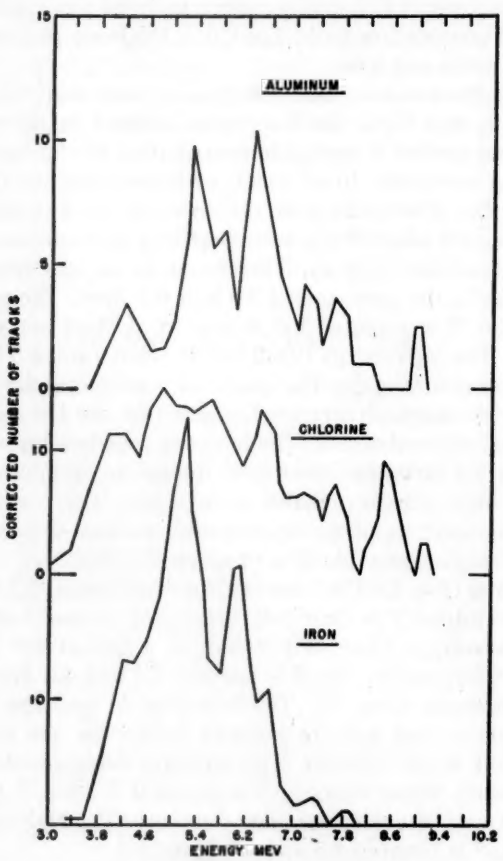

FIG. 5. Neutron capture gamma-ray spectra of aluminum, chlorine, and iron.

VI. CONCLUSION

The D_2O soaked plate technique of studying neutron capture gamma-ray spectra yields results which give a general picture of the shapes of such spectra. The poor resolving power of the method does not allow one to determine with any good accuracy line structure in the spectra. The results on the nine elements that are reported are rather surprising and indicate that a theory of the spectra based on a statistical nuclear model is not valid. The results suggest a dependence of

[9] H. A. Bethe and R. F. Bacher, Rev. Mod. Phys. 9, 231 (1937).

[10] C. O. Muehlhause, Phys. Rev. 79, 219 (1950).

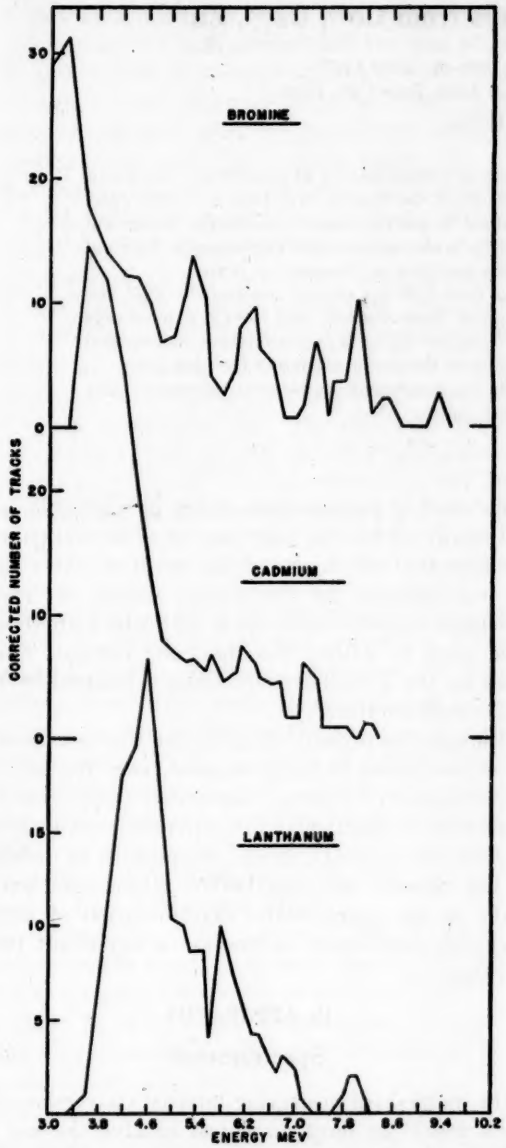

FIG. 6. Neutron capture gamma-ray spectra of bromine, cadmium, and lanthanum.

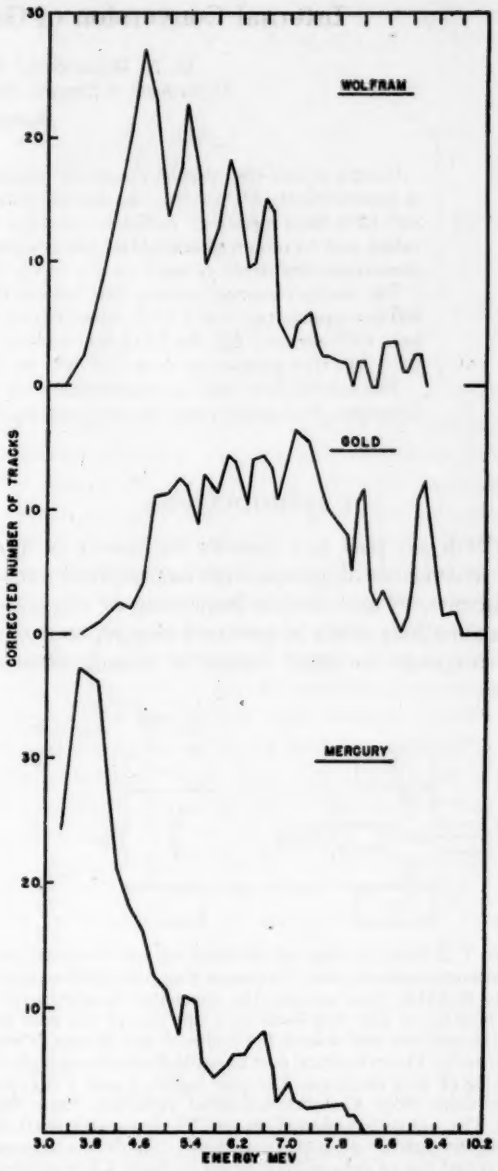

FIG. 7. Neutron capture gamma-ray spectra of wolfram, gold, and mercury.

the spectral shapes on the odd-even character of the compound nuclei which emit the spectra.

It is a pleasure to acknowledge the advice and assistance of the many people who have aided in the above research. Most of the very tedious plate searching was done by Louise Kollman. Without her help the work would have progressed at a much slower pace. John Dalman constructed the plate holders and assisted in setting up the apparatus. Drs. Albert Wattenberg and Morton Hamermesh were of incalculable help in offering advice and encouragement in the many discussions that were held as the research progressed.

Internal Conversion of Gamma-Rays from Co^{60}, Cs^{134}, Zn^{65}

M. A. WAGGONER,* M. L. MOON, AND A. ROBERTS**
Department of Physics, State University of Iowa, Iowa City, Iowa
(Received June 30, 1950)

Using a double-coil, thin-lens magnetic beta-ray spectrometer of transmission 2.40 percent and line width of approximately 3.0 percent, the internal conversion coefficients of the gamma-rays from Co^{60}, Cs^{134}, and Zn^{65} have been measured. Sufficient precision has been attained in several cases to verify the theoretical values and to obtain unambiguous identification of the multipole character of the gamma-rays. Internal conversion coefficients as small as 10^{-5} can be measured with a precision of 5 percent or better.

The results obtained indicate that both of the gamma-rays from Co^{60} are electric quadrupole (*EQ*), the 560-kev gamma-ray from Cs^{134} is either *EQ* or *MD* or a mixture of these, the 602- and 799-kev gamma-rays from Cs^{134} are both *EQ*, the 1.114-Mev gamma-ray from Zn^{65} is either *EQ* or *MD* or a mixture of these and the 1.363-Mev gamma-ray from Cs^{134} may be *EQ*. Further data on the decay scheme of Cs^{134} are given.

The results show that in combination with angular correlation measurements internal conversion data determine the angular momenta and parities of excited nuclear states.

I. INTRODUCTION

OVER the past two decades the theory of internal conversion of gamma-rays has received numerous treatments,[1–12] each author improving or changing the approximations made in previous papers, or extending the treatment to other values of atomic number or atomic shell or gamma-rays energy or multipole order, until finally within the past year or so several papers[1,2] have appeared which give as the result of rather elaborate calculations the theoretical values of internal conversion coefficients for the *K* shell which are thought to be good to within less than one percent. Similar values for the *L* shell are now being calculated by Rose and his collaborators.[1]

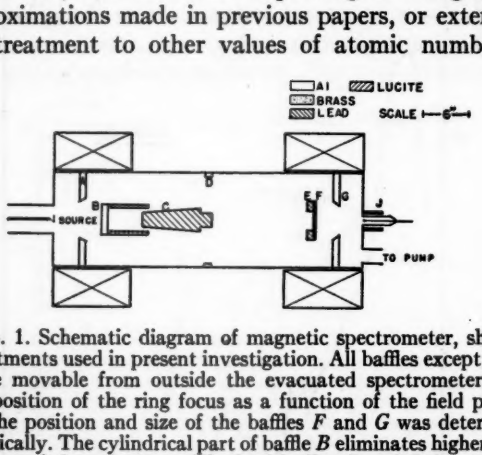

FIG. 1. Schematic diagram of magnetic spectrometer, showing adjustments used in present investigation. All baffles except *C* and *D* are movable from outside the evacuated spectrometer tube. The position of the ring focus as a function of the field pattern and the position and size of the baffles *F* and *G* was determined empirically. The cylindrical part of baffle *B* eliminates higher order focusing of slow electrons. The lead baffles *E* and *J* decrease the background from Compton-scattered radiation from the lens coils. The source is mounted on an "O" ring-sealed shaft and inserted through an air-lock (not shown). With the arrangement shown 660 lbs. of copper take 20 kw to focus 4.5-Mev electrons; with both coils at the center one-fourth as much power is required, but the transmission is decreased. The coils are wound with $1\frac{1}{8}$" by 0.022" copper strip, each coil containing three pairs of pies separated by water-cooled hollow disks.

Although the present status of the theory of internal conversion seems to be quite good, very few accurate measurements of internal conversion coefficients have been made (in particular for conversion coefficients of less than one percent). It was our purpose in undertaking the present investigation to attain sufficient accuracy in the experimental determination of internal conversion coefficients to provide a significant test of the theory.

II. APPARATUS

Spectrometer

The methods of measuring internal conversion coefficients which we have employed involve the use of a double-coil, thin-lens beta-ray spectrometer in which some care has been taken to eliminate background. The one we have used is shown in Fig. 1. In its essential parts it is patterned after the thin-lens magnetic spectrometer described by Deutsch, Elliott, and Evans[13] except for the modification of ring focusing which Frankel[14] and others[15,16] have discussed. The particular adjustment of the spectrometer which we have employed in the present investigation is as indicated in Fig. 1. The half-angle of the cone described by baffles *F* and *G* and the counter is approximately 30°. With this adjustment the transmission of the spectrometer is 2.40 percent and the line width (defined below) about 3.0 percent.

The argon- and alcohol-filled Geiger-Mueller counters

* Now at Vassar College.
** Now at University of Rochester.
[1] Rose, Goertzel, Spinrad, Harr, and Strong, Phys. Rev. **76**, 184 (1949).
[2] John R. Reitz, Phys. Rev. **77**, 10 (1950); C. L. Longmire and H. Brown, Phys. Rev. **75**, 264 (1949).
[3] R. Schafroth, Helv. Phys. Acta **21**, 499 (1948).
[4] S. D. Drell, Phys. Rev. **75**, 132 (1949).
[5] I. S. Lowen and N. Tralli, Phys. Rev. **75**, 529 (1949).
[6] B. A. Griffith and J. P. Stanley, Phys. Rev. **75**, 534 (1949).
[7] Hulme, Mott, and Oppenheimer, Proc. Roy. Soc. **A155**, 315 (1936).
[8] H. M. Taylor and N. F. Mott, Proc. Roy. Soc. **A142**, 215 (1933).
[9] H. M. Taylor and N. F. Mott, Proc. Roy. Soc. **A138**, 665 (1932).
[10] M. H. Hebb and G. E. Uhlenbeck, Physica **5**, 605 (1938).
[11] S. M. Dancoff and P. Morrison, Phys. Rev. **55**, 122 (1939).
[12] M. H. Hebb and E. Nelson, Phys. Rev. **58**, 486 (1940).
[13] Deutsch, Elliot, and Evans, Rev. Sci. Inst. **15**, 178 (1944).
[14] S. Frankel, Phys. Rev. **73**, 804 (1948).
[15] J. W. M. DuMond, Rev. Sci. Inst. **20**, 160 (1949).
[16] E. Persico, Rev. Sci. Inst. **20**, 191 (1949).

used had mica windows which were thick enough to begin affecting the data around 120 kev and to cut off at 50 kev. Although such counters are self-quenching, best results were obtained when a Neher-Pickering quench circuit was used in conjunction with them. Corrections were made for counting losses.

The sources used were mounted on a brass ring, $\frac{1}{64}''$ thick, $\frac{1}{2}''$ o.d. and $\frac{3}{8}''$ i.d., across which was stretched a thin three-ply laminated film (zapon-Formvar-zapon) or a LC-600 film. Some of the sources were covered with a single zapon film. Each of these films was less than 30 $\mu g/cm^2$. Care was taken to eliminate any possible effects due to source charging on several of the stronger sources, but no such effects were ever observed. For the external conversion measurements an aluminum absorber ($\frac{1}{16}''$ thick) and lead converter (0.001″ thick) were attached to the brass ring from which the source was supported.

Calibration

The constant of the spectrometer, $k \equiv H\rho/i$, was determined by using the internal conversion lines from Co^{60} and the crystal spectroscopy value[17] for the corresponding gamma-ray energies. Appropriate correction was made for the horizontal component of the earth's magnetic field parallel to which the magnetic axis of the spectrometer was aligned. The vertical component of the earth's field was cancelled out to within 1.5 percent throughout the entire volume of the spectrometer by means of two large Helmholtz coils of a design described by Lyddane and Ruark.[18]

The line width of the spectrometer was determined as a function of source size using the highly converted 625-kev internal conversion line of Cs^{137}. For source sizes from 1.5 to 5.5 mm in diameter the increase in line width with diameter was found to be 1.3 percent of the line width per millimeter.

While in principle the transmission could be calculated if the electron orbits were known in detail, we have preferred to measure it experimentally. Consider, for example, a radioactive isotope which has the decay scheme shown in Fig. 2.

Let: t = transmission of spectrometer = fraction of emitted particles of a given energy detected by the counter; N, N_e, N_γ = number of disintegrations, number of internal conversion electrons, and number of gamma-rays, respectively, from the source per unit time; r_α = counting rate at the peak of the conversion line from an infinitely thin source; w = line width = width of a rectangle of height r_α having the same area as the observed internal conversion line; A = area of the momentum plot of the beta-ray spectrum, i.e., number of observed beta-rays per unit time per unit momentum *versus* momentum. It follows from these definitions

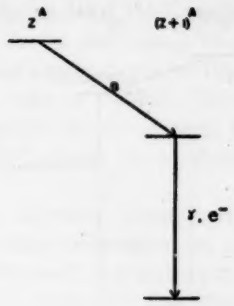

FIG. 2. Hypothetical decay scheme.

that

$$t = (A/(Nw)).$$

(This equation is adequate as long as the curvature of the beta-ray spectrum is negligible over the range of w.)

The line width being known, in order to determine the transmission of the spectrometer it is necessary to determine A/N as a function of source size. To do this we used three high specific activity Co^{60} sources (approximately two microcuries each) of less than 0.016 mg/cm^2 average thickness and with diameters from 3.0 to 5.0 mm. The absolute strength, N, of each of these sources was obtained by coincidence measurements. The value of A for each of these sources was obtained from a momentum plot of the beta-ray spectrum which had been reconstructed from the Fermi plot of that spectrum. This reconstruction procedure was necessary since the thickness of the counter window did not permit us to obtain valid data below about 120 kev. Thus points for the momentum plot in this energy region were obtained by extrapolating to zero the straight Fermi plot (allowed shape) observed at higher energies. With an exit window 2.0 cm in diameter, the transmission of the spectrometer for sources ranging in diameter from 3.0 to 5.0 mm was found to be constant and equal to 2.40 percent.

After an accurate value of the internal conversion coefficient is obtained for an isotope which can be accurately calibrated, the measurement of the transmission is considerably simplified. Then it is necessary to measure just the strength N of the source and the counting rate r_α at the peak of the internal conversion line for this source. The value of transmission is then given by $t = r_\alpha/(N\alpha)$. [See Eq. (2) below.] The results given in this paper for Co^{60} make this readily possible.

III. METHODS OF MEASURING α

From the definitions given above, it follows[19] that

$$\alpha = N_e/N_\gamma = r_\alpha/(N_\gamma t) = (r_\alpha/Nt)(1+\alpha) = [(Nt/r_\alpha)-1]^{-1}. \quad (1)$$

For $\alpha \ll 1$ this reduces to

$$\alpha = r_\alpha/(Nt). \quad (2)$$

[17] Lind, Brown, and DuMond, Phys. Rev. **76**, 591, 1838 (1949).
[18] R. H. Lyddane and A. E. Ruark, Rev. Sci. Inst. **10**, 253 (1939).
[19] We make the assumption that the coefficients of internal pair conversion and all other possible modes of decay are small compared to unity. See M. E. Rose, Phys. Rev. **76**, 678 (1949).

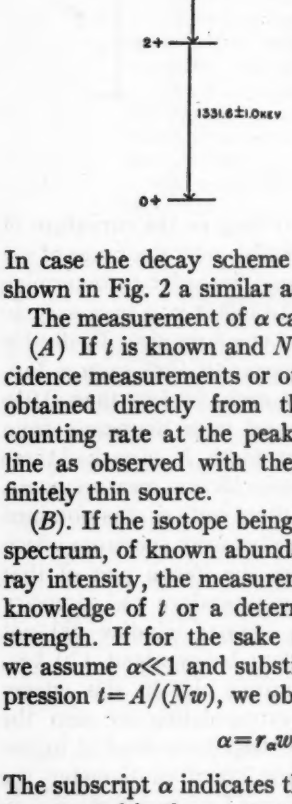

FIG. 3. Decay scheme of Co^{60}; assignment of spins and parities to the nuclear levels involved in the decay of Co^{60}. The assignments are based on polarization and angular correlation measurements, Gamow-Teller selection rules, the allowed shape of the spectrum and the absence of decay to the 2; even level of Ni^{60}. The shell model predicts a $p_{3/2}f_{7/2}$ configuration.

In case the decay scheme is more complex than that shown in Fig. 2 a similar analysis can be made.

The measurement of α can be made by two methods:

(*A*) If t is known and N can be determined by coincidence measurements or other methods, then α can be obtained directly from the measurement of r_α, the counting rate at the peak of the internal conversion line as observed with the spectrometer using an infinitely thin source.

(*B*). If the isotope being investigated has a beta-ray spectrum, of known abundance relative to the gamma-ray intensity, the measurement of α does not require a knowledge of t or a determination of absolute source strength. If for the sake of simplicity in illustration we assume $\alpha \ll 1$ and substitute for t in Eq. (2) the expression $t=A/(Nw)$, we obtain

$$\alpha = r_\alpha w N / A N_\alpha. \tag{3}$$

The subscript α indicates that N_α is the strength of the source used in the measurement of r_α, whereas N is the strength of the source used in obtaining A. Thus only the comparison measurement of source strengths, N/N_α, need be made. In addition r_α, the diameter of the source (and thus w) and the area A under the momentum plot of the beta-ray spectrum must be measured.

When the value of N_γ needed in the calculation of internal conversion coefficients cannot be determined by means of coincidence measurements or integration of a beta-ray spectrum, the value of N_γ must be determined by some other method. One such method is by comparing the photoelectric conversion line of the gamma-ray of unknown intensity with that of a gamma-ray of known intensity, using identical radiators. In practice, however, this method encounters at least two difficulties: uncertainty as to the correct dependence of the photoelectric cross section on energy, and of the effects of the anisotropy and scattering of the photoelectrons. In the cases discussed in this paper, wherever the method of external conversion comparison has been used to determine N_γ the energies of the gammas being compared are sufficiently alike that the errors due to the above difficulties are quite small. We have therefore neglected the effect of anisotropy and used Gray's[20] empirical formula, which seems to be the best available, for the photoelectric cross-section ratios. We intend to publish in a subsequent paper other results which are more seriously affected by the above mentioned difficulties with the method of external conversion comparison.

IV. EXPERIMENTAL RESULTS

A. Cobalt 60

The decay scheme[21] for Co^{60} is shown in Fig. 3. The gamma-ray energies have been measured accurately by Lind, Brown, and DuMond[17] using a crystal spectrograph. The value given for the end point of the beta-ray spectrum is the one we have determined from the Fermi plots of data on three different Co^{60} sources (same sources and data used in obtaining A/N in the measurement of the transmission of the spectrometer). Previous work[21] had indicated the beta-ray spectrum to have an allowed shape and our results are in agreement with this. The order of emission of the two gamma-rays is known from the work of Peacock.[22]

Brady and Deutsch[23] have studied the angular correlation of the gamma-rays of Co^{60} and found them both to be quadrupole with the spins of the three nuclear levels involved having the values 0, 2, 4. Angular correlation measurements, however, cannot distinguish between electric and magnetic radiation and therefore the parities of the nuclear levels cannot be fixed from these results. Measurement of the internal conversion coefficients for these two gamma-rays will determine the exact type of radiation and thus fix the parities of these nuclear levels relative to each other (as well as checking on the spin assignments). Recent measurements of Metzger and Deutsch[24] of the polarization-directional correlation of the gamma-rays indicate that the levels all have the same parity.

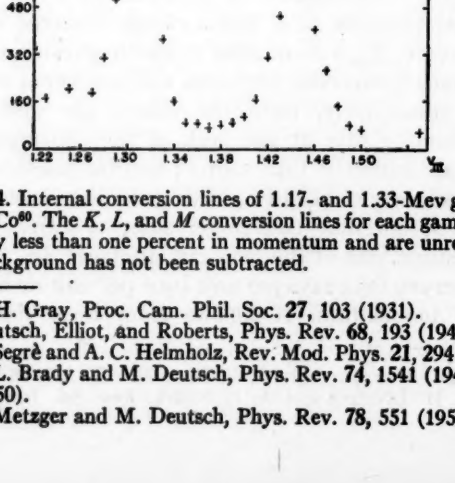

FIG. 4. Internal conversion lines of 1.17- and 1.33-Mev gamma-rays of Co^{60}. The K, L, and M conversion lines for each gamma-ray differ by less than one percent in momentum and are unresolved. The background has not been subtracted.

[20] L. H. Gray, Proc. Cam. Phil. Soc. **27**, 103 (1931).
[21] Deutsch, Elliot, and Roberts, Phys. Rev. **68**, 193 (1945).
[22] E. Segrè and A. C. Helmholz, Rev. Mod. Phys. **21**, 294 (1949).
[23] E. L. Brady and M. Deutsch, Phys. Rev. **74**, 1541 (1948); **78**, 558 (1950).
[24] F. Metzger and M. Deutsch, Phys. Rev. **78**, 551 (1950).

TABLE I. Internal conversion in excited states of $_{28}Ni^{60}$.*

Gamma-ray energy in Mev	$\alpha \times 10^4$ exp	Theoretical values of internal conversion coefficients *EQ*	*MD*	Classification of radiation
1.1715	1.733±0.061	1.545×10^{-4}	1.387×10^{-4}	*EQ*
1.3316	1.286±0.035	1.175×10^{-4}	1.034×10^{-4}	*EQ*

* The experimental values are for the $K+L+M$ conversion, unresolved. The theoretical values given are obtained by interpolation from the results given by Rose and his collaborators (see reference 1). The internal conversion coefficients for all types of radiation except magnetic dipole differ from that of electric quadrupole by a factor two or more and are therefore not given in this table.

The internal conversion coefficients in this case can be measured[25] by method B; i.e., using Eq. (3). In this case A and r_α cannot be measured with the same source since α is of the order of 10^{-4}. Therefore r_α was measured for three different Co^{60} sources of strengths varying from 60.5 to 85.8 microcuries and average thickness less than 0.20 mg/cm². A plot of a typical set of the data obtained for r_α is shown in Fig. 4. The rising background on the left is due to Compton electrons from the source which have end points at the potentiometer readings $V_{III}=1.128$ and 1.274 for the 1.17- and 1.33-Mev gamma-rays, respectively. A was measured for three different Co^{60} sources of strengths varying from 2.5 to 3.9 microcuries and average thickness less than 0.016 mg/cm² in the manner described above. The line width, w, was already known as a function of source size and the values of N/N_α were obtained by comparison of gamma-intensities.

The values we have obtained for the coefficients of conversion in the K, L, and M shells together (unresolved) for the two gamma-rays involved in the decay of Co^{60} and the theoretical[1] values of the conversion coefficients for the K shell for electric quadrupole (EQ) and magnetic dipole (MD) radiation are given in Table I. The conversion coefficients for all types of radiation except MD differ from that for EQ by a factor two or more. Supposing $L+M$ conversion[11] and screening[2] effects to contribute about 10 percent, our results classify both gamma-rays as EQ radiation. Since the selection rules for EQ radiation are $|I+I'| \geqslant 2 \geqslant |I-I'|$; no parity change, comparison of our results with angular correlation and polarization measurements fixes the spins and parities of the three Ni^{60} nuclear levels involved in the decay of Co^{60} as 0, 2, 4; same. If we assume the ground state of $_{28}Ni^{60}$ has even parity, then all three levels have even parity.

Once having assigned these spins and parities to the three Ni^{60} levels the fact that the beta-decay to the 4; even level has an allowed shape and no beta-decay to the 2; even or 0; even level is observed permits us to draw some tentative conclusions as to the spin and parity of the Co^{60} nuclear level. The present experiment permits us to place an upper limit of 0.1 percent on beta-decay to the 2; even level. Assuming that decay to the 2; even level must be at least once more forbidden than the observed decay and using Gamow-Teller selection rules, possible assignments to the Co^{60} level would be 4; even, 5; even or 5; odd. Thus the assignment of spins and parities to the nuclear levels involved in the decay of Co^{60} would be as shown in Fig. 3.

Although the agreement between theoretical and experimental values of the internal conversion coefficients seems quite good, more exact comparison cannot be made until the theoretical values for the effects of $L+M$ conversion and screening have been calculated. The present results are in agreement with those of Deutsch and Siegbahn[26] within the relatively large error (approximately 30 percent) of the latter. The classification of both gamma-rays as EQ now seems unambiguous.

B. Cesium 134

The decay scheme of Cs^{134} has been investigated by Siegbahn and Deutsch[27,28] and Elliot and Bell[29] with coincidence and spectrometer techniques. They found gamma-rays of energies 568, 602, 799, and 1350 kev and beta-rays with endpoints of 658 kev and approximately 90 kev. Coincidence and intensity measurements indicated that the three lowest energy gammas were in cascade and the 568-kev gamma-ray was first, but the order of the 799- and 602-kev gamma-rays was not determined. The 1.35-Mev gamma-ray was not definitely located in the decay scheme.

Elliot and Bell[29] obtained a straight (allowed shape) Fermi plot for both beta-spectra and determined the branching ratio of the beta-decay by two different methods. The values they obtained for the ratio of the number of 90 kev to the number of 658-kev beta-rays were about 0.25 and 0.28. Siegbahn and Deutsch[28] also measured this ratio by two methods and obtained the values 0.26±0.08 and 0.32±0.08. Meem and Maienschein[30] give the value 0.34±0.05. Siegbahn and

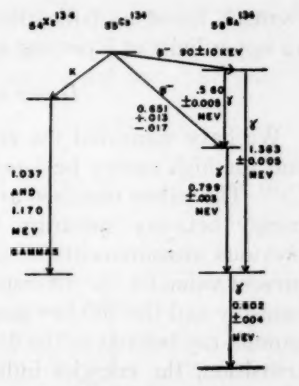

FIG. 5. Tentative decay scheme for Cs^{134}.

[25] Our results for Co^{60} have already been reported in a letter, Phys. Rev. 78, 295 (1950).

[26] M. Deutsch and K. Siegbahn, Phys. Rev. 77, 680 (1950).
[27] K. Siegbahn and M. Deutsch, Phys. Rev. 71, 483 (1947).
[28] K. Siegbahn and M. Deutsch, Phys. Rev. 73, 410(L) (1948).
[29] L. G. Elliot and R. E. Bell, Phys. Rev. 72, 979(L) (1947).
[30] J. L. Meem, Jr. and F. Maienschein, Phys. Rev. 76, 328 (1949).

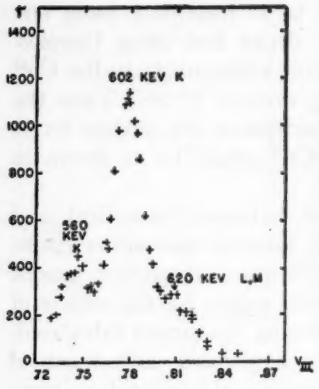

FIG. 6. Internal conversion lines of 560- and 602-kev gamma-rays of Cs^{134}. Fermi plot *II* (Fig. 9) has been subtracted as background. Note the incomplete resolution of the two *K* conversion lines and the partial resolution of the *L* conversion line of the 602-kev gamma-ray.

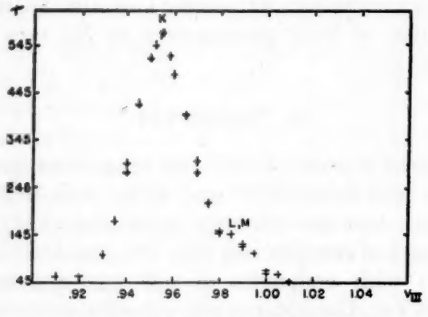

FIG. 7. Internal conversion line of 799-kev gamma-ray of Cs^{134}.

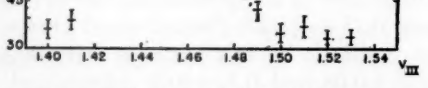

FIG. 8. Internal conversion line of 1.363-Mev gamma-ray of Cs^{134}.

Deutsch found no indication of *K*-capture and placed an upper limit of 5 percent on it.

Decay scheme

We have measured the energies of the gamma-rays and the high energy beta-ray involved in the decay of Cs^{134}. The values obtained are shown in Fig. 5. The low energy beta-ray spectrum was not investigated but previous measurements[29,30] are in agreement with the present value for the difference in energy of the 651-kev beta-ray and the 560-kev gamma-ray. If the 1.363-Mev gamma-ray belongs in the decay scheme as a cross-over transition, the energies indicate it to be a cross-over of the 560- and 799-kev gamma-rays. The fact that the energies add up correctly is not conclusive evidence for so assigning it, of course. Dr. R. Holland of this department has observed coincidences between the 90-kev beta-ray and the 1.363-Mev gamma-ray. His results indicate that 80±20 percent of the 1.363-Mev gamma-rays coincide with the 90-kev beta-rays. Thus we feel justified in saying that at least part of the 1.363-Mev gamma-rays belong in the decay scheme as an alternate transition to the 560, 799-kev cascade.

In our investigation of Cs^{134} we found, in addition to the internal conversion lines corresponding to the four gamma-rays previously observed, two conversion lines of energies 1.002 and 1.135 Mev of intensities about half of that of the 1.363-Mev gamma-ray conversion line. Sufficient evidence is not available to permit us to say definitely whether these are perhaps due to impurities or belong to a *K*-capture branch. The intensities and energies of these gamma-rays do not permit us to place them in the beta-ray decay branch. The height of the conversion lines of these gamma-rays were watched over a period of four months and there was no significant change of these lines with respect to that of the 1.363-Mev gamma-ray. Thus the assignment of these gamma-rays to an impurity seems unlikely. If they do belong to a *K*-capture branch, the corresponding gamma-ray energies would be 1.03 and 1.17 Mev and their intensities indicate that less than 4 percent of the disintegrations proceed in this manner. All of the experimental results discussed here are independent of the origin and assignment of these gamma-rays.

We thus *tentatively* propose as the decay scheme of Cs^{134} the one shown in Fig. 5.

Angular correlation[23] measurements for the 602- and 799-kev gamma-rays indicate that the spins of the first three $_{56}Ba^{134}$ nuclear levels are probably 0, 2, 4. These results are not completely unambiguous, but they do show definitely that the spin assignments cannot be anything which give rise to a very great anisotropy such as 0, 2, 0, for example. The polarization-directional correlation measurements[24] indicate that if the 0, 2, 4 spin assignment is correct, the levels all have the same parity.

It is clear that the measurement of internal conversion coefficients in the case of Cs^{134} involves some practical difficulties. Not only is the decay scheme somewhat in doubt, which presents a very serious problem, but there are also other difficulties. The 560- and 602-kev

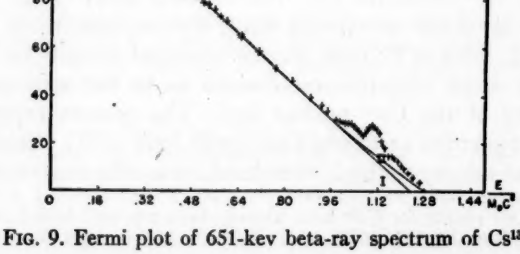

FIG. 9. Fermi plot of 651-kev beta-ray spectrum of Cs^{134}.

TABLE II. Internal conversion in excited states of $_{56}Ba^{134}$, calculated for two values of the beta-branching ratio, b, and for a relative abundance, z, of the 1.363-Mev gamma-ray to the 651-kev beta-ray of 0.058 (see reference 32).

	$\alpha_{560}\times10^3$	$\alpha_{602}\times10^3$	$\alpha_{799}\times10^3$	$\alpha_{1363}\times10^4$
Experimental values for				
b 265/735	8.2±1.0	5.31±0.23	2.55±0.06	6.20±0.34
b 30/70	6.7±0.8	5.06±0.22	2.41±0.06	6.20±0.34
Theoretical values				
ED	2.25	~2	1.06	3.87
EQ	6.17	5.25	2.63	8.5
MD	9.75	8.13	4.12	13
EO	15.40	12	6	18
MQ	20	20		
Classification of radiation	*EQ* and/ or *MD*	*EQ*	EQ	?

gamma-rays do not differ sufficiently in energy to be completely resolved (the L line of the 560 and the K line of the 602-kev gamma-ray will not be resolved at all). Both the 560- and 602-kev lines are superimposed on the high energy beta spectrum and near its end point. The 90-kev beta-spectrum is of such low energy that it is difficult to investigate. The branching ratios are not accurately known. The decay scheme is sufficiently complicated to make determination of source strengths by coincidence methods difficult. Consequently our results for Cs^{134} are not complete. We have taken as the basis of our calculations the decay scheme indicated in Fig. 5. The calculations have been carried through for two different values of the beta-ray branching ratio, namely, 265/735 and 30/70.

1.363-Mev gamma-ray

The number of 1.363-Mev gamma-ray transitions was determined by comparison with the external conversion line of the 1.332-Mev gamma-ray of a Co^{60} source of known strength, appropriate allowance being made for the change in photoelectric cross section with energy.[31]

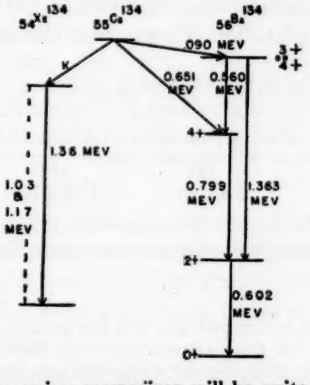

FIG. 10. Tentative assignment of spins and parities to the nuclear levels involved in the decay of Cs^{134}. We have assumed the 0, 2, 4 spin assignment to the first three Ba^{134} levels as indicated by angular correlation measurements to be correct. The shell model predicts a $g_{7/2}d_{3/2}$ configuration. Decay to the 2; even level of Ba^{134} is not present to as much as 0.1 percent.

[31] The method of external conversion comparison will be quite accurate in this case since we are comparing gamma-rays of very nearly the same energy.

The conversion coefficient could then be obtained by determining the value of r_α for the 1.363-Mev line since $\alpha=r_\alpha/(N_\gamma t)$. Thus the value of the internal conversion coefficient for the 1.363-Mev gamma-ray is independent of all the difficulties with branching ratios and so forth.

560-, 602- and 799-kev gamma-rays

The measurement of the internal conversion coefficients for the other gamma-rays can be made by either of the methods previously discussed. Because of the difficulties with the decay scheme we have found it convenient to use the second method, i.e., Eq. (3), and express our results in terms of two parameters:

b=the beta-branching ratio≡number of 90-kev beta-rays divided by the number of 651-kev beta-rays,

z≡the ratio of the number of 1.363-Mev gamma-rays to the number of 651-kev beta-rays.

This will permit the calculations to be repeated when more accurate values of the beta-branching ratio are obtained as well as making it clear just how the various internal conversion coefficients are affected by the 1.363-Mev gamma-cross-over transition.

The internal conversion coefficients can also be determined by the first method, i.e., $\alpha=r_\alpha/(N_\gamma t)$, if an absolute value for N_γ can be obtained. We have done this by determining the number of 651-kev beta-rays by coincidence techniques. The results obtained are entirely consistent with those obtained from Eq. (3).

In the determination of the internal conversion coefficients by Eq. (3) we have used the 651-kev beta-spectrum to obtain the value of A. The value of r_α for all the gamma-rays (except the 1.363 Mev) could be obtained from the same source. Thus N/N_α was simply an expression in terms of z and b which gave the ratio of the number of gamma-rays of the particular energy concerned to the number of 651-kev beta-rays in the assumed decay scheme.

The Cs^{134} sources used in obtaining A and the value of r_α for all except the 1.363-Mev gamma-ray were approximately 4 microcuries, 4 mm in diameter, and had an average thickness of less than 0.3 mg/cm². The sources

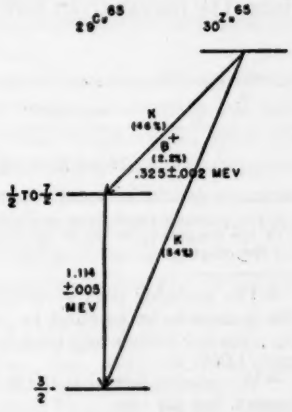

FIG. 11. Decay scheme of Zn^{65} according to previous work (references 34–38). The branching ratios are not relevant to the measurement of the conversion coefficient.

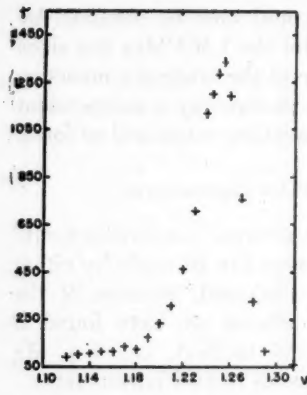

FIG. 12. Internal conversion line of 1.114-Mev gamma-ray of Zn^{65}. The distortion of the line is caused by finite source thickness.

used in obtaining r_α for the 1.363-Mev gamma-ray were about 10 times stronger and 4.5 mm in diameter.

Typical experimental data on the internal conversion lines of Cs^{134} are shown in Figs. 6–8.

Beta-Ray Spectrum Shape

In addition to the above mentioned difficulties another was encountered. In order to obtain A it was necessary to reconstruct the momentum plot of the 651-kev beta-ray spectrum from the Fermi plot by extrapolating the latter to zero. Contrary to the results of Elliot and Bell[29] we did not obtain a straight Fermi plot for this spectrum, but one slightly convex toward the energy axis at the high energy end. This curvature, found for two sources, was more than could be accounted for on the basis of the effect of the internal conversion lines which occur in this region. The Fermi plot for one of the sources is shown in Fig. 9. We have drawn two different curves through the data: I is a straight line and II is a smooth curve which coincides with I at lower energies but which is so chosen at the high energy end that the internal conversion lines of the 560- and 602-kev gamma-rays have the correct widths. Although the value of A (and consequently the value of z) is changed only about 0.3 percent by this difference in the shape of the Fermi plot at the high energy end, the values of r_α for the 560- and 602-kev gamma-rays are very sensitive to this shape since the beta-ray spectrum must be subtracted as background from these lines. The results given here are based on Fermi plot II. No attempt to find a correction factor to straighten this plot has been made.

The number of 651-kev beta-rays was also determined by coincidence methods. Although the results obtained were consistent with those obtained by integration of the beta-ray spectrum, they do not permit one to choose between the two Fermi plots since the coincidence method requires the use of the beta-branching ratio which is rather inaccurately known at the present time.

The average value of z obtained from two separate measurements is 0.0582 ± 0.0012.

Results

Expressed in terms of b and z the values obtained for the internal conversion coefficients are[32] as follows:

$$\alpha_{560}=(2.46\pm0.30)\times10^{-3}/(b-z),$$
$$\alpha_{602}=(7.22\pm0.13)\times10^{-3}/(1+b),$$
$$\alpha_{799}=(3.32\pm0.08)\times10^{-3}/(1+b-z),$$
$$\alpha_{1363}=(6.20\pm0.34)\times10^{-4}.$$

A summary of the calculations of the experimental values for the internal conversion coefficients of Cs^{134} and comparable theoretical values[1] is given in Table II. All of the experimental values are for the K shell only.

These results indicate that the 600- and 799-kev gamma-rays are both EQ. Comparison of these results with angular[33] correlation and polarization-directional correlation measurements fixes the spins and parities of the first three $_{56}Ba^{134}$ levels as 0, 2, 4; same. If we assume the ground level of $_{56}Ba^{134}$ to be 0; even, then the spins and parities of the first three Ba^{134} nuclear levels are as shown in Fig. 10.

The dependence of α_{560} on both b and the shape of the Fermi plot does not permit us to say whether the 560-kev gamma-ray is EQ, MD or a mixture of these. In any case, however, it seems clear that the selection rules obeyed by this transition are $|I+I'|\geq2\geq|I-I'|$; no parity change. Thus we would assign a spin between 2 and 6 and an even parity to the highest excited level of Ba^{134}. We shall return to the discussion of this assignment later.

As previously noted, the value of the internal conversion coefficient for the 1.363-Mev gamma-ray is quite independent of errors in the branching ratio and Fermi plot. Yet if we accept the theoretical values, the value

TABLE III. Internal conversion in excited state of $_{29}Cu^{65}$

α_K(exp)*	Theoretical values† of internal conversion coefficients for K shell				
	ED	*EQ*	*EO*	*MD*	*MQ*
$(2.28\pm0.26)\times10^{-4}$	1.2×10^{-4}	1.84×10^{-4}	5.4×10^{-4}	1.74×10^{-4}	5.0×10^{-4}

* The probable error given does not include error in value used for the ratio of the photoelectric cross sections for 1.114- and 1.172-Mev gamma-rays, 1.10, nor possible error due to external conversion in the source.
† See reference 1.

[32] The probable error given for the internal conversion coefficient of the 560- and 602-kev gamma-rays does not include error in r_α due to error in background, i.e., error in Fermi plot. The error given for the internal conversion coefficient of the 1.363-Mev gamma-ray does not include any error in the value taken for the ratio of the photoelectric cross sections for 1.332- and 1.363-Mev gamma-rays, 1.046.

[33] We assume here that the 0, 2, 4 spin assignment indicated by angular correlation measurements (but not unambiguously) is correct. See the text.

TABLE IV. Complete tabulation of experimental results.

Isotope	E_γ(Mev)	Source number	
Co^{60}	1.1715	6	1.745×10^{-4}
		10	1.795×10^{-4}
		11	1.658×10^{-4}
			Av. 1.733×10^{-4}
	1.3315	6	1.290×10^{-4}
		10	1.283×10^{-4}
		11	1.286×10^{-4}
			Av. 1.286×10^{-4}
Cs^{134}	0.560	1	$\frac{2.44}{b-z}\times10^{-3}$
		6	$\frac{2.48}{b-z}\times10^{-3}$
			Av. $\frac{2.46}{b-z}\times10^{-3}$
	0.602	1	$\frac{7.19}{1+b}\pm10^{-3}$
		6	$\frac{7.24}{1+b}\times10^{-3}$
			Av. $\frac{7.22}{1+b}\times10^{-3}$
	0.799	1	$\frac{3.37}{1+b-z}\times10^{-3}$
		11	$\frac{3.34}{1+b-z}\times10^{-3}$
			Av. $\frac{3.32}{1+b-z}\times10^{-3}$
Cs^{134}	1.363	5	5.94×10^{-4}
		9	6.45×10^{-4}
			Av. 6.20×10^{-4}
Zn^{65}	1.114	11	2.38×10^{-4}
		12	2.18×10^{-4}
			Av. 2.28×10^{-4}

$(6.20\pm0.34)\times10^{-4}$ which was obtained is not plausible for a single gamma-ray. According to the theoretical values α_{1363} cannot have a value between 3.87 and 8.5×10^{-4} unless we wish to consider the possibility of combining *ED* and *EO* radiation. The large difference in the theoretical half-lives of these types of radiation makes such a combination very unlikely, however.

There are at least five possible explanations of this anomalous conversion coefficient. First, the sources used were not extremely thin and as a result perhaps the conversion line is spread out and the peak value r_α is smaller than it should be. From a careful study of the conversion lines from three different Cs^{134} sources this effect was found to be small, however. (See Fig. 8.) This small correction has been made. (The value of r_α used in obtaining α_{1363} is that obtained by dividing the area under the observed conversion line by the appropriate line width, allowance being made for the effect of the *L* line on the line width.)

Second would be the possible effect of external conversion of the gamma-rays in the source itself. (See discussion with regard to this point under the results for Zn^{65}.) This would cause the observed value to be at most about 3 percent too high.

Third, perhaps the value used for the ratio of photoelectric cross sections for the 1.332- and 1.363-Mev gamma-rays is not correct. These two energies are close enough, however, that any error in this ratio, 1.046, cannot be large.

Fourth, perhaps the 1.363-Mev gamma-ray does not belong to Ba^{134} at all, but to some other isotope. This explanation is ruled out, however, on the basis of Holland's results that 80 ± 20 percent of the 1.363-Mev gamma-rays coincide with the 90-kev beta-rays.

Fifth, perhaps not *all* of the 1.363-Mev gamma-rays belong in the decay scheme as assumed, but part of them belong to a *K*-capture branch or even to another isotope.

Of these proposed explanations it is only the last one that the present evidence does not rule out. If about 40 percent of these conversion electrons belong to an *ED* gamma-ray in a *K*-capture branch (the gamma-ray energy would be 1.360 Mev), the conversion coefficient would be as observed provided the cross-over transition in the beta-decay branch is *EQ*. This would mean a spin of 2, 3, or 4 (and even parity) for the highest excited nuclear level of Ba^{134}. The absence of beta-decay to the first excited level (2; even) of Ba^{134} would rule out the assignment of 2; even to the highest excited level, assuming the existence of only the Gamow-Teller selection rules.

Thus if the above explanation is correct the assignment of spins and parities to the Ba^{134} nuclear levels would be as shown in Fig. 10. Whether this is the correct explanation or not present evidence does not permit us to decide.

C. Zinc 65

The decay scheme[34–38] of Zn^{65} is shown in Fig. 11. The energies given there are those reported by Mann, Rankin, and Daykin.[35] The value of the gamma-ray energy obtained in the present experiment is 1.112 ±0.007 Mev. The positron spectrum was not investigated, but previous work[35,36] indicates that it has an allowed shape. None of the branching ratios are relevant to the present investigation. In the case of Zn^{65} the internal conversion coefficient of its 1.11-Mev gamma-ray can be measured by either of the methods previously discussed. However, since the number of disintegrations leading to the 1.11 Mev excited state is easily measured whereas the *fraction* of disintegrations occurring by positron decay and leading to the 1.11-Mev excited state is not accurately known, we have used the first method, i.e., $\alpha=r_\alpha/(N_\gamma t)$.

The value of r_α was obtained for two Zn^{65} sources of diameters 4.45 mm and average thicknesses 2.2 and 2.6 mg/cm². The corresponding values of N_γ were obtained by means of gamma-comparison measurements with three other Zn^{65} sources for which the external conversion lines of the 1.11-Mev gamma-ray were compared with the external conversion lines of the 1.17-Mev gamma-ray of two Co^{60} sources of known strengths,

[34] Deutsch, Roberts, and Elliot, Phys. Rev. 71, 389 (1942).
[35] Mann, Rankin, and Daykin, Phys. Rev. 76, 1719 (1949).
[36] W. C. Peacock, Plut. Proj. Rep., Mon. N-432, 56 (Dec. 1947).
[37] Jensen, Laslett, and Pratt, Phys. Rev. 75, 458 (1949).
[38] W. M. Good and W. C. Peacock, Phys. Rev. 69, 680 (1946).

appropriate allowance being made for the dependence of the photoelectric cross section on energy. The error due to the inaccuracy in the knowledge of the variation of the photoelectric cross section with energy and the effect of anisotropy will be small here if we compare the 1.11- and 1.17-Mev gamma-rays since the difference in energy is small.

A typical example of the data obtained for r_α is shown in Fig. 12. Because of the thickness of the Zn^{65} sources used in obtaining the internal conversion line, these lines were spread over a wider energy range than that due to the finite resolution of the spectrometer. As a result the value of r at the peak of the conversion line is not the actual value of r_α, but is too small.[39] The actual value of r_α is obtained by determining the area under the internal conversion line and dividing by the line width (due to the finite resolution of the spectrometer) corresponding to that particular diameter source. Appropriate allowance must, of course, be made for the effect of the L and M lines on the line width.

The experimental values obtained and the relevant theoretical values[1] of the conversion coefficients for the K shell are given in Table III.

The experimental accuracy attainable with the relatively low specific activity Zn^{65} available and the uncertainty concerning the dependence of the photoelectric cross section on energy and the effect of anisotropy in the emission of the photo-electrons do not permit us to classify the gamma-radiation unambiguously. However, the above results seem to indicate that the radiation is EQ or MD or a mixture of these. Thus the parity of the excited state in Cu^{65} is the same as that of the ground state.

The theoretical values for EQ and MD radiation lie outside the experimental error by an amount which is of doubtful significance. One cannot account for the large observed coefficient on the basis of the effect of photo-electrons produced in the relatively thick source. These photo-electrons would add to the height of the external conversion line observed and the corresponding absorption would decrease the height of the observed external conversion line. Since $\alpha=r_\alpha/(N_\gamma t)$, the effect on α could be rather large if the product of the effective thickness of the source and the photoelectric absorption coefficient for this energy gamma-ray in Zn^{65} were appreciable compared to α. Using the values of photoelectric cross sections given by Hulme and collaborators[40] and supposing the effective path length in the approximately 2.5 mg/cm^2 ZnS source to be less than 10^{-3} cm, one would estimate as an upper limit on the value of (μx) about 3×10^{-6}. This would cause the observed internal conversion coefficient to be about 2 percent too high. This effect alone is thus not enough to account for the large coefficient observed. (See Table III.)

[39] This is similar to the dependence of the height of an external conversion line on the thickness of the converter. See Hornyak, Lauritsen, and Rasmussen, Phys. Rev. **76**, 731 (1949).

[40] Hulme, McDougall, Buckingham, and Fowler, Proc. Roy. Soc. **A149**, 131 (1935).

V. CONCLUSIONS

Of the seven gamma-rays reported on here (see Table IV) the measured internal conversion coefficients of four (the 1.17 and 1.33 Mev of Co^{60} and the 602 and 799 kev of Cs^{134}) agree very well both with the angular correlation and polarization measurements and with the theoretical values obtained by careful interpolations from the calculations of Rose and collaborators,[1] one value (that for the 1.11 Mev of Zn^{65}) is slightly too high and the experimental accuracy on another (the 560 kev of Cs^{134}) is not good enough to permit an accurate comparison with theory. The observed value for the 1.363-Mev gamma-ray of Cs^{134} does not agree with the theoretical results if the experimental calculations are based on the decay scheme for Cs^{134} shown in Fig. 5. Thus in the majority of the cases the agreement between experiment and theory is quite satisfactory. Further work must be done on the decay scheme of Cs^{134} to check the proposed explanation for the disagreement between experiment and theory in the case of the 1.363-Mev gamma-ray of Cs^{134}. It is noteworthy that all six of the excited nuclear levels observed in the present experiment have the same parity as their respective ground states.

In conclusion we may note the following:

(1) The results for Co^{60} and the two abundant gamma-rays of Cs^{134} are in excellent agreement with the theoretical values of Rose *et al.* and may be taken as verifying the theory, since independent evidence of the nature of these gamma-rays is available. Accordingly, the results of internal conversion measurements can be taken as positive identification of the multipole character of the gamma-ray, except in those cases in which different multipoles give indistinguishable coefficients.

(2) Internal conversion coefficients of 10^{-5} or even less can be measured with a precision of 5 percent or better. The 1.363-Mev gamma-ray of Cs^{134} gives one conversion electron for every 40,000 disintegrations and does not by any means represent the limits of the instrumental technique.

(3) In combination with angular correlation measurements, internal conversion coefficients can establish uniquely both the angular momenta and parities of excited nuclear states; in this respect they are probably more useful than the often ambiguous polarization correlations.

The radioactive materials used in this investigation were obtained from the Oak Ridge National Laboratory, Union Carbide and Carbon Corp. We should like to express our appreciation to Dr. R. Holland of this department for the coincidence measurements with the Cs^{134}, to Dr. A. Popov of the University's chemistry department for valuable aid and advice in the preparation of the radioactive sources, to Mr. J. G. Sentinella and the physics shop who fabricated the spectrometer for us, and to Dr. W. R. Arnold and Mr. P. Malmberg who assisted in the construction of the spectrometer and associated equipment.

The Rotational Structure of the Ultraviolet Band System of the P_2 Molecule

E. J. MARAIS AND H. VERLEGER
National Physical Laboratory, South African Council for Scientific and Industrial Research, Pretoria, South Africa
(Received November 25, 1949)

In continuation of the investigation by one of us (E.J.M.) further emission bands of the ultraviolet band system of the diatomic phosphorus molecule have been analyzed, and the vibrational and rotational constants calculated, taking the observed perturbations into consideration.

I. INTRODUCTION

A SERIES of emission bands of the ultraviolet $^1\Sigma_u^+ - {}^1\Sigma_g^+$-band spectrum of the P_2 molecule was previously photographed by one of us[1] in the third and fourth orders of a 21-ft. concave grating in a Paschen mounting at the Merensky Institute of Physics, University of Stellenbosch. These bands were analyzed and strong rotational perturbations were verified or found in the $v'=5$, 7, 8, and 9 vibrational levels of the upper electronic state. Furthermore, it was shown that the abnormality which was previously ascribed[2] to a vibrational perturbation in the $v'=5$ level, could be attributed to a rotational perturbation in this level. Since additional bands were photographed with the same experimental set-up, it appeared to be of value to analyze these and to recalculate the molecular constants taking the perturbations into consideration. The newly calculated constants of the new bands are given in this paper. In the following publication[3] the manner in which the investigation of the perturbations in the upper electronic state led to the molecular constants will be indicated.

II. VIBRATIONAL CONSTANTS

The following rotational bands were newly analyzed:[4] 3–16, 4–17, 4–18, 6–22, 7–27, 8–25, 8–26, 8–29, 9–27, 9–30, 10–30, and 11–32. The ν_0-values of these individual transitions were calculated and are given in the second column of Table I. In this table the results of Herzberg, Herzberg and Milne[5] on the 0–5, 0–6, 0–7 absorption, and 2–15 and 3–16 emission bands are also tabulated. In column 3 of Table I the ν_0-values are given calculated according to the newly computed formula:

$$\nu = 46787.282 + (472.62v' - 2.600v'^2 + 0.0235v'^3) - (777.62v'' - 2.8118v''^2 - 0.00533v''^3).$$

Column 4 shows the difference $(\nu_{0\text{exp}} - \nu_{0\text{cal}})$.

The vibrational constants for both states, which were calculated according to the usual methods, are tabulated in Table II.

The vibrational levels of the upper $^1\Sigma_u^+$-state can be taken from Table III. The experimental values in this table are average values, where more than one transition to the particular levels were measured. The maximum deviation of the average values from the individual measurements amounts to ± 0.05 cm^{-1}. The average value for $v'=0$ differs by an amount of ± 0.3 from the three individual values of Herzberg. The difference between the experimental and the calculated G-values of this level amounts to -0.27 cm^{-1}, so that the conclusion that this level is unperturbed seems to be legitimate. This is important for the later perturbation considerations.

In column 2 of Table III the experimental G-values are given, in column 3 the calculated values are shown and in column 4 the differences between the experimental and calculated values are given.

If the difference G'(experimental)$-G'$(calculated) is plotted against the vibrational quantum number v', one gets the dependence indicated in Fig. 1. The dotted

TABLE I. Band origins of the ultraviolet $^1\Sigma_u^+ \rightarrow {}^1\Sigma_g^+$ system of P_2.

Transition	ν_0 experimental	ν_0 calculated	ν_0 exp-ν_0 cal	v'
3–16	36484.56	36482.114	+2.45	3
4–17	36257.42	36256.923	+0.50	4
4–18	35583.08	35582.614	+0.47	4
5–20	37703.28	34703.280	±0.00	5
5–21	34047.66	34047.664	±0.00	5
6–21	34494.90	34493.823	+1.08	6
6–22	33845.62	33844.503	+1.12	6
6–23	33202.58	33201.510	+1.07	6
7–23	33643.27	33643.315	−0.05	7
7–24	33006.62	33006.682	−0.06	7
7–27	31135.18	31135.255	−0.08	7
8–25	32814.01	32814.030	−0.02	8
8–26	32190.21	32190.211	±0.00	8
8–27	31572.67	31572.847	−0.18	8
8–28	30961.79	30961.969	−0.18	8
8–29	30357.59	30357.611	−0.02	8
9–27	32006.46	32006.366	+0.11	9
9–28	31395.41	31395.489	−0.08	9
9–29	30791.09	30791.131	−0.04	9
9–30	30193.45	30193.324	+0.13	9
10–29	31220.41	31220.719	−0.31	10
10–30	30622.53	30622.912	−0.38	10
10–31	30031.39	30031.688	−0.30	10
11–31	30456.89	30457.486	−0.60	11
11–32	29872.29	29872.877	−0.60	11
0–5	42969.92	42970.143	−0.22	0
0–6	42223.39	42223.938	−0.55	0
0–7 } 4	41483.56	41483.548	+0.01	0
2–15	36713.85	36698.654	+5.20	2
3–16	36484.56	36482.114	+2.45	3

[1] E. J. Marais, Phys. Rev. **70**, 499 (1946).
[2] Compare the bibliography in reference 1.
[3] S. M. Naudé and H. Verleger, Phys. Rev. following paper.
[4] See Doctors Thesis of E. J. Marais, University of Stellenbosch, 1945.
[5] Herzberg, Herzberg, and Milne, Can. J. Research **18A**, 139 (1940).

curve follows from the data due to Herzberg.[6] Herzberg and his collaborators[4] have shown that the previously suspected[5] vibrational perturbation in $v'=2$ is a strong rotational perturbation. This would mean that also for $v'=2$ the curve proceeds towards zero.

Whereas there is no linear relation between $\Delta G'$ and the vibrational quantum numbers in the upper electronic state, a linear relation does exist between $\Sigma G''$ and the vibrational quantum numbers in the lower electronic state. This makes it possible to calculate the dissociation energy in the lower state according to the formula

$$D_0=\omega_0^2/4\omega_0x_0 \quad \text{and} \quad D_e=\omega_e^2/4\omega_ex_e.$$

Thus the following upper limit values for the dissociation energies in the ground state are obtained

$$D_0=153.663 \text{ kcal./mole chem.}=6.66\text{ev},$$

and

$$D_e=155.216 \text{ kcal./mole chem.}=6.73\text{ev}.$$

If one attempts to find the v_{max} value according to Birge and Sponer,[7] for which the distance between two levels becomes zero, we find

$$G(v)=\omega_e(v+\tfrac{1}{2})-\omega_ex_e(v+\tfrac{1}{2})^2+\cdots$$

or

$$dG(v)/dv=\omega_e-2\omega_ex_e(v+\tfrac{1}{2})+\cdots$$

or

$$V_{max}+\tfrac{1}{2}=\omega_e/2\omega_ex_e.$$

The heat of dissociation is then given by:

$$D=G(v_{max})-G(0).$$

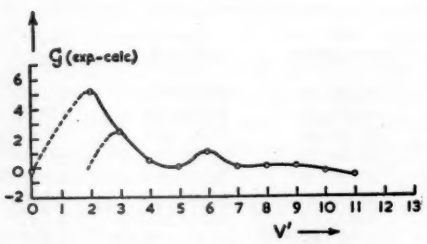

FIG. 1. $G_{exp}-G_{cal}$ as a function of v'.

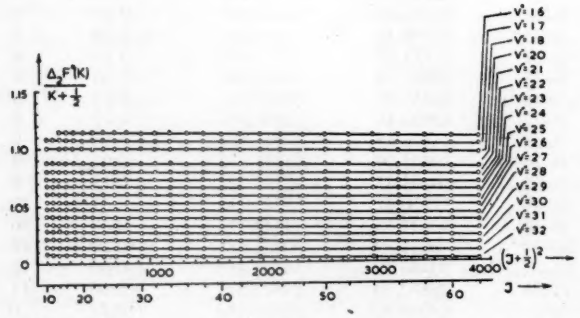

FIG. 2. Plot of the combination differences for the lower electronic state.

[6] G. Herzberg, Ann. d. Physik 15, 677 (1932).
[7] R. T. Birge and H. Sponer, Phys. Rev. 28, 259 (1926).

TABLE II. Vibrational constants.

Lower electronic state $^1\Sigma_g^+$	Upper electronic state $^1\Sigma_u^+$
$\omega_e''=+780.4278$ cm^{-1}	$\omega_e'=+475.2217$ cm^{-1}
$\omega_e''x_e''=+2.8038$	$\omega_e'x_e'=+2.6035$
$\omega_e''y_e''=-0.00533$	$\omega_e'y_e'=+0.0235$
$k_e''=5.5567\times10^5$ dyne/cm	$k_e'=2.0604\times10^5$ dyne/cm

TABLE III. G-values.

v'	G'(exp.)	G'(cal.)	G'(exp.-cal.)
0	46787.01	46787.282	−0.27
1	——	47257.324	——
2	47727.510	47722.310	+5.20
3	48184.822	48182.377	+2.45
4	48638.148	48637.666	+0.48
5	49088.320	49088.320	±0.00
6	49535.566	49534.478	+1.08
7	49976.220	49976.283	−0.06
8	50413.895	50413.874	+0.02
9	50847.394	50847.394	±0.00
10	51276.656	51276.982	−0.33
11	51702.193	51702.781	−0.59

or

$$D_e=(\omega_e^2/4\omega_ex_e)-\tfrac{1}{2}\omega_e.$$

From this one finds the upper limit of the value:

$$D_e=154.101 \text{ kcal./mole chem.}=6.68 \text{ ev}.$$

III. ROTATIONAL CONSTANTS

The rotational constants were calculated from the combination differences according to the usual graphical method. If $\Delta_2F(J)/(J+\frac{1}{2})$ is plotted as a function of $(J+\frac{1}{2})^2$, the ordinate value for $(J+\frac{1}{2})^2=0$ gives the $4B$ value, and the line gradient $8D$. This method has the advantage that slight irregularities can easily be detected in the rotational structure of a vibrational level. Whereas smooth curves are obtained for all of the vibrational levels of the lower electronic state (Fig. 2), strong departures from the smooth curve are found at several J-values in the vibrational levels $v'=5$, 7, 8, and 9 of the upper electronic state (see Fig. 3). These departures are treated as rotational perturbations. The remaining vibrational levels of the upper electronic state in the investigated region are not rotationally perturbed (Fig. 4). In the above mentioned rotationally perturbed vibrational levels no vibrational perturbations could be detected. For them the criterion of the departure of a vibrational level from the normal position is used. The rotational constants for the rotational states of a vibrational level, whose curves proceed unperturbed, were calculated in the usual way without applying a correction. These values are tabulated in Table IV as well as the B-values for the perturbed vibrational levels, which were corrected by taking into consideration the vibrational perturbations. The fact that it was found that the $\Delta_2G(J)/(J+\frac{1}{2})$ curves of the ground-state vibrational levels proceeded normally is

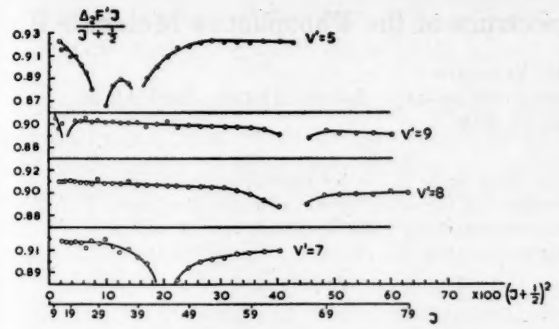

FIG. 3. Plot of the combination differences for the upper electronic state showing perturbations.

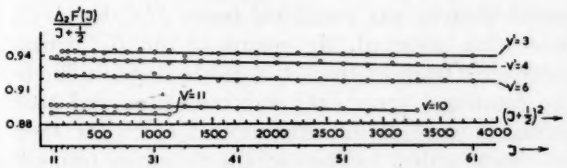

FIG. 4. Plot of the combination differences for the upper electronic state showing no perturbation.

one of the reasons for building up the vibrational levels of the upper state on those of the lower state according to the perturbation treatment, which is described below.[3]

In Table IV the values of the rotational constants B_v and D_v are tabulated, which were calculated on the basis of the following values of the equilibrium constants

$$B_e'=0.24166, \quad B_e''=0.30624,$$
$$\alpha_e'=0.00165, \quad \alpha_e''=0.00167.$$

The differences B_v(calculated)$-B_v$(experimental) are also given.

For the moment of inertia and internuclear distance in both states the following values were found using the new Birge values of constants

$$I_e'=115.809\times10^{-40} \text{ g cm}^2,$$
$$I_e''=91.388\times10^{-40} \text{ g cm}^2,$$
$$r_e'=2.122\times10^{-8} \text{ cm},$$
$$r_e''=1.885\times10^{-8} \text{ cm}.$$

TABLE IV. Rotational constants.

v'	B_v'(exp)	B_v'(cal)	B_v'(cal)-B_v'(exp)	D_v'
3	0.23598	0.23588	−0.00010	−0.00000025
4	0.23427	0.23423	−0.00004	−0.00000025
5	0.23259	0.23258	−0.00001	−0.00000025
6	0.23083	0.23093	+0.00010	−0.00000025
7	0.22923	0.22928	−0.00005	−0.00000024
8	0.22768	0.22763	−0.00005	−0.00000024
9	0.22605	0.22598	−0.00007	−0.00000024
10	0.22432	0.22433	+0.00001	−0.00000024
11	0.22272	0.22268	−0.00004	−0.00000024
v''	B_v''(exp)	B_v''(cal)	B_v''(cal)-B_v''(exp)	D_v''
16	0.27867	0.27868	+0.00001	−0.00000018
17	0.27699	0.27701	+0.00002	−0.00000018
18	0.27530	0.27534	+0.00004	−0.00000018
19	——	0.27367	——	——
20	0.27205	0.27200	−0.00005	−0.00000018
21	0.27036	0.27033	−0.00003	−0.00000018
22	0.26868	0.26866	−0.00002	−0.00000017
23	0.26707	0.26699	−0.00008	−0.00000017
24	0.26535	0.26532	−0.00003	−0.00000017
25	0.26367	0.26365	−0.00002	−0.00000017
26	0.26198	0.26198	±0.0	−0.00000017
27	0.26033	0.26031	−0.00002	−0.00000017
28	0.25867	0.25864	−0.00003	−0.00000017
29	0.25696	0.25697	+0.00001	−0.00000017
30	0.25532	0.25530	−0.00002	−0.00000017
31	0.25365	0.25363	−0.00002	−0.00000017
32	0.25200	0.25196	−0.00004	−0.00000017

We wish to thank Dr. S. M. Naudé for valuable discussions with us on the problem.

This paper is published with the permission of the South African Council for Scientific and Industrial Research.

The Perturbations in the Ultraviolet Band Spectrum of the Phosphorus Molecule P_2

S. M. NAUDÉ AND H. VERLEGER
National Physical Laboratory, South African Council for Scientific and Industrial Research, Pretoria, South Africa
(Received November 25, 1949)

The perturbations which have been observed in the upper state of the $^1\Sigma_u^+-{}^1\Sigma_g^+$ system of the P_2 molecule are discussed, the term values and the rotational constants of the unperturbed terms are computed, and the approximate term values and B values of the unknown perturbing terms determined. A $^3\Sigma_u^+$ and a $^1\Sigma_u^{s+}$ terms have been assumed as unknown perturbing terms.

I. INTRODUCTION

RECENTLY Herzberg, Herzberg, and Milne,[1] Marais,[2] and Marais and Verleger[3] have shown that the vibrational states with $v'>0$ of the upper state of the $^1\Sigma_u^+-{}^1\Sigma_g^+$ system of the P_2 molecule are perturbed partly by vibrational and partly by rotational perturbations. On the other hand, the vibrational and rotational levels of the lower state of the molecule show a normal behavior. Hitherto no explanation could be given for the behavior of the unperturbed terms of the upper state and the calculation of the constants on the basis of the perturbed terms always contained an element of uncertainty. Although the perturbing terms are not known, a consideration of the perturbations should make possible the accurate determination of the constants of the upper state and, furthermore, should allow conclusions concerning the nature of the perturbing terms.

The theory of the perturbations in band spectra has been worked out by Kronig[4] and by A. Budó and I. Kovács.[5] Budó and Kovács[5] have been able to show that perturbations between a $^3\Sigma$ and a $^1\Sigma$ state show the same behavior as perturbations between a $^1\Sigma$ and a $^1\Pi$ state.

II. THE PERTURBATIONS IN THE UPPER STATE OF THE ULTRAVIOLET P_2 BANDS

Let us consider the perturbations which occur in the bands of the P_2 molecule which have been studied by Marais[2] and Marais and Verleger.[3] From the normal behavior of the $\Delta_2F''(J)/J+\frac{1}{2}$ curves, and the systematic dependence of the v_0'' and B_v'' values, we conclude that the vibrational and rotational levels of the lower state are quite normal. On the other hand, the corresponding curves of the upper state show deviations from normal. The vibrational states $v'=3$, 4, 6, 10 and 11 are displaced owing to vibrational perturbations and the vibrational states $v'=5$, 7, 8 and 9 are irregular owing to rotational perturbations.

The rotational terms of the lower state (which is also the ground state) were first determined. The combination differences $\Delta_2F''(J)$ for $J=1$, 3, 5, $\cdots$ were added whereby the rotational terms $F(J)$ for $J=2$, 4, 6$\cdots$ were obtained. By means of the B_v'' and D_v'' values, determined from the combination differences, the rotational term $F(1)$ was calculated and to this value the combination differences $\Delta_2F''(J)$ for $J=2$, 4, 6$\cdots$ were added. In this way the rotational terms $F(J)$ for $J=3$, 5, 7$\cdots$ were obtained. These term values were then compared with the values which were computed by means of the determined B_v'' and D_v'' values. In this way the partly unobserved combination differences were averaged out. Moreover, this method allows a possibility of finding errors.

From the ground levels established in this way the rotational terms of the upper vibrational state which combine with these levels, were obtained by adding the wave numbers of the P or R lines to the corresponding rotational terms of the ground state. If P and R lines were available for the calculation of a term value, then the average value of the two term values obtained was taken. After the rotational term values were known, the origins of the bands could be determined. In the case of a $^1\Sigma-{}^1\Sigma$ transition this is given directly by the wave number difference of the corresponding nuclear vibrational levels for $J=0$.

The B values of the lower state which have been determined from the combination differences, are final owing to the absence of perturbations. The B values of the upper state were also determined initially from the combination differences. These values, however, have only a provisional character and are employed in order to be able at all to carry through a perturbation consideration. To begin with the discrepancies between the observed perturbed term values and the term values calculated by means of these provisional B values were plotted as a function of the rotational quantum number J. From this provisional perturbation curve the position of the perturbation maximum could be ascertained. From this position the conclusion is justified that the mutually perturbing terms must have the same energy at this point. We have, therefore, a numerical relation between $\Delta\nu$ and ΔB, for the J value is known. Now we are able to plot the actual perturbation curves, to determine the perturbation constants and to correct

[1] Herzberg, Herzberg, and Milne, Can. J. Research **18A**, 139 (1940).
[2] E. J. Marais, Phys. Rev. **70**, 499 (1946).
[3] E. J. Marais and H. Verleger, Phys. Rev. **80**, 429 (1950).
[4] R. de L. Kronig, Zeits. f. Physik **46**, 814 (1928); **50**, 347 (1928); Band Spectra and Molecular Structure (Cambridge University Press, London, 1930).
[5] A. Budó and I. Kovács, Zeits. f. Physik **11**, 633 (1939).

the B values. By means of $\Delta\nu$ and ΔB we further have information about the ν and B values of the perturbing term.

The curves representing the perturbations in the individual vibrational levels are given in Figs. 1–3. Since two closely adjacent perturbations are present in the vibrational level $v'=5$, a dotted curve is plotted next to the full curve representing the experimental results. The dotted curve represents the state of affairs which would exist in this state according to our perturbation considerations, if each perturbation were present alone without the influence of the other.

III. THE PERTURBATIONS IN THE $v'=3$ LEVEL

All rotational terms of this vibrational state are displaced to higher energy values with a constant amount for the smaller J values; i.e., the perturbing term must lie lower. Moreover, the perturbation decreases only gradually with increasing rotational quantum number. This leads to the conclusion that the mutually perturbing terms draw apart with increasing J. Consequently one can expect a B_v value for the perturbing term which is smaller than that of the perturbed term and differs only slightly from this B_v value. From the above we must conclude that the perturbing term is a Σ term.

IV. THE PERTURBATION IN THE $v'=4$ LEVEL

Also in this vibrational state the rotational states are displaced towards higher energy values with a constant amount, although smaller than above. This indicates again that the perturbing term lies lower than the perturbed term and that the perturbing term has a B_v value which is slightly smaller than that of the perturbed term. It also follows here that the unknown perturbing term must be a Σ term.

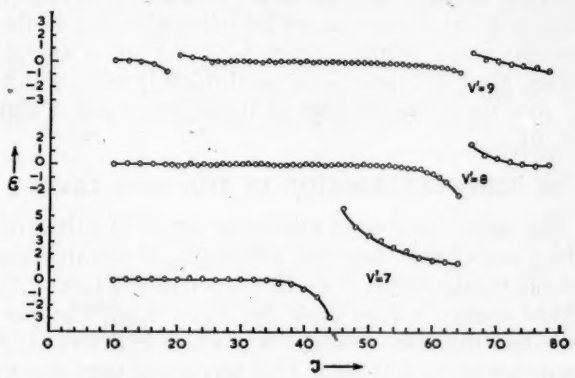

FIG. 1. Perturbations in the vibrational levels $v'=7$, 8, 9.

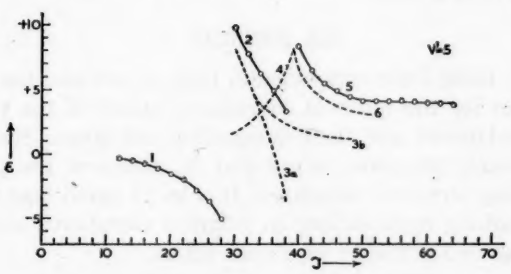

FIG. 2. Perturbations in the vibrational level $v'=5$.

V. THE PERTURBATION IN THE $v'=5$ LEVEL

It is more difficult to distinguish between the perturbations in the $v'=5$ level. It is clear, however, that the rotational states are not all equally perturbed in the sense of a vibrational perturbation but that the perturbing term values cross each other. The course of the perturbation curve does not tend towards zero after the perturbations die away, but towards a constant value. This indicates that we are concerned with an A perturbation here. We will now attempt to determine the position and the absolute amount of each perturbation individually.

If one plots the absolute amounts of the perturbations $|\epsilon|$ against J (Fig. 4), the perturbation increases systematically from the initial observed line with rotational quantum number $J=12$ along a normal curve to a maximum value of $|\epsilon|=8.0$ at $J=30$ (curve 1). The experimental displacements for $J=30$ and for $J=32$ to 36 (curve 2) are, however, greater than could be anticipated and it is natural to consider these experimental values as the sum of the first perturbation at $J=30$ and the second at $J=39$. Both perturbations lie so close together that they influence each other mutually. If one makes this assumption, curve 2 can be resolved into two curves of the form 3a and 4 of which 3a corresponds to the first perturbation at $J=30$. If the second perturbation at $J=39$ were not present, a curve of the form 3b could be expected for the fading out of the first perturbation at $J=30$. This leads one to surmise that a B perturbation is responsible for the first perturbation. Curve 4 which results from this consideration would represent the course of the values for the perturbation at $J=39$, if the first perturbation were absent. The experimental values of curve 5 have now to be corrected accordingly. The amounts of the correction can be ascertained from curve 3b for the first perturbation. As a result we get curve 6 which gives, taken together with curve 4, the maximum of the second perturbation at $J=39$.

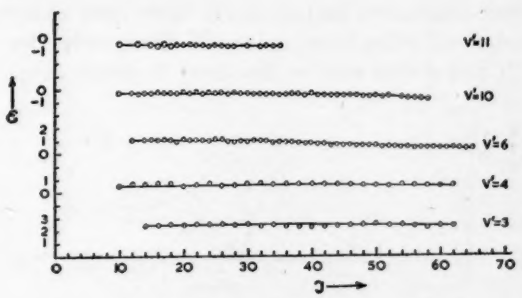

FIG. 3. Perturbations in the vibrational levels $v'=3$, 4, 6, 10, 11.

The perturbing terms in this state must be assumed to be a Σ and a Π term, which is also plausible seeing that the two perturbation positions lie so close together.

Calculations based on these considerations give the following values:

$$\nu_\Sigma = 49087 \text{ cm}^{-1}, \quad \nu_\Pi = 49108 \text{ cm}^{-1},$$
$$B_\Sigma = 0.234 \text{ cm}^{-1}, \quad B_\Pi = 0.230 \text{ cm}^{-1}.$$

VI. THE PERTURBATION IN THE $v'=6$ LEVEL

Here, just as in the $v'=3$ and $v'=4$ levels, all rotational levels are also displaced upwards. This must be caused by a perturbing term which lies lower. The perturbation changes with increasing rotational quantum number. The mutually perturbing terms therefore draw further apart with increasing J. Here we can also assume that the B value of the perturbing Π term is smaller than that of the perturbed Σ term.

VII. THE PERTURBATION IN THE $v'=7$ LEVEL

In the $v'=7$ level we have a simple case of a rotational perturbation. The terms with small rotational quantum numbers are unperturbed and the maximum divergence takes place only at $J=45.5$ (Fig. 5). Initially the known perturbed terms are pressed downwards by an unknown higher term. The term curves cross each other at $J=45.5$ and the known terms are now displaced upwards. The perturbation dies away with increasing J values. However, it does not return to zero, but tends towards a constant positive value in this case, which can again be considered as a criterion for an A perturbation. The perturbing term can therefore, be a Π term and the calculation of the data gives:

$$\nu_\Pi = 49940 \text{ cm}^{-1}, \quad B_\Pi = 0.234 \text{ cm}^{-1}.$$

VIII. THE PERTURBATION IN THE $v'=8$ LEVEL

In this level the known Σ state is crossed at $J=64.5$ by an unknown state (Fig. 6). After reaching a maximum the perturbation returns to zero. We, therefore, have a B perturbation here. For the unknown perturbing Σ term we get:

$$\nu_\Sigma = 50419 \text{ cm}^{-1}, \quad B_\Sigma = 0.226 \text{ cm}^{-1}.$$

IX. THE PERTURBATION IN THE $v'=9$ LEVEL

Three rotational perturbations have been observed in the $v'=9$ vibrational state. Of these only two at $J=19$ and $J=65$ can be discussed in detail (Fig. 5).

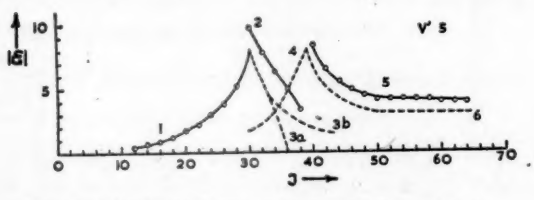

FIG. 4. Absolute values of the perturbations in the vibrational level $v'=5$.

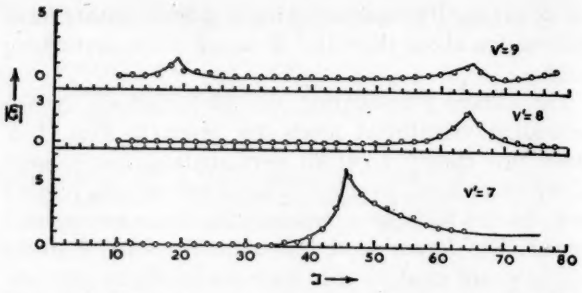

FIG. 5. Absolute values of the perturbations in the vibrational levels $v'=7, 8, 9$.

The further course of the third perturbation at $J=78$ could not be followed further owing to the predissociation[6] which occurs at these energy values. The first perturbation at $J=19$ is again a characteristic example of a B perturbation. A Σ-term can be assumed as the crossing term. A perturbation consideration of the second perturbation at $J=65$ is not completely possible owing to the third perturbation following closely upon it. It can be presumed, however, that this is due to a crossing Π-term. We have:

$$\nu_\Sigma = 50856 \text{ cm}^{-1}, \quad \nu_\Pi = 51053 \text{ cm}^{-1},$$
$$B_\Sigma = 0.214 \text{ cm}^{-1}, \quad B_\Pi = 0.224 \text{ cm}^{-1}.$$

X. THE PERTURBATION IN THE $v'=10$ LEVEL

The rotational levels with smaller J values are again displaced towards lower energy values with a small but measurable amount. This is caused by a perturbing Σ term of higher energy value. With increasing rotational quantum number ($J=60$) a considerable irregularity appears whose course cannot be followed owing to the predissociation[6] which occurs here. At these energy values, however, there lies a perturbing Π term, which fits into the series of other Π terms (see Table I and Fig. 6).

XI. THE PERTURBATION IN THE $v'=11$ LEVEL

The small number of rotational states of this level which have been observed, are displaced towards the smaller energy values, for which a perturbing term with higher energy values must be responsible. The perturbation increases slowly with J which indicates an A perturbation by a Π term. This perturbing term should have a v and a B value which is slightly greater than the perturbed Σ term.

XII. RESULTS

In Table I the experimental term values and the B_v values for the different vibrational states of the perturbed terms and their designation are given. Simultaneously the term values and B_v values of the perturbing terms are tabulated. It is to be noted that the perturbing terms belong to different vibrational states of the two unknown electronic terms.

[6] G. Herzberg, Ann. d. Physik **15**, 677 (1932).

TABLE I. Term values and B_v values for the perturbed vibrational states.

Known perturbed term				Unknown perturbing terms				
Designation	v'	B_v	Term value	Designation	v	B_v	Term value	Perturbs
	3	0.23598	48184.822	$^1\Sigma^*$	$x+1$	$<B_{^1\Sigma v'=3}$	48180	$v'=3$
	4	0.23427	48638.148	$^1\Sigma^*$	$x+2$	$<B_{^1\Sigma v'=4}$	48636	$v'=4$
	5	0.23259	49088.320	$^1\Sigma^*$	$x+3$	0.234	49087	$v'=5$
	6	0.23083	49535.566	$^1\Sigma^*$	$x+4$	——	(49535)	——
$^1\Sigma_u^+$	7	0.22923	49976.220	$^1\Sigma^*$	$x+5$	——	(49979)	——
	8	0.22768	50413.895	$^1\Sigma^*$	$x+6$	0.226	50419	$v'=8$
	9	0.22605	50847.394	$^1\Sigma^*$	$x+7$	0.214	50856	$v'=9$
	10	0.22432	51276.656	$^1\Sigma^*$	$x+8$	$>B_{^1\Sigma v'=10}$	51278	$v'=10$
	11	0.22272	51702.193	$^3\Sigma$	$y+1$	0.230	49108	$v'=5$
				$^3\Sigma$	$y+2$	$<B_{^1\Sigma v'=6}$	49533	$v'=6$
				$^3\Sigma$	$y+3$	0.234	49940	$v'=7$
				$^3\Sigma$	$y+4$	——	(50329)	——
				$^3\Sigma$	$y+5$	——	(50700)	——
				$^3\Sigma$	$y+6$	0.224	51053	$v'=9$
				$^3\Sigma$	$y+7$	——	(51388)	——
				$^3\Sigma$	$y+8$	$>B_{^1\Sigma v'=11}$	51705	$v'=11$

In Fig. 6 the positions of the known $^1\Sigma_u^+$ terms and both the unknown $^1\Sigma_u^+$ and $^3\Sigma_u^+$ terms are represented graphically.

The final designation of the unknown terms was determined as a result of the following considerations. According to Kronig[4] the perturbing terms should be $^1\Sigma$ and $^1\Pi$ states respectively, a designation which was also proposed by Marais[2] as far as the one term is concerned. As Herzberg[6] has already pointed out, however, the interruption of the rotational structure in the $v'=10$ and $v'=11$ levels is due to predissociation and the state causing this predissociation can only be a $^3\Sigma_u^+$ or $^3\Pi_u$ term. According to this the $^1\Sigma_u^+$ term is perturbed in such a way by the $^3\Sigma_u^+$ or $^3\Pi_u$ state that the potential curves form maxima for large nuclear separations which are greater for greater J-values. The intersections lie lower than the predissociation limit. The predissociation therefore only occurs after the molecules in the predissociation state $^1\Sigma_u^+$ have more energy than at these maxima. This is also the reason why higher rotational levels in $v'=9$ and $v'=10$ are more stable than the lower levels in $v'=11$.

It is very probable now that this state ($^3\Sigma_u^+$ or $^3\Pi_u$) which is responsible for the predissociation is also the state which causes the perturbations in these and other vibrational levels of the $^1\Sigma_u^+$ state. Furthermore, since

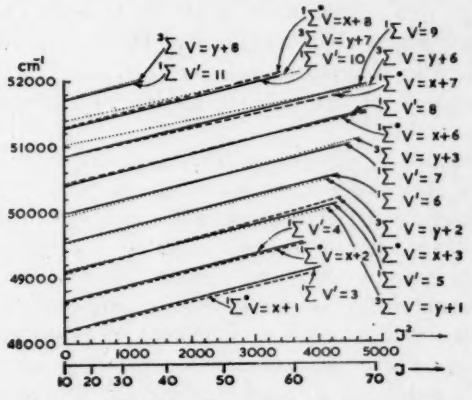

FIG. 6. Positions of the known $^1\Sigma_u^+$ and the unknown $^1\Sigma_u^{*+}$ and $^3\Sigma_u^+$ terms.

Budó and Kovács[5] showed that perturbations between a $^3\Sigma$ and a $^1\Delta$ state are similar to perturbations between a $^1\Pi$ and a $^1\Sigma$ state, we have to ascribe the A perturbations of Kronig's $^1\Pi$ state to a $^3\Sigma$ state. We therefore conclude that the perturbations are caused by $^1\Sigma_u^{*+}$ and $^3\Sigma_u^+$ states.

This paper is published with the permission of the South African Council for Scientific and Industrial Research.

The Forces Exerted on Dislocations and the Stress Fields Produced by Them

M. PEACH AND J. S. KOEHLER*
Carnegie Institute of Technology, Pittsburgh, Pennsylvania
(Received May 4, 1950)

It is shown that the force $d\mathbf{F}$ exerted on a line element $\mathbf{v}d\sigma$ of a dislocation with Burgers vector $\mathbf{f}$ by a stress τ is given by $d\mathbf{F}=-\mathbf{v}\times(\mathbf{f}\cdot\tau)d\sigma$. An analogy is drawn between the behavior of a closed line dislocation in a stress field and the behavior of a closed current-carrying loop in a field of magnetic induction. Then formulas for the stress components caused at any point of an infinite elastically isotropic crystal by a line element of a general Burgers dislocation are deduced from Burger's expressions for the displacements (see Sec. III(C)). These formulas bear a close analogy to the Biot-Savart formula of electromagnetic theory. Both of these results taken together constitute a complete system for the investigation of the mutual interaction of dislocations in an infinite elastically isotropic crystal.

I. INTRODUCTION

THIS paper aims to answer the following two questions. (1) How does a given dislocation interact with a given stress field? (2) How do two dislocations interact with each other? The first problem is treated with complete generality. The second problem is discussed for the case of an infinite isotropically elastic crystal.

In Section I, we describe the Burgers dislocation. In Section II, we obtain a result which gives the force on an element of a Burgers dislocation in a given external stress field. This force bears a certain analogy to the formula giving the force on a current element in a magnetic field. In Section III expressions are given for the stresses produced by a line element of a Burgers dislocation. These expressions are obtained from previously published formulas[1] giving the displacements produced by an element of a dislocation.

The results given constitute a complete system for the investigation of the behavior of a dislocation in a stress field and, within the limits mentioned, the interaction of dislocations with one another.

Let us create a Burgers dislocation in a crystal (Fig. 1). The crystal is cut along a surface (i.e., the hatched surface in Fig. 1). Next remove a cylinder of material of radius r_0 having as axis the line ABCDA bounding the cut surface. Give one face of the cut surface an arbitrary displacement $\mathbf{f}$ relative to the other face. Rejoin the two faces of the cut in their displaced position. Finally replace the atoms originally lying inside the cylinder of radius r_0. The block now contains a Burgers dislocation lying along ABCDA. If $\mathbf{f}$ is not parallel to the surface of the cut it will be necessary either to remove a thin slice of material on the cut surface or to add it when the translation is accomplished. r_0 is chosen large enough so that outside this cylinder the classical theory of elasticity can be used. If $\mathbf{f}$ is one atomic distance r_0 turns out to be two or three lattice parameters.[2]

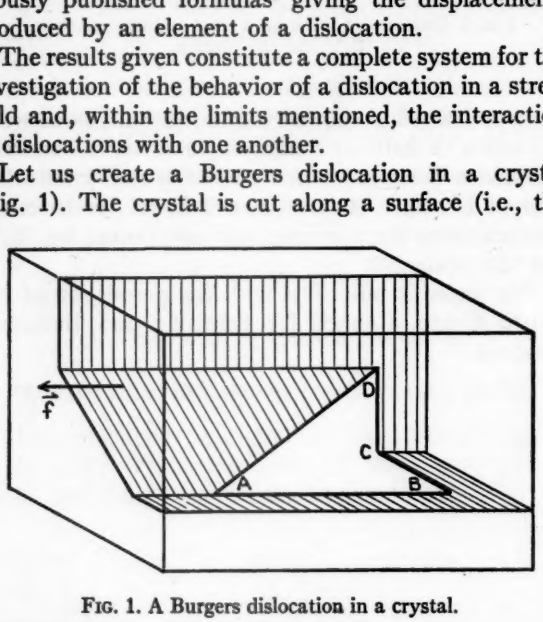

FIG. 1. A Burgers dislocation in a crystal.

The discussion given in the present paper enables one to treat the behavior of that portion of the crystal which behaves elastically. In the case of a Burgers dislocation this excludes only the region inside the cylinder r_0. In the case of two half-dislocations[3] one must exclude a slab of material a few atoms thick lying along that portion of the slip plane which joins the two half-dislocations. In many cases the changes in the arrangement of dislocations and other sources of stress are such that only relatively minor changes in stress occur in the excluded regions. For such situations elastic calculations such as those given in this paper are valuable.

II. FORCE ON AN ELEMENT OF A BURGERS DISLOCATION

(A). Sign Convention

The vector $\mathbf{f}$ is the Burgers vector of the dislocation. The sign of this vector can be determined by adopting the following convention. Figure 2 shows the positive sense of description of the dislocation line, the positive outward normal $\mathbf{n}$ of the dislocation surface, and the positive sense of description of a closed curve linking the dislocation line. If one crosses the cut surface going in the direction of the outward normal $\mathbf{n}$, he goes from the cut surface No. 1 to the cut surface No. 2. We shall

* This research constitutes a portion of a thesis submitted by M. O. Peach in partial fulfillment of the requirements for the degree of Doctor of Science at Carnegie Institute of Technology. This work was supported in part by ONR.

[1] W. G. Burgers, Proc. Akad. v. Wettensch. (Amsterdam), 42, 293 (1939).

[2] J. S. Koehler, Phys. Rev. 60, 397 (1941).

[3] R. D. Heidenreich and W. Shockley, Bristol Conference Report on Strength of Solids (1948).

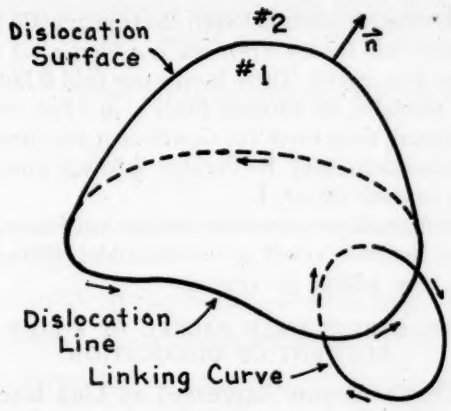

FIG. 2. Sign conventions for general dislocation.

in all cases obtain the dislocation by translating surface No. 1 through the distance **f** while surface No. 2 is held fixed.

(B). Fundamental Principle

If, in constructing the dislocation shown in Fig. 1, we had cut the block along any other surface having ABCDA as its sole internal boundary, the final physical state of the block would have been identical with that produced above. In other words the distribution of displacements and strains in a crystal containing a dislocation depends only on the configuration of the dislocation line and the Burgers vector.

This result is established[4] in Love's treatise. The argument is based on the definition of strain, the compatibility equations, and the assumption of a continuous stress distribution in the dislocated body. It is independent of the elastic properties of the body except that it is assumed that the continuity of stress implies a continuity of the strains. In particular, the result holds for elastically anisotropic crystals as well as isotropic bodies.

(C). Force on a Line Element of Dislocation in a Stress Field

Consider a rigid dislocation Γ having a vector **f**. Let $d\sigma$ be a line element of the dislocation in the direction shown (Fig. 3). The dislocation is immersed in a stress field described by the tensor τ

$$\tau=\begin{pmatrix}\tau_{xx} & \tau_{xy} & \tau_{xz}\\ \tau_{xy} & \tau_{yy} & \tau_{yz}\\ \tau_{xz} & \tau_{yz} & \tau_{zz}\end{pmatrix},$$

where the components τ_{ij} are scalar functions of position.

The dislocation possesses energy W (interaction energy with stress field) by reason of the presence of the stress field τ. The stress field does *not* include the stress field caused by the dislocation itself but includes that due to all other sources. We wish to calculate change in energy $\Delta W=W'-W$ caused by giving it an infinitesimal translation $d\mathbf{s}$ in an arbitrary direction, thus bringing it into a new position Γ' where it possesses (interaction) energy W'.

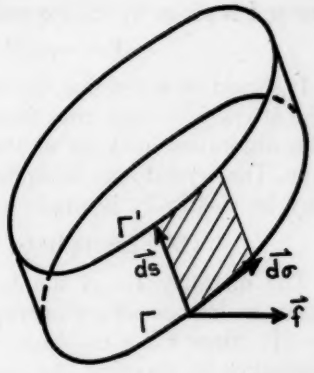

FIG. 3. Infinitesimal displacement of a dislocation.

Erect a cylinder on Γ with generators parallel to $d\mathbf{s}$ and extending to the surface of the crystal. We know we can construct the dislocation Γ by cutting the crystal along the surface of this cylinder and displacing the material inside the cylinder by a translation **f**. We know further that the interaction energy W of Γ with the stress field τ can be computed[5] by evaluating the work done on the surface of this cylinder during this displacement by the stress field τ. Similarly, the energy W' is the work done by τ on the surface of the cylinder erected on Γ' during the displacement **f**. It follows that $\Delta W=W'-W$ is the negative of the work done by τ on that portion of the cylindrical surface having Γ and Γ' as bases. Consider an element of this surface, $d\sigma\times d\mathbf{s}$, a vector element (Fig. 3) of area with normal pointing outward from the cylinder. The force on this area[6] is $\tau\cdot(d\sigma\times d\mathbf{s})$. Then the work done is $\mathbf{f}\cdot\{\tau\cdot(d\sigma\times d\mathbf{s})\}$ on this element. The total work $-\Delta W=\int_\sigma \mathbf{f}\cdot\{\tau\cdot(d\sigma\times d\mathbf{s})\}$. The force acting on the dislocation in the direction of $d\mathbf{s}$ is then $-\partial W/\partial s=+\int_\sigma \mathbf{f}\cdot\{\tau\cdot(d\sigma\times\lambda)\}$, where $d\sigma=\nu d\sigma$ and $d\mathbf{s}=\lambda ds$, λ and ν being unit vectors. Then, since τ is symmetric,

$$\mathbf{F}_\lambda=-\int_\sigma\{(\mathbf{f}\cdot\tau)\cdot(\lambda\times\nu)\}d\sigma.$$

Since the integration is on $d\sigma$ we may interpret the integrand as being the λ-component of force acting on an element of length $d\sigma$ of the dislocation. This can be written as

$$d\mathbf{F}_\lambda=-\lambda\cdot\{\nu\times(\mathbf{f}\cdot\tau)\}d\sigma.$$

It follows that the resultant force $d\mathbf{F}$, in a stress field τ, on an element $\nu d\sigma$ of a dislocation having a

[4] A. E. H. Love, *A Treatise on the Mathematical Theory of Elasticity* (Cambridge University Press, London, 1927).

[5] A. H. Cottrell, *Progress in Metal Physics* (Interscience Publishers, Inc., New York, 1949), p. 85.

[6] For notation see L. Page, *Introduction of Theoretical Physics* (D. Van Nostrand Company, Inc., New York, 1928), p. 34.

vector $\mathbf{f}$ is given by the expression[7]

$$d\mathbf{F}=-\nu\times(\mathbf{f}\cdot\tau)d\sigma.$$

It should be noted that this formula is very general.[8] The stress field may arise from any source whatever. The dislocation may be of the most general Burgers type. The crystal may be finite or infinite. The crystal may be elastically isotropic or elastically anisotropic.

(D). Immediate Deductions

The quantity $\mathbf{f}\cdot\tau$ is simply the vector traction τ_f across an element of area perpendicular to $\mathbf{f}$ multiplied by $|\mathbf{f}|$. Since $\mathbf{f}$ is a constant vector there is no loss of generality in choosing the x-axis parallel to $\mathbf{f}$. Then $\tau_f=\mathbf{i}\tau_{xx}+\mathbf{j}\tau_{yx}+\mathbf{k}\tau_{zx}$. Moreover τ_f is a solenoidal vector, for

$$div\tau_f=\frac{\partial\tau_{xx}}{\partial x}+\frac{\partial\tau_{yx}}{\partial y}+\frac{\partial\tau_{zx}}{\partial z}$$

and this last expression equated to zero is one of the three equilibrium equations of elasticity theory for the case where body forces can be neglected. The formula for the force on a line element of dislocation becomes $d\mathbf{F}=-|\mathbf{f}|\nu\times\tau_f d\sigma$ and this is exactly analogous to the formula $d\mathbf{F}=(i/c)\nu\times\mathbf{B}d\sigma$ from electromagnetic theory. The behavior of a dislocation in the vector field τ_f is exactly the same as that of a current-carrying wire in the vector field $\mathbf{B}$. In particular, one can introduce the concept of lines of force and arrive at a result that a dislocation loop will tend to move in such a way as to link with the greatest possible number of lines. Whether it actually will move depends upon the atomic constraints, just as whether a current loop will move depends upon the mechanical constraints imposed upon it. The only motion which is easily possible for a dislocation is motion in its slip plane. Any other motion requires the simultaneous breaking of so many atomic bonds as to be virtually impossible at ordinary temperatures, except in so far as diffusion of holes and extra atoms allows such motions to proceed. Greater freedom may be expected at high temperatures. One motion which is possible for dislocation loops which is not possible for current loops is a motion in which the length of the loop increases. The loop length will increase if sufficient energy is supplied to furnish the increased self energy corresponding to the increase in length of the loop and the energy lost (converted into heat) in overcoming the atomic constraints. If the stress system is reversed the field τ_f will be reversed, and since the dislocation loop is not free to rotate through 180° to align itself with the field but is bound to the slip plane, it will try to reduce its area as much as possible.

[7] The force on a dislocation given by J. S. Koehler, reference 2, differs slightly from that obtained above because he did not use an energetically closed system. This discrepancy will be dealt with in detail in a later paper, together with other discrepancies which exist in the literature.

[8] Shockley and Read have obtained a formula which gives the component in the slip direction of the force on an edge dislocation produced by any externally applied shear stress. T. W. Read and W. Shockley, Phys. Rev. 78, 275 (1950).

A difference appears between electromagnetic theory and dislocation theory when one considers a set of dislocations in a crystal. There is only one field $\mathbf{B}$ but there are, for example, six different fields τ_f in a face centered cubic crystal, since there are six different slip directions. The dislocations may be divided into six groups according to their vectors $\mathbf{f}$.

If electrostatic or other non-mechanical forces act on a crystal the fields τ_f will not be solenoidal; there will be sources of τ_f within the crystal.

III. STRESS FIELD CAUSED BY A LINE ELEMENT OF DISLOCATION

(A). Displacements Expressed as Line Integrals

In the paper[1] in which Burgers introduced the concept of a Burgers dislocation he also gave explicit expressions for the components of displacement caused by a general dislocation in an infinite, elastically isotropic crystal. Each expression contained three terms, of which two were given as line integrals over the dislocation curve, and the remaining one as a surface integral over an arbitrary surface bounded by the dislocation curve. He pointed out that the surface integral could be replaced by a line integral but did not express it as such. The problem of replacing the surface integral by a line integral does not have a unique solution, but one can choose a symmetric solution which enables the x-component of displacement to be written as follows;[9]

$$\begin{aligned}u_1=\frac{1}{4\pi}\int_\sigma\Bigg\{&\frac{d\xi_1}{d\sigma}\Bigg[f_1\frac{YZ}{3R}\left(\frac{1}{Z^2+X^2}-\frac{1}{X^2+Y^2}\right)\\&+X\frac{K}{R^3}(-f_2Z+f_3Y)\Bigg]\\&+\frac{d\xi_2}{d\sigma}\Bigg[f_1\frac{ZX}{3R}\left(\frac{1}{X^2+Y^2}-\frac{1}{Y^2+Z^2}\right)\\&+X\frac{K}{R^3}(-f_3X+f_1Z)-\frac{(1-K)}{R}f_3\Bigg]\\&+\frac{d\xi_3}{d\sigma}\Bigg[f_1\frac{XY}{3R}\left(\frac{1}{Y^2+Z^2}-\frac{1}{Z^2+X^2}\right)\\&+X\frac{K}{R^3}(-f_1Y+f_2X)+\frac{(1-K)}{R}f_2\Bigg]\Bigg\}d\sigma.\end{aligned}$$

From this the expressions for u_2 and u_3 can be obtained by simultaneous cyclic permutation of the three sets of quantities (ξ_1,ξ_2,ξ_3), (X,Y,Z), and (f_1,f_2,f_3). The quantities appearing in this equation are defined as follows:

$$X=x-\xi_1,\quad Y=y-\xi_2,\quad Z=z-\xi_3,$$
$$R=(X^2+Y^2+Z^2)^{\frac{1}{2}},$$

[9] This formula can be obtained from Eq. (21) and (5) of reference 1 by writing (5) as a line integral. The connection between the line and surface integral is given by Stoke's theorem. Thereafter it is necessary to find a vector potential for the field $\mathbf{r}/r^3$.

x, y, z are coordinates of the field point ξ_1, ξ_2, ξ_3 are coordinates of the source point, i.e., a point on the dislocation line.

f_1, f_2, f_3 are the components of the Burgers vector

$$K=\frac{\lambda+\mu}{\lambda+2\mu}, \quad 1-K=\frac{\mu}{\lambda+2\mu}.$$

λ and μ are the Lamé constants of isotropic elasticity theory. (Figure 4.)

(B). Strain Components Expressed as Line Integrals

The strain components are defined (Love's definitions)

$$e_{xx}=\partial u_1/\partial x, \text{ etc.} \quad e_{yz}=\partial u_2/\partial z+\partial u_3/\partial y, \text{ etc.}$$

An elementary though somewhat tedious calculation then gives the following line integral expressions:

$$e_{xx}=\frac{1}{4\pi}\int_\sigma\left\{\frac{d\xi_1}{d\sigma}\left[Kf_2\left(\frac{3ZX^2}{R^5}-\frac{Z}{R^3}\right)-Kf_3\left(\frac{3YX^2}{R^5}-\frac{Y}{R^3}\right)\right]\right.$$
$$+\frac{d\xi_2}{d\sigma}\left[f_3\left(\{1-3K\}\frac{X}{R^3}+3K\frac{X^3}{R^5}\right)\right.$$
$$\left.-f_1\left(\{1-K\}\frac{Z}{R^3}+3K\frac{ZX^2}{R^5}\right)\right]$$
$$+\frac{d\xi_3}{d\sigma}\left[f_1\left(\{1-K\}\frac{Y}{R^3}+3K\frac{YX^2}{R^5}\right)\right.$$
$$\left.\left.\left.-f_2\left(\{1-3K\}\frac{X}{R^3}+3K\frac{X^3}{R^5}\right)\right]\right\}d\sigma,$$

$$e_{yz}=\frac{1}{4\pi}\int_\sigma\left\{\frac{d\xi_1}{d\sigma}\left[Kf_2\left(\frac{6YZ^2}{R^5}-\frac{2Y}{R^3}\right)-Kf_3\left(\frac{6ZY^2}{R^5}-\frac{2Z}{R^3}\right)\right]\right.$$
$$+\frac{d\xi_2}{d\sigma}\left[f_2\left(\frac{X}{R^3}\right)+f_3K\left(\frac{6XYZ}{R^5}\right)\right.$$
$$\left.-f_1\left(\{1-2K\}\frac{Y}{R^3}+6K\frac{YZ^2}{R^5}\right)\right]$$
$$+\frac{d\xi_3}{d\sigma}\left[f_3\left(-\frac{X}{R^3}\right)+f_1\left(\{1-2K\}\frac{Z}{R^3}+6K\frac{ZY^2}{R^5}\right)\right.$$
$$\left.\left.\left.-f_3K\left(\frac{6XYZ}{R^5}\right)\right]\right\}d\sigma.$$

The other normal strain components can be obtained from e_{xx} by simultaneous cyclic permutation of variables and the other shear strain components can similarly be obtained from e_{yz}.

(C). Stress Components

The stress components are related to the strain components by

$$\tau_{xx}=\lambda\Delta+2\mu e_{xx}, \text{ etc.} \quad \tau_{yz}=\mu e_{yz}, \text{ etc.},$$

where $\Delta=e_{xx}+e_{yy}+e_{zz}$.

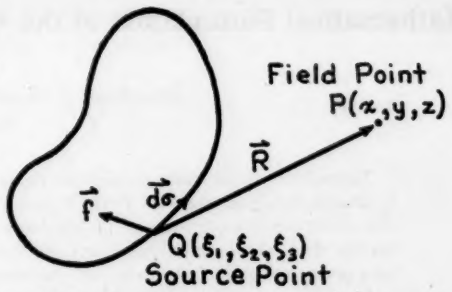

FIG. 4. Sketch showing the quantities which appear in the formulas for displacement, strain, and stress caused by a line element of dislocation.

Line integral expressions for the stresses are

$$\tau_{xx}=\frac{1}{4\pi}\int_\sigma\left\{\frac{d\xi_1}{d\sigma}\left[f_2\left(3L\frac{ZX^2}{R^5}-M\frac{Z}{R^3}\right)\right.\right.$$
$$\left.-f_3\left(3L\frac{YX^2}{R^5}-M\frac{Y}{R^3}\right)\right]$$
$$+\frac{d\xi_2}{d\sigma}\left[f_3\left(3L\frac{X^3}{R^5}-L\frac{X}{R^3}\right)-f_1\left(3L\frac{ZX^2}{R^5}+L\frac{Z}{R^3}\right)\right]$$
$$+\frac{d\xi_3}{d\sigma}\left[f_1\left(3L\frac{YX^2}{R^5}+L\frac{Y}{R^3}\right)\right.$$
$$\left.\left.\left.-f_2\left(3L\frac{X^3}{R^5}-L\frac{X}{R^3}\right)\right]\right\}d\sigma,$$

$$\tau_{yz}=\frac{1}{4\pi}\int_\sigma\left\{\frac{d\xi_1}{d\sigma}\left[f_2\left(3L\frac{YZ^2}{R^5}-L\frac{Y}{R^3}\right)\right.\right.$$
$$\left.-f_3\left(3L\frac{Y^2Z}{R^5}-L\frac{Z}{R^3}\right)\right]+\frac{d\xi_2}{d\sigma}\left[f_2\left(\mu\frac{X}{R^3}\right)\right.$$
$$+f_3\left(3L\frac{XYZ}{R^5}\right)-f_1\left(3L\frac{YZ^2}{R^3}-N\frac{Y}{R^3}\right)\Big]$$
$$+\frac{d\xi_3}{d\sigma}\left[f_3\left(-\mu\frac{X}{R^3}\right)+f_1\left(3L\frac{ZY^2}{R^5}-N\frac{Z}{R^3}\right)\right.$$
$$\left.\left.\left.-f_2\left(3L\frac{XYZ}{R^5}\right)\right]\right\}d\sigma,$$

where

$$L=\frac{2\lambda\mu+2\mu^2}{\lambda+2\mu}, \quad M=\frac{2\mu^2}{\lambda+2\mu}, \quad N=\frac{\lambda\mu}{\lambda+2\mu}.$$

The above integrations are on $d\sigma$. Hence the integrands can be interpreted as the stress produced at a point (x, y, z) by a line element $d\sigma$ of dislocation located at (ξ_1, ξ_2, ξ_3). It is clear that we have reached a result which, for an infinite elastically isotropic crystal, performs the same function as the formula

$$d\mathbf{B}=(\mu i/c)d\sigma\times\mathbf{r}/r^3$$

from electromagnetic theory. This result, together with the result of Section III, provide a complete system for investigating the mutual interaction of dislocations.

PHYSICAL REVIEW VOLUME 80, NUMBER 3 NOVEMBER 1, 1950

Mathematical Formulation of the Quantum Theory of Electromagnetic Interaction

R. P. FEYNMAN*
Department of Physics, Cornell University, Ithaca, New York
(Received June 8, 1950)

The validity of the rules given in previous papers for the solution of problems in quantum electrodynamics is established. Starting with Fermi's formulation of the field as a set of harmonic oscillators, the effect of the oscillators is integrated out in the Lagrangian form of quantum mechanics. There results an expression for the effect of all virtual photons valid to all orders in $e^2/\hbar c$. It is shown that evaluation of this expression as a power series in $e^2/\hbar c$ gives just the terms expected by the aforementioned rules.

In addition, a relation is established between the amplitude for a given process in an arbitrary unquantized potential and in a quantum electrodynamical field. This relation permits a simple general statement of the laws of quantum electrodynamics.

A description, in Lagrangian quantum-mechanical form, of particles satisfying the Klein-Gordon equation is given in an Appendix. It involves the use of an extra parameter analogous to proper time to describe the trajectory of the particle in four dimensions.

A second Appendix discusses, in the special case of photons, the problem of finding what real processes are implied by the formula for virtual processes.

Problems of the divergences of electrodynamics are not discussed.

1. INTRODUCTION

IN two previous papers[1] rules were given for the calculation of the matrix element for any process in electrodynamics, to each order in $e^2/\hbar c$. No complete proof of the equivalence of these rules to the conventional electrodynamics was given in these papers. Secondly, no closed expression was given valid to all orders in $e^2/\hbar c$. In this paper these formal omissions will be remedied.[2]

In paper **II** it was pointed out that for many problems in electrodynamics the Hamiltonian method is not advantageous, and might be replaced by the over-all space-time point of view of a direct particle interaction. It was also mentioned that the Lagrangian form of quantum mechanics[3] was useful in this connection. The rules given in paper **II** were, in fact, first deduced in this form of quantum mechanics. We shall give this derivation here.

The advantage of a Lagrangian form of quantum mechanics is that in a system with interacting parts it permits a separation of the problem such that the motion of any part can be analyzed or solved first, and the results of this solution may then be used in the solution of the motion of the other parts. This separation is especially useful in quantum electrodynamics which represents the interaction of matter with the electromagnetic field. The electromagnetic field is an especially simple system and its behavior can be analyzed completely. What we shall show is that the net effect of the field is a delayed interaction of the particles. It is possible to do this easily only if it is not necessary at the same time to analyze completely the motion of the particles. The only advantage in our problems of the form of quantum mechanics in **C** is to permit one to separate these aspects of the problem. There are a number of disadvantages, however, such as a lack of familiarity, the apparent (but not real) necessity for dealing with matter in non-relativistic approximation, and at times a cumbersome mathematical notation and method, as well as the fact that a great deal of useful information that is known about operators cannot be directly applied.

It is also possible to separate the field and particle aspects of a problem in a manner which uses operators and Hamiltonians in a way that is much more familiar. One abandons the notation that the order of action of operators depends on their written position on the paper and substitutes some other convention (such that the order of operators is that of the time to which they refer). The increase in manipulative facility which accompanies this change in notation makes it easier to represent and to analyze the formal problems in electrodynamics. The method requires some discussion, however, and will be described in a succeeding paper. In this paper we shall give the derivations of the formulas of **II** by means of the form of quantum mechanics given in **C**.

The problem of interaction of matter and field will be analyzed by first solving for the behavior of the field in terms of the coordinates of the matter, and finally discussing the behavior of the matter (by matter is actually meant the electrons and positrons). That is to say, we shall first eliminate the field variables from the equations of motion of the electrons and then discuss the behavior of the electrons. In this way all of the rules given in the paper **II** will be derived.

Actually, the straightforward elimination of the field

* Now at the California Institute of Technology, Pasadena, California.

[1] R. P. Feynman, Phys. Rev. **76**, 749 (1949), hereafter called **I**, and Phys. Rev. **76**, 769 (1949), hereafter called **II**.

[2] See in this connection also the papers of S. Tomonaga, Phys. Rev. **74**, 224 (1948); S. Kanesawa and S. Tomonaga, Prog. Theoret. Phys. **3**, 101 (1948); J. Schwinger, Phys. Rev. **76**, 790 (1949); F. Dyson, Phys. Rev. **75**, 1736 (1949); W. Pauli and F. Villars, Rev. Mod. Phys. **21**, 434 (1949). The papers cited give references to previous work.

[3] R. P. Feynman, Rev. Mod. Phys. **20**, 367 (1948), hereafter called **C**.

variables will lead at first to an expression for the behavior of an arbitrary number of Dirac electrons. Since the number of electrons might be infinite, this can be used directly to find the behavior of the electrons according to hole theory by imagining that nearly all the negative energy states are occupied by electrons. But, at least in the case of motion in a fixed potential, it has been shown that this hole theory picture is equivalent to one in which a positron is represented as an electron whose space-time trajectory has had its time direction reversed. To show that this same picture may be used in quantum electrodynamics when the potentials are not fixed, a special argument is made based on a study of the relationship of quantum electrodynamics to motion in a fixed potential. Finally, it is pointed out that this relationship is quite general and might be used for a general statement of the laws of quantum electrodynamics.

Charges obeying the Klein-Gordon equation can be analyzed by a special formalism given in Appendix A. A fifth parameter is used to specify the four-dimensional trajectory so that the Lagrangian form of quantum mechanics can be used. Appendix B discusses in more detail the relation of real and virtual photon emission. An equation for the propagation of a self-interacting electron is given in Appendix C.

In the demonstration which follows we shall restrict ourselves temporarily to cases in which the particle's motion is non-relativistic, but the transition of the final formulas to the relativistic case is direct, and the proof could have been kept relativistic throughout.

The transverse part of the electromagnetic field will be represented as an assemblage of independent harmonic oscillators each interacting with the particles, as suggested by Fermi.[4] We use the notation of Heitler.[5]

2. QUANTUM ELECTRODYNAMICS IN LAGRANGIAN FORM

The Hamiltonian for a set of non-relativistic particles interacting with radiation is, classically, $H=H_p+H_I+H_c+H_{tr}$, where $H_p+H_I=\sum_n \frac{1}{2}m_n^{-1}(\mathbf{p}_n-e_n\mathbf{A}^{tr}(\mathbf{x}_n))^2$ is the Hamiltonian of the particles of mass m_n, charge e_n, coordinate $\mathbf{x}_n$ and momentum $\mathbf{p}_n$ and their interaction with the transverse part of the electromagnetic field. This field can be expanded into plane waves

$$\mathbf{A}^{tr}(\mathbf{x})=(8\pi)^{\frac{1}{2}}\sum_{\mathbf{K}}[\mathbf{e}_1(q_{\mathbf{K}}^{(1)}\cos(\mathbf{K}\cdot\mathbf{x})+q_{\mathbf{K}}^{(3)}\sin(\mathbf{K}\cdot\mathbf{x}))+\mathbf{e}_2(q_{\mathbf{K}}^{(2)}\cos(\mathbf{K}\cdot\mathbf{x})+q_{\mathbf{K}}^{(4)}\sin(\mathbf{K}\cdot\mathbf{x}))] \quad (1)$$

where $\mathbf{e}_1$ and $\mathbf{e}_2$ are two orthogonal polarization vectors at right angles to the propagation vector $\mathbf{K}$, magnitude k. The sum over $\mathbf{K}$ means, if normalized to unit volume, $\frac{1}{2}\int d^3\mathbf{K}/8\pi^3$, and each $q_{\mathbf{K}}^{(r)}$ can be considered as the coordinate of a harmonic oscillator. (The factor $\frac{1}{2}$ arises for the mode corresponding to $\mathbf{K}$ and to $-\mathbf{K}$ is the same.) The Hamiltonian of the transverse field represented as oscillators is

$$H_{tr}=\frac{1}{2}\sum_{\mathbf{K}}\sum_{r=1}^{4}((p_{\mathbf{K}}^{(r)})^2+k^2(q_{\mathbf{K}}^{(r)})^2)$$

where $p_{\mathbf{K}}^{(r)}$ is the momentum conjugate to $q_{\mathbf{K}}^{(r)}$. The longitudinal part of the field has been replaced by the Coulomb interaction,[6]

$$H_c=\tfrac{1}{2}\sum_n\sum_m e_ne_m/r_{nm}$$

where $r_{nm}^2=(\mathbf{x}_n-\mathbf{x}_m)^2$. As is well known,[4] when this Hamiltonian is quantized one arrives at the usual theory of quantum electrodynamics. To express these laws of quantum electrodynamics one can equally well use the Lagrangian form of quantum mechanics to describe this set of oscillators and particles. The classical Lagrangian equivalent to this Hamiltonian is $L=L_p+L_I+L_c+L_{tr}$ where

$$L_p=\tfrac{1}{2}\sum_n m_n\dot{\mathbf{x}}_n^2 \quad (2a)$$

$$L_I=\sum_n e_n\dot{\mathbf{x}}_n\cdot\mathbf{A}^{tr}(\mathbf{x}_n) \quad (2b)$$

$$L_{tr}=\tfrac{1}{2}\sum_{\mathbf{K}}\sum_r((\dot{q}_{\mathbf{K}}^{(r)})^2-k^2(q_{\mathbf{K}}^{(r)})^2) \quad (2c)$$

$$L_c=-\tfrac{1}{2}\sum_n\sum_m e_ne_m/r_{mn}. \quad (2d)$$

When this Lagrangian is used in the Lagrangian forms of quantum mechanics of C, what it leads to is, of course, mathematically equivalent to the result of using the Hamiltonian H in the ordinary way, and is therefore equivalent to the more usual forms of quantum electrodynamics (at least for non-relativistic particles). We may, therefore, proceed by using this Lagrangian form of quantum electrodynamics, with the assurance that the results obtained must agree with those obtained from the more usual Hamiltonian form.

The Lagrangian enters through the statement that the functional which carries the system from one state to another is $\exp(iS)$ where

$$S=\int L dt=S_p+S_I+S_c+S_{tr}. \quad (3)$$

The time integrals must be written as Riemann sums with some care; for example,

$$S_I=\sum_n\int e_n\dot{\mathbf{x}}_n(t)\cdot\mathbf{A}^{tr}(\mathbf{x}_n(t))dt \quad (4)$$

becomes according to C, Eq. (19)

$$S_I=\sum_n\sum_i\tfrac{1}{2}e_n(\mathbf{x}_{n,i+1}-\mathbf{x}_{n,i})\cdot(\mathbf{A}^{tr}(\mathbf{x}_{n,i+1})+\mathbf{A}^{tr}(\mathbf{x}_{n,i})) \quad (5)$$

so that the velocity $\dot{\mathbf{x}}_{n,i}$ which multiplies $\mathbf{A}^{tr}(\mathbf{x}_{n,i})$ is

$$\dot{\mathbf{x}}_{n,i}=\tfrac{1}{2}\epsilon^{-1}(\mathbf{x}_{n,i+1}-\mathbf{x}_{n,i})+\tfrac{1}{2}\epsilon^{-1}(\mathbf{x}_{n,i}-\mathbf{x}_{n,i-1}). \quad (6)$$

[4] E. Fermi, Rev. Mod. Phys. 4, 87 (1932).

[5] W. Heitler, *The Quantum Theory of Radiation*, second edition (Oxford University Press, London, 1944).

[6] The term in the sum for $n=m$ is obviously infinite but must be included for relativistic invariance. Our problem here is to re-express the usual (and divergent) form of electrodynamics in the form given in II. Modifications for dealing with the divergences are discussed in II and we shall not discuss them further here.

In the Lagrangian form it is possible to eliminate the transverse oscillators as is discussed in **C**, Section 13. One must specify, however, the initial and final state of all oscillators. We shall first choose the special, simple case that all oscillators are in their ground states initially and finally, so that all photons are virtual. Later we do the more general case in which real quanta are present initially or finally. We ask, then, for the amplitude for finding no quanta present and the particles in state $\chi_{t''}$ at time t'', if at time t' the particles were in state $\psi_{t'}$ and no quanta were present.

The method of eliminating field oscillators is described in Section 13 of **C**. We shall simply carry out the elimination here using the notation and equations of **C**. To do this, for simplicity, we first consider in the next section the case of a particle or a system of particles interacting with a single oscillator, rather than the entire assemblage of the electromagnetic field.

3. FORCED HARMONIC OSCILLATOR

We consider a harmonic oscillator, coordinate q, Lagrangian $L=\frac{1}{2}(\dot{q}^2-\omega^2q^2)$ interacting with a particle or system of particles, action S_p, through a term in the Lagrangian $q(t)\gamma(t)$ where $\gamma(t)$ is a function of the coordinates (symbolized as x) of the particle. The precise form of $\gamma(t)$ for each oscillator of the electromagnetic field is given in the next section. We ask for the amplitude that at some time t'' the particles are in state $\chi_{t''}$ and the oscillator is in, say, an eigenstate m of energy $\omega(m+\frac{1}{2})$ (units are chosen such that $\hbar=c=1$) when it is given that at a previous time t' the particles were in state $\psi_{t'}$ and the oscillator in n. The amplitude for this is the transition amplitude [see **C**, Eq. (61)]

$$\langle\chi_{t''}\varphi_m|1|\psi_{t'}\varphi_n\rangle_{S_p+S_0+S_I}$$
$$=\int\int\chi_{t''}^*(x_{t''})\varphi_m^*(q_{t''})\exp i(S_p+S_0+S_I)$$
$$\cdot\varphi_n(q_{t'})\psi_{t'}(x_{t'})dx_{t''}dx_{t'}dq_{t''}dq_{t'}\mathfrak{D}x(t)\mathfrak{D}q(t) \quad (7)$$

where x represents the variables describing the particle, S_p is the action calculated classically for the particles for a given path going from coordinate $x_{t'}$ at t' to $x_{t''}$ at t'', S_0 is the action $\int\frac{1}{2}(\dot{q}^2-\omega^2q^2)dt$ for any path of the oscillator going from $q_{t'}$ at t' to $q_{t''}$ at t'', while

$$S_I=\int q(t)\gamma(t)dt, \quad (8)$$

the action of interaction, is a functional of both $q(t)$ and $x(t)$, the paths of oscillator and particles. The symbols $\mathfrak{D}x(t)$ and $\mathfrak{D}q(t)$ represent a summation over all possible paths of particles and oscillator which go between the given end points in the sense defined in **C**, Eq. (9). (That is, assuming time to proceed in infinitesimal steps, ϵ, an integral over all values of the coordinates x and q corresponding to each instant in time, suitably normalized.)

The problem may be broken in two. The result can be written as an integral over all paths of the particles only, of $(\exp iS_p)\cdot G_{mn}$:

$$\langle\chi_{t''}\varphi_m|1|\psi_{t'}\varphi_n\rangle_{S_p+S_0+S_I}=\langle\chi_{t''}|G_{mn}|\psi_{t'}\rangle_{S_p} \quad (9)$$

where G_{mn} is a functional of the path of the particles alone (since it depends on $\gamma(t)$) given by

$$G_{mn}=\left\langle\varphi_m\left|\exp i\int q(t)\gamma(t)dt\right|\varphi_n\right\rangle_{S_0}$$
$$=\int\varphi_m^*(q_{t''})\exp i(S_0+S_I)\varphi_n(q_{t'})dq_{t'}dq_{t''}\mathfrak{D}q(t)$$
$$=\int\varphi_m^*(q_j)\exp i\epsilon\sum_{i=0}^{j-1}[\tfrac{1}{2}\epsilon^{-2}(q_{i+1}-q_i)^2-\tfrac{1}{2}\omega^2q_i^2+q_i\gamma_i]$$
$$\cdot\varphi_n(q_0)dq_0a^{-1}dq_1a^{-1}dq_2\cdots a^{-1}dq_j \quad (10)$$

where we have written the $\mathfrak{D}q(t)$ out explicitly (and have set $a=(2\pi i\epsilon)^{\frac{1}{2}}$, $t''-t'=j\epsilon$, $q_{t'}=q_0$, $q_{t''}=q_j$). The last form can be written as

$$G_{mn}=\int\varphi_m^*(q_j)k(q_j,t'';q_0,t')\varphi_n(q_0)dq_0dq_j \quad (11)$$

where $k(q_j,t'';q_0,t')$ is the kernel [as in **I**, Eq. (2)] for a forced harmonic oscillator giving the amplitude for arrival at q_j at time t'' if at time t' it was known to be at q_0. According to **C** it is given by

$$k(q_j,t'';q_0,t')=(2\pi i\omega^{-1}\sin\omega(t''-t'))^{-\frac{1}{2}}$$
$$\times\exp iQ(q_j,t'';q_0,t') \quad (12)$$

where $Q(q_j,t'';q_0,t')$ is the action calculated along the classical path between the end points $q_j,t'';q_0,t'$, and is given explicitly in **C**.[7] It is

[7] That (12) is correct, at least insofar as it depends on q_0, can be seen directly as follows. Let $\bar{q}(t)$ be the classical path which satisfies the boundary condition $\bar{q}(t')=q_0$, $\bar{q}(t'')=q_j$. Then in the integral defining k replace each of the variables q_i by $q_i=\bar{q}_i+y_i$, $(\bar{q}_i=\bar{q}(t_i))$, that is, use the displacement y_i from the classical path $\bar{q}_i$ as the coordinate rather than the absolute position. With the substitution $q_i=\bar{q}_i+y_i$ in the action

$$S_0+S_I=\int(\tfrac{1}{2}\dot{q}^2-\tfrac{1}{2}\omega^2q^2+\gamma q)dt$$
$$=\int(\tfrac{1}{2}\dot{\bar{q}}^2-\tfrac{1}{2}\omega^2\bar{q}^2+\gamma\bar{q})dt+\int(\tfrac{1}{2}\dot{y}^2-\tfrac{1}{2}\omega^2y^2)dt$$

the terms linear in y drop out by integrations by parts using the equation of motion $\ddot{\bar{q}}=-\omega^2\bar{q}+\gamma(t)$ for the classical path, and the boundary conditions $y(t')=y(t'')=0$. That this should occur should occasion no surprise, for the action functional is an extremum at $q(t)=\bar{q}(t)$ so that it will only depend to second order in the displacements y from this extremal orbit $\bar{q}(t)$. Further, since the action functional is quadratic to begin with, it cannot depend on y more than quadratically. Hence

$$S_0+S_I=Q+\int(\tfrac{1}{2}\dot{y}^2-\tfrac{1}{2}\omega^2y^2)dt$$

so that since $dq_i=dy_i$,

$$k(q_j,t'';q_0,t')=\exp(iQ)\int\exp\left(i\int\tfrac{1}{2}(\dot{y}^2-\omega^2y^2)dt\right)\mathfrak{D}y(t).$$

The factor following the $\exp iQ$ is the amplitude for a free oscillator to proceed from $y=0$ at $t=t'$ to $y=0$ at $t=t''$ and does not there-

$$Q=\frac{\omega}{2\sin\omega(t''-t')}\Big[(q_j^2+q_0^2)\cos\omega(t''-t')-2q_jq_0$$
$$+\frac{2q_j}{\omega}\int_{t'}^{t''}\gamma(t)\sin\omega(t-t')dt$$
$$+\frac{2q_0}{\omega}\int_{t'}^{t''}\gamma(t)\sin\omega(t''-t)dt$$
$$-\frac{2}{\omega^2}\int_{t'}^{t''}\int_{t'}^{t}\gamma(t)\gamma(s)\sin\omega(t''-t)$$
$$\times\sin\omega(s-t')dsdt\Big]. \quad (13)$$

The solution of the motion of the oscillator can now be completed by substituting (12) and (13) into (11) and performing the integrals. The simplest case is for $m, n=0$ for which case[8]

$$\varphi_0(q_0)=(\omega/\pi)^{\frac{1}{4}}\exp(-\tfrac{1}{2}\omega q_0^2)\exp(-\tfrac{1}{2}i\omega t')$$

so that the integrals on q_0, q_j are just Gaussian integrals. There results

$$G_{00}=\exp\left(-\frac{1}{2}\omega^{-1}\int_{t'}^{t''}\int_{t'}^{t}\exp(-i\omega(t-s))\gamma(t)\gamma(s)dtds\right)$$

a result of fundamental importance in the succeeding developments. By replacing $t-s$ by its absolute value $|t-s|$ we may integrate both variables over the entire range and divide by 2. We will henceforth make the results more general by extending the limits on the integrals from $-\infty$ to $+\infty$. Thus if one wishes to study the effect on a particle of interaction with an oscillator for just the period t' to t'' one may use

$$G_{00}=\exp\left(-\frac{1}{4\omega}\int_{-\infty}^{\infty}\int_{-\infty}^{\infty}\times\exp(-i\omega|t-s|)\gamma(t)\gamma(s)dtds\right) \quad (14)$$

imagining in this case that the interaction $\gamma(t)$ is zero outside these limits. We defer to a later section the discussion of other values of m, n.

Since G_{00} is simply an exponential, we can write it as $\exp(iI)$, consider that the complete "action" for the system of particles is $S=S_p+I$ and that one computes transition elements with this "action" instead of S_p (see C, Sec. 12). The functional I, which is given by

$$I=\tfrac{1}{4}i\omega^{-1}\int\int\exp(-i\omega|t-s|)\gamma(s)\gamma(t)dsdt \quad (15)$$

is complex, however; we shall speak of it as the complex action. It describes the fact that the system at one time can affect itself at a different time by means of a temporary storage of energy in the oscillator. When there are several independent oscillators with different interactions, the effect, if they are all in the lowest state at t' and t'', is the product of their separate G_{00} contributions. Thus the complex action is additive, being the sum of contributions like (15) for each of the several oscillators.

4. VIRTUAL TRANSITIONS IN THE ELECTROMAGNETIC FIELD

We can now apply these results to eliminate the transverse field oscillators of the Lagrangian (2). At first we can limit ourselves to the case of purely virtual transitions in the electromagnetic field, so that there is no photon in the field at t' and t''. That is, all of the field oscillators are making transitions from ground state to ground state.

The $\gamma_{\mathbf{K}}^{(r)}$ corresponding to each oscillator $q_{\mathbf{K}}^{(r)}$ is found from the interaction term L_I [Eq. (2b)], substituting the value of $\mathbf{A}^{tr}(\mathbf{x})$ given in (1). There results, for example,

$$\gamma_{\mathbf{K}}^{(1)}=(8\pi)^{\frac{1}{2}}\textstyle\sum_n e_n(\mathbf{e}_1\cdot\mathbf{x}'_n)\cos(\mathbf{K}\cdot\mathbf{x}_n)$$
$$\gamma_{\mathbf{K}}^{(3)}=(8\pi)^{\frac{1}{2}}\textstyle\sum_n e_n(\mathbf{e}_1\cdot\mathbf{x}'_n)\sin(\mathbf{K}\cdot\mathbf{x}_n) \quad (16)$$

the corresponding results for $\gamma_{\mathbf{K}}^{(2)}$, $\gamma_{\mathbf{K}}^{(4)}$ replace $\mathbf{e}_1$ by $\mathbf{e}_2$.

The complex action resulting from oscillator of coordinate $q_{\mathbf{K}}^{(1)}$ is therefore

$$I_{\mathbf{K}}^{(1)}=\frac{8\pi i}{4k}\sum_n\sum_m\int\int e_ne_m\exp(-ik|t-s|)(\mathbf{e}_1\cdot\mathbf{x}'_n(t))$$
$$\times(\mathbf{e}_1\cdot\mathbf{x}'_m(s))\cdot\cos(\mathbf{K}\cdot\mathbf{x}_n(t))\cos(\mathbf{K}\cdot\mathbf{x}_m(s))dsdt.$$

The term $I_{\mathbf{K}}^{(3)}$ exchanges the cosines for sines, so in the sum $I_{\mathbf{K}}^{(1)}+I_{\mathbf{K}}^{(3)}$ the product of the two cosines, $\cos A\cdot\cos B$ is replaced by $(\cos A\cos B+\sin A\sin B)$ or $\cos(A-B)$. The terms $I_{\mathbf{K}}^{(2)}+I_{\mathbf{K}}^{(4)}$ give the same result with $\mathbf{e}_2$ replacing $\mathbf{e}_1$. The sum $(\mathbf{e}_1\cdot\mathbf{V})(\mathbf{e}_1\cdot\mathbf{V}')+(\mathbf{e}_2\cdot\mathbf{V})(\mathbf{e}_2\cdot\mathbf{V}')$ is $(\mathbf{V}\cdot\mathbf{V}')-k^{-2}(\mathbf{K}\cdot\mathbf{V})(\mathbf{K}\cdot\mathbf{V}')$ since it is the sum of the products of vector components in two orthogonal directions, so that if we add the product in the third direction (that of $\mathbf{K}$) we construct the complete scalar product. Summing over all $\mathbf{K}$ then, since $\sum_{\mathbf{K}}=\frac{1}{2}\int d^3\mathbf{K}/8\pi^3$ we find for the total complex action of all of the transverse oscillators,

$$I_{tr}=i\sum_n\sum_m\int_{t'}^{t''}dt\int_{t'}^{t''}ds\int e_ne_m\exp(-ik|t-s|)$$
$$\times[\mathbf{x}'_n(t)\cdot\mathbf{x}'_m(s)-k^{-2}(\mathbf{K}\cdot\mathbf{x}'_n(t))(\mathbf{K}\cdot\mathbf{x}'_m(s))]$$
$$\cdot\cos(\mathbf{K}\cdot(\mathbf{x}_n(t)-\mathbf{x}_m(s)))d^3\mathbf{K}/8\pi^2k. \quad (17)$$

---

fore depend on q_0, q_j, or $\gamma(t)$, being a function only of $t''-t'$. [That it is actually $(2\pi i\omega^{-1}\sin\omega(t''-t'))^{-\frac{1}{2}}$ can be demonstrated either by direct integration of the y variables or by using some normalizing property of the kernels k, for example that G_{00} for the case $\gamma=0$ must equal unity.] The expression for Q given in C on page 386 is in error, the quantities q_0 and q_j should be interchanged.

[8] It is most convenient to define the state φ_n with the phase factor $\exp[-i\omega(n+\frac{1}{2})t']$ and the final state with the factor $\exp[-i\omega(m+\frac{1}{2})t'']$ so that the results will not depend on the particular times t', t'' chosen.

This is to be added to S_p+S_e to obtain the complete action of the system with the oscillators removed.

The term in $(\mathbf{K}\cdot\dot{\mathbf{x}}_n(t))(\mathbf{K}\cdot\dot{\mathbf{x}}_m(s))$ can be simplified by integration by parts with respect to t and with respect to s [note that $\exp(-ik|t-s|)$ has a discontinuous slope at $t=s$, or break the integration up into two regions]. One finds

$$I_{tr}=R-I_c+I_{\text{transient}} \tag{18}$$

where

$$R=-i\sum_n\sum_m\int_{t'}^{t''}dt\int_{t'}^{t''}ds\int e_ne_m \times\exp(-ik|t-s|)(1-\dot{\mathbf{x}}_n(t)\cdot\dot{\mathbf{x}}_m(s)) \cdot\cos\mathbf{K}\cdot(\mathbf{x}_n(t)-\mathbf{x}_m(s))d^3\mathbf{K}/8\pi^2k \tag{19}$$

and

$$I_c=-\sum_n\sum_m\int_{t'}^{t''}dt\int e_ne_m \times\cos\mathbf{K}\cdot(\mathbf{x}_n(t)-\mathbf{x}_m(t))d^3\mathbf{K}/4\pi^2k^2 \tag{20}$$

comes from the discontinuity in slope of $\exp(-ik|t-s|)$ at $t=s$. Since

$$\int\cos(\mathbf{K}\cdot\mathbf{R})d^3\mathbf{K}/4\pi^2k^2=\int_0^\infty(kr)^{-1}\sin(kr)dk/\pi=(2r)^{-1}$$

this term I_c just cancels the Coulomb interaction term $S_c=\int L_c dt$. The term

$$\begin{aligned}I_{\text{transient}}=-\sum_n\sum_m e_ne_m\int\frac{d^3\mathbf{K}}{4\pi^2k^2}\\ \times\Big\{\int_{t'}^{t''}[\exp(-ik(t''-t))\cos\mathbf{K}\cdot(\mathbf{x}_n(t'')-\mathbf{x}_m(t))\\ +\exp(-ik(t-t'))\cos\mathbf{K}\cdot(\mathbf{x}_n(t)-\mathbf{x}_m(t'))]dt\\ +(2k)^{-1}i[\cos\mathbf{K}\cdot(\mathbf{x}_n(t'')-\mathbf{x}_m(t''))\\ +\cos\mathbf{K}\cdot(\mathbf{x}_n(t')-\mathbf{x}_m(t'))\\ -2\exp(-ik(t''-t'))\cos\mathbf{K}\cdot(\mathbf{x}_n(t')-\mathbf{x}_m(t''))]\Big\}.\end{aligned} \tag{21}$$

is one which comes from the limits of integration at t' and t'', and involves the coordinates of the particle at either one of these times or the other. If t' and t'' are considered to be exceedingly far in the past and future, there is no correlation to be expected between these temporally distant coordinates and the present ones, so the effects of $I_{\text{transient}}$ will cancel out quantum mechanically by interference. This transient was produced by the sudden turning on of the interaction of field and particles at t' and its sudden removal at t''. Alternatively we can imagine the charges to be turned on after t' adiabatically and turned off slowly before t'' (in this case, in the term L_c, the charges should also be considered as varying with time). In this case, in the limit, $I_{\text{transient}}$ is zero.[9] Hereafter we shall drop the transient term and consider the range of integration of t to be from $-\infty$ to $+\infty$, imagining, if one needs a definition, that the charges vary with time and vanish in the direction of either limit.

To simplify R we need the integral

$$J=\int\exp(-ik|t|)\cos(\mathbf{K}\cdot\mathbf{R})d^3\mathbf{K}/8\pi^2k =\int_0^\infty\exp(-ik|t|)\sin(kr)dk/2\pi r \tag{22}$$

where r is the length of the vector $\mathbf{R}$. Now

$$\int_0^\infty\exp(-ikx)dk=\lim_{\epsilon\to0}(-i(x-i\epsilon)^{-1}) =-ix^{-1}+\pi\delta(x)=\pi\delta_+(x)$$

where the equation serves to define $\delta_+(x)$ [as in II, Eq. (3)]. Hence, expanding $\sin(kr)$ in exponentials find

$$\begin{aligned}J&=-(4\pi r)^{-1}((|t|-r)^{-1}-(|t|+r)^{-1}) +(4ir)^{-1}(\delta(|t|-r)-\delta(|t|+r))\\ &=-(2\pi)^{-1}(t^2-r^2)^{-1}+(2i)^{-1}\delta(t^2-r^2) =-\tfrac{1}{2}i\delta_+(t^2-r^2)\end{aligned} \tag{23}$$

where we have used the fact that

$$\delta(t^2-r^2)=(2r)^{-1}(\delta(|t|-r)+\delta(|t|+r))$$

and that $\delta(|t|+r)=0$ since both $|t|$ and r are necessarily positive.

Substitution of these results into (19) gives finally,

$$R=-\frac{1}{2}\sum_n\sum_m\int_{-\infty}^{+\infty}\int_{-\infty}^{+\infty}e_ne_m(1-\dot{\mathbf{x}}_n(t)\cdot\dot{\mathbf{x}}_m(s)) \times\delta_+((t-s)^2-(\mathbf{x}_n(t)-\mathbf{x}_m(s))^2)dtds. \tag{24}$$

The total complex action of the system is then[10] S_p+R. Or, what amounts to the same thing; to obtain

[9] One can obtain the final result, that the total interaction is just R, in a formal manner starting from the Hamiltonian from which the longitudinal oscillators have not yet been eliminated. There are for each $\mathbf{K}$ and cos or sin, four oscillators $q_{\mu\mathbf{K}}$ corresponding to the three components of the vector potential ($\mu=1$, 2, 3) and the scalar potential ($\mu=4$). It must then be assumed that the wave functions of the initial and final state of the $\mathbf{K}$ oscillators is the function $(k/\pi)\exp[-\frac{1}{2}k(q_{1\mathbf{K}}^2+q_{2\mathbf{K}}^2+q_{3\mathbf{K}}^2-q_{4\mathbf{K}}^2)]$. The wave function suggested here has only formal significance, of course, because the dependence on $q_{4\mathbf{K}}$ is not square integrable, and cannot be normalized. If each oscillator were assumed actually in the ground state, the sign of the $q_{4\mathbf{K}}$ term would be changed to positive, and the sign of the frequency in the contribution of these oscillators would be reversed (they would have negative energy).

[10] The classical action for this problem is just $Sp+R'$ where R' is the real part of the expression (24). In view of the generalization of the Lagrangian formulation of quantum mechanics suggested in Section 12 of C, one might have anticipated that R would have been simply R'. This corresponds, however, to boundary conditions other than no quanta present in past and future. It is harder to interpret physically. For a system enclosed in a light tight box, however, it appears likely that both R and R' lead to the same results.

transition amplitudes including the effects of the field we must calculate the transition element of $\exp(iR)$:

$$\langle\chi_{t''}|\exp iR|\psi_{t'}\rangle s_p \tag{25}$$

under the action S_p of the particles, excluding interaction. Expression (24) for R must be considered to be written in the usual manner as a Riemann sum and the expression (25) interpreted as defined in **C** [Eq. (39)]. Expression (6) must be used for $\mathbf{x}'_n$ at time t.

Expression (25), with (24), then contains all the effects of virtual quanta on a (at least non-relativistic) system according to quantum electrodynamics. It contains the effects to all orders in $e^2/\hbar c$ in a single expression. If expanded in a power series in $e^2/\hbar c$, the various terms give the expressions to the corresponding order obtained by the diagrams and methods of **II**. We illustrate this by an example in the next section.

5. EXAMPLE OF APPLICATION OF EXPRESSION (25)

We shall not be much concerned with the non-relativistic case here, as the relativistic case given below is as simple and more interesting. It is, however, very similar and at this stage it is worth giving an example to show how expressions resulting from (25) are to be interpreted according to the rules of **C**. For example, consider the case of a single electron, coordinate $\mathbf{x}$, either free or in an external given potential (contained for simplicity in S_p, not in[11] R). Its interaction with the field produces a reaction back on itself given by R as in (24) but in which we keep only a single term corresponding to $m=n$. Assume the effect of R to be small and expand $\exp(iR)$ as $1+iR$. Let us find the amplitude at time t'' of finding the electron in a state ψ with no quanta emitted, if at time t' it was in the same state. It is

$$\langle\psi_{t''}|1+iR|\psi_{t'}\rangle s_p=\langle\psi_{t''}|1|\psi_{t'}\rangle s_p+i\langle\psi_{t''}|R|\psi_{t'}\rangle s_p$$

where $\langle\psi_{t''}|1|\psi_{t'}\rangle s_p=\exp[-iE(t''-t')]$ if E is the energy of the state, and

$$\langle\psi_{t''}|R|\psi_{t'}\rangle s_p=-\tfrac{1}{2}e^2\int_{t'}^{t''}dt\int_{t'}^{t''}ds\langle\psi_{t''}|(1-\mathbf{x}'_t\cdot\mathbf{x}'_s)\times\delta_+((t-s)^2-(\mathbf{x}_t-\mathbf{x}_s)^2)|\psi_{t'}\rangle s_p. \tag{26}$$

Here $\mathbf{x}_s=\mathbf{x}(s)$, etc. In (26) we shall limit the range of integrations by assuming $s<t$, and double the result.

The expression within the brackets $\langle\ \rangle s_p$ on the right-hand side of (26) can be evaluated by the methods described in **C** [Eq. (29)]. An expression such as (26) can also be evaluated directly in terms of the propagation kernel $K(2,1)$ [see **I**, Eq. (2)] for an electron moving in the given potential.

The term $\mathbf{x}'_s\cdot\mathbf{x}'_t$ in the non-relativistic case produces an interesting complication which does not have an analog for the relativistic case with the Dirac equation. We discuss it below, but for a moment consider in further detail expression (26) but with the factor $(1-\mathbf{x}'_s\cdot\mathbf{x}'_t)$ replaced simply by unity.

The kernel $K(2,1)$ is defined and discussed in **I**. From its definition as the amplitude that the electron be found at $\mathbf{x}_2$ at time t_2, if at t_1 it was at $\mathbf{x}_1$, we have

$$K(\mathbf{x}_2,t_2;\mathbf{x}_1,t_1)=\langle\delta(\mathbf{x}-\mathbf{x}_2)_{t_2}|1|\delta(\mathbf{x}-\mathbf{x}_1)_{t_1}\rangle s_p \tag{27}$$

that is, more simply $K(2,1)$ is the sum of $\exp(iS_p)$ over all paths which go from space time point 1 to 2.

In the integrations over all paths implied by the symbol in (26) we can first integrate over all the $\mathbf{x}_i$ variables corresponding to times t_i from t' to s, not inclusive, the result being a factor $K(\mathbf{x}_s,s;\mathbf{x}_{t'},t')$ according to (27). Next we integrate on the variables between s and t not inclusive, giving a factor $K(\mathbf{x}_t,t;\mathbf{x}_s,s)$ and finally on those between t and t'' giving $K(\mathbf{x}_{t''},t'';\mathbf{x}_t,t)$. Hence the left-hand term in (26) excluding the $\mathbf{x}'_t\cdot\mathbf{x}'_s$ factor is

$$-e^2\int dt\int ds\int\psi^*(\mathbf{x}_{t''},t'')K(\mathbf{x}_{t''},t'';\mathbf{x}_t,t)\delta_+((t-s)^2-(\mathbf{x}_t-\mathbf{x}_s)^2)\cdot K(\mathbf{x}_t,t;\mathbf{x}_s,s)K(\mathbf{x}_s,s;\mathbf{x}_{t'},t')\times\psi(\mathbf{x}_{t'},t')d^3\mathbf{x}_{t''}d^3\mathbf{x}_td^3\mathbf{x}_sd^3\mathbf{x}_{t'} \tag{28}$$

which in improved notation and in the relativistic case is essentially the result given in **II**.

We have made use of a special case of a principle which may be stated more generally as

$$\begin{aligned}\langle\chi_{t''}|F(\mathbf{x}_1,t_1;\mathbf{x}_2,t_2;\cdots\mathbf{x}_k,t_k)|\psi_{t'}\rangle s_p&=\int\chi^*(\mathbf{x}_{t''})K(\mathbf{x}_{t''},t'';\mathbf{x}_1,t_1)\cdot K(\mathbf{x}_1,t_1;\mathbf{x}_2,t_2)\cdots\\&\times K(\mathbf{x}_{k-1},t_{k-1};\mathbf{x}_k,t_k)K(\mathbf{x}_k,t_k;\mathbf{x}_{t'},t')\\&\cdot F(\mathbf{x}_1,t_1;\mathbf{x}_2,t_2;\cdots\mathbf{x}_k,t_k)\psi(\mathbf{x}_{t'})\\&\times d^3\mathbf{x}_{t''}d^3\mathbf{x}_1d^3\mathbf{x}_2\cdots d^3\mathbf{x}_kd^3\mathbf{x}_{t'}\end{aligned} \tag{29}$$

where F is any function of the coordinate $\mathbf{x}_1$ at time t_1, $\mathbf{x}_2$ at t_2 up to $\mathbf{x}_k$, t_k, and, it is important to notice, we have assumed $t''>t_1>t_2>\cdots t_k>t'$.

Expressions of higher order arising for example from R^2 are more complicated as there are quantities referring to several different times mixed up, but they all can be interpreted readily. One simply breaks up the ranges of integrations of the time variables into parts such that in each the order of time of each variable is definite. One then interprets each part by formula (29).

[11] One can show from (25) how the correlated effect of many atoms at a distance produces on a given system the effects of an external potential. Formula (24) yields the result that this potential is that obtained from Liénard and Wiechert by retarded waves arising from the charges and currents resulting from the distant atoms making transitions. Assume the wave functions χ and ψ can be split into products of wave functions for system and distant atoms and expand $\exp(iR)$ assuming the effect of any individual distant atom is small. Coulomb potentials arise even from nearby particles if they are moving slowly.

As a simple example we may refer to the problem of the transition element

$$\left\langle \chi_{t''} \middle| \int U(\mathbf{x}(t), t)dt \int V(\mathbf{x}(s), s)ds \middle| \psi_{t'} \right\rangle$$

arising, say, in the cross term in U and V in an ordinary second order perturbation problem (disregarding radiation) with perturbation potential $U(\mathbf{x}, t)+V(\mathbf{x}, t)$. In the integration on s and t which should include the entire range of time for each, we can split the range of s into two parts, $s<t$ and $s>t$. In the first case, $s<t$, the potential V acts earlier than U, and in the other range, vice versa, so that

$$\begin{aligned}
&\left\langle \chi_{t''} \middle| \int U(\mathbf{x}_t, t)dt \int V(\mathbf{x}_s, s)ds \middle| \psi_{t'} \right\rangle \\
&= \int_{t'}^{t''} dt \int_{t'}^{t} ds \int \chi^*(\mathbf{x}_{t''})K(\mathbf{x}_{t''}, t''; \mathbf{x}_t, t) \\
&\times U(\mathbf{x}_t, t)K(\mathbf{x}_t, t; \mathbf{x}_s, s)V(\mathbf{x}_s, s) \\
&\cdot K(\mathbf{x}_s, s; \mathbf{x}_{t'}, t')\psi(\mathbf{x}_{t'})d^3\mathbf{x}_{t''}d^3\mathbf{x}_t d^3\mathbf{x}_s d^3\mathbf{x}_{t'} \\
&+ \int_{t'}^{t''} dt \int_{t}^{t''} ds \int \chi^*(\mathbf{x}_{t''})K(\mathbf{x}_{t''}, t''; \mathbf{x}_s, s) \\
&\times V(\mathbf{x}_s, s)K(\mathbf{x}_s, s; \mathbf{x}_t, t)U(\mathbf{x}_t, t) \\
&\cdot K(\mathbf{x}_t, t; \mathbf{x}_{t'}, t')\psi(\mathbf{x}_{t'})d^3\mathbf{x}_{t''}d^3\mathbf{x}_s d^3\mathbf{x}_t d^3\mathbf{x}_{t'} \qquad (30)
\end{aligned}$$

so that the single expression on the left is represented by two terms analogous to the two terms required in analyzing the Compton effect. It is in this way that the several terms and their corresponding diagrams corresponding to each process arise when an attempt is made to represent the transition elements of single expressions involving time integrals in terms of the propagation kernels K.

It remains to study in more detail the term in (26) arising from $\mathbf{x}^\cdot(t)\cdot\mathbf{x}^\cdot(s)$ in the interaction. The interpretation of such expressions is considered in detail in **C**, and we must refer to Eqs. (39) through (50) of that paper for a more thorough analysis. A similar type of term also arises in the Lagrangian formulation in simpler problems, for example the transition element

$$\left\langle \chi_{t''} \middle| \int \mathbf{x}^\cdot(t)\cdot\mathbf{A}(\mathbf{x}(t), t)dt \int \mathbf{x}^\cdot(s)\cdot\mathbf{B}(\mathbf{x}(s), s)ds \middle| \psi_{t'} \right\rangle$$

arising say, in the cross term in **A** and **B** in a second-order perturbation problem for a particle in a perturbing vector potential $\mathbf{A}(\mathbf{x}, t)+\mathbf{B}(\mathbf{x}, t)$. The time integrals must first be written as Riemannian sums, the velocity (see (6)) being replaced by $\mathbf{x}^\cdot=\frac{1}{2}\epsilon^{-1}(\mathbf{x}_{i+1}-\mathbf{x}_i)+\frac{1}{2}\epsilon^{-1}(\mathbf{x}_i-\mathbf{x}_{i-1})$ so that we ask for the transition element of

$$\sum_i\sum_j [\tfrac{1}{2}(\mathbf{x}_{i+1}-\mathbf{x}_i)+\tfrac{1}{2}(\mathbf{x}_i-\mathbf{x}_{i-1})]\cdot\mathbf{A}(\mathbf{x}_i, t_i) \times[\tfrac{1}{2}(\mathbf{x}_{j+1}-\mathbf{x}_j)+\tfrac{1}{2}(\mathbf{x}_j-\mathbf{x}_{j-1})]\cdot\mathbf{B}(\mathbf{x}_j, t_j). \qquad (31)$$

In **C** it is shown that when converted to operator notation the quantity $(x_{i-1}-x_i)/\epsilon$ is equivalent (nearly, see below) to an operator,

$$(x_{i+1}-x_i)/\epsilon \rightarrow i(Hx-xH) \qquad (32)$$

operating in order indicated by the time index i (that is after x_l's for $l\leq i$ and before all x_l's for $l>i$). In non-relativistic mechanics $i(Hx-xH)$ is the momentum operator p_x divided by the mass m. Thus in (31) the expression $[\frac{1}{2}(\mathbf{x}_{i+1}-\mathbf{x}_i)+\frac{1}{2}(\mathbf{x}_i-\mathbf{x}_{i-1})]\cdot\mathbf{A}(\mathbf{x}_i, t_i)$ becomes $\epsilon(\mathbf{p}\cdot\mathbf{A}+\mathbf{A}\cdot\mathbf{p})/2m$. Here again we must split the sum into two regions $j<i$ and $j>i$ so the quantities in the usual notation will operate in the right order such that eventually (31) becomes identical with the right-hand side of Eq. (30) but with $U(\mathbf{x}_t, t)$ replaced by the operator

$$\frac{1}{2m}\left(\frac{1}{i}\frac{\partial}{\partial\mathbf{x}_t}\cdot\mathbf{A}(\mathbf{x}_t, t)+\mathbf{A}(\mathbf{x}_t, t)\cdot\frac{1}{i}\frac{\partial}{\partial\mathbf{x}_t}\right)$$

standing in the same place, and with the operator

$$\frac{1}{2m}\left(\frac{1}{i}\frac{\partial}{\partial\mathbf{x}_s}\cdot\mathbf{B}(\mathbf{x}_s, s)+\frac{1}{i}\mathbf{B}(\mathbf{x}_s, s)\cdot\frac{\partial}{\partial\mathbf{x}_s}\right)$$

standing in the place of $V(\mathbf{x}_s, s)$. The sums and factors ϵ have now become $\int dt\int ds$.

This is nearly but not quite correct, however, as there is an additional term coming from the terms in the sum corresponding to the special values, $j=i$, $j=i+1$ and $j=i-1$. We have tacitly assumed from the appearance of the expression (31) that, for a given i, the contribution from just three such special terms is of order ϵ^2. But this is not true. Although the expected contribution of a term like $(x_{i+1}-x_i)(x_{j+1}-x_j)$ for $j\neq i$ is indeed of order ϵ^2, the expected contribution of $(x_{i+1}-x_i)^2$ is $+ie\epsilon m^{-1}$ [**C**, Eq. (50)], that is, of order ϵ. In non-relativistic mechanics the velocities are unlimited and in very short times ϵ the amplitude diffuses a distance proportional to the square root of the time. Making use of this equation then we see that the additional contribution from these terms is essentially

$$ie\epsilon m^{-1}\sum_i \mathbf{A}(\mathbf{x}_i, t_i)\cdot\mathbf{B}(\mathbf{x}_i, t_i) = ie m^{-1}\int \mathbf{A}(\mathbf{x}(t), t)\cdot\mathbf{B}(\mathbf{x}(t), t)dt$$

when summed on all i. This has the same effect as a first-order perturbation due to a potential $\mathbf{A}\cdot\mathbf{B}/m$. Added to the term involving the momentum operators

we therefore have an additional term[12]

$$\frac{i}{m}\int_{t'}^{t''} dt \int \chi^*(\mathbf{x}_{t''})K(\mathbf{x}_{t''}, t''; \mathbf{x}_t, t)\mathbf{A}(\mathbf{x}_t, t)\cdot\mathbf{B}(\mathbf{x}_t, t) \cdot K(\mathbf{x}_t, t; \mathbf{x}_{t'}, t')\psi(\mathbf{x}_{t'})d^3\mathbf{x}_{t''}d^3\mathbf{x}_t d^3\mathbf{x}_{t'}. \quad (33)$$

In the usual Hamiltonian theory this term arises, of course, from the term $\mathbf{A}^2/2m$ in the expansion of the Hamiltonian

$$H=(2m)^{-1}(\mathbf{p}-\mathbf{A})^2=(2m)^{-1}(\mathbf{p}^2-\mathbf{p}\cdot\mathbf{A}-\mathbf{A}\cdot\mathbf{p}+\mathbf{A}^2)$$

while the other term arises from the second-order action of $\mathbf{p}\cdot\mathbf{A}+\mathbf{A}\cdot\mathbf{p}$. We shall not be interested in non-relativistic quantum electrodynamics in detail. The situation is simpler for Dirac electrons. For particles satisfying the Klein-Gordon equation (discussed in Appendix A) the situation is very similar to a four-dimensional analog of the non-relativistic case given here.

6. EXTENSION TO DIRAC PARTICLES

Expressions (24) and (25) and their proof can be readily generalized to the relativistic case according to the one electron theory of Dirac. We shall discuss the hole theory later. In the non-relativistic case we began with the proposition that the amplitude for a particle to proceed from one point to another is the sum over paths of $\exp(iS_p)$, that is, we have for example for a transition element

$$\langle\chi|1|\psi\rangle=\lim_{\epsilon\to 0}\int\cdots\int\chi^*(\mathbf{x}_N)\Phi_p(\mathbf{x}_N, \mathbf{x}_{N-1}, \cdots\mathbf{x}_0) \cdot\psi(\mathbf{x}_0)d^3\mathbf{x}_0 d^3\mathbf{x}_1\cdots d^3\mathbf{x}_N \quad (34)$$

where for $\exp(iS_p)$ we have written Φ_p, that is more precisely,

$$\Phi_p=\Pi_i A^{-1}\exp iS(\mathbf{x}_{i+1}, \mathbf{x}_i).$$

As discussed in C this form is related to the usual form of quantum mechanics through the observation that

$$(\mathbf{x}_{i+1}|\mathbf{x}_i)_\epsilon=A^{-1}\exp[iS(\mathbf{x}_{i+1}, \mathbf{x}_i)] \quad (35)$$

where $(\mathbf{x}_{i+1}|\mathbf{x}_i)_\epsilon$ is the transformation matrix from a representation in which $\mathbf{x}$ is diagonal at time t_i to one in which $\mathbf{x}$ is diagonal at time $t_{i+1}=t_i+\epsilon$ (so that it is identical to $K_0(\mathbf{x}_{i+1}, t_{i+1}; \mathbf{x}_i, t_i)$ for the small time interval ϵ). Hence the amplitude for a given path can also be written

$$\Phi_p=\Pi_i(\mathbf{x}_{i+1}|\mathbf{x}_i)_\epsilon \quad (36)$$

for which form, of course, (34) is exact irrespective of whether $(\mathbf{x}_{i+1}|\mathbf{x}_i)_\epsilon$ can be expressed in the simple form (35).

For a Dirac electron the $(\mathbf{x}_{i+1}|\mathbf{x}_i)_\epsilon$ is a 4×4 matrix (or $4^N\times4^N$ if we deal with N electrons) but the expression (34) with (36) is still correct (as it is in fact for any quantum-mechanical system with a sufficiently general definition of the coordinate $\mathbf{x}_i$). The product (36) now involves operators, the order in which the factors are to be taken is the order in which the terms appear in time.

For a Dirac particle in a vector and scalar potential (times the electron charge e) $\mathbf{A}(\mathbf{x}, t)$, $A_4(\mathbf{x}, t)$, the quantity $(\mathbf{x}_{i+1}|\mathbf{x}_i)_\epsilon^{(A)}$ is related to that of a free particle to the first order in ϵ as

$$(\mathbf{x}_{i+1}|\mathbf{x}_i)_\epsilon^{(A)}=(\mathbf{x}_{i+1}|\mathbf{x}_i)_\epsilon^{(0)}\exp[-i(\epsilon A_4(\mathbf{x}_i, t_i) -(\mathbf{x}_{i+1}-\mathbf{x}_i)\cdot\mathbf{A}(\mathbf{x}_i, t_i))]. \quad (37)$$

This can be verified directly by substitution into the Dirac equation.[13] It neglects the variation of $\mathbf{A}$ and A_4 with time and space during the short interval ϵ. This produces errors only of order ϵ^2 in the Dirac case for the expected square velocity $(\mathbf{x}_{i+1}-\mathbf{x}_i)^2/\epsilon^2$ during the interval ϵ is finite (equaling the square of the velocity of light) rather than being of order $1/\epsilon$ as in the non-relativistic case. [This makes the relativistic case somewhat simpler in that it is not necessary to define the velocity as carefully as in (6); $(\mathbf{x}_{i+1}-\mathbf{x}_i)/\epsilon$ is sufficiently exact, and no term analogous to (33) arises.]

Thus $\Phi_p^{(A)}$ differs from that for a free particle, $\Phi_p^{(0)}$, by a factor $\Pi_i\exp-i(\epsilon A_4(\mathbf{x}_i, t_i)-(\mathbf{x}_{i+1}-\mathbf{x}_i)\cdot\mathbf{A}(\mathbf{x}_i, t_i))$ which in the limit can be written as

$$\exp\left\{-i\int[A_4(\mathbf{x}(t), t)-\mathbf{x}^\cdot(t)\cdot\mathbf{A}(\mathbf{x}(t), t)]dt\right\} \quad (38)$$

exactly as in the non-relativistic case.

The case of a Dirac particle interacting with the quantum-mechanical oscillators representing the field may now be studied. Since the dependence of $\Phi_p^{(A)}$ on $\mathbf{A}$, A_4 is through the same factor as in the non-relativistic case, when $\mathbf{A}$, A_4 are expressed in terms of the oscillator coordinates q, the dependence of Φ on the oscillator coordinates q is unchanged. Hence the entire analysis of the preceding sections which concern the results of the integration over oscillator coordinates can be carried through unchanged and the results will be expression (25) with formula (24) for R. Expression (25) is now interpreted as

$$\langle\chi_{t''}|\exp iR|\psi_{t'}\rangle=\lim_{\epsilon\to 0}\int\chi^*(\mathbf{x}_{t''}^{(1)}, \mathbf{x}_{t''}^{(2)}\cdots) \times\prod_n(\Phi_{p,n}^{(0)}d^3\mathbf{x}_{t''-\epsilon}^{(n)}\cdots d^3\mathbf{x}_{t'}^{(n)}) \cdot\exp(iR)\psi(\mathbf{x}_{t'}^{(1)}, \mathbf{x}_{t'}^{(2)}\cdots) \quad (39)$$

[12] The term corresponding to this for the self-energy expression (26) would give an integral over $\delta_+((t-t')^2-(\mathbf{x}_t-\mathbf{x}_t)^2)$ which is evidently infinite and leads to the quadratically divergent self-energy. There is no such term for the Dirac electron, but there is for Klein-Gordon particles. We shall not discuss the infinities in this paper as they have already been discussed in II.

[13] Alternatively, note that Eq. (37) is exact for arbitrarily large ϵ if the potential A_μ is constant. For if the potential in the Dirac equation is the gradient of a scalar function $A_\mu=\partial\chi/\partial x_\mu$ the potential may be removed by replacing the wave function by $\psi=\exp(-i\chi)\psi'$ (gauge transformation). This alters the kernel by a factor $\exp[-i(\chi(2)-\chi(1))]$ owing to the change in the initial and final wave functions. A constant potential A_μ is the gradient of $\chi=A_\mu x_\mu$ and can be completely removed by this gauge transformation, so that the kernel differs from that of a free particle by the factor $\exp[-i(A_\mu x_{\mu 2}-A_\mu x_{\mu 1})]$ as in (37).

where $\Phi_{p,n}^{(0)}$, the amplitude for a particular path for particle n is simply the expression (36) where $(\mathbf{x}_{i+1}|\mathbf{x}_i)_\epsilon$ is the kernel $K_{0,n}(\mathbf{x}_{i+1}^{(n)}, t_{i+1}; \mathbf{x}_i^{(n)}, t_i)$ for a free electron according to the one electron Dirac theory, with the matrices which appear operating on the spinor indices corresponding to particle (n) and the order of all operations being determined by the time indices.

For calculational purposes we can, as before, expand R as a power series and evaluate the various terms in the same manner as for the non-relativistic case. In such an expansion the quantity $\mathbf{x}^\cdot(t)$ is replaced, as we have seen in (32), by the operator $i(H\mathbf{x}-\mathbf{x}H)$, that is, in this case by $\boldsymbol{\alpha}$ operating at the corresponding time. There is no further complicated term analogous to (33) arising in this case, for the expected value of $(x_{i+1}-x_i)^2$ is now of order ϵ^2 rather than ϵ.

For example, for self-energy one sees that expression (28) will be (with other terms coming from those with $\mathbf{x}^\cdot(t)$ replaced by $\boldsymbol{\alpha}$ and with the usual β in back of each K_0 because of the definition of K_0 in relativity theory)

$$\langle\psi_{t''}|R|\psi_{t'}\rangle_{S_p}=-e^2\int\psi^*(\mathbf{x}_{t''})K_0(\mathbf{x}_{t''},t'';\mathbf{x}_t,t)\beta\alpha_\mu \cdot\delta_+((t-s)^2-(\mathbf{x}_t-\mathbf{x}_s)^2)K_0(\mathbf{x}_t,t;\mathbf{x}_s,s)\beta\alpha_\mu \cdot K_0(\mathbf{x}_s,s;\mathbf{x}_{t'},t')\beta\psi(\mathbf{x}_{t'})d^3\mathbf{x}_{t''}d^3\mathbf{x}_t d^3\mathbf{x}_s d^3\mathbf{x}_{t'}dtds, \quad (40)$$

where $\alpha_4=1$, $\alpha_{1,2,3}=\alpha_{x,y,z}$ and a sum on the repeated index μ is implied in the usual way; $a_\mu b_\mu=a_4b_4-a_1b_1-a_2b_2-a_3b_3$. One can change $\beta\alpha_\mu$ to γ_μ and ψ^* to $\bar{\psi}\beta$. In this manner all of the rules referring to virtual photons discussed in II are deduced; but with the difference that K_0 is used instead of K_+ and we have the Dirac one electron theory with negative energy states (although we may have any number of such electrons).

7. EXTENSION TO POSITRON THEORY

Since in (39) we have an arbitrary number of electrons, we can deal with the hole theory in the usual manner by imagining that we have an infinite number of electrons in negative energy states.

On the other hand, in paper I on the theory of positrons, it was shown that the results of the hole theory in a system with a given external potential A_μ were equivalent to those of the Dirac one electron theory if one replaced the propagation kernel, K_0, by a different one, K_+, and multiplied the resultant amplitude by factor C_v involving A_μ. We must now see how this relation, derived in the case of external potentials, can also be carried over in electrodynamics to be useful in simplifying expressions involving the infinite sea of electrons.

To do this we study in greater detail the relation between a problem involving virtual photons and one involving purely external potentials. In using (25) we shall assume in accordance with the hole theory that the number of electrons is infinite, but that they all have the same charge, e. Let the states $\psi_{t'}$, $\chi_{t''}$, represent the vacuum plus perhaps a number of real electrons in positive energy states and perhaps also some empty negative energy states. Let us call the amplitude for the transition in an external potential B_μ, but *excluding virtual photons*, $T_0[B]$, a functional of $B_\mu(1)$. We have seen (38)

$$T_0[B]=\langle\chi_{t''}|\exp iP|\psi_{t'}\rangle \quad (41)$$

where

$$P=-\sum_n\int[B_4(\mathbf{x}^{(n)}(t),t)-\mathbf{x}^{\cdot(n)}(t)\cdot\mathbf{B}(\mathbf{x}^{(n)}(t),t)]dt$$

by (38). We can write this as

$$P=-\sum_n\int B_\mu(x_\nu^{(n)}(t))\dot{x}_\mu^{(n)}(t)dt$$

where $x_4(t)=t$ and $\dot{x}_4=1$, the other values of μ corresponding to space variables. The corresponding amplitude for the same process in the same potential, but *including* all the virtual photons we may call,

$$T_{e^2}[B]=\langle\chi_{t''}|\exp(iR)\exp(iP)|\psi_{t'}\rangle. \quad (42)$$

Now let us consider the effect on $T_{e^2}[B]$ of changing the coupling e^2 of the virtual photons. Differentiating (42) with respect to e^2 which appears only [14] in R we find

$$dT_{e^2}[B]/d(e^2)=\left\langle\chi_{t''}\middle|-\frac{i}{2}\sum_n\sum_m\int\int dtds\dot{x}_\mu^{(n)}(t)\dot{x}_\mu^{(m)}(s)\cdot\delta_+((x_\nu^{(n)}(t)-x_\nu^{(m)}(s))^2)\exp i(R+P)\middle|\psi_{t'}\right\rangle. \quad (43)$$

We can also study the first-order effect of a change of B_μ:

$$\delta T_{e^2}[B]/\delta B_\mu(1)=-i\left\langle\chi_{t''}\middle|\sum_n\int dt\dot{x}_\mu^{(n)}\delta^4(x_\alpha^{(n)}(t)-x_{\alpha,1})\cdot\exp i(R+P)\middle|\psi_{t'}\right\rangle \quad (44)$$

where $x_{\alpha,1}$ is the field point at which the derivative with respect to B_μ is taken[15] and the term (current density) $-\sum_n\int dt\dot{x}_\mu^{(n)}(t)\delta^4(x_\alpha^{(n)}(t)-x_{\alpha,1})$ is just $\delta P/\delta B_\mu(1)$. The function $\delta^4(x_\alpha^{(n)}-x_{\alpha,1})$ means $\delta(x_4^{(n)}-x_{4,1})$

[14] In changing the charge e^2 we mean to vary only the degree to which virtual photons are important. We do not contemplate changes in the influence of the external potentials. If one wishes, as e is raised the strength of the potential is decreased proportionally so that B_μ, the potential times the charge e, is held constant.

[15] The functional derivative is defined such that if $T[B]$ is a number depending on the functions $B_\mu(1)$, the first order variation in T produced by a change from B_μ to $B_\mu+\Delta B_\mu$ is given by

$$T[B+\Delta B]-T[B]=\int(\delta T[B]/\delta B_\mu(1))\Delta B_\mu(1)d\tau_1$$

the integral extending over all four-space $x_{\alpha,1}$.

$\times\delta(x_3^{(n)}-x_{3,1})\delta(x_2^{(n)}-x_{2,1})\delta(x_1^{(n)}-x_{1,1})$ that is, $\delta(2,1)$ with $x_{\alpha,2}=x_\alpha^{(n)}(t)$. A second variation of T gives, by differentiation of (44) with respect to $B_\nu(2)$,

$$\delta^2T_{e2}[B]/\delta B_\mu(1)\delta B_\nu(2)$$
$$=-\left\langle\chi_{l'}\left|\sum_n\sum_m\int dt\int ds\dot{x}_\mu^{(n)}(t)\dot{x}_\nu^{(m)}(s)\right.\right.$$
$$\cdot\delta^4(x_\alpha^{(n)}(t)-x_{\alpha,1})\delta^4(x_\beta^{(m)}(s)-x_{\beta,2})$$
$$\left.\left.\times\exp i(R+P)\right|\psi_{l'}\right\rangle. \tag{45}$$

Comparison of this with (43) shows that

$$dT_{e2}[B]/d(e^2)=\tfrac{1}{2}i\int\int(\delta^2T_{e2}[B]/\delta B_\mu(1)\delta B_\mu(2))$$
$$\times\delta_+(s_{12}^2)d\tau_1d\tau_2$$

where $s_{12}^2=(x_{\mu,1}-x_{\mu,2})(x_{\mu,1}-x_{\mu,2})$.

We now proceed to use this equation to prove the validity of the rules given in **II** for electrodynamics. This we do by the following argument. The equation can be looked upon as a differential equation for $T_{e2}[B]$. It determines $T_{e2}[B]$ uniquely if $T_0[B]$ is known. We have shown it is valid for the hole theory of positrons. But in **I** we have given formulas for calculating $T_0[B]$ whose correctness relative to the hole theory we have there demonstrated. Hence we have shown that the $T_{e2}[B]$ obtained by solving (45) with the initial condition $T_0[B]$ as given by the rules in **I** will be equal to that given for the same problem by the second quantization theory of the Dirac matter field coupled with the quantized electromagnetic field. But it is evident (the argument is given in the next paragraph) that the rules[16] given in **II** constitute a solution in power series in e^2 of the Eq. (45) [which for $e^2=0$ reduce to the $T_0[B]$ given in **I**]. Hence the rules in **II** must give, to each order in e^2, the matrix element for any process that would be calculated by the usual theory of second quantization of the matter and electromagnetic fields. This is what we aimed to prove.

That the rules of **II** represent, in a power series expansion, a solution of (45) is clear. For the rules there given may be stated as follows: Suppose that we have a process to order k in e^2 (i.e., having k virtual photons) and order n in the external potential B_μ. Then, *the matrix element for the process with one more virtual photon and two less potentials is that obtained from the previous matrix by choosing from the n potentials a pair, say $B_\mu(1)$ acting at 1 and $B_\nu(2)$ acting at 2, replacing them by $ie^2\delta_{\mu\nu}\delta_+(s_{12}^2)$, adding the results for each way of choosing the pair, and dividing by $k+1$, the present number of photons.* The matrix with no virtual photons ($k=0$) being given to any n by the rules of **I**, this permits terms to all orders in e^2 to be derived by recursion. It is evident that the rule in italics is that of **II**, and equally evident that it is a word expression of Eq. (45). [The factor $\frac{1}{2}$ in (45) arises since in integrating over all $d\tau_1$ and $d\tau_2$ we count each pair twice. The division by $k+1$ is required by the rules of **II** for, there, each diagram is to be taken only once, while in the rule given above we say what to do to add one extra virtual photon to k others. But which one of the $k+1$ is to be identified at the last photon added is irrelevant. It agrees with (45) of course for it is canceled on differentiating with respect to e^2 the factor $(e^2)^{k+1}$ for the $(k+1)$ photons.]

8. GENERALIZED FORMULATION OF QUANTUM ELECTRODYNAMICS

The relation implied by (45) between the formal solution for the amplitude for a process in an arbitrary unquantized external potential to that in a quantized field appears to be of much wider generality. We shall discuss the relation from a more general point of view here (still limiting ourselves to the case of no photons in initial or final state).

In earlier sections we pointed out that as a consequence of the Lagrangian form of quantum mechanics the aspects of the particles' motions and the behavior of the field could be analyzed separately. What we did was to integrate over the field oscillator coordinates first. We could, in principle, have integrated over the particle variables first. That is, we first solve the problem with the action of the particles and their interaction with the field and then multiply by the exponential of the action of the field and integrate over all the field oscillator coordinates. (For simplicity of discussion let us put aside from detailed special consideration the questions involving the separation of the longitudinal and transverse parts of the field.[9]) Now the integral over the particle coordinates for a given process is precisely the integral required for the analysis of the motion of the particles in an unquantized potential. With this observation we may suggest a generalization to all types of systems.

Let us suppose the formal solution for the amplitude for some given process with matter in an external potential $B_\mu(1)$ is some numerical quantity T_0. We mean matter in a more general sense now, for the motion of the matter may be described by the Dirac equation, or by the Klein-Gordon equation, or may involve charged or neutral particles other than electrons and positrons in any manner whatsoever. The quantity T_0 depends of course on the potential function $B_\mu(1)$; that is, it is a functional $T_0[B]$ of this potential. We

[16] That is, of course, those rules of **II** which apply to the unmodified electrodynamics of Dirac electrons. (The limitation excluding real photons in the initial and final states is removed in Sec. 8.) The same arguments clearly apply to nucleons interacting via neutral vector mesons, vector coupling. Other couplings require a minor extension of the argument. The modification to the $(\mathbf{x}_{i+1}|\mathbf{x}_i)_\epsilon$, as in (37), produced by some couplings cannot very easily be written without using operators in the exponents. These operators can be treated as numbers if their order of operation is maintained to be always their order in time. This idea will be discussed and applied more generally in a succeeding paper.

assume we have some expression for it in terms of B_μ (exact, or to some desired degree of approximation in the strength of the potential).

Then the answer $T_{el}[B]$ to the corresponding problem in quantum electrodynamics is $T_0[A_\mu(1)+B_\mu(1)] \times \exp(iS_0)$ summed over all possible distributions of field $A_\mu(1)$, wherein S_0 is the action for the field $S_0 = -(8\pi c^2)^{-1}\sum_\mu \int((\partial A_\mu/\partial t)^2 - (\nabla A_\mu)^2)d^3\mathbf{x}dt$ the sum on μ carrying the usual minus sign for space components.

If $F[A]$ is any functional of $A_\mu(1)$ we shall represent by ${}_0|F[A]|_0$ this superposition of $F[A]\exp(iS_0)$ over distributions of A_μ for the case in which there are no photons in initial or final state. That is, we have

$$T_{el}[B] = {}_0|T_0[A+B]|_0. \tag{46}$$

The evaluation of ${}_0|F[A]|_0$ directly from the definition of the operation ${}_0|\ \ |_0$ is not necessary. We can give the result in another way. We first note that the operation is linear,

$${}_0|F_1[A]+F_2[A]|_0 = {}_0|F_1[A]|_0 + {}_0|F_2[A]|_0 \tag{47}$$

so that if F is represented as a sum of terms each term can be analyzed separately. We have studied essentially the case in which $F[A]$ is an exponential function. In fact, what we have done in Section 4 may be repeated with slight modification to show that

$${}_0\left|\exp\left(-i\int j_\mu(1)A_\mu(1)d\tau_1\right)\right|_0$$

$$= \exp\left(-\tfrac{1}{2}ie^2\int\int j_\mu(1)j_\mu(2)\delta_+(s_{12}^2)d\tau_1 d\tau_2\right) \tag{48}$$

where $j_\mu(1)$ is an arbitrary function of position and time for each value of μ.

Although this gives the evaluation of ${}_0|\ \ |_0$ for only a particular functional of A_μ the appearance of the arbitrary function $j_\mu(1)$ makes it sufficiently general to permit the evaluation for any other functional. For it is to be expected that any functional can be represented as a superposition of exponentials with different functions $j_\mu(1)$ (by analogy with the principle of Fourier integrals for ordinary functions). Then, by (47), the result of the operation is the corresponding superposition of expressions equal to the right-hand side of (48) with the various j's substituted for j_μ.

In many applications $F[A]$ can be given as a power series in A_μ:

$$F[A] = f_0 + \int f_\mu(1)A_\mu(1)d\tau_1$$

$$+ \int\int f_{\mu\nu}(1,2)A_\mu(1)A_\nu(2)d\tau_1 d\tau_2 + \cdots \tag{49}$$

where $f_0, f_\mu(1), f_{\mu\nu}(1,2)\cdots$ are known numerical functions independent of A_μ. Then by (47)

$${}_0|F[A]|_0 = f_0 + \int f_\mu(1){}_0|A_\mu(1)|_0 d\tau_1$$

$$+ \int\int f_{\mu\nu}(1,2){}_0|A_\mu(1)A_\nu(2)|_0 d\tau_1 d\tau_2 + \cdots \tag{50}$$

where we set ${}_0|1|_0 = 1$ (from (48) with $j_\mu = 0$). We can work out expressions for the successive powers of A_μ by differentiating both sides of (48) successively with respect to j_μ and setting $j_\mu = 0$ in each derivative. For example, the first variation (derivative) of (48) with respect to $j_\mu(3)$ gives

$${}_0\left|-iA_\mu(3)\exp\left(-i\int j_\nu(1)A_\nu(1)d\tau_1\right)\right|_0$$

$$= -ie^2\int \delta_+(s_{34}^2)j_\mu(4)d\tau_4$$

$$\times\exp\left(-\tfrac{1}{2}ie^2\int\int j_\nu(1)j_\nu(2)\delta_+(s_{12}^2)d\tau_1 d\tau_2\right). \tag{51}$$

Setting $j_\mu = 0$ gives

$${}_0|A_\mu(3)|_0 = 0.$$

Differentiating (51) again with respect to $j_\nu(4)$ and setting $j_\nu = 0$ shows

$${}_0|A_\mu(3)A_\nu(4)|_0 = ie^2\delta_{\mu\nu}\delta_+(s_{34}^2) \tag{52}$$

and so on for higher powers. These results may be substituted into (50). Clearly therefore when $T_0[B+A]$ in (46) is expanded in a power series and the successive terms are computed in this way, we obtain the results given in **II**.

It is evident that (46), (47), (48) imply that $T_{el}[B]$ satisfies the differential equation (45) and conversely (45) with the definition (46) implies (47) and (48). For if $T_0[B]$ is an exponential

$$T_0[B] = \exp\left(-i\int j_\mu(1)B_\mu(1)d\tau_1\right) \tag{53}$$

we have from (46), (48) that

$$T_{el}[B] = \exp\left[-\tfrac{1}{2}ie^2\int\int j_\mu(1)j_\mu(2)\delta_+(s_{12}^2)d\tau_1 d\tau_2\right]$$

$$\cdot\exp\left[-i\int j_\nu(1)B_\nu(1)d\tau_1\right]. \tag{54}$$

Direct substitution of this into Eq. (45) shows it to be a solution satisfying the boundary condition (53). Since the differential equation (45) is linear, if $T_0[B]$ is a superposition of exponentials, the corresponding superposition of solutions (54) is also a solution.

Many of the formal representations of the matter system (such as that of second quantization of Dirac electrons) represent the interaction with a fixed potential in a formal exponential form such as the left-hand side of (48), except that $j_\mu(1)$ is an operator instead of a numerical function. Equation (48) may still be used if care is exercised in defining the order of the operators on the right-hand side. The succeeding paper will discuss this in more detail.

Equation (45) or its solution (46), (47), (48) constitutes a very general and convenient formulation of the laws of quantum electrodynamics for virtual processes. Its relativistic invariance is evident if it is assumed that the unquantized theory giving $T_0[B]$ is invariant. It has been proved to be equivalent to the usual formulation for Dirac electrons and positrons (for Klein-Gordon particles see Appendix A). It is suggested that it is of wide generality. It is expressed in a form which has meaning even if it is impossible to express the matter system in Hamiltonian form; in fact, it only requires the existence of an amplitude for fixed potentials which obeys the principle of superposition of amplitudes. If $T_0[B]$ is known in power series in B, calculations of $T_{e^2}[B]$ in a power series of e^2 can be made directly using the italicized rule of Sec. 7. The limitation to virtual quanta is removed in the next section.

On the other hand, the formulation is unsatisfactory because for situations of importance it gives divergent results, even if $T_0[B]$ is finite. The modification proposed in II of replacing $\delta_+(s_{12}^2)$ in (45), (48) by $f_+(s_{12}^2)$ is not satisfactory owing to the loss of the theorems of conservation of energy or probability discussed in II at the end of Sec. 6. There is the additional difficulty in positron theory that even $T_0[B]$ is infinite to begin with (vacuum polarization). Computational ways of avoiding these troubles are given in II and in the references of footnote 2.

9. CASE OF REAL PHOTONS

The case in which there are real photons in the initial or the final state can be worked out from the beginning in the same manner.[17] We first consider the case of a system interacting with a single oscillator. From this result the generalization will be evident. This time we shall calculate the transition element between an initial state in which the particle is in state $\psi_{t'}$ and the oscillator is in its nth eigenstate (i.e., there are n photons in the field) to a final state with particle in $\chi_{t''}$, oscillator in mth level. As we have already discussed, when the coordinates of the oscillator are eliminated the result is the transition element $\langle\chi_{t''}|G_{mn}|\psi_{t'}\rangle$ where

$$G_{mn}=\int \varphi_m^*(q_j)k(q_j,t'';q_0,t')\varphi_n(q_0)dq_0dq_j \quad (11)$$

where φ_m, φ_n are the wave functions[8] for the oscillator in state m, n and k is given in (12). The G_{mn} can be evaluated most easily by calculating the generating function

$$g(X,Y)=\sum_m\sum_n G_{mn}X^mY^n(m!n!)^{-\frac{1}{2}} \quad (55)$$

for arbitrary X, Y. If expression (11) is substituted in the left-hand side of (55), the expression can be simplified by use of the generating function relation for the eigenfunctions[8] of the harmonic oscillator

$$\sum_n \varphi_n(q_0)Y^n(n!)^{-\frac{1}{2}}=(\omega/\pi)^{\frac{1}{4}}\exp(-\tfrac{1}{2}i\omega t')\times\exp\tfrac{1}{2}[\omega q_0^2-(Y\exp[-i\omega t']-(2\omega)^{\frac{1}{2}}q_0)^2]$$

Using a similar expansion for the φ_m^* one is left with the exponential of a quadratic function of q_0 and q_j. The integration on q_0 and q_j is then easily performed to give

$$g(X,Y)=G_{00}\exp(XY+i\beta^*X+i\beta Y) \quad (56)$$

from which expansion in powers of X and Y and comparison to (11) gives the final result

$$G_{mn}=G_{00}(m!n!)^{-\frac{1}{2}}\sum_r \frac{m!}{(m-r)!r!}\frac{n!}{(n-r)!r!}\times r!(i\beta^*)^{m-r}(i\beta)^{n-r} \quad (57)$$

where G_{00} is given in (14) and

$$\beta=(2\omega)^{-\frac{1}{2}}\int_{t'}^{t''}\gamma(t)\exp(-i\omega t)dt,$$
$$\beta^*=(2\omega)^{-\frac{1}{2}}\int_{t'}^{t''}\gamma(t)\exp(+i\omega t)dt, \quad (58)$$

and the sum on r is to go from 0 to m or to n whichever is the smaller. (The sum can be expressed as a Laguerre polynomial but there is no advantage in this.)

Formula (57) is readily understandable. Consider first a simple case of absorption of one photon. Initially we have one photon and finally none. The amplitude for this is the transition element of $G_{01}=i\beta G_{00}$ or $\langle\chi_{t''}|i\beta G_{00}|\psi_{t'}\rangle$. This is the same as would result if we asked for the transition element for a problem in which all photons are virtual but there was present a perturbing potential $-(2\omega)^{-\frac{1}{2}}\gamma(t)\exp(-i\omega t)$ and we required the first-order effect of this potential. Hence photon absorption is like the first order action of a potential varying in time as $\gamma(t)\exp(-i\omega t)$ that is with a positive frequency (i.e., the sign of the coefficient of t in the exponential corresponds to positive energy). The amplitude for emission of one photon involves $G_{10}=i\beta^*G_{00}$, which is the same result except that the potential has negative frequency. Thus we begin by interpreting $i\beta^*$ as the amplitude for emission of one photon $i\beta$ as the amplitude for absorption of one.

Next for the general case of n photons initially and m finally we may understand (57) as follows. We first

[17] For an alternative method starting directly from the formula (24) for virtual photons, see Appendix B.

neglect Bose statistics and imagine the photons as individual distinct particles. If we start with n and end with m this process may occur in several different ways. The particle may absorb in total $n-r$ of the photons and the final m photons will represent r of the photons which were present originally plus $m-r$ new photons emitted by the particle. In this case the $n-r$ which are to be absorbed may be chosen from among the original n in $n!/(n-r)!r!$ different ways, and each contributes a factor $i\beta$, the amplitude for absorption of a photon. Which of the $m-r$ photons from among the m are emitted can be chosen in $m!/(m-r)!r!$ different ways and each photon contributes a factor $i\beta^*$ in amplitude. The initial r photons which do not interact with the particle can be re-arranged among the final r in $r!$ ways. We must sum over the alternatives corresponding to different values of r. Thus the form of G_{mn} can be understood. The remaining factor $(m!)^{-\frac{1}{2}}(n!)^{-\frac{1}{2}}$ may be interpreted as saying that in computing probabilities (which therefore involves the square of G_{mn}) the photons may be considered as independent but that if m are actually equal the statistical weight of each of the states which can be made by rearranging the m equal photons is only $1/m!$. This is the content of Bose statistics; that m equal particles in a given state represents just one state, i.e., has statistical weight unity, rather than the $m!$ statistical weight which would result if it is imagined that the particles and states can be identified and rearranged in $m!$ different ways. This holds for both the initial and final states of course. From this rule about the statistical weights of states the derivation of the blackbody distribution law follows.

The actual electromagnetic field is represented as a host of oscillators each of which behaves independently and produces its own factor such as G_{mn}. Initial or final states may also be linear combinations of states in which one or another oscillator is excited. The results for this case are of course the corresponding linear combination of transition elements.

For photons of a given direction of polarization and for sin or cos waves the explicit expression for β can be obtained directly from (58) by substituting the formulas (16) for the γ's for the corresponding oscillator. It is more convenient to use the linear combination corresponding to running waves. Thus we find the amplitude for absorption of a photon of momentum $\mathbf{K}$, frequency $k=(\mathbf{K}\cdot\mathbf{K})^{\frac{1}{2}}$ polarized in direction $\mathbf{e}$ is given by including a factor i times

$$\beta_{\mathbf{K},\mathbf{e}}=(4\pi)^{\frac{1}{2}}(2k)^{-\frac{1}{2}}\sum_n e_n\int_{t'}^{t''}\exp(-ikt)\times\exp(i\mathbf{K}\cdot\mathbf{x}_n(t))\mathbf{e}\cdot\dot{\mathbf{x}}_n(t)dt \quad (59)$$

in the transition element (25). The density of states in momentum space is now $(2\pi)^{-3}d^3\mathbf{K}$. The amplitude for emission is just i times the complex conjugate of this expression, or what amounts to the same thing, the same expression with the sign of the four vector k_μ reversed. Since the factor (59) is exactly the first-order effect of a vector potential

$$\mathbf{A}^{PH}=(2\pi/k)^{\frac{1}{2}}\mathbf{e}\exp(-i(kt-\mathbf{K}\cdot\mathbf{x}))$$

of the corresponding classical wave, we have derived the rules for handling real photons discussed in **II**.

We can express this directly in terms of the quantity $T_{e2}[B]$, the amplitude for a given transition without emission of a photon. What we have said is that the amplitude for absorption of just one photon whose classical wave form is $A_\mu{}^{PH}(1)$ (time variation $\exp(-ikt_1)$ corresponding to positive energy k) is proportional to the first order (in ϵ) change produced in $T_{e2}[B]$ on changing B to $B+\epsilon A^{PH}$. That is, more exactly,

$$\int(\delta T_{e2}[B]/\delta B_\mu(1))A_\mu{}^{PH}(1)d\tau_1 \quad (60)$$

is the amplitude for absorption by the particle system of one photon, A^{PH}. (A superposition argument shows the expression to be valid not only for plane waves, but for spherical waves, etc., as given by the form of A^{PH}.) The amplitude for emission is the same expression but with the sign of the frequency reversed in A^{PH}. The amplitude that the system absorbs two photons with waves $A_\mu{}^{PH_1}$ and $A_\nu{}^{PH_2}$ is obtained from the next derivative,

$$\int\int(\delta^2 T_{e2}[B]/\delta B_\mu(1)\delta B_\nu(2))A_\mu{}^{PH_1}(1)A_\nu{}^{PH_2}(2)d\tau_1 d\tau_2,$$

the same expression holding for the absorption of one and emission of the other, or emission of both depending on the sign of the time dependence of A^{PH_1} and A^{PH_2}. Larger photon numbers correspond to higher derivatives, absorption of l_1 emission of l_2 requiring the (l_1+l_2) derivaties. When two or more of the photons are exactly the same (e.g., $A^{PH_1}=A^{PH_2}$) the same expression holds for the amplitude that l_1 are absorbed by the system while l_2 are emitted. However, the statement that initially n of a kind are present and m of this kind are present finally, does not imply $l_1=n$ and $l_2=m$. It is possible that only $n-r=l_1$ were absorbed by the system and $m-r=l_2$ emitted, and that r remained from initial to final state without interaction. This term is weighed by the combinatorial coefficient $(m!n!)^{-\frac{1}{2}}\binom{m}{r}\binom{n}{r}r!$ and summed over the possibilities for r as explained in connection with (57). Thus once the amplitude for virtual processes is known, that for real photon processes can be obtained by differentiation.

It is possible, of course, to deal with situations in which the electromagnetic field is not in a definite state after the interaction. For example, we might ask for the total probability of a given process, such as a scattering, without regard for the number of photons emitted. This is done of course by squaring the ampli-

tude for the emission of m photons of a given kind and summing on all m. Actually the sums and integrations over the oscillator momenta can usually easily be performed analytically. For example, the amplitude, starting from vacuum and ending with m photons of a given kind, is by (56) just

$$G_{m0}=(m!)^{-\frac{1}{2}}G_{00}(i\beta^*)^m. \tag{61}$$

The square of the amplitude summed on m requires the product of two such expressions (the $\gamma(l)$ in the β of one and in the other will have to be kept separately) summed on m:

$$\sum_m G_{m0}^*G_{m0}'=\sum_m G_{00}^*G_{00}'(m!)^{-1}\beta^m(\beta'^*)^m$$
$$=G_{00}^*G_{00}'\exp(\beta\beta'^*).$$

In the resulting expression the sum over all oscillators is easily done. Such expressions can be of use in the analysis in a direct manner of problems of line width, of the Bloch-Nordsieck infra-red problem, and of statistical mechanical problems, but no such applications will be made here.

The author appreciates his opportunities to discuss these matters with Professor H. A. Bethe and Professer J. Ashkin, and the help of Mr. M. Baranger with the manuscript.

APPENDIX A. THE KLEIN-GORDON EQUATION

In this Appendix we describe a formulation of the equations for a particle of spin zero which was first used to obtain the rules given in II for such particles. The complete physical significance of the equations has not been analyzed thoroughly so that it may be preferable to derive the rules directly from the second quantization formulation of Pauli and Weisskopf. This can be done in a manner analogous to the derivation of the rules for the Dirac equation given in I or from the Schwinger-Tomonaga formulation[2] in a manner described, for example, by Rohrlich.[18] The formulation given here is therefore not necessary for a description of spin zero particles but is given only for its own interest as an alternative to the formulation of second quantization.

We start with the Klein-Gordon equation

$$(i\partial/\partial x_\mu-A_\mu)^2\psi=m^2\psi \tag{1A}$$

for the wave function ψ of a particle of mass m in a given external potential A_μ. We shall try to represent this in a manner analogous to the formulation of quantum mechanics in C. That is, we try to represent the amplitude for a particle to get from one point to another as a sum over all trajectories of an amplitude $\exp(iS)$ where S is the classical action for a given trajectory. To maintain the relativistic invariance in evidence the idea suggests itself of describing a trajectory in space-time by giving the four variables $x_\mu(u)$ as functions of some fifth parameter u (rather than expressing x_1, x_2, x_3 in terms of x_4). As we expect to represent paths which may reverse themselves in time (to represent pair production, etc., as in I) this is certainly a more convenient representation, for all four functions $x_\mu(u)$ may be considered as functions of a parameter u (somewhat analogous to proper time) which increase as we go along the trajectory, whether the trajectory is proceeding forward ($dx_4/du>0$) or backward ($dx_4/du<0$) in time.[19] We shall then have a new type of wave function $\varphi(x, u)$ a function of five variables, x standing for the four x_μ. It gives the amplitude for arrival at point x_μ with a certain value of the parameter u. We shall suppose that this wave function satisfies the equation

$$i\partial\varphi/\partial u=-\tfrac{1}{2}(i\partial/\partial x_\mu-A_\mu)^2\varphi \tag{2A}$$

which is seen to be analogous to the time-dependent Schrödinger equation, u replacing the time and the four coordinates of space-time x_μ replacing the usual three coordinates of space.

Since the potentials $A_\mu(x)$ are functions only of coordinates x_μ and are independent of u, the equation is separable in u and we can write a special solution in the form $\varphi=\exp(\frac{1}{2}im^2u)\psi(x)$ where $\psi(x)$, a function of the coordinates x_μ only, satisfies (1A) and the eigenvalue $\frac{1}{2}m^2$ conjugate to u is related to the mass m of the particle. Equation (2A) is therefore equivalent to the Klein-Gordon Eq. (1A) provided we ask in the end only for the solution of (1A) corresponding to the eigenvalue $\frac{1}{2}m^2$ for the quantity conjugate to u.

We may now proceed to represent Eq. (2A) in Lagrangian form in general and without regard to this eigenvalue condition. Only in the final solutions need we apply the eigenvalue condition. That is, if we have some special solution $\varphi(x, u)$ of (2A) we can select that part corresponding to the eigenvalue $\frac{1}{2}m^2$ by calculating

$$\psi(x)=\int_{-\infty}^{\infty}\exp(-\tfrac{1}{2}im^2u)\varphi(x, u)du$$

and thereby obtain a solution ψ of Eq. (1A).

Since (2A) is so closely analogous to the Schrödinger equation, it is easily written in the Lagrangian form described in C, simply by working by analogy. For example if $\varphi(x, u)$ is known at one value of u its value at a slightly larger value $u+\epsilon$ is given by

$$\varphi(x, u+\epsilon)=\int \exp i\epsilon\left[-\frac{(x_\mu-x_\mu')^2}{2\epsilon^2}-\frac{1}{2}\left(\frac{x_\mu-x_\mu'}{\epsilon}\right)(A_\mu(x)+A_\mu(x'))\right]$$
$$\cdot\varphi(x', u)d^4\tau_{x'}(2\pi i\epsilon)^{-2}(-2\pi i\epsilon)^{-\frac{1}{2}} \tag{3A}$$

where $(x_\mu-x_\mu')^2$ means $(x_\mu-x_\mu')(x_\mu-x_\mu')$, $d^4\tau_{x'}=dx_1'dx_2'dx_3'dx_4'$ and the sign of the normalizing factor is changed for the x_4 component since the component has the reversed sign in its quadratic coefficient in the exponential, in accordance with our summation convention $a_\mu b_\mu=a_4b_4-a_1b_1-a_2b_2-a_3b_3$. Equation (3A), as can be verified readily as described in C, Sec. 6, is equivalent to first order in ϵ, to Eq. (2A). Hence, by repeated use of this equation the wave function at $u_0=n\epsilon$ can be represented in terms of that at $u=0$ by:

$$\varphi(x_{\nu, n}, u_0)=\int \exp-\frac{i\epsilon}{2}\sum_{i=1}^{n}\left[\left(\frac{x_{\mu, i}-x_{\mu, i-1}}{\epsilon}\right)^2\right.$$
$$\left.+\epsilon^{-1}(x_{\mu, i}-x_{\mu, i-1})(A_\mu(x_i)+A_\mu(x_{i-1}))\right]$$
$$\cdot\varphi(x_{\nu, 0}, 0)\prod_{i=0}^{n-1}(d^4\tau_i/4\pi^2\epsilon^2 i). \tag{4A}$$

That is, roughly, the amplitude for getting from one point to another with a given value of u_0 is the sum over all trajectories of $\exp(iS)$ where

$$S=-\int_0^{u_0}[\tfrac{1}{2}(dx_\mu/du)^2+(dx_\mu/du)A_\mu(x)]du, \tag{5A}$$

when sufficient care is taken to define the quantities, as in C. This completes the formulation for particles in a fixed potential but a few words of description may be in order.

In the first place in the special case of a free particle we can define a kernal $k^{(0)}(x, u_0; x', 0)$ for arrival from x_μ', 0 to x_μ at u_0 as the sum over all trajectories between these points of $\exp-i\int_0^{u_0}\frac{1}{2}(dx_\mu/du)^2du$. Then for this case we have

$$\varphi(x, u_0)=\int k^{(0)}(x, u_0; x', 0)\varphi(x', 0)d^4\tau_{x'} \tag{6A}$$

and it is easily verified that k_0 is given by

$$k^{(0)}(x, u_0; x', 0)=(4\pi^2u_0^2i)^{-1}\exp-i(x_\mu-x_\mu')^2/2u_0 \tag{7A}$$

for $u_0>0$ and by 0, by definition, for $u_0<0$. The corresponding

[18] F. Rohrlich (to be published).

[19] The physical ideas involved in such a description are discussed in detail by Y. Nambu, Prog. Theor. Phys. 5, 82 (1950). An equation of type (2A) extended to the case of Dirac electrons has been studied by V. Fock, Physik Zeits. Sowjetunion 12, 404 (1937).

kernel of importance when we select the eigenvalue $\frac{1}{2}m^2$ is[20]

$$2iI_+(x,x')=\int_{-\infty}^{\infty}k^{(0)}(x,u_0;x',0)\exp(-\tfrac{1}{2}im^2u_0)du_0$$
$$=\int_0^{\infty}du_0(4\pi^2u_0^2i)^{-1}\exp-\tfrac{1}{2}i(m^2u_0+u_0^{-1}(x_\mu-x_\mu')^2) \quad (8A)$$

(the last extends only from $u_0=0$ since k_0 is zero for negative u_0) which is identical to the I_+ defined in II.[21] This may be seen readily by studying the Fourier transform, for the transform of the integrand on the right-hand side is

$$\int(4\pi^2u_0^2i)^{-1}\exp(ip\cdot x)\exp-\tfrac{1}{2}i(m^2u_0+x_\mu^2/u_0)d^4\tau_x$$
$$=\exp-\tfrac{1}{2}iu_0(m^2-p_\mu^2)$$

so that the u_0 integration gives for the transform of I_+ just $1/(p_\mu^2-m^2)$ with the pole defined exactly as in II. Thus we are automatically representing the positrons as trajectories with the time sense reversed.

If $\Phi^{(0)}[x(u)]=\exp-i\int_0^{u_0}\frac{1}{2}(dx_\mu/du)^2du$ is the amplitude for a given trajectory $x_\nu(u)$ for a free particle, then the amplitude in a potential is

$$\Phi^{(A)}[x(u)]=\Phi^{(0)}[x(u)]\exp-i\int_0^{u_0}(dx_\mu/du)A_\mu(x)du. \quad (9A)$$

If desired this may be studied by perturbation methods by expanding the exponential in powers of A_μ.

For interpretation, the integral in (9A) must be written as a Riemann sum, and if a perturbation expansion is made, care must be taken with the terms quadratic in the velocity, for the effect of $(x_{\mu,i+1}-x_{\mu,i})(x_{\nu,i+1}-x_{\nu,i})$ is not of order ϵ^2 but is $-i\delta_{\mu\nu}\epsilon$. The "velocity" dx_μ/du becomes the momentum operator $p_\mu=+i\partial/\partial x_\mu$ operating half before and half after A_μ, just as in the non-relativistic Schrödinger equation discussed in Sec. 5. Furthermore, in exactly the same manner as in that case, but here in four dimensions, a term quadratic in A_μ arises in the second-order perturbation terms from the coincidence of two velocities for the same value of u.

As an example, the kernal $k^{(A)}(x,u_0;x',0)$ for proceeding from $x_\mu',0$ to x_μ,u_0 in a potential A_μ differs from $k^{(0)}$ to first order in A_μ by a term

$$-i\int_0^{u_0}duk^{(0)}(x,u_0;y,u)\tfrac{1}{2}(p_\mu A_\mu(y)+A_\mu(y)p_\mu)k^{(0)}(y,u;x',0)d\tau_y$$

the p_μ here meaning $+i\partial/\partial y_\mu$. The kernel of importance on selecting the eigenvalue $\frac{1}{2}m^2$ is obtained by multiplying this by $\exp(-\frac{1}{2}im^2u_0)$ and integrating u_0 from 0 to ∞. The kernel $k^{(0)}(x,u_0;y,u)$ depends only on $u'=u_0-u$ and in the integrals on u and u_0; $\int_0^\infty du_0\int_0^{u_0}du\exp(-\frac{1}{2}im^2u_0)\cdots$, can be written, on interchanging the order of integration and changing variables to u and u', $\int_0^\infty du\int_0^\infty du'\exp(-\frac{1}{2}im^2(u+u'))\cdots$. Now the integral on u' converts $k^{(0)}(x,u_0;y,u)$ to $2iI_+(x,y)$ by (8A), while that on u converts $k^{(0)}(y,u;x',0)$ to $2iI_+(y,x')$, so the result becomes

$$\int 2iI_+(x,y)(p_\mu A_\mu+A_\mu p_\mu)I_+(y,x')d^4\tau_y$$

as expected. The same principle works to any order so that the rules for a single Klein-Gordon particle in external potentials given in II, Section 9, are deduced.

The transition to quantum electrodynamics is simple for in (5A) we already have a transition amplitude represented as a sum (over trajectories, and eventually u_0) of terms, in each of which the potential appears in exponential form. We may make use of the general relation (54). Hence, for example, one finds for the case of no photons in the initial and final states, in the presence of an external potential B_μ, the amplitude that a particle proceeds from $(x_\mu',0)$ to (x_μ,u_0) is the sum over all trajectories of the quantity

$$\exp-i\left[\frac{1}{2}\int_0^{u_0}\left(\frac{dx_\mu}{du}\right)^2du+\int_0^{u_0}\frac{dx_\mu}{du}B_\mu(x(u))du\right.$$
$$\left.+\frac{e^2}{2}\int_0^{u_0}\int_0^{u_0}\frac{dx_\mu(u)}{du}\frac{dx_\nu(u')}{du'}\delta_+((x_\mu(u)-x_\mu(u'))^2)dudu'\right]. \quad (10A)$$

This result must be multiplied by $\exp(-\frac{1}{2}im^2u_0)$ and integrated on u_0 from zero to infinity to express the action of a Klein-Gordon particle acting on itself through virtual photons. The integrals are interpreted as Riemann sums, and if perturbation expansions are made, the necessary care is taken with the terms quadratic in velocity. When there are several particles (other than the virtual pairs already included) one use a separate u for each, and writes the amplitude for each set of trajectories as the exponental of $-i$ times

$$\frac{1}{2}\sum_n\int_0^{u_0^{(n)}}\left(\frac{dx_\mu^{(n)}}{du}\right)^2du+\sum_n\int_0^{u_0^{(n)}}\frac{dx_\mu^{(n)}}{du}B_\mu(x_\mu^{(n)}(u))du$$
$$+\frac{e^2}{2}\sum_n\sum_m\int_0^{u_0^{(n)}}\int_0^{u_0^{(m)}}\frac{dx_\nu^{(n)}(u)}{du}\frac{dx_\nu^{(m)}(u')}{du'}$$
$$\times\delta_+((x_\mu^{(n)}(u)-x_\mu^{(m)}(u'))^2)dudu', \quad (11A)$$

where $x_\mu^{(n)}(u)$ are the coordinates of the trajectory of the nth particle.[22] The solution should depend on the $u_0^{(n)}$ as $\exp(-\frac{1}{2}im^2\Sigma_n u_0^{(n)})$.

Actually, knowledge of the motion of a single charge implies a great deal about the behavior of several charges. For a pair which eventually may turn out to be a virtual pair may appear in the short run as two "other particles." As a virtual pair, that is, as the reverse section of a very long and complicated single track we know its behavior by (10A). We can assume that such a section can be looked at equally well, for a limited duration at least, as being due to other unconnected particles. This then implies a definite law of interaction of particles if the self-action (10A) of a single particle is known. (This is similar to the relation of real and virtual photon processes discussed in detail in Appendix B.) It is possible that a detailed analysis of this could show that (10A) implied that (11A) was correct for many particles. There is even reason to believe that the law of Bose-Einstein statistics and the expression for contributions from closed loops could be deduced by following this argument. This has not yet been analyzed completely, however, so we must leave this formulation in an incomplete form. The expression for closed loops should come out to be $C_v=\exp+L$ where L, the contribution from a

[20] The factor $2i$ in front of I_+ is simply to make the definition of I_+ here agree with that in I and II. In II it operates with $\mathbf{p}\cdot\mathbf{A}+\mathbf{A}\cdot\mathbf{p}$ as a perturbation. But the perturbation coming from (3A) in a natural way by expansion of the exponential is $-\frac{1}{2}i(\mathbf{p}\cdot\mathbf{A}+\mathbf{A}\cdot\mathbf{p})$.

[21] Expression (8A) is closely related to Schwinger's parametric integral representation of these functions. For example, (8A) becomes formula (45) of F. Dyson, Phys. Rev. **75**, 486 (1949) for $\Delta_F=\Delta^{(1)}-2i\bar{\Delta}=2iI_+$ if $(2\alpha)^{-1}$ is substituted for u_0.

[22] The form (10A) suggests another interesting possibility for avoiding the divergences of quantum electrodynamics in this case. The divergences arise from the δ_+ function when $u=u'$. We might restrict the integration in the double integral such that $|u-u'|>\delta$ where δ is some finite quantity, very small compared with m^{-2}. More generally, we could keep the region $u=u'$ from contributing by including in the integrand a factor $F(u-u')$ where $F(x)\to1$ for x large compared to some δ, and $F(0)=0$ (e.g., $F(x)$ acts qualitatively like $1-\exp(-x^2\delta^{-2})$. (Another way might be to replace u by a discontinuous variable, that is, we do not use the limit in (4A) as $\epsilon\to0$ but set $\epsilon=\delta$.) The idea is that two interactions would contribute very little in amplitude if they followed one another too rapidly in u. It is easily verified that this makes the otherwise divergent integrals finite. But whether the resulting formulas make good physical sense is hard to see. The action of a potential would now depend on the value of u so that Eq. (2A), or its equivalent, would not be separable in u so that $\frac{1}{2}m^2$ would no longer be a strict eigenvalue for all disturbances. High energy potentials could excite states corresponding to other eigenvalues, possibly thereby corresponding to other masses. This note is meant only as a speculation, for not enough work has been done in this direction to make sure that a reasonable physical theory can be developed along these lines. (What little work has been done was not promising.) Analogous modifications can also be made for Dirac electrons.

single loop, is

$$L=2\int_0^\infty l(u_0)\exp(-\tfrac{1}{2}im^2u_0)du_0/u_0$$

where $l(u_0)$ is the sum over all trajectories which close on themselves ($x_\mu(u_0)=x_\mu(0)$) of $\exp(iS)$ with S given in (5A), and a final integration $d\tau_{x(0)}$ on $x_\mu(0)$ is made. This is equivalent to putting

$$l(u_0)=\int(k^{(A)}(x,u_0;x,0)-k^{(0)}(x,u_0;x,0))d\tau_x.$$

The term $k^{(0)}$ is subtracted only to simplify convergence problems (as adding a constant independent of A_μ to L has no effect).

APPENDIX B. THE RELATION OF REAL AND VIRTUAL PROCESSES

If one has a general formula for all virtual processes he should be able to find the formulas and states involved in real processes. That is to say, we should be able to deduce the formulas of Section 9 directly from the formulation (24), (25) (or its generalized equivalent such as (46), (48)) without having to go all the way back to the more usual formulation. We discuss this problem here.

That this possibility exists can be seen from the consideration that what looks like a real process from one point of view may appear as a virtual process occurring over a more extended time.

For example, if we wish to study a given real process, such as the scattering of light, we can, if we wish, include in principle the source, scatterer, and eventual absorber of the scattered light in our analysis. We may imagine that no photon is present initially, and that the source then emits light (the energy coming say from kinetic energy in the source). The light is then scattered and eventually absorbed (becoming kinetic energy in the absorber). From this point of view the process is virtual; that is, we start with no photons and end with none. Thus we can analyze the process by means of our formula for virtual processes, and obtain the formulas for real processes by attempting to break the analysis into parts corresponding to emission, scattering, and absorption.[22]

To put the problem in a more general way, consider the amplitude for some transition from a state empty of photons far in the past (time t') to a similar one far in the future ($t=t''$). Suppose the time interval to be split into three regions a, b, c in some convenient manner, so that region b is an interval $t_2>t>t_1$ around the present time that we wish to study. Region a, $(t_1>t>t')$, precedes b, and c, $(t''>t>t_2)$, follows b. We want to see how it comes about that the phenomena during b can be analyzed by a study of transitions $g_{ji}(b)$ between some initial state i at time t_1 (which no longer need be photon-free), to some other final state j at time t_2. The states i and j are members of a large class which we will have to find out how to specify. (The single index i is used to represent a large number of quantum numbers, so that different values of i will correspond to having various numbers of various kinds of photons in the field, etc.) Our problem is to represent the over-all transition amplitude, $g(a,b,c)$, as a sum over various values of i,j of a product of three amplitudes,

$$g(a,b,c)=\Sigma_i\,\Sigma_j\,g_{0j}(c)g_{ji}(b)g_{i0}(a);\qquad(1B)$$

first the amplitude that during the interval a the vacuum state makes transition to some state i, then the amplitude that during b the transition to j is made, and finally in c the amplitude that the transition from j to some photon-free state 0 is completed.

The mathematical problem of splitting $g(a,b,c)$ is made definite by the further condition that $g_{ji}(b)$ for given i,j must not involve the coordinates of the particles for times corresponding to regions a or c, $g_{i0}(a)$ must involve those only in region a, and $g_{0j}(c)$ only in c.

To become acquainted with what is involved, suppose first that we do not have a problem involving virtual photons, but just the transition of a one-dimensional Schrödinger particle going in a long time interval from, say, the origin o to the origin o, and ask what states i we shall need for intermediary time intervals. We must solve the problem (1B) where $g(a,b,c)$ is the sum over all trajectories going from o at t' to o at t'' of $\exp iS$ where $S=\int L dt$. The integral may be split into three parts $S=S_a+S_b+S_c$ corresponding to the three ranges of time. Then $\exp(iS)=\exp(iS_c)\cdot\exp(iS_b)\cdot\exp(iS_a)$ and the separation (1B) is accomplished by taking for $g_{i0}(a)$ the sum over all trajectories lying in a from o to some end point x_{t_1} of $\exp(iS_a)$, for $g_{ji}(b)$ the sum over trajectories in b of $\exp(iS_b)$ between end points x_{t_1} and x_{t_2}, and for $g_{0j}(c)$ the sum of $\exp(iS_c)$ over the section of the trajectory lying in c and going from x_{t_2} to o. Then the sum on i and j can be taken to be the integrals on x_{t_1}, x_{t_2} respectively. Hence the various states i can be taken to correspond to particles being at various coordinates x. (Of course any other representation of the states in the sense of Dirac's transformation theory could be used equally well. Which one, whether coordinate, momentum, or energy level representation, is of course just a matter of convenience and we cannot determine that simply from (1B).)

We can consider next the problem including virtual photons. That is, $g(a,b,c)$ now contains an additional factor $\exp(iR)$ where R involves a double integral $\int\int$ over all time. Those parts of the index i which correspond to the particle states can be taken in the same way as though R were absent. We study now the extra complexities in the states produced by splitting the R. Let us first (solely for simplicity of the argument) take the case that there are only two regions a, c separated by time t_0 and try to expand

$$g(a,c)=\Sigma_i\,g_{0i}(c)g_{i0}(a).$$

The factor $\exp(iR)$ involves R as a double integral which can be split into three parts $\int_a\int_a+\int_c\int_c+\int_a\int_c$ for the first of which both t, s are in a, for the second both are in c, for the third one is in a the other in c. Writing $\exp(iR)$ as $\exp(iR_{cc})\cdot\exp(iR_{aa})\cdot\exp(iR_{ac})$ shows that the factors R_{cc} and R_{aa} produce no new problems for they can be taken bodily into $g_{0i}(c)$ and $g_{i0}(a)$ respectively. However, we must disentangle the variables which are mixed up in $\exp(iR_{ac})$.

The expression for R_{ac} is just twice (24) but with the integral on s extending over the range a and that for t extending over c. Thus $\exp(iR_{ac})$ contains the variables for times in a and in c in a quite complicated mixture. Our problem is to write $\exp(iR_{ac})$ as a sum over possibly a vast class of states i of the product of two parts, like $h_i'(c)h_i(a)$, each of which involves the coordinates in one interval alone.

This separation may be made in many different ways, corresponding to various possible representations of the state of the electromagnetic field. We choose a particular one. First we can expand the exponential, $\exp(iR_{ac})$, in a power series, as $\Sigma_n\,i^n(n!)^{-1}(R_{ac})^n$. The states i can therefore be subdivided into subclasses corresponding to an integer n which we can interpret as the number of quanta in the field at time t_0. The amplitude for the case $n=0$ clearly just involves $\exp(iR_{aa})$ and $\exp(iR_{cc})$ in the way that it should if we interpret these as the amplitudes for regions a and c, respectively, of making a transition between a state of zero photons and another state of zero photons.

Next consider the case $n=1$. This implies an additional factor in the transitional element; the factor R_{ac}. The variables are still mixed up. But an easy way to perform the separation suggests itself. Namely, expand the $\delta_+((t-s)^2-(\mathbf{x}_n(t)-\mathbf{x}_m(s))^2)$ in R_{ac} as a Fourier integral as

$$i\int\exp(-ik|t-s|)\exp(-i\mathbf{K}\cdot(\mathbf{x}_n(t)-\mathbf{x}_m(s))d^3\mathbf{K}/4\pi^2k.$$

[22] The formulas for real processes deduced in this way are strictly limited to the case in which the light comes from sources which are originally dark, and that eventually all light emitted is absorbed again. We can only extend it to the case for which these restrictions do not hold by hypothesis, namely, that the details of the scattering process are independent of these characteristics of the light source and of the eventual disposition of the scattered light. The argument of the text gives a method for discovering formulas for real processes when no more than the formula for virtual processes is at hand. But with this method belief in the general validity of the resulting formulas must rest on the physical reasonableness of the above-mentioned hypothesis.

For the exponential can be written immediately as a product of $\exp+i(\mathbf{K}\cdot\mathbf{x}_m(s))$, a function only of coordinates for times s in a (suppose $s<t$), and $\exp-i\mathbf{K}\cdot\mathbf{x}_n(t)$ (a function only of coordinates during interval c). The integral on $d^3\mathbf{K}$ can be symbolized as a sum over states i characterized by the value of $\mathbf{K}$. Thus the state with $n=1$ must be further characterized by specifying a vector $\mathbf{K}$, interpreted as the momentum of the photon. Finally the factor $(1-\mathbf{x}^*_n(t)\cdot\mathbf{x}^*_m(s))$ in R_{ac} is simply the sum of four parts each of which is already split (namely 1, and each of the three components in the vector scalar product). Hence each photon of momentum $\mathbf{K}$ must still be characterized by specifying it as one of four varieties; that is, there are four polarizations.[24] Thus in trying to represent the effect of the past a on the future c we are lead to invent photons of four polarizations and characterized by a propagation vector $\mathbf{K}$.

The term for a given polarization and value of $\mathbf{K}$ (for $n=1$) is clearly just $-\beta_c\beta_a^*$ where the β_a is defined in (59) but with the time integral extending just over region a, while β_c is the same expression with the integration over region c. Hence the amplitude for transition during interval a from a state with no quanta to a state with one in a given state of polarization and momentum is calculated by inclusion of an extra factor $i\beta_a^*$ in the transition element. Absorption in region c corresponds to a factor $i\beta_c$.

We next turn to the case $n=2$. This requires analysis of R_{ac}^2. The δ_+ can be expanded again as a Fourier integral, but for each of the two δ_+ in $\frac{1}{2}R_{ac}^2$ we have a value of $\mathbf{K}$ which may be different. Thus we say, we have two photons, one of momentum $\mathbf{K}$ and one momentum $\mathbf{K}'$ and we sum over all values of $\mathbf{K}$ and $\mathbf{K}'$. (Similarly each photon is characterized by its own independent polarization index.) The factor $\frac{1}{2}$ can be taken into account neatly by asserting that we count each possible pair of photons as constituting just one state at time t_0. Then the $\frac{1}{2}$ arises for the sum over all $\mathbf{K}$, $\mathbf{K}'$ (and polarizations) counts each pair twice. On the other hand, for the terms representing two identical photons ($\mathbf{K}=\mathbf{K}'$) of like polarization, the $\frac{1}{2}$ cannot be so interpreted. Instead we invent the rule that a state of two like photons has statistical weight $\frac{1}{2}$ as great as that calculated as though the photons were different. This, generalized to n identical photons, is the rule of Bose statistics.

The higher values of n offer no problem. The $1/n!$ is interpreted combinatorially for different photons, and as a statistical factor when some are identical. For example, for all n identical one obtains a factor $(n!)^{-1}(-\beta_c\beta_a^*)^n$ so that $(n!)^{-\frac{1}{2}}(i\beta_a^*)^n$ can be interpreted as the amplitude for emission (from no initial photons) of n identical photons, in complete agreement with (61) for G_{m0}.

To obtain the amplitude for transitions in which neither the initial nor the final state is empty of photons we must consider the more general case of the division into three time regions (1B). This time we see that the factor which involves the coordinates in an entangled manner is $\exp i(R_{ab}+R_{bc}+R_{ac})$. It is to be expanded in the form $\Sigma_i\Sigma_j h_i''(c)h_{ij}'(b)h_j(a)$. Again the expansion in power series and development in Fourier series with a polarization sum will solve the problem. Thus the exponential is $\Sigma_r\Sigma_{l_1}\Sigma_{l_2}(iR_{ac})^r(iR_{ab})^{l_1}(iR_{bc})^{l_2}(l_1!)^{-1}(l_2!)^{-1}(r!)^{-1}$. Now the R are written as Fourier series, one of the terms containing l_1+l_2+r variables $\mathbf{K}$. Since l_1+r involve a, l_2+r involve c and l_1+l_2 involve b, this term will give the amplitude that l_1+r photons are emitted during the interval a, of those l_1 are absorbed during b but the remaining r, along with l_2 new ones emitted during b go on to be absorbed during the interval c. We have therefore $n=l_1+r$ photons in the state at time t_1 when b begins, and $m=l_2+r$ at t_2 when b is over. They each are characterized by momentum vectors and polarizations. When these are different the factors $(l_1!)^{-1}(l_2!)^{-1}(r!)^{-1}$ are absorbed combinatorially. When some are equal we must invoke the rule of the statistical weights. For example, suppose all l_1+l_2+r photons are identical. Then $R_{ab}=i\beta_b\beta_a^*$, $R_{bc}=i\beta_c\beta_b^*$, $R_{ac}=i\beta_c\beta_a^*$ so that our sum is

$$\Sigma_{l_1}\Sigma_{l_2}\Sigma_r(l_1!l_2!r!)^{-1}(i\beta_c)^{l_2+r}(i\beta_b)^{l_1}(i\beta_b^*)^{l_2}(i\beta_a^*)^{l_1+r}.$$

Putting $m=l_2+r$, $n=l_1+r$, this is the sum on n and m of

$$(i\beta_c)^m(m!)^{-\frac{1}{2}}[\Sigma_r(m!n!)^{\frac{1}{2}}((m-r)!(n-r)!r!)^{-1}\times(i\beta_b^*)^{m-r}(i\beta_b)^{n-r}](n!)^{-\frac{1}{2}}(i\beta_a^*)^n.$$

The last factor we have seen is the amplitude for emission of n photons during interval a, while the first factor is the amplitude for absorption of m during c. The sum is therefore the factor for transition from n to m identical photons, in accordance with (57). We see the significance of the simple generating function (56).

We have therefore found rules for real photons in terms of those for virtual. The real photons are a way of representing and keeping track of those aspects of the past behavior which may influence the future.

If one starts from a theory involving an arbitrary modification of the direct interaction δ_+ (or in more general situations) it is possible in this way to discover what kinds of states and physical entities will be involved if one tries to represent in the present all the information needed to predict the future. With the Hamiltonian method, which begins by assuming such a representation, it is difficult to suggest modifications of a general kind, for one cannot formulate the problem without having a complete representation of the characteristics of the intermediate states, the particles involved in interaction, etc. It is quite possible (in the author's opinion, it is very likely) that we may discover that in nature the relation of past and future is so intimate for short durations that no simple representation of a present may exist. In such a case a theory could not find expression in Hamiltonian form.

An exactly similar analysis can be made just as easily starting with the general forms (46), (48). Also a coordinate representation of the photons could have been used instead of the familiar momentum one. One can deduce the rules (60), (61). Nothing essentially different is involved physically, however, so we shall not pursue the subject further here. Since they imply[23] all the rules for real photons, Eqs. (46), (47), (48) constitute a compact statement of all the laws of quantum electrodynamics. But they give divergent results. Can the result *after* charge and mass renormalization also be expressed to all orders in $e^2/\hbar c$ in a simple way?

APPENDIX C. DIFFERENTIAL EQUATION FOR ELECTRON PROPAGATION

An attempt has been made to find a differential wave equation for the propagation of an electron interacting with itself, analogous to the Dirac equation, but containing terms representing the self-action. Neglecting all effects of closed loops, one such equation has been found, but not much has been done with it. It is reported here for whatever value it may have.

An electron acting upon itself is, from one point of view, a complex system of a particle and a field of an indefinite number of photons. To find a differential law of propagation of such a system we must ask first what quantities known at one instant will permit the calculation of these same quantities an instant later. Clearly, a knowledge of the position of the particle is not enough. We should need to specify: (1) the amplitude that the electron is at x and there are no photons in the field, (2) the amplitude the electron is at x and there is one photon of such and such a kind in the field, (3) the amplitude there are two photons, etc. That is, a series of functions of ever increasing numbers of variables. Following this view, we shall be led to the wave equation of the theory of second quantization.

We may also take a different view. Suppose we know a quantity $\Phi_e 2[B, x]$, a spinor function of x_μ, and functional of $B_\mu(1)$, defined as the amplitude that an electron arrives at x_μ with no photon in the field when it moves in an arbitrary external unquantized potential $B_\mu(1)$. We allow the electron also to interact with itself,

[24] Usually only two polarizations transverse to the propagation vector $\mathbf{K}$ are used. This can be accomplished by a further rearrangement of terms corresponding to the reverse of the steps leading from (17) to (19). We omit the details here as it is well-known that either formulation gives the same results. See II, Section 8.

but $\Phi_e 2$ is the amplitude at a given instant that there happens to be no photons present. As we have seen, a complete knowledge of this functional will also tell us the amplitude that the electron arrives at x and there is just one photon, of form $A_\mu^{PH}(1)$ present. It is, from (60), $\int(\delta\Phi_e 2[B,x]/\delta B_\mu(1))A_\mu^{PH}(1)d\tau_1$.

Higher numbers of photons correspond to higher functional derivatives of $\Phi_e 2$. Therefore, $\Phi_e 2[B,x]$ contains all the information requisite for describing the state of the electron-photon system, and we may expect to find a differential equation for it. Actually it satisfies ($\nabla=\gamma_\mu\partial/\partial x_\mu$, $B=\gamma_\mu B_\mu$),

$$(i\nabla-m)\Phi_e 2[B,x]=B(x)\Phi_e 2[B,x]+ie^2\gamma_\mu\int\delta_+(s_{x1}^2)(\delta\Phi_e 2[B,x]/\delta B_\mu(1))d\tau_1 \quad (1C)$$

as may be seen from a physical argument.[25] The operator $(i\nabla-m)$ operating on the x coordinate of $\Phi_e 2$ should equal, from Dirac's equation, the changes in $\Phi_e 2$ as we go from one position x to a neighboring position due to the action of vector potentials. The term $B(x)\Phi_e 2$ is the effect of the external potential. But $\Phi_e 2$ may also change for at the first position x we may have had a photon present (amplitude that it was emitted at another point 1 is $\delta\Phi_e 2/\delta B_\mu(1)$) which was absorbed at x (amplitude photon released at 1 gets to x is $\delta_+(s_{x1}^2)$ where s_{x1}^2 is the squared invariant distance from 1 to x) acting as a vector potential there (factor γ_μ). Effects of vacuum polarization are left out.

Expansion of the solution of (1C) in a power series in B and e^2 starting from a free particle solution for a single electron, produces a series of terms which agree with the rules of II for action of potentials and virtual photons to various orders. It is another matter to use such an equation for the practical solution of a problem to all orders in e^2. It might be possible to represent the self-energy problem as the variational problem for m, stemming from (1C). The δ_+ will first have to be modified to obtain a convergent result.

We are not in need of the general solution of (1C). (In fact, we have it in (46), (48) in terms of the solution $T_0[B]=\Phi_0[B,x]$ of the ordinary Dirac equation $(i\nabla-m)\Phi_0[B,x]=B\Phi_0[B,x]$. The general solution is too complicated, for complete knowledge of the motion of a self-acting electron in an arbitrary potential is essentially all of electrodynamics (because of the kind of relation of real and virtual processes discussed for photons in Appendix B, extended also to real and virtual pairs). Furthermore, it is easy to see that other quantities also satisfy (1C). Consider a system of many electrons, and single out some one for consideration, supposing all the others go from some definite initial state i to some definite final state f. Let $\Phi_e 2[B,x]$ be the amplitude that the special electron arrives at x, there are no photons present, and the other electrons go from i to f when there is an external potential B_μ present (which B_μ also acts on the other electrons). Then $\Phi_e 2$ also satisfies (1C). Likewise the amplitude with closed loops (all other electrons go vacuum to vacuum) also satisfies (1C) including all vacuum polarization effects. The various problems correspond to different assumptions as to the dependence of $\Phi_e 2[B,x]$ on B_μ in the limit of zero e^2. The Eq. (1C) without further boundary conditions is probably too general to be useful.

[25] Its general validity can also be demonstrated mathematically from (45). The amplitude for arriving at x with no photons in the field with virtual photon coupling e^2 is a transition amplitude. It must, therefore, satisfy (45) with $T_e 2[B]=\Phi_e 2[B,x]$ for any x. Hence show that the quantity

$$C_e 2[B,x]=(i\nabla-m-B(x))\Phi_e 2[B,x]-ie^2\gamma_\mu\int\delta_+(s_{x1}^2)(\delta\Phi_e 2[B,x]/\delta B_\mu(1))d\tau_1$$

also satisfies Eq. (45) by substituting $C_e 2[B,x]$ for $T_e 2[B]$ in (45) and using the fact that $\Phi_e 2[B,x]$ satisfies (45). Hence if $C_0[B,x]=0$ then $C_e 2[B,x]=0$ for all e^2. But $C_e 2[B,x]=0$ means that $\Phi_e 2[B,x]$ satisfies (1C). Therefore, that solution $\Phi_e^2[B,x]$ of (45) which also satisfies $(i\nabla-m-B(x))\Phi_0[B,x]=0$ (the propagation of a free electron without virtual photons) is a solution of (1C) as we wished to show. Equation (1C) may be more convenient than (45) for some purposes for it does not involve differentiation with respect to the coupling constant, and is more analogous to a wave equation.

PHYSICAL REVIEW VOLUME 80, NUMBER 3 NOVEMBER 1, 1950

On the Ordering Effect of Antiferromagnetism

YIN-YUAN LI
Department of Physics, University of Illinois, Urbana, Illinois

(Received June 19, 1950)

It is shown with the Heisenberg model that in general the Curie temperature of antiferromagnetism depends on the external field. It is also predicted that when an antiferromagnetic crystal with face-centered cubic or close-packed hexagonal magnetic lattice is kept at sufficiently low temperatures, its neutron diffraction pattern should show a transition from that due to an order of the $\alpha\beta$-type to that of the $\alpha\beta_3$-type as the applied field is greatly increased. When the Ising model is assumed, a quasichemical statistical theory shows that a latent heat and sudden disappearance of the neutron diffraction pattern should be observed in the antiferromagnetic transition of a face-centered cubic magnetic lattice. However, this cannot be predicted with assurance, since the Ising model is not reliable.

THE effect of antiferromagnetism[1] was recently shown by Shull and Smart[2] using the new technique of neutron diffraction in the same manner as the x-ray diffraction pattern of alloys revealing the order-disorder effect. The physical characteristics of the antiferromagnetic effect and of the atomic ordering effect in alloys are so closely parallel[3] that we shall be able to say much concerning the former effect by drawing an analogy with the well-developed theory of the latter. In treating either problem we may consider the lattice structure[4] as made up of two or more sets of

[1] See the review article J. H. Van Vleck, Rev. Mod. Phys. 17, 45 (1945).

[2] C. G. Shull and J. S. Smart, Phys. Rev. 76, 1256 (1949).

[3] Peierls first pointed out the close analogy between ferromagnetism and the order-disorder problem of adsorption. See R. Peierls, Proc. Camb. Phil. Soc. 32, 477 (1936).

[4] In this paper the term *lattice* spoken of in connection with the antiferromagnetic effect usually does not mean the crystal lattice. Shull and Smart proved by the neutron diffraction method that in MnO only Mn atoms take part in the spin ordering effect. This should be a common feature for antiferromagnetic salts. The face-centered cubic lattice of Mn^{++} in MnO is what we must consider, though MnO crystallizes in a simple cubic structure of NaCl type. The lattice of the antiferromagnets in a crystal will be referred as *magnetic lattice.*

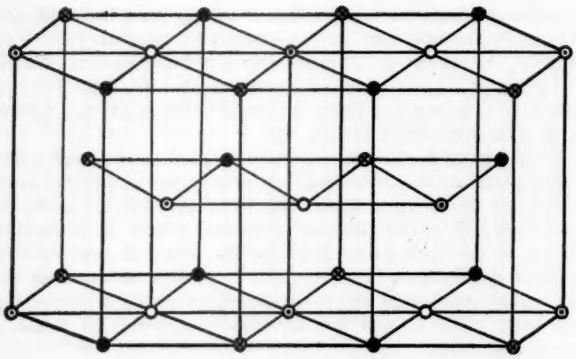

FIG. 1. The decomposition of a close-packed hexagonal lattice into four sub-lattices as described in the text. The sites on different sub-lattices are represented by different symbols. *The symbol ● in the second layer should be replaced by ⊗ and vice versa.*

interpenetrating sub-lattices. In the present problem the spin interaction is given by

$$V=-2J\sum_{l\neq m}\mathbf{S}_l\cdot\mathbf{S}_m-(eh/2\pi mc)\sum_l\mathbf{S}_l\cdot\mathbf{H}, \qquad (1)$$

where J is the exchange integral, being negative for the case of antiferromagnetism, $\mathbf{S}_l$ the electronic spin of the lth atom, and $\mathbf{H}$ the intensity of the applied field. As usual, the first summation is only taken over the nearest atoms.

Van Vleck[5] has applied the Weiss-Heisenberg method of ferromagnetism to the problem of antiferromagnetism. His treatment was limited to the cases of simple cubic and body-centered cubic structures. In the face-centered cubic or close-packed hexagonal lattice some of the nearest neighbors of a given atom are nearest neighbors between themselves and a theoretical treatment must consider at least more than two sets of sub-lattices. As shown in the literature,[6] the face-centered cubic lattice can be decomposed into four simple cubic sub-lattices. This conventional decomposition is quite reasonable and has shown its usefulness in many other problems. Similarly, a close-packed hexagonal lattice may be considered as a composition of four sub-lattices as shown in Fig. 1. In both cases none of the twelve neighbors are found on the same sub-lattice as the central atom and four of them are found on each one of the other three sub-lattices. The situation becomes more complicated than that considered by Van Vleck using two sets of sub-lattices. We shall use the parameter σ to stand for $\mathbf{S}/S$, where $\mathbf{S}$ is the (average) spin per atom in the whole system and S is the spin quantum number of the atom. Similarly, we use σ_i for the corresponding quantity of the ith sub-lattice. Evidently these quantities are connected by the relation

$$\sum r_i\sigma_i=\sigma, \qquad (2)$$

if Nr_i is the number of atomic sites contained in the ith sub-lattice, with N being the total number of the sites in the whole lattice. For both of the particular example presented above we have $i=1,2,3,4$, and $r_i=\frac{1}{4}$. A negas tive exchange integral requires $\sigma=0$ when no external field is applied, but the σ_i's do not *all* vanish when the temperature is below a certain Curie point: this effect is usually called *spontaneous* antiferromagnetism. With non-vanishing external field strength $\sigma\neq 0$ and at sufficiently low temperatures the σ_i's do not equal σ, since they tend to interlock themselves. A minimization of the energy (1) with a certain value of σ gives the equilibrium state at very low temperatures. Therefore, we can obtain the equilibrium state simply by seeking the arrangement of spins which contains for a given value of σ the largest number of antiparallel pairs of nearest neighbors. When $\sigma=0$ (i.e., at $\mathbf{H}=0$), the equilibrium state is $\sigma_1=\sigma_3=1$ and $\sigma_2=\sigma_4=-1$ (all σ_i's in a certain direction); i.e., at the absolute zero of temperature and in the absence of an applied field the four sub-lattices group into two equal sets, one with all spins parallel to a certain direction and the other with all spins antiparallel. With the increasing of the applied field σ increases from zero to unity. When $\sigma=\frac{1}{2}$, the stable state is $\sigma_1=\sigma_2=\sigma_3=1$ and $\sigma_4=-1$; i.e., all spins in three sub-lattices are parallel and all those in the other are antiparallel to a certain direction. Beside these two *most* ordered states we have $\sigma_1=\sigma_3=1$ and $\sigma_2=\sigma_4=2\sigma-1$ as the stable state for small σ, and $\sigma_1=\sigma_2=\sigma_3\neq\sigma_4$ for the values of σ lying in a certain region around $\frac{1}{2}$. (We shall call the state $\sigma_1=\sigma_3\neq\sigma_2=\sigma_4$ the $\alpha\beta$-structure and the state $\sigma_1=\sigma_2=\sigma_3\neq\sigma_4$ the $\alpha\beta_3$-structure.) The first *most* ordered state corresponds to ordered alloys such as $\frac{1}{2}$Au$\frac{1}{2}$Cu (slightly tetragonal) and the latter corresponds to $\frac{1}{4}$Au$\frac{3}{4}$Cu (cubic) or $\frac{1}{4}$Cd$\frac{3}{4}$Mg (hexagonal). We may conclude that *when an antiferromagnetic crystal with face-centered cubic (or close-packed hexagonal) magnetic lattices is kept at sufficiently low temperatures, the neutron diffraction pattern should gradually change from that of an order of $\alpha\beta$-type to that of $\alpha\beta_3$-type as the applied field is greatly increased.* Without a quantitative analysis we can only predict the following details. As the applied field increases from zero, the intensity of the $\alpha\beta$-superstructure lines becomes weaker with stronger background until the lines fade away. As σ approaches $\frac{1}{2}$, the $\alpha\beta_3$-superstructure lines begin to appear; their intensity reaches a maximum when $\sigma=\frac{1}{2}$ and then gradually fades out as $\mathbf{H}$ increases. Between $\sigma=0$ and $\frac{1}{2}$ there may exist a completely disordered region where no diffraction pattern of either group can be observed; i.e., as $\mathbf{H}$ increases strongly, the $\alpha\beta$-lines may disappear before the emerging of the $\alpha\beta_3$-lines. If the two-phase equilibrium gives a lower *free energy* than either a pure $\alpha\beta$- or $\alpha\beta_3$-structure, both the two sets of lines will show up simultaneously in this intermediate region, indicating the coexistence of both the ordered phases in different domains. Since the susceptibility of antiferromagnetic crystals is only about 10^{-4} per gram, an applied field of the order of 10^5 gauss

[5] J. H. Van Vleck, J. Chem. Phys. **9**, 85 (1941). For earlier works see L. Néel, Ann. de Physique **17**, 64 (1932); **5**, 256 (1936) and F. Bitter, Phys. Rev. **54**, 79 (1937).

[6] See Fig. 27 of F. C. Nix and W. Shockley, Rev. Mod. Phys. **10**, 1 (1938).

must be used to *complete* this transition. However, a gradual transition should be observable even with a much lower applied field. The phenomenon of a transition of the neutron diffraction pattern may also occur for antiferromagnetic crystals with magnetic lattice more complicated than the face-centered cubic and the close-packed hexagonal ones.

The same effect of the applied field not only brings the spins of the whole crystal leaning to a certain orientation but must also hinder the antiparallel interlock between the spins on one sub-lattice and those on another sub-lattice. This means that the Curie temperature must decrease when **H** increases from zero. In order to render this clear we draw an analogy with the theory of atomic order-disorder: in correspondence to the order parameters and the atomic ratio in the theory of atomic superstructure[7] we define $\theta_i=\frac{1}{2}(1-\sigma_i)$ and $\theta=\frac{1}{2}(1-\sigma)$. (Equation (2) becomes $\sum_i r_i\theta_i=\theta$ and $\theta=\frac{1}{2}$ when $\mathbf{H}=0$.) The only difference between these two problems is that the variables here are vectors which in the theory of atomic order are scalars. Both experimental and theoretical findings have shown that the order-disorder Curie temperature[8] depends remarkably on the atomic ratio and the Curie temperature always has a maximum at $\theta=\frac{1}{2}$. Actually Squire[9] did observe the decreasing of the antiferromagnetic Curie temperature T_c with the increase of **H** a few years ago. In Fig. 4 of his paper we can see that T_c of MnSe decreases steadily from ca. 166°K to ca. 160°K when **H** increases from 3 gauss to 10 gauss. No attention has been paid to this fact. One might doubt this evidence because only three sets of data with different values of H were recorded by Squire, and there might have been a lag between the temperature of the specimen and that of the thermocouple. This issue could be certainly decided by neutron diffraction experiments. In passing we should mention that Eq. (9) of Van Vleck's paper[5] implies that the Curie temperature of antiferromagnetic transition must be a function of the applied field strength.

We should mention that the validity of the conclusions reached above is subject to the imperfection of the Heisenberg model adopted in our considerations. It is quite possible that the effects of electron migration are appreciable. We also have neglected all other factors of influence such as the thermal vibrations, the change of atomic space with the applied field, etc. Evidently a quantitative analysis of the present theory would not produce results worth the labor involved.

The difference between the theories of spontaneous antiferromagnetism and the superstructure in alloys shrinks to a mere change of notation when the Ising model of magnetism is assumed. In this model the spin

[7] See C. N. Yang and Y. Y. Li, Chinese J. Phys. **7**, 59 (1947); Y. Y. Li, J. Chem. Phys. **17**, 447 (1949). The latter will be referred as reference 1.

[8] See E. E. Easthope, Proc. Camb. Phil. Soc. **33**, 502 (1937). Also reference 1.

[9] C. F. Squire, Phys. Rev. **56**, 922 (1939).

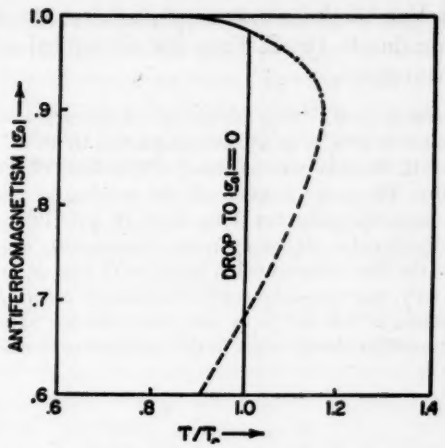

FIG. 2. The degree of antiferromagnetism $\sigma_0=\sigma_1-\sigma_2$ *vs.* temperature curve obtained with the Ising model and quasichemical statistics.

stable metastable unstable

The degree of antiferromagnetism does not drop appreciably until T becomes higher than 0.8 T_c.

per atom is oriented either parallel or antiparallel to a specified direction; i.e., the vector spin is replaced by a scalar. The theory of order for the copper-gold alloy system has been developed to such a stage that the predicted phase diagram and type of transition agree very well with the experimental findings (see reference 1). Figure 2 is taken from reference 1 by substituting v of reference 1 by $|J|$.[10] The transition is of the first order occurring at $T_c=0.7306|J|/k$, and the spontaneous ($\mathbf{H}=0$) antiferromagnetism drops from 0.893 to zero at the transition, releasing a latent heat $Q=0.228|J|$ per mole. These figures evidently cannot be used for even a semiquantitative prediction of the effect of antiferromagnetism. The properties of the Ising model are rather far from those of the true antiferromagnet, although the two have some characteristics in common. The only purpose in giving Fig. 2 here is to show that it should not be a surprise if a latent heat and a sudden vanishing of the neutron diffraction pattern were to be observed during the experimental investigation of antiferromagnetism of more complicated crystalline structure when the temperature passes through a certain point. This transition does not involve a change of crystal structure.

The author is deeply indebted to Professors F. Seitz

[10] Analogously to Eq. (26) of reference 1, the distribution function for the present problem with $S=\frac{1}{2}$ and zero applied field is

$$\varphi=X^{\frac{1}{2}}+2(\mu_1+\mu_2)+(\mu_1^2+\mu_2^2+4\mu_1\mu_2)X^{-\frac{1}{2}}+2\mu_1\mu_2(\mu_1+\mu_2)+\mu_1^2\mu_2^2X^{\frac{1}{2}},$$

where $X=\exp 2J/kT$. When we substitute μ_1 and μ_2 respectively with $\mu_1X^{\frac{1}{2}}$ and $\mu_2X^{\frac{1}{2}}$, we have

$$\varphi=X^{\frac{1}{2}}[1+2(\mu_1+\mu_2)+(\mu_1^2+\mu_2^2+4\mu_1\mu_2)X+2\mu_1\mu_2(\mu_1+\mu_2)X^2+\mu_1^2\mu_2^2X^3].$$

This transformation of the parameter μ's does not change the form of the equations which relate μ's to θ_1, θ_2, and T, but render the whole problem identical to that of the order-disorder of $\frac{1}{2}$Au$\frac{1}{2}$Cu if we identify $|J|$ with v there.

and J. H. Van Vleck for their helpful advice. My sincere thanks are due to Dr. F. Fumi for his critical reading of the manuscript.

Notes added in proof.—After this article was submitted for publication, a series of articles on antiferromagnetism by P. W. Anderson and G. H. Wannier was published (Phys. Rev. **79**, 350; 357; 705 (1950)). The exact solution of the problem of antiferromagnetic Ising triangular net (Phys. Rev. **79**, 357 (1950)) shows that it is disordered at all temperatures. Consequently it is speculated that the face-centered cubic lattice, with nearest exchange couplings only, may not sustain antiferromagnetic ordering. However, as shown in this article by the quasi-chemical approximation the transition should occur in the face-centered cubic lattice of Ising spins and is one *of the first order*. These results will not be disproved when an exact solution of the same problem is carried out. We also learned that C. G. Shull has found a rather unexpected ordering of Mn^{++} in MnO: Each of the four simple cubic sub-lattices is arranged antiferromagnetically within itself, while the sub-lattices are either completely uncorrelated, or are correlated in such a way that the spins in a set of (111) planes are all parallel (Phys. Rev. **79**, 350 (1950)). This indicates that instead of the direct exchange force the most effective (not necessarily the strongest) force is that between the next-nearest neighboring Mn^{++} ions which are separated by an 0^{--} ion. If we consider the so-called superexchange interaction instead of the nearest interaction, we surely get the observed pattern (with the sub-lattices completely uncorrelated). However, the assumption is again an over-simplified one.

PHYSICAL REVIEW VOLUME 80, NUMBER 3 NOVEMBER 1, 1950

The Irreducible Volume Character of Events. I. A Theory of the Elementary Particles and of Fundamental Length*†

B. T. DARLING
Mendenhall Laboratory of Physics, Ohio State University, Columbus, Ohio
(Received January 31, 1950)

In this series of papers a theory of elementary particles is presented based on the postulates that the elementary particles are a material process and that with every such process there is associated an inherent irreducible volume of space-time. The equations of motion are obtained from the wave equations of Dirac, Maxwell, etc., through a two-step correspondence principle consisting of replacing these equations by self-adjoint partial difference equations and then integrating these over the group manifold of the closed real orthogonal group G in four-dimensional space. This introduces a new fundamental constant of the dimensions of a length, the difference step ω. The resulting equations are relativistically invariant integro-difference equations in a complex four-dimensional space. They give a quantized mass spectrum when ω is purely imaginary. This paper treats only the Dirac equation. Section 1 sketches the basic physical ideas from which we work. Section 2 carries out the mathematical realization of the ideas of Section 1, obtains the fundamental integro-difference equation (2.2) for spin ½ processes, points out that space is a four-dimensional *complex* continuum, and defines the *dynasphere*. Section 3 transforms the integro-difference equation into an equivalent partial differential equation of infinite order (3.10). The operator functions in (3.10) are the Bessel functions $J_1(z)$ and $J_2(z)$ when the radius ($i\omega$) of the dynasphere is purely imaginary. Section 4 gives the general solution of (3.10) and deduces the mass quantization condition. In keeping with our basic postulates all elementary charged particles of spin ½ must be embraced by this mass quantization condition which is the case for the electron, proton, and μ-meson (predicted mass 218.76 e.m.u. [electron mass units]) with the fundamental length $\omega=4.538\times10^{-13}$ cm (one-half percent larger than the classical electron diameter). This possibility is due to the rather remarkable properties of the mass quantization condition (4.4). There is an infinite number of roots not uniformly spaced and indeed not uniformly non-uniform in this respect: first there is one *very* small positive root which gives the electron; the next positive root reaches way out to give on a mass scale the μ-meson at 218 e.m.u.; the distance on the mass scale to the next root suffers a sudden drop to 139 e.m.u., the spacing thereafter dropping uniformly to the asymptotic value of 133.69 e.m.u. The proton is the thirteenth in the series. Table I of this section lists the first sixteen masses. All of these particles have the same magnitude of electronic charge since they are just different states of the same matter equation. Section 5 gives two alternatives for the neutral particles. In one we simply set the charge to zero and obtain one zero mass particle and an infinite number close in mass to those of the charged particles (the electron excluded). In the other we further change to a real radius for the dynasphere, in which case we have only one real zero mass. On this alternative we have only one elementary neutral particle of spin ½—the neutrino—and (combined with Section 4) the only elementary particles with non-vanishing rest mass are charged (and conversely), the universality of charge being simply identified with the existence of the particle. Since there is no neutral particle between the neutrino and the μ-meson on either alternative we can predict that the μ^0-particle postulated by Tiomno and Wheeler for the decay of the μ-meson must be a neutrino, that is, $\mu\rightarrow e+2\nu$.

INTRODUCTION

THE wave mechanics corresponds to classical mechanics through an alteration of the kinetic energy by the replacement $p\rightarrow-i\hbar\partial/\partial q$. A new fundamental constant is thereby introduced. In the limit $h\rightarrow0$, the new mechanics reduces to the old. We here propose a further generalization of the nature of a

* The expression, "The Volume Character of Events," is adopted by permission from R. D. Carmichael's 1932 notes on "A Tensor Theory (in the difference calculus) for Atomic Phenomena." His ideas were in somewhat the same direction as my own independent efforts initiated in 1934 on a difference geometry. The present theory, contrary to those efforts, places the volume character of events in the phenomenological process rather than in the geometry of space.

† To meet space limitations, this paper is a condensed version of two papers originally submitted. Those interested in more detail may obtain copies of the two original papers by writing the Department of Physics at the Ohio State University. Revised manuscript received July 19, 1950.

correspondence principle. We replace any of the wave equations such as Maxwell's, Dirac's, Proca's, etc., by self-adjoint difference equations involving a new constant of the dimensions of a length, the difference step ω, and then average over the four-dimensional rotation group. The new equations are relativistically invariant and reduce in the limit $\omega \to 0$ to the original wave equations. These equations with ω purely imaginary lead to a quantized mass spectrum. In this paper we confine our attention to the Dirac equation. The resulting Eq. (2.2) with imaginary ω, or equivalently (3.10), is assumed to describe all elementary charged particles of spin $\frac{1}{2}$ including in particular the electron, μ-meson, and proton.

Born[1] has proposed a method of quantization of mass according to different spin, but in his case the electron and proton are treated as exceptional and on a different footing from his quantization method. Heisenberg[2] has advocated a fundamental length and inferred its connection to the quantization of mass. Blokhinzev[3] has considered wave fields with a spectrum of masses. The development presented in this paper is more related to the work of Heisenberg and Blokhinzev than to that of Born. Section 1 points out that we do not consider space to be quantized as is proposed by Snyder, Flint, and others,[4] nor discrete as is proposed by Schild.[5]

1. THE IRREDUCIBLE VOLUME CHARACTER OF EVENTS

The guiding principle which we shall use throughout these papers is the following. Creation, continued existence, and annihilation of particles are considered as aspects of a material process.[6] This material process—through which a transformation from non-particle (field) to particle occurs—is governed by the *same* structure whether the transformation involves the creation of one or of several particles (of same or of different natures), or of their motion in continued existence. The individual particle is not a permanently existing "thing in itself," but its mode of existence is in material process.[7] Next we assume that this material process requires a volume in space-time that cannot be reduced to zero; that is, with every process is associated an inherent irreducible volume. This "volume" is not a property of space as such, for example, we do not assume that space is discrete; on the contrary, we shall give reasons for believing that space forms a continuum. The "volume" character will be imposed on the laws (equations of motion) of the process rather than on the associated space; however, some of the properties of space will need to be extended to accommodate the volume character of events.

In keeping with the above guiding principle we first consider the motion in continued existence of a free particle. With the exception of the properties of spin, three relations stand at the basis of the quantum theory of a "free" particle:

(1) The Einstein equation $E^2/c^2 - p^2 = m^2c^2$.
(2) The de Broglie equation $\lambda = h/p$ together with $(E = h\nu)$.
(3) The wave function $\psi = \exp(i\mathbf{p}\cdot\mathbf{r}/\hbar)$ together with the identification

$$p_x = -i\hbar\partial/\partial x \cdots, \quad p_0 = i\hbar\partial/\partial x_0$$

where $x_0 = ct$ and $p_0 = E/c$.

Arguments can be given that these relations should be preserved and consequently we assume *that the relations (1) to (3) are valid without restriction. The energy and momentum then are the characteristic values of the corresponding operators, and the rest mass the characteristic value of the operator obtained from the relation (1).*

The operators of momentum and energy are the operators corresponding to infinitesimal displacements parallel to the axes. In consequence, we are forced to assume that space is continuous and not discrete like a lattice. If further we wish to be consistent with the requirement of relativistic invariance, we must also exclude a "lattice" space.[5] It seems clear that space is infinitely divisible.

We reach the conclusion (mentioned above) that the volume character of events manifests itself in the dynamical equations specifying the motion. Let us consider a single "free" electron which we shall for the moment picture as a small sphere. Any infinitesimal displacement of this electron is possible and classically we may picture its motion taking place in this way (or via the operators of momentum and energy) *so long as we are concerned only with the individual particle aspect of the process.* Now consider the opposite aspect of the process—the field aspect. Here we see that there must be something to take account of the "impenetrability" of our spherical electrons. Taking one sphere in an arbitrarily chosen position, we can surround it with others whose centers can be as close but no closer than their diameters. Hence, from any arbitrary position, the dynamical law must relate to positions a diameter away. The dynamical law ceases to be a differential law and becomes a law expressible in the difference calculus.

[1] M. Born, Rev. Mod. Phys. **21**, 463 (1949).
[2] W. Heisenberg, Ann. d. Physik **32**, 20 (1938); Zeits. f. Physik **110**, 251 (1938), **120**, 513, 673 (1942–43).
[3] D. Blokhinzev, J. Phys. USSR **11**, 72 (1947).
[4] H. S. Snyder, Phys. Rev. **71**, 38 (1947); H. T. Flint, Phys. Rev. **74**, 209 (1948), Nature **163**, 131 (1949).
[5] A. Schild, Can. J. Math. **1**, 29 (1949).
[6] For example, the Dirac equation used in the usual manner to obtain the behavior of an electron in an external electromagnetic field illustrates the individual particle aspect of motion in continued existence, whereas the same equation with second quantization illustrates the many particle or field aspect embracing as it does the creation and annihilation of particles. The originally submitted papers contained an analysis of the particle concept (classical and quantum) leading up to the above principle as well as some elaboration on its meaning.
[7] The elementary particles are mutable. The very way, for example, an electron exists is through this possibility of change. Consequently, the great stability and seeming immutability of electrons and protons, etc., must *not* be assumed but must be explained. It would seem that the Poincaré stresses do not offer such an explanation since then the particle would be absolutely immutable.

We now drop our appeal to spherical electrons and retain only the essence of the requirement—namely, *the fundamental dynamical law must be expressed by means of finite difference equations* (taken in their analytical sense, e.g., as treated by Nörlund[8] where the functions must be analytic functions of a continuous variable).[9] Relativistic invariance forces us a step further, i.e., into integro difference equations, so that *the basic laws of motion will be expressible as integro-difference equations*. When we replace the differential laws by appropriate difference laws, we carry over the "spin" structure of the equations unchanged so that in the limit when our "fundamental" length approaches zero, we just obtain the usual differential laws.

2. THE FUNDAMENTAL INTEGRO-DIFFERENCE EQUATION FOR SPIN ½ PROCESSES; THE COMPLEX CHARACTER OF SPACE

We generalize from the wave mechanical equations in a two-step process. First we replace the differential equations by self-adjoint difference equations.[10] This involves introducing a new fundamental quantity, the difference step ω. These equations are not relativistically invariant. In order to recoup this property we then average these difference equations over the four-dimensional rotation group G (not the Lorentz group Γ which cannot be used since it is not closed). The result is invariant under the Lorentz group because of the intimate connection between the two groups.[11]

Applying this procedure to the Dirac equation in the form given by Pauli[12] we obtain from the first step the self-adjoint difference equation[13]

$$\{\gamma_\lambda \Delta_\lambda \nabla_\lambda + \kappa \nabla\}\psi = 0$$

in which $\kappa = mc/h$, λ runs from 1 to 4 with $x_4 = ix_0 = ict$, and the other symbols have the following definitions:

$$\Delta_\lambda \psi = [\psi(x_\lambda + \Delta x_\lambda) - \psi(x_\lambda - \Delta x_\lambda)]/2\Delta x_\lambda$$
$$_\lambda\nabla\psi = [\psi(x_\lambda + \Delta x_\lambda) + \psi(x_\lambda - \Delta x_\lambda)]/2,$$

where we have indicated only the altered variable, the others being held fixed, and

$$\nabla\psi = \prod_{\beta=1}^{4} {}_\beta\nabla\psi = {}_1\nabla {}_2\nabla {}_3\nabla {}_4\nabla\psi$$

$$\nabla_\lambda\psi = \prod_{\beta\neq\lambda} {}_\beta\nabla\psi \quad \text{or} \quad \nabla_1\psi = {}_2\nabla {}_3\nabla {}_4\nabla\psi \quad \text{etc.}$$

In the next step we choose any point of space (x_λ) and with this as origin set up a rotating set of axes (denoted by a prime) along which we make our displacements $\Delta x_\lambda'$. If $(r_{\lambda\sigma})$ is an element of the rotation group G connecting the primed to the unprimed axes, we have

$$\Delta x_\sigma = r_{\lambda\sigma}\Delta x_\lambda'$$
$$\gamma_\lambda' = r_{\lambda\sigma}\gamma_\sigma,$$

summation over repeated index understood. But we do *not* transform the space x_σ; the point x_σ serves only as the origin from which we make our displacements. Thus, for example,

$$\Delta_2'\psi(x_1x_2x_3x_4) = [\psi(x_1 + r_{21}\Delta x_2',\ x_2 + r_{22}\Delta x_2',\ x_3 + r_{23}\Delta x_2',\ x_4 + r_{24}\Delta x_2')$$
$$- \psi(x_1 - r_{21}\Delta x_2',\ x_2 - r_{22}\Delta x_2',\ x_3 - r_{23}\Delta x_2',\ x_4 - r_{24}\Delta x_2')]/2\Delta x_2' \quad (2.1)$$

and similarly for the other partial operations. It is apparent that we always refer our displacement in the primed system back to the unprimed system since the function $\psi(x)$ is specified in this system. The difference equations in all the primed systems must be formed identically to one another; hence in the primed system the displacement vectors along the axes must be constants independent of $r_{\lambda\sigma}$:

$$\Delta x_1' : (\omega_1,\ 0,\ 0,\ 0)$$
$$\Delta x_2' : (0,\ \omega_2,\ 0,\ 0)$$
$$\Delta x_3' : (0,\ 0,\ \omega_3,\ 0)$$
$$\Delta x_4' : (0,\ 0,\ 0,\ \omega_4),$$

the ω_λ being constants. But there are operations of the group G which will interchange any pair of the primed axes so that if we are to have a unique displacement for any axis we must set $\omega_1 = \omega_2 = \omega_3 = \omega_4$. For the time being let this common value be denoted by ω.

Since ψ is analytic it has a Taylor expansion and we

[8] N. E. Nörlund, *Vorlesungen Über Differenzenrechnung* (J. W. Edwards, Ann Arbor, 1945).

[9] The entrance of a "fundamental" length into the equations of motion of a single individual is incomprehensible, but becomes understandable in the field aspect on the basis we have explained here. In view of the above statements we expect the magnitude of the difference step ω entering the difference equations to be equal to the classical electron diameter.

[10] The original papers contain a development of the theory of self-adjoint partial difference equations and the transcription of the Dirac, Maxwell, and Proca equations as such. A Green's theorem for partial difference equations and finite integration (and playing the same role as the usual Green's theorem for partial differential equations) exists; the equations of physics (as difference equations) can be obtained from a Lagrange expression by variation; the appropriate current densities satisfy a generalized type of continuity theorem. None of this material can be found elsewhere; in fact there is very little literature even on partial difference equations.

[11] For the relation of Γ to G consult, for example, Francis D. Murnaghan, *The Theory of Group Representations* (Johns Hopkins Press, Baltimore, 1938). This book also gives a thorough treatment of the theory of integration over a group manifold. In this latter connection one should also consult E. Wigner, *Gruppentheorie und ihre Anwendung auf die Quanten Mechanic der Atomspektren*, (J. W. Edwards, Ann Arbor, 1944).

[12] W. Pauli, *Handbuch der Physik* Vol. 24, p. 220. J. W. Edwards, Ann Arbor, 1943. There is no limitation involved in this choice of starting equation since all other forms amount to different choices of the matrices, whereas, what we do only affects the differential operators.

[13] This form is uniquely determined by the requirement of self-adjointness (see originally submitted papers). The operator ∇ of the last term is essential, a fact that can only be appreciated through the complete details. Its importance to physical consequences will be mentioned later.

shall find it convenient to write such expressions as (2.1) in the form

$$\Delta_\lambda'\psi=\left[\exp\left(\frac{\omega r_{\lambda\sigma}\partial}{\partial x_\sigma}\right)-\exp\left(\frac{-\omega r_{\lambda\sigma}\partial}{\partial x_\sigma}\right)\right]\Big/2\omega\psi.$$

If dG' is an element of volume on the group manifold in the neighborhood of the primed frame then, with the preceding specifications, we may write our basic integro-difference equation for spin $\frac{1}{2}$ material processes as

$$\int\left\{\gamma_\lambda'\Delta_\lambda'\nabla_\lambda'\psi+\kappa\nabla'\psi\right\}dG'\Big/\int dG'=0, \quad (2.2)$$

the integration being over the group manifold of the four-dimensional rotation group.

It is apparent that the difference steps sweep out under the group G a sphere of radius ω about the point (x_σ). We shall call this sphere the "dynasphere." It is also apparent that if ω is real the projections on the fixed axes of any point on this sphere are real, so that $\Delta x_k(k=1-3)$ are real, whereas Δt is purely imaginary since $\Delta t=-i/c\Delta x_4$ and Δx_4 is real. On the other hand, if ω is purely imaginary (the case required for quantization of mass, see later) then Δx_k are purely imaginary, whereas now Δt is real. Hence as soon as we introduce the integration over the group G in our basic law we are at the same time introducing purely complex displacements either in time or in space. Thus in order to write our equations of motion we must extend space to be a four-dimensional complex continuum, the space of observation being the subspace for which $x_k=$ real, $x_4=$ purely imaginary, while the dynasphere and the displacements entering the equations of motion are not confined to this subspace. A point in the observer's subspace is *not* dynamically connected to any other point in the observer's subspace but it is so connected to all points of the dynasphere with it as center.[14]

3. THE EQUIVALENT PARTIAL DIFFERENTIAL EQUATION OF INFINITE ORDER

We introduce the notation $u_\rho=\partial/\partial x_\rho$, $u^2=\sum u_\rho^2=\sum\partial^2/\partial x_\rho^2$ and treat these operators as algebraic quantities as is usual in the operational calculus.[15,16] If we set $\Omega_\lambda=i\omega r_{\lambda\rho}u_\rho$, then Eq. (2.2) with ω replaced by $i\omega$ may be written

$$\int\left\{\sum_{\lambda\sigma}r_{\lambda\sigma}\gamma_\sigma\frac{e^{\Omega_\lambda}-e^{-\Omega_\lambda}}{2i\omega}\prod_\lambda\frac{e^{\Omega_\beta}+e^{-\Omega_\beta}}{2}+\kappa\prod\frac{e^{\Omega_\beta}+e^{-\Omega_\beta}}{2}\right\}dG\Big/\int dG\psi=0, \quad (3.1)$$

where $\prod$ is the product of all similar terms for $\beta=1$ to 4, and $\prod_\lambda$ does not contain the factor $\beta=\lambda$.

Let the function $g(u)=g(u_1, u_2, u_3, u_4)$ be defined by

$$g(u)=\frac{1}{16}\prod(e^{\Omega_\beta}+e^{-\Omega_\beta}). \quad (3.2)$$

Then

$$\partial g/\partial u_\sigma=\frac{1}{16}\sum_\lambda i\omega r_{\lambda\sigma}(e^{\Omega_\lambda}-e^{-\Omega_\lambda})\prod_\lambda(e^{\Omega_\beta}+e^{-\Omega_\beta}),$$

and so

$$-\frac{1}{\omega^2}\sum\gamma_\sigma\frac{\partial g}{\partial u_\sigma}=\sum_{\lambda\sigma}r_{\lambda\sigma}\gamma_\sigma\frac{e^{\Omega_\lambda}-e^{-\Omega_\lambda}}{2i\omega}\prod_\lambda\frac{e^{\Omega_\beta}+e^{-\Omega_\beta}}{2}$$

is just the first term in the integrand of (3.1). Hence we can write (3.1) as

$$\int\left\{-\frac{1}{\omega^2}\sum_\sigma\gamma_\sigma\frac{\partial g}{\partial u_\sigma}+\kappa g(u)\right\}dG\Big/\int dG\psi=0. \quad (3.3)$$

Or if we introduce the function $f(u)=f(u_1, u_2, u_3, u_4)$ defined by

$$f(u)=\int g(u)dG\Big/\int dG, \quad (3.4)$$

Eq. (3.3) becomes

$$\left\{-\frac{1}{\omega^2}\sum_\sigma\gamma_\sigma\frac{\partial}{\partial u_\sigma}f(u)+\kappa f(u)\right\}\psi=0. \quad (3.5)$$

In order to evaluate (3.4) we write

$$g(u)=\frac{1}{16}\sum_{+,-}\exp[i\omega(\pm r_{1\rho}\pm r_{2\rho}\pm r_{3\rho}\pm r_{4\rho})u_\rho],$$

where the sum is over all combinations of signs. But the 16 points $i\omega(\pm r_{1\rho}\pm r_{2\rho}\pm r_{3\rho}\pm r_{4\rho})$ all lie on the dynasphere, and since each point sweeps out the entire dynasphere under G, we need only consider one of them, say with the plus sign throughout, so that

$$\int g(u)dG=\int\exp[i\omega(r_{1\rho}+r_{2\rho}+r_{3\rho}+r_{4\rho})u_\rho]dG.$$

Notice that $\omega(r_{1\rho}+r_{2\rho}+r_{3\rho}+r_{4\rho})$ is just the ρ-component in the unprimed coordinate system of a vector $2\omega=(\omega, \omega, \omega, \omega)$ in the primed coordinate system. Hence the argument in the exponential is equal to the scalar

[14] J. L. S. Hatton, *The Imaginary in Geometry* (Cambridge University Press, London, 1920). J. L. Coolidge, *The Geometry of the Complex Domain* (Oxford University Press, London, 1924).

[15] H. T. Davis, *The Theory of Linear Operators* (The Principia Press, Bloomington, Indiana, 1936). This book contains a good bibliography of the literature on differential equations of infinite order.

[16] Of the many books treating the subject of operational calculus, we mention two: N. W. McLachlan, *Complex Variable and Operational Calculus* (Cambridge University Press, London, 1939). H. S. Carslaw and J. C. Jaeger, *Operational Methods in Applied Mathematics* (Clarendon Press, Oxford, 1941).

TABLE I. Calculated positive and negative masses for the first sixteen masses of the spin ½ family according to Eq. (3.10).

Root number n	Zero of $J_3(z)=0$ $z_n{}^0$	Root of Eq. (4.8) z_n	Mass values μ_n (units of e.m.u.)		Consecutive mass differences $\mu_{n+1}-\mu_n$
0			1		
1	5.136	−5.131 5.14	−218.34 218.76	0.42	217.76
2	8.417	−8.412 8.423	−357.95 358.42	0.47	139.66
3	11.620	−11.614 11.626	−494.21 494.72	0.51	136.30
4	14.796	−14.790 14.802	−629.35 629.86	0.51	135.14
5	17.960	−17.954 17.966	−763.99 764.50	0.51	134.64
6	21.117	−21.111 21.123	−898.33 898.84	0.51	134.34
7	24.270	−24.264 24.276	−1032.50 1033.01	0.51	134.17
8	27.42	27.42	1166.79		133.78
9	30.57	30.57	1300.83		134.04
10	33.72	33.72	1434.87		134.04
11	36.86	36.86	1568.91		134.04
12	40.01	40.01	1702.53		133.62
13	43.15	43.16	−1836.03 1836.57	0.54	134.04
14	46.30	46.30	1969.76		133.19
15	49.44	49.44	2104.23		134.47
16	52.59	52.59	2237.42		133.19

product

$$2\omega u\cos\theta,$$

where θ is the angle between $\mathbf{u}$ and $2\boldsymbol{\omega}$. As $r_{\lambda\rho}$ in the integral runs over G the vector $2\boldsymbol{\omega}$ sweeps over a sphere, each position receiving equal weight which is proportional to the element of "area" of the sphere. We can in this way replace the integration over the group manifold by an integration over the surface of this sphere.

Choosing spherical coordinates $(R, \theta, \lambda, \alpha)$, where R is the radius vector, θ is the angle with the x_4 axis, λ is the co latitude, and α the longitude of the component of $\mathbf{R}$ normal to x_4, then an easy calculation shows that the "solid angle" subtended by an element of "area" of the four-dimensional sphere is

$$d\Omega=\sin^2\theta\sin\lambda d\theta d\lambda d\alpha.$$

The range of variation is $0\leqslant\theta\leqslant\pi$, $0\leqslant\lambda\leqslant\pi$, $0\leqslant\alpha\leqslant 2\pi$. We have $\int d\Omega=2\pi^2$ and

$$f(u)=\frac{1}{2\pi^2}\int e^{i2\omega u\cos\theta}d\Omega=\frac{2}{\pi}\int_0^\pi e^{i2\omega u\cos\theta}\sin^2\theta d\theta. \quad (3.6)$$

Set $z_\rho=2\omega u_\rho$, $z=2\omega u$; then from the Bessel function

$$J_0(z)=\frac{1}{2\pi}\int_0^{2\pi}e^{iz\cos\theta}d\theta, \quad (3.7)$$

it is easy to show that

$$f(u)=2[J_0''(z)+J_0(z)]=2J_1(z)/z. \quad (3.8)$$

Furthermore,

$$\frac{\partial f}{\partial u_\sigma}=\frac{df}{du}\frac{\partial u}{\partial u_\sigma}=8\omega^2\frac{d}{zdz}\left(\frac{J_1}{z}\right)u_\sigma=-8\omega^2\frac{J_2}{z^2}u_\sigma. \quad (3.9)$$

Putting these results into Eq. (3.5) it becomes

$$\left\{\frac{8J_2(z)}{z^2}\sum_\sigma\gamma_\sigma\frac{\partial}{\partial x_\sigma}+\kappa\frac{2J_1(z)}{z}\right\}\psi=0. \quad (3.10)$$

This is the partial differential equation of infinite order equivalent to the above integro-difference Eq. (2.2) or (3.1). The operator z enters only to even powers. J_1 and J_2 are Bessel's functions of order one and two.[17] Equation (3.10) is obviously invariant under the complete Lorentz group. The adjoint equation to (3.10) is

$$D_\sigma\varphi\gamma_\sigma-M\varphi=0, \quad (3.11)$$

where

$$D_\sigma=[8J_2(z)/z^2]\partial/\partial x_\sigma \quad (3.12)$$

$$M=\kappa 2J_1(z)/z. \quad (3.13)$$

In this form of statement of the fundamental law, all reference to the dynasphere and the complex nature of space is obscured since only operations in the observer's (real) subspace are involved in the equation. This fact owes itself to the assumed analytical character of the wave function.

4. QUANTIZATION OF REST MASS

We have now to consider those solutions of (3.10) or (2.2)[18] which are of physical interest. In accordance with Section 1 the solutions that we are interested in will be a superposition of plane wave functions for particles of different rest masses μ, such as

$$\psi(\mathbf{p},\mu)=\exp(ip_\sigma x_\sigma/\hbar), \quad (4.1)$$

with $\mathbf{p}$ and μ connected by the equation

$$\sum_\sigma p_\sigma{}^2=-\mu^2c^2. \quad (4.2)$$

The general solution is

$$\psi=\sum_{\mathbf{p}\mu}a(\mathbf{p}\mu)\psi(\mathbf{p}\mu),$$

where the $a(\mathbf{p}\mu)$ are arbitrary spinor coefficients. The summation over μ is only over those values admitted by Eq. (3.10).

The allowed values of μ may be determined by substituting (4.1) into (3.10). The operator $z=2\omega\mu c/\hbar$, and

[17] Whittaker and Watson, *Modern Analysis* (Cambridge University Press, London, 1927), fourth edition, p. 355.

[18] We note that the substitution of (4.1) into (2.2) directly will lead to the same results as substitution into (3.10) and would involve the same type of transformations as were made in the preceding section.

the equation is satisfied if $\mu/m=zJ_1/4J_2$. Setting $\omega=\beta e^2/mc^2$, where β is a number of order of magnitude unity, we find that z must be a root of

$$J_2(z)/J_1(z)=\beta e^2/2\hbar c \tag{4.3a}$$

and that the mass corresponding to this root is given by

$$\mu/m=\hbar cz/e^2 2\beta. \tag{4.3b}$$

Taking the value of the fine structure constant[19] as 1/137.027 we obtain

$$\beta/274.054=J_2/J_1 \tag{4.4a}$$

and

$$\mu/m=68.515z/\beta. \tag{4.4b}$$

The small value of the left-hand side of Eq. (4.4a) shows that its roots will lie close to those of $J_2(z)=0$. Since the roots of J_2 and J_1 are never coincident and are real, there will be an infinite number of real values of z satisfying (4.4a) so that (4.4b) will yield an infinite number of masses μ. The roots of J_2 are not uniformly spaced being wider in the beginning and then narrowing down to an asymptotic value of $z_{n+1}-z_n\sim\pi$. This value may be compared with the first root (other than $z=0$ which we shall denote as the zeroth root) of J_2, that is, $z_1=5.136$.

By expanding the Bessel functions about the origin, the smallest or zeroth root of (4.4a) yields the electron mass

$$\mu_0\cong[1-\tfrac{1}{6}\beta^2(e^2/\hbar c)^2]m\cong m.$$

Since $\mu_0=m$ to an extremely high approximation, the difference between μ_0 and m being much less than the error of observation, we may take m to be the electron mass. We also see that μ_0 is very insensitive to the value of β.

So far β is undetermined. The fitting of one observed mass would determine β and all the other predicted masses uniquely. From the discussion of Section 1 we expected ω to be equal to the diameter of the classical electron, for which $\beta=8/5=1.6$. This value of β is such that all masses are slightly high, the thirteenth being close but slightly greater than that of the proton. Adjusting β so that[19] $\mu_{13}=1836.57$ e.m.u. [electron mass units] we get $\beta=1.610$, the corresponding value of $\omega=4.538\times10^{-13}$ cm.

With this value of β and a table of Bessel functions,[20] the masses of the spin $\frac{1}{2}$ family have been calculated and are given in Table I.

From Table I one sees that with the exception of the electron the masses occur in positive and negative pairs, the negative partner being slightly smaller in magnitude because the negative root of (4.4a) is slightly smaller than the corresponding positive root due to the oddness of the function $J_1(z)$. The last column shows consecutive mass differences and reflects a peculiarity of the Bessel function J_2 which reaches way out for its first (nonzero) root, and so fixes the first mass pair at 218 e.m.u. in good agreement with the observed most probable value of the cosmic-ray μ-meson.[21] Besides the correct prediction of mass the spin is predicted to be $\frac{1}{2}$ in agreement with experiment.[22] As to the other masses[23] predicted in Table I, one can only say at present that experiment[24] indicates the possible existence of several mesons but there are not enough data to determine masses and other properties. The asymptotic spacing of the masses is 133.69 e.m.u.

We see that Eq. (2.2) with complex radius of the dynasphere, or equivalently (3.10), is the field equation of a charged material process, the particles of different rest mass being but different states of this field. Among these particles is the electron, the μ-meson, and the proton. But one charge parameter "e" is introduced when the electromagnetic potentials are introduced into the matter field equation (2.2) or (3.10). Consequently, *according to our principle of Section 1 in the individual particle aspect all particles have the same charge (except for sign).*[25]

5. THE NEUTRINO

If we consider the equation for the charged particles in some such form as that of reference 25, then on putting the charge equal to zero, the mass term drops out so that for neutral particles we should have the equation

$$(8J_2(z)/z^2)\gamma_\lambda u_\lambda\psi=0.$$

This equation describes an infinite number of particles, one of which has zero rest mass. The other masses are determined from $J_2(z)=0$ and sandwich between the charged mass pairs given in Table I. However, these

[19] J. W. M. Dumond and E. Richard Cohen, Rev. Mod. Phys. 21, 651 (1949).

[20] *Tables of the Bessel Functions of the First Kind* (Harvard Computation Laboratory), Vols. 3 and 4.

[21] R. B. Brode, Rev. Mod. Phys. 21, 37 (1949).

[22] R. F. Christy and S. Kusaka, Phys. Rev. 59, 414 (1941); R. E. Lapp, Phys. Rev. 64, 255 (1943); S. Belenky, J. Phys. USSR, 10, 144 (1946).

[23] The importance of the operator ∇ required by the condition of self-adjointness of the difference operators may be seen by replacing the term $2\kappa J_1 z$ to which it gives rise simply by κ. There is then a greatest mass. If we take this to be the proton then again it turns out to be the thirteenth. In this case $\beta=1.561$ and $\mu_1=223.5$ e.m.u., and the positive and negative masses no longer occur in close pairs. The experimental value (reference 21) for the mass of the cosmic-ray μ-meson is 218 ± 5 e.m.u., so that the agreement is somewhat worsened when ∇ is dropped. A complete mass table for this case is contained in the original papers.

[24] G. D. Rochester and C. C. Butler, Nature 160, 855 (1947); Brown, Camerini, Fowler, Muirhead, Powell, and Ritson, Nature 163, 82 (1949); Seriff, Leighton, Hsiao, Cowan, and Anderson, Phys. Rev. 78, 290 (1950); J. B. Harding, Phil. Mag. 41, 405 (1950); Alixanjan, Alihanov, Morosov, Muschelishvili, and Hrinyan, J. Exp. Theor. Phys. 18, 673 (1948). I wish to express my appreciation to Professor J. D. Kurbatov for preparing for me an English abridgment of this paper.

[25] If we introduce the potentials through a gauge transformation and if we set $u_\lambda\rightarrow U_\lambda=u_\lambda-(ie/\hbar c)A_\lambda$, $z\rightarrow Z=2\omega\gamma_\lambda U_\lambda$, then the mass quantization condition (4.4) is rigorously maintained. The equation (3.10) may be written $[(2J_2/Z)+\beta(e^2/\hbar c)J_1/Z]\psi=0$. It has for general solution $\psi=\Sigma\psi_n$ where ψ_n is a solution of $(Z+z_n)\psi_n=0$ and z_n is a root of (4.4a). The last equation in ordinary notation is $\{\gamma_\lambda[u_\lambda-(ie/\hbar c)A_\lambda]+(\mu_n c/\hbar)\}\psi_n=0$. It is further evident that all particles are stable, the electromagnetic field not producing any intertransformation of particles.

neutral particles do not involve the spin in any intrinsic way, since for them ψ is essentially a solution of $J_2(z)\psi=0$.

The last remark suggests as an alternative that we change to a real radius for the dynasphere so that for neutral processes we have

$$(8I_2(z)/z^2)\gamma_\lambda u_\lambda\psi=0.$$

This equation has one real rest mass which is zero and an infinite number of purely imaginary ones. The latter may be entirely excluded from consideration as being physically meaningless. We are then left with the one zero mass particle which involves the spin intrinsically and may be identified with the neutrino. On this picture there is only one elementary neutral particle of spin $\frac{1}{2}$, the neutrino. The neutron would not be an elementary particle. It would be consistent with this picture to assert that *all elementary particles of non-vanishing rest mass are also charged, and conversely, all charged particles have non-vanishing rest mass.* This statement may be considered as a resurgence of an old idea, the electrical nature of mass.[26] However, we see that the idea here receives an entirely new form. We have no direct connection between the mass of a particle and its radius. In fact, the particle itself has no radius. The existence of the particles with different rest masses as obtained in Section 4 arises in a manner completely outside the classical electromagnetic theory of mass. Finally, *all these elementary particles have the same charge (except for sign), this fact being reduced simply to the bare existence of the particle.*

On either of these alternatives the non-existence of a meson of spin $\frac{1}{2}$ of mass between that of the electron and the μ-meson allows us to predict that the meson postulated by Tiomno and Wheeler[27] for the decay of the μ-meson according to the scheme $\mu\rightarrow e+\nu+\mu^0$ must be a neutrino.

[26] H. A. Lorentz, *The Theory of Electrons, Columbia Lectures* (MacMillan Company, Ltd., London, 1909). J. Frenkel, *Lehrbuch der Electrodynamik* (Verlag. Julius Springer Berlin, 1926). G. A. Schott, *Electromagnetic Radiation* (Cambridge University Press, London, 1912).

[27] J. Tiomno and J. A. Wheeler, Rev. Mod. Phys. **21**, 144 (1949).

SUMMARY

It is suggested that the creation, continued existence, and annihilation of elementary particles be considered as aspects of a material process which requires an irreducible volume in space-time. The mathematical formulation of this idea is carried out through a correspondence type of generalization of the wave equations of Maxwell, Dirac, etc., and involves the introduction of a new constant ω of the dimensions of a length.

This paper applies the method to the Dirac equation. A quantized spectrum of masses is obtained in terms of the electron mass m and the length ω. This spectrum of masses should give all elementary charged particles of spin $\frac{1}{2}$. If we take for ω the classical electron diameter then the mass of the proton is one-half percent too high and consequently ω has been adjusted upward by one-half percent in order to fit the mass of the proton. $\omega=4.538\times10^{-13}$ cm. Between the electron and proton there are twelve particles (see Table I). The first one has a predicted mass of 218.76 e.m.u.—in agreement with experimental values for the μ-meson—and since its spin is $\frac{1}{2}$, in agreement with experiment, this particle may be identified as the μ-meson. With reference to the other particles experimental evidence indicates that there are other mesons between the μ-meson and proton but there is not sufficient data to determine masses and other properties. There is predicted an infinite number of particles beyond the proton (but see reference 23 of Section 4) with an asymptotic mass spacing of 133.69 e.m.u. All the particles are predicted to have the same magnitude of electrical charge.

There are at present two unresolved possibilities for the neutral particles (see Section 5). In either case the three-particle decay of the μ-meson into spin $\frac{1}{2}$ particles is predicted to be $\mu\rightarrow e+2\nu$ (since there is no neutral spin $\frac{1}{2}$ particle between the neutrino and μ-meson).

Finally, this paper leaves open the questions of stability and intertransformation of particles. These questions depend not alone on the spin $\frac{1}{2}$ family of particles.

Letters to the Editor

PUBLICATION of brief reports of important discoveries in physics may be secured by addressing them to this department. The closing date for this department is five weeks prior to the date of issue. No proof will be sent to the authors. The Board of Editors does not hold itself responsible for the opinions expressed by the correspondents. Communications should not exceed 600 words in length.

Mass-Spectrographic Identification of Cm^{243} and Cm^{244}

F. L. REYNOLDS, E. K. HULET, AND K. STREET, JR.
Radiation Laboratory and Department of Chemistry, University of California, Berkeley, California*
September 7, 1950

THE isotopes Cm^{243} and Cm^{244} have been identified mass-spectrographically. The curium fraction from a long neutron irradiation of Am^{241} was separated chemically and its isotopic composition determined by means of the 60° focusing mass spectrograph used in this laboratory for work with radioactive isotopes. A thermal ion source was used and the ions were recorded photographically. Figure 1 is a reproduction of the plate obtained.

The Am^{241} which is responsible for the rather intense line at mass 241 and the much fainter line at mass 257 ($Am^{241}O^+$) represents a very small fraction of the initial Am^{241} target material that was not successfully separated in the chemistry. The line at mass 254 is due to $Pu^{238}O^+$ which grew in from the alpha-decay of Cm^{242} after the chemical separation. The Cm^{242} appears to a small extent as the metal at mass 242 and much more intensely as $Cm^{242}O^+$ at mass 258. The ghost line one-third of a mass unit to the right of mass 258 is a characteristic of the machine and appears often on intense spectra. The isotopes Cm^{243} and Cm^{244} because of their small abundances are detected only at the more intense oxide masses 259 and 260.

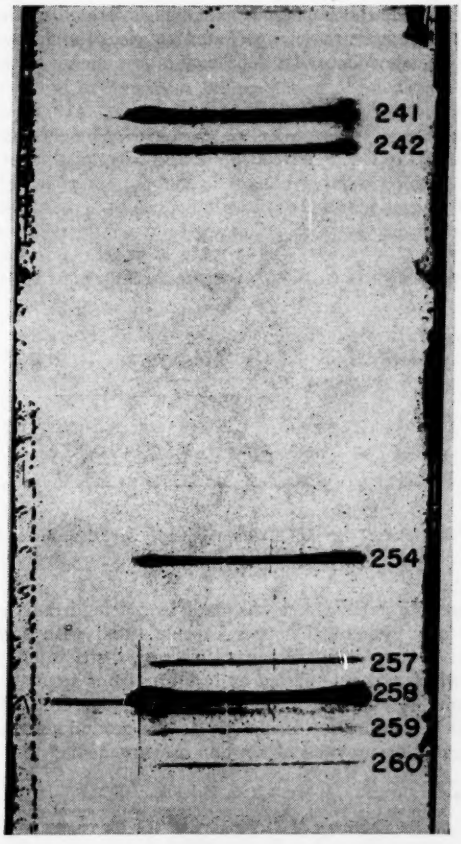

FIG. 1. Isotopic composition of the curium fraction from a long neutron irradiation of Am^{241}.

A photometer tracing of the plate gave the semiquantitative information that Cm^{243} and Cm^{244} are of about equal abundance in this sample and that each is about 1 percent as abundant as Cm^{242}.

The Cm^{243} was produced by the following sequence of nuclear reactions:

$$\begin{array}{c} Cm^{242}(n,\gamma)Cm^{243} \\ \uparrow \beta^-(16\text{ hr.}) \\ Am^{241}(n,\gamma)Am^{242m}. \end{array}$$

The Cm^{244} was undoubtedly produced both by neutron capture in the Cm^{243} formed as above and also by the following path:[1]

$$\begin{array}{c} Cm^{244} \\ \uparrow \beta^-(\sim 25\text{ min.}) \\ Am^{241}(n,\gamma)Am^{242}(n,\gamma)Am^{243}(n,\gamma)Am^{244}. \end{array}$$

Alpha-particles ascribed to Cm^{243} have been seen previously,[2,3] but the mass spectrographic identification of Cm^{244} represents the first definite evidence for this isotope.

From the energy balances involved one expects Cm^{243} to be slightly unstable with respect to orbital electron capture,[1] or possibly beta-stable. The alpha-decay systematics[4] predict that Cm^{244} is beta-stable with an alpha-decay half-life of years.

We would like to express our appreciation to Dr. S. G. Thompson for his very valuable assistance in carrying out this work.

* This work was performed under the auspices of the AEC.
[1] Street, Ghiorso, and Seaborg, Phys. Rev. 79, 530 (1950).
[2] Street, Thompson, and Ghiorso (unpublished work).
[3] Rasmussen, Reynolds, Thompson, and Ghiorso, Phys. Rev. 80, 475 (1950).
[4] Perlman, Ghiorso, and Seaborg, Phys. Rev. 77, 26 (1950).

P–N Junctions Prepared by Impurity Diffusion

R. N. HALL AND W. C. DUNLAP
General Electric Research Laboratory, Schenectady, New York
September 8, 1950

WHEN $P-N$ barriers in a semiconductor are formed by the solidification of a melt, the concentrations of the different impurities which are present vary nearly linearly with distance from the barrier. The rectification properties of such barriers depend upon the donor and acceptor impurity gradients in such a manner that as the net concentration gradient is increased, the forward characteristic improves while the inverse breakdown voltage decreases.

By using a distinctly non-linear impurity distribution as indicated by Fig. 1, it is possible to construct rectifiers which combine the good forward characteristic of a large impurity gradient with the high inverse breakdown voltage of a barrier having a small impurity gradient. In the blocking direction, the potential drop is largely confined to a thin "barrier layer" within which the impurity concentration varies slowly. In the forward direction, holes and electrons are drawn in opposite directions across the rectifier from the regions of high impurity concentration where a copious supply of carriers is available. If the layers of high impurity concentration are not too greatly separated, space charge potentials due to recombination of holes and electrons can be made small and good forward characteristics are obtained.

The non-linear impurity distribution which is required may be obtained by thermal diffusion of donor and acceptor impurities into opposite sides of a wafer of semiconductor. Germanium diodes have been prepared in this manner which will withstand inverse potentials of the order of 100 volts and which will pass 500 amp./cm² at one volt in the forward direction. The charac-

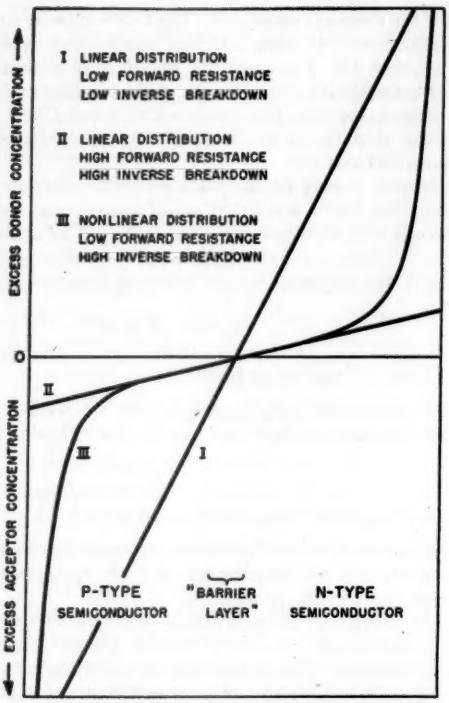

FIG. 1. Impurity distributions in semiconductor rectifiers.

teristics of these rectifiers are similar to those of selenium or copper oxide units except that the current densities are approximately 1000 times greater in the germanium units. Satisfactory rectifiers may be made from *N*- or *P*-type germanium having a resistivity of 5 ohm-cm or more.

When a rectifier is prepared by the diffusion of donor and acceptor impurities into the opposite sides of a wafer of extrinsic semiconductor, the barrier is located near one surface where the concentrations of donors and acceptors are equal. Accurate location of the barrier by means of a potential probe is possible and affords a sensitive method for the measurement of the diffusion of donor and acceptor impurities into semiconductors.

The Beta-Disintegration of Th^{233}

M. E. BUNKER, L. M. LANGER,* AND R. J. D. MOFFAT*
Los Alamos Scientific Laboratory,† Los Alamos, New Mexico
September 8, 1950

THE 23.3-minute activity of Th^{233} has been studied in a magnetic lens spectrometer.[1] Sources were prepared by irradiating ThO_2 with neutrons in the thermal column of a nuclear reactor. The above decay rate was obtained by direct measurement for over eight half-lives and was also checked in the spectrometer. Sources were about 0.5 inch in diameter. The spectrometer was adjusted at a resolution of six percent during the investigation. Detection was by means of a 3.6-mg/cm² mica end-window counter.

The momentum distribution of the beta-particles is shown in Fig. 1 and the corresponding Fermi plot is shown in Fig. 2. There is clearly only one group of beta-rays. The extrapolated end point is 1.23±0.01 Mev. At high energies the Fermi plot is a straight line as might be expected, since the comparative half-life is only $ft \sim 10^6$. From the nuclear shell model one might expect this transition to involve a change of parity. The transition, therefore, appears to be of the once-forbidden type with a spin change of 0 or 1.

The downward deviation of the Fermi plot at low energy cannot be ascribed to source thickness or to counter window cut-off and is not fully understood. The data represented by circles were obtained using a source with 16 mg/cm² surface density mounted on 0.0002-inch aluminum backing. In order to examine the possibility that the apparent deficiency of low energy particles was due to source thickness, another source, with surface density of 0.6 mg/cm² mounted on a thin Zapon film, was studied in the spectrometer. These data are represented by triangles in Figs. 1 and 2. It is apparent that the use of a much thinner source

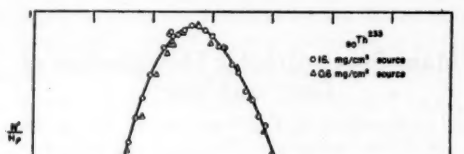

FIG. 1. Beta-spectrum of Th^{233}.

merely served to accentuate the downward deviation at low energy. This fall-off could possibly be due to a low energy defocusing effect in the spectrometer, although no other beta-ray spectrum analyzed with this instrument has exhibited any such deviation until below 200 kev. For example, the RaE spectrum, which has about the same end point and is located in the same part of the periodic table, was found to yield its characteristic shape, with no evidence of a deficiency of low energy electrons as reported above.

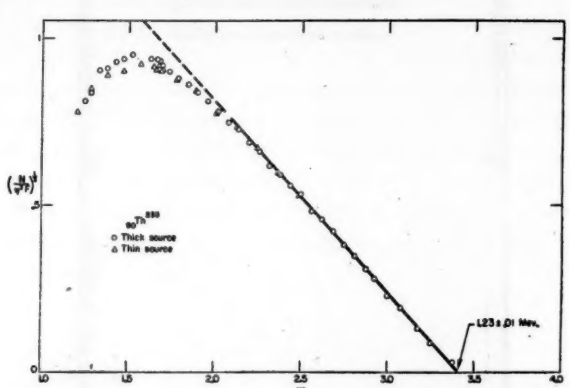

FIG. 2. Fermi plot of the data. The values for *F* were determined from the curves prepared by Moszkowski.

A search for gamma-rays was made by placing irradiated ThO_2 powder in a cylindrical copper capsule fitted with a uranium radiator. A very weak secondary electron distribution was observed which was interpreted as resulting from bremsstrahlung.[2] There was no evidence of photo-electron peaks. It is concluded that the beta-transition is directly to the ground state of Pa^{233}, as suggested by previous absorption measurements.[2]

* Indiana University, Bloomington, Indiana.
† This document is based on work performed under government contract for the Los Alamos Scientific Laboratory of the University of California.
[1] L. M. Langer, Phys. Rev. **77**, 50 (1950).
[2] Seaborg, Gofman, and Stoughton, Plutonium Project Report CN-126 (June, 1942), unpublished.

On the Angular Distribution of 3.1-Mev Neutrons Scattered by Protons

YUKIYASU ODA, JUMPEI SANADA, AND SHOTARO YAMABE
Physics Department, Osaka University, Osaka, Japan
August 21, 1950

THE angular distribution of the scattering of fast neutrons by protons has been usually studied by analyzing the recoil protons. Therefore, the results are concerned with the neutrons which are scattered backwards. They showed an isotropic distribution at the energy of *d–d* neutrons. On the other hand, the angular distribution in the forward direction has been studied by Kikuchi, Aoki, and Wakatsuki.[1] They used ring scatterers and an ionization chamber filled with methane or hydrogen gas at high pressure to detect the scattered neutrons. The peculiarity of this method is that it gives the absolute value of the differential scattering cross section. The values of the differential scattering cross sections at different angles thus obtained were equal to each other within the experimental error. But the absolute values were only about a half of $\sigma_0/4\pi$, where σ_0 is the total scattering cross section for the proton. If correct, the result indicated a strong asymmetry in the scattering. The experiment has been repeated, since by some improvements of the apparatus a larger intensity of neutrons became available and better geometric conditions could be used. We raised the sensitivity of detection by increasing the number of hydrogen atoms in the ionization chamber and by using more scattering materials. The other arrangements were almost the same as those used in the previous experiments. The monoenergetic neutrons used were from the *d–d* reaction and were produced in a thick heavy water ice target by an unanalyzed beam of 100μamp. of 300-kev. deuterium ions. The ring scatterers were of paraffin, graphite, water, quartz, and silicon.

We measured the ratio $\Delta I/I_0$, where ΔI is the increase of the ionization current in the ionization chamber when the ring scatterer was placed in position, and I_0 is the ionization current produced by neutrons coming directly from the target. We computed the scattering by a proton by subtracting the contribution of carbon and oxygen from the scattering of paraffin and water, respectively. In this case, we made the assumption that the ionization current in the ionization chamber produced by neutrons, which lost their energy through the collision with protons, was proportional to the product of the energy after collision and the total scattering cross section of neutrons at that energy. We used for the values of the total scattering cross section the data obtained by C. L. Bailey, *et al.*[2]

Our results are summarized in Table I and are shown in Fig. 1.

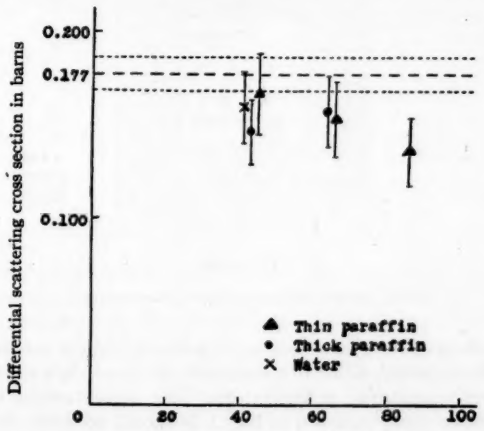

FIG. 1. Differential scattering cross section in c.m. system. Dotted line indicates $\sigma_0/4\pi$, where σ_0 is the total scattering cross section.

The errors involved in these values of the cross section came mainly from the errors involved in the total scattering cross section which was used in the calculation of the sensitivity of the ionization chamber. From these results we conclude that the angular distribution in the forward direction is consistent with isotropic scattering. The cause of the discrepancy with the former results is not clear.

TABLE I. The differential scattering cross section of 3.1-Mev neutrons scattered by protons in the center-of-mass system.

Scattering angle in c.m. system in deg.	Scatterer and its weight in grams	$(\Delta I/I_0)_{\text{proton}}$ in %	Differential cross section in c.m. system in barns
44±10	Paraffin 50.7	2.19±0.07	0.166±0.022
	Paraffin 94.9	3.10±0.05	0.146±0.017
	Water 94.1	2.32±0.06	0.159±0.019
66±10	Paraffin 71.8	2.06±0.06	0.153±0.020
	Paraffin 141.4	3.38±0.07	0.157±0.019
86±10	Paraffin 95.4	1.63±0.06	0.136±0.019

Total cross section $\sigma_0/4\pi = 0.177 \pm 0.009$ barn

We wish to express our gratitude to Professors S. Kikuchi and T. Wakatsuki for their advice and encouragement throughout the progress of this work.

[1] Kikuchi, Aoki, and Wakatsuki, Proc. Phys. Math. Soc. Japan 21, 410 (1939); T. Wakatsuki, Proc. Phys. Math. Soc. Japan 22, 430 (1940).
[2] C. L. Bailey, *et al.*, Phys. Rev. 70, 583 (1946).

Infra-Red Absorption of Hydrogen Induced by Foreign Gases

M. F. CRAWFORD, H. L. WELSH, J. C. F. MACDONALD,* AND J. L. LOCKE†
McLennan Laboratory, University of Toronto, Toronto, Canada
August 14, 1950

THE vibrations of O_2, N_2, and H_2, and the symmetrical mode of CO_2, all normally inactive in infra-red absorption, are rendered active by intermolecular forces in the compressed gas.[1] The absorption was attributed to the dipole moment arising from the distortion of the charge distribution of the absorbing molecule during a collision. This interpretation is substantiated by the effect of foreign gases added to the absorbing gas; N_2 added to O_2, N_2 and He to H_2. More complete data on the absorption induced in H_2 by He, A, and N_2 are presented here.

Hydrogen at a given pressure was admitted to the cell, 85 cm in length, and the foreign gas added at partial pressures up to 100 atmospheres. Several partial pressures of hydrogen in the range 10 to 50 atmospheres were used. The enhancement due to the foreign gas was obtained by subtracting the absorption of the H_2 alone from the absorption of the mixture. Over the pressure ranges used the integrated absorption coefficient of the enhancement varies linearly with the product of the foreign gas density and the hydrogen density, and can therefore be expressed as a specific absorption coefficient. The specific absorption coefficients are given in Table I.

The effectiveness of He and A in increasing the induced absorption is of special significance. Mizushima[2] has interpreted the absorption observed in O_2 and H_2 in terms of the polarization of the absorbing molecule by the quadrupole fields of the surrounding molecules. Since the rare gas atoms possess no quadrupole field, the absorption induced by these atoms in H_2 cannot

TABLE I. Coefficient of induced absorption.

	(cm^{-1} $sec.^{-1}$ per molecule H_2) (per molecule foreign gas per cm^3)	(cm^{-1} $sec.^{-1}$ per atmos. H_2) (per atmos. foreign gas at 0°C)
H_2-He	0.0744×10^{-30}	0.00537×10^{19}
H_2-A	0.233×10^{-30}	0.0168×10^{19}
H_2-N_2	0.257×10^{-30}	0.0185×10^{19}
H_2-H_2	0.105×10^{-30}	0.00759×10^{19}

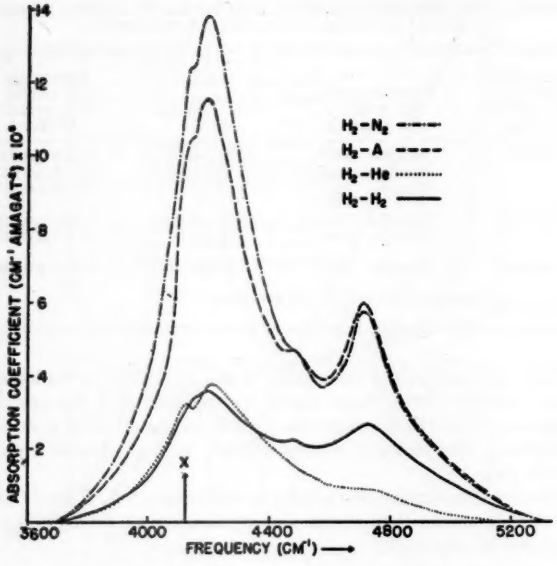

FIG. 1. Contours of the induced infra-red absorption of hydrogen.

be explained by the quadrupole field effect, and must be due to induction by close collisions. H_2 and N_2 have quadrupole moments, but the absorption in pure H_2 and in the H_2-N_2 mixture must also be mainly collision induced, since on hydrogen He is nearly as effective as H_2 and A is nearly as effective as N_2. The comparable intensities of the Q- and S-branches in H_2, N_2, and O_2 is further evidence that the quadrupole field effect is relatively unimportant. Mizushima's calculation predicts an intensity distribution similar to that in the Raman effect in which for these molecules the intensity of the Q-branch is many fold more intense than the other branches.

The contours of the absorption in H_2 induced by the foreign gases are reproduced in Fig. 1. For A and N_2 the $S(0)$ and $S(1)$ rotational lines are quite prominent, but for He they are appreciably weaker relative to the Q-branch. A contour for pure H_2 is shown for comparison. The frequency calibration, obtained with Edser-Butler fringes,[3] is more accurate than that for the previously published contour.[1] It is now evident that the frequency of the peak of the Q-branch for pure H_2 and for each mixture is 40 to 50 cm^{-1} higher than the vibrational frequency of the free molecule. All contours show a weak sharper component marked X; it is barely apparent in the H_2 contour in Fig. 1, but is more prominent at higher densities. This component cannot be assigned to the rotational fine structure of the band, and as yet its origin is speculative.

The large half-width of the rotational lines, about 320 cm^{-1} at room temperature, is a notable feature of the induced absorption of H_2. This indicates that the duration of the perturbation is short, and hence that close collisions are causative. The induced absorption of H_2 cooled by liquid air has been recorded, and the half-width of the lines is markedly reduced. The half-width appears to be proportional to the square root of the absolute temperature, and thus proportional to the thermal velocity. This dependence further confirms the hypothesis that the absorption in H_2 is caused by a dipole moment induced mainly by the overlap forces operative during a close two-body collision.

* Holder of a Studentship under the National Research Council of Canada.

† Now at The Dominion Observatory, Ottawa, Canada.

[1] Crawford, Welsh, and Locke, Phys. Rev. **75**, 1607 (1949). Welsh, Crawford, and Locke, Phys. Rev. **76**, 580 (1949).

[2] M. Mizushima, Phys. Rev. **76**, 1268 (1949).

[3] W. Ewart Williams, *Applications of Interferometry* (Methuen and Company, Ltd., London, 1930), p. 101.

Excitation Function of the Reaction $C^{12}(\gamma,p)B^{11}$

A. K. MANN AND J. HALPERN
University of Pennsylvania, Philadelphia, Pennsylvania*
September 18, 1950

IT is the purpose of this note to describe a measurement of the yield curve of the reaction $C^{12}(\gamma,p)B^{11}$, using the University of Pennsylvania 25-Mev betatron. The data of this experiment when combined with knowledge of the incident photon energy spectrum permit the calculation of the absolute total cross section of the reaction as a function of energy.

The arrangement of the apparatus employed in the experiment is shown in Fig. 1. The collimated x-ray beam has an angular divergence of 0.22 degree. The cross section of the beam at the target position is a sharply defined circle $\frac{5}{32}$ in. in diameter. The target is a slab of graphite approximately one sq. in. in area and 38 mg-cm^2 thick, placed such that the target surface makes an angle of 30° with the x-ray beam. The proton detectors are scintillation counters each of which consists of an RCA 5819 phototube, a silver activated ZnS screen supported in a vertical plane by 0.1 cm thick glass backing, and a hemispherical aluminum reflector in which there is a thin (0.00035-in. aluminum) window to permit the entrance of photo-protons. The area of the ZnS screen is 1 cm^2. Since the scattering chamber is not evacuated, protons emitted from the target traverse approximately 7.3 cm of air before striking the detector screen. The two scintillation counters are operated independently. The output pulses from each of the photo-tubes are fed into separate cathode followers, amplifiers, discriminators, and scaling circuits, all of conventional design.

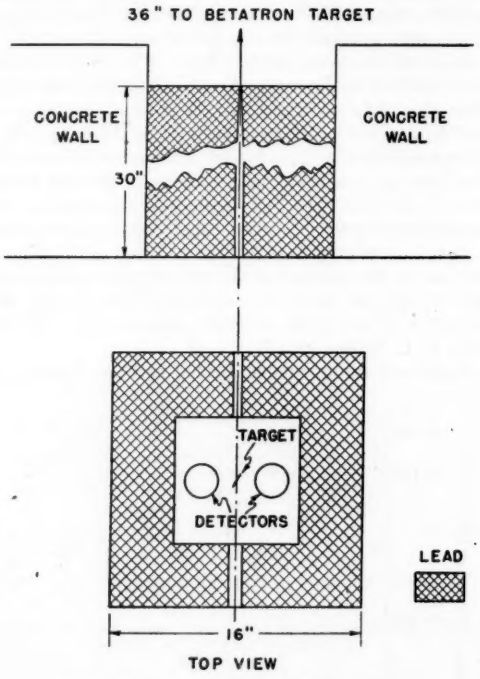

FIG. 1. General arrangement of apparatus.

The data of the experiment are a series of integral bias curves, each curve corresponding to a maximum energy of the x-ray beam. A direct comparison of the integral bias curves results in the yield curve which is shown in Fig. 2. It should be noted that the data in Fig. 2 were obtained using only one of the scintillation counters. The yield curve from the other counter is identical with that in Fig. 2 except for a 10 percent difference in the scale of the ordinate. This difference might easily result from a difference in the geometry of the two counters.

The approximate energy spectrum of the betatron x-ray beam

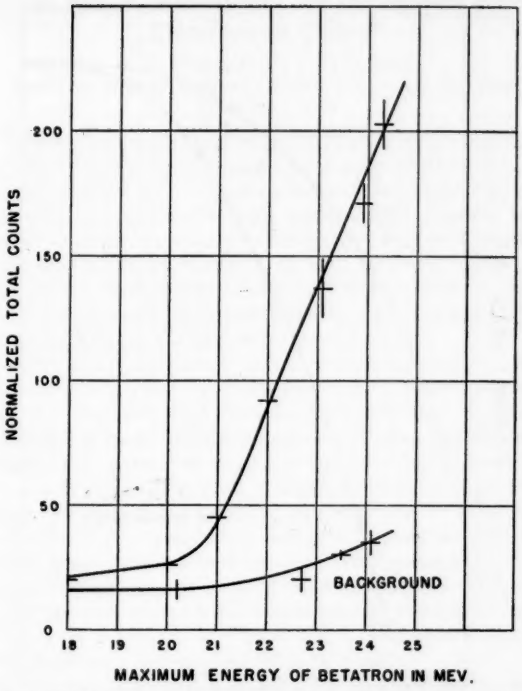

FIG. 2. Yield curve $C^{12}(\gamma,p)B^{11}$. The total counts at each energy are normalized to the same number of roentgens as measured by an ionization chamber.

for any given maximum energy is known.[1] Using these results and our yield curve, the excitation function shown in Fig. 3 is obtained.

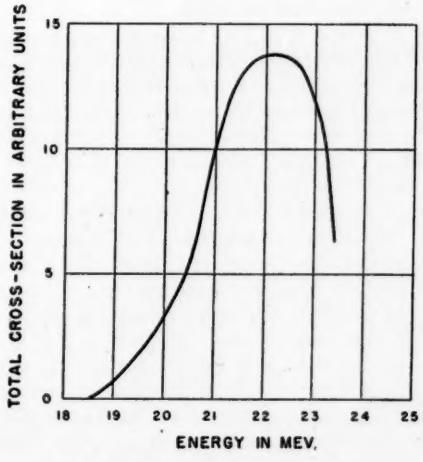

FIG. 3. Excitation function $C^{12}(\gamma,p)B^{11}$.

Since the yield curve is that of a thick (4.8-Mev) target, and since the protons must possess an energy of at least 2 Mev in order to reach the detector, the threshold of this excitation function is probably too high and its shape near the threshold is distorted. However, the threshold calculated from the mass values is 16 Mev. If the proton barrier and air absorption are taken into account, then the value of the threshold in Fig. 3 is within one Mev of the expected value. From the known geometry of the experimental arrangement and the effective target thickness, it is possible to assign an absolute value of 1×10^{-26} cm² to the cross section at the peak of the excitation function. It should be emphasized that this value has not been corrected for counter efficiency and target absorption, and therefore represents a lower limit of the actual value. We estimate that the upper limit does not exceed this value by more than a factor of five.

We are at present applying the techniques described here to a survey of the relative yields and angular distributions of photoprotons from various elements and are continuing the investigation of $\gamma-p$ excitation functions.

Each of us wishes to acknowledge a grant from the Committee on the Advancement of Research of the University of Pennsylvania.

* This work was supported in part by the joint program of the ONR and AEC.

[1] H. W. Koch and R. E. Carter, Phys. Rev. 77, 165 (1950); R. N. H. Haslam *et al.*, Phys. Rev. 80, 318 (1950). We are indebted to Professor Katz for a private communication.

The Isotopes of Xenon and Krypton in Pitchblende and the Spontaneous Fission of U^{238}

J. MACNAMARA AND H. G. THODE
Department of Chemistry, McMaster University, Hamilton, Ontario, Canada
August 31, 1950

IT has been known for some time that the uranium nucleus undergoes spontaneous fission.[1,2] Recent values for the spontaneous fission half-life of uranium range from $(1.3\pm0.2)10^{16}$ to $(1.9\pm0.1)10^{16}$ years.[3-5] Since the spontaneous fission rate for U^{235} has been found to be approximately the same as that for natural uranium,[6] the spontaneous fission rate of natural uranium will be essentially that of the much more abundant isotope, U^{238}. The small concentration of plutonium in pitchblende[7] would seem to preclude the possibility of appreciable neutron fission of U^{235}.

As one would expect a similar distribution of fission fragments originating in the spontaneous fission of U^{238} as in the neutron fission of U^{235}, especially in the neighborhood of the 82-neutron shell, appreciable quantities of fission product krypton and xenon should be present in pitchblende. Since very little is known of the fission products from the spontaneous fission of uranium, experiments were designed to extract these rare gases with the hope that sufficient quantities could be obtained for mass spectrometer investigations. During the course of this work Khlopin, Gerling, and Baranovskaya[8] reported a much higher ratio of Xe to Kr in pitchblende than is normally found in the atmosphere, indicating the presence of appreciable quantities of fission product xenon.

The rare gases in a sample of pitchblende from Great Bear Lake, Canada, have now been extracted, purified, and analyzed with a mass spectrometer. The purified gas samples analyzed contained about 5×10^{-4} c.c. at N.T.P. of total xenon and krypton. Five fission product isotopes of xenon (Xe^{129}, Xe^{131}, Xe^{132}, Xe^{134}, Xe^{136}), and three of krypton (Kr^{83}, Kr^{84}, Kr^{86}) have been identified. The samples also contained some normal xenon and krypton as indicated by the presence of non-fission product isotopes in abundances proportional to their concentration in normal atmospheric gases.

Thus it was possible to determine with considerable accuracy the ratio of fission product to normal material. The ratios of fission product xenon to normal xenon and fission product krypton to normal krypton were 4:1 and 1:24, respectively.

The abundance data for the fission product isotopes of xenon and krypton are given in Table I.

TABLE I. The abundance data for the fission product isotopes of xenon and krypton from the spontaneous fission of U^{238}.

Xenon		Krypton	
Mass	Yield[a] (percent)	Mass	Yield[b] (percent)
129	0.088 ±0.013	83	0.12 ±0.01
131	0.74 ±0.02	84	0.45 ±0.05
132	3.46 ±0.025	86	1.64 ±0.15
134	5.10 ±0.014		
136	6.00		

[a] Xe^{136} taken as 6.00 percent.
[b] Xe/Kr ratio taken as 7.0.

It is interesting to note that Xe^{129} is a product in the spontaneous fission of U^{238}. This is not surprising, since the half-life of I^{129} is estimated[9] to be 10^8 yr., or about 1/14 the age of the pitchblende sample.[10] By extracting the xenon from pitchblende of different ages and determining the abundance of Xe^{129}, relative to another stable isotope of xenon, it is hoped to obtain a more accurate half-life for I^{129}.

Figure 1 is a mass fission yield curve obtained by plotting the data of Table I. The curve will vary slightly depending on the yield value assigned to Xe^{136} and to the ratio of xenon to krypton formed in the fission process. The ratio of xenon to krypton of 7.0 used in the calculations was determined by direct mass spectrometer measurements and is a preliminary value. The results indicate an asymmetrical mass fission yield curve similar to that obtained in the fission of U^{234} and U^{236} with maxima at approximately 95 and 140 in agreement with the results of Whitehouse and Galbraith.[11] The higher ratio of Xe to Kr found, however, would indicate a shifting of the whole mass fission yield curve toward the heavier masses which would be expected for the spontaneous fission of U^{238}. The relatively high yield of Xe^{132} is of particular interest. It can be seen from Figs. 1 and 2 that the fission yield of this isotope is about 65 percent above the smooth curve drawn through yield values for the other xenon isotopes. Since the relative precision of these yield values is better than one percent (except for Xe^{129}), it is clear that Xe^{132} has an abnormally high yield.

The fine structure previously reported in the mass fission yield curve for U^{236} fission[12] appears also in the neighborhood of nuclides with 82 neutrons, but the high yields occur at Xe^{133} and Xe^{134}, not Xe^{132}. This shifting of the fine structure to the lower masses would be expected, if we accepted the hypothesis of Glendenin[13] to account for these abnormal yields.

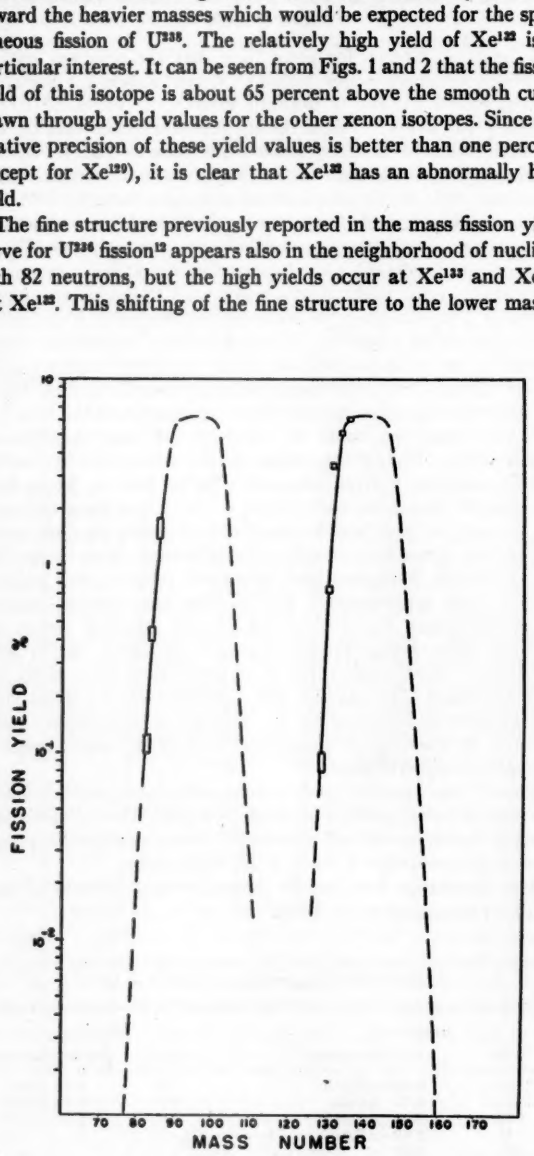

FIG. 1. Mass fission yield curve for spontaneous fission of U^{238}.

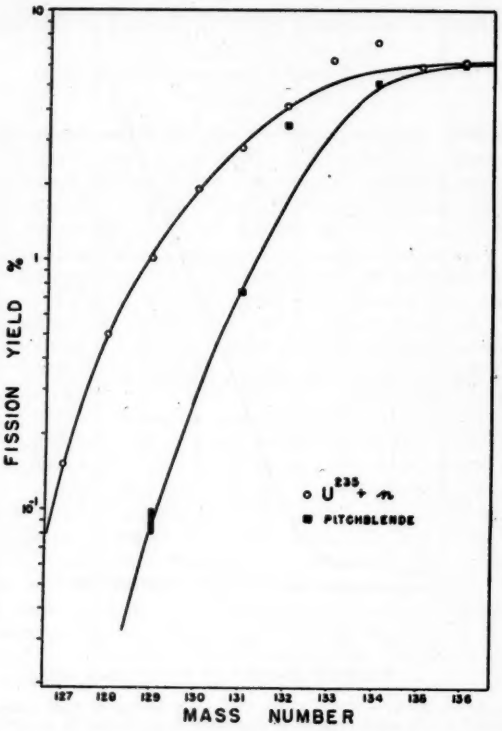

FIG. 2. Mass fission yield curve for the fission of U^{236} and U^{238} showing fine structure.

A careful investigation of the relative abundances of the argon isotopes occluded in the pitchblende sample showed less than a three percent variation in the argon 40 to argon 36 ratio when compared with atmospheric argon. This would seem to indicate that there is little fractionation of the xenon and krypton isotopes due to different rates of diffusion out of the mineral.

Experiments are in progress to determine actual volumes of fission product xenon and krypton in pitchblende samples of different ages. These determinations will yield an accurate ratio of Xe to Kr and will make possible estimates of the total amount of fission per gram of uranium for geophysical age studies. Also, similar studies are under way with thorium minerals to determine the extent of spontaneous fission of thorium.

The authors wish to thank M. Dubeck for his assistance in preparing the samples and R. F. Errington and the Eldorado Mining and Refining Company, Limited for the samples of pitchblende. We also wish to acknowledge the financial assistance from the National Research Council of Canada.

[1] K. A. Petrzhak and G. N. Flerov, J. Phys. U.S.S.R. 3, 275 (1940); Chem. Abs. 35, 4677[1] (1941).
[2] G. N. Flerov and K. A. Petrzhak, Phys. Rev. 58, 89 (1940).
[3] N. A. Perfilov, J. Phys. U.S.S.R. 11, No. 3 (1947), Chem. Abs. 42, 2864 (b) (1948).
[4] H. Yagoda and N. Kaplan, Phys. Rev. 76, 702 (1949).
[5] W. Maurer and H. Pose, Zeits. f. Physik 121, 285 (1943).
[6] R. R. Williams, *Principles of Nuclear Chemistry* (D. Van Nostrand and Company, Inc., New York, 1950), p. 27.
[7] Peppard, Studier, Gergel, Mason, Sullivan, and Mech, paper presented at 118th Meeting of American Chemical Society, Chicago, September 1950.
[8] Khlopin, Gerling, and Baranovskaya, Bull. Acad. Sci. U.R.S.S. Classe. Sci. Chim. 599-604, 1947; Chem. Abs. 42, 3664[a], (1948).
[9] S. Katcoff, Phys. Rev. 71, 826 (1947).
[10] A. O. Nier, Phys. Rev. 55, 153 (1939).
[11] W. G. Whitehouse and W. Galbraith, Phil. Mag. 41 (May, 1950).
[12] Macnamara, Collins, and Thode, Phys. Rev. 78, 129 (1950).
[13] L. E. Glendenin, Phys. Rev. 75, 337 (1949).

On Range-Momentum Measurements for Electrons in Gases*

G. F. O'NEILL† AND W. T. SCOTT‡
Brookhaven National Laboratory, Upton, Long Island, New York
September 5, 1950

THE high pressure cloud chamber offers a convenient means for determining the range-momentum relations for slow electrons in gases. The purpose of this note is to report on some preliminary measurements made with a high pressure cloud chamber described previously.[1] Gamma-rays from Na^{24} produced Compton electrons of momenta up to 1.1 Mev/c, which were investigated in hydrogen and helium at 136 atmospheres pressure and with a regionally calibrated magnetic field of approximately 4000 gauss. The vapor was a water-alcohol mixture.

Because of the high energy loss in the dense gases, the particles were bent into spirals (Fig. 1) instead of the circles found at low pressure. Thus, each track that can be seen to its end could be used to give a range-momentum relation. A good fraction of the statistical fluctuation was eliminated by excluding trucks having high energy knock-ons, with accompanying sudden curvature changes. To obviate the necessity for corrections for drift in the line of sight, only regular spirals nearly in the plane of the cloud chamber were chosen. The curvatures were measured by fitting circles at approximately 1-cm intervals along the path. The results of measurements on four tracks in helium and three in hydrogen are given by the points in Figs. 2 and 3. The large amount of useful data available from each track is evident.

An analysis of scattering induced curvature in high pressure gases will be given in a later paper. It has been found that with the 4000-gauss magnetic field about 1/10 of the curvature was due to scattering. In a heavier gas, such as argon, the scattering curvature is about equal to the magnetic curvature. A stronger magnetic field (such as that in the high pressure chamber with a 36,000-gauss magnetic field nearing completion at the Brookhaven Laboratory) would be necessary to use this method of obtaining the range-momentum relation in argon at this pressure, and, of course, a high range of energies would have to be used.

FIG. 1. Electron spirals in helium, showing one useful track (actual diameter 3 cm) and several others.

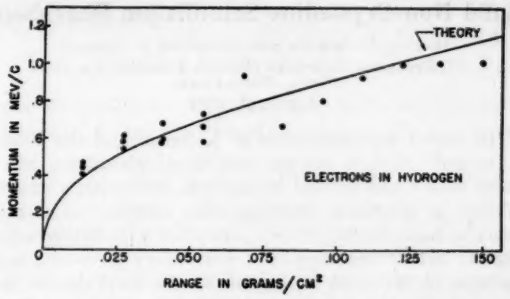

FIG. 2. Experimental and theoretical range-momentum relation for electrons in helium.

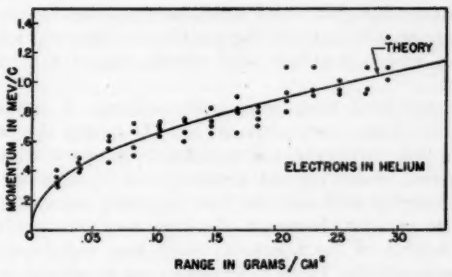

FIG. 3. Experimental and theoretical range-momentum relation for electrons in hydrogen.

It is of interest to compare these experimental points with the usual energy loss theory. Radiation loss can be neglected, as the only cases of importance would be the relatively rare emission of a large fraction of the energy in one photon, resulting in a detectable sudden change of curvature. No tracks with such curvature changes were included.

The collision loss was calculated from Eq. (76) of Møller,[2] with use of Rossi and Greisen's formula[3] for small energy losses. The value of the ionization potential $I(Z)$ was taken from experiments of Mano[4] on alpha-particle ranges. A knock-on electron was considered as being certainly visible if its energy was 64 kev $=mc^2/8$, and this value was used as an upper limit in the integration of Møller's formula. Numerical integration was used above 375 kev/c momentum loss; below this value a curve of the form $pc=AR^{0.43}$ was used,[5] using the ordinate and slope of the integrated curve at $pc=375$ kev to determine R at this point, and then finding A.

The resulting curves are given in Figs. 2 and 3. It is evident that even a few tracks give a reasonable confirmation of the theory, and that this method is capable of yielding rather accurate results.

We wish to acknowledge the advice and assistance of A. R. Hoke, W. A. Tuttle, and R. P. Shutt in connection with the operation of the cloud chamber at Brookhaven.

* Research carried out at Brookhaven National Laboratory, under the auspices of the AEC.
† Now at Fordham University. The experimental work here reported was performed by the first-named author at Brookhaven National Laboratory as part of a Ph.D. thesis at Fordham University.
‡ On summer leave from Smith College, Northampton, Massachusetts.
[1] Johnson, Benedetti, and Shutt, Rev. Sci. Inst. 14, 265 (1943).
[2] C. Møller, Ann. d. Physik 14, 531 (1934).
[3] B. Rossi and K. Greisen, Rev. Mod. Phys. 13, 240 (1941).
[4] G. Mano, Ann. de Physique 1, 407 (1934).
[5] This formula was derived by fitting a power-law expression to curves in D. J. X. Montgomery, *Cosmic-Ray Physics* (Princeton University Press, Princeton, 1949).

Solid Non-Crystalline Scintillation Phosphors

MARVIN G. SCHORR AND FRANKLIN L. TORNEY
Physics and Electronics Division, Tracerlab, Inc., Boston, Massachusetts
August 31, 1950

THE recent announcements of Kallman[1] and the Princeton group[2,3] of their success with liquid phosphors, and particularly with terphenylated metaxylene, immediately raises the possibility of obtaining counting solid solutions of terphenyl, anthracene, naphthacene, stilbene, and other scintillating materials in organic plastic materials. For low energy beta-counting the advantages of the solid is obvious, as are they also in ease of preparation as compared to crystal growing.

We have found that 0.5 percent terphenyl in *m*-xylene, when rapidly frozen so that the terphenyl does not leave the solution, will count Co^{60} gamma-rays. The counting efficiency when frozen was about one-half that of the liquid, but the solid was very cloudy so that presumably much of the scintillation light was lost in the phosphor. Frozen *m*-xylene itself counts, but at a much lower efficiency.

More successful have been solid solutions of terphenyl in polystyrene. These were prepared by: (1) mixing the terphenyl in molten polystyrene; (2) polymerizing a solution of styrene with a one percent benzoil peroxide catalyst; and (3) without the catalyst. All counted well, but the best phosphor resulted from the use of the catalyst. However, the other methods involved protracted heating of the solutions, which may well have affected their characteristics. Large clear masses are obtainable with terphenyl percentages at least up to two percent. The effects of terphenyl concentration on counting rates are given in Fig. 1.

The scintillation pulses have been investigated with both 1P21 photo-multipliers in a two-channel coincidence circuit and a single 5819 tube cooled with dry ice. The counting efficiency for gammas and betas is comparable to that obtained with clear stilbene crystals. Viewing of the pulses on a synchroscope shows them to have a rise and decay time of less than 0.05 μsec. with pulse heights somewhat smaller than those obtained from stilbene. Typical plots of counting rate for Cs^{137} gamma-rays as a function of photo-multiplier voltage for a five percent terphenyl polymer and a polymer containing 10 percent dissolved *trans*-stilbene are shown in Fig. 2. A curve for a clear, single stilbene crystal is included as reference. The reason for the smaller plateau slopes of the plastics is not completely understood, but may be due to less aftercounting in the phosphor. The synchroscope shows a much smaller occurrence of secondary pulses following the scintillation than is observed with crystalline phosphors. As the tube voltage is raised, these secondaries can start giving multiple counts. A detailed investigation of the concentration and purity of the materials, effects of catalysts, and response to different types of radiation is underway. Other materials will also be studied.

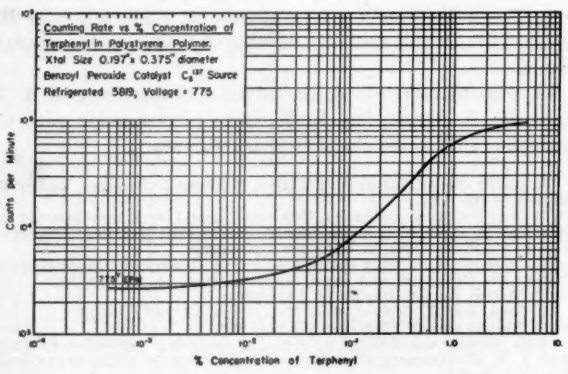
Counting Rate vs % Concentration of Terphenyl in Polystyrene Polymer.
Xtal Size 0.197"x 0.375" diameter
Benzoyl Peroxide Catalyst
Refrigerated 5819, Voltage = 775
Counts per Minute
% Concentration of Terphenyl

FIG. 1. Effect of terphenyl concentration on counting efficiency of plastic.

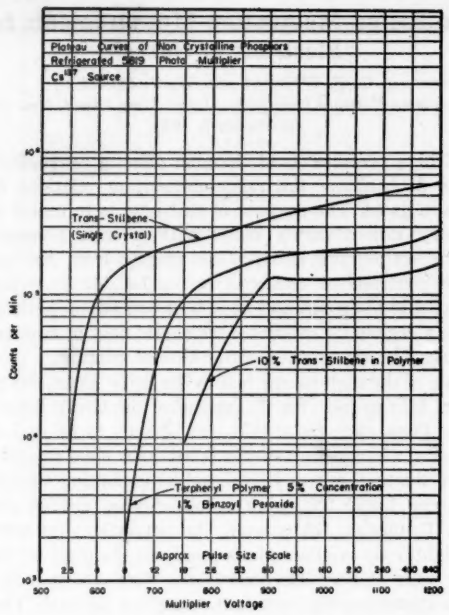

FIG. 2. Counting plateaus for plastics and a clear single crystal of stilbene.

The mechanism here seems distinct from that involved in the work of Robinson, *et al.*[4] in which crystalline zinc sulfide was imbedded in plastic.

It would seem quite reasonable to suppose that much of the observed counting in commercial polystyrene, Lucite, and quartz may be due to small terphenyl-like impurities.

The phosphor samples were prepared by Dr. J. Bornstein of these laboratories; the possibilities of solid solution phosphors were first pointed out to us by Dr. Walter Juda of Ionics, Inc.

[1] H. Kallman, Phys. Rev. **78**, 621 (1950).
[2] G. T. Reynolds, Nucleonics **6**, 68, (May, 1950).
[3] Reynolds, Harrison, and Salvini, Phys. Rev. **78**, 488 (1950).
[4] Robinson, Cook, and Jefferson, J. Chem. Phys. **18**, 148 (1950).

On the μ-Meson Decay*

G. G. HARRIS AND T. J. B. SHANLEY
Palmer Physical Laboratory, Princeton University, Princeton, New Jersey
August 4, 1950

AN experiment is being performed to investigate the energy of the gamma-rays resulting from the capture of negative μ-mesons in lead. This experiment is an extension of work initiated by Chang,[1] and differs from the previous work in that the cloud chamber is in a magnetic field of 2200 gauss. The chamber expansion is controlled by a Geiger counter telescope that selects events in which a particle stops in the chamber foil system.

During the course of the experiment several pictures have been obtained showing positive and negative mesons stopping in the gas of the chamber. One of these events is considered of interest because of the low energy of the decay particle. Observation of momentum and ionization serve to identify the decay product as a positron. The momentum of the decay particle is 6.2 ± 1.7 Mev/c, corresponding to a positron energy of 5.7 ± 1.8 Mev. Interest in the event arises from the fact that the observations of Leighton *et al.*[2] indicate that the probability of a decay product of such a low energy is very small.

* Assisted by the ONR.
[1] W. Y. Chang, Rev. Mod. Phys. **21**, 166 (1949).
[2] Leighton, Anderson, and Seriff, Phys. Rev. **75**, 1432 (1949).

Variational Methods in Collision Problems

TOSIO KATO
Department of Physics, Tokyo University, Tokyo, Japan
June 22, 1950

RECENTLY variational methods have been applied successfully to scattering problems by several authors. However, it appears to be rather strange that so many different methods have been proposed for the one simple problem of scattering by a center of force. In the present note we wish to point out some simple relations existing among these apparently independent procedures.

For simplicity consider the radial wave equation for S-scattering

$$L[u]\equiv d^2u/dr^2+k^2u+W(r)u=0. \tag{1}$$

Let us normalize the trial wave function by the conditions

$$u(0)=0, \quad u(r)\to\cos(kr+\theta)+\lambda\sin(kr+\theta), \quad r\to\infty, \tag{2}$$

in which θ is a fixed constant (usually zero or $\pi/2$) and λ is an adjustable parameter. For the correct wave function λ is connected with the phase, η, by the relation $\lambda=\cot(\eta-\theta)$.

It is easily shown that

$$\delta\int_0^\infty uL[u]dr=k\delta\lambda$$

for the correct wave function, $u=u_0$. In other words, the functional

$$F\equiv F[u]=k\lambda-\int_0^\infty uL[u]dr \tag{3}$$

is stationary for $u=u_0$ and is equal to $k\cot(\eta-\theta)$ since $L[u_0]=0$. If we set $\theta=\pi/2$ (hence $\lambda=-\tan\eta$), we have the variational method originally due to Kohn[1] and equivalent also to Huang's method[2] if we make a slight modification in the latter.

The methods of Hulthén[3] and Schwinger[4] can also be derived directly from (3) with $\theta=0$ (hence $\lambda=\cot\eta$). To show this, it is convenient to set

$$\begin{aligned} &u=\cos(kr)-y+\lambda\sin(kr),\\ &y(0)=1, \quad y\to0 \text{ as } r\to\infty. \end{aligned} \tag{4}$$

Substitution of (4) into (3) and integration by parts yields

$$F=F_H\equiv-J+2(k-N)\lambda-k\eta_B\lambda^2, \tag{5}$$

with

$$\begin{aligned} &J=\int_0^\infty[k^2y^2-(dy/dr)^2+W(\cos(kr)-y)^2]dr,\\ &N=\int_0^\infty\sin(kr)\cdot[\cos(kr)-y]Wdr, \quad k\eta_B=\int_0^\infty\sin^2kr\cdot Wdr. \end{aligned} \tag{6}$$

Here y contains some adjustable constants $c_1, c_2, \cdots$. To make F_H stationary we set

$$\partial F_H/\partial c_n=0, \quad \partial F_H/\partial\lambda=0,$$

or

$$\partial J/\partial c_n+2\lambda\partial N/\partial c_n=0, \quad (n=1, 2, \cdots), \tag{7}$$

$$k\eta_B\lambda=k-N. \tag{8}$$

These equations are in complete agreement with those of Hulthén's second method.[5] Furthermore, we have by (5) and (8)

$$F_H=-J+(k-N)\lambda=k\lambda-\Delta, \quad \Delta=J+\lambda N. \tag{9}$$

Since (9) should give $k\cot\eta$ correctly up to the first order, this also coincides with his result:[6] $\cot\eta=\lambda-k^{-1}\Delta$. Thus Hulthén's second method is equivalent to our (3) with $\theta=0$, and hence it is based on the correct variation principle, although his original derivation is not very simple. Also it will be noted that his method gives $k\cot\eta$ *explicitly* as the stationary value[7] of (3).

Next, consider the functional

$$F_s=F_H+\int_0^\infty(L[u])^2W^{-1}dr. \tag{10}$$

An application of the variation principle to F_s leads to the same results as those given above, *for the second term on the right-hand side of (10) vanishes for the correct solution, together with its variation.* On substituting (4) into (10) and integrating by parts, we obtain, setting $z=\cos(kr)-y$,

$$F_s=\int_0^\infty(d^2z/dr^2+k^2z)^2W^{-1}dr+\int_0^\infty z(d^2z/dr^2+k^2z)dr. \tag{11}$$

Setting $d^2z/dr^2+k^2z=-Wv$, and noting that $z\to\cos(kr)$ as $r\to\infty$, we obtain from Green's theorem

$$z(r)=\int_0^\infty G(r, r')W(r')v(r')dr', \tag{12}$$

where $G(r, r')$ is the Green's function used in Schwinger's method.[8] In this way we find

$$F_s=\int_0^\infty Wv^2dr-\int_0^\infty Wvdr\int_0^\infty G(r, r')W(r')v(r')dr'. \tag{13}$$

It will be noted that

$$k^{-1}\int_0^\infty Wv\sin(kr)dr=1$$

by virtue of the condition $y(0)=1$. If we remove this restriction on v and write (13) in a homogeneous form by the well-known method, F_s becomes just the expression for $k\cot\eta$ in Schwinger's method,[9] which is thus connected with Hulthén's by the simple relation (10). Sometimes it would be convenient to use the former in the form (10) which does not contain a double integral, in contrast to (13). *An interesting consequence of (10) is that the Schwinger method always gives a larger (smaller) value of $k\cot\eta$ than does Hulthén's if $W(r)\geqq0$ [$W(r)\leqq0$] everywhere.* It can even be shown that it gives an upper (lower) bound for $k\cot\eta$ if W is not too strong (more precisely, if $|\eta|<\pi$).[10]

These results can be extended to more general cases (higher angular momentum, inclusion of Coulomb potential).

[1] W. Kohn, Phys. Rev. **74**, 1763 (1948), Eq. (2.14).
[2] S. Huang, Phys. Rev. **76**, 1878 (1949).
[3] L. Hulthén, K. Fysiogr. Sällsk. Lund Föohandl. **14**, No. 21 (1944); Arkiv. Mat. Astr. Fys. **35A**, No. 25 (1948).
[4] J. Schwinger, Phys. Rev. **72**, 742 (1947); **78**, 135 (1950). J. M. Blatt and J. D. Jackson, Phys. Rev. **76**, 18 (1949).
[5] See reference 3, second paper, Eqs. (23) and (24).
[6] See reference 5, Eq. (36).
[7] His first method (reference 3, first paper) can also be derived easily from our standpoint. We have only to replace (8) by $\int uL[u]dr=0$; this changes the trial function, u, only by a first-order quantity and hence F is unaffected to the first order. Since F reduces to $k\lambda$ in this case, this is exactly equivalent to the first method of Hulthén.
[8] J. M. Blatt and J. D. Jackson, reference 4, Eq. (2.7).
[9] See reference 8, Eq. (2.11). It will be remarked that our function, v, does not necessarily satisfy the boundary condition $v(0)=0$. But this is not essential, for it follows for the correct solution automatically from the variation principle (natural boundary condition).
[10] The proof will be given elsewhere together with generalizations.

Mass Assignments of Alpha-Active Isotopes in the Rare-Earth Region*

J. O. RASMUSSEN, F. L. REYNOLDS, S. G. THOMPSON, AND A. GHIORSO
Radiation Laboratory and Department of Chemistry, University of California, Berkeley, California
September 7, 1950

IN a previous communication from this laboratory, the production of alpha-radioactivity in the rare-earth elements was reported.[1] The suggestion was made that this might be due to the influence of the stable configuration of 82 neutrons on the daughter nuclides and some likely isotopic assignments were proposed on this basis. We have succeeded in testing this suggestion through the use of the mass spectrograph to make an isotopic assignment for one of the major artificial rare-earth alpha-activities with the result that this explanation seems to be confirmed.

The mass assignment of the alpha-emitting terbium isotope of 4.0-hr. half-life and 4.0-Mev alpha-particle energy was made by performing a mass spectrographic separation of terbium activity onto a photographic plate and detecting alpha-activity by a transfer plate technique. The terbium activity (6×10^7 alpha-disintegrations per minute at end of a 5-hr. bombardment) was produced by bombardment of 30 mg of gadolinium oxide with 150-Mev protons in the 184-inch cyclotron, and rapid chemical separation was made by elution from cation exchange columns

with 1/4 μg terbium carrier added before elution. The equipment and method used in the separations were essentially as described previously in the work by Thompson *et al.* on the new element berkelium.[2] Two column separations were made in order to remove all of the gadolinium, the first column of 1.0 cm diameter, the second of 2 mm diameter. One-fourth μg of samarium nitrate in solution was added to the active terbium fraction before mass spectrographic separation to serve as an internal mass standard. The products of the mass spectrographic separation in the 60° slit-type mass spectrograph, using a thermal ionization source from a tungsten filament, were collected on an Eastman III-0 photographic plate. Before development this plate was left face to face with an Eastman NTA transfer plate for a day. After development the collection plate showed solid lines at the mass numbers corresponding to all the stable samarium isotopes (as both Sm^+ and SmO^+) and to stable terbium (as Tb^+). The transfer plate was searched with a microscope for alpha-tracks. A concentration of alpha-tracks was observed on the transfer plate only in a region corresponding to mass 149. The 4-hr. terbium alpha-activity was the only alpha-activity here present in large enough amount to be detected by this technique. Tb^{149} has 84 neutrons and would thus be expected to have the maximum alpha-decay energy of the terbium isotopes in this mass region.

The suggestion was also made in the previous communication[1] that the long-known natural radioactivity of samarium might be assigned to Sm^{147} or Sm^{148}, rather than to Sm^{152}, since this assignment would be more consistent with decay toward the stable configuration of 82 neutrons (on this basis the most alpha-unstable samarium isotope would be Sm^{146}, and its anomalous absence from nature would thus be explained). This hypothesis has also been tested and it has been found that a major part of this natural radioactivity should indeed be assigned to Sm^{147}. The possibility that there may be also some alpha-radioactivity of nearly the same energy associated with Sm^{148} has not been ruled out.

A sample of isotopically pure Sm^{147} was obtained by ion exchange chemical separation from an 0.8 mg amount of Pm^{147} (a beta-emitter variously reported as 2.26-yr.[3] or 3.7-yr.[4] half-life) which had been allowed to decay for about a year. This samarium sample was analyzed in an optical spark spectrograph to establish its chemical purity, in the mass spectrograph to prove the material was isotopically pure mass 147, and was examined for alpha-activity in an ionization chamber with differential pulse-height analyzer, which affords an alpha-energy determination in addition to detection. Alpha-activity of the same energy as that of the natural samarium alpha-activity was observed. The specific alpha-activity of this small sample of Sm^{147} has not yet been accurately determined, but it is roughly of the order of magnitude to account for the total alpha-activity observed in natural samarium.

Dempster[5] had previously come to the conclusion that the natural samarium alpha-activity should be assigned to Sm^{147} on the basis of a continuance of his work using isotopic separation with the mass spectrograph together with the photograph technique for detection.

We are grateful for the advice and suggestions of Glenn T. Seaborg. We wish to thank Dr. John Swartout of Oak Ridge National Laboratory for making available to us the Pm^{147}. The help of J. C. Conway and M. F. Moore in the spectrographic analysis is also gratefully acknowledged. We wish also to thank J. T. Vale and the crew of the 184-inch cyclotron for their assistance in this work.

* This work was performed under the auspices of the AEC.

[1] Thompson, Ghiorso, Rasmussen, and Seaborg, Phys. Rev. **76**, 1406 (1949).

[2] Thompson, Cunningham, and Seaborg, J. Am. Chem. Soc. **72**, 2798 (1950).

[3] Ingram, Hayden, and Hess, Phys. Rev. **79**, 271 (1950).

[4] J. A. Seiler and L. Winsberg, *Radiochemical Studies: The Fission Products* (McGraw-Hill Book Company, Inc., New York), National Nuclear Energy Series, Plutonium Project Record, Vol. 9B (to be published).

[5] A. J. Dempster, tentative result given in Argonne National Laboratory Report ANL-4355 (October, 1949), unpublished.

Magnetic Shielding Constant of H_2

G. F. Newell
Physics Department, University of Illinois, Urbana, Illinois
September 20, 1950

RECENT investigations of the magnetic shielding effects in the H_2 molecule[1-3] have shown that, to calculate $-\Delta H/H$, the fractional change of the magnetic field H at a nucleus due to the electrons, it is necessary to know the average value of r^{-1}. Here r is the distance of one of the electrons from the nucleus considered and the average must be taken over the electron distribution of the ground state of H_2.

The electronic wave function derived previously by the author[4] is used to determine average r^{-1} as a function of the internuclear distance R. The results are given in Table I.

Averaging these values over the zero-point vibration of the molecule gives average $r^{-1}=0.904\pm0.003$. The error is estimated following the procedure used in reference 4 to determine the error in the electric field gradient. Further assurance of the reliability of the estimated limits of error is obtained by comparison with the known error of the electron energy[4] calculated from this wave function. Since average r^{-1} is $\frac{1}{4}$ of the potential energy of the molecule excluding the mutual repulsion of the two electrons, it is one of the major contributions to the energy of the molecule. The percentage error given for average r^{-1} is comparable to the percentage error in the energy of the electron distribution, as one would expect it to be.

TABLE I. Average r^{-1} as a function of the internuclear separation R. r^{-1} and R are given in atomic units.

R	Average r^{-1}
1.2	0.982
1.3	0.946
1.4	0.915
1.5	0.886

The formula for the magnetic shielding constant of H_2 as given by Ramsey[2] is

$$\sigma=-\Delta H/H=\tfrac{1}{3}\alpha^2(\text{average } r^{-1}) -(\alpha^2a_0R^2/6\mu_N)[(2Z\mu_N/R^3)-(\mu' H_r/MJ)].$$

The notation is essentially that used by Ramsey (Eq. (24) of reference 2).

A new value $(3.21\pm0.01)\times10^{-5}$ obtained for the first term of σ is to be compared with the value $3.2_4\times10^{-5}$ given by Anderson[1] using Nordsieck's wave function[5] and the value 3.16×10^{-5} by Hylleraas and Skavlem.[3] The latter two values are those at the equilibrium value of R and are not averages over the molecular vibration. This explains the difference between the present value and Anderson's; the present calculation giving 3.25×10^{-5} at the equilibrium position $R=1.4$. The Hylleraas and Skavlem value was obtained from a much less accurate wave function.

The second term of σ is given by Ramsey as $(0.56\pm0.01)\times10^{-5}$, the error being only that due to the experimental error in H_r. Anderson[6] has pointed out that the molecular vibration contributes an additional source of error in this term. A correction for this is less easily made here than in the first term because H_r is not known as a function of R. An experimentally measured value of H_r, which itself corresponds to an average over the molecular vibration, is known, however. A theoretical expression[2] for H_r is composed of integrals containing the factor r^{-3}. For this reason, we assume that $H_r(R)$ varies as R^{-n}, choose $n\sim3$, and require that the average of $H_r(R)$ be 13.66 as given by Ramsey.

The average value of the second term of σ calculated in this way becomes 0.55×10^{-5}. Because of the uncertainty of the assumptions made above, the error of this is taken to be 5 percent, which would correspond to an error in n of about ±1.5.

The resulting expression for σ is

$$\sigma=(3.21\pm0.01)\times10^{-5}-(0.55\pm0.03)\times10^{-5}$$
$$=(2.66\pm0.03)\times10^{-5}.$$

The error in σ given above is smaller than is necessary in order to correct any experimental data obtained thus far. Greater accuracy than this will undoubtedly be necessary, however, for some future experiments.

[1] H. L. Anderson, Phys. Rev. **76**, 1460 (1949).
[2] N. F. Ramsey, Phys. Rev. **78**, 699 (1950).
[3] E. Hylleraas and S. Skavlem, Phys. Rev. **79**, 117 (1950).
[4] G. F. Newell, Phys. Rev. **78**, 711 (1950).
[5] A. Nordsieck, Phys. Rev. **58**, 310 (1940).
[6] H. L. Anderson, private communication.

Scintillation Decay Times*

ARNE LUNDBY
Institute for Nuclear Studies, University of Chicago, Chicago, Illinois
August 21, 1950

THE decay curves for the scintillation of some molecular crystals, excited by nuclear γ-rays, have been determined using a delayed coincidence apparatus. The results are given in Fig. 1 and Table I.

In the experimental arrangement, one or two 1P21 photo-multipliers were used to detect the photons emitted by the crystals. The output from the ninth dynode of the multipliers was fed through RG 7/U coaxial cables (used as delay lines) and amplified in distributed amplifiers before being applied to a germanium diode coincidence circuit. The photo-multipliers were either excited by separate crystals or by one crystal placed between them. The decay curves were measured by varying the relative length of the RG 7/U cables in the two channels.

By varying the bias on the coincidence discriminator, one can select coincidences due to a superposition of one, two, three, etc., photon pulses in the non-delayed channel with the pulses in the delayed channel. For delays exceeding the width of the pulses at the input of the coincidence circuit, the coincidence rate is then given by $\Sigma_{n\geq1}A_n\exp(-nt_d/\tau)$. τ is the decay time of the scintillation, t_d is the time delay, n is essentially the number of single photon pulses contributing to the recorded coincidence pulse from the non-delayed channel, and A_n are constants independent of t_d. The present experiment was so arranged as to record coincidences due to three or more photons only. This was done in order to obtain an effective discrimination between the true coincidence pulses and large single pulses feeding through the coincidence circuit. Furthermore, this procedure leads to an increased resolving power in delayed coincidence experiments. The half-width of the delayed coincidence curve for radiations following each other in instantaneous succession is independent of the pulse sizes in the two channels, and the coincidence rate decays with a time constant which is three times the lifetime of the crystal. The contribution from coincidences due to relatively large pulses being generated by one or two photons in the non-delayed channel or pulses due to four or more photons was observed for lower, respectively higher discriminator bias settings. In Fig. 1, the measurements corresponding to the term $\exp(-3t_d/\tau)$ are shown. The crystals and the photo-multipliers were operated at room temperature (+24°C). In order to obtain an estimate of the width of the pulses due to single electrons released from the cathode (curve F, Fig. 1), self-coincidences of thermal noise pulses from one multiplier were recorded or, alternatively, a strong Co^{60} γ-ray source was inserted between the multipliers.

The 1,4-diphenylbutadiene and the *para*-terphenyl were used in the form of microcrystalline powder[1] in Lucite containers. The luminescence of the Lucite was negligible. The *trans*-stilbene,[2] anthracene,[3] and naphthalene[4] were available as transparent crystals.

The average lifetimes of the excited crystals, being three times the decay periods deduced from the curves in Fig. 1, are listed in Table I.

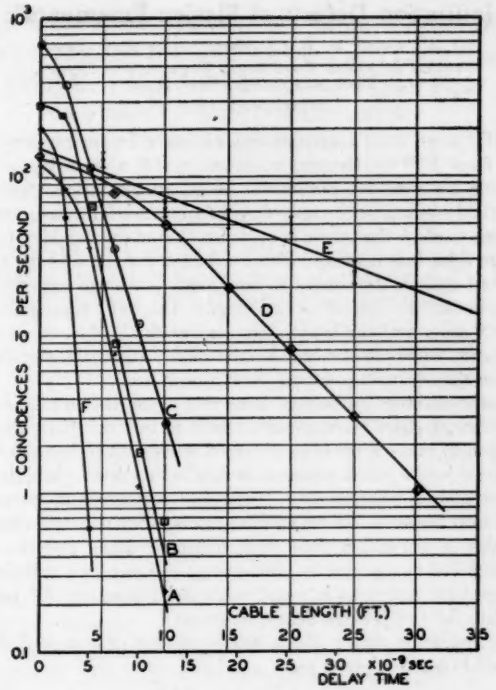

FIG. 1. The decay curves $\exp(-3t_d/\tau)$ of scintillations from: A: 1,4-diphenylbutadiene, B: *p*-terphenyl, C: *t*-stilbene, D: anthracene, and E: naphthalene. Curve F represents noise pulses. The ordinates of curve E have been multiplied by a factor of 1000. This curve also runs through a point with coordinates (55 ft., 0.004 ± 0.001 sec.$^{-1}$).

TABLE I. Decay times of scintillation crystals.

Crystal	$\tau(1/e)$ in 10^{-9} sec.
p-terphenyl	4.2
1,4-diphenylbutadiene	4.2
t-stilbene	5.7
anthracene	24
naphthalene	60

The curvature of the decay curves near the ordinate axis in Fig. 1 is caused either by saturation of the multipliers or by a superposition of pulses due to several photons. This was demonstrated by recording triple coincidences between multiplier anode pulses of different integral charge and the fast double coincidences. For the large pulses, the curvature was much more predominant while for the small pulses it disappeared.

The width of the pulses due to single electrons liberated from the cathode of the photo-multiplier (curve F, Fig. 1) is apparently determined by the rise time of the distribution amplifiers (2.6×10^{-9} sec.). This was borne out by experiments without amplifiers preceding the coincidence circuit, giving a pulse width $\lesssim10^{-9}$ sec., which is in general agreement with the value calculated by Sard[5] and with the experimental results of Post and Shiren.[6] The decay constants reported here are all in the expected range of agreement with the values calculated by Kasha[7] from optical data.

I am indebted to Dr. H. L. Anderson for help throughout this work. Dr. M. Kasha has given me much valuable information.

* This work was performed with the joint support of the ONR and AEC.
[1] Obtained from Larco Nuclear Instrument Company.
[2] Grown by E. Tajima using stilbene purified from that obtained from Eastman Kodak Company.
[3] Obtained from the Harshaw Chemical Company.
[4] Reagent Merck's naphthalene recrystalized about seven times from ethyl alcohol. Obtained from M. Kasha.
[5] R. D. Sard, J. App. Phys. **17**, 768 (1946).
[6] R. F. Post and N. S. Shiren, Phys. Rev. **78**, 80 (1950).
[7] M. Kasha, *Scintillation Counters. Qualitative Treatment of the Molecular Optical Parameters* (to be published).

Ionization Defects of Fission Fragments*

J. K. KNIPP, R. B. LEACHMAN,† AND R. C. LING
Institute for Atomic Research and Department of Physics, Iowa State College, Ames, Iowa
September 5, 1950

THE mean total kinetic energy of fission fragments produced from U^{235} by thermal neutrons is still a quantity of considerable uncertainty. Estimates[1] based on ionization yields are appreciably less than the only direct (calorimetric) measurement.[2] We wish to show that there is evidence that about 2.5 Mev for the average light fragment and about 4.2 Mev for the average heavy fragment escape detection in the usual ionization experiments. These ionization defects occur because the light fragment loses about 5 Mev, and the heavy fragment about 8 Mev, to recoiling gas atoms, which themselves have a reduced ionization efficiency because they in turn produce recoil atoms, etc.

Double-chamber ionization data[3] give a distribution in ratio of ionization of pairs of fragments which is broader than the distribution in ratio of energies obtained from data on masses.[4] The difference in the distributions is somewhat reduced when the dispersion arising from neutron recoil and instrumental errors are taken into account. The remaining discrepancy is attributed to a variation in ionization yield with fragment mass. For the most probable fission asymmetry, the energy to ionization ratio of the average light fragment is found to be approximately 3.7 percent less than for the average heavy fragment.[5]

The ionization defect Δ of a heavy particle of energy E that is stopped in a gas is given by

$$\Delta=\int_0^E dE\lambda(E)\int_0^{E_m'} dE'k(E,E')\chi'(E'), \qquad (1)$$

where $\lambda=[1+(b^e/b^r)]^{-1}$ is a function of the energy determined by the ratio b^e/b^r of the stopping cross sections for loss of energy to excitation and ionization and to atomic recoil, respectively, and

$$k(E,E')=\sigma(E,E')E'\Big/\int_0^{E_m'} dE'\sigma(E,E')E'.$$

Here $\sigma(E,E')$ is the cross section per unit energy range for the production of a recoil atom of energy E'; E_m' is the maximum energy transferred to an atom and $\chi'(E')$ is $1-(\omega^eI'/E')$, where I' is the number of ion pairs resulting from a gas atom of energy E' and ω^e is the energy loss per ion pair of an atom the energy of which is very high. We have

$$d(E'\chi')/dE'=\lambda'\int_0^{E'} dE''k'(E',E'')\chi'(E''), \quad \chi'(0)=1, \qquad (2)$$

in which primed quantities are similarly defined for a gas atom in its own gas.

Reasonable estimates for the ratios of stopping cross sections for low velocities can be made from the analysis of the ionization by recoil particles from alpha-decay.[6] Atomic scattering is approximately spherically symmetrical in the center of gravity system below particle velocities of the order of

$$\left[2m\left(\frac{M+M'}{MM'}\right)ZZ'(Z^{\frac{1}{3}}+Z'^{\frac{1}{3}})^{\frac{1}{2}}\right]^{\frac{1}{2}}\frac{e^2}{\hbar}$$

and very nearly coulomb with minor screening above this velocity.[7] Correspondingly, $k(E,E')$ is $2E'/E_m'^2$ and

$$\left\{2E'\ln\left[\frac{2M'}{M+M'}\frac{E}{ZZ'\epsilon_0(Z^{\frac{1}{3}}+Z'^{\frac{1}{3}})^{\frac{1}{2}}}\right]\right\}^{-1}$$

(except outside the screening radius, where it is zero), respectively. Ratios of stopping cross sections for intermediate and high velocities can be estimated by well-known methods.

In this manner it is possible to make a crude calculation of the behavior of the solution of (2). It is found, for instance, that an ionization defect $\Delta'\approx 0.8$ Mev for a very energetic argon particle in argon is not unreasonable, and that $\chi'=0.5$ at about 350 kev. Numerical integration of (1) leads to 0.94 and 0.975 as probable values of the ionization efficiencies in argon gas of the heavy and light fission fragments from U^{235} by thermal neutrons, respectively. The ratio of efficiencies is 0.964. The remarkable agreement with that found from the analysis of the fragment pair distributions must be regarded as largely accidental, because of the approximate nature of both considerations.

* Work performed in part at the Ames Laboratory of the AEC.
† Now at Los Alamos Scientific Laboratory, Los Alamos, New Mexico.
[1] 156 Mev by Brunton and Hanna, Can. J. Research **A28**, 190 (1950); 162 Mev by Jentschke, Zeits. F. Physik **120**, 165 (1943); about 155 Mev, when corrected for foil losses, by Flammersfeld, Jensen, and Gentner, Zeits. f. Physik **120**, 450 (1943).
[2] 165±8 Mev by Henderson, Phys. Rev. **58**, 774 (1940).
[3] D. C. Brunton and G. C. Hanna, reference 1; M. Deutsch and M. Ramsey, MDDC 945 (1946); W. Jentsche, reference 1; Flammersfeld, Jensen, and Gentner, reference 1.
[4] Plutonium Project Report, Rev. Mod. Phys. **18**, 513 (1946).
[5] R. B. Leachman, Phys. Rev. **79**, 197 (1950). Details of this analysis and other considerations will be presented in papers submitted to the Physical Review.
[6] Knipp, Leachman, and Ling, Phys. Rev. **80**, 478 (1950).
[7] N. Bohr, D. Kgl. Danske Vidensk. Selskab, Mat.-fys. Medd. **15**, No. 8 (1948).

Nuclear Spins of the 2.62-Mev and 3.20-Mev Excited States of Thorium *D*

H. E. PETCH AND M. W. JOHNS
Department of Physics, McMaster University, Hamilton, Canada
September 18, 1950

APPROXIMATELY 70 percent of the beta-disintegrations of Th*C*″ are followed by two gamma-rays of energy 0.58 and 2.62 Mev; these involve the three energy states 0, 2.62, and 3.20 Mev of Th*D*. By comparison of the measured internal conversion coefficients with the calculations of Hulme *et al.*[1] and by consideration of the degree of forbiddenness of the beta-spectra, Oppenheimer[2] and Arnoult[3] have assigned spins 0, 2, 3 to these levels. Martin and Richardson[4] on the basis of their recent measurements of internal conversion coefficients and the theoretical calculations of Rose *et al.*[5] have decided that the spins of these levels are 0, 1, 3. Bell and Elliott[6] after an unsuccessful search for the 3.20-Mev cross-over transition, have concluded that the spin of the 3.20-Mev level could be either 3 or 4.

Since the angular correlation function for two successive gamma-rays is very sensitive to the spin changes and multipolarities involved,[7,8] a determination of this function provides an independent approach to the problem. For this purpose we have used a coincidence circuit of resolving time 5×10^{-9} sec., similar to that constructed by Bell and Petch,[9] with two anthracene scintillation counters to investigate the angular correlation of successive gamma-rays resulting from the decay of Th*C*″. The coincidences observed were almost all due to the 0.58- and 2.62-Mev gamma-rays. Counts for ten-minute periods were taken alternately at the 90° position and at a chosen θ-position until at least 10,000 coincidences had been recorded at each. This procedure was carried out in 15° steps from $\theta=90°$ to 180°. Chance coincidences, obtained directly by introducing a delay of 5×10^{-8} sec. into one channel preceding the mixing stage of the circuit, were subtracted from the number of observed coincidences. The apparatus, when tested on the Co^{60} gamma-rays, gave a correlation function which conformed very closely to the published results of Brady and Deutsch.[10]

Figure 1 records the results of a series of experiments planned to obtain the correlation function for the 0.58- and 2.62-Mev gamma-rays from Th*D*. A complete set of points (series *A*) was recorded with an instrumental angular resolution of 12°, using sources of initial strength of about 0.3 mc of thorium active deposit on thin aluminum foil packed into a thin wall brass or Bakelite capsule of inside diameter 2 mm. To obtain better resolution and better statistics the measurements were repeated (series *B*) with an instrumental resolution of 7°, using a 1.5-mc source of radiothorium in equilibrium with its products sealed in a platinum capsule of diameter 5 mm enclosed in a brass container. In both series the front surfaces of the anthracene crystals were covered with 2 mm of lead. Since, according to Arnoult and Oppenheimer, the weak 0.27-Mev gamma is also in cascade with the 2.62-Mev radiation, series *B* was repeated with 4 mm of lead over each

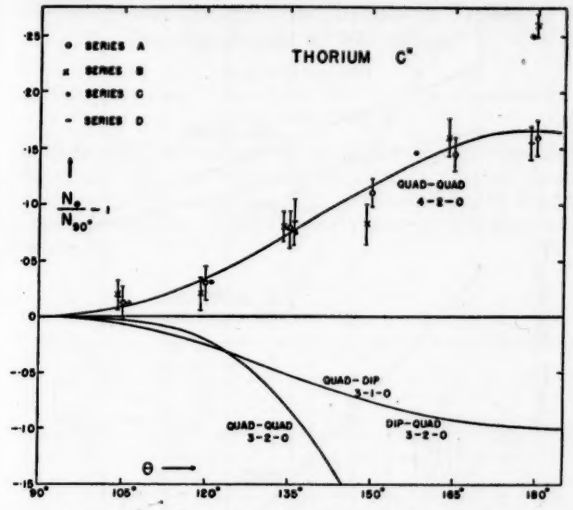

FIG. 1. A comparison of the angular correlation function of the ThC'' gamma-rays with the theoretical functions.

crystal to remove the contribution of this gamma-ray. These points agreed so closely with the results obtained with 2-mm shielding that they have been averaged with them as part of series *B*.

Series *C* was taken by H. E. Petch at Chalk River during the summer of 1949 with a different instrument, using a 1-mc radiothorium source in equilibrium with its products which was enclosed in a platinum capsule. The agreement with series *B* is within the statistical error. Since *B* and *C* agree closely with *A* except at the 180° position, where the effect of annihilation radiation following pair production in the container might be important, the 180° and 135° positions were repeated as series *D* with 2.5 cm of lead over one crystal to remove the contribution of this radiation.

It is obvious from Fig. 1 that, when the effect of annihilation radiation is removed, all the series are consistent and in very good agreement with the theoretical correlation function for 4–2–0 quadrupole-quadrupole transitions.

In each of the three disintegration schemes referred to above a weak gamma-ray of energy over 0.5 Mev is in cascade with the 2.62-Mev radiation. Since the contribution of this radiation could not be removed by shielding, the experimental results may be slightly distorted by its presence. However, considering the low intensity of this radiation, it is impossible that the distortion could be sufficient to make our results consistent with either of the spin assignments 3–1–0 or 3–2–0. The correlation functions for these spin assignments (see Fig. 1) are widely different from the 4–2–0 function.

On the basis of our measurements, both the 0.58 and 2.62 gamma-rays of Th*D* are electric quadrupole radiations and the spins of the three levels involved are 0–2–4. This conclusion is consistent with the results of Bell and Elliott's experiments but in clear contradiction to the conclusion of Martin and Richardson that the 2.62-Mev radiation is magnetic dipole in nature.

We wish to express our gratitude to Dr. R. E. Bell and Dr. B. B. Kinsey of the Chalk River laboratories for helpful discussions and assistance. The financial support received from the Research Council of Ontario and the National Research Council of Canada is gratefully acknowledged.

[1] Hulme, Mott, and Oppenheimer, Proc. Roy. Soc. **A155**, 315 (1936).
[2] F. Oppenheimer, Proc. Camb. Phil. Soc. **32**, 328 (1936).
[3] R. Arnoult, Ann. de physique, 11e Serie, 241 (1939).
[4] D. G. E. Martin and H. O. W. Richardson, Proc. Phys. Soc. London, **A63**, 223 (1950).
[5] M. E. Rose *et al.*, AEC Report U-550 (1950).
[6] R. E. Bell and L. G. Elliott, Can. J. Research **A26**, 379 (1948).
[7] D. R. Hamilton, Phys. Rev. **58**, 122 (1940).
[8] G. Goertzel, Phys. Rev. **70**, 897 (1946).
[9] R. E. Bell and H. W. Petch, Phys. Rev. **76**, 1409 (1949).
[10] E. L. Brady and M. Deutsch, Phys. Rev. **78**, 558 (1950).

The Barometric Effect for Large Cosmic-Ray Bursts under Thick Absorbers at 11,500 Feet Elevation and the Absorption Mean Free Path for Very High Energy Nuclear Collisions*

THOMAS G. STINCHCOMB
Department of Physics, University of Chicago, Chicago, Illinois
September 15, 1950

A CARNEGIE model "C" ionization chamber together with Geiger counter circuits to detect air showers has been in operation at Climax, Colorado (elevation, 11,500 feet or 675 g/cm²). The arrangement was similar to that used by Fahy and Schein.[1] The chamber was shielded with a spherical absorber of 12-cm lead, and the frequencies of bursts of 200 particles and greater which were not in coincidence with air showers were noted. Because of the large variations in atmospheric pressure from December, 1949, to April, 1950, the barometric effect for the radiation producing these bursts was obtained.

The results, shown in Fig. 1, indicate that the ratio of the burst frequency (*A*) at low barometric pressure to that at high barometric pressure (*B*) is 1.187±4.3 percent. A correction is applied, since the chamber records bursts produced by radiation from all directions. The result is that the frequencies of bursts produced by vertical radiation have the ratio 1.167±4.3 percent. The pressure difference was 11.4 g/cm². This gives a mean absorption path in air of 74±21 g/cm² or a barometric coefficient of −1.8 (±0.5 percent) per mm Hg.

Some of these bursts are caused by energic μ-mesons just as at sea level.[3] These should show very little absorption in the air between Climax (11,500 feet) and sea level. To allow for these, Lapp's data[3] for the burst frequencies at sea level (Cheltenham,

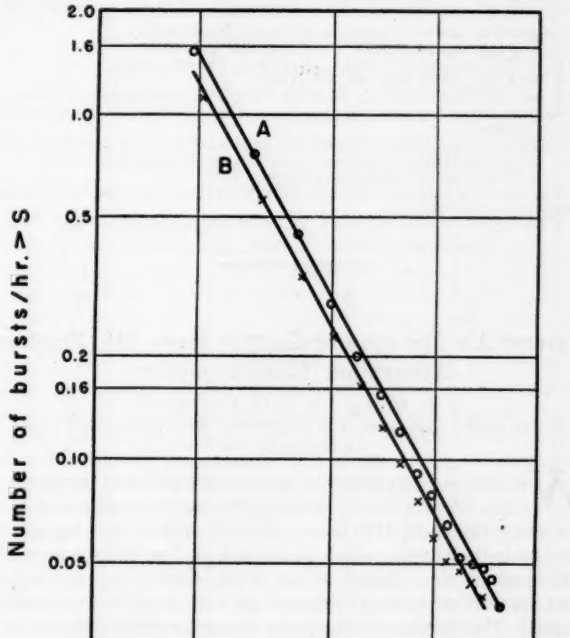

FIG. 1. Distribution of burst sizes. Curve *A* refers to 1145 bursts obtained in 735.8 hours at an average pressure of 486.86 mm Hg. Curve *B* refers to 1008 bursts obtained in 884.0 hours at an average pressure of 495.26 mm Hg.

Maryland) are used. We find that 14.7 percent of the bursts at low barometer and 17.4 percent at high barometer are due to μ-mesons and must be subtracted. The resulting ratio is 1.227 ± 5.2 percent, which becomes 1.207 ± 5.2 percent when similarly corrected for bursts produced by non-vertical radiation. This corresponds to a mean absorption path in air of 61 ± 17 g/cm^2 and to a barometric coefficient[4] of -2.2 (±0.6) percent per mm Hg. It is noteworthy to point out that the mean free path of 61 g/cm^2 corresponds to a cross section for nuclear collisions, which is very nearly equal to the cross-sectional area of an air nucleus.

The energy necessary to produce the electronic cascades of which these bursts consist is of the order of 10^8 ev per particle.[3] Hence, we are dealing with energies of 2×10^{10} ev and greater. This large absorption in air indicates that for these energies elastic scattering is practically zero. The bursts at Climax, then (except those produced by μ-mesons), probably originate from primary protons and perhaps to some extent from first generation π-mesons. If one assumes that the bursts come from the decay of neutral mesons which comprise $\frac{1}{3}$ of all mesons produced, one finds that 6×10^{10} ev must go into meson production in the collision which produces a burst of 200 particles. This represents a lower limit to the energy of our bursts producing radiation.

Assuming an angular distribution corresponding to an exponential absorption of 9 or 10 mean paths,[5] a vertical flux of 0.5×10^{-6} particles cm^{-2} sec.$^{-1}$ steradian^{-1} is obtained at an atmospheric depth of 675 g/cm^2 (Climax) for energies $E>6\times10^{10}$ ev. This corresponds to a vertical flux at the top of the atmosphere of the order of magnitude of 0.004 to 0.01 particles cm^{-2} sec.$^{-1}$ steradian^{-1}, and this is not in disagreement with Winckler's estimate[6] of 0.004 particles cm^{-2} sec.$^{-1}$ steradian^{-1} for energies greater[7] than 6×10^{10} ev.

The author is indebted to his sponsor, Professor Marcel Schein, for many valuable discussions and suggestions. The Carnegie ionization chamber was provided through the courtesy of the Carnegie Institution of Washington. Thanks are also due to the Climax Molybdenum Company for its hospitality and cooperation.

* Assisted by the joint program of the ONR and AEC.
[1] E. F. Fahy and M. Schein, Phys. Rev. **75**, 207 (1949).
[2] R. F. Christy and S. Kusaka, Phys. Rev. **59**, 405 (1941).
[3] R. E. Lapp, Phys. Rev. **69**, 321 (1946).
[4] A second-order correction to these results may be necessary after a better comparison between this chamber and the Cheltenham chamber has been completed.
[5] Preliminary analysis of experiments on the zenith angle dependence of burst producing radiation indicates that this assumption is justified.
[6] J. R. Winckler, private communication, 1950.
[7] The details of this and other experiments on these large bursts are being prepared for publication.

Narrow Air Showers of Cosmic Rays. III. Further Absorption Measurements

J. P. N. Wei and C. G. Montgomery
Sloane Physics Laboratory, Yale University, New Haven, Connecticut*
September 18, 1950

We have recently reported two determinations of the absorption curve of narrow showers. The first[1] of these, performed at Climax, Colorado, 3510 meters altitude, showed only a gradual decrease in the counting rate with increase in absorber; the second,[2] performed in New Haven at sea level, showed a more rapid decrease (soft component) followed by a flat portion (hard component). The counter arrangements were somewhat different for the two experiments. To attempt to resolve the discrepancy we have effectively duplicated the Climax arrangement and repeated the measurements at sea level. Four trays of counters were used as indicated in Fig. 1. In addition in all cases a large fifth tray, separated from the others horizontally by one meter or more, was employed to eliminate the effects of extensive showers. In the Climax experiment coincidences *ABC* not accompanied by an extensive shower were measured and the absorption curve is reproduced in Fig. 1. The New Haven curve for the same coincidences shows a smaller slope but is the same shape as the Climax curve.

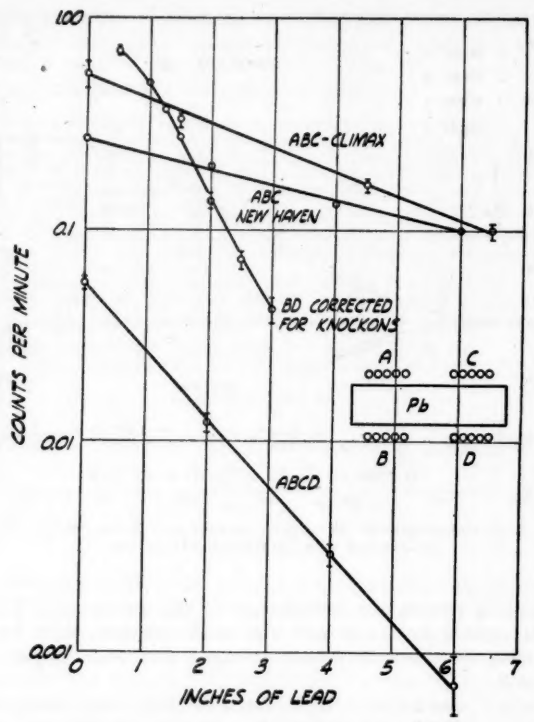

FIG. 1. Absorption curves for narrow showers. All data have been corrected by subtraction of the contribution of extensive showers.

In the experiment recently reported,[2] coincidences *BD* were recorded and the resultant curve is given in Fig. 2 of reference 2. It seems likely that the flat portion of the curve is best interpreted as caused by single mesons accompanied by one or more knock-on electrons. Except for small thicknesses, it is therefore permissible to subtract the hard component and the resultant curve is shown in Fig. 3 of reference 2 and reproduced in the accompanying figure here. The coincidences *ABCD* were also measured, and these data are plotted in Fig. 1. The slope is much larger than that for the *ABC* coincidences but not much different from the corrected *BD* curve.

The situation is thus very similar to that which obtains for extensive showers. When two counters are covered with lead, the absorption curve is steeper than that obtained when only one counter is covered.[3] The ratio of slopes of the two absorption curves for the narrow showers is much greater, however, than this same ratio for extensive ones. This is easily understood, since an absorber placed over a counter is equivalent to a reduction in the area of the counter. If α is the fractional equivalent reduction in area, then it can be shown[4] that, for α small compared with unity, the counting rate for an arrangement with a single counter covered by absorber is proportional to α. If the absorber covers two counters, the counting rate is proportional to α^γ, where γ is the exponent in the integral density distribution function for the showers. We have already shown[1] that the variation of counting rate with area is more rapid for the narrow showers than for the extensive ones and hence the effective value of γ is larger for narrow showers. The absorption data thus confirm this.

* Assisted by the joint program of the ONR and AEC.
[1] J. Wei and C. G. Montgomery, Phys. Rev. **76**, 1488 (1949).
[2] J. P. N. Wei, Phys. Rev. **79**, 670 (1950).
[3] See reference 2, Fig. 5, and other papers there cited.
[4] D. Broadbent and L. Jánossy, Proc. Roy. Soc. **A192**, 364 (1948).

Neutron Energy Distribution in Proton Bombardment of Beryllium*

DAVID BODANSKY†
Nuclear Laboratory, Harvard University, Cambridge, Massachusetts
September 5, 1950

A MEASUREMENT has been made of the energy distribution of the neutrons emitted in the forward direction from a one-eighth-in. thick beryllium target bombarded by the 110-Mev internal proton beam of the Harvard cyclotron. The results are shown in Fig. 1.

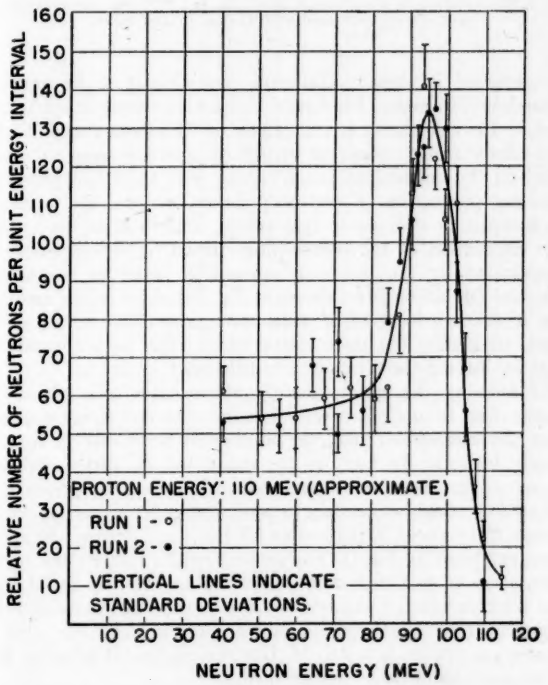
RELATIVE NUMBER OF NEUTRONS PER UNIT ENERGY INTERVAL
NEUTRON ENERGY (MEV)
PROTON ENERGY: 110 MEV (APPROXIMATE)
RUN 1 - ○
RUN 2 - •
VERTICAL LINES INDICATE STANDARD DEVIATIONS.

FIG. 1. Neutron energy distribution with beryllium target.

The neutrons from the target passed through a collimating hole in the concrete shielding surrounding the cyclotron and fell upon two one-fourth-in.-thick polyethylene scatterers. The recoil protons from the scatterers were counted by anthracene scintillation counters used in triple coincidence telescopes. One telescope system was used as a monitor. The second telescope system consisted of four individual scintillation counters directed at the second scatterer at an angle of 15 degrees with the neutron beam.

In the second system the difference in the triple coincidence rates of counters 1, 2, and 3 and counters 1, 2, and 4 (numbered away from the scatterer) was due to the stopping power of the anthracene crystal of counter 3. By interposing different thicknesses of aluminum absorber between counters 1 and 2, data were obtained for a differential proton range distribution. The measurement was repeated with a carbon scatterer of appropriate thickness and a polyethylene-carbon subtraction performed to give the number of protons arising from neutron-proton scattering.

The recoil proton energy was calculated from the range in the aluminum absorbers and the anthracene crystals. The corresponding incident neutron energy was found from the relativistic two-body collision equation. In calculating the number of neutrons per unit energy interval, the recoil proton counts observed with a given aluminum absorber were multiplied by a correction factor. The numerator of this factor uses Berkeley data[2] at 40 and 90 Mev to account for the energy dependence of neutron-proton scattering. To interpolate and extrapolate over the experimental energy range the differential cross section for neutron-proton scattering was assumed to vary as $1/(A+E_n)^2$ where E_n is the energy in the laboratory system of the incident neutrons.[3] At a given angle A should be constant, and was evaluated to fit the Berkeley data for recoil protons at 15 degrees. The denominator of the correction factor accounts for the energy dependence of the width of the interval in initial energies of the recoil protons which stop in the crystal of counter 3. The correction factor used was $(127+E_n)^2/(dE/dx)E_p$, where E_p is the energy of the recoil protons.

The measured neutron energy distribution from a beryllium target was peaked at 95 Mev and showed no other marked peaks in the energy interval 40 to 110 Mev. The stable orbit energy of the incident protons in the cyclotron was calculated from the magnetic field and target radius to be 114 Mev. Effects arising from oscillations of the proton beam and multiple traversals of the target may cause a significant spread and reduction in the energy of the protons actually striking the target. Hence, the observed peak in the neutron energy distribution may be at a lower energy and may be wider than the peak which would be obtained with a 114-Mev monoenergetic proton beam.

Preliminary results of a similar measurement with a carbon target do not show the marked high energy peak obtained with the beryllium target.

The writer is deeply appreciative of the advice and encouragement given him by Professor N. F. Ramsey under whose direction the work was performed. He is greatly indebted to R. W. Birge, W. G. Cross, J. A. Hofmann, and many others for valuable suggestions and assistance.

* Assisted by the joint program of the ONR and AEC.
† AEC Predoctoral Fellow. Now at Columbia University.
[1] The experimental arrangement was strongly influenced by the experiment of Hadley, *et al.*, Phys. Rev. 75, 351 (1949).
[2] Hadley, *et al.*, reference 1.
[3] This form of the dependence was suggested by Dr. M. L. Goldberger.

Scattering and Polarization of Neutrons in an Iron Single Crystal*

D. J. HUGHES
Brookhaven National Laboratory, Upton, New York
AND
M. T. BURGY AND W. E. WOOLF
Argonne National Laboratory, Chicago, Illinois
September 15, 1950

IN 1947 Halpern,[1] stimulated by work of Shull and Wollan[2] that indicated excessive incoherent neutron scattering, suggested the use of iron single crystals to reveal the source of the incoherent scattering. When slow neutrons are transmitted through a single crystal (oriented so that no Bragg scattering occurs), only incoherent scattering is observed. Halpern pointed out that of the three main sources of incoherent scattering, isotope disorder, spin-dependent scattering, and inelastic lattice scattering, only the last would be affected by a magnetic field and hence capable of producing neutron polarization. By measuring the neutron polarization as well as the transmission with an iron crystal, it would then be possible to isolate the inelastic scattering. Although most of the diffuse scattering observed by Shull and Wollan later proved to be instrumental[3] (multiple scattering in the samples), it was important to investigate the iron single crystal because of the large polarization effects which had been observed in polycrystals[4,5] compared to theoretical estimates.[6] Halpern, Hamermesh, and Johnson[6] had subtracted 2.5 barns of isotope disorder scattering from the cross section of iron in their calculation of neutron polarization and it seemed likely that the isotope effect was actually much smaller.

A single crystal of iron, 2×2×3 cm, containing 10 percent (by weight) of silicon was obtained from Professor Kaufmann of M.I.T. The total cross section of the single crystal, measured with monoenergetic neutrons obtained with the Argonne "chopper," is shown in Fig. 1, together with earlier results for a polycrystalline

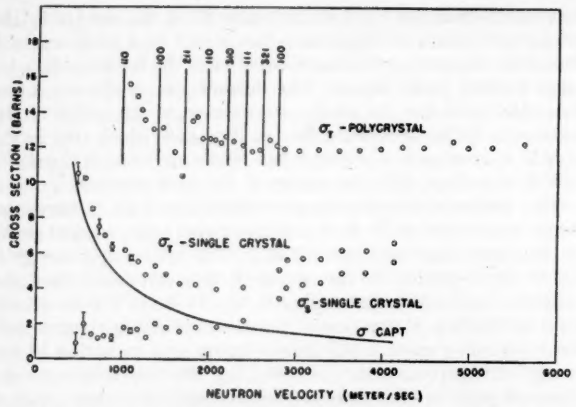

FIG. 1. Measured total cross sections of an iron polycrystal and a single crystal of iron-silicon. The scattering cross section of the single crystal, σ_S, obtained by subtraction of capture, is also shown. The vertical lines are the limiting velocities for reflection by lattice planes, marked with the appropriate Miller indices.

sample. The single crystal cross section is much smaller than that of the polycrystal, especially in the region just above the "cut-off" velocity (980 meters per sec., below which velocity the polycrystal exhibits no coherent scattering). The points marked σ_S are those for the single crystal after subtraction of the capture cross section, taken as 1/v and equal to 2.45 b at 2200 m/s for iron. (The single crystal cross sections of Fig. 1 all refer to the "average atom" in the crystal, containing 18 percent silicon atoms.) After an additional 0.40 b is subtracted from the single crystal points, to take account of the incoherent scattering caused by the assumed random location of the silicon atoms, the remaining scattering, shown in Fig. 2, represents the incoherent scattering of the

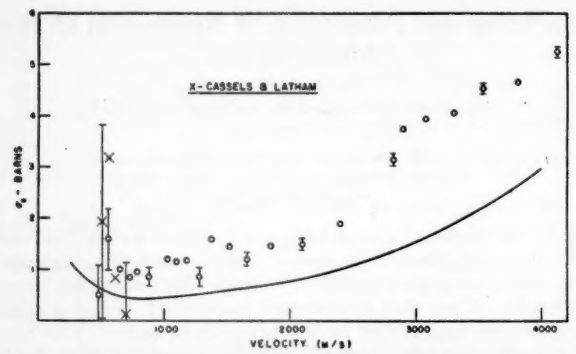

FIG. 2. The incoherent scattering of the iron-silicon single crystal after subtraction of the calculated scattering resulting from the assumed random location of the silicon atoms. Results of Cassels and Latham and the calculated inelastic scattering (Weinstock) are shown for comparison.

crystal. Some points obtained by Cassels and Latham[7] are also shown (we have re-analyzed their data, using 2.45 b for capture instead of their 2.2 b), as well as the inelastic scattering calculated by Cassels and Latham from the theory developed by Weinstock.[8] The variation of the incoherent scattering with velocity suggests that the scattering is mainly inelastic and about twice the calculated value. Both spin-dependent and isotope disorder scattering, in contrast to the inelastic scattering, would show no change with neutron velocity.

The polarization, which would result from inelastic scattering but not from other incoherent scattering, was next sought and found by magnetizing the crystal in a field of 11,000 oersteds and measuring the single[1,6] transmission effect, E_s. E_s is the fractional increase in transmitted neutron intensity resulting from magnetization to saturation. The measured points for an iron thickness of 2.97 cm are compared in Fig. 3 with the effect calculated from

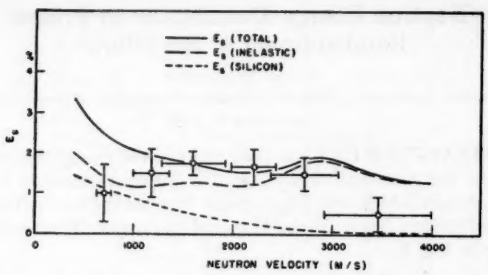

FIG. 3. Observed single transmission effect, E_s, in a 2.97-cm single crystal of iron-silicon compared with the calculated value.

the observed incoherent scattering assuming it to be entirely inelastic and isotropic. The form factor for the magnetic scattering used in the calculation is that given by Steinberger and Wick.[9] The silicon atoms constitute irregularities in the magnetic scattering of the magnetized single crystal, and there will be corresponding production of neutron polarization from the resulting incoherence, in addition to that arising from inelastic scattering. The calculation of the polarization caused by silicon atoms is complicated by the unknown amount of order in the silicon location. The silicon effect shown in Fig. 3 is based on the assumption of random location; if order were present the silicon effect would be smaller but the inelastic effect larger by a comparable amount, leaving the total almost unchanged.

Considering the results mainly above 1200 m/s where the silicon effect is small, it is seen that the observed E_s is consistent with the assumption that the incoherent scattering in iron is largely inelastic. In fact, as the calculated E_s varies with the square of the inelastic scattering cross section, the presence of only 0.25 b of spin-dependent or isotope disorder scattering would change E_s by about 50 percent at 1500 m/s and destroy the agreement exhibited by Fig. 3. The present results support the recent calculation of polarization in polycrystalline iron by Steinberger and Wick[9] in which it was assumed that most of the total scattering (coherent plus incoherent) produces polarization. We wish to express our gratitude to Dr. M. Hamermesh for his generous help in the analysis of these measurements.

* Research carried out under contract with the AEC.
[1] O. Halpern, Phys. Rev. **72**, 260 (1947).
[2] C. G. Shull and E. O. Wollan, Phys. Rev. **72**, 168 (1947).
[3] E. O. Wolland and C. G. Shull, Phys. Rev. **73**, 830 (1948).
[4] Bloch, Condit, and Staub, Phys. Rev. **70**, 972 (1946).
[5] Hughes, Wallace, and Holtzman, Phys. Rev. **73**, 1277 (1948).
[6] Halpern, Hamermesh, and Johnson, Phys. Rev. **59**, 986 (1941); M. Hamermesh, Phys. Rev. **61**, 17 (1942).
[7] J. M. Cassels and R. Latham, Phys. Rev. **74**, 103 (1948).
[8] R. Weinstock, Phys. Rev. **65**, 1 (1944).
[9] J. Steinberger and G. C. Wick, Phys. Rev. **76**, 994 (1949).

A 3×10^{-9} Sec. Isomeric State in $_{63}Eu^{153}$

F. K. McGowan
Oak Ridge National Laboratory, Oak Ridge, Tennessee*
September 15, 1950

AN excited state in Eu^{153} with a half-life $(3.0\pm0.3)\times10^{-9}$ sec. has been observed with a delayed coincidence scintillation spectrometer. The position of the metastable state in the disintegration scheme has been determined.

The delayed coincidence scintillation spectrometer employing anthracene with Type 5819 multiplier tubes as detectors is similar to that described in a previous letter.[1] The video amplifier sections have been replaced with Hewlett Packard 460A wide-band amplifiers. With this apparatus the existence of the short-lived isomeric state[2] of Yb^{170} (1.6×10^{-9} sec.) was confirmed.

Sm^{153} (47 hr.) is known to decay by a 0.78-Mev beta-ray branch leading to an excited state of Eu^{153}. This state is de-excited by γ-ray transitions in cascade[3] corresponding to 69 and 103 kev

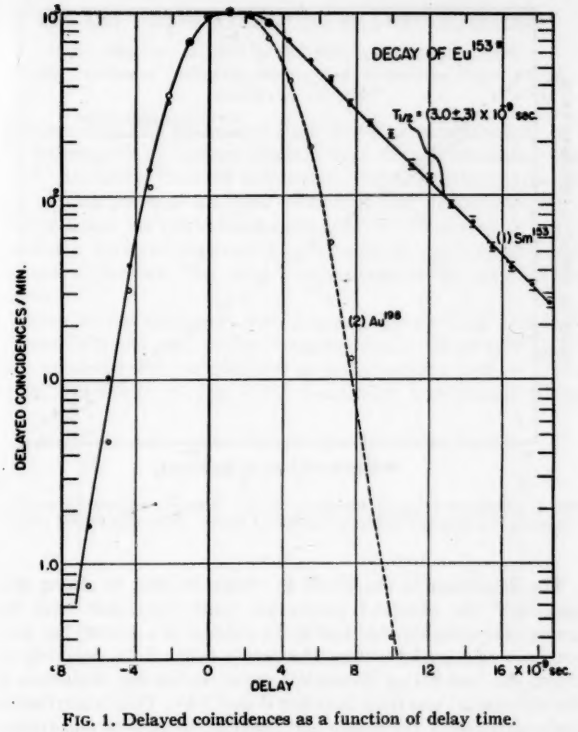

FIG. 1. Delayed coincidences as a function of delay time.

which are strongly converted.[4] In Fig. 1, curve (1), the number of coincidences are plotted as a function of delay time obtained with a source of Sm^{153}. This delayed coincidence resolution curve was recorded by exciting one channel of the delayed coincidence apparatus by the nuclear beta-rays and the other channel by the L, M, or N internal conversion electrons of the 103-kev γ-rays. Without a change in the apparatus, a resolution curve for prompt coincidences was obtained between the 411-kev γ-rays or internal conversion electrons and 85- to 110-kev nuclear beta-rays with a source of Au^{198}. Curve (2) shows the result of such a measurement. Thus, for delay $T \geqslant 8\times10^{-9}$ sec. the half-life of Eu^{153*} may be determined from the slope of curve (1).

The spectrum of the radiation announcing the formation of the metastable state appears to be a simple beta-ray distribution unaccompanied by γ-rays. This information plus the fact that the decay curve for Eu^{153*} was obtained selecting coincidences between the nuclear beta-rays and the L, M, or N internal conversion electrons of the 103-kev γ-ray fixes the position of the metastable state at 172 kev above the ground state of Eu.

Measurements of the internal conversion electron spectrum of the delayed radiation indicate the presence of the 69- and 103-kev γ-rays. The relative heights of the K conversion peak of the 103-kev γ-ray (superimposed on the L, M, and N conversion lines of the 69-kev γ-ray) and the $L+M+N$ conversion peak of the 103-kev γ-ray indicates that the amount of internal conversion in the L shell is comparable to that in the K shell. Also, the spectrum of the unconverted and delayed electromagnetic radiation shows the presence of two peaks which are attributed to the K x-ray of Eu and the 69-kev γ-ray. These observations favor the idea that the isomeric transition is the 103-kev transition.

From the energy and half-life of this isomeric state the transition is probably electric quadrupole or a combination of electric quadrupole and magnetic dipole radiation.

* This document is based on work performed for the Atomic Energy Project at Oak Ridge National Laboratory.
[1] F. K. McGowan, Phys. Rev. **79**, 404 (1950).
[2] R. E. Bell and R. L. Graham, Phys. Rev. **78**, 490 (1950).
[3] S. B. Burson and B. O. Muehlhause, Phys. Rev. **74**, 1264 (1948).
[4] R. D. Hill, Phys. Rev. **74**, 78 (1948).

Radiofrequency Spectrum of D_2 in a Magnetic Field*

H. G. KOLSKY,† T. E. PHIPPS, JR.,‡ N. F. RAMSEY, AND H. B. SILSBEE
Lyman Laboratory of Physics, Harvard University, Cambridge, Massachusetts
September 14, 1950

THE radiofrequency spectrum of D_2 in a magnetic field of about 1616 gauss has been investigated by means of a molecular beam apparatus[1] of improved resolution. The molecules of the beam are cooled to the temperature of liquid N_2, so that most of them are in the zeroth and first rotational states. They traverse a path of total length 269 cm. Experimental evaluation of the frequency separations of the six first rotational state resonances permits more accurate determination of D_2 molecular and nuclear constants. In the customary notation,[2] the results are

$$H' = 13.43\pm0.06 \text{ gauss},$$
$$S_D = \tfrac{1}{2}(H''+H''') = 19.301\pm0.015 \text{ gauss},$$
$$H''' = -5e^2qQ/4\mu_D = 86.11\pm0.08 \text{ gauss},$$
$$-qQ = (1.2931\pm0.0012)\times10^3 \text{ cm}^{-1},$$
$$Q = (2.739\pm0.016)\times10^{-27} \text{ cm}^2.$$

The error in the above value of the quadrupole moment of the deuteron is largely the consequence of error in the newly calculated value[3] of q.

Improved accuracy of the present results is to be attributed chiefly to three factors: (a) increased length of the apparatus, (b) variation of frequency instead of magnetic field, (c) use of a recently developed technique[4] of applying the radiofrequency current in two separated sections near the ends of the homogeneous magnetic field. The latter method, involving only the average effect of the field along the molecular path, minimizes the results of field inhomogeneities, which otherwise are found in the present apparatus to be rather serious. Line widths in the new method are very close to theoretical. Instead of turning the oscillator on and off, as in customary operation, we found it advantageous to change the phase of one r-f end section 180° relative to the other. By recording the sense as well as the magnitude of the resulting signal, one can obtain a resonance curve of the same shape (near resonance) as the customary one[1,4] but having double the effective amplitude. Experimental curves of this type are shown in Fig. 1. Moreover, the phase-shifting method greatly reduces r-f pick-up changes in the detector circuit by eliminating r-f current amplitude changes.

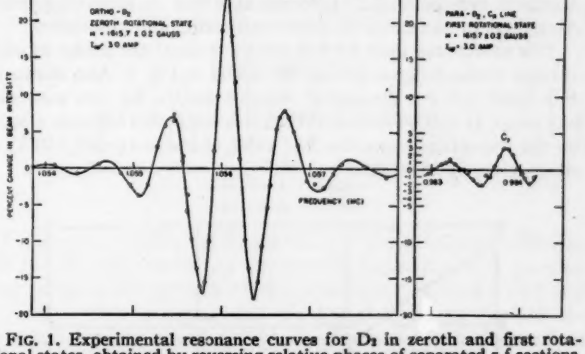

FIG. 1. Experimental resonance curves for D_2 in zeroth and first rotational states, obtained by reversing relative phases of separated r-f sections. Relative intensities are in approximate agreement with theory.

Acknowledgment is made to the Isotopes Division of the AEC for D_2 and D_2O used in the current investigations. These are continuing, and will be more fully reported later.

* This work was assisted by the joint program of the ONR and AEC.
† AEC Fellow.
‡ NRC Fellow.
[1] Kolsky, Phipps, Ramsey, and Silsbee, Phys. Rev. **79**, 883 (1950).
[2] Kellogg, Rabi, Ramsey, and Zacharias, Phys. Rev. **57**, 677 (1940).
[3] G. F. Newell, Phys. Rev. **78**, 711 (1950).
[4] N. F. Ramsey, Phys. Rev. **78**, 695 (1950).

The Beta-Spectrum of Sulfur 35 in the Range of 0–30 Kilovolts*

LEONARD GROSS† AND DONALD R. HAMILTON
Palmer Physical Laboratory, Princeton University, Princeton, New Jersey
September 19, 1950

THERE have been three separate investigations[1–3] of the beta-spectrum of S^{35} with magnetic spectrometers and thin sources. There is substantial agreement on the end point (167, 169, 166 kv respectively); the spectrum agrees with theory above the voltages (70, 40, and 16 kv respectively) at which deviations due to source or window effects may be expected. (See points *K*, *F*, *H* in Fig. 3, reference 5.) Cockcroft and Insch,[4] using a proportional counter, find marked deviations from theory below 80 kv.

The electrostatic beta-spectrograph described in more detail elsewhere[5] has been used[6] to investigate the spectrum of S^{35} in the range 0–30 kv. In the hemispherical structure of this spectrograph, electrons move radially outward, encountering a retarding radial electric field in the region between two hemispherical grids (diameters 8 and 12 inches); observation, as a function of retarding voltage, of the FP-54 measured current to a collector (diameter 16 in.) yields the integral spectrum. Fine grid mesh and large ratio of grid diameter to source size (0.3 in. diameter) give momentum resolution one-third percent. High vacuum, graphite electrode coating, an electron-absorbing backstop behind the source, and use of the larger grid as a suppressor grid for the collector serve to minimize secondary effects (see below).

From the theoretical differential spectrum of Fig. 1, the 0–30 kv range should include 36 percent of the S^{35} electrons. The monotonic decrease of intensity with increasing electron energy is an effect of the Coulomb correction.[7–9] (Note that in reference 7, column 1 for S^{35} has an extra zero after the decimal.)

The S^{35} source was prepared from Oak Ridge carrier-free sulfuric acid in 0.1 normal hydrochloric acid. A thin collodion film 3×10^{-6} cm in thickness[6] was used as backing; since the acid solution breaks this film, 0.7 cc of the active solution (0.5 millicurie) was evaporated to dryness, the residue dissolved in distilled water, and the resulting solution vacuum-desiccated on the backing film. From the constitution of distilled water and the Oak Ridge solution, it seems probable that the resulting deposit had an average thickness ≤ 0.4 $\mu g/cm^2$. Microscope and radioautograph analysis indicated local thicknesses larger by a factor 20, i.e. ≤ 8.0 $\mu g/cm^2$. This gives, according to the semi-empirical equation,[5]

$$V_c = 1700[Z^2(g/cm^2)/A]^{\frac{1}{3}} \text{ kv},$$

a critical voltage $V_c \leq 12$ kilovolts at which to expect spectrum deviations to be caused by source scattering and absorption.

This source was used for five complete runs; the points at each voltage were averaged, giving the points in Fig. 2. Also shown in this figure are the theoretical integral spectra for two values of end point. It will be seen that the observed points fall very closely on the theoretical curve for that value of the end point, 168.3 kv, which gives the best fit.

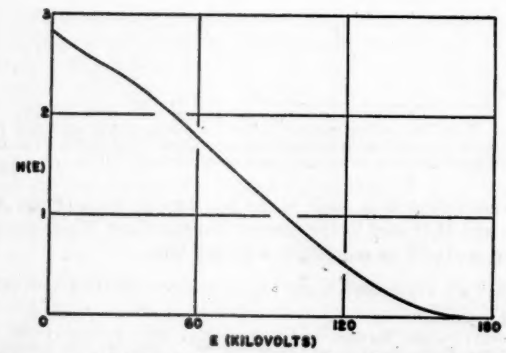

FIG. 1. Theoretical differential beta-spectrum for S^{35}, calculated for 170-kv end point.

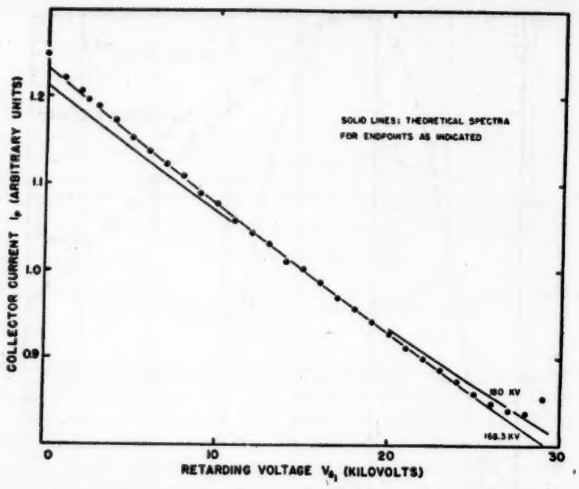

FIG. 2. Observed integral spectrum for S^{35} (points); calculated integral spectra, for two end points as indicated (lines). Note suppressed zero.

The deviations in the 25–30 kv range are due to strong field emission;[5] the observed points are quite consistent with the strong field emission observed in the absence of a source, but have not been corrected for this. The points below 5 kv definitely lie above the best-fitting theoretical curve, indicating deviations in the differential spectrum between 6 and 7 kv. This is ascribed to backscattering in the source and backing; in view of uncertainty in source thickness and in the constant in Eq. (4) reference 5, deviations at higher voltages would not have been surprising.

The theoretical integral spectrum for another end point, 180 kv, as shown in Fig. 2, indicate the sensitivity of the low energy integral spectrum to the end point. The experimental points discriminate between 168.3 and 168.3 ± 1 kv. Including errors in this end point due to the voltage scale of Fig. 5 (±1 kv) and to secondary electronic effects as analyzed in detail in the manner outlined in reference 5 (±2 kv), the end point as obtained from Fig. 2 in all probability lies in the range 168.3 ± 4 kv. The good agreement with previous values is significant not as verification of these values, but primarily as confirmation of the theory of beta-decay as applied to the low energy range here investigated.

The most fundamental way of comparing theory and experiment is to compare intensities not in the integral but in the differential spectrum. Even if the points in Fig. 2 had no scatter, the uncertainty in voltage measurement, in secondary electronic effects, and in value of magnetic-spectrograph end point would not allow one to predict the slope of the observed integral spectrum to better than two percent. Adding to this the uncertainty of slope arising from scatter of points, one may say that the total number of electrons between 6 and 25 kv deviates from theory by at most $\pm2\frac{1}{2}$ percent; for any 7 kv range between 5 and 25 kv, by ±4 percent; for any 2 kv range, by ±8 percent. And in the latter case, any excess could of course not occur uniformly throughout the 6–25 kv range.

We are indebted to Mr. W. P. Alford for assistance with many of the measurements involved here. One of the authors (L.G.) was the recipient of an AEC predoctoral fellowship (1948–1949) during the course of this work. The S^{35} was obtained from the Isotopes Division of the Oak Ridge National Laboratory.

* This work assisted by the joint program of the ONR and AEC.
† Now at Hughes Aircraft Company, Culver City, California.
[1] Langer, Motz, and Price, Phys. Rev. 77, 789 (1950).
[2] J. L. Berggren and R. K. Osborne, Phys. Rev. 74, 1240 (1948).
[3] R. D. Albert and C. S. Wu, Phys. Rev. 74, 847 (1948).
[4] A. L. Cockroft and J. G. M. Insch, Phil. Mag. 40, 1014 (1949).
[5] D. R. Hamilton and L. Gross (to be published in Rev. Sci. Inst.
[6] L. Gross and D. R. Hamilton, Phys. Rev. 78, 318 (1950).
[7] C. Longmire and H. Brown, Phys. Rev. 75, 264 (1949).
[8] C. Longmire and H. Brown, Phys. Rev. 75, 1182 (1949).
[9] J. R. Reitz, Phys. Rev. 77, 10 (1950).

On the Phase Transition in Lead Zirconate

GEN SHIRANE, ETSURO SAWAGUCHI, AND AKITSU TAKEDA
Tokyo Institute of Technology, Oh-okayama, Meguro-ku, Tokyo, Japan
September 14, 1950

IT was found by Waku and Hori[1] that lead zirconate may be a ferroelectric of barium titanate type with a transition near 220°C. Recently, Roberts[2] has investigated the dielectric properties of this material and has confirmed that it becomes ferroelectric below the Curie temperature, 236°C. With respect to this transition, we have observed the anomalies of specific heat and of thermal expansion. The main results obtained will be described below.

Ceramic lead zirconates were prepared by sintering a mixture of pure ZrO_2 and pure PbO at temperatures of about 1100°C. We first measured the permittivity at temperatures from −160 to 300°C. As shown in Fig. 1 we found only one transition near

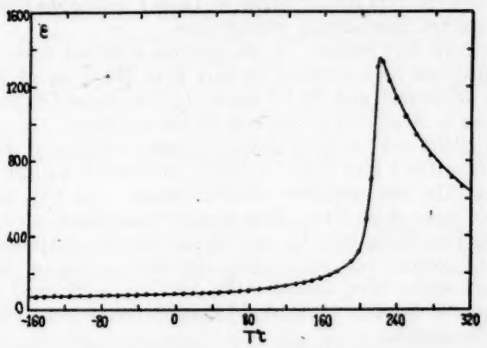

FIG. 1. Permittivity *vs.* temperature curve, measured at 1 Mc/sec. and 2v/cm.

222°C, in contrast to the three transitions known in barium titanate. Near the Curie point the permittivity increases very sharply and the maximum value is more than 15 times its value at room temperature.

In order to obtain more detailed information concerning this transition, we have measured the specific heat using an adiabatic calorimeter of Nagasaki-Takagi type.[3] The sample of about 40 g was heated in a glass vessel at the rate of about 1°C/min. One of the results is shown in Fig. 2. There is a rather large specific heat

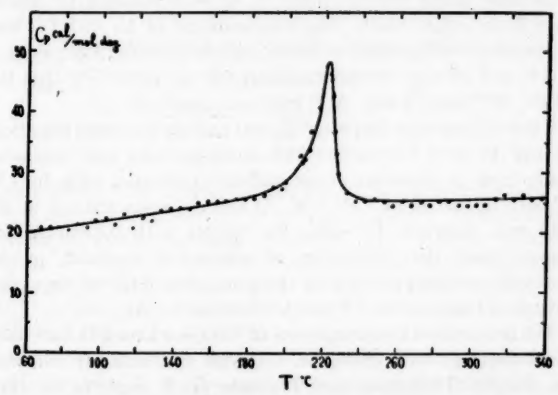

FIG. 2. Specific heat *vs.* temperature curve.

anomaly at the Curie point. The transition energy is about 400 cal./mole and the entropy change calculated from the heat absorbed is found to be about 0.4 R. This transition energy is remarkably large compared with that of barium titanate; the latter[4] is about 40 cal./mole. For the present it is difficult to determine whether there is a latent heat.

We have measured the thermal expansion of this ceramic by a simple dilatometer consisting of silica rods and an optical lever. We have used a specimen 3 cm in length, and have been able to detect the dilatation $\Delta l/l$ of about 3×10^{-6}. Figure 3 shows

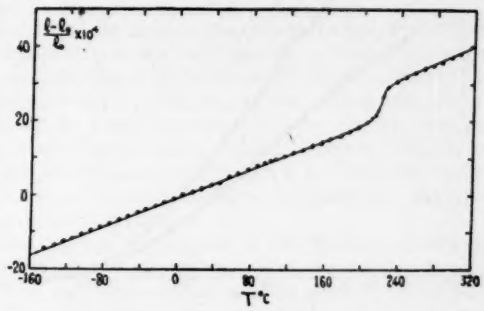

FIG. 3. Length *vs.* temperature curve.

$(l-l_0)/l_0$ as a function of the temperature, where l_0 represents the length at 0°C. There is an anomalous volume expansion at the transitional region and the linear expansion coefficient becomes maximum at 223°C. The volume change $\Delta V/V$ during the transition is about 2.7×10^{-2} namely 0.18A³ per unit cell provided the lattice constant $a=4.1$A. This large anomalous volume expansion is to be contrasted with a small volume contraction of $BaTiO_3$ at 120°C. The linear expansion coefficients are almost the same in both phases below and above the Curie point; they are both about 9.5×10^{-6}.

After all, it will probably be said that the nature of the ferroelectric transition in lead zirconate is very different from the well-known phase change in barium titanate. For an explanation of this transition, further investigations on the dielectric properties and the crystal structure of this material will be required. Detailed results will shortly be reported in the *Journal of the Physical Society of Japan.*

In conclusion we wish to express our sincere thanks to Mr. J. Hori for stimulating our interest in this problem and also to Professor Y. Takagi for his encouragement in the course of this research.

[1] S. Waku and J. Hori, private communication (summer, 1949).
[2] S. Roberts, J. Am. Cer. Soc. 33, 63 (1950).
[3] S. Nagasaki and Y. Takagi, J. App. Phys. Japan 17, 104 (1948).
[4] Horwood, Popper, and Rushman, Nature 160, 58 (1947); S. Sawada and G. Shirane, J. Phys. Soc. Japan 4, 52 (1949).

A Two-Day Xe^{133} Isomer

B. H. KETELLE, A. R. BROSI, AND H. ZELDES
Chemistry Division, Oak Ridge National Laboratory, Oak Ridge, Tennessee
September 15, 1950

IN a recent publication Bergström and Thulin[1] reported 196-kev and 227-kev conversion electrons corresponding to a gamma-ray energy of 232 kev in Xe^{133}. They found the conversion electrons to decay with the same half-life (~5.5 days) as the 345-kev maximum energy beta-radiation. On the basis of their observations they proposed a decay scheme in which both the 232-kev gamma-transition and the well-known 345-kev beta-transition are from a single metastable level in Xe^{133}.

In attempting to confirm the observations of Bergström and Thulin the beta-energy distribution of fission product xenon which was highly purified from other gaseous fission products including krypton has been measured. The source mounting was the same as that used in previous work[2] on the Kr^{85} beta-spectrum. The observed energy distribution obtained with a thin lens spectrometer 11 days after the irradiation is shown as curve A in Fig. 1. Curve B in Fig. 1 shows the energy distribution 20 days

FIG. 1. Curve A. Beta-spectrum of Xe^{133} 11 days after bombardment. Curve B. Beta-spectrum of same source 20 days later with ordinate scale multiplied by 10.

later. It can be seen that the 196-kev conversion line has essentially disappeared in curve B. This shows that the 232-kev gamma-ray decayed with a shorter half-life than the 5.3-day beta-radiation.

The decay of the unconverted 232-kev gamma-ray, which was found in low intensity, was measured with a Tl activated NaI scintillation spectrometer. This gave a half-life of approximately 2 days in agreement with the observed decay of the 196-kev conversion electrons.

This 232-kev gamma-ray is undoubtedly the same as the 232-kev gamma-ray found by Bergström and Thulin and is therefore associated with the decay of an isomer of mass 133. Their suggestion that the 232-kev gamma-ray is emitted in an isomeric transition in Xe^{133} is probably correct. However, the half-life of 2-day is not the same as that of the 5.3-day beta-decay and therefore the two transitions cannot occur from a single metastable level in Xe^{133} as proposed in their decay scheme.

Bergström and Thulin have pointed out that the level assignments in the decay scheme they proposed were consistent with the nuclear shell model of Mayer.[3] This theory is also consistent with the experimental results reported here provided that the assignment of the 2-day metastable level is $h_{11/2}$ and the 5.3-day ground-state assignment is $d_{3/2}$.

It is hoped that work now in progress on parent-daughter relationships and internal conversion coefficients will help to establish decay schemes for I^{133} and Xe^{133}.

[1] I. Bergström and S. Thulin, Phys. Rev. 79, 538 (1950).
[2] Zeldes, Ketelle, and Brosi, Phys. Rev. 79, 901 (1950).
[3] M. G. Mayer, Phys. Rev. 78, 16 (1950).

Acceleration of Stripped C^{12} and C^{13} Nuclei in the Cyclotron*

J. F. MILLER, J. G. HAMILTON, T. M. PURNAM, H. R. HAYMOND, AND G. B. ROSSI
Crocker Laboratory, Divisions of Physics, Medical Physics, Medicine, and Radiology, University of California, Berkeley and San Francisco, California
September 11, 1950

THE acceleration of stripped C^{12} and O^{16} nuclei in the cyclotron has been reported.[1-4] The significance of this feat was limited by the fact that the obtainable intensities were far too small to produce a sufficient number of nuclear reactions to permit the detection of radio-isotopes formed by the transmutation of target nuclei by these heavy ions. The discovery of the transuranic elements has given considerable impetus to attempts to achieve this. For the last four years, a program to increase the intensities of accelerated heavy ions has been under way at the Crocker Laboratory using the 60-in. cyclotron. This program has included attempts to accelerate B^{10}, B^{11}, C^{12}, C^{13}, N^{14}, O^{16}, O^{17}, O^{18}, and F^{19}.

TABLE I. Ranges and energies of accelerated nuclei of He^4, C^{12}, and C^{13}.

Particle	Measured range (mg/cm^2 Al)	Expected range	Measured energy (Mev)	Expected energy (Mev)
$_2He^4$	158±2	158	38.6±0.4	38.6
$_6C^{12}$	53.5±2	54	115±2.4	116
$_6C^{13}$	55.5±2	58	122±2.5	125

To date, detectable intensities of completely stripped C^{12} and C^{13} ions have been observed. A hooded capillary ion source gave the best results. The source gas for the production of carbon ions was CO_2. Range determinations using aluminum absorbers were made and the data is summarized in Table I, giving the measured and expected range-energy relationships.

The maximum intensity of the external deflected beam of C^{12} ions that has been obtained to date is of the order of 10^5 C^{12} nuclei per second, and 10^4 C^{13} nuclei. In the case of C^{13}, material enriched to 50 percent of this isotope was employed.

Aluminum and gold were selected as target elements as they can be obtained in a high degree of purity and possess a single stable isotope. The transmutation products sought were Cl^{34} and the light isotopes of astatine. These possess conveniently short half-lives and may be isolated by relatively simple chemical procedures. The At isotopes were particularly attractive in view of the fact that the lighter ones, notably At^{203}, At^{204}, and At^{205} could not be produced in the 60-in. cyclotron by the ever-present contamination of alpha-particles.

Internal targets of Al and Au were bombarded. The 33-min. positron emitting Cl^{34} and the[5] 24-min. At^{205}, were chemically isolated and identified by the character of their radiations and rates of radioactive decay. Further proof identification was made of At^{205} by the use of the alpha-particle pulse analyzer developed by Ghiorso who made these determinations for us. The yields were in the range of from 0.1 to 0.002 microcurie. Assuming the cross section for the production of Cl^{34} from Al to be in the range of 0.1 barn, the internal C^{12} beam was estimated to be of the order of 10^8 ions per second. The nuclear reactions for the production of these two radio-isotopes are presumably $Al^{27}(C^{12}, \alpha n)Cl^{34}$, $Au^{197}(C^{12}, 4n)At^{205}$.

Internal target bombardment of Al with stripped C^{13} nuclei gave inconclusive results. The bombardment of Au with C^{13} ions produced a small amount of alpha-particle activity. The presence of 11- and 25-min. components suggests the possibility that the 7-min. At^{203} and 24-min. At^{205} had been produced.

Control runs were made to rule out radioactive contamination. Al and Au were bombarded with alpha-particles and runs were made using an argon arc at the magnetic resonance value for C^{12}. In both instances, no Cl^{34} from Al and no alpha-activity in the gold was observed. Covering the targets with 0.3-mil Al foil demonstrated that sputtering of radioactive materials in the cyclotron could not account for the production of Cl^{34} or the alpha-particle activity in the C^{12} and C^{13} bombarded Au.

The interest and encouragement of Professor Ernest O. Lawrence is acknowledge with gratitude. We wish to thank Mr. Ghiorso, Dr. Stanley Thompson, and Professor G. T. Seaborg for their valuable assistance and advice which greatly facilitated these experiments. The cooperation and aid of the 60-in. cyclotron crew were invaluable.

* This work has been performed in part under contract with the AEC.
[1] L. W. Alvarez, Phys. Rev. 58, 192 (1940).
[2] C. A. Tobias, Ph.D. thesis, University of California, 1941.
[3] R. I. Condit, Ph.D. thesis, University of California, 1942, and Phys. Rev. 62, 301 (1942).
[4] York, Hildebrand, Putnam, and Hamilton, Phys. Rev. 70, 446 (1946).
[5] Barton, Ghiorso, and Perlman, private communication.

Values of μ_p, F, and M_p/m_e Using the Omegatron

H. SOMMER, H. A. THOMAS, AND J. A. HIPPLE
National Bureau of Standards, Washington, D. C.
September 1, 1950

IN an earlier note,[1] we described a method of measuring the cyclotron frequency of ions with an instrument which we called the omegatron. In illustration of the promise of this method, we presented a preliminary value of the ratio of the cyclotron frequency of the proton ν_c to its precessional frequency ν_n in the same magnetic field. Because this preliminary value has been used by others in several publications, we feel that our most recent results should be made available, although further work will probably improve the accuracy.

A careful study made it apparent that the resonant frequency could be shifted by more than 1 part in 5000 by sufficiently varied operating conditions. A consistent method of correcting for these shifts, which are attributable largely to space charge, has now been developed. Since the frequency shift is proportional to the mass, the true cyclotron frequency can be determined by using the isotopic weights of the ions. The frequency shift can thus be determined by making measurements under identical experimental conditions on several masses. Consistent results for the proton have been obtained by correcting with H_2^+, D_2^+, and H_2O^+. A detailed description will be presented later. Our result is now

$$\nu_n/\nu_c = 2.79268 \pm 0.00006,$$

where ν_n was measured in water. This ratio is μ_p, the proton moment in nuclear magnetons[2] (without diamagnetic correction). Using the gyromagnetic ratio of the proton,[3]

$$\gamma_p = (2.67523 \pm 0.00006) \times 10^4 \text{ sec.}^{-1} \text{ gauss}^{-1}$$

(no diamagnetic correction), and the isotopic weight of the proton,[4] $A_p = 1.007580$, the faraday is

$$F = 9652.03 \pm 0.3 \text{ e.m.u./g (physical scale)}.$$

Combining our result on the frequency ratio with the measurement of Gardner and Purcell[5] one obtains

$$M_p/m_e = 1836.12 \pm 0.05.$$

[1] Hipple, Sommer, and Thomas, Phys. Rev. **76**, 1877 (1949).
[2] L. W. Alvarez and F. Bloch, Phys. Rev. **57**, 111 (1940).
[3] Thomas, Driscoll, and Hipple, Phys. Rev. **78**, 787 (1950).
[4] K. T. Bainbridge, "Isotopic Weights of the Fundamental Isotopes," Preliminary Report No. 1, Nat. Res. Council (June, 1948).
[5] J. H. Gardner and E. M. Purcell, Phys. Rev. **76**, 1262 (1949).

A New Method for Determining the Value of the Faraday

D. NORMAN CRAIG AND JAMES I. HOFFMAN
National Bureau of Standards, Washington, D. C.
September 1, 1950

IN a program on the redetermination of the value of the faraday at the National Bureau of Standards twelve determinations were made during the summer of 1949 by anodically oxidizing Bureau of Standards Standard Sodium Oxalate No. 40e in a sulfuric acid solution. As much as 12 g of oxalate was oxidized in a single determination. The average of all but the first result is 9651.93±0.26 e.m.u. Eq^{-1} (physical scale). The first result obtained is omitted from the average because it was agreed that a result obtained in a pilot run should not be averaged with the rest. Its inclusion would change the average less than 1 part in 100,000.

Final publication of the results is being delayed because the authors wish to assure themselves that the reaction,

$$C_2O_4^{--} - 2e \rightarrow 2CO_2,$$

is a pure one. All the evidence so far obtained indicates that this is so, but several additional rather difficult experiments will be required to verify the conclusions on the purity of the reaction. The final determinations are to be made by oxidizing an equivalent weight (67 g) of sodium oxalate. Tests have shown that this can be done. The purity of the sodium oxalate is taken as 99.96$_0$ percent. This value was most painstakingly established by the analytical work of H. B. Knowles and W. Stanley Clabaugh of this Bureau.

The value of the faraday determined electrolytically by the use of sodium oxalate should be of interest to those workers interested in the re-evaluation of the fundamental atomic constants[1,2] because the atomic weights of sodium, carbon, and oxygen are involved instead of the more conventional silver. Furthermore, approximately one-half of the sodium oxalate molecule, $Na_2C_2O_4$, consists of oxygen, whose atomic weight is given by definition. As far as the authors know, this reaction has never before been used to determine a value of the faraday.

Another part of the program at this Bureau is concerned with the anodic solution of pure silver and the cathodic deposition of silver in an electrolyte containing silver perchlorate and perchloric acid. The preliminary results obtained with the two methods involving silver are slightly higher than those obtained with oxalate, but the work has not progressed to the point where final values can be given. However, the average of all the results (25) obtained by the three methods is 9652.33±0.62 e.m.u. Eq^{-1} (physical scale).

In accordance with DuMond's suggestion (Phys. Rev. **77**, 411 (1950)) our values for one gram of singly charged ions of unit isotopic weight might be expressed on the physical scale as 9651.93±0.26 e.m.u./g and 9652.33±0.62 e.m.u./g, respectively. The electrochemist, however, prefers the definition in terms of an equivalent because this definition is an operational one.

[1] J. W. M. DuMond, Phys. Rev. **75**, 1267 (1949).
[2] J. A. Bearden and H. M. Watts, *A Reevaluation of the Fundamental Atomic Constants* (The Johns Hopkins University Radiation Laboratory, July 31, 1950).

Selection Rules for Closed Loop Processes

C. B. VAN WYK
University of Natal, Pietermaritzburg, South Africa
June 28, 1950

TRANSITIONS which can be described by closed loop Feynman diagrams[1] are sometimes forbidden by the symmetry existing between particles and antiparticles. Furry[2] dealt with the case in which electrons and positrons are the particles associated with the closed loop.

A proof of Furry's theorem which can be modified easily for the nucleon case is given in this note. The proof is so modified as to apply to the case of closed nucleon loops connecting meson lines.

The existence of a matrix C such that

$$X^T = \pm C \times C^{-1} \tag{1}$$

is well known.[3] Here X is a Dirac matrix and T denotes the operation of transposition. The upper sign holds for[4]

$$X = 1, \quad \gamma_\mu\gamma_\nu\gamma_\sigma(\mu \neq \nu \neq \sigma), \quad \gamma_1\gamma_2\gamma_3\gamma_4,$$

while the lower sign holds for

$$X = \gamma_\mu, \quad \gamma_\mu\gamma_\nu(\mu \neq \nu).$$

The first (second) group of matrices is called even (odd).

Consider the transition

$$\beta_1 \rightarrow \beta_2 + \beta_3 \tag{2}$$

between three neutral bosons (photons or neutral mesons), the process taking place by means of the virtual creation and annihilation of fermions. According to reference 1, the Feynman diagram will be a closed triangle of fermion and antifermion lines with boson lines at the vertices.

Let X_i ($i = 1, 2, 3$) be the Dirac matrices for the fermion-boson interactions. Suppose the fermion and antifermion are created

with the annihilation of B_1 and after the fermion has emitted B_2, the Fermi particles are annihilated with the emission of B_3. A second way in which this process can take place is obtained if the antifermion emits B_2. The triangles in the two cases differ only in the directions of the Feynman arrows.

The only difference in the matrix elements for the two transitions is that the first one contains the trace of the matrix

$$X=X_1(p_1-m)^{-1}X_2(p_2-m)^{-1}X_3(p_3-m)^{-1},$$

while the second contains the trace of the matrix

$$X'=X_1(-p_3-m)^{-1}X_3(-p_2-m)^{-1}X_2(-p_1-m)^{-1},$$

where p_i are appropriate functions of the energy-momentum four-vectors of bosons and Fermi particles combined with γ_μ according to Feynman. The minus signs of p_i in X' occur in the usual way when the behavior of fermions is contrasted with that of antifermions.

By Eq. (1)

$$X'^T=(-)^r CXC^{-1},$$

where r of the matrices X_i satisfy Eq. (1) with the minus sign. Taking the traces of the matrices makes it at once evident that the contributions of the two processes cancel each other if r is odd.

Other contributions to the total matrix element are obtained by permuting the processes involving B_i, which means orienting the triangle in different ways with respect to the time direction. These contributions can similarly be grouped into pairs.

For the sake of simplicity we have considered a triangular loop, but it is obvious that the above argument can be generalized for any closed loop. Hence, we have Furry's theorem for transitions between neutral bosons: processes associated with closed loops which can be traversed in opposite directions are forbidden if an odd number of odd Dirac matrices are associated with that closed loop.

Analogous selection rules can be formulated for the case where the bosons in Eq. (2) are neutral and charged mesons. In this case, to every way in which a transition can take place, there corresponds a second way which is obtained by replacing in the Feynman triangle, protons (neutrons) by antineutrons (antiprotons) or vice versa.

Let the contribution of the first process depend on the trace of

$$X=X_1\tau_i(p_1-m)^{-1}X_2\tau_j(p_2-m)^{-1}X_3\tau_k(p_3-m)^{-1},$$

where τ_i ($i=1, 2, 3$) are the isotopic spin matrices. The contribution from the second process then contains

$$X'=X_1\tau_1\tau_i\tau_1(-p_3-m)^{-1}X_3\tau_1\tau_k\tau_1(-p_2-m)^{-1}\times X_2\tau_1\tau_j\tau_1(-p_1-m)^{-1},$$

where the introduction of τ_1 effects the above replacements. Since

$$\tau_1\tau_i{}^T=\tau_i\tau_1 \quad (i=1, 2),$$
$$\tau_1\tau_3{}^T=-\tau_3\tau_1,$$

it follows that

$$X'^T=(-)^{r+s}CXC^{-1},$$

where r denotes the number of odd matrices among X_i ($i=1, 2, 3$), and s the number of neutral mesons.

This result can be generalized as follows for transitions between neutral and charged mesons via nucleons: Transitions between charged and neutral mesons associated with reversible closed nucleon loops are forbidden if the sum of the number of odd Dirac interaction matrices and the number of neutral mesons is odd.

The first theorem plays a fundamental role in a process like vacuum polarization. The second theorem will apply in cases where, for instance, a heavy charged meson decays into a lighter charged meson and a neutral one. Thus far no such decay process has been observed.

[1] R. P. Feynman, Phys. Rev. 76, 769 (1949).
[2] W. H. Furry, Phys. Rev. 51, 125 (1937).
[3] W. Pauli, Rev. Mod. Phys. 13, 203 (1941). Our C equals Pauli's C times γ_4.
[4] The γ-matrices are defined as in reference 1.

Disintegration of He^3 by Fast Neutrons*

J. H. Coon
University of California, Los Alamos Scientific Laboratory, Los Alamos, New Mexico
September 18, 1950

THE large cross section found to exist for the $He^3(n,p)T$ reaction at thermal neutron energy[1-3] indicates that this reaction may be investigated with relative ease for fast neutrons. Such an investigation has been carried out using techniques similar to those previously described.[2]

A proportional counter having a known sensitive volume was filled with a 31.4-cc sample of pure He^3 to which was added Kr at suitable pressure. Nearly monenergetic neutrons were produced at various energies in the range from 0.4 to 3.0 Mev by use of the two reactions: $T(p,n)He^3$ and $D(d,n)He^3$. The number of disintegrations induced in the He^3 by these neutrons was measured with the counter and neutron source located in well-defined geometry.

The absolute number of neutrons entering the counter was determined by use of a "long counter,"[4] the sensitivity of which was calibrated against the half-gram Ra-Be source No. 44 whose neutron source strength has been measured by Walker.[5]

The disintegration pulses were sorted by a 10-channel pulse-height analyzer. For the determination of the total number of disintegrations the pulse-height distribution curves were extrapolated (using an estimation of "wall effect") to zero pulse height, and the area under the curve was obtained numerically. The area under the extrapolated portion ranged from 20 to 45 percent of the total. It is estimated that the uncertainty of the extrapolation may introduce errors of from 15 to 20 percent in the cross-section determinations.

Measured cross-section values are indicated by the circles plotted in Fig. 1. The estimated probable error, including a guess

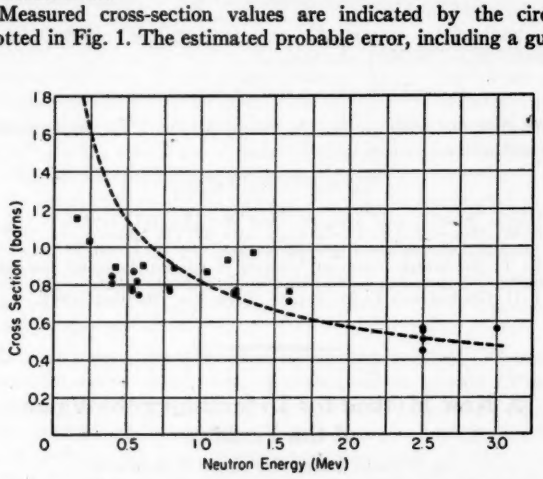

FIG. 1. Cross section for the reaction $He^3(n,p)T$ as a function of neutron energy. Directly measured values are indicated by circles. Values deduced by detailed balancing from measurements of the inverse reaction are indicated by squares. The solid curve is deduced by the $1/v$-law.

of systematic errors, is ± 30 percent. For comparison, the $1/v$-law dependence is shown as a dashed curve, though it it not to be expected that the data follow such a dependence. The results of King and Goldstein[3] for neutron absorption in the thermal region were used to deduce the $1/v$-curve.

The data of Jarvis, *et al.*[6] for the cross section of the inverse reaction, *viz.* $T(p,n)He^3$, may be compared with the present measurements by the principle of detailed balancing. The squares in Fig. 1 indicate values deduced from their data. Within experimental errors the two sets of values agree.

* Work done under the auspices of the AEC.
[1] Batchelor, Eppstein, Flowers, and Whittaker, Nature 163, 211 (1949).
[2] J. H. Coon and R. A Nobles, Phys. Rev. 75, 1358 (1949).
[3] L. D. P. King and Louis Goldstein, Phys. Rev. 75, 1366 (1949).
[4] A. O. Hansen and J. L. McKibben, Phys. Rev. 72, 673 (1947).
[5] R. L. Walker, MDDC 414, LADC 155, October, 1946, unpublished.
[6] Jarvis, Hemmendinger, Argo, and Taschek, Phys. Rev. 79, 929 (1950).

Internal Conversion of Gamma-Ray From Cs^{137}

M. A. WAGGONER
Department of Physics, State University of Iowa, Iowa City, Iowa*
September 15, 1950

THE decay scheme of Cs^{137} has been investigated previously by several research workers and been shown to consist of (1) a beta-decay ($E_0=0.518$ Mev) to a metastable state of Ba^{137} followed by a gamma-transition to the ground state, and (2) a beta-decay directly to the ground state of Ba^{137}. Although the higher energy beta-group was observed in the present investigation, no special attempt was made to measure its energy or abundance. The work of Osaba[1] indicates that between two and five percent of the total number of disintegrations proceed in this manner and that the end point of this high energy beta-group is about 1.18 Mev.

The present work yields (1) a value of 0.625 Mev for the energy of the peak of the K internal conversion line, (2) a value of 0.518 Mev for the end point of the low energy beta-group, and (3) a spectrum shape for the 0.518-Mev beta-group which gives a straight Fermi plot when corrected by the correction factor[2] G' and thus indicates that this transition involves a spin change of two with a change of parity. All of these results are in agreement with those of Osaba.

The spins of the ground states of Ba^{137} and Cs^{137} are known[3,4] to be 3/2 and 7/2, respectively.

The internal conversion coefficient for the 0.663-Mev gamma-ray has been measured by the group at Indiana[5] and by Osaba.[1] The values obtained were 0.118 and 0.081, respectively. Neither of these values is in close agreement with any of the theoretical values of Rose and his collaborators.[6]

The purpose of the present investigation has been to measure the internal conversion coefficient of the gamma-ray and recheck the shape of the low energy beta-spectrum. The observed shape of the low energy beta-spectrum is as stated above. The internal conversion coefficient has been measured by two methods. The internal conversion coefficient for the K shell is defined as the ratio of the number of electrons ejected from the K shell to the number of gamma-rays which are emitted. The number of K electrons ejected can be readily obtained by observing the internal conversion line with a beta-ray spectrometer. The one used by us is the double-coil, thin-lens magnetic spectrometer described briefly in a recent paper[7] by Waggoner, Moon, and Roberts and more fully in another paper now in press. The difficulty lines in determining the number of gamma-rays. This cannot be done by means of the standard coincidence techniques, since the Ba^{137} excited state is a metastable state. The first method we employed was to compare the external conversion line of the Cs^{137} gamma-ray with those obtained with identical converters from gamma-ray sources of other elements which could be calibrated by coincidence techniques. Appropriate allowance must, of course, be made for the dependence of the photoelectric absorption coefficient on energy. The empirical formula of Gray[8] was used to obtain the ratios of absorption coefficients. The values obtained for the internal conversion coefficient for the K shell by this method are 0.0969 and 0.0972 to give an average value of 0.097 ± 0.003. (The probable error quoted does not include the possible error in the ratios of photoelectric absorption coefficients used.) Because of the uncertainty as to the accuracy of the ratio of the photoelectric absorption coefficients used we wished to measure the internal conversion coefficient by another method. The second method employed was to compare the areas under the beta-ray spectrum and the internal conversion line. Since window thickness did not permit us to obtain valid data below about 120 kev, in order to obtain a complete momentum plot of the beta-ray spectrum it was necessary to obtain points for the momentum plot in the region below about 120 kev by extrapolating to zero the straight Fermi plot (correction factor G') observed at higher energies. Two independent values were obtained: 0.0986 and 0.0952 to give an average value of 0.097 ± 0.005 for the internal conversion coefficient for the K shell.

Comparison of the experimental values and the theoretical values[6] of the internal conversion coefficient for the K shell: $E(2^4)=0.025$, $E(2^5)=0.053$, $M(2^3)=0.045$, $M(2^4)=0.094$, $M(2^5)=0.25$ indicates that the gamma-ray is $M(2^4)$-pole radiation. Using the known spins of the ground states of Ba^{137} and Cs^{137} and assuming even parity for the ground state of Ba^{137} these results would indicate that the spins and parities of the Ba^{137}, Ba^{137*}, and Cs^{137} nuclear levels involved in the radioactive decay of Cs^{137} were 3/2, 11/2, 7/2; even, odd, even. This result is in agreement with the low abundance of the high energy beta-group (a spin change of two and no parity change places the transition in the second-forbidden class according to Gamow-Teller selection rules), the observed shape of the low energy beta-ray spectrum, Gamow-Teller selection rules and the Fermi theory for forbidden spectra, and the known half-life for the metastable state of Ba^{137} as well as the results of the nuclear shell model which predicts the same parity (even) for the ground states of Cs^{137} and Ba^{137}.

The author wishes to express her thanks to Dr. A. Roberts under whose direction this investigation was begun and to Mr. M. L. Moon who assisted in the construction and maintenance of the apparatus used.

* Present address: Department of Physics, Vassar College, Poughkeepsie, New York.

[1] J. S. Osaba, Phys. Rev. 76, 345 (1949).
[2] J. S. Osaba, Phys. Rev. 76, 345 (1949); E. J. Konopinski and G. E. Uhlenbeck, Phys. Rev. 60, 308 (1941); E. J. Konopinski, Rev. Mod. Phys. 15, 226 (1943).
[3] Davis, Nagle, and Zacharias, Phys. Rev. 76, 1068 (1949).
[4] Goldsmith and Inglis, *The Properties of Atomic Nuclei. I. Spins, Magnetic Moments and Electric Quadrupole Moments*, Brookhaven National Laboratory, October 1, 1948.
[5] C. L. Peacock, Phys. Rev. 76, 186 (1949).
[6] Rose, Goertzel, Spinrad, Harr, and Strong, Phys. Rev. 76, 184 (1949).
[7] Waggoner, Moon, and Roberts, Phys. Rev. 78, 295 (1950).
[8] L. H. Gray, Proc. Camb. Phil. Soc. 27, 103 (1931).

The Solar Atmosphere and the Origin of Radiofrequency Radiation

S. A. KORFF AND Y. BEERS
New York University, University Heights, New York, New York
September 18, 1950

RECENTLY a number of papers have appeared in this and other journals discussing radio noise measurements and interpreting these in terms of solar origin. Occasionally these interpretations draw a quite non-physical picture of conditions on the sun. Without wishing to criticize particular papers, we wish to point out a few relevant physical considerations.

First, the atmosphere of the sun is not, except in the broadest and most general sense, in equilibrium. Yet our concepts of temperature and radiation are usually based on equilibrium considerations. Pressures are extremely low, and one does not have to go far up above the photosphere to be in a region of free paths kilometers long. Through this rarified gas an enormous flux of radiant energy is pouring in one predominant direction. Our gas-kinetic concept of temperature as determined by atomic velocities is easily misinterpreted here. Since collisions are infrequent, there will be neither equipartition nor Maxwellian velocity distributions. Yet individual atoms as a result of repeated Compton encounters with the great flux of photons will acquire very high velocities, corresponding to temperatures of millions of degrees. But if a quantity of dense substance containing a hypothetical thermometer were placed here, the indicated temperature would be substantially below that of the photosphere, as the mass would receive energy from one direction and radiate in all directions.

Second, while ionization can be accomplished in a stepwise manner, recombination which depends on the square of the ion-density, is improbable because of the low pressures. A hydrogen atom does not have to absorb in one process a quantum equal to or greater than the Lyman series limit in order to lose its electron. The radiation flux is great enough to cause the higher energy levels of atoms to be well populated, as the Fraunhofer spectrum shows. Since the Balmer series appears strongly in absorption, there must be many hydrogen atoms in the second level and higher. Each

absorption act results in the momentum of the quantum being partly transferred to the atom, and these momenta have mainly one direction. The subsequent re-radiation is spherically symmetrical except insofar as stimulated emission may take place. The pressure of radiation is more important than thermal collisions in supporting the outer atmosphere against solar gravity.

This same situation obtains in certain diffuse nebulas. From the degree of excitation and ionization and from the character of the radiation one infers high temperatures. Millions of degrees are often cited in the literature. For true thermal equilibrium such temperatures would indeed be required. But the gas in most nebulas would be considered to be an excellent vacuum in most laboratories and its constituent atoms would not be in thermal equilibrium. It is important to recall the fictitious nature of these temperatures in considering mechanisms for the origin of cosmic radiation. The temperature of cosmic-ray particles, with with energies of some ten Bev would be around 10^{14} degrees. Nebulas are not "blackbodies."

Third, we cannot always correctly infer the temperature of a source from the noise-radiation which it emits. Clearly, if there are enough charges circulating about a sunspot to produce a field of thousands of gauss over many thousand square miles, there will also be enough charges in irregular, and hence accelerated, motion to produce abundant radiofrequency radiation. The irregular character of this motion would be expected to result in the radiation of continuum-like noise rather than particular frequencies, though at any one time one particular frequency or set of frequencies may be preferentially radiated. The radiofrequency radiation therefore will not necessarily be truly thermal.

No doubt much confusion is the result of a temptation to attach physical significance to the equivalent noise temperature T. This is a quantity used to express the available power of a source of noise. It is defined as the fictitious temperature of a resistor whose Johnson noise would have an available power equal to that of the source under observation. The convenience in this specification lies in the fact that the result is independent of the band width of the detecting device and the internal resistance of the source. The band width need never be measured, and the temperature T is determined directly. Whatever the method of measurement, however, it merely gives information in regard to power and nothing concerning the details of the mechanism of the origin. In most cases, of which the measurement of solar or celestial noise is one, the temperature T is purely a convenient fiction to which no direct physical significance can be attached.

Erratum: A Ferroelectric Curie Point in $KTaO_3$ at Very Low Temperatures

[Phys. Rev. 79, 885 (1950)]

J. K. Hulm, B. T. Matthias, and E. A. Long
Institute for the Study of Metals, University of Chicago, Chicago, Illinois

September 19, 1950

THROUGH a regrettable error, the word "ferromagnetic" was substituted for "ferroelectric" in the title of this Letter to the Editor as printed.

Proton-Proton Scattering at 100 Mev

R. W. Birge
Harvard University, Cambridge, Massachusetts

September 12, 1950

THE recent operation of the Harvard 95-in. cyclotron has made possible proton-proton scattering experiments in the 100-Mev region. The experiment described here is similar to one in progress at Rochester,[1] in that the equipment is placed directly inside the vacuum tank of the cyclotron.

The internal proton beam was intercepted by a ten-mil polyethylene foil mounted in the median plane of the magnet gap.

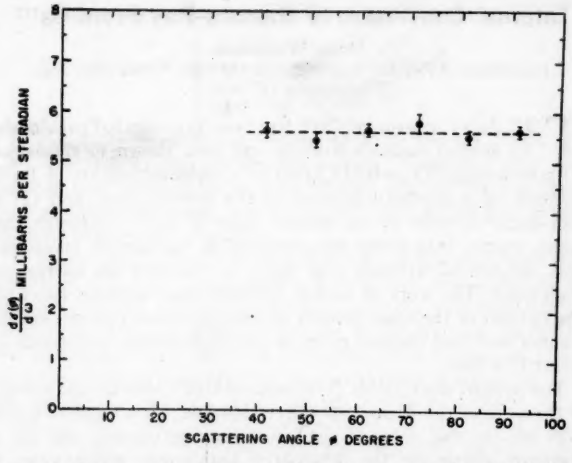

FIG. 1. Proton-proton differential scattering cross section at 100 Mev *versus* scattering angle in the center-of-mass system. Absolute value based on $C^{12}(p,pn)C^{11}$ cross section equal to 70 mb. The standard deviations shown are due only to the statistical fluctuations in the number of protons counted.

Anthracene scintillation crystals placed above and below the median plane counted the scattered and recoil protons in coincidence as in the method of Wilson and Creutz.[2] The light flashes from the crystals were transmitted through seven-foot Lucite rods to RCA 5819 photo-multiplier tubes placed in magnetic shields. The positions of the counters depended on the angle to be studied, but in all cases only those protons scattered in a vertical plane were counted. One counter defined the solid angle while the other counter was made much larger in order to detect all recoils associated with the protons entering the defining counter. The larger counter could be moved by remote control from the cyclotron control room. A plateau was obtained when the coincidence rate was plotted as a function of position of this counter. A delayed coincidence rate was used as a measure of the accidental coincidences.

To obtain suitable counting rates, the beam current of the cyclotron was reduced to about 10^{-12} amp. This was accomplished by shutting off the hydrogen supply and by placing flaps on the edge of the dee to reduce the height of the gap. Helium was let into the system to maintain the ion source arc, in order that the hydrogen remaining in the system would be ionized at the tank center as desired. In order to reduce the possibility of protons undergoing multiple traversals of the target, a beam height clipper with a one-fourth-in. gap was placed on the opposite side of the tank from the target. The multiple scattering in the target was sufficient to cause the protons to hit the clipper after one or two traversals.

For each scattering run the beam current was monitored by measuring the C^{11} positron activity formed in the polyethylene foil. Since the cross section for the formation of C^{11} is known,[3] it is possible to get an absolute differential cross section. However, the absolute value may be in error by as much as 20 percent whereas the relative angular cross section should be correct to better than 10 percent.

The differential scattering cross section in the center-of-mass system, shown in Fig. 1, appears to be isotropic within statistical deviation over the range of angles measured. Further details will be published at a later date.[4]

I wish to express my sincere appreciation to Professor N. F. Ramsey, under whose direction this work was performed.

[1] C. L. Oxley, Phys. Rev. 76, 461 (1949).
[2] R. R. Wilson and E. C. Creutz, Phys. Rev. 71, 339 (1947).
[3] W. W. Chupp and E. M. McMillan, Phys. Rev. 72, 873 (1947); E. M. McMillan and R. D. Miller, Phys. Rev. 73, 80 (1948); Aamodt, Peterson, and Phillips, Phys. Rev. 78, 87 (1950).
[4] A more detailed description has been given in a Ph.D. thesis presented to Harvard University.

On the Directional Correlation of Successive Nuclear Radiations

J. A. SPIERS
The Clarendon Laboratory, Oxford, England
September 18, 1950

IN a recent paper with the above title, Falkoff and Uhlenbeck[1] quote a general expression for the angular correlation function $W(\theta)$ between successive nuclear emissions:

$$W(\theta)=\sum_{M_0M_1M_2} P_{M_0M_1}(0)P_{M_1M_2}(\theta), \quad (1)$$

where M_0, M_1, M_2 are the z-components of total angular momentum of the possible spin orientations ("sub-levels") of the initial, intermediate, and final nuclear states, respectively; $P_{M_0M_1}(0)$ $P_{M_0M_1}(0)$ is the relative probability of emission of the first particle along the direction $\theta=0$ (axis of quantization) and $P_{M_1M_2}(\theta)$ the relative probability of emission of the second particle along a direction making an angle θ with this axis.

This expression has hitherto only been verified for particular applications. A general proof, involving only properties of the angular momentum, can be given as follows. The transitions in which the first and second particles, respectively, are emitted can be written

$$\psi J_0M_0 \rightarrow \sum_{j_1a_1} A_{j_1a_1} \sum_{m_1+M_1=M_0} C^{J_0J_1j_1}_{M_1m_1} \psi J_1M_1\phi^{(1)}_{j_1m_1a_1}, \quad (2)$$

$$\psi J_1M_1 \rightarrow \sum_{j_2a_2} A_{j_2a_2} \sum_{m_2+M_2=M_1} C^{J_1J_2j_2}_{M_2m_2} \psi J_2M_2\phi^{(2)}_{j_2m_2a_2}. \quad (3)$$

Here the C's are the usual Wigner coefficients, ψ's are nuclear wave functions, ϕ's are wave functions of the emitted particles with quantized total angular momenta (intrinsic spin plus orbital) j_1m_1, j_2m_2; a_1, a_2 denote any other quantities, e.g., polarization, required to specify the ϕ-states completely; $A_{j_1a_1}$ and $A_{j_2a_2}$ are complex amplitudes related to the transition probabilities for the various possible values of j_1a_1, j_2a_2, respectively.

Define

$$\Phi^{(1)}_{M_0M_1}=\sum_{j_1a_1} A_{j_1a_1} C^{J_0J_1j_1}_{M_1,\,M_0-M_1} \phi^{(1)}_{j_1,\,M_0-M_1,\,a_1}, \quad (4)$$

$$\Phi^{(2)}_{M_1M_2}=\sum_{j_2a_2} A_{j_2a_2} C^{J_1J_2j_2}_{M_2,\,M_1-M_2} \phi^{(2)}_{j_2,\,M_1-M_2,\,a_2}. \quad (5)$$

The final state $\psi_f{}^{M_0}$ of the system as a whole (after emission of both particles) can then be written, using (2)–(5), as

$$\psi_f{}^{M_0}=\sum_{M_1M_2} \Phi^{(1)}_{M_0M_1}\Phi^{(2)}_{M_1M_2}\psi J_2M_2. \quad (6)$$

Hence, by integrating the square modulus of $\psi_f{}^{M_0}$ over all nuclear variables and summing over spin orientations, we obtain the probability

$$W(\theta_1\phi_1,\,\theta_2\phi_2)=\sum_{M_0}\sum_{\sigma_1\sigma_2}\sum_{M_2}\sum_{M_1} |\Sigma\Phi^{(1)}_{M_0M_1}(r_1\sigma_1)\cdot\Phi^{(2)}_{M_1M_2}(r_2\sigma_2)|^2. \quad (7)$$

($r_1\equiv r_1\theta_1\phi_1$ are the coordinates of the first particle, σ_1 the z-component of its intrinsic (spin) angular momentum, and similarly for the second particle. r_1 and r_2 are assumed to be given some large but constant value in expression (7).)

The crux of the proof is to show that the summation over M_1 can also be brought outside the square modulus when we put $\theta_1=\phi_1=0$. Now the wave function of an emitted particle of intrinsic spin S has the form

$$\phi_{jma}(r\theta\phi\sigma)=\sum_{l=|j-s|}^{l=j+s} a_l C^{jlS}_{m-\sigma,\,\sigma} f_l(r)Y_l{}^{m-\sigma}(\theta,\phi). \quad (8)$$

The quantities a_l are constants depending on the state of polarization of the particle.

From (8) it can be seen that $\phi_{jma}(r_100\sigma_1)=0$ unless $\sigma_1=m_1$, hence that $\Phi^{(1)}_{M_0M_1}(r_100\sigma_1)=0$ unless $M_0-M_1=\sigma_1$. Thus there is only one value of M_1 which gives a non-vanishing term in expression (7) for given values of M_0, σ_1, and we may write

$$W(00,\,\theta_2\phi_2)=\sum_{M_0M_1M_2}\{\Sigma|\Phi^{(1)}_{M_0M_1}(r_100\sigma_1)|^2\cdot\Sigma|\Phi^{(2)}_{M_1M_2}(r_2\theta_2\phi_2\sigma_2)|^2\}, \quad (9)$$

whence the expression (1) follows immediately.

The argument given above applies to photons as well as to nuclear particle emissions; in this case the wave functions ϕ_{jma} are replaced by the Heitler spherical wave expansions for the electromagnetic vector potential[2] which can be put in the form (8) with $S=1$; also with a slight increase in complexity to β-emissions, (occurrence of suitable combinations of electron and neutrino "large" and "small" components, each of the form (8) with $S=\frac{1}{2}$, instead of single particle functions).

It should be pointed out incidentally that the absence of interference between transitions via different intermediate levels implied by (1) enables this expression to be put in the more symmetrical form[3]

$$W(\theta)=\sum_{M_0M_1M_1'M_2} P_{M_0M_1}(0)\cdot[D^{J_1}_{M_1M_2}{}'(\theta)]^*\cdot P_{M_1'M_2}(0), \quad (10)$$

where $D^{J_1}_{M_1M_1}{}'(\theta)$ is the irreducible representation of the spatial rotation group of order J_1; a form which is useful when the emitted particles (or photons) have high angular momentum (or multipole order), since the relative probabilities have only to be evaluated for emission along the axis of quantization.[4]

[1] D. L. Falkoff and G. E. Uhlenbeck, Phys. Rev. 79, 323 (1950) (Eq. (2a), with a slight change in notation).
[2] G. Goertzel, Phys. Rev. 70, 897 (1946); D. S. Ling and D. L. Falkoff, Phys. Rev. 76, 1639 (1949).
[3] J. A. Spiers, *Directional Effects in Radioactivity*, Nat. Res. Council of Canada, Chalk River, Ontario, April, 1949, p. 13. Goertzel, reference 2, verifies this expression for the particular case of $\gamma-\gamma$ correlation.
[4] This expression was used to calculate the correlation functions given in J. A. Spiers, Phys. Rev. 78, 75 (1950).

A Note on Neutron-Deficient Europium Activities*

GEOFFREY WILKINSON† AND HARRY G. HICKS‡
Radiation Laboratory and Department of Chemistry, University of California, Berkeley, California
September 13, 1950

A STUDY has been made of europium activities produced by bombardment of samarium oxide with 10-Mev protons from the 60-in. Crocker Laboratory cyclotron. The techniques of bombardment, chemical separation by ion exchange resin-column procedures, and determination of radiation characteristics by measurements with beryllium, aluminum, and lead absorbers have been described previously.[1]

In addition to the very long-lived activities Eu^{154}, Eu^{152}, and possibly lighter europium isotopes which have not been individually resolved, proton bombardment of samarium produces activities of half-lives 15.0±0.5 hours, 14±1 days, and 54±1 days.

The 15-hr. activity was determined by study on a simple magnetic spectrometer and decayed with emission of positrons of maximum energy 1.8 Mev. The negative sweep showed beta-particles of maximum energy approximately 1.8 Mev decaying with the half-life of the well-known 9.2-hr. Eu^{152} activity. The decay and lead absorption curves of the electromagnetic radiations were complex and difficult to resolve but no evidence of gamma-radiation harder than about 0.5 Mev associated with the 15-hr. activity was found. From the ratios of negative to positive electrons, of the total electron to electromagnetic radiations, and the known[2] K/β^--ratio of 0.22 for the 9.2-hr. Eu^{152}, and assuming 0.5 percent counting efficiency for the soft gamma-radiation in the standard argon-alcohol tubes used, the ratio γ/β^+ for the 15-hr. activity was found to be 2 to 2.3, showing that orbital electron capture accounts for less than about one-third of the disintegrations. On these assumptions the yield of the 15-hr. activity was

about one-third that of the 9.2-hr. activity in the proton bombardment of samarium suggesting allocation to mass 150.

A europium activity of half-life 27 hours, decaying by positron-emission, was reported to be formed by $(n,2n)$ reactions in europium[2] while recently a 15-hr. activity was produced by bombardment of europium with 23-Mev gamma-rays, presumably by (γ,n) reaction;[4] no radiation characteristics were given for these activities. Allocation of the 15-hr. activity to mass 150 seems therefore to be fairly certain.

In addition to very long-lived activities (5.3-yr. Eu^{154} and 5.2-yr. Eu^{152}), two additional activities of half-lives 14 ± 1 days and 54 ± 1 days were observed in the chemically separated europium fraction. The radiation characteristics were obtained by resolution of decay and aluminum, beryllium, and lead absorption curves after subtraction of the experimentally determined contributions of the long-lived activities. The 14-day activity decays with emission of soft electrons of about 100-kev energy, L and K x-rays, and a hard gamma-ray of around 1-Mev energy; the curves were rather difficult to resolve. The 54-day activity showed electrons of approximately 0.4-Mev energy, L and K x-radiations, and gamma-rays of energies about 0.4 Mev and 1.0 Mev. The ratios of various radiations of the 54-day activity corrected for counting efficiencies of x- and gamma-radiation, absorption in counter windows, etc., were $\sim$0.4 Mev e^-: L x-ray: K x-ray: $\sim$0.4-Mev gamma-ray: 1.0-Mev gamma-ray $=\sim0.05:\sim0.7:1:\sim0.3:\sim0.3$.

No positrons were observed in the radiations of either the 14-day or the 54-day activity and both presumably decay by orbital electron capture with gamma-rays arising from subsequent transitions. Marinsky and Glendenin have independently reported[5] similar activities in the europium fraction from deuteron bombarded samarium and have allocated the 14-day and 54-day activities to masses 149 and 147, respectively. The present data agree closely with this earlier work.

Of the europium isotopes which could be formed by (p,n) reactions in samarium, only Eu^{144} and Eu^{148} have not yet been observed; both might be expected to have short half-lives. In the present work half-lives less than a few hours would not have been detected.

* This work was done under the auspices of the AEC.
† Present address: Chemistry Department, Massachusetts Institute of Technology, Cambridge, Massachusetts.
‡ Present address: Chemistry Division, General Electric Company, Hanford Works, Richland, Washington.
[1] G. Wilkinson and H. G. Hicks, Phys. Rev. **75**, 1370 (1949).
[2] J. H. Reynolds and M. G. Inghram, Phys. Rev. **75**, 1500 (1949).
[3] M. L. Pool and L. L. Quill, Phys. Rev. **53**, 437 (1938).
[4] F. D. S. Butement, Nature **165**, 149 (1950).
[5] J. A. Marinsky and L. E. Glendenin, *Radiochemical Studies: The Fission Products* (McGraw-Hill Book Company, Inc., New York) (to be published), Paper No. 336, National Nuclear Energy Series, Plutonium Project Record, Vol. 9.

The Stars Initiated by Gamma-Rays

SEISHI KIKUCHI
Laboratory of Nuclear Studies, Cornell University, Ithaca, New York
September 14, 1950

WHILE the stars initiated by π-mesons, alpha-particles,[1] deuterons,[2] protons,[3] and neutrons[4] have been investigated by the photographic emulsion method, little is known about the stars initiated by gamma-rays. The following is a brief report of an experiment on the stars initiated by 300-Mev synchrotron gamma-rays.

Ilford C2 plates, 100-μ thick and insensitive to electrons, were exposed directly in the beam of gamma-rays about 3.3 meters from the synchrotron target. The intensity of the beam at the axis of the beam measured by a Victoreen Condenser r-meter behind a one-eighth-inch thick lead converter was about 600 r per hour. An exposure of a few minutes was most suitable to get a clear picture of the stars. An area of about 7.5 cm^2 was scanned and 750 stars were observed. That at least most of them are not due to π-mesons emitted by gamma-rays is clear from the difference in features of the stars in this case from that of π-meson stars. The fact that the most of the stars are obviously not associated with π-meson tracks also provides strong evidence that they are not due to π-mesons. A probability consideration shows that it is highly improbable that they are due to neutrons emitted by gamma-rays from the glass plate on which the emulsion is fixed or from the emulsion itself.

TABLE I. Distribution of prongs.

		2	3	4	5	6	7
Number of prongs							
Number of events		103*	64	57	24	4	1
Relative number of events relative to 3-prong star	gamma-rays	160	100	89	38	6.4	1.6
	π-mesons	180	100	51	12	—	—

* This figure is subjected to a larger error compared with other figures since two-prong stars are easily confused with a single track suffering a large angle scattering. Only such cases were counted where either the grain density is obviously different in both prongs or it was obvious from the change in grain density that the both prongs started from the point where they meet.

Two hundred and fifty-two stars obtained from one-third of the total area scanned were examined rather carefully. About 4 or 5 of them were suspected to be due to π-mesons. The distribution of prongs in the stars observed is shown in Table I. Prongs shorter than 5μ are not counted. The stars with four or more prongs are more abundant in this case than in the meson-produced stars.

To show the energy distribution of prongs more or less quantitatively the prongs were classified in five groups A, B, C, D, and E according to their energies. The energy of each prong was estimated by its range or by the visual comparison of the grain density with that of tracks of known residual ranges. In the latter case the accuracy is very low. The results are shown in Table II.

The exact comparison with the case of π-meson is difficult because of the large error involved in these figures. But it seems[5] that the prongs are on the average more energetic in this case than in the case of π-mesons.

TABLE II. Energy distribution of prongs.

A	B	C	D	E
>4500μ	4500–600μ	600–50μ	50–5μ	<5μ
60–30 Mev	30–10 Mev	10–2 Mev	2–0.2 Mev	<0.2 Mev
39	109	427	181	67

The cross section of the process averaged over all kind of atoms except hydrogen is estimated to be 4×10^{-28} cm^2. In this estimation the result of Blocker, Kenny, and Panofsky[6] was used, assuming that the r-value of the intensity at the beam axis 1 meter from the synchrotron target determined by us would give the same value as measured by the Berkeley method. The small difference in energy is also ignored. The error arising from these circumstances together with those arising from the inaccuracy involved in this experiment was estimated to be a factor of 5. The cross section is close to that for the π-meson production.

Many thanks are due to Professor R. R. Wilson for valuable suggestions and discussions, to other members of the laboratory for discussions as well as for the operation of the synchrotron and to Mrs. M. R. Keck for her valuable help in examining the plates.

[1] E. Gardner, Phys. Rev. **75**, 379 (1949).
[2] E. Gardner and V. Peterson, Phys. Rev. **75**, 364 (1949).
[3] Camerini, Fowler, Lock, and Muirhead, Phil. Mag. **41**, 413 (1950).
[4] Smith, Gardner, and Bradner, UCRL 527, November 23, 1949.
[5] See for instance W. B. Cleston and L. J. B. Goldfarb, Phys. Rev. **78**, 683 (1950).
[6] Blocker, Kenny, and Panofsky, Phys. Rev. **79**, 419 (1950).

The Relation between Phase Stability and First-Order Focusing in Linear Accelerators

EDWIN M. MCMILLAN
Radiation Laboratory, Department of Physics, University of California, Berkeley, California
September 11, 1950

IT is well known that phase stability and first-order focusing are incompatible in a simple linear accelerator without foils or grids in the path of the particles.[1] However, various attempts have been made to design more complicated field shapes and time variations that will circumvent this limitation. A general proof that the limitation exists in all cases was made by the author in 1945 but was not published at that time. This proof is given below.

A particle of charge e moves parallel to the z-axis with velocity v and is acted on by fields $\mathbf{E}$ and $\mathbf{H}$, which are periodic in time and nearly periodic along the z-axis. The time period is T and the corresponding repeat length L is equal to vT. Changes in velocity and direction during one repeat length will be neglected; this is what we mean by the term "first order." The time corresponding to the position z is then given by $t_0+(z/v)$, where t_0 is an arbitrary starting time.

The focusing effect depends on the x and y force components F_x and F_y, whose mean values are given by

$$\bar{F}_x=(e/vT)\int_0^L[E_x-(v/c)H_y]dz,$$
$$\bar{F}_y=(e/vT)\int_0^L[E_y+(v/c)H_x]dz, \tag{1}$$

the field components being evaluated at the position and corresponding time of the moving particle. If the line of motion is chosen so that both these forces vanish, the restoring force constants toward this line are

$$k_x=-\partial\bar{F}_x/\partial x, \quad k_y=-\partial\bar{F}_y/\partial y. \tag{2}$$

From Eqs. (1) and (2) we get

$$k_x+k_y=(e/vT)\int_0^L\{-[(\partial E_x/\partial x)+(\partial E_y/\partial y)]+(v/c)[(\partial H_y/\partial x)-(\partial H_x/\partial y)]\}dz. \tag{3}$$

With the aid of the Maxwell equations $\mathrm{div}\mathbf{E}=0$,

$$\mathrm{curl}\mathbf{H}=(1/c)\partial\mathbf{E}/\partial t,$$

this becomes

$$k_x+k_y=(e/vT)\int_0^L[(\partial E_x/\partial z)+(v/c^2)\partial E_x/\partial t]dz. \tag{4}$$

Finally, since $\partial/\partial z=(d/dz)-(1/v)\partial/\partial t$, we can write

$$k_x+k_y=(e/vT)[E_x]_0^L-(e/v^2T)(1-v^2/c^2)\int_0^L(\partial E_x/\partial t)dz. \tag{5}$$

Next consider the energy gain ΔW during one period, given by

$$\Delta W=e\int_0^L E_x dz. \tag{6}$$

This depends on the starting time t_0, and its rate of change with t_0 is

$$\partial(\Delta W)/\partial t_0=e\int_0^L(\partial E_x/\partial t)dz. \tag{7}$$

Combining Eqs. (5) and (7), we obtain the relation

$$k_x+k_y=(e/vT)[E_x]_0^L-(1/v^2T)(1-v^2/c^2)\partial(\Delta W)/\partial t_0. \tag{8}$$

Now, in order to have phase stability, $\partial(\Delta W)/\partial t_0$ must be positive, since an increasing t_0 means that the particle is too slow and therefore has an energy defficiency. In order to have focusing, both k_x and k_y must be positive; this is clearly incompatible with the above requirement unless some help is obtained from the first term on the right of Eq. (8). This term depends on the difference in E_x experienced by the particle on leaving and entering the repeat length, and is obviously zero in the absence of foils or grids. With a foil placed so that the field strength on one side is zero, it is determined by the field strength on the other side at the instant the particle enters the foil. (The repeat length must be taken as ending at the foil, since the field equations used are not valid inside a conductor.) In the case of a grid, the effect is essentially the same, even though there is no field discontinuity through a grid opening; the focusing force can then be considered as arising from the charge lying between the equilibrium path and the displaced path.

[1] V. K. Zworykin, Morton, Ramberg, Hillier, and Vance, *Electron Optics and the Electron Microscope* (John Wiley & Sons, Inc., 1945), pp. 660–664; Ginzton, Hansen, and Kennedy, Rev. Sci. Inst. 19, 89 (1948).

Production of π^+-Mesons by X-Rays as a Function of Atomic Number*

R. F. MOZLEY
Radiation Laboratory, Department of Physics, University of California, Berkeley, California
July 31, 1950

THE electronic method of meson detection developed by Steinberger and Bishop[1] has been used to study the relative cross sections of various elements for production of π^+-mesons by x-rays.

This study has been made at an angle of 90±8 degrees to the x-ray beam, at approximately 317-Mev synchrotron energy, and at meson energies of 42±7 Mev and 76±6 Mev. The targets used were of identical shape and approximately 1.5 g/cm² for both x-ray beam and mesons. With two exceptions the targets were of approximately equivalent meson ranges. The tin and lead targets were of about 1/10 the range, and corrections of about 10 percent were required for this. The other corrections required for meson range, attenuation of the x-ray beam, inpurities,[2] and decay of mesons in flight were of the order of 2 percent or less in most cases. No correction has been made for nuclear scattering or nuclear absorption of the mesons in the absorbers. The hydrogen cross section was obtained by a polyethylene, carbon subtraction.

The values of the relative cross sections per proton in the nucleus are given in Table I in arbitrary units.

TABLE I. Relative cross sections per proton for the production of π^+-mesons by x-rays from the synchrotron.

Element	42 Mev	Standard deviation[a] (percent)	76 Mev	Standard deviation[a] (percent)
H	6.6	17	8.07	11
Li	3.32	10	2.80	11
Be	2.82	11	2.13	10
B	3.02	11	2.28	15
C	2.60	6	1.93	5
Al	2.50	11	1.68	9
Cu	1.92	19	1.17	15
Sn	1.66	25	0.51	55
Pb	0.51	91	0.80	65

[a] Additional non-statistical errors may be as large as 10 percent for hydrogen, tin, and lead, and 5 percent for the others.

Steinberger, Panofsky, and Steller have made similar measurements as yet unpublished[3] on the yields of 75 Mev *neutral* mesons, using the method described in their recent paper.[4] Relative cross sections were obtained for hydrogen, lithium, beryllium, carbon, aluminum, copper, and lead. When these are tabulated in terms of the cross section per nucleon, σ_{π^0}/A, and arbitrarily normalized to the σ_{π^+}/Z data at beryllium, all except hydrogen agree within the statistical error. Their hydrogen value is approximately the same as the lithium cross section per nucleon.

It is apparent from the above that at least two factors contribute to the decrease of σ/Z with atomic number, one dependent on and the other independent of the meson charge. Chew and Lewis[5] have suggested that for π^+-mesons σ/Z may be higher for hydrogen than for other elements, since the exclusion principle limits the phase space available for the residual neutron. For other

elements lower neutron states are occupied. Such an effect would be less with neutral mesons, since the residual nucleon does not have a changed sign.

The further decrease of σ_{π^+}/Z and σ_{π^0}/A with atomic number is not incompatible with the possibility that only the nucleons on the surface of the nucleus take part in the production of mesons. The decrease cannot readily be explained by screening of the internal nucleons from the x-rays and hence possibly may be caused by an interaction of the outgoing π-mesons with the nucleons.

If it is assumed that such an interaction is the entire cause of the effect, a calculation can be made of the mean free path of mesons in nuclear matter. Although the calculated decrease is relatively insensitive to the mean free path assumed, the data are incompatible with a mean free path greater than approximately five times the proton radius.

It is a pleasure to acknowledge the assistance of Dr. J. Steinberger in all parts of this experiment. I wish also to express my gratitude to Professors E. McMillan and W. K. H. Panofsky for their interest and advice. My sincere thanks also go to Mr. Walter Gibbins and the entire synchrotron crew.

* This work was sponsored by the AEC.
[1] J. L. Steinberger and A. S. Bishop, Phys. Rev. **78**, 493 (1950).
[2] Analysis of purity performed by Conway and Moore.
[3] Steinberger, Panofsky, and Steller have kindly allowed me to quote their as yet unpublished work.
[4] Steinberger, Panofsky, and Steller, Phys. Rev. **78**, 802 (1950).
[5] G. Chew, private communication.

Isotope Shift in the Atomic Spectrum of Carbon

CLYDE R. BURNETT
University of Wisconsin, Madison, Wisconsin*
September 18, 1950

THE isotope shift between C^{12} and C^{13} in the λ2837 doublet in C II has been resolved and previous results[1] on λ2478 and C I have been verified. The observed shifts are given in Table I. In each case the C^{13} was found to be shifted to lower frequency. The normal mass effect can be calculated readily from the change in the Rydberg constant with a result of $+0.142$ cm^{-1} for λ2478 and $+0.124$ cm^{-1} for λ2837, leaving the algebraic differences from the observed values to be accounted for by the "specific mass effect."[2]

TABLE I. Isotope shifts for carbon.

		λ	Observed shift (cm^{-1})
C II	$2s2p^2\ ^2S_{1/2}-2s^23p\ ^2P_{3/2}$	2836.7	-0.612 ± 0.002
	$2s2p^2\ ^2S_{1/2}-2s^23p\ ^2P_{1/2}$	2837.6	-0.623 ± 0.003
C I	$2p^2\ ^1S_0-2p3s\ ^1P_1$	2478.5	-0.156 ± 0.003

The hyperfine structure due to the magnetic moment in C^{13} was too small to be observed. Resolution of the isotope shifts was obtained by use of a Fabry-Perot interferometer with aluminized mirrors of approximately 75 percent reflectivity, crossed with a quartz Littrow spectrograph.

The carbon spectrum was obtained from a Schüler liquid-air cooled hollow cathode source of the type developed by Arroe and Mack,[3] charged with KCN enriched with 63 percent C^{13}. A static helium supply[3] provided the carrier gas, and the hollow cathodes were made from both aluminum and magnesium.

Measurements were made with 4-, 4.5-, and 12-mm spacers for the C II doublet and with a 15-mm spacer for the C I line. Positive identification of the components was made by two procedures. In one of these, some $KC^{12}N$ was added to the cathode and the resultant relative change in intensities noted. Also exposures were taken on adjacent sections of the spectrograph slit with no change in the positions of the interferometer and photographic plate, first with a cathode containing the enriched sample and then with another cathode containing ordinary KCN.

I wish to express my thanks to Professor J. E. Mack, under whose direction this research was begun, for his interest and advice during progress of the work.

* Project supported by the ONR.
[1] J. R. Holmes, Phys. Rev. **77**, 745 (1950).
[2] D. S. Hughes and C. Eckart, Phys. Rev. **36**, 694 (1930).
[3] O. H. Arroe and J. E. Mack, J. Opt. Soc. Am. **40**, 386 (1950).